Title

Total Synthesis of Topologically Complex Natural Products: Aconitine-Type Diterpenoid Alkaloids, Simplified Analogs and Sesterterpene Somaliensene A

Author

Doering, Nicolle Ashley

Publication Date

2020

Peer reviewed|Thesis/dissertation

Total Synthesis of Topologically Complex Natural Products: Aconitine-Type Diterpenoid Alkaloids, Simplified Analogs and Sesterterpene Somaliensene A

by

Nicolle A. Doering

A dissertation submitted in partial satisfaction of the

requirements for the degree of

Doctor of Philosophy

in

Chemistry

in the

Graduate Division

of the

University of California, Berkeley

Committee in charge:

Professor Richmond Sarpong, Chair
Professor Thomas J. Maimone
Professor Polina V. Lishko

Spring 2020

Total Synthesis of Topologically Complex Natural Products: Aconitine-Type Diterpenoid Alkaloids, Simplified Analogs and Sesterterpene Somaliensene A

Abstract

Total Synthesis of Topologically Complex Natural Products: Aconitine-Type Diterpenoid Alkaloids, Simplified Analogs and Sesterterpene Somaliensene A

by

Nicolle A. Doering

Doctor of Philosophy in Chemistry

University of California, Berkeley

Professor Richmond Sarpong, Chair

The synthesis of aconitine-type diterpenoid alkaloids and analogs thereof has been completed. The first chapter of this dissertation introduces the diterpenoid alkaloid natural products and seminal studies toward their synthesis. The second chapter details strategies used to construct the polycyclic scaffolds of these highly bridged molecules, including both previous synthetic work and our own total synthesis of weisaconitine D. The third chapter focuses on the biological activity of these natural products and synthesis of analogs thereof to enable structure–activity relationship studies. The final chapter details ongoing studies regarding the rearrangement of strained [3.1.1] bicycles for use in terpene synthesis.

Chapter 1 includes discussion of the classification and biological activity of these topologically complex natural products. Seminal syntheses by both Nagata and Wiesner of two relatively simple diterpenoid alkaloids, atisine and garryine, are discussed alongside Wiesner's later synthesis of the more highly bridged talatisamine.

Chapter 2 details how the use of bond-network analysis can provide clues on how to put together these highly caged scaffolds. The efficacy of this approach is evaluated in the context of eight modern syntheses of hetidine- and hetisine-type diterpenoid alkaloids. Bond-network analysis is then applied to the retrosynthesis of the aconitine-type diterpenoid alkaloids, identifying key disconnections that were ultimately applied successfully in the total synthesis of weisaconitine D. Two late-stage bicyclization strategies—the originally planned meta-π-arene photocycloaddition and an alternative Diels–Alder cycloaddition/Wagner–Meerwein rearrangement sequence—are discussed.

Chapter 3 includes further discussion of the biological activity of the aconitine-type diterpenoid alkaloids, focusing on their modulation of voltage-gated sodium ion channels. The effects of two representative compounds, aconitine and lappaconitine, were evaluated in collaboration with Dr. David Hackos of Genentech and used as the starting point for structure–activity relationship studies using simplified analogs of these diterpenoid alkaloids. The design and synthesis of these analogs is discussed.

Chapter 4 focuses on the synthesis and rearrangement of strained [3.1.1] bicycles as part of an ongoing effort to synthesize terpene natural products. Discussion includes synthetic progress toward the sesterterpene somaliensene A from carvone using a strategy featuring cyclization and deoxygenation, as well as toward the diterpene xishacorene B from verbenone using a strategy featuring rearrangement and ring expansion.

To my parents,
who will understand almost nothing discussed in this dissertation, but will (pretend to) read it nonetheless,
my sister,
whom I wish the best of luck as she starts her own PhD,
and Jaxx,
who won't care about any of this because it's not edible.

Contents

Acknowledgements

I would like to begin by thanking all of the members of the Sarpong lab, past and present, for being so welcoming and creating a group that felt more like family than a collection of co-workers. Given the long hours we all spent in the lab, this has always been one of the biggest selling points of the lab in my mind.

I would particularly like to thank all of my labmates in 847 Latimer over the years, as well as my labmates Brian and Danilo from my brief stint working in 844. It was a pleasure working with all of you. I really appreciate all of the helpful discussions at white boards, fume hoods, in the NMR room, and all of the places in between.

Of all of my labmates, one person really stood out as an excellent mentor. Kevin, I don't even know where to start thanking you. I could not have asked for a better mentor as an incoming grad student. You were endlessly patient with me, answering my many questions and taking the time to make sure I knew the best way to do everything. I know you had a lot on your plate, but you never made me feel as though you didn't have time for me. You also made a great late-night lab buddy. Our room was sadly lacking in night owls after you left.

Additionally, thank you to all of the other wonderful scientists with whom I have had the opportunity to collaborate, both within the group and externally. Krissada, Kim, and Kerry: it was great to work with you in the lab. I'm not sure why I only ended up working directly with people whose names start with "K" but, weird coincidences aside, I could not have asked for a better set of teammates. Shelby, it was great to be the last of the diterpenoid alkaloid subgroup with you. Writing review articles with you and with Prof. Hoffmann was really interesting and felt like a fitting end to the diterpenoid alkaloid story.

Of course, my acknowledgements of all of the people in the Sarpong lab would not be complete without acknowledgement of Prof. Richmond Sarpong himself. Richmond, it has been a privilege to be a part of your research group. We may not have always seen eye-to-eye, but you have always been a great mentor and supported me in both my research and career goals. I appreciate your commitment to our ongoing education and your high standards for science communication, as well as how hard you work to keep abreast of everyone's research progress. I know it isn't easy to stay up-to-date on all of the projects in such a large group and am thankful that you do it anyway.

To Dr. Dave Hackos and the rest of the team at Genentech, thank you for bringing me on as a summer intern. I had no formal training in electrophysiology (review articles and YouTube videos can only get you so far) going into the summer and had no experience working with cells, but you took a chance on me anyway. I really appreciate the time you took to explain *why* and not just *how*.

Hasan, thank you for all of your hard work keeping the NMR facility up and running. Between Latimer being Latimer, power shutoffs, and the apparent inability of us users to follow instructions, it is nothing short of extraordinary that you have managed to keep the facility from imploding, let alone how dramatically you have improved it in the last few years. Thank you to Kathy, Yinka, and Dave for all of your help with computations. The Molecular Graphics & Computational Facility is an amazing resource that wouldn't exist without you. I would also like to

thank Antonio and Nick for acquiring and solving all of the X-ray crystal structures that appear in this dissertation, as well as Lynn, Joel, and the rest of the graduate office for all of their administrative help. Meggie, many thanks for all you do to keep the Sarpong lab running.

I also owe endless gratitude to the friends outside of the Sarpong lab who kept me (mostly) sane throughout this journey. Alexis, thank you for introducing me to the Society of Women in the Physical Sciences and to Iota Sigma Pi. Being a woman in STEM can be isolating sometimes, but joining SWPS and ISP helped me to feel like part of a larger community of women.

Amélie, (Yes, this section is alphabetized. This should cause you absolutely no surprise.) thank you for being an amazing roommate. I will miss margarita/GNT nights on the couch when you head back to Europe. Also, for the record, I 100% blame you for the small fortune I now spend on yarn to feed my crochet addiction. My only consolation is that you are equally addicted to knitting, so I am not the only little old lady in our apartment. I'm going to hold you to your promise that we will continue to craft together via Skype even if it means that I will have to actually drag myself out of bed before noon on a weekend.

Jenna & Morgan, thanks for putting up with my ridiculous schedule all this time. Our paths have diverged a lot over the last 20 years, but I'm glad we have all found things that we are passionate about and have been able to find the time to meet up in person periodically. While that's going to get a lot harder when Jenna moves to Japan or Norway on us, I'm sure we'll figure it out.

Zach, I'm not sure you count as a friend from outside of the Sarpong lab. For all that you had "left" the lab by the time that we met, I think you spent enough time in 847 to count as a labmate given how often you visited Paul or me. Thank you for being a great friend and mentor. Your enthusiasm never fails to brighten my day. I always really enjoy chatting with you on our probably-too-frequent bubble tea outings.

As I thank all of the amazing people who helped me make it through the last five years, I also want to take a moment to thank all of the people who got me to Berkeley in the first place. As I tell the students I meet through the BASIS (Bay Area Scientists in Schools) program, this year I would have been in the 21st grade if we kept counting on past high school. I like that sentiment because, no matter that it sometimes feels like the time before grad school was a lifetime ago, it is a reminder that graduate school does not exist in a vacuum. As such, I want to thank a few of the people who set me up for success in my chosen path.

Mrs. Phillips, thank you for pushing me to do better. You were the first to teach me the difference between completing tasks and actually engaging with the material. My dad always said that you were the one who taught me how to learn. Also, thank you for failing me in handwriting. I now have handwriting more comparable to type than the chicken scratch to which I subjected you.

Coach Nacho Zarate, thank you for teaching me discipline, persistence, and the value of hard work. I'm guessing you never expected to end up in the acknowledgements of a chemistry dissertation, but I never would have made it through the last five years if not for the lessons I learned playing soccer on your team.

Mr. Widler, thank you for introducing me to chemistry. You (and all of other teachers I had at Franklin) did an amazing job of making the course material interesting and understandable.

Entering UC Santa Barbara, everyone told us that high school was a lot easier than college and we would need to step up our game to do well, but we were ready for it because of you.

Armen, it was a pleasure to do my undergraduate research in your lab. Thank you for providing the mentorship I needed while also allowing me the freedom to begin to find myself as an independent researcher. Jeff and Aaron, you were great mentors and labmates. Beyond teaching me all of the lab skills I needed to do well in grad school, I thank you and the rest of the Zakarian lab for making me feel welcome and included in the lab. I never felt isolated despite being the only undergrad and/or the only woman for large portions of the three years I spent in the lab. The poker nights and lab beach volleyball are some of my favorite memories from Santa Barbara (even if I never did manage to break even at poker).

Last, but certainly not least, are my parents and the rest of the family. I can't even begin to express how much your love and support has meant to me throughout the years. Dad, I'm sorry I didn't end up with a degree in computer science. Apparently, no amount of decimal–binary conversion in the car on the way to soccer practice could overcome the draw to chemistry. Mom, thanks for always being willing to talk things through with me even when the "u got 5 min?" text turns into an hour on the phone. Special thanks to Jaxx as well for keeping me company while I wrote this dissertation in quarantine. My room is covered in dog fur, but it was worth it.

This is by no means a comprehensive list of all of the people to whom I am grateful; so many people have touched my life that I could never do justice to such a list. Therefore, I close with a simple thank you to all of the people I have had the opportunity to learn from and work with along the way. I could not have done it without you.

Chapter 1

An introduction to the diterpenoid alkaloids

The diterpenoid alkaloids are a collection of over 1,200 complex, bridged, polycyclic natural products derived primarily from flowering plants in the *Aconitum*, *Consolida*, and *Delphinium* genera.[1–3] Categorized as C_{18}-, C_{19}-, or C_{20}-diterpenoid alkaloids based on the number of carbon atoms comprising their cores, these natural products arise biosynthetically through various rearrangements of geranylgeranylpyrophosphate (see Section 2.1.1 for further discussion). The topological complexity of these multiply-bridged scaffolds, as well as the potent biological activities of multiple members of the family, explain why this class of molecules has continued to be of interest to the scientific community for over a century.[4,5]

The diterpenoid alkaloids are known to possess analgesic, anti-inflammatory, anti-arrhythmic, and other pharmacological activities.[1–3] The plants from which these pseudoalkaloids are isolated have long been used in traditional medicine for the treatment of pain and cardiovascular diseases. In fact, Guan-fu base A (**1.1**, Figure 1.1) is marketed as an anti-arrhythmic agent in China.[6] Perhaps most intriguing is the ability of some diterpenoid alkaloids to modulate voltage-gated sodium (Na_V) or potassium (K_V) ion channels.[7] For example, aconitine (**1.3**) is a Na_V channel activator.[8] However, structurally related lappaconitine (**1.5**) is a Na_V channel blocker.[9] The potential for these molecules to act as subtype-selective ion channel modulators has significant implications for treating channelopathies without causing undesirable side effect profiles.[10,11] However, few of these secondary metabolites have been studied for their function due to inadequate accessibility. Developing synthesis strategies that provide access to a variety of these natural products and related unnatural analogs would facilitate studies into their structure–activity relationships and provide myriad opportunities for clinical applications (see Section 3.1 for further discussion).

Early studies on the synthesis of these structurally complex molecules were conducted in the 1960s and 1970s.[12] Among the first diterpenoid alkaloids to be synthesized were atisine (**1.2**) and garryine (**1.24**), which were explored contemporaneously by Nagata and Wiesner, among others.[13] Wiesner went on to synthesize the first aconitine-type diterpenoid alkaloid, talatisamine (**1.4**).[14] While lengthy, these contributions set the stage for the field and provided inspiration that can still be seen in modern syntheses, such that of weisaconitine D (**1.6**) by our laboratory. Recent approaches to diterpenoid alkaloid synthesis are the focus of Chapter 2.

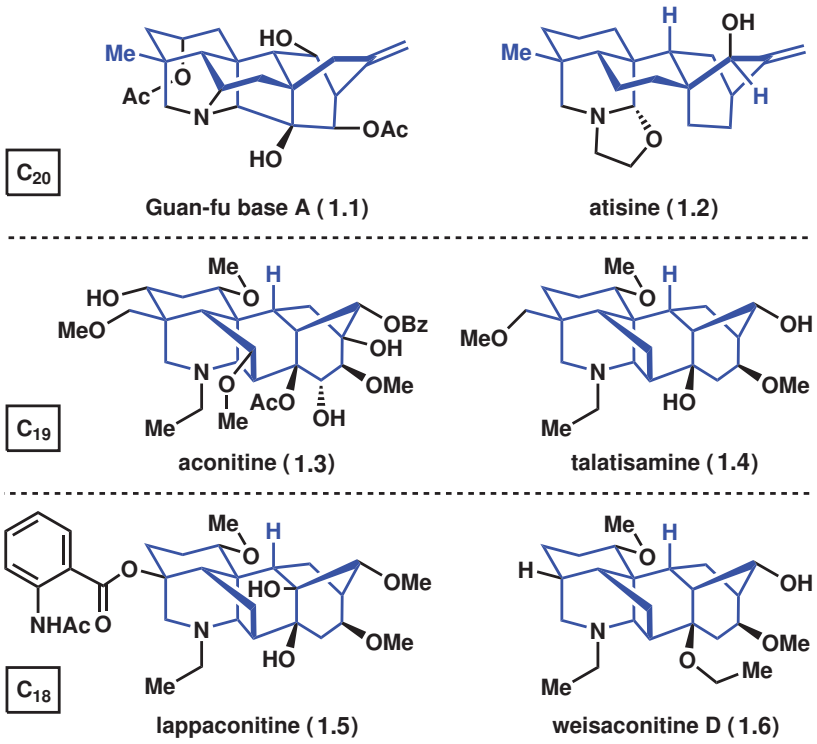

Figure 1.1: Selected examples of diterpenoid alkaloids.

1.1 Seminal syntheses by Nagata and co-workers

1.1.1 The first diterpenoid alkaloid total synthesis: atisine

Nagata's synthesis of atisine (**1.2**) began from a simple tricycle (**1.7**), which could be advanced in four steps to nitrile **1.8** (Scheme 1.1).[15] Treatment of this nitrile with base in aqueous methanol converted the cyano group to a primary amide, which spontaneously engaged the aldehyde group to give a hemiaminal (the new bond is highlighted in blue). This hemiaminal could be trapped with triethyl orthoformate to give tetracycle **1.9** as an inconsequential mixture of diastereomers, which could be advanced together through a series of reduction steps to give enone **1.10**. From there, a sequence of four additional steps effected what was formally 1,4-addition of an acetyl group into enone **1.10** to give diketone **1.11**. An intramolecular aldol reaction then forged [3.2.1] bicycle **1.12**, which was transformed into mesylate **1.13** through acetylation, ketone reduction, and mesylation of the resultant secondary alcohol. Mesylate **1.13** fragmented under basic conditions, the alkoxide adding into the acetate carbonyl and inducing cleavage of the C–C bond marked in red with concomitant elimination of the mesylate to give terminal alkene **1.14**. This constituted a net dehydration of diketone **1.11**. Alkene **1.14** was converted into primary mesylate **1.15** in five steps, setting the stage for cyclization to give a [2.2.2] bicycle (**1.16**) containing the complete pentacyclic core of atisine. Ketone **1.16** then underwent a series of functional group manipulations to give allylic alcohol **1.17**, the conversion of which to atisine had been previously reported by Pelletier and Parthasarathy in a relay synthesis from the natural product.[16] This thus constituted the first total synthesis of a diterpenoid alkaloid.

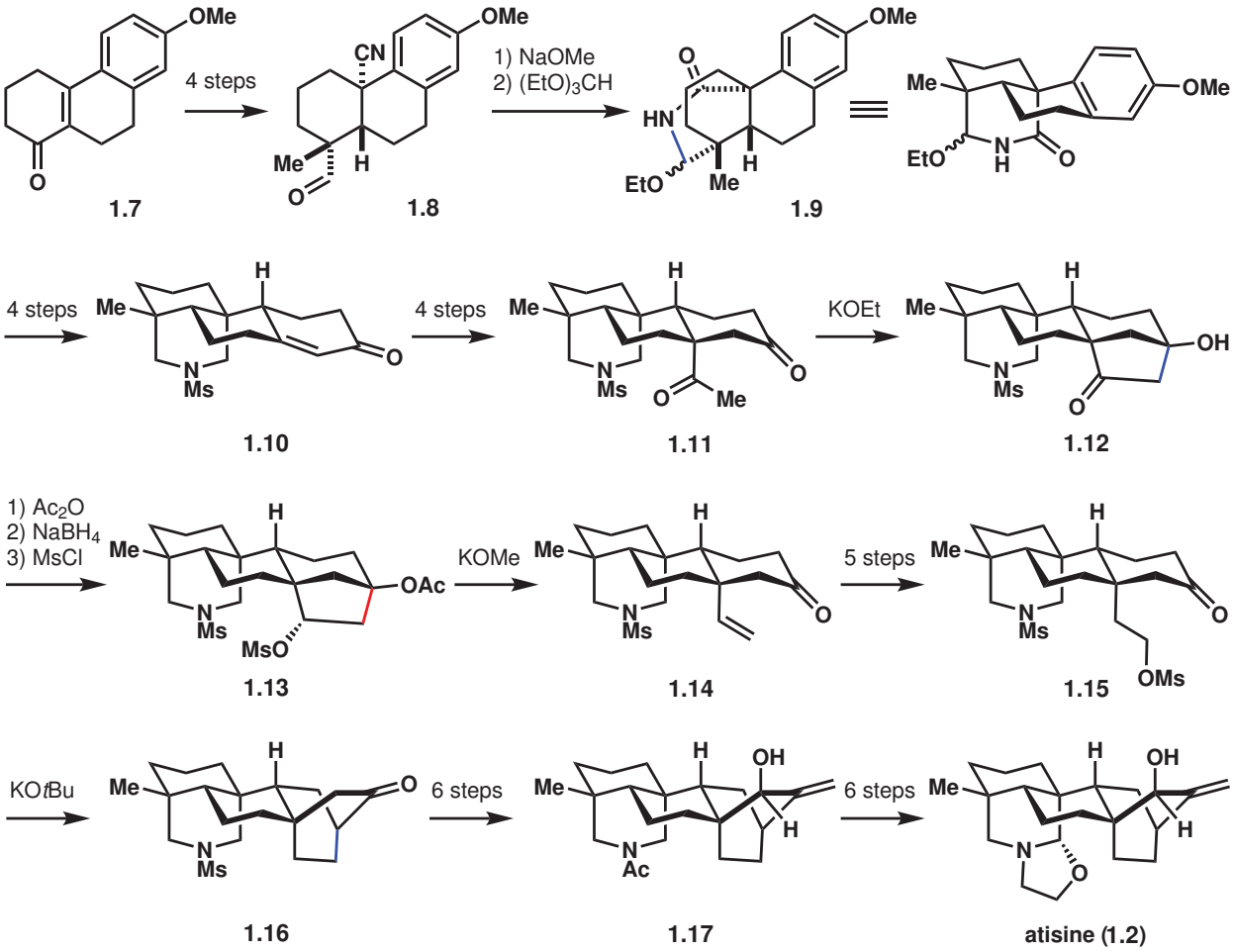

Scheme 1.1: Nagata's synthesis of C_{20}-diterpenoid alkaloid atisine.

1.1.2 Scaffold hopping through Wagner–Meerwein rearrangement: a formal synthesis of veatchine

Intercepting bicyclo[3.2.1] intermediate **1.13** from their previous synthesis, Nagata and co-workers then went on to complete formal syntheses of garryine (**1.24**) and isomeric diterpenoid alkaloid veatchine (**1.25**, Scheme 1.2).[17] The mesylate group of **1.13** was eliminated and the resultant alkene subjected to hydroboration–oxidation, followed by treatment with *p*-bromophenylsulfonic chloride to give brosylate **1.18**. This brosylate underwent a key Wagner–Meerwein rearrangement under basic conditions with the bond highlighted in red migrating to displace the brosylate group and give rearranged ketone **1.19**. Wittig olefination then gave terminal alkene **1.20**, which was converted to allylic bromide **1.21** in three further steps. From there, stereoselective epoxidation of the trisubstituted alkene and subsequent debromination with zinc gave allylic alcohol **1.22**. Ethyl carbamate **1.22** was then converted into the corresponding ethanolamine (**1.23**), which Wiesner and co-workers had previously shown to yield garryine (**1.24**) upon oxidation with OsO_4.[18] Further conversion of garryine to veatchine (**1.25**) had been reported by Pelletier and Kawazu.[19] This therefore constituted a formal synthesis of both gar-

ryine and veatchine.

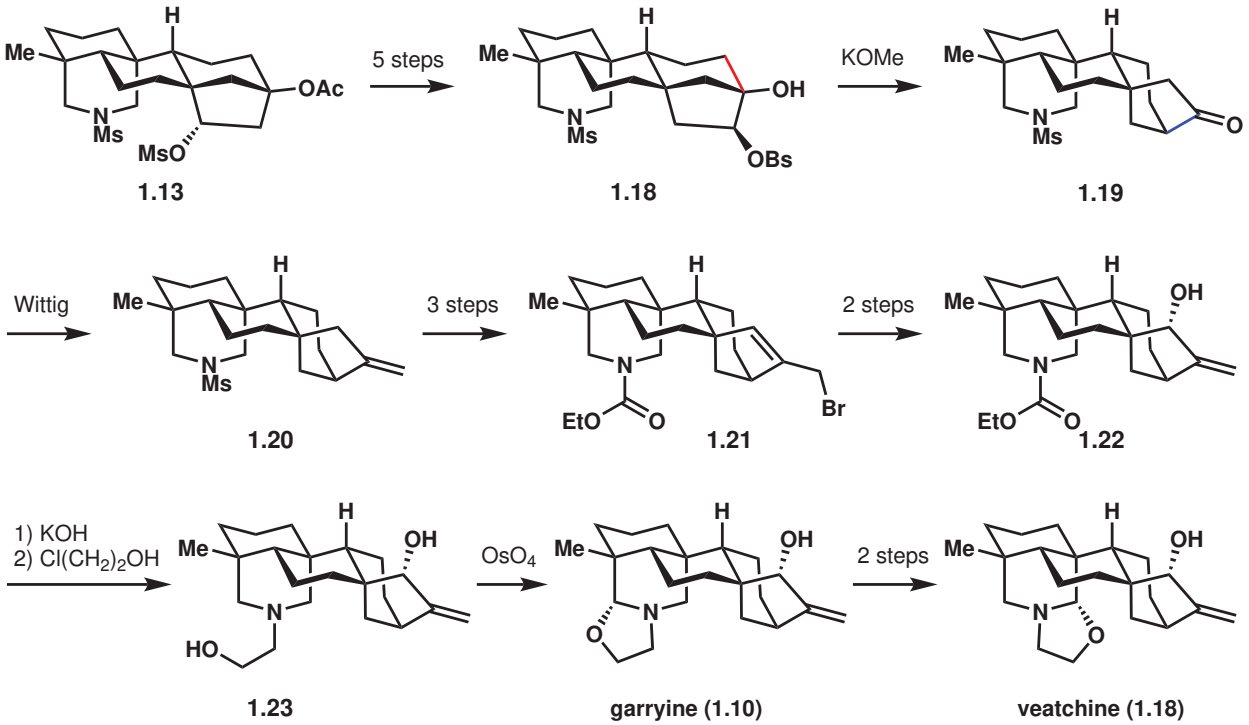

Scheme 1.2: Nagata's synthesis of garryine and veatchine utilizing a key Wagner–Meerwein rearrangement.

1.2 Seminal syntheses by Wiesner and co-workers

Contemporaneously with Nagata, Wiesner and co-workers were also exploring diterpenoid alkaloid synthesis, both through relay synthesis from the natural products themselves to aid in structure confirmation, as well through total synthesis.

1.2.1 The first synthesis of an optically active diterpenoid alkaloid: garryine

Wiesner's synthesis began with a modified Robinson annulation that joined quaternary ammonium salt **1.26** and γ-ketoester **1.27** to give tricycle **1.28** (Scheme 1.3).[20] Hydrogenation and subsequent conversion of the carboxylic acid group to an azide gave tricycle **1.29**, which underwent Curtius rearrangement to the corresponding isocyanate upon heating to reflux in benzene. Treatment of this isocyanate intermediate with acid induced cyclization to afford amide **1.30**, which was advanced to acetamide **1.31** in five steps. From there, hydrogenation of phenol **1.31** and oxidation of the cyclohexanol using Collins reagent gave ketone **1.32**. Site-selective α-functionalization to give ketoaldehyde **1.33** was achieved in an additional five steps. Aldol cyclization under acidic conditions then forged a [3.2.1] bicycle to complete the core of garryine and afford alcohol **1.34**. Four redox manipulation steps gave ketone **1.35**, which then underwent α-acetoxylation with lead(IV) tetraacetate and subsequent Wittig olefination to give allylic acetate **1.36**. Finally, dissolving metal reduction and conversion of the resultant secondary

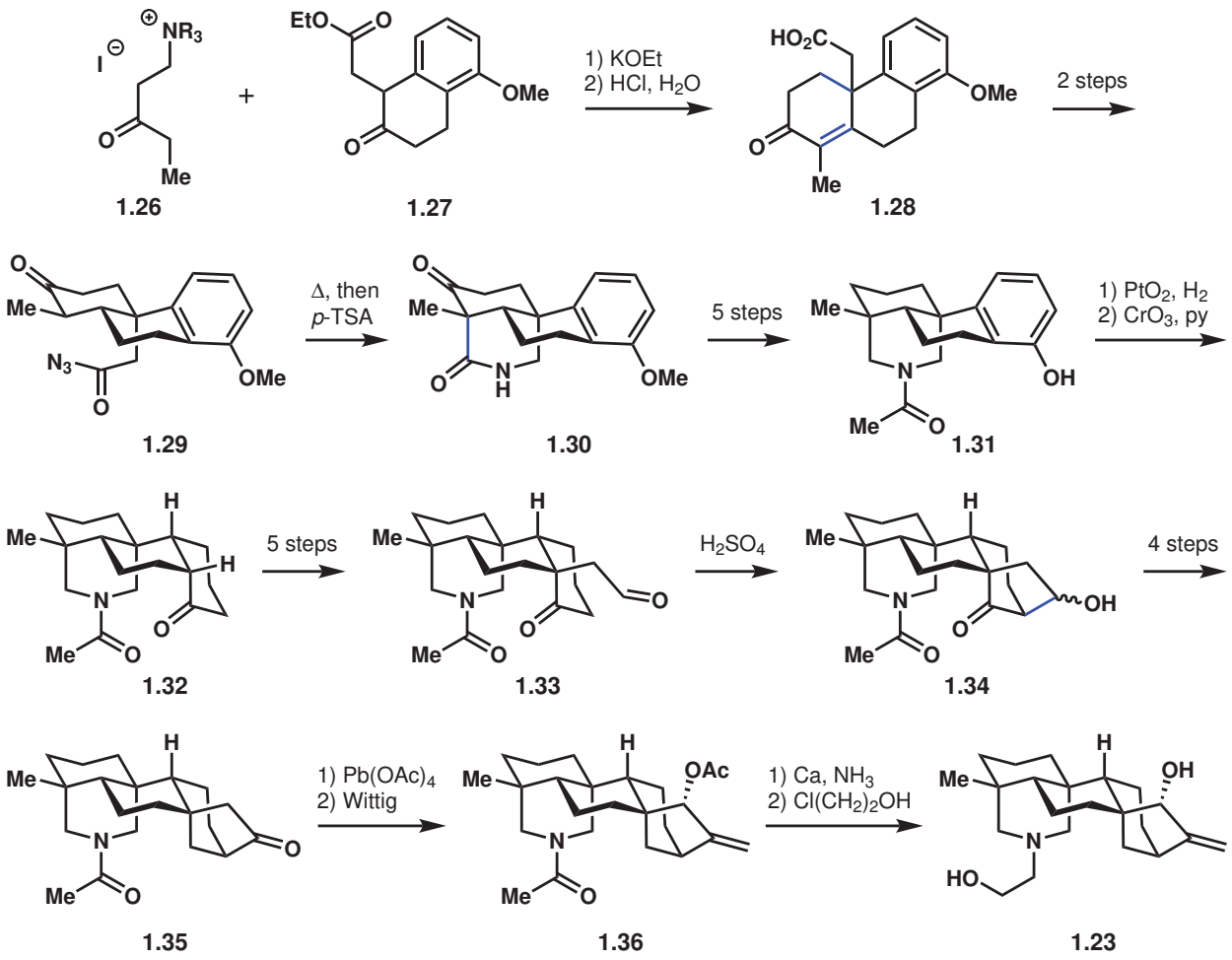

Scheme 1.3: Wiesners's formal synthesis of garryine and veatchine.

amine to an ethanolamine gave pentacycle **1.23**, the same intermediate synthesized by Nagata and co-workers[17] to intercept previous relay syntheses (see Section 1.1.2).

Wiesner later reported the first synthesis of an optically active diterpenoid alkaloid by performing a chiral resolution of late-stage intermediate **1.35** (Scheme 1.4).[21] This was accomplished by first protecting ketone **1.35** as a ketal, then cleaving the acetyl group to give the corresponding secondary amine (**1.37**), which was then reprotected as a mesylate. Cleavage of the ketal under acidic conditions revealed the ketone, which could then be reduced to the corresponding alcohol (**1.38**). This alcohol was obtained as a single diastereomer of unknown geometry. Esterification of **1.38** upon heating with succinic anhydride (**1.39**) and base gave carboxylic acid **1.40**, which underwent chiral resolution by complexation with the alkaloid brucine (**1.41**), which is readily isolated from the seeds of *Strychnos nux-vomica*.[22] Upon separation of the two salts by selective precipitation of the undesired diastereomer, each salt could be decomposed to give resolved **1.40**, the desired enantiomer of which was converted in four steps to optically pure intermediate **1.35** for use in the synthesis of garryine and veatchine. In all previous syntheses, scalemic intermediates had been achieved only by degradation of the natural products themselves.

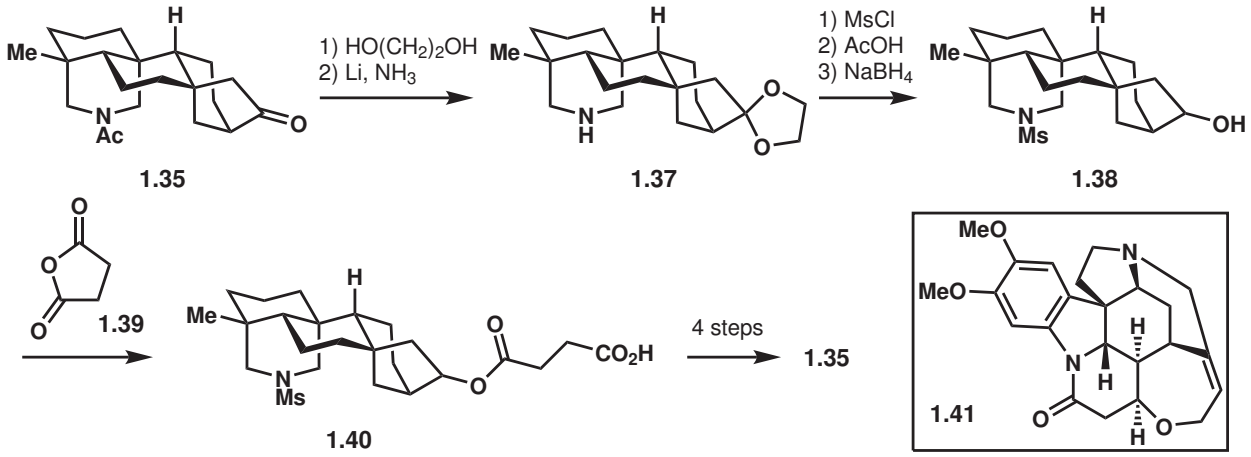

Scheme 1.4: Chiral resolution of pentacycle **1.35** through complexation with brucine (**1.41**).

1.2.2 Total synthesis of atisine using a key photocycloaddition

Wiesner and co-workers were also able to leverage tetracycle **1.30** from their garryine synthesis to complete a formal synthesis of atisine using an allene photocycloaddition approach (Scheme 1.5).[23] In this synthesis, ketone **1.30** was first reduced to give anisole **1.42**, which then underwent Birch reduction to a methyl enol ether that was, in turn, converted to the corresponding enone (**1.43**) under acidic conditions. Upon treatment with allene under photochemical conditions, enone **1.43** participated in a [2+2] cycloaddition to give cyclobutene **1.44**. This cycloadduct underwent four refunctionalization steps to give ketone **1.45**, which was then reduced to give alcohol **1.46** as a single diastereomer of undetermined configuration. Upon cleav-

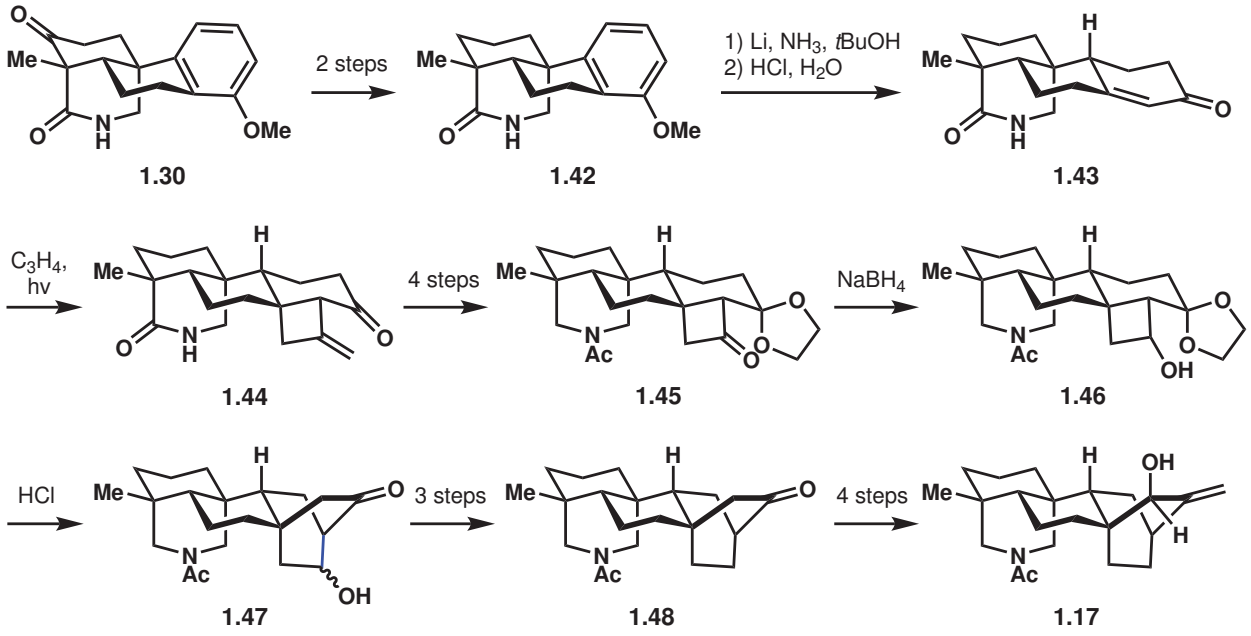

Scheme 1.5: Wiesner's synthesis of atisine using a key allene photocycloaddition.

age of the ketal in **1.46**, the resulant β-ketoalcohol underwent spontaneous retro-aldol ring opening and reclosure on the other side of the oxo group to give [2.2.2] bicycle **1.47** as an inconsequential mixture of epimers. The hydroxy group was removed in a series of three steps to afford racemic **1.48**, which was identical to an optically active sample obtained through degradation of atisine (**1.2**).[16] Optically active ketone **1.48** was then advanced to the analogous allylic alcohol (**1.17**) in four additional steps, intercepting Nagata's route (see Scheme 1.1) to complete a formal synthesis of atisine.

1.2.3 Rearrangement of the atisine skeleton: total synthesis of talatisamine

Building upon the strategies used in syntheses of atisine and garryine by both his own laboratory and that of Nagata, Wiesner later published the total synthesis of a more highly oxygenated hexacyclic diterpenoid alkaloid, talatisamine (**1.4**).[14] Talatisamine contains a rearranged [3.2.1] bicycle, as well as an additional carbocycle relative to garryine and atisine. Wiesner's synthesis began with a Diels–Alder cycloaddition between oxygenated diene **1.49** and vinyl nitrile **1.50** to give a 1:1 mixture of cycloadducts **1.51** and **1.52** (Scheme 1.6). Wiesner postulated that this lack of selectivity could be attributed to the fact that both the anisole ring and the cyano group are capable of stabilizing *endo*-interactions with the diene. Each of these adducts could be advanced to ketone **1.53** in five steps. In the case of isomer **1.51**, the stereocenter adjacent to the cyano group (marked with a *) was epimerized under basic conditions upon hydrolysis of the acetyl group, the resultant β-cyanoalcohol undergoing retro-aldol ring opening and closure to the lower energy *cis*-diastereomer. Ketone **1.53** was converted into homologated aldehyde **1.54** in six additional steps. From there, a formal hydrogenation of the tetra-substituted alkene gave *trans*-decalin **1.55**, which was advanced to dimesylate **1.56** through α-functionalization of the aldehyde, global reduction, and treatment with mesyl chloride. Mesylate **1.56** cyclized under basic conditions to give tetracycle **1.57**. The mesyl group on the nitrogen atom was then replaced with an acetyl group and the anisole ring reduced to afford enone **1.58**.

Enone **1.58** was then advanced to [2.2.2] bicycle **1.59** in an allene photocycloaddition/rearrangement sequence analogous to that used in Wiesner's earlier atisine synthesis (see Scheme 1.5, **1.43** to **1.47**). In this case, cyclization to the [2.2.2] bicycle gave only the desired β-hydroxy isomer, the methoxy group presumably imposing greater steric constraints on the system than were present in the previous synthesis. Alcohol **1.59** was then advanced to tosylate **1.60**, the substrate for the key Wagner–Meerwein rearrangement. Upon heating in DMSO and tetramethylguanidine, a 1,2-alkyl shift (migrating bond is marked in red) and loss of the tosylate gave a tertiary carbocation from which two isomeric alkenes (**1.61**) arose. The isomer in which the olefin was exocyclic to the newly formed [3.2.1] bicycle was then treated with $LiAlH_4$ to give tertiary amine **1.62**, which was also synthesized by degradation of natural talatisamine. Continuing on with the optically pure **1.62** obtained in this manner, Wiesner completed the synthesis of talatisamine through ketal cleavage, reduction of the resultant ketone, and oxidation with mercuric acetate[24] to forge the final C–C bond α to the amine. This synthesis relied heavily on cycloadditions and skeletal rearrangements, as opposed to the sequential annulations by intramolecular cyclization more commonly utilized in other early syntheses. While Wiesner's synthesis of talatisamine was not the first to use any one of these transformations, the prioriti-

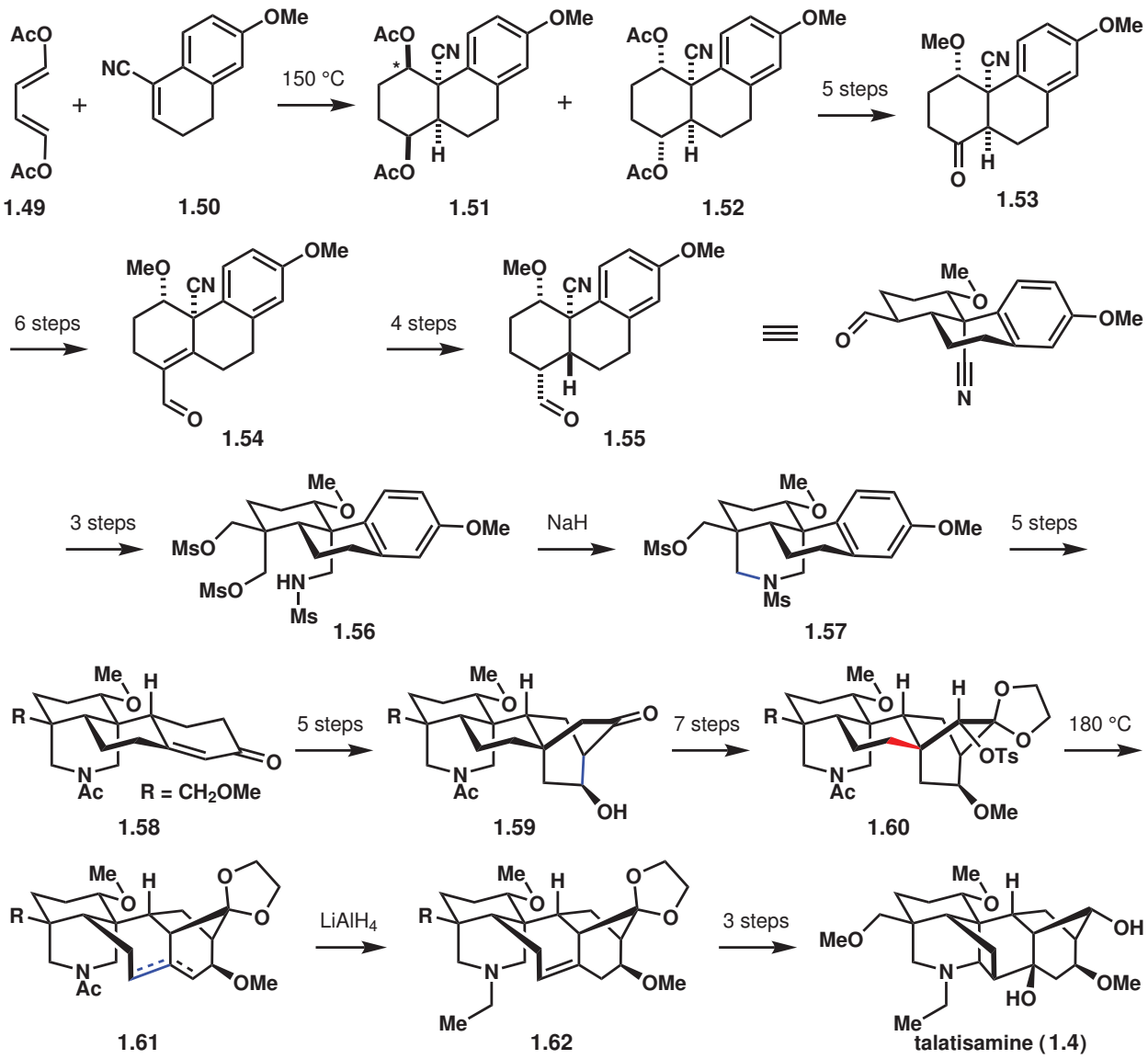

Scheme 1.6: Wiesner's synthesis of talatisamine utilizing key cycloadditions and a late-stage Wagner–Meerwein rearrangement.

zation of these approaches over others marked a change in overall strategy that has persisted in more recent work. Ring construction strategies in modern diterpenoid alkaloid syntheses are discussed in Chapter 2.

1.3 References

1. Atta-ur-Rahman; Choudhary, M. I. *Nat. Prod. Rep.* **1999**, *16*, 619–635.
2. Wang, F. P.; Chen, Q. H.; Liu, X. Y. *Nat. Prod. Rep.* **2010**, *27*, 529–570.
3. Wang, X. W.; Xie, H. *Drugs Future* **1999**, *24*, 877–882.
4. Cash, J. T.; Dunstan, W. R. *Philos. Trans. R. Soc. B Biol. Sci.* **1898**, *190*, 239–393.
5. Cherney, E. C.; Baran, P. S. *Isr. J. Chem.* **2011**, *51*, 391–405.

6. Sun, J. et al. *Drug Metab. Dispos.* **2015**, *43*, 713–724.
7. Ameri, A. *Prog. Neurobiol.* **1998**, *56*, 211–235.
8. Fujita, Y.; Terui, K.; Fujita, M.; Kakizaki, A.; Sato, N.; Oikawa, K.; Aoki, H.; Takahashi, K.; Endo, S. *J. Anal. Toxicol.* **2007**, *31*, 132–137.
9. Wang, F.-P.; Chen, Q.-H. In *Alkaloids. Chem. Biol.* Cordell, G. A., Ed.; Academic Press: San Diego, 2010; Vol. 69, pp 1–577.
10. Stevens, M.; Peigneur, S.; Tytgat, J. *Front. Pharmacol.* **2011**, *2*, DOI: 10.3389/fphar.2011.00071.
11. Borcsa, B.; Fodor, L.; Csupor, D.; Forgo, P.; Molnár, A.; Hohmann, J. *Planta Med.* **2014**, *80*, 231–236.
12. (a) Pelletier, S. W.; Mody, N. V. *Alkaloids Chem. Physiol.* **1981**, 99–216; (b) Pelletier, S. W. *Experientia* **1964**, *20*, 1–10; (c) Wiesner, K.; Valenta, Z. In *Prog. Chem. Org. Nat. Prod.* Springer Vienna: Vienna, 1958, pp 26–89; (d) Wiesner, K. *Chem. Soc. Rev.* **1977**, *6*, 413–430.
13. (a) ApSimon, J. W.; Edwards, O. E. *Can. J. Chem.* **1962**, *40*, 896–902; (b) Findlay, J. A.; Henry, W. A.; Jain, T. C.; Valenta, Z.; Wiesner, K.; Wong, C. M. *Tetrahedron Lett.* **1962**, *3*, 869–872; (c) Bell, R. A.; Ireland, R. E. *Tetrahedron Lett.* **1963**, *4*, 269–273; (d) Ogiso, A.; Shimizu, B.; Iwai, I. *Chem. Pharm. Bull. (Tokyo).* **1963**, *11*, 770–774; (e) Ogiso, A.; Iwai, I. *Chem. Pharm. Bull. (Tokyo).* **1964**, *12*, 820–824; (f) Masamune, S. *J. Am. Chem. Soc.* **1964**, *86*, 291–292; (g) Masamune, S. *J. Am. Chem. Soc.* **1964**, *86*, 288–289; (h) Bell, R. A.; Ireland, R. E.; Partyka, R. A. *J. Org. Chem.* **1966**, *31*, 2530–2536; (i) Turner, R. B.; Diana, G. D.; Fodor, G. E.; Gebert, K.; Simmons, D. L.; Rao, A. S.; Roos, O.; Wirth, W. *J. Am. Chem. Soc.* **1966**, *88*, 1786–1792; (j) Turner, R. B.; Gänshirt, K. H.; Shaw, P. E.; Tauber, J. D. *J. Am. Chem. Soc.* **1966**, *88*, 1776–1785.
14. (a) Wiesner, K.; Tsai, T. Y.; Huber, K.; Bolton, S. E.; Vlahov, R. *J. Am. Chem. Soc.* **1974**, *96*, 4990–4992; (b) Wiesner, K. *Pure Appl. Chem.* **1975**, *41*, 93–112.
15. (a) Nagata, W.; Sugasawa, T.; Narisada, M.; Wakabayashi, T.; Hayase, Y. *J. Am. Chem. Soc.* **1963**, *85*, 2342–2343; (b) Nagata, W.; Sugasawa, T.; Narisada, M.; Wakabayashi, T.; Hayase, Y. *J. Am. Chem. Soc.* **1967**, *89*, 1483–1499.
16. Pelletier, S. W.; Parthasarathy, P. C. *Tetrahedron Lett.* **1963**, *4*, 205–208.
17. (a) Nagata, W.; Narisada, M.; Wakabayashi, T.; Sugasawa, T. *J. Am. Chem. Soc.* **1964**, *86*, 929–930; (b) Nagata, W.; Narisada, M.; Wakabayashi, T.; Sugasawa, T. *J. Am. Chem. Soc.* **1967**, *89*, 1499–1504.
18. Wiesner, K.; Taylor, W. I.; Figdor, S. K.; Bartlett, M. F.; Armstrong, J. R.; Edwards, J. A. *Chem. Ber.* **1953**, *86*, 800–816.
19. Pelletier, S. W.; Kawazu, K. *Chem. Ind.* **1963**, *47*, 1879–1880.
20. (a) Valenta, Z.; Wiesner, K.; Wong, C. M. *Tetrahedron Lett.* **1964**, *5*, 2437–2442; (b) Guthrie, R. W.; Henry, W. A.; Immer, H.; Wong, C. M.; Valenta, Z.; Wiesner, K. *Collect. Czechoslov. Chem. Commun.* **1966**, *31*, 602–621.
21. Wiesner, K.; Komlossy, Z. I.; Philipp, A.; Valenta, Z. *Experientia* **1970**, *26*, 471.
22. Bhati, R.; Singh, A.; Saharan, V.; Ram, V. A.; Bhandari, A. *J. Ayurveda Integr. Med.* **2012**, *3*, 80–84.
23. Guthrie, R. W.; Valenta, Z.; Wiesner, K. *Tetrahedron Lett.* **1966**, *7*, 4645–4654.
24. Edwards, O. E. *Chem. Commun.* **1965**, 318–319.

Chapter 2

Ring construction strategies toward diterpenoid alkaloid frameworks

2.1 A case for bond-network analysis in the synthesis of bridged polycyclic complex molecules: hetidine and hetisine diterpenoid alkaloids*

Retrosynthesis has been adopted as the standard approach to identifying synthetic strategies to construct organic molecules. For many practitioners of organic synthesis, generating a synthetic plan for the preparation of a complex molecule without undertaking a retrosynthetic analysis is unfathomable.[1] Retrosynthesis, which involves breaking the bonds that will be formed in the forward (synthetic) direction, is often guided by knowledge of known transformations to forge those bonds. Over the years, the way in which retrosynthetic analyses are conducted has been formalized, led principally by the "Logic of Chemical Synthesis" introduced by Corey.[2]

In one approach to retrosynthesis, the bonds chosen for disconnection are marked on the structure of the target molecule and designated as the *bondset* for the intended synthesis.[3] The selection of the individual bonds to be included in a bondset hinges on the topology of the target framework, as well as upon consideration of which functional groups in the target structure may be leveraged to achieve bond formation in the course of the forward synthesis. Thus, consideration of both how to minimize structural complexity in the retrosynthetic direction, as well as what reactions can be employed in the synthetic direction, are taken into account in retrosynthetic analyses.

Because a bondset does not specify the sequence in which individual bonds are to be forged in the synthetic direction, the order in which the bonds are broken must also be considered. In the end, the sequence that emerges for bond formation should correspond to an efficient forward synthesis, in which the attributes of a convergent versus linear synthesis are maximized.[3] In general, step count in complex molecule synthesis is minimized when an exponential increase

*Reproduced from Doering, N. A.; Sarpong, R.; Hoffmann, R. W. *Angew. Chem. Int. Ed.*, **2020**, *59*, ASAP. DOI: 10.1002/anie.201909656. Copyright 2020 Gesellschaft Deutscher Chemiker, Wiley-VCH.

in target-relevant structural complexity of the intermediates is achieved en route to the target.[4] In the context of a retrosynthesis, this requires judicious choice of disconnections that will lead to maximal simplification at each stage.

Ultimately, the step count and elegance of a synthesis are heavily influenced by the choice of *which* bonds are placed in the bondset and *when* they are generated in the forward synthesis.

2.1.1 Topology-oriented approach to retrosynthesis of diterpenoid alkaloids

While several hundred diterpenoid alkaloids have been structurally characterized,[5] only a handful of these intricate molecules had been synthesized in the laboratory at the beginning of the 21st century.[6] Notably, after highly insightful seminal contributions by Wiesner[7] on delphinine type alkaloids (see Chapter 1), synthetic studies toward the diterpenoid alkaloids lay practically dormant for almost thirty years. Only in the last two decades have these natural products come back into focus as targets for chemical synthesis.[8] Likely, the lack of synthetic progress toward the diterpenoid alkaloids can be attributed to the challenge posed by the structural complexity of their multiply-bridged polycyclic skeletons, as illustrated by the hexacyclic hetidines and the heptacyclic hetisines (Figure 2.1).

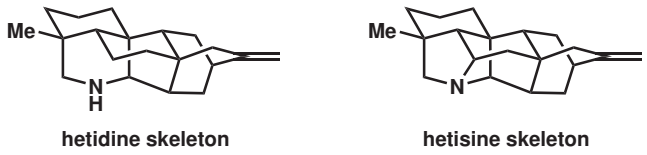

Figure 2.1: Hetidine and hetisine skeletons.

Given the complex framework of the diterpenoid alkaloids, a first level of analysis in generating a plan for their syntheses is to focus on the molecular skeleton. Hence, a bondset might be generated without regard for the functional groups. Clearly, to disregard the importance of functional groups in determining the bondset, or to postpone it to a later phase of planning, is unusual because, throughout the 20th century, chemists adhered to synthesis strategies that prioritize functional group considerations (functional group oriented synthesis).[9] Yet, in biosynthesis of terpenes and hence terpene-derived (terpenoid) alkaloids, nature follows a different scenario.[10] The molecular framework of terpenoid molecules is assembled first from a linear precursor containing all the carbon atoms in a 'cyclase' phase, followed by a second 'oxidase' phase, in which the skeleton is decorated with functional groups through oxygenation. In terpenoid alkaloids, nitrogen atom incorporation is believed to occur through Mannich condensation or Prins cyclization (with participation of a hydride), either immediately prior to or during the oxidase phase.[11]

Unsurprisingly, the way in which terpenoids are constructed in nature has been challenging to mimic in the laboratory setting.[12] Even though mimicking the 'cyclase' phase through a cationic polyene cascade is well-established,[13] accompanying rearrangement steps (*e.g.*, methyl shifts, Wagner–Meerwein type rearrangements) can be low yielding in some cases. Still, the advent of position-selective C–H activation/functionalization reactions has paved the way for several

impressive syntheses of terpenoids.[14] Thus, while the relatively limited ability to mimic the oxidase phase prevents the synthetic chemist from pursuing a truly biomimetic approach to terpenoid synthesis at present, we may still take our cue from nature and consider the skeleton of these topologically complex molecules, independent of functional groups, in the initial phase of designing a retrosynthesis.

2.1.2 Identifying a bondset

If retrosynthetic analyses were guided solely by the reactions one would seek to employ in the forward sense, they would be inherently biased toward transformations already known to the practitioner. On the other hand, topological analysis of the target, which is carried out without regard for functional groups, may identify different disconnections. Because development of new modes of reactivity is a goal of synthesis, this more objective method can illuminate gaps in the known chemical space. In the case of bridged polycycles, such as longifolene (**2.1**, Figure 2.2), the most highly bridged ring (see **2.1a**) incarnates the complexity of the system and is thus the focus of most topology-based retrosyntheses of these scaffolds.

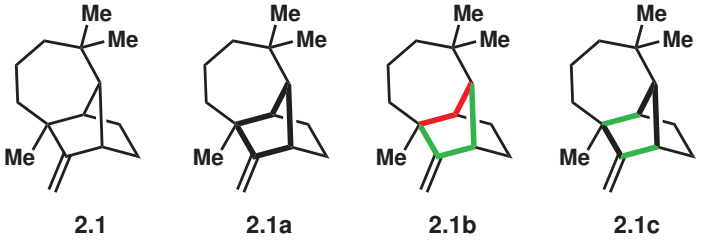

Figure 2.2: Bond-network analysis of the maximally bridged ring of longifolene (**2.1**).

As the most highly bridged ring is necessarily central to a polycyclic ring system, it would seem reasonable to select this ring as the starting point for a synthesis, and to sequentially anellate all the other rings to this central platform. Such an anellation approach would, however, lead to a synthesis with, at best, an inefficient linear increase in complexity.[†]

An alternative approach to synthesis planning was pointed out by Corey in 1975.[16] Corey recognized that retrosynthetic disconnection of certain bonds in the most highly bridged ring would lead to the greatest reduction in structural complexity. To identify these bonds, one must first identify all sites at which each primary ring[‡] is bridged, keeping in mind that an atom may be bridging relative to one ring but not to another. In the case of **2.1**, the maximally bridged ring is easily identified (see emphasis in **2.1a**). For more highly bridged polycycles, it may be beneficial to automate this portion of retrosynthesis, a feature that Corey and co-workers built into LHASA[16] and Sarpong and co-workers have since adapted into a web-based program.[17]

[†]While there is not one agreed upon metric for describing the complexity of a molecule, most definitions consider the topological bond network and/or the likely difficulty of the synthetic transformations needed to build that network. Multiple complexity indices have been developed to quantify the complexity of structures involved in a synthesis.[4,15] These indices lend themselves to a graphical representation of reaction sequences and provide a basis for semi-empirical comparison of (potential) syntheses.

[‡]A primary ring in a polycyclic structure is a ring that is not an envelope of two or more smaller bridged or fused rings. Such envelope rings are considered to be secondary rings.[16]

It is important to note that not every bond in the most highly bridged ring provides equal simplification upon disconnection. For example, disconnection of some bonds in **2.1** (marked red in **2.1b**) would generate a precursor with a primary ring larger than seven-membered, which is considered to be challenging to construct in the forward synthesis direction.[16] Therefore, the remaining bonds in the bondset (marked green in **2.1b**) are designated as *strategic*. The formation of these bonds in the synthesis direction would lead to a significant increase in complexity. Further analysis[16] must be applied to rank the merits and importance of the individual bonds marked in green. This additional analysis includes considerations of whether bridging is drastically reduced in the retrosynthetic direction, whether the change in complexity is maximized,[4] and whether dangling substituents are minimized as one disconnects the strategic bonds.

For molecules that incorporate heteroatoms into their skeleton, separate consideration must be given to any C–X bonds to determine whether these bonds should be considered strategic.[16] This is due to the relative ease of forming C–X bonds (the X group is inherently a functional group). Therefore, only a subset of Corey's rules apply. Importantly, C–X bonds may be considered strategic even if they are part of a large ring or one that is not maximally bridged.

Corey network analysis essentially identifies which skeletal bond(s) of a target are best constructed last in a synthesis. It therefore defines the skeleton of a penultimate intermediate that lacks either the most highly bridged ring or a strategic C–X bond. This intermediate is subjected to network analysis to identify strategic bond(s) for the next disconnection. In doing so recursively,[17] one generates a complete bondset, as well as timing for each ring-closing step in the forward synthesis. At one extreme, an open-chain precursor containing all skeletal atoms of the target would be generated[18] and that precursor would then be advanced through n steps into a polycycle that possesses n rings, each synthetic step closing one additional ring.

An even more rapid increase in complexity would be provided by reactions that form two skeletal bonds at a time, such as cycloadditions,[19] or (if target relevant) greater than two bonds at a time. Such bicyclizations (or polycyclizations) close multiple rings in one stroke. When this concept is applied to the most highly bridged ring, bonds other than those well-suited to one-bond disconnection, *cf.* **2.1b**, may be considered for two-bond (bond pair) disconnection (see **2.1c**). This version of Corey network analysis, which has been modified to allow consideration of multi-bond disconnections in the context of the maximally bridged ring,[§] is referred to herein as bond-network analysis.

Selecting one of several strategic bonds for disconnection is where we see that bond-network analysis does not fully supplant the idea of functional group oriented synthesis, but instead complements it. Retrosynthetic disconnections should be chosen at this level to take advantage of inherent functionality in the target molecule where possible, minimizing the number of peripheral modifications required in the forward synthesis. The introduction of additional

[§]When outlining the procedure for network analysis, Corey et al. specifically disclude disconnections that involve multiple bonds from network analysis, stating that such disconnections would be found through transform-oriented strategies (see ref. 16, page 6122). In his later book "The Logic of Chemical Synthesis", Corey includes a paragraph that discusses the possibility of two-bond disconnections, which would correlate to cycloadditions in a forward synthesis (see ref. 2, page 44). In both cases, such a discussion is limited to disconnection of a maximum of two bonds at once and separates bond pair disconnection from the considerations laid out in the context of strategic single-bond disconnection.

functional handles (and the attendant increase in step count) should be balanced against their ability to facilitate efficient skeletal bond formation.

This approach should enable a rational plan to synthesize complex polycyclic targets, such as the bridged, architecturally intricate diterpenoid alkaloids. A critical evaluation of eight relatively recent total syntheses of the hexacyclic hetidine and heptacyclic hetisine classes of alkaloids provides a sense of the state of the art. Particular attention is directed to how well each synthesis adheres to the concept of bond-network analysis.

2.1.3 Hetidine syntheses

In the hetidine skeleton[¶](**2.2**, Figure 2.3), ring F is recognized as the most highly bridged ring (see **2.2a** for emphasis). This ring is anellated to an aza-bicyclo[3.3.1]nonane skeleton (rings A and E), as well as to a bicyclo[2.2.2]octane ring system (rings C and D). Hence, retrosynthetic disconnection of either bond C9–C10 or bond C14–C20 in ring F would generate the most significant simplification (see **2.2b**) if the analysis were restricted to single bond disconnections. The set of strategic bonds also includes the two C–N bonds.

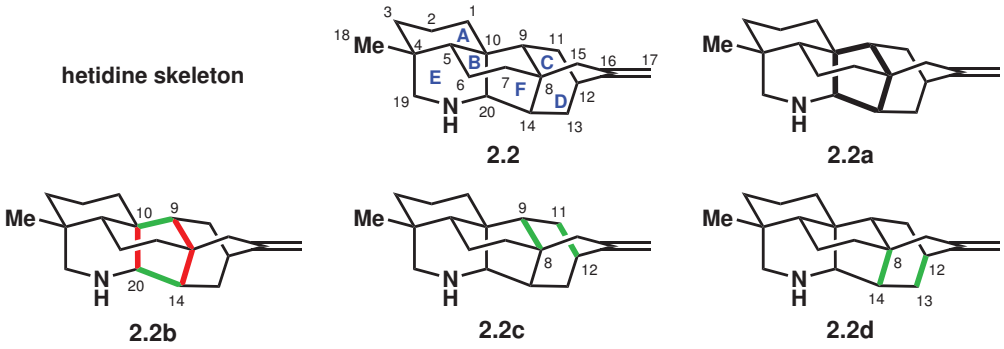

Figure 2.3: Bond-network analysis of the maximally bridged ring of the hetidine skeleton.

A different picture arises when two-bond disconnections (such as the Diels–Alder transform) are considered. To attain maximal retrosynthetic simplification, one of the rings targeted for two-bond disconnection should still be the most highly bridged ring. Of note, bonds targeted for two-bond disconnection may differ from those designated as strategic for one-bond disconnection. Examples of possible two-bond disconnections of the hetidine skeleton are shown in **2.2c** and **2.2d**.

To address the question of where the community currently stands with regard to achieving the total synthesis of these bridged polycycles, we analyze the reported syntheses of hetidine derivatives. These analyses emphasize the framework-forming transformations of intermediates that already contain most or all of the skeletal atoms.

[¶]The primary rings of the hetidine scaffold have been defined as follows: A (C1-C2-C3-C4-C5-C10); B(C5-C6-C7-C8-C9-C10); C (C11-C12-C16-C15-C8-C9); D (C12-C13-C14-C8-C15-C16); E (C4-C5-C10-C20-N-C19); F (C8-C9-C10-C20-C14).

In their synthesis of a hetidine core structure, Sarpong and co-workers[20] sought to employ a late-stage formal bicyclization to construct the [2.2.2] bicycle resident in the framework (Scheme 2.1). The key bond forming process started from a precursor (**2.3**) that contained rings A and D,

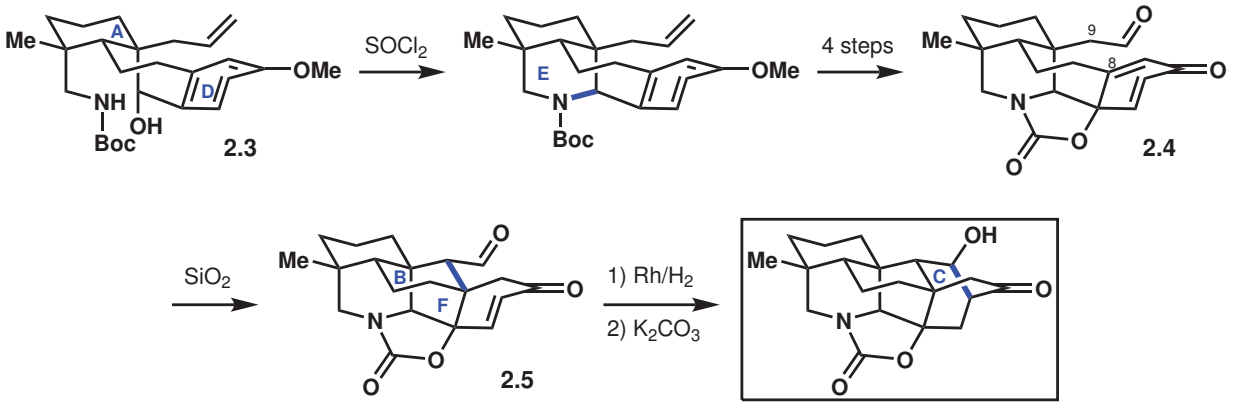

Scheme 2.1: Key cyclization steps from the Sarpong synthesis of a hetidine core structure.[20]

which were connected by parts of rings B and F. From there, they constructed the aza-bicyclo-[3.3.1]nonane system by closing ring E. Thereafter, a series of refunctionalization steps led to dearomatized intermediate **2.4**. Isomerization to **2.5** closed rings F and B by forming the C8–C9 bond, which is a strategic bond so long as ring C is not yet closed. The latter ring was closed in the final ascent from **2.5** to give the heptacyclic target. This synthesis followed a retrosynthetic plan that was identified using bond-network analysis that suggested a late stage closure of rings C and F through a bicyclization (*cf.* **2.2c**). However, the analysis did not predicate a *one-step* bicyclization, rather leaving room for variants in the forward synthetic direction.

In their approach to the hetidine framework, Qin and co-workers[21] started the late-stage cyclization phase of their synthesis from a tricyclic precursor (**2.6**, Scheme 2.2) that already pos-

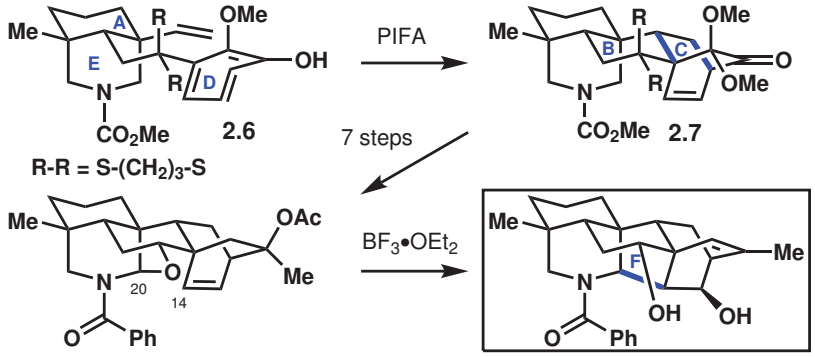

Scheme 2.2: Late-stage ring formation steps in Qin synthesis of a hetidine derivative.[21]

sessed an aza-bicyclo[3.3.1]nonane system (rings A and E) and an attached ring D. The first key transformation was a bicyclization that simultaneously formed rings B and C to give ketal **2.7**. Then followed seven refunctionalization steps before ring F was closed at the strategic C14–C20 bond. In accordance with bond-network analysis, the final ring formed in the

Qin approach was the maximally bridged ring. The well-precedented oxidative dearomatization/intramolecular Diels–Alder cascade[22] to forge the bicyclo[2.2.2] framework that preceded the final bond-forming step to construct the hetidine skeleton was powerfully applied in this context.

The Li group's approach to the highly bridged polycyclic framework of septedine[23] started from tricyclic precursor **2.8**, in which rings A, B, and C were already anellated (Scheme 2.3). A bi-

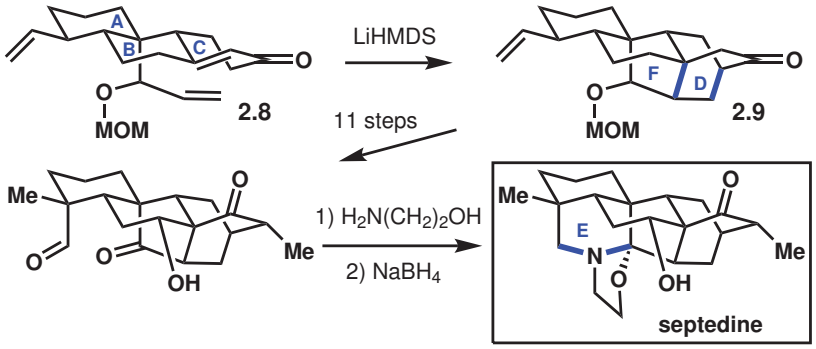

Scheme 2.3: Synthesis of the hetidine-type natural product septedine by Li and co-workers.[23]

cyclization simultaneously closed rings D and F to give pentacycle **2.9**. This Diels–Alder-type cycloaddition deviates from that seen in the other alkaloid syntheses discussed here in that it is initiated by enolate formation rather than by oxidative dearomatization to a masked *o*-quinone. With **2.9** in hand, several steps were undertaken to adjust the peripheral substituents, before ring E was closed in a final sequence to access septedine. The Li approach adhered to a strategy that conforms to bond-network analysis in that a bicyclization is employed to construct the maximally bridged ring in the penultimate cyclization step of the synthesis, and in the final step forging strategic C–N bonds to close ring E. In addition, the Li approach to septedine contained elements of a potentially biomimetic approach in that the nitrogen atom was incorporated at a late stage through a condensation/reduction with ethanolamine.

Ma and co-workers[24] addressed the synthesis of the proposed structure of navirine C in a synthesis (Scheme 2.4) that conceptually resembles that of Qin[21] (vide supra) although these ef-

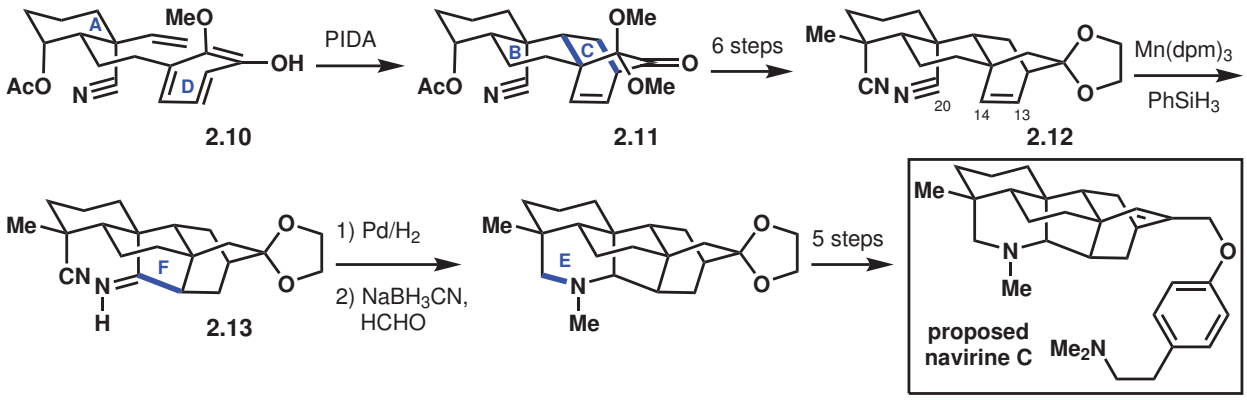

Scheme 2.4: Ma's synthesis of the proposed structure of navirine C.[24]

forts were likely pursued contemporaneously. The conceptual similarities are readily apparent in both the retrosynthetic disconnections chosen and how the starting material (**2.10**) for the Ma synthesis resembles compound **2.6** in the Qin synthesis. However, in Ma's case, ring E had yet to be closed, avoiding complications that would have arisen regarding position-selective (C19 vs. C20) attachments to ring E.

The first step involved the well-established oxidative dearomatization of ring D, which led to the formation of the [2.2.2] bicycle within **2.11** and the simultaneous closure of rings B and C. At this stage, following five refunctionalization steps to generate **2.12**, Ma employed a hydrogen-atom transfer[25] to the C13–C14 double bond in order to close ring F via the strategic C14–C20 bond. This process generated **2.13** with the necessary functionality for the concluding formation of ring E. Overall, this synthesis may be thought of as a hybrid approach combining elements of bond-network analysis with bio-inspiration. The nitrogen atom resident in the hetidine framework is introduced early in the form of a nitrile group, which is critical to the later construction of the maximally bridged ring F in a manner somewhat reminiscent of the Mannich approach proposed for the biosynthesis of the related aconitine skeleton.[26] In this way, the disconnections identified by Ma and co-workers in their synthesis are potentially biomimetic, but the actual reactions employed in the forward sense are quite dissimilar from the conditions likely in the biosynthesis.

To facilitate comparison of the four syntheses of hetidine derivatives, the following overview illustrates the bondset and timing adopted by each group for the assembly of the hexacyclic skeleton (Figure 2.4). A dominant feature in all four syntheses is the focus on a cycloaddition

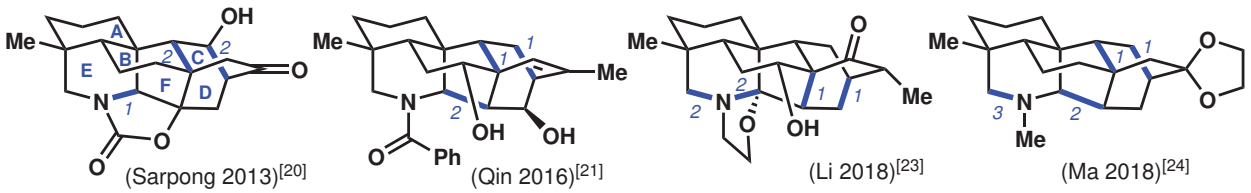

Stage	Rings
At Start	A, D
Closure 1)	E
Closure 2)	B, C, F

Stage	Rings
At Start	A, E, D
Closure 1)	B, C
Closure 2)	F

Stage	Rings
At Start	A, B, C
Closure 1)	D, F
Closure 2)	E

Stage	Rings
At Start	A, D
Closure 1)	B, C
Closure 2)	F
Closure 3)	E

Figure 2.4: Comparison of ring closure strategies employed in hetidine scaffold syntheses.

approach to the bicyclo[2.2.2]octane portion (rings C and D) of the hetidines. Each synthesis incorporates one of these two rings at an early stage to facilitate a bicyclization. Additionally, none of the syntheses started with a completed ring F, which was therefore closed somewhere along the synthesis route. To what extent did the individual researchers avail themselves of bond-network analysis? This would be reflected in the closure of ring F in the last skeletal C–C bond-forming step. This holds for Qin's synthesis[21] of a hetidine derivative, which featured early installation of the nitrogen-containing ring E, then followed an optimal plan to assemble the hexacyclic skeleton, ending with formation of the strategic C14–C20 bond. Likewise, Ma[24] formed the C14–C20 bond as part of the endgame in conjunction with the closure of ring E at the C19–N bond. These approaches are contrasted by the syntheses executed by Sarpong[20]

and Li[23], in which the researchers instead closed ring F through bicyclization strategies that utilized bonds that were not considered strategic for one-bond disconnection. Nonetheless, all four syntheses adhere to the suggestions of the expanded bond-network analysis in their own way, showcasing how this type of analysis guides retrosyntheses without prescribing the transformations to be used in the forward synthesis.

2.1.4 Hetisine syntheses

The heptacyclic hetisine skeleton‖ (**2.14**, Figure 2.5) contains two primary rings (F and G, labeled differently from the hetidines) which are equally highly bridged. Application of bond-network analysis[16] to the hetisine skeleton unveils, with regard to ring G, a result illustrated in **2.14a** where two strategic bonds (C14–C20, C9–C10, shown in green) emerge—similar to the analysis that was carried out with the hetidines (*cf.* **2.2a**). Bond-network analysis of the other maximally bridged ring (*i.e.*, ring F) reveals two strategic bonds (N–C6, N–C20), as indicated in **2.14b**.

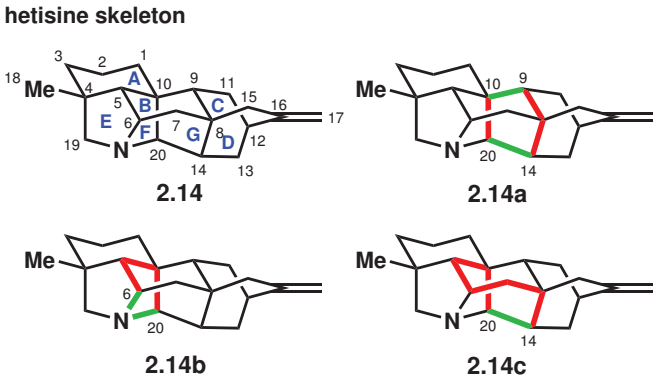

Figure 2.5: Bond-network analysis of the maximally bridged ring of the hetisine skeleton.

As examination of the two primary rings (*i.e.*, F and G) did not point to a singularly attractive synthetic pathway, it would be appropriate to extend the analysis to a four- to seven-membered secondary ring.[16] For the hetisine skeleton **2.14**, this applies to the highly bridged envelope of rings B and G, *cf.* **2.14c**. Yet, bond-network analysis of this ring bond-network analysis doesn't reveal any further options for late-stage closure of this ring; the only strategic bond is shared with ring G. Rather, many bonds in this ring being red-flagged for one-bond disconnection suggests—and here is a twist of the network analysis—this ring could instead be generated early and maintained throughout the synthesis as the majority of strategic disconnections would leave it intact.

The existing syntheses of hetisine natural products and their closely related derivatives are summarized in the following schemes with emphasis on transformations that contribute directly to the formation of skeletal bonds.

‖The primary rings of the hetisine scaffold have been defined as follows: A (C1-C2-C3-C4-C5-C10); B (C5-C6-C7-C8-C9-C10); C (C11-C12-C16-C15-C8-C9); D (C12-C13-C14-C8-C15-C16); E (C4-C5-C6-N-C19); F (C5-C6-N-C20-C10); G (C8-C9-C10-C20-C14).

In their synthesis of the hetisine alkaloid nominine, Muratake/Natsume[27] utilized tricyclic precursor **2.15**, comprising rings A, B, and an envelope of rings C and D of the target structure (Scheme 2.5). They rigidified the system by closing bond C14–C20, *i.e.*, ring G. A lengthy se-

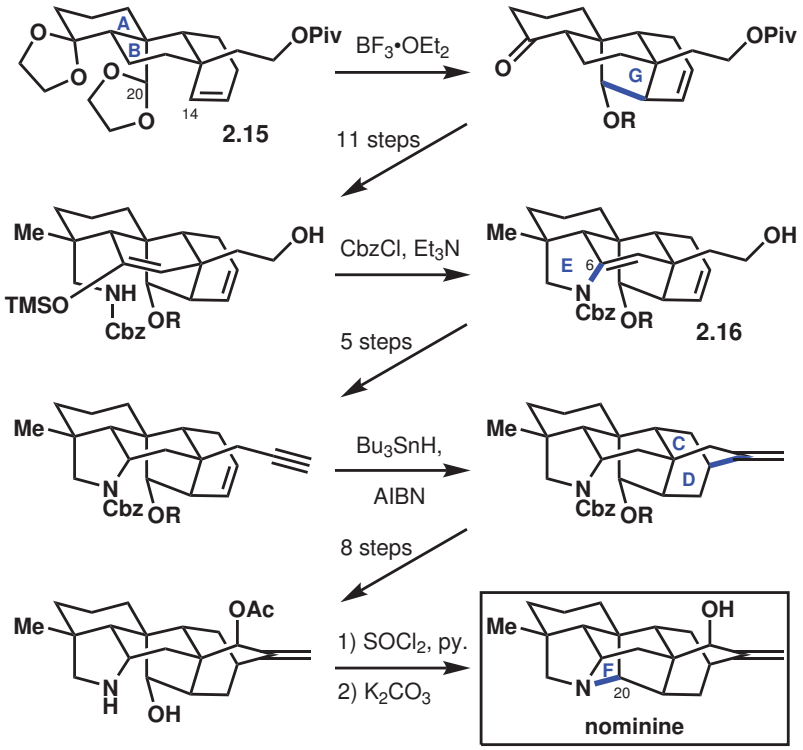

Scheme 2.5: Synthesis of hetisine-type alkaloid nominine by Muratake and Natsume.[27]

quence following C14–C20 bond formation culminated in the closure of ring E by forming the C6–N bond to give carbamate **2.16**. Muratake/Natsume then addressed the assembly of the bicyclo[2.2.2] ring system (rings C and D), followed by several steps to adjust the functionality therein. It was only at the very end of the synthesis that the C20–N bond was formed to close ring F, in accord with bond-network analysis, *cf.* **2.14b**. While the penultimate ring closure to form ring C did not involve the maximally bridged ring at that stage, all other ring-closing steps did align with the bond-network analysis.

A second synthesis of nominine by Peese/Gin[28] followed a drastically different approach, focusing on the early generation of the two most highly bridged rings (Scheme 2.6). The advanced intermediate that was employed (**2.17**) contained ring A connected via C19 to an isoquinolinium moiety, representing ring D and elements of rings F and G. The ascent to the nominine skeleton was initiated through an inventive 1,3-dipolar cycloaddition that closed rings E and F. After six refunctionalization steps, a second bicyclization closed rings B, C and G in a Diels–Alder reaction. In both bicyclization steps, bonds were formed that were undesirable for one-bond disconnection approaches based on bond-network analysis (see Figure 2.5). Foremost, this synthesis impresses by its rapid increase in target-relevant complexity, advancing from the starting tricycle to the heptacyclic hetisine structure in only two skeleton building steps. This underscores the power of bicyclization reactions in the synthesis of bridged polycyclic targets.

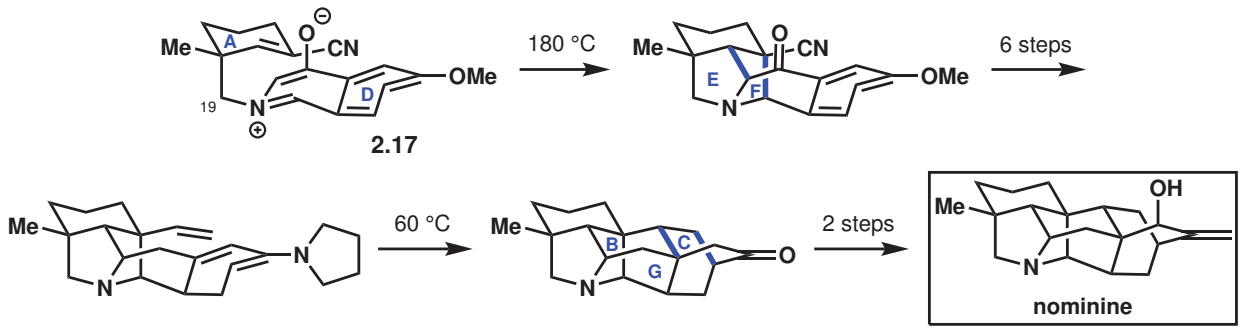

Scheme 2.6: Late-stage cyclization steps in the synthesis of nominine by Peese and Gin.[28]

In their synthesis of spirasine IV, Zhang and co-workers[29] initiated their final set of ring-forming reactions from a rather simple precursor (**2.18**, Scheme 2.7) possessing only two directly connected rings (A and C). Essential skeletal atoms for rings B, D, F, and G were attached to this

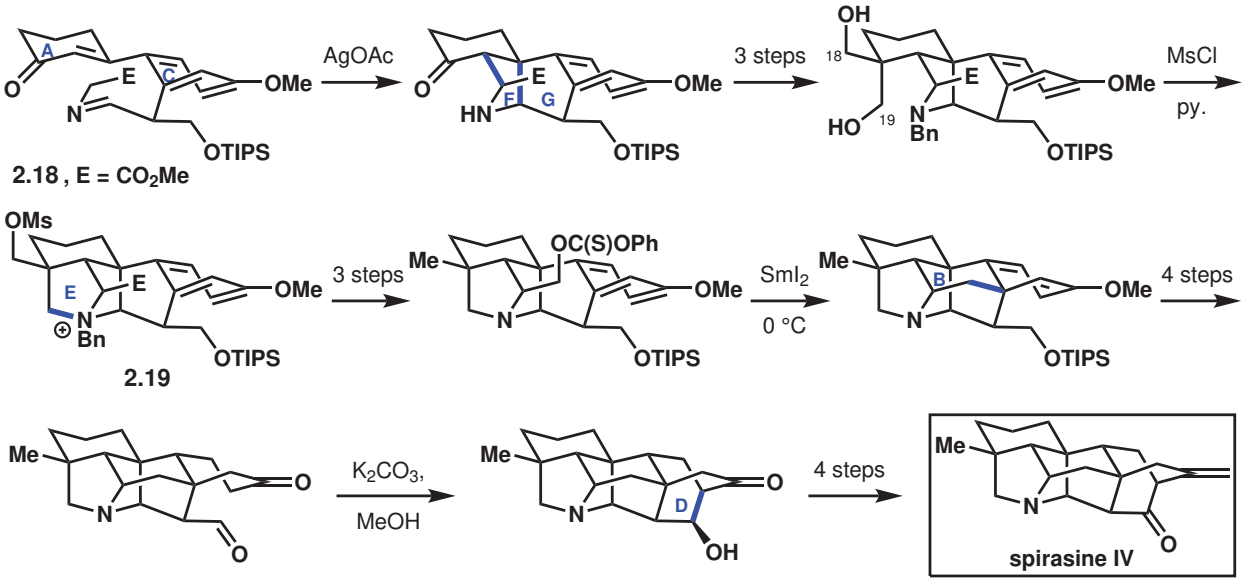

Scheme 2.7: Introduction of bridged rings in spirasine IV by Zhang and co-workers.[29]

bicycle, facilitating their subsequent assembly. The ring-formations were initiated by a 1,3-dipolar cycloaddition to form rings F and G, a similar approach as in the Peese/Gin synthesis.[28] At this stage, the remaining atoms, C18 and C19, of ring E were introduced, and ring E was closed to afford pentacyclic intermediate **2.19**. After a few refunctionalization steps, ring B was closed through a free radical addition to the aromatic ring C. Another series of functional group adjustments set the stage for an aldol reaction to close ring D and complete the synthesis in four additional steps. Overall, the synthetic approach adopted here is of the anellation type, where "construction of the most highly bridged core occurs first followed by subsequent crocheting of the remaining rings". Nonetheless, the synthetic ascent to the hetisine skeleton as a target is marked by a steady increase in complexity over the four steps that lead to the skeleton. It eschews the principles of bond-network analysis, but profits from a well-chosen starting point.

In their synthesis of cossonidine, Sarpong and co-workers[30] drew upon the group's prior synthe-

sis[20] of a navirine precursor by using a tricyclic starting compound (**2.20**, Scheme 2.8) containing rings A and D connected by an envelope of rings B and G, realizing the analysis depicted by **2.14c**. As in the previous synthesis of the hetidine framework, they first forged the C20–N bond.

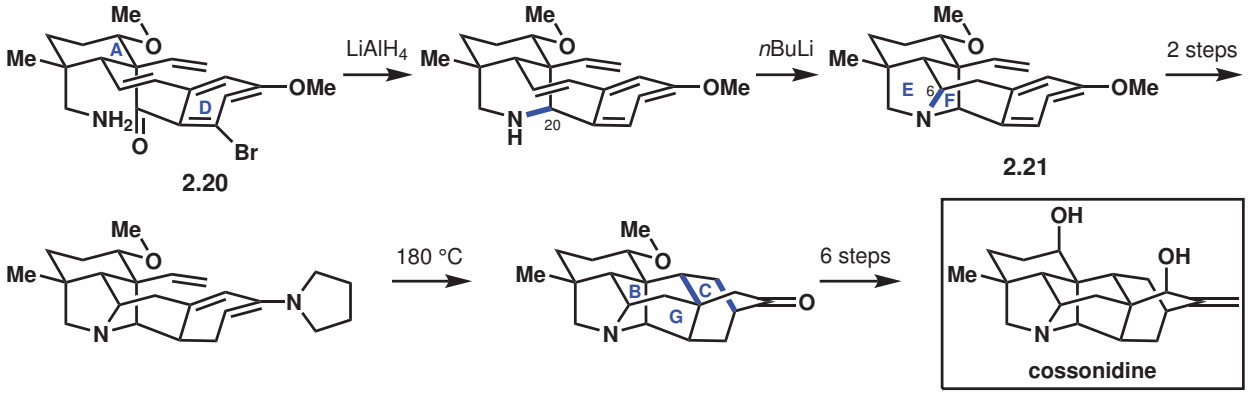

Scheme 2.8: Closure of bridged rings in cossonidine synthesis by Sarpong and co-workers.[30]

This was followed immediately by C6–N bond formation, closing rings E and F to give pentacycle **2.21**. The ultimate heptacyclic skeleton was reached following Peese/Gin's precedent[28] by closing rings B and C in a Diels–Alder reaction. Finally, the functionalities were adjusted in a series of redox manipulation steps to reach cossonidine in a sequence that does not quite give an exponential increase in complexity, but does fully align with bond-network analysis.

To facilitate a comparison of the four syntheses of hetisine derivatives in the context of bond-network analysis, the following overview illustrates the bondset and timing of bond formation chosen by the different groups for the assembly of the heptacyclic skeleton (Figure 2.6).**

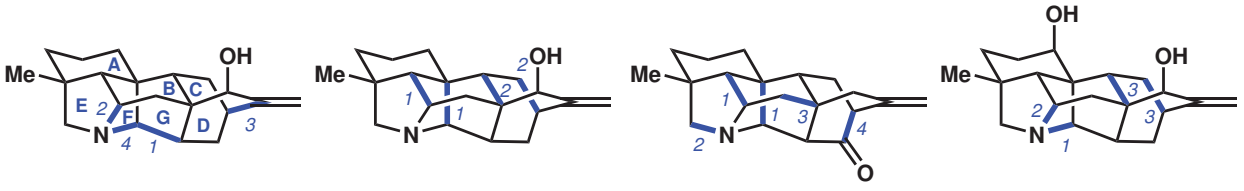

(Muratake/Natsume 2004)[27]

Stage	Rings
At Start	A, B, (C,D)
Closure 1)	G
Closure 2)	E
Closure 3)	C, D
Closure 4)	F

(Peese/Gin 2008)[28]

Stage	Rings
At Start	A, D
Closure 1)	E, F
Closure 2)	B, C, G

(Zhang 2018)[29]

Stage	Rings
At Start	A, C
Closure 1)	F, G
Closure 2)	E
Closure 3)	B
Closure 4)	D

(Sarpong 2018)[30]

Stage	Rings
At Start	A, D, (B,G)
Closure 1)	(E,F)
Closure 2)	E, F
Closure 3)	B, C, G

Figure 2.6: Comparison of ring closure strategies in sysntheses of hetisine-type natural products.

As with the hetidine syntheses, bicyclizations are embraced in constructing the hetisine skeleton. These powerful transformations dramatically reduce the number of ring-closing steps required. Another unifying theme that emerged was the manner in which each research group

**Herein, an envelope of two rings is denoted using the two ring letters in parentheses and separated by a comma. For example, (C,D) refers to an envelope of rings C and D.

leveraged the nitrogen atom inherent in the framework of the hetisines for strategic bond formation. This is immediately apparent in the three syntheses which utilize a C–N bond to close rings directly, but is also instrumental to the 1,3-dipolar cycloaddition strategies used in both the Zhang[29] and the Peese/Gin[28] syntheses.

2.1.5 Summary and outlook

Sections 2.1.3 and 2.1.4 detailed the state of the art in the synthesis of bridged polycyclic skeletons. To what extent did the scientists behind these syntheses avail themselves of the considerations outlined in Section 2.1.2? A full answer to that question would require knowledge of all disconnections considered, including the original retrosynthesis and any failed routes. While this is unfortunately not feasible, one can still discern that the majority of the syntheses described here have several features in common, which provide insight into the elements of a successful synthesis.

First, each of the syntheses of bridged polycyclic diterpenoid alkaloids covered here comprise two phases. The first phase addresses reaching a fully assembled 'base camp' (*i.e.*, a key intermediate compound), which already contains a number of connected rings (in the present examples, two or three), but with the rigidifying bridges yet to be installed. Attached to the skeleton of the key intermediate are side chains, which provide the skeletal atoms of the yet-to-be-closed rings. The second phase of the syntheses comprises the elevation of the key intermediate to the desired hexa- or heptacyclic skeleton of the target by forming strategic bonds to forge the bridging rings. While 'phase one' efforts are not reviewed in the present context, the efforts of 'phase two' are highlighted, albeit without significant discussion relating to the functionality present in the target structures.

A second trend apparent across the eight syntheses is the preference for bicyclization reactions, which achieve particularly rapid increases in target-relevant complexity. In seven of the eight examples, bicyclization reactions were employed, most often for the construction of the bicyclo[2.2.2]octane ring system present in both the hetidine and hetisine scaffolds.

The anellation approach to build bridged polycyclic compounds via early introduction of the maximally bridged ring (as discussed in Section 2.1.2) is adumbrated in only one of the eight syntheses covered (spirasine IV by Zhang[29]). The remainder of the syntheses that were surveyed largely follow bond-network analysis at the retrosynthetic level, even if these disconnections did not translate perfectly to the forward synthesis (see the synthesis of the hetidine core by Sarpong[20]). It is our opinion that a bond-network analysis approach to retrosynthesis is not consistently employed or considered by the synthetic community at present, but that the degree to which the precepts of bond-network analysis are adhered in reported syntheses nevertheless validates the principles outlined in Section 2.1.2.

On the other hand, bond network analysis may not necessarily be the most effective approach in all cases, depending on the functional groupings on a target molecule. This latter situation is particularly appreciated in light of previous reports,[31] in which solely following a bond-network analysis in forward syntheses led to conflicts with the functionalities that needed to be generated. Still, there is value in the fact that bond-network analysis sometimes suggests discon-

nections where the forward synthesis has no precedent and a new reaction may need to be developed. Finding creative solutions to challenging problems that may arise in this manner is the lifeblood of organic synthesis. Reaction development enables synthesis, which in turn highlights areas where further reaction development is needed. That cycle advances the frontiers of chemistry and can be driven forward by looking for strategies to accomplish these objectively identified disconnections, especially when we challenge ourselves to exploit native functionality to do so.

On the basis of the widespread application—conscious or unconscious—of bond-network analysis in successful syntheses of hetidine- and hetisine-type diterpenoid alkaloids, one should consider undertaking a bond-network analysis when planning the synthesis of a bridged polycyclic target structure, performing recursive network analyses in order to obtain hints on disconnections to give key intermediates. Searching within these hints for the potential application of bicyclization strategies is of paramount importance in assuring a rapid increase in complexity. The final stage in the planning process would then be to ascertain the compatibility of the intended bondset with the functionalities present in the target structure, as well as to consider which transform- and functional group-based strategies may be employed to capitalize upon the disconnections identified through bond-network analysis.

2.2 Synthesis of aconitine-type diterpenoid alkaloids*

Attracted by the challenges associated with the architectural complexity, as well as opportunities to learn about the biological function of diterpenoid alkaloid natural products (see Chapter 3), our laboratory embarked on a total synthesis campaign targeting members of the C_{18}-, C_{19}-, and C_{20}-diterpenoid alkaloids[11,33,34] with varying substitution and oxygenation patterns decorating their framework. These efforts have led to the first syntheses of aconitine-type diterpenoid alkaloids weisaconitine D (C_{18}, **1.6**, Figure 2.7) and liljestrandinine (C_{19}, **2.22**),[17] as well as of the previously discussed cossonidine (C_{20}, **2.23**, see Scheme 2.8).[30]

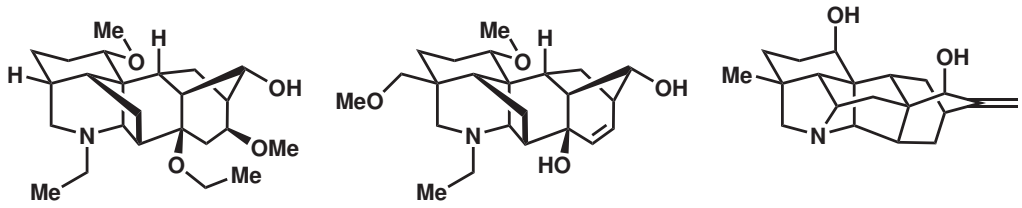

Figure 2.7: Selected diterpenoid alkaloids synthesized in the Sarpong laboratory.

2.2.1 Retrosynthesis of weisaconitine D guided by bond-network analysis

As with the hetidines and hetisines, bond-network analysis can be applied iteratively to guide retrosynthesis of the hexacyclic aconitine framework. Applying bond-network analysis to this

*Reproduced in part from Kou, K. G. M.; Kulyk, S.; Marth, C. J.; Lee, J. C.; Doering, N. A.; Li, B. X.; Gallego, G. M.; Lebold, T. P.; Sarpong, R. *J. Am. Chem. Soc.* **2017**, *139*, 13882–13896.[32] Copyright 2017 American Chemical Society.

highly bridged framework, as exemplified by weisaconitine D (**1.6**, Figure 2.8), we analyzed each of the individual rings to determine which was the most highly bridged. In this case, ring B con-

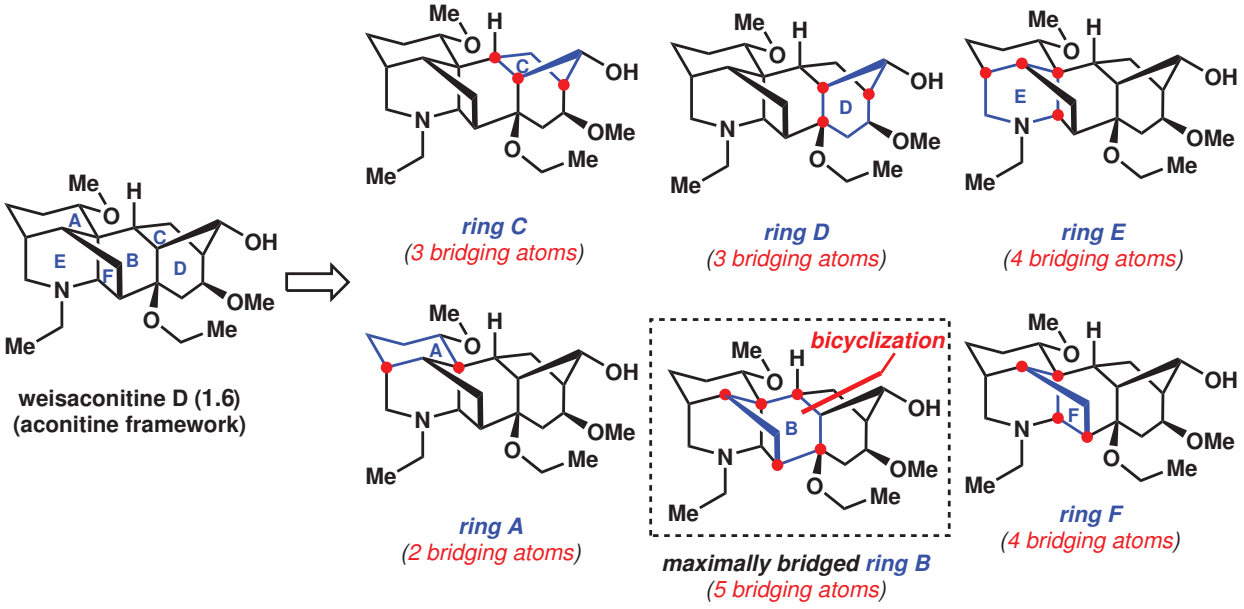

Figure 2.8: Bond-network analysis of weisaconitine D. The red dots indicate bridging atoms.

tains five bridging atoms, rings E and F four bridging atoms, ring C contains three bridging atoms, ring D three bridging atoms, and ring A two bridging atoms. Having identified ring B as the maximally bridged ring, we envisioned a bicyclization transform that effectively simplifies the target to tricyclic vinyl arene **2.24** (Scheme 2.9). In the forward sense, this operation forges two bonds and three new rings in a single step. Similarly, applying network analysis to intermediate **2.24** yields the piperidine ring E as the maximally bridged system with four bridging atoms. Since the piperidine ring also contains a nitrogen atom (a functional group), we reasoned that its disconnection would provide the greatest simplification, thus leading back to fused AF ring system **2.25** that contains no bridging elements. The protected amine functionality of **2.25** can arise from a hydration and Hofmann rearrangement sequence on nitrile **2.26**, which in turn can be prepared from vinyl nitrile **2.27** through a conjugate arylation reaction and transformation of the methyl ester. This intermediate can be further simplified to hydrindenone **2.28**, which can be accessed in >20 g quantities using a Diels–Alder reaction.[35]

Using network analysis, we determined that a bicyclization reaction to form the BCD ring systems would be most effective in directly assembling the target hexacyclic structure. To achieve this, we imagined a late-stage *meta*-π-arene photocycloaddition between the alkene and arene groups of vinyl arene **2.29** (Scheme 2.10). Photoexcitation of the arene component with UV irradiation was expected to lead to formation of an exciplex where concerted σ-bond formations would occur to generate diradical **2.30**. Spontaneous collapse of the diradical intermediate would form vinyl cyclopropane **2.31**.[36] Subsequent oxidation of the alkene to epoxide **2.32** could be followed by an acid-mediated cyclopropane fragmentation and epoxide ring-opening to furnish diketone **2.33**.[37,38] This approach would be unlike the proposed biosynthesis of the aconitine-type diterpenoid alkaloids that contain the bicyclo[3.2.1]octane CD ring system, and

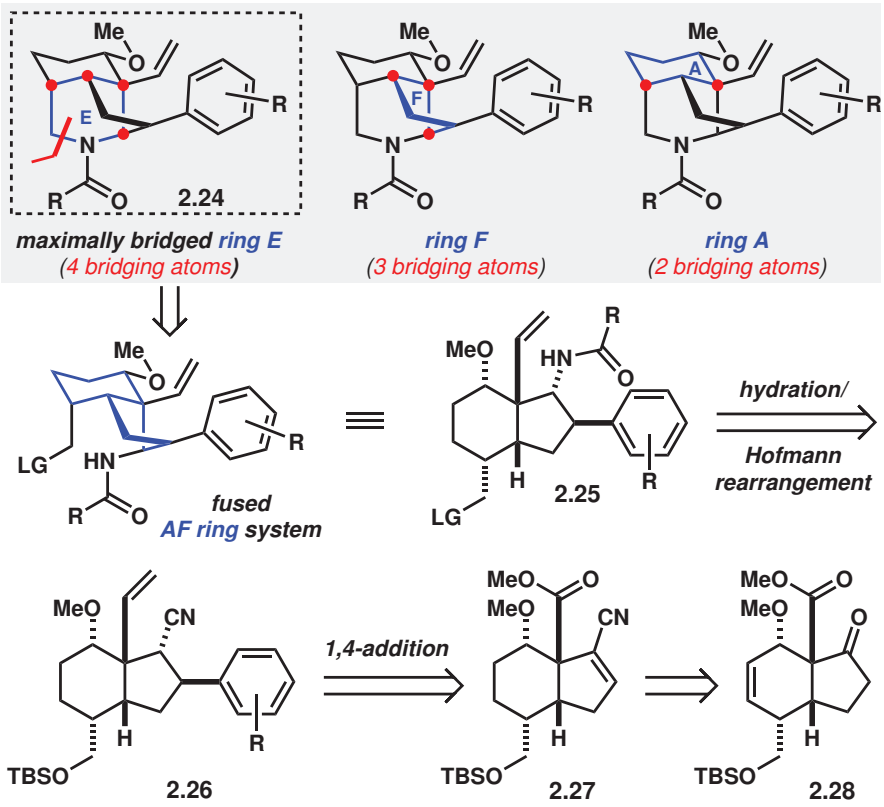

Scheme 2.9: Retrosynthetic analysis of aconitine-type natural products, as guided by bond-network analysis. The red dots indicate bridging atoms.

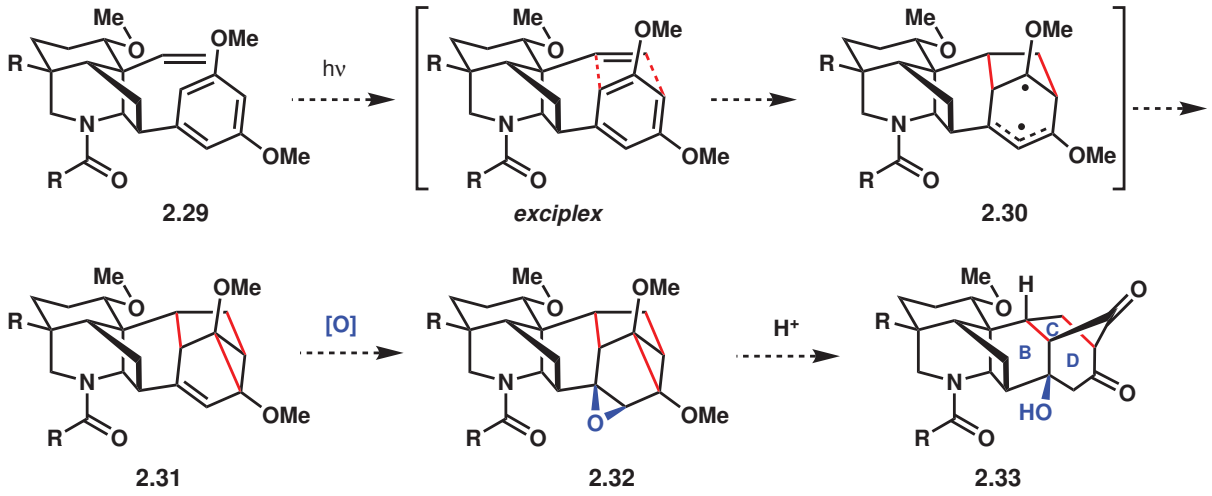

Scheme 2.10: Proposed *meta*-π-arene photocycloaddition approach to the BCD ring system.

would provide a more direct route to the desired carbon framework. We chose to introduce a methoxy-substituted aromatic ring (see **2.29**) because the arene oxygens would be native to many of our target natural products. In addition, electron-rich methoxy groups direct *meta*-π-functionalization to sites ortho to it, permitting us to take maximum advantage of the substituents inherent to the target structures in streamlining our synthesis.

2.2.2 Synthesis of the bicyclization precursor

The synthesis begins with dimethylation of 1,4-butynediol (**2.34**, Scheme 2.11) followed by $NaNH_2$-promoted elimination/isomerization to generate enyne **2.35** in 60% yield.[39] A two-step

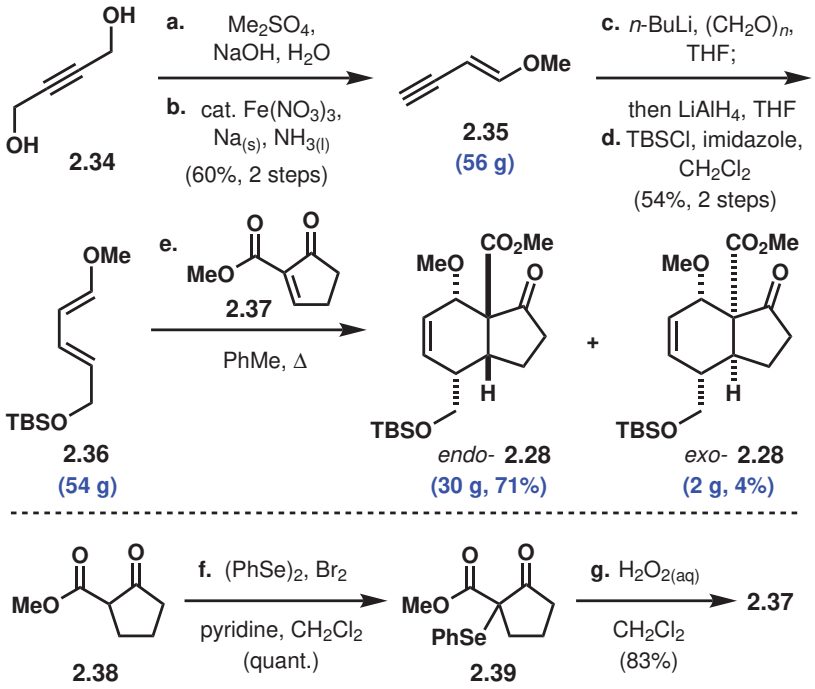

Scheme 2.11: Decagram-scale synthesis of diene **2.36** and cycloadducts **2.28**.

sequence involving alkylation of the terminal alkyne with paraformaldehyde and subsequent reduction of the propargyl alkyne with $LiAlH_4$, followed by TBS-protection of the primary alcohol yielded diene **2.36**,[40] which can be prepared on 54 g scale in a single pass. Heating a two-equivalent excess of diene **2.36** with dienophile **2.37** (prepared from α-selenation of β-ketoester **2.38**, followed by selenoxide elimination from **2.39**)[41] resulted in formation of the desired *endo*-cycloadduct (**2.28**) as the major product in 71% yield along with the *exo*-diastereomer in 4% yield.

The alkene group in hydrindenone *endo*-**2.28** was hydrogenated with Pd/C as the catalyst, and the ketone group converted to the vinyl triflate by treatment with LiHMDS and $PhNTf_2$ in 88% yield over the two steps (Scheme 2.12). The resulting vinyl triflate was then converted to vinyl nitrile **2.27** in 78% yield by a Pd- and Cu-catalyzed cyanation protocol using NaCN.[42] Introducing the electron-rich aromatic group onto the vinyl nitrile was accomplished using a Rh-catalyzed 1,4-addition reaction developed by the Hayashi group, providing *trans*-β-aryl nitrile

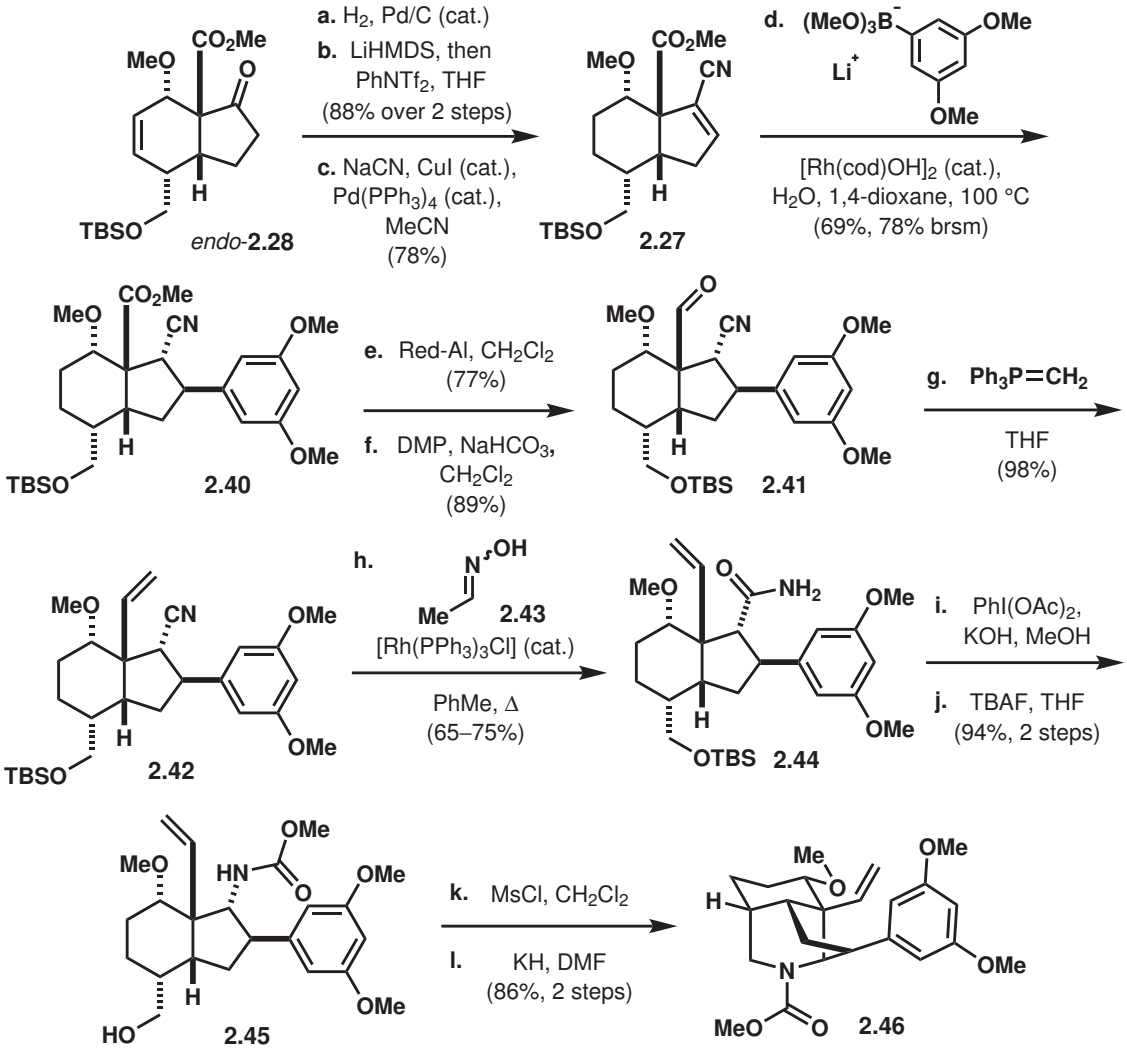

Scheme 2.12: Synthesis of vinyl arene intermediate **2.46** for photocycloaddition.

2.40 in 69% yield (78% brsm).[43] The ester moiety was selectively reduced to the primary alcohol with Red-Al, leaving the nitrile intact (77%). The primary hydroxy group was oxidized to aldehyde **2.41** (89%), which was subsequently methylenated to alkene **2.42** (98%). In the presence of acid-labile functionalities such as the silyl ether, hydration of the nitrile to afford primary amide **2.44** proceeds in 65–75% yield under anhydrous conditions employing Wilkinson's catalyst and acetaldoxime as the water-equivalent.[44] Hypervalent iodine-mediated Hofmann rearrangement of **2.44** in methanol solvent formed the corresponding methyl carbamate which was then subjected to TBAF-mediated deprotection to reveal alcohol **2.45** in 94% yield over two steps. Successive activation of the alcohol as the mesylate and treatment with KH in DMF resulted in cyclization to piperidine **2.46** (88% yield over two steps), which served as our substrate for photocycloaddition studies.

2.2.3 *meta*-π-Arene bicyclization approach

Irradiation of a solution of vinyl arene **2.46** in C_6D_6 with 254 nm UV light resulted in the formation of diastereomeric [2+2]-cycloadducts **2.47** and **2.48** (Scheme 2.13) via *ortho*-π-arene pho-

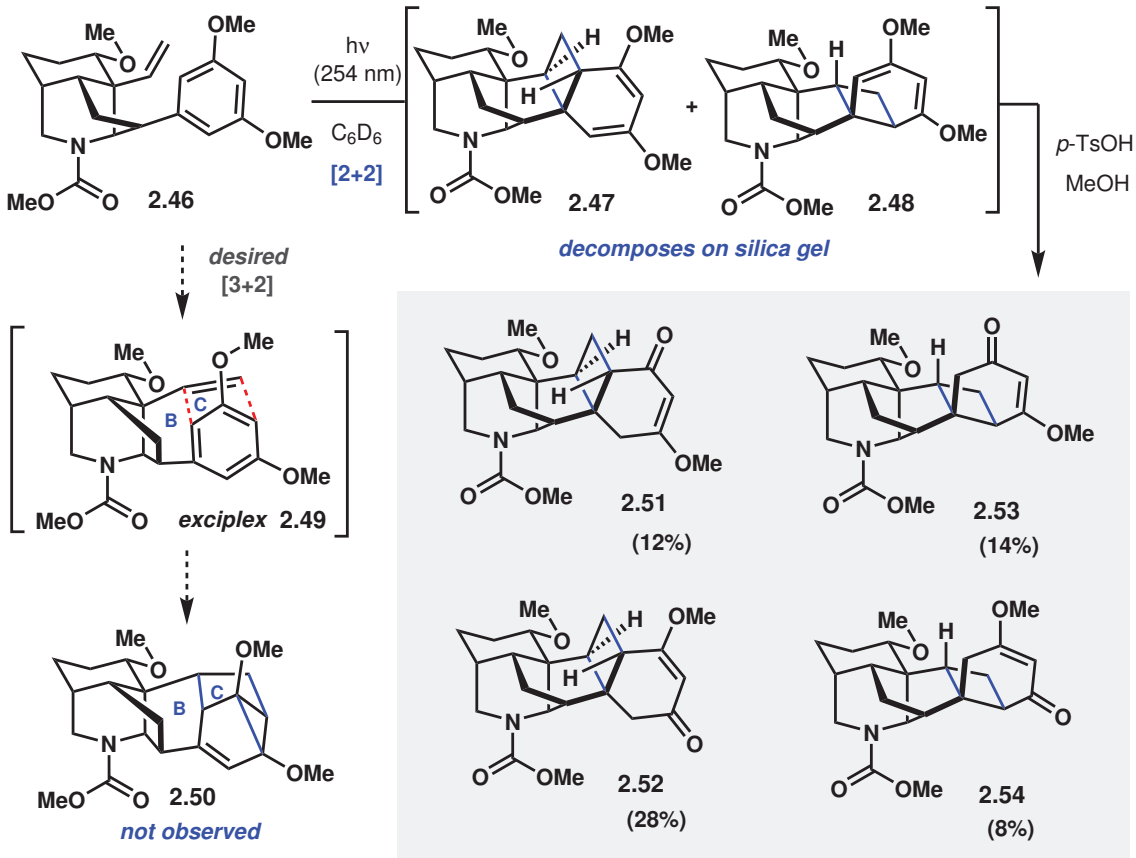

Scheme 2.13: Exploration of alkene–arene photocycloadditions.

tocycloaddition. Products arising from formation of exciplex **2.49** and the desired (3+2) *meta*-π-arene photocycloaddition pathway were not observed (*e.g.*, **2.50**). Using 310 nm UV light gave a

similar outcome by ^{1}H NMR analysis. Attempts to isolate these cycloadducts by silica gel chromatography resulted in their decomposition to a mixture of hydrolyzed products. However, reconstituting this mixture of **2.47** and **2.48** in methanol with *p*-TsOH fully converted the bis-enol ether intermediates to an isomeric mixture of hexacyclic, vinylogous esters **2.51**, **2.52**, **2.54**, and **2.53**† in 12%, 28%, 8%, and 14% yields, respectively. Initial studies conducted in quartz NMR tubes provided insufficient material to fully characterize these cycloadducts. Attempts to scale the reaction up in quartz test tubes resulted in greatly decreased conversion compared to the original experiments, despite extended reaction times. Switching to a flow chemistry apparatus, in which thin tubing was coiled around a medium-pressure Hg lamp, led to a significant increase in reaction rate such that full conversion of vinyl arene **2.46** was achieved in two hours. This setup also enabled us to run the reaction on >100 mg scale, facilitating unambiguous characterization of three of the cycloadducts by single-crystal X-ray crystallography (Figure 2.9).

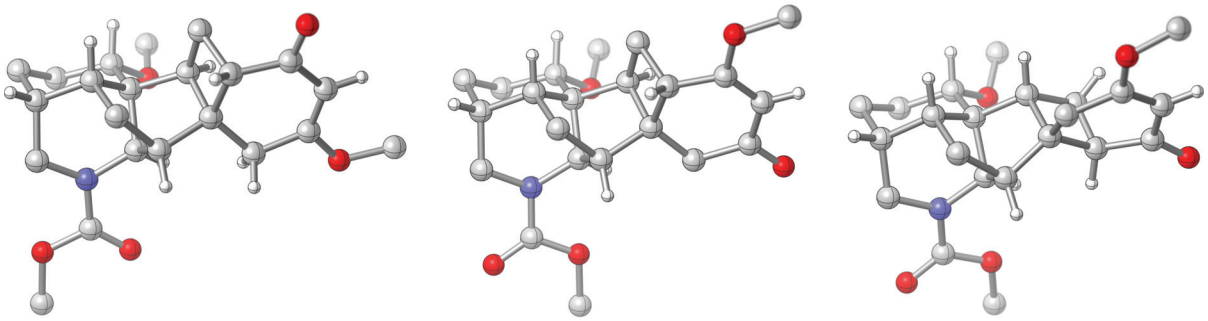

Figure 2.9: X-ray structures of [2+2]-cycloadducts **2.51** (left), **2.52** (center), and **2.54** (right) visualized with CYLview.

UV irradiation in other non-polar solvents such as cyclohexane and toluene at room temperature or 4 °C had minimal effect on reactivity, and the use of methanol as solvent partially facilitated hydrolysis of photocycloadducts **2.47** and **2.48**. The lack of (3+2) reactivity is likely due to the developing strain that is imposed by tethering the alkene meta to the methoxy-directing groups, a substitution pattern that has not been demonstrated to undergo *meta*-π-arene photocycloaddition.[45] To help alleviate strain, bicyclic vinyl arenes **2.42** and **2.55** (precursors to alcohol **2.45**) were subjected to 254 nm UV irradiation (Scheme 2.14a). However, reducing strain by

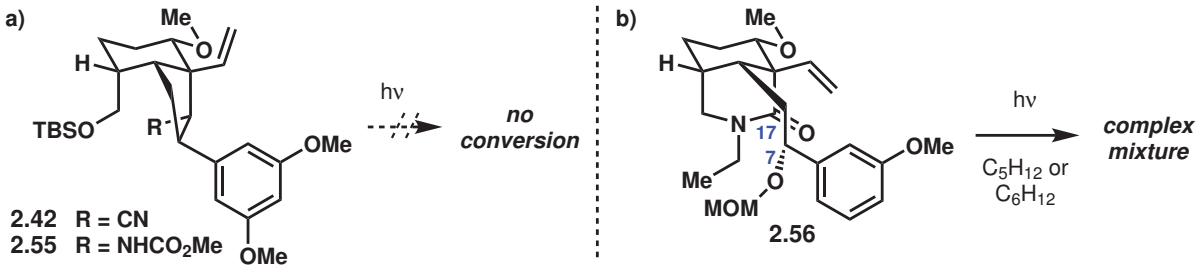

Scheme 2.14: Alternate alkene–arene photocycloaddition substrates.

†The structure of **2.53** is presumed, but not unambiguously confirmed. See experimental details for discussion.

not having the piperidine ring in place resulted in no reactivity, likely due to the system being unable to adopt an energetically-accessible, reactive conformation.

Based on similar reasoning, a less constrained vinyl arene (**2.56**) lacking the C7–C17 bond was prepared and irradiated with 254 nm UV light (Scheme 2.14b). While reactive, this substrate gave rise to a complex mixture of products that could not be easily purified. To test whether the lack of (3+2) reactivity could be due to a high barrier in forming a strained 6-membered ring B, we designed substrate **2.57** where the alkene is tethered ortho to the methoxy-group (Scheme 2.15). In this case, if a (3+2) photocycloaddition was to occur through exciplex **2.58**

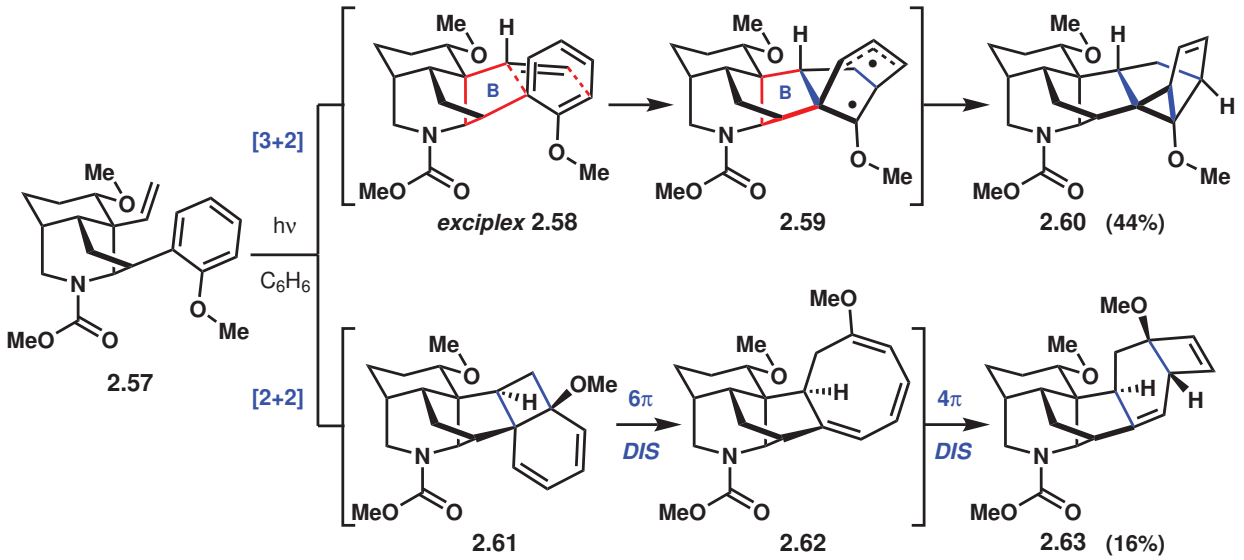

Scheme 2.15: Alkene–arene photocycloaddition with ortho tether.

and diradical **2.59**, a more favorable 5-membered ring B (highlighted in red) would form. This hypothesis proved correct, providing (3+2)-cycloadduct **2.60** as the major product in 44% yield. The [2+2] cycloaddition pathway was also operative to a small extent, affording cyclobutene-bearing **2.63** in 16% yield. This product differs from the previously observed *ortho*-photocycloaddition reactions (*cf.* Scheme 2.13) in that cyclobutene intermediate **2.61** bearing a tertiary methoxy group formed from the initial photochemical [2+2]-cycloaddition, undergoes spontaneous 6π-electrocyclic ring opening to cyclooctatriene **2.62**, followed by a final photochemical 4π-electrocyclic ring closing process to arrive at **2.63**. These products, however, could not be easily advanced to weisaconitine D (**1.6**. The structures of both **2.60** and **2.63** were confirmed by X-ray crystallography (Figure 2.10).

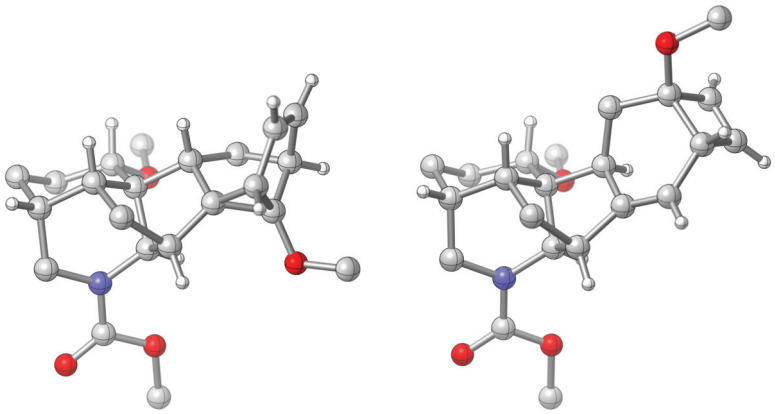

Figure 2.10: X-ray structures of (3+2)-cycloadduct **2.60** (left) and cyclobutene **2.63** (right) visualized with CYLview.

2.2.4 A revised approach: Diels–Alder/Wagner–Meerwein rearrangement

An alternative bicyclization disconnection that still retrosynthetically cleaves the maximally bridged ring B of the aconitine-type framework involves a [4+2]-cycloaddition between the alkene and the arene system following oxidative dearomatization of tetracycle **2.66** (Scheme 2.16). The product will contain a bicyclo[2.2.2]octane system characteristic of the denudatine-type

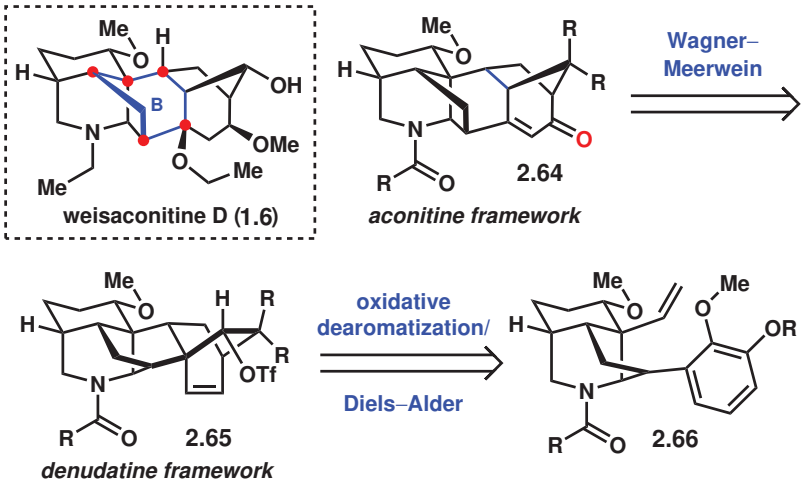

Scheme 2.16: Revised retrosynthetic plan.

molecules that will need to be rearranged to give the bicyclo[3.2.1] CD-ring system. Since nature employs such an isomerization in the biosynthesis of numerous diterpenes by rearranging the diterpene skeleton of denudatine alkaloids to that of the aconite skeleton,[46–49] we reasoned that this approach could offer promising opportunities for developing a divergent synthesis. In fact, Wagner–Meerwein-type rearrangement of a bicyclo[2.2.2]octane to the corresponding bicyclo[3.2.1]octane was first reported in 1949[50,51] by Doering et al. and successfully applied to early syntheses of the diterpenoid alkaloids talatisamine[7b] (**1.4**, see Section 1.2.3) and 13-desoxydelphonine[52] by Wiesner and co-workers. We thus targeted hexacycle **2.65**, which ex-

hibits the denudatine framework, with the intention of rearranging it to **2.64**, which exhibits the aconitine framework, via an oxidative Wagner–Meerwein rearrangement.

The synthesis of the denudatine framework commences with the 1,4-arylation of vinyl nitrile **2.27** using aryl boronate ester **2.67** to form β-aryl nitrile **2.68** (Scheme 2.17), which was then advanced through a similar sequence to that illustrated in Scheme 2.12 to give tetracycle **2.69**. Subsequent cleavage of the MOM protecting group with HCl and oxidative dearomatization

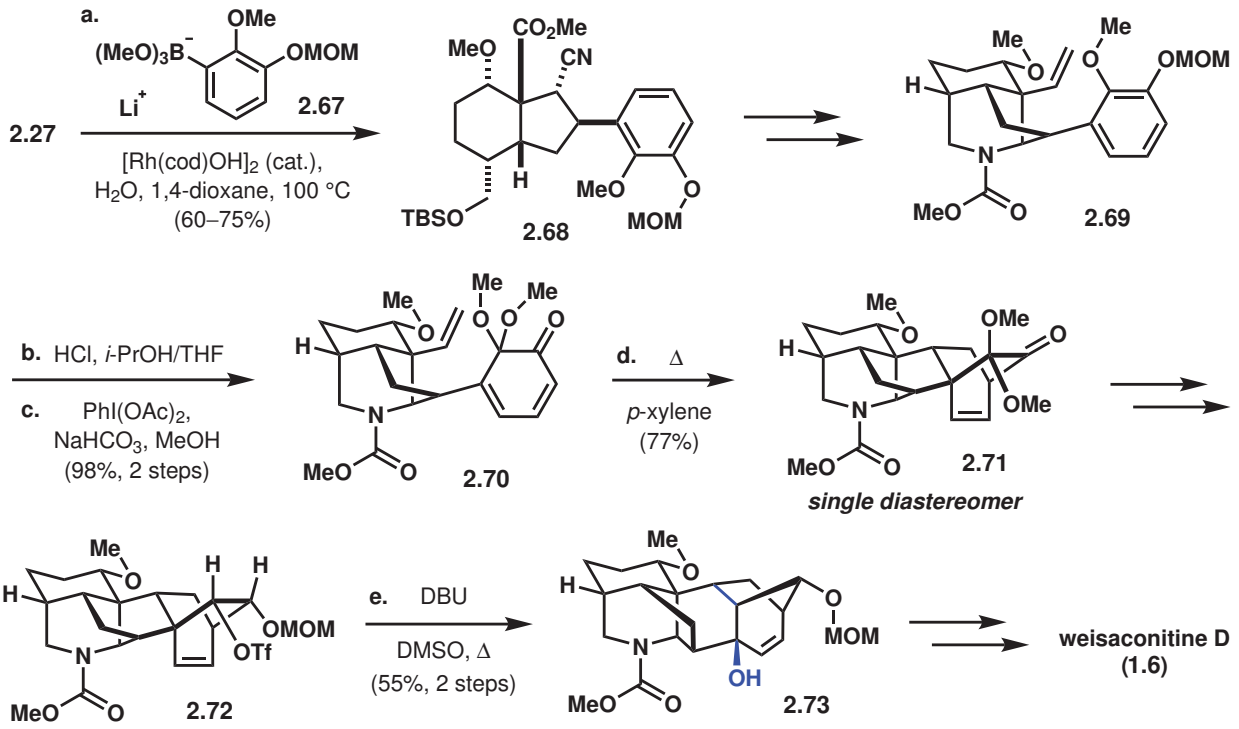

Scheme 2.17: Synthesis of weisaconitine D using a key Wagner–Meerwein rearrangement.

with $PhI(OAc)_2$ in methanol furnishes dienone **2.70**, the immediate precursor to intramolecular Diels–Alder cycloaddition, in 98% yield over two steps. Heating a solution of **2.70** in *p*-xylene to 150 °C in a sealed flask induces the intramolecular [4+2]-cycloaddition to provide the desired hexacycle (**2.71**) as a single diastereomer in 77% yield. Redox and protecting group manipulation of **2.71** affords triflate **2.72**, which undergoes Wagner–Meerwein rearrangement when heated in a mixture of DBU and DMSO to give allylic alcohol **2.73** as the only observable product. Allylic alcohol **2.73** bears the desired bicyclo[3.2.1]octene system that can be advanced to weisaconitine D (**1.6**) in another eight steps.

2.3 Experimental contributors

Terry P. Lebold (T. P. L.) contributed to the conceptualization of the synthetic route with significant synthetic contributions made to the early portion of the synthesis. T. P. L. and Gary M. Gallego (G. M. G.) established a large-scale synthesis of **2.28**. Jack C. Lee (J. C. L.) conceptualized the nitrile as a nitrogen atom surrogate and developed conditions for the conjugate addition of the functionalized arene (**2.24** to **2.40**). Christopher J. Marth (C. J. M.) and Kevin

G. M. Kou (K. G. M. K.) then optimized this key transformation. G. M. G. developed the route from **2.40** to the bicyclization precursors, as well as the Diels–Alder cycloaddition to form **2.71**. C. J. M. developed the key Wagner–Meerwein rearrangement. C. J. M. and J. C. L. developed the route to advance [3.2.1] bicycle **2.73** to weisaconitine D (**1.6**). K. G. M. K., with the help of Svitlana Kulyk (S. K.) and Nicolle A. Doering (N. A. D.), optimized the route to weisaconitine D. Bicyclization reactions in the failed *meta*-π-arene approach were initially explored by C. J. M. and S. K., then followed up on by K. G. M. K. and N. A. D. Scale up of these reactions to enable structural characterization was developed by N. A. D.

2.4 Materials and methods

Solvents and reagents. Unless noted below, commercial reagents were purchased from Sigma Aldrich, Acros Organics, Chem-Impex, Combi-blocks, TCI, and/or Alfa Aesar, and used without additional purification. Solvents were purchased from Fisher Scientific, Acros Organics, Alfa Aesar, and Sigma Aldrich. Tetrahydrofuran (THF), diethyl ether (Et_2O), acetonitrile (CH_3CN), benzene, methanol (MeOH), and triethylamine (Et_3N) were sparged with argon and dried by passing through alumina columns using argon in a Glass Contour solvent purification system. Dichloromethane (CH_2Cl_2) was freshly distilled over calcium hydride under a N_2 atmosphere prior to each use. DMSO and toluene (PhMe) were distilled over calcium hydride under a N_2 atmosphere, degassed via freeze–pump–thaw (3 cycles), and stored over 4 Å molecular sieves in a Schlenk flask under N_2. Dimethoxyethane (DME), *p*-xylene, dimethylformamide (DMF), MeLi solution, *n*-BuLi solution, LiHMDS solution, Red-Al solution, and pyridine were purchased in Aldrich SureSeal, Acros AcroSeal, or Alfa Aesar ChemSeal bottling, and used directly. 1,4-Dioxane was purchased in AcroSeal bottling (99.5%, anhydrous, stabilized, over 4 Å molecular sieves) and additionally sparged with N_2 prior to use. $B(OMe)_3$ was distilled over calcium hydride, degassed via freeze-pump-thaw (3 cycles), and stored under N_2 in a Schlenk flask.

Reaction setup, progress monitoring, and product purification. Unless otherwise noted in the experimental procedures, reactions were carried out in flame or oven-dried glassware under a positive pressure of N_2 in anhydrous solvents using standard Schlenk techniques. Reaction temperatures above rt (22–23 °C) were controlled by an IKA temperature modulator and monitored using liquid-in-glass thermometers. Reaction progresses were monitored using a combination of LC–MS analysis (via a Shimadzu LCMS-2020 (UFLC) equipped with the LC-20AD solvent delivery system, a SPD-20AV prominence UV/Vis detector (SPD-M20A Photo Diode Array), and a Thermo Scientific Hypersil GOLD HPLC column (5 μm particle size, 4.6 x 50 mm)), and thin-layer chromatography (TLC) on Silicycle Siliaplates (glass backed, extra hard layer, 60 Å, 250 μm thickness, F254 indicator). Visualization of the developed plates was performed under UV-light (254 nm) irradiation, and then gently heated with $KMnO_4$, *p*-anisaldehyde, or ceric ammonium molybdate stains. Purification and isolation of products were performed via silica gel chromatography (both column and preparative thin-layer chromatography). Flash column chromatography was performed with either glass columns using Silicycle silica gel (40–63 μm particle size) or with a Yamazen Smart Flash EPCLC W-Prep 2XY (dual channel) automated flash chromatography system on prefilled, premium, universal columns using ACS grade solvents. Organic solutions were concentrated under reduced pressure on a Heidolph temperature-controlled rotary evaporator equipped with a dry ice/isopropanol condenser or a

Büchi temperature-controlled rotary evaporator equipped with an Ecodyst Ecochyll system.

Analytical instrumentation. NMR spectral data were obtained using deuterated solvents were obtained from Cambridge Isotope Laboratories, Inc. ^{1}H NMR and ^{13}C NMR data were recorded on Bruker AVB-400, AVQ-400, AV-500, DRX-500, AV-600, or CRYO-900 MHz spectrometers using $CDCl_3$, C_6D_6, or D_2O solvents, typically at 20–23 °C. Variable temperature (VT) experiments, typically between 60–70 °C (in C_6D_6), were performed for compounds that exist as rotamers at rt. Chemical shifts (δ) are reported in ppm relative to the residual solvent signal (δ 7.26 for ^{1}H NMR, δ 77.16 for ^{13}C NMR in $CDCl_3$, δ 7.16 for ^{1}H NMR, δ 128.06 for ^{13}C NMR in C_6D_6, and δ 4.79 for D_2O).[53] When ^{13}C signals appear weak and/or broad (with poor signal/noise ratios), especially for variable temperature (VT) experiments, HSQC spectra are acquired to confirm signal authenticity. Data for ^{1}H NMR spectroscopy are reported as follows; chemical shift (δ ppm), multiplicity (s = singlet, bs = broad singlet, d = doublet, t = triplet, q = quartet, m = multiplet, dd = doublet of doublets, dt = doublet of triplets), coupling constant (Hz), integration. Data for ^{13}C NMR spectroscopy are reported in terms of chemical shift (δ ppm). ^{13}C NMR chemical shifts are reported to one decimal place; a second decimal place is included when two closely spaced, but distinct, signals resonate within 0.1 ppm of each other.

IR spectroscopic data were recorded on a Bruker ALPHA FT-IR spectrophotometer using a diamond attenuated total reflectance (ATR) accessory. Samples are loaded onto the diamond surface either neat or as a solution in organic solvent and the data acquired after the solvent had evaporated.

Mass spectral data were obtained from: 1) the QB3/Chemistry Mass Spectrometry Facility at the University of California, Berkeley, on a Finnigan/Thermo LTQ-FT instrument (ESI), and the data acquired and processed using the Xcalibur software, and 2) the Catalysis Facility of Lawrence Berkeley National Laboratory (supported by the Director, Office of Science, of the US Department of Energy under contract no. DE-AC02-05CH11231) using a PerkinElmer AxION 2 TOF-MS. X-Ray data were collected on a Bruker APEX-II CCD diffractometer with Mo-Kα radiation (λ = 0.71073 Å) or a MicroStar-H X8 APEX-II diffractometer with Cu-Kα radiation (λ = 1.54178 Å) (supported by an NIH Shared Instrumentation Grant S10-RR027172). CYLview (Legault, C. Y., Université de Sherbrooke, 2009) was used for graphic rendering.

2.5 Experimental details

The synthesis and characterization data for compounds **2.27**, **2.56**, **2.57**, and **2.67**–**2.73** have been previously reported by us and are not reproduced here.[17,54,55] Procedures and characterization data for all new compounds are provided.

2.5.1 Synthesis of photocycloaddition precursor 2.46

Enyne 2.35. 2-Butyne-1,4-diol (**2.34**, 141 g, 1.64 mol) was suspended in deionized H_2O (270 mL) in a 2 L round bottom flask equipped with magnetic stirring bar, and stirred until most of the solids had dissolved. The flask was immersed in an ice/water bath, and a solution of NaOH (148 g in 250 mL H_2O, 3.70 mol) was added to the reaction flask under air. To the cold reaction

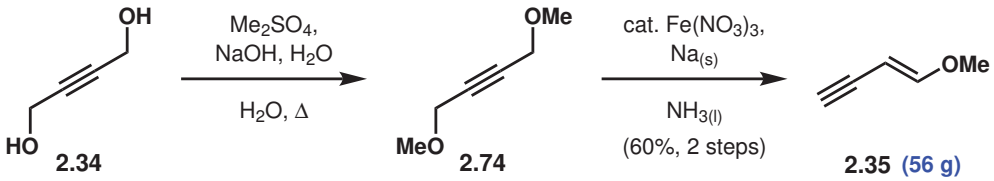

mixture was added Me_2SO_4 (346 mL, 3.65 mol) over 30 min via addition funnel. This process was exothermic, which was evident during the addition of the final 30 mL of Me_2SO_4. A reflux condenser was attached and the resulting biphasic mixture heated to 90–100 °C for 2.5 h using a heating mantle. The reaction was cooled to rt, and the organic and aqueous layers were separated. The aqueous layer was extracted with Et_2O (2 x 200 mL). The combined organic extract was washed with brine (150 mL), dried over Na_2SO_4, filtered, and concentrated *in vacuo* to give dimethoxy-2-butyne (**2.74**, 169 g) as a light yellow liquid. Care should be taken to minimize vacuum exposure and reduce product loss due to its volatility. This material was pure by ^{1}H NMR analysis and was used in the subsequent reaction without purification. ^{1}H NMR (300 MHz, $CDCl_3$) δ 4.15 (s, 4H), 3.39 (s, 6H).

$NH_{3(g)}$ was condensed into a flame-dried 2 L two-neck round bottom flask that was precooled to –78 °C in a dry ice/acetone bath, and equipped with a magnetic stirring bar and cold finger condenser (filled with dry ice in acetone). The condensation process was allowed to proceed until approximately 1 L of $NH_{3(l)}$ had been collected. A balloon was attached to a neck of the flask through a septum to qualitatively monitor NH_3 pressure over the course of the condensation; the balloon was subsequently replaced with a N_2 inlet line. The $Na_{(s)}$ (40.8 g, 1.18 mol) was rinsed with hexanes and cut into approximately 20 x 1 cm^3 cubes. One piece of $Na_{(s)}$ was added, followed by a catalytic amount of $Fe(NO_3)_3 \cdot 9H_2O$ (0.924 g, 3.82 mmol) to produce a dark purple mixture. The remainder of $Na_{(s)}$ was carefully added in 20 s intervals. The N_2 inlet line was replaced with an oil bubbler to monitor hydrogen gas generation. The reaction mixture was stirred at –78 °C for 2 h, at which point hydrogen gas evolution had ceased. The oil bubbler was removed and the N_2 inlet line was re-attached. Crude butyne **2.74** (83.3 g, 730 mmol) was added via syringe pump (1 mL/min). After complete addition of the starting material, the reaction mixture was stirred for an additional 1 h at –78 °C. While ensuring adequate N_2 flow through the reaction flask, NH_3 was carefully evaporated over 2 h by removing the dry ice bath and allowing the reaction vessel to gradually warm to rt. After most NH_3 had evaporated, Et_2O (250 mL) was slowly added to the reaction mixture. The reaction mixture was then cooled in an ice/water bath, and quenched by dropwise addition of H_2O (250 mL). The resulting dark brown suspension was filtered through Celite (rinsing with 200 mL Et_2O). The resulting dark brown filtrate was extracted with Et_2O (2 x 100 mL), and the combined organic extract was washed with brine (100 mL), dried over Na_2SO_4, and filtered. To minimize loss of the volatile product, the rotovap was not used. Instead, most of the Et_2O solvent was removed by distillation at 40–50 °C to give a volatile brown liquid (90.1 g, 2:3 **2.35**:Et_2O by ^{1}H NMR analysis, ~440 mmol, 60% over 2 steps). The material was used directly without further purification. ^{1}H NMR (400 MHz, $CDCl_3$) δ6.95 (d, J = 12.9 Hz, 1H), 4.82 (dd, J = 12.9, 2.4 Hz, 1H), 3.60 (s, 3H), 2.72 (dd, J = 2.4, 0.5 Hz, 1H).

Diene 2.36. Crude enyne **2.35** (2:3 **2.35**/Et_2O, approximately 440 mmol) was diluted with THF under N_2 in a flame-dried 2 L round bottom flask equipped with a magnetic stirring bar. The solution was cooled to –78 °C in a dry ice/acetone bath, and *n*-BuLi (2.5 M in hexanes, 228

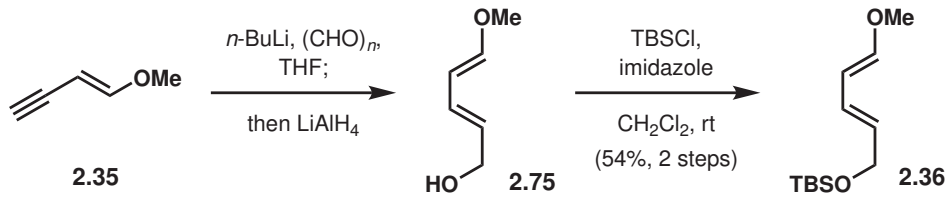

mL, 570 mmol) was added over 30 min via addition funnel. The cold bath was replaced with a water bath at rt, and the dark brown reaction mixture was stirred at rt for 1 h. This mixture was then cooled in an ice/water bath, and paraformaldehyde (20.3 g, 676 mmol) was added in one portion. The reaction mixture was gradually warmed to rt, stirring for 17 h. The resulting mixture was cooled in an ice/water bath, and $LiAlH_4$ (25.0 g, 658 mmol) was carefully added in 12 portions. The brown slurry was gradually warmed to rt over 90 min. Finally, the reaction mixture was cooled in an ice/water bath and carefully quenched using Fieser–Fieser work-up conditions (10 mL EtOAc, 24.3 mL H_2O, 24.3 mL 15% aqueous NaOH, and 3 x 24.3 mL H_2O were added dropwise to the reaction mixture, respectively). The crude mixture was filtered through Celite, and concentrated *in vacuo* to obtain dienol **2.75** as a yellow liquid (40.6 g). This material was used without further purification. ^{1}H NMR (400 MHz, C_6D_6) δ 6.44 (d, J = 12.5 Hz, 1H), 5.94 (dd, J = 26.8, 9.8 Hz, 1H), 5.52 (dtt, J = 15.1, 6.3, 0.7 Hz, 1H), 5.43 (dd, J = 12.5, 10.6 Hz, 1H), 3.97–3.91 (m, 2H), 3.08 (d, J = 0.7 Hz, 3H), 1.04 (s, 1H). Because the addition of $LiAlH_4$ was added directly to the reaction mixture without prior workup or reconstitution of the reaction mixture in an alternative solvent, we regard this as a single-step reaction.

Crude dienol **2.75** (40.6 g) was dissolved in anhydrous CH_2Cl_2 (600 mL) under N_2 in a 2 L round bottom flask, equipped with magnetic stir bar, and the reaction flask was immersed in a water bath at rt. Imidazole (52.5 g, 771 mmol) was added in 3–5 g portions, followed by TBSCl (64.3 g, 427 mmol) in 5–10 g portions. The reaction mixture was stirred under N_2 at rt for 9 h, during which time a light orange precipitate formed. The reaction mixture was quenched by addition of a saturated solution of $NaHCO_3$ (saturated aqueous, 300 mL). The aqueous and organics layers were separated, and the organic layer was washed with brine (100 mL), dried over Na_2SO_4, filtered, and concentrated *in vacuo* to give an orange liquid. Purification via column chromatography (eluting with 0–4% EtOAc in hexanes) gave the title product as a light, yellow liquid (54.0 g, 54% over 2 steps). ^{1}H NMR (400 MHz, C_6D_6) δ 6.46 (d, J = 12.5 Hz, 1H), 6.12 (ddtd, J = 15.0, 10.6, 1.5, 0.6 Hz, 1H), 5.60 (dtt, J = 15.1, 5.5, 0.6 Hz, 1H), 5.48 (dd, J = 12.5, 10.7 Hz, 1H), 4.16 (dd, J = 5.6, 1.5 Hz, 2H), 3.07 (s, 3H), 1.01 (s, 9H), 0.10 (s, 6H); ^{1}H NMR (400 MHz, $CDCl_3$) δ 6.58 (d, J = 12.6 Hz, 1H), 6.20–5.94 (m, 1H), 5.69–5.39 (m, 2H), 4.18 (dd, J = 5.6, 1.5 Hz, 2H), 3.58 (s, 3H), 0.91 (s, 9H), 0.07 (s, 6H). The spectroscopic data obtained are consistent with those previously reported in the literature.[17] This product decomposes in $CDCl_3$ and the NMR sample should be discarded. Reconstituting a $CDCl_3$ NMR sample with the bulk of the material results in gradual decomposition of the whole batch of material. The pure diene can be stored in the freezer for several months with no change in activity.

***endo*- and *exo*-Hydrindenone 2.28.** A 500 mL Schlenk flask was charged with methyl 5-oxocyclopent-1-ene-1-carboxylate (**2.76**, 17.6 g, 1 equiv), diene **2.36** (54.0 g, 1.9 equiv), and PhMe (250 mL). The resulting mixture was carefully evacuated (on a Schlenk manifold) and backfilled with N_2. The Schlenk flask was sealed and the vessel heated to 100 °C for 10 h. [In our hands, the

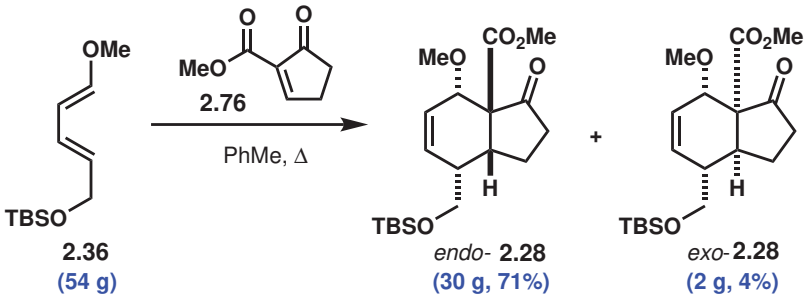

use of 1.9–2.2 equiv of diene suppresses polymerization. The use of excess, equimolar, or "aged" dienophile generally results in a substantial amount of polymerization, and yields an insoluble "tar" by the end of the reaction. We noticed that the color of the crude reaction mixture is often an indicator for whether or not the reaction is successful; reaction mixtures that turn dark red/black often give significant amounts of polymeric side-products while reaction mixtures that remain light in color over the during of the heating process provide high yields of the Diels–Alder cycloadducts.] The resulting light orange mixture was cooled to rt and concentrated *in vacuo*. Purification by gradient flash chromatography (using 1.7 L of silica gel) eluting with 2–20% EtOAc in hexanes gave the desired *endo*-hydrindenone **2.28** as a pale yellow liquid (29.6 g, 71%). The *exo*-diastereomer was isolated as a white solid (2.07g, 4.5%). The spectroscopic data obtained are consistent with those previously reported in the literature.[17]

endo-**2.28**. ^{1}H NMR (400 MHz, $CDCl_3$) δ 5.99 (ddd, *J* = 10.4, 4.3, 2.7 Hz, 1H), 5.75–5.67 (m, 1H), 4.35 (dq, *J* = 3.2, 1.0 Hz, 1H), 3.73 (s, 3H), 3.71–3.52 (m, 2H), 3.31 (s, 3H), 2.99 (dt, *J* = 12.9, 6.6 Hz, 1H), 2.48 (q, *J* = 8.3 Hz, 1H), 2.38 (ddd, *J* = 18.8, 8.4, 1.6 Hz, 1H), 2.24 (ddd, *J* = 18.9, 10.2, 8.7 Hz, 1H), 2.02–1.81 (m, 2H), 0.89 (s, 9H), 0.06 (s, 6H).

exo-**2.28**. Mp 75–78 °C. The melting range reported previously (61–65 °C)[17] was measured using material that was not completely pure. ^{1}H NMR (400 MHz, $CDCl_3$) δ 5.94 (ddd, *J* = 10.2, 4.3, 1.7 Hz, 1H), 5.89 (dd, *J* = 10.4, 2.6 Hz, 1H), 4.26 (d, *J* = 3.9 Hz, 1H), 3.72 (s, 3H), 3.69 (dd, *J* = 9.6, 6.1 Hz, 1H), 3.55 (dd, *J* = 9.5, 7.4 Hz, 1H), 3.29 (s, 3H), 2.84–2.66 (m, 1H), 2.36–2.24 (m, 1H), 2.22–2.03 (m, 2H), 1.97–1.77 (m, 2H), 0.88 (s, 9H), 0.04 (s, 6H).

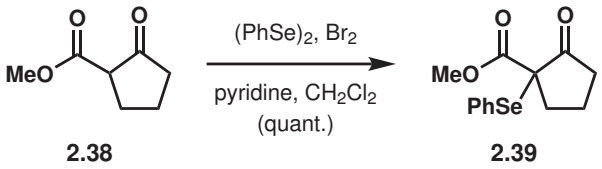

Selenide 2.39. To a solution of diphenyl diselenide (50.7 g, 162 mmol, 1 equiv) in CH_2Cl_2 (500 mL) was added bromine (8.25 mL, 162 mmol, 0.99 equiv). The reaction mixture turned red-black and an orange precipitate started to form on the sides of the flask. The reaction mixture was stirred at rt for 1.5 h, then cooled in an ice/water bath. Pyridine (32.7 mL, 406 mmol, 2.5 equiv) was added and the reaction mixture was stirred for 10 min. β-Ketoester **2.38** (39.4 mL, 292 mmol, 1.8 equiv) was added dropwise and the reaction mixture was stirred in the ice/water bath for 1.5 h, before being warmed to rt and stirred for an additional 3.5 h. The reaction mixture was then added to a separatory funnel with 1 M HCl (aqueous, 100 mL) and shaken vigorously. The organic layer was separated, then washed with 1 M HCl (aqueous, 100 mL), followed by

$NaHCO_3$ (saturated aqueous, 100 mL) and brine (50 mL). The organic extract was dried over anhydrous Na_2SO_4, filtered, and concentrated *in vacuo* to afford the crude product **2.39** (95.3 g) as a dark red oil. Purification by flash chromatography eluting with 14–35% EtOAc in hexanes gave the product as a yellow oil (86.8 g, quant.). ^{1}H NMR (300 MHz, $CDCl_3$) δ 7.64–7.59 (m, 2H), 7.45–7.38 (m, 1H), 7.36–7.29 (m, 2H), 3.74 (s, 3H), 2.59–2.48 (m, 2H), 2.38–2.24 (m, 1H), 2.13–1.87 (m, 3H). The ^{1}H NMR data obtained are consistent with those reported in the literature.[56] The ^{13}C NMR data has not been previously reported and is therefore provided here: (125 MHz, $CDCl_3$) δ 207.2, 170.9, 137.5, 129.8, 129.0, 126.3, 58.6, 52.9, 36.8, 34.0, 19.0.

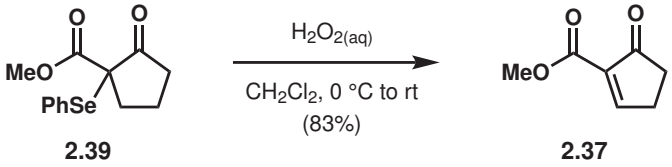

Dienophile 2.37. Selenide **2.39** (45.05 g, 152 mmol, 1 equiv) was dissolved in CH_2Cl_2 (380 mL) under air, then cooled in an ice/water bath. A 30 wt % aqueous solution of H_2O_2 (20.8 mL, 306 mmol, 2 equiv) was added dropwise to the vigorously stirring solution. The reaction mixture turns from light yellow to a dark yellow homogeneous solution, before forming a precipitate to give a light yellow suspension. The reaction mixture was gradually allowed to warm to rt over 3 h, at which time it was cooled in an ice/water bath, and additional H_2O_2 solution (30%, 8.7 mL, 77 mmol, 0.5 equiv) was added dropwise. The reaction was gradually warmed to rt, stirring for an additional 2 h, before being cooled in an ice/water bath again. Additional H_2O_2 solution (30%, 5.2 mL, 53 mmol, 0.35 equiv) was added dropwise, at which point the reaction mixture became a white suspension and TLC analysis indicated complete consumption of selenide **2.39**. The white suspension was diluted with H_2O (100 mL) and the biphasic mixture shaken vigorously. The layers were separated and the organic layer was washed with a solution of $NaHCO_3$ (saturated aqueous, 2 x 100 mL), H_2O (100 mL), and brine (100 mL), then dried over anhydrous Na_2SO_4, filtered, and concentrated *in vacuo* to yield a dark yellow liquid (17.6 g, 83%). ^{1}H NMR (400 MHz, $CDCl_3$) δ 8.43 (t, J = 2.7 Hz, 1H), 3.84 (s, 3H), 2.75 (dt, J = 7.8, 2.8 Hz, 2H), 2.60–2.54 (m, 2H). The spectroscopic data obtained are consistent with those reported in the literature.[56]

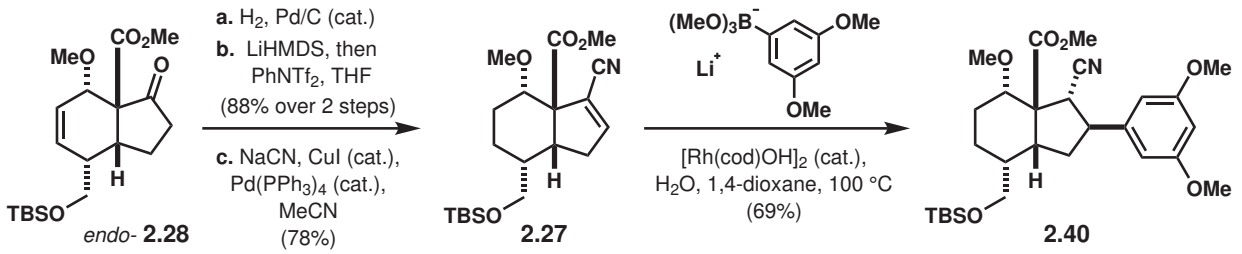

Nature **2015**, *528*, 493.
JACS **2016**, *138*, 10830.

***trans*-β-Aryl nitrile 2.40.** The three-step sequence leading to vinyl nitrile **2.27** has previously been reported by us.[17,54] The aryl boronate ester was prepared in situ. 1-Bromo-3,5-dimethoxybenzene (1.73 g, 7.95 mmol, 3 equiv) was dissolved in Et_2O (18 mL) under N_2 in a 250 mL Schlenk flask. The solution was cooled to –78 °C and a solution of *n*-BuLi (1.65 M in hexanes, 5.0 mL, 8.25 mmol, 3.1 equiv) was added. The resulting mixture was maintained at –78 °C for

10 min, then stirred at rt for 30 min. The turbid mixture was then cooled to –40 °C and $B(OMe)_3$ (890 µL, 7.98 mmol, 3 equiv) was added. The cold bath was subsequently removed and the reaction mixture was stirred at rt for 2.5 h, at which time the solvent was carefully evaporated *in vacuo* using a Schlenk manifold to give the boronate ester as a white foam. The Schlenk flask was brought into a nitrogen-filled glovebox and the boronate ester was dissolved in 1,4-dioxane (26 mL). $[Rh(cod)OH]_2$ (75 mg, 0.16 mmol, 0.06 equiv) and vinyl nitrile **2.27** (1.00 g, 1 equiv) were subsequently added. The mixture was stirred at ambient glovebox temperature (~30 °C) for 2 h until a homogeneous solution was achieved, at which time H_2O (145 µL, 8.05 mmol, 3.3 equiv) was added and the reaction mixture heated to 100 °C for 24 h. The reaction was cooled to rt, filtered over Celite, and concentrated *in vacuo*. With a 99:1 CH_2Cl_2/Et_2O mixture, purification by gradient flash chromatography eluting with 0–100% of this solvent mixture as the strong eluent and hexanes as the weak eluent, then flushing the column with 9:1 CH_2Cl_2/Et_2O gave a 85:15 mixture of product **2.40**/starting material **2.27** (1.06 g, 69% yield corrected for starting material). This mixture was used in the subsequent reaction without further purification. However, for characterization purposes, this material can be additionally purified via a second cycle of gradient flash chromatography eluting with 0–15% EtOAc in hexanes. ^{1}H NMR data obtained from this experiment is reported: ^{1}H NMR (500 MHz, $CDCl_3$) δ 6.42 (d, *J* = 2.2 Hz, 2H), 6.33 (t, *J* = 2.2 Hz, 1H), 3.97 (br. s, 1H), 3.79 (s, 6H), 3.73 (s, 3H), 3.68 (ddd, *J* = 11.4, 8.4, 2.8 Hz, 1H), 3.43 (s, 3H), 3.42 (s, 1H), 3.41 (s, 1H), 3.08 (d, *J* = 8.4 Hz, 1H), 3.00 (ddd, *J* = 13.6, 8.9, 4.8 Hz, 1H), 2.41 (q, *J* = 12.6 Hz, 1H), 2.12–2.06 (m, 1H), 2.02–1.95 (m, 1H), 1.74 (ddd, *J* = 12.4, 9.0, 2.9 Hz, 1H), 1.50–1.27 (m, 3H), 0.88 (s, 9H), 0.03 (s, 3H), 0.01 (s, 3H); ^{13}C NMR (126 MHz, $CDCl_3$) δ 173.2, 161.3, 148.0, 120.1, 105.0, 98.7, 77.0, 66.3, 60.4, 57.0, 55.5, 52.9, 49.7, 47.2, 43.3, 38.2, 32.8, 26.0, 24.8, 18.4, 16.6, –5.3. IR (ATR, thin film): 2951, 2929, 2856, 1730, 1595, 1460, 1430, 1250, 1206, 1156, 1119, 1102, 1081, 833, 775, 733 cm^{-1}. HRMS (ESI+) *m/z* calc'd for $C_{28}H_{43}NO_6SiNa$ $[M+Na]^+$: 540.2752, found: 540.2747.

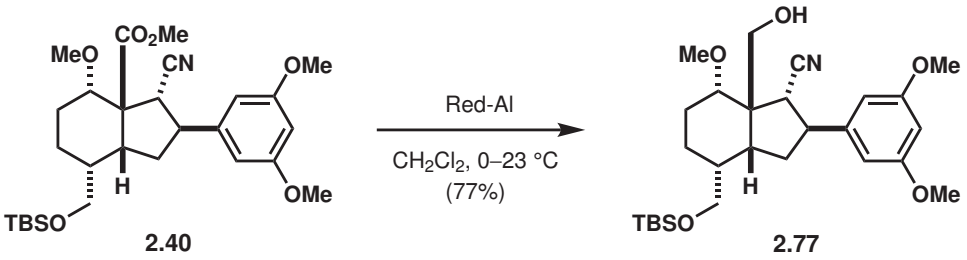

2.40 2.77

Alcohol 2.77. Ester **2.40** (85:15 mixture of **2.40**/**2.27**, 1.06 g, 1.81 mmol corrected for impurity, 1 equiv) was dissolved in CH_2Cl_2 (18 mL) and cooled to 0 °C under N_2. A solution of Red-Al (70 wt.% in PhMe, 2.5 mL, 8.7 mmol, 4.8 equiv) was added and the resulting mixture stirred at 0 °C for 1 h, then at rt for 4.5 h. The turbid mixture was diluted with THF (20 mL), cooled to 0 °C, and quenched by sequential addition of H_2O (50 µL), 15% NaOH (aqueous, 50 µL), and H_2O (150 µL), and stirred at 0 °C for 2 h. The resulting slurry was filtered through Celite, which was additionally washed with THF (30 mL). The filtrate was concentrated *in vacuo* and purified by gradient flash chromatography (eluting with 17–38% EtOAc in hexanes) to give the product as a white solid (681 mg, 77%). Mp 165–166 °C. ^{1}H NMR (500 MHz, C_6D_6) δ 6.65 (d, *J* = 2.1 Hz, 2H), 6.45 (t, *J* = 2.0 Hz, 1H), 3.91–3.83 (m, 1H), 3.37 (s, 6H), 3.32 (s, 1H), 3.30 (s, 1H), 3.29 (s, 3H), 3.23 (d, *J* = 11.5 Hz, 2H), 3.17 (d, *J* = 8.5 Hz, 1H), 3.09 (d, *J* = 11.2 Hz, 1H), 2.52 (ddd, *J* = 13.2, 9.1, 5.0 Hz, 1H), 2.41 (q, *J* = 12.2 Hz, 1H), 1.78–1.57 (m, 4H), 1.34 (qd, *J* = 13.3, 2.9 Hz, 1H), 1.23–1.16 (m,

1H), 1.05–0.98 (m, 1H), 0.98 (s, 9H), 0.03 (s, 3H), 0.02 (s, 3H); ^{13}C NMR (126 MHz, C_6D_6) δ 161.9, 149.7, 121.5, 105.4, 99.1, 78.0, 66.7, 63.6, 56.9, 55.8, 54.9, 49.3, 45.4, 39.9, 37.8, 34.0, 26.2, 24.2, 18.5, 17.4, –5.2, –5.3. IR (ATR, thin film): 3461, 2953, 2931, 2896, 2855, 2241, 1610, 1592, 1461, 1328, 1300, 1249, 1205, 1162, 1097, 1068, 1003, 831, 814, 773 cm^{-1}. HRMS (ESI+) *m/z* calc'd for $C_{27}H_{43}NO_5SiNa$ [M+Na]$^+$: 512.2803, found 512.2802.

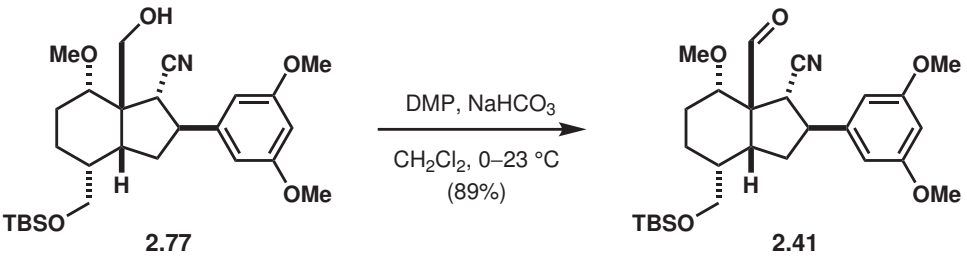

Aldehyde 2.41. A 50 mL round bottom flask was charged with alcohol **2.77** (699 mg, 1 equiv), $NaHCO_3$ (480 mg, 4 equiv), and CH_2Cl_2 (15 mL) and maintained under an atmosphere of N_2. This mixture was cooled to 0 °C and DMP (910 mg, 1.5 equiv) was added in one portion. The resulting yellow suspension was gradually allowed to warm to rt, stirring for 8 h, then diluted with H_2O (~20 mL), thoroughly mixed. The biphasic layers were separated and the aqueous layer extracted with CH_2Cl_2 (2 x 10 mL). The combined organic extract was washed with brine (20 mL), dried over anhydrous Na_2SO_4, filtered, and concentrated *in vacuo*. Purification by gradient flash chromatography (eluting with 0–18% EtOAc in hexanes) gave aldehyde **2.41** as a colorless liquid (619 mg, 89%). ^{1}H NMR (500 MHz, $CDCl_3$) δ 9.45 (s, 1H), 6.42 (d, *J* = 2.2 Hz, 2H), 6.34 (t, *J* = 2.2 Hz, 1H), 3.86 (br. s, 1H), 3.78 (s, 6H), 3.74 (ddd, *J* = 11.5, 8.6, 2.9 Hz, 1H), 3.48–3.44 (m, 1H), 3.44 (s, 3H), 3.41–3.35 (m, 1H), 2.92 (d, *J* = 8.5 Hz, 1H), 2.79 (ddd, *J* = 13.3, 8.7, 4.8 Hz, 1H), 2.45 (q, *J* = 12.5 Hz, 1H), 2.14 (dt, *J* = 11.6, 3.1 Hz, 1H), 1.87 (ddd, *J* = 12.2, 8.8, 2.9 Hz, 1H), 1.78–1.67 (m, 1H), 1.44–1.31 (m, 3H), 0.88 (s, 9H), 0.02 (s, 3H), 0.02 (s, 3H); ^{13}C NMR (126 MHz, $CDCl_3$, 25 °C) δ 200.3, 161.4, 147.4, 119.1, 105.0, 98.8, 75.4, 66.0, 63.9, 57.1, 55.5, 49.8, 44.1, 42.6, 38.7, 32.7, 26.0, 24.7, 18.4, 16.3, –5.3. IR (ATR, neat): 2951, 2929, 2890, 2856, 2241 (weak), 1726, 1606, 1596, 1460, 1429, 1256, 1207, 1157, 1123, 1098, 1085, 1070, 836, 776 cm^{-1}. HRMS (ESI+) *m/z* calc'd for $C_{27}H_{41}NO_5SiNa$ [M+Na]$^+$: 510.2646, found 510.2649.

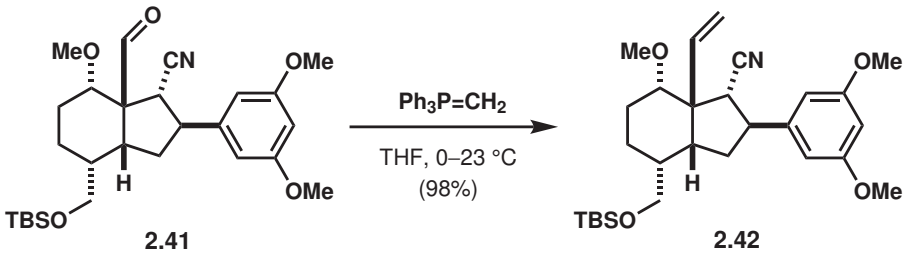

Alkene 2.42. Ph_3PMeBr (588 mg, 1.3 equiv) was suspended in THF (5 mL) under a N_2 atmosphere and to this was added a solution of LiHMDS (1.0 M in THF, 1.6 mL, 1.27 equiv). The resulting mixture was heated to 70 °C for 1 h, then cooled to 0 °C. A solution of the aldehyde (614 mg, 1 equiv) in THF (3 mL + 2 mL for rinsing) was added to the cold reaction mixture via cannula. The reaction mixture was gradually allowed to warm to rt, stirring for 24 h, and then quenched with H_2O (10 mL). The layers were separated and the aqueous layer was additionally extracted with EtOAc (3 x 10 mL). The combined organic extract was washed with brine (10

mL), dried over anhydrous Na_2SO_4, filtered, and concentrated *in vacuo*. Purification by gradient flash chromatography (Yamazen, eluting with 0–12% EtOAc in hexanes) gave the product as a white solid, 600 mg, 98%. Mp 87–88 °C. ^{1}H NMR (500 MHz, $CDCl_3$) δ 6.40 (d, *J* = 2.2 Hz, 2H), 6.33 (t, *J* = 2.2 Hz, 1H), 5.88 (dd, *J* = 17.7, 11.0 Hz, 1H), 5.27 (d, *J* = 17.7 Hz, 1H), 5.20 (d, *J* = 11.0 Hz, 1H), 3.79 (s, 6H), 3.66 (ddd, *J* = 10.8, 8.8, 2.8 Hz, 1H), 3.50 (s, 1H), 3.46–3.39 (m, 2H), 3.41 (s, 3H), 2.68 (d, *J* = 8.7 Hz, 1H), 2.52–2.37 (m, 2H), 2.02–1.88 (m, 2H), 1.78–1.70 (m, 1H), 1.4–1.29 (m, 3H), 0.89 (s, 9H), 0.04 (s, 3H), 0.02 (s, 3H); ^{13}C NMR (126 MHz, $CDCl_3$) δ 161.2, 148.7, 141.2, 120.9, 115.5, 105.1, 98.5, 80.0, 66.4, 56.8, 55.4 (contains overlapping quaternary carbon adjacent to alkene based on HSQC analysis), 50.1, 49.1, 44.6, 37.8, 33.1, 26.1, 23.7, 18.4, 17.0, -5.3. IR (ATR, solid): 3463, 2954, 2926, 2901, 1675, 1610, 1591, 1458, 1205, 1162, 1088, 834, 775 cm^{-1}. HRMS (ESI+) *m/z* calc'd for $C_{28}H_{43}NO_4SiNa$ $[M+Na]^+$: 508.2854, found 508.2860.

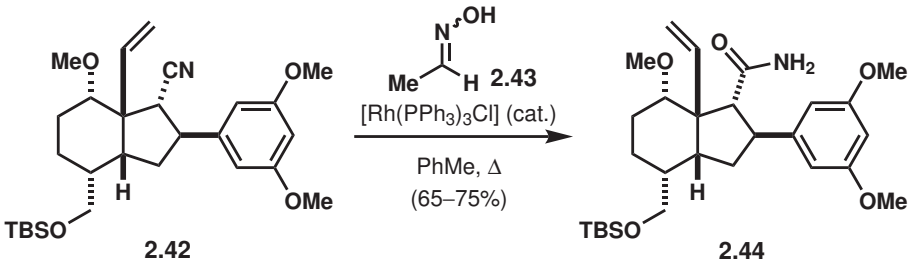

Primary amide 2.44. A 25 mL round bottom flask was charged with nitrile **2.42** (590 mg, 1 equiv) and $[Rh(PPh_3)_3Cl]$ (112 mg, 0.1 equiv). A reflux condenser was attached and the system was purged with N_2. Acetaldoxime (**2.43**, 2 mL, 27 equiv) and PhMe (3 mL) were subsequently added via syringe through the reflux condenser. The reaction mixture was heated to 125–135 °C for 11 h, then cooled to rt, diluted with 1:1 EtOAc/hexanes (15 mL), filtered over Celite (rinsed with 15 mL EtOAc), and concentrated *in vacuo*. [Alternatively, it is possible to dilute the hot reaction mixture with EtOAc and directly dry load the material onto silica gel. However, the crude reaction mixture (upon cooling and provided enough time) completely crystallizes. In this case, gentle heating to re-dissolve the crude mixture is ideal prior to dry loading on silica gel.] Purification by gradient flash chromatography (eluting with 0–17% EtOAc in hexanes) returned the unreacted starting material **2.42** (165 mg, 28% recovery). Gradually increasing the gradient to 70% EtOAc in hexanes gave primary amide **2.44** as a light cream-colored solid (395 mg, 65%, 90% yield brsm). A 75% yield for **2.44** was obtained in a separate reaction that was run on the same scale by reducing the volume of PhMe from 3 mL to 1 mL and heating at 125–135 °C for 7 h. Mp 157–159 °C (the white solid became glassy at 141 °C). ^{1}H NMR (500 MHz, C_6D_6) δ 6.82 (s, 1H), 6.74 (d, *J* = 2.3 Hz, 2H), 6.41 (t, *J* = 2.2 Hz, 1H), 5.84 (dd, *J* = 17.9, 11.1 Hz, 1H), 5.22 (s, 1H), 5.01 (d, *J* = 17.7 Hz, 1H), 4.96 (d, *J* = 11.2 Hz, 1H), 4.15 (ddd, *J* = 10.9, 8.8, 2.7 Hz, 1H), 3.70 (br. s, 1H), 3.39–3.36 (m, 2H), 3.37 (s, 6H), 3.17 (s, 3H), 2.86 (d, *J* = 8.6 Hz, 1H), 2.66–2.51 (m, 2H), 1.94 (dtd, *J* = 11.7, 7.5, 3.8 Hz, 1H), 1.82–1.70 (m, 2H), 1.44 (qd, *J* = 12.7, 3.0 Hz, 1H), 1.29 (tt, *J* = 13.4, 2.6 Hz, 1H), 1.23 (dd, *J* = 12.4, 3.3 Hz, 1H), 0.99 (s, 9H), 0.03 (s, 3H), 0.03 (s, 3H). ^{13}C NMR (126 MHz, C_6D_6) δ 174.7, 161.9, 152.1, 145.7, 113.9, 105.9, 98.3, 78.9, 66.8, 65.5, 56.7, 55.6, 54.9, 46.6, 46.1, 38.2, 34.0, 26.2, 24.3, 18.5, 17.7, –5.2, –5.3. IR (ATR, thin film): 3463, 3334, 3277, 3186 (br., weak), 2927, 2856, 1674, 1607, 1590, 1471, 1456, 1311, 1266, 1249, 1208, 1162, 1092, 1066, 834, 821, 774, 708, 666 cm^{-1}. HRMS (ESI+) *m/z* calc'd for $C_{28}H_{45}NO_5SiNa$ $[M+Na]^+$: 526.3959, found 526.2963.

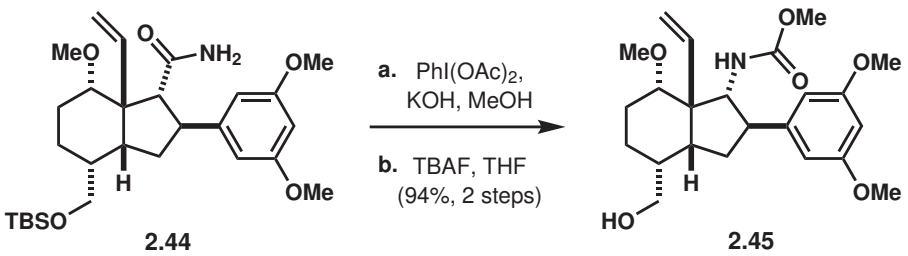

Alcohol 2.45. Amide **2.44** (860 mg, 1 equiv) was suspended in MeOH (17 mL) and cooled in an ice/water bath under N_2. Finely crushed KOH (322 mg, 3.3 equiv) was added and the resulting turbid solution was stirred for 2 min before $PhI(OAc)_2$ (715 mg, 1.3 equiv) was added. The reaction mixture was stirred at 0 °C for 30 min and then at rt for 2.5 h. The MeOH solvent was carefully evaporated *in vacuo* using a rotovap. The residue obtained in this manner was diluted with H_2O (15 mL) and extracted with EtOAc (3 x 10 mL). The combined organic extract was washed with brine (10 mL), dried over anhydrous Na_2SO_4, filtered, and concentrated *in vacuo* to give crude carbamate intermediate **2.55** (986 mg; contained a small amount of iodobenzene byproduct based on ^{1}H NMR analysis), which was used directly without purification.

The crude material (986 mg) was dissolved in THF (17 mL) under air and a solution of TBAF (1 M in THF, 3.4 mL, 2 equiv) was added. The reaction mixture was stirred at rt for 10 h, then carefully concentrated *in vacuo* to remove THF. The residue obtained in this manner was reconstituted in EtOAc (20 mL) and washed with H_2O (10 mL), brine (10 mL), dried over anhydrous Na_2SO_4, filtered, and concentrated *in vacuo*. Purification by gradient flash chromatography (Yamazen, eluting with 38–58% EtOAc in hexanes) gave alcohol **2.45** as a white solid (672 mg, 94% over two steps). This compound exists as a 4.8:1 mixture of rotamers in C_6D_6 at 21 °C. The resonances coalesce at 70 °C in C_6D_6. ^{1}H NMR (500 MHz, C_6D_6, 70 °C) δ 6.71 (s, 2H), 6.41 (t, *J* = 2.2 Hz, 1H), 5.79 (dd, *J* = 17.6, 11.3 Hz, 1H), 5.18 (d, *J* = 17.7 Hz, 1H), 5.06 (d, *J* = 11.2 Hz, 1H), 5.01 (d, *J* = 10.5 Hz, 1H), 4.59 (br. s, 1H), 3.47 (s, 6H), 3.39 (s, 3H), 3.30–3.24 (m, 2H), 3.24–3.15 (m, 2H), 2.91 (s, 3H), 2.45 (ddd, *J* = 13.2, 8.6, 4.8 Hz, 1H), 2.33 (q, *J* = 12.3 Hz, 1H), 1.80–1.72 (m, 1H), 1.72–1.61 (m, 2H), 1.30–1.13 (m, 3H), 0.72 (s, 1H). ^{13}C NMR (126 MHz, C_6D_6, 70 °C) δ 161.8, 157.0 (br. weak), 149.7, 143.4, 113.9, 106.0, 99.0, 79.4, 68.5 (br. weak), 66.0, 55.05, 55.02, 54.5, 52.3, 51.7, 42.8, 38.4, 32.1, 23.5, 17.7. IR (ATR, thin film): 3445 (br.), 2936, 2876, 2838, 1712, 1606, 1595, 1507, 1459, 1428, 1347, 1290, 1258, 1206, 1152, 1105, 1071 cm^{-1}. HRMS (ESI+) *m/z* calc'd for $C_{23}H_{33}NO_6K$ $[M+K]^+$: 458.1940, found 458.1936.

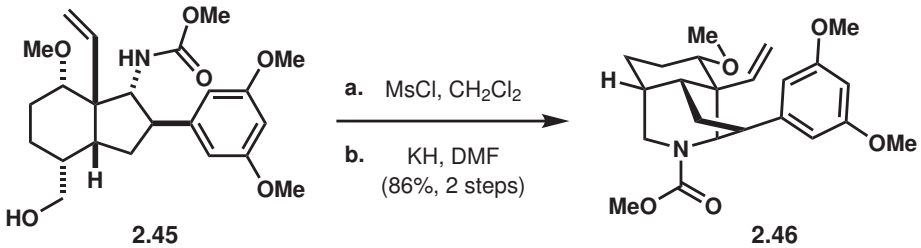

Tetracycle 2.46. Alcohol **2.45** (252 mg, 1 equiv) was dissolved in CH_2Cl_2 under N_2. MsCl (70 µL, 1.5 equiv) and Et_3N (0.42 mL, 5 equiv) were successively added via syringe and the yellow reaction mixture was stirred at rt for 2 h, at which time LC-MS analysis indicated full conversion

of the starting material to the corresponding mesylate. The reaction was quenched by addition of a saturated solution of $NaHCO_3$ (20 mL) and the product extracted with CH_2Cl_2 (3 x 10 mL). The combined organic extract was washed with brine (20 mL), dried over anhydrous Na_2SO_4, filtered, and concentrated *in vacuo* to give the mesylate as a yellow foam (314 mg). This material was sufficiently pure by ^{1}H NMR analysis and used without further purification.

The crude mesylate (314 mg) was additionally dried by azeotropic distillation with benzene, and then dissolved in DMF (6 mL) under N_2. KH (washed with 3 x 1 mL hexanes, 36.5 mg, 1.5 equiv) was added in one portion and the reaction mixture stirred at rt for 12 h, at which time LC-MS analysis indicated incomplete conversion of starting material (<50%). Therefore additional KH (32.5 mg, 0.81 equiv) was added and the resulting slurry heated to 60 °C for 4 h. The reaction mixture was quenched by addition of H_2O (60 mL) and brine (10 mL), and then extracted with CH_2Cl_2 (3 x 25 mL). The combined organic extract was washed with brine (20 mL), dried over anhydrous Na_2SO_4, filtered, and concentrated *in vacuo*. Purification by gradient flash chromatography (Yamazen, eluting with 23–45% EtOAc in hexanes) gave tetracycle **2.46** as a viscous, colorless liquid (208 mg, 86% over two steps). This compound exists as a 1.4:1 mixture of rotamers in C_6D_6 at 25 °C. Increasing the temperature to 70 °C did not result in complete coalescence of the rotameric resonances. Major rotamer: ^{1}H NMR (700 MHz, C_6D_6, 25 °C) δ 6.72 (s, 2H), 6.42 (s, 1H), 5.76 (dd, *J* = 17.4, 10.9 Hz, 1H), 5.29 (s, 1H), 4.86 (d, *J* = 17.8 Hz, 1H), 4.78 (d, *J* = 10.9 Hz, 1H), 3.98 (d, *J* = 13.7 Hz, 1H), 3.58 (s, 3H), 3.39 (s, 6H), 3.15–3.09 (m, 1H), 3.05 (s, 3H), 3.02–2.97 (m, 2H), 2.25 (dt, *J* = 13.2, 6.4 Hz, 1H), 1.88–1.78 (m, 2H), 1.78–1.69 (m, 1H), 1.63–1.54 (m, 1H), 1.46–1.40 (m, 1H), 1.33–1.25 (br. m, 1H), 1.25–1.13 (m, 1H); Minor rotamer: ^{1}H NMR (700 MHz, C_6D_6, 25 °C) δ 6.96 (s, 2H), 6.43 (s, 1H), 5.78 (dd, *J* = 17.0, 10.9 Hz, 1H), 5.61 (s, 1H), 4.90 (d, *J* = 18.1 Hz, 1H), 4.79 (d, *J* = 10.7 Hz, 1H), 3.60–3.56 (m, 1H), 3.54 (s, 3H), 3.46 (s, 6H), 3.15–3.09 (m, 1H), 3.03 (s, 3H), 3.02–2.97 (m, 1H), 2.94 (dd, *J* = 12.8, 4.5 Hz, 1H), 2.34 (dt, *J* = 13.1, 6.4 Hz, 1H), 1.88–1.78 (m, 2H), 1.78–1.69 (m, 1H), 1.63–1.54 (m, 1H), 1.46–1.40 (m, 1H), 1.33–1.25 (m, 1H), 1.25–1.13 (m, 1H); ^{13}C NMR (176 MHz, C_6D_6, 25 °C, mixture of rotamers) δ 161.4, 161.3, 155.4, 155.2, 146.0, 145.9, 145.0, 144.9, 113.5, 113.4, 106.3, 106.2, 98.2, 97.8, 85.5, 85.3, 65.2, 65.0, 57.3, 57.2, 54.9, 54.7, 52.7, 52.52, 52.45, 52.3, 49.1, 48.9, 44.1 (both rotamers), 43.9, 43.8, 33.2, 33.0, 30.8, 30.6, 30.3, 30.1, 25.3, 25.0. The ^{13}C signals for the two rotamers coalesce at 70 °C: ^{13}C NMR (126 MHz, C_6D_6, 70 °C) δ 161.5, 155.3, 146.1, 145.1, 113.5, 106.6, 98.5 (br.), 85.5, 65.3, 57.3, 55.0, 52.9, 52.3, 49.2, 44.7, 44.0, 33.5, 31.1, 30.4, 25.3. IR (ATR, thin film): 2954, 2933, 2873, 2856, 1696, 1586, 1447, 1402, 1366, 1354, 1327, 1311, 1292, 1241, 1205, 1177, 1153, 1117, 1097 cm^{-1}. HRMS (ESI+) *m/z* calc'd for $C_{23}H_{31}NO_5Na$ $[M+Na]^+$: 424.2094, found 424.2115.

2.5.2 Photocycloaddition studies with arene 2.46

In a N_2-filled glovebox, vinyl arene **2.46** (20.7 mg, 0.051 mmol) was dissolved in C_6D_6 (0.55 mL) and the resulting solution was transferred to a quartz NMR tube. The quartz NMR tube was sealed, removed from the glovebox, and irradiated with UV-C light (254 nm) in a Rayonet photobox at rt for 24 h to give a mixture of **2.47** and **2.48** (tentatively assigned by LC-MS analysis) as the major products. The resulting solution was concentrated *in vacuo* to give the crude mixture of products as a yellow film (19.7 mg), which was reconstituted in MeOH (1 mL). *p*-TsOH · H_2O (19.6 mg, 0.103 mmol, 2 equiv) was added and the reaction mixture stirred at rt for 1 h.

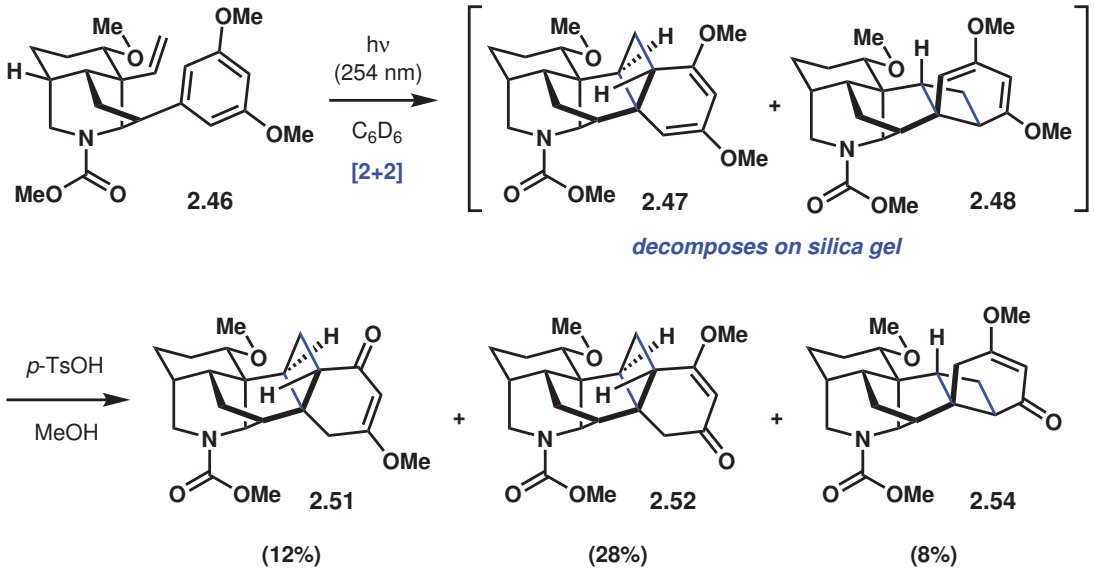

A saturated solution of $NaHCO_3$ (1 mL) was added and the resulting mixture was concentrated under a gentle stream of air (to remove MeOH). The aqueous mixture obtained in this manner was extracted with CH_2Cl_2 (3 × 0.5 mL). The combined organic extract was filtered through a plug of anhydrous Na_2SO_4 and concentrated *in vacuo*.

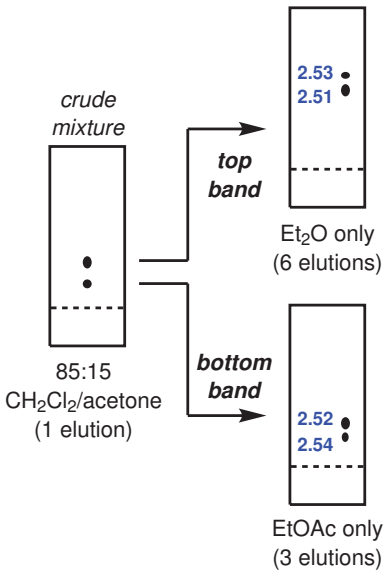

TLC analyses of photocycloadducts

Purification and isolation of photocycloadducts **2.51**, **2.52**, and **2.54** were achieved through multiple cycles of preparative-TLC elutions. The crude mixture was first subjected to preparative-TLC eluting with 15% acetone in CH_2Cl_2 (1 elution), resulting in the isolation of two bands, both containing a mixture of two compounds. Each band was isolated and resubjected to preparative-TLC: the material isolated from the top band was eluted with Et_2O (6 elutions) and the material isolated from the bottom band was eluted with EtOAc (6 elutions), yielding **2.51** (2.5 mg, 12% after 2 steps), **2.52** (5.6 mg, 28% after 2 steps), **2.54** (1.7 mg, 8% after 2 steps) and an unidentified product **2.53** (2.8 mg, 14% after 2 steps). HRMS analysis of compound **2.53** suggests a chemical formula of $C_{22}H_{29}NO_5$, which is consistent with the structure being a constitutional isomer of **2.51**, **2.52** and **2.54**. HRMS (ESI+) *m/z* calc'd for $C_{22}H_{29}NO_5Na$ $[M+Na]^+$: 410.1938, found 410.1938. We were unable to crystallize this compound to enable unambiguous characterization.

Photocycloadduct 2.51. White solid. This compound exists as a 1.3:1 mixture of rotamers in C_6D_6 at 25 °C. The rotameric signals do not fully coalesce at temperatures up to 50 °C. NMR characterization of the rotameric mixture at 25 °C is presented. ^{1}H NMR (700 MHz, C_6D_6, 25 °C, mixture of rotamers) δ 5.48 (d, *J* = 1.7 Hz, 1.3H), 5.46 (d, *J* = 1.7 Hz, 1H), 4.83 (s, 1H), 4.47 (s, 1.3H), 3.68 (d, *J* = 13.5 Hz, 1.3H), 3.50 (s, 3H), 3.43 (s, 4H), 3.36–3.31 (m, 3H), 3.22 (dd, *J* = 13.2, 7.0 Hz, 1H), 2.93 (s, 4H), 2.92 (s, 3H), 2.91 (s, 4H), 2.88 (m, 3H), 2.82 (td, *J* = 11.1, 10.5, 6.5 Hz, 4H), 2.67–2.59 (m, 3.6H), 2.47 (d, *J* = 18.1 Hz, 1.3H), 2.27–2.14 (m,

5H), 2.00–1.92 (m, 2.6H), 1.81 (dd, *J* = 14.5, 7.8 Hz, 1H), 1.77 (q, *J* = 8.2, 7.8 Hz, 2.6H), 1.66–1.56 (m, 7H). ^{13}C NMR (151 MHz, C_6D_6) δ 200.1, 200.0, 175.0, 174.4, 156.0 (2 carbons), 101.5, 101.3, 77.24, 77.17, 61.3, 61.0, 56.32, 56.29, 54.9, 54.8, 52.9, 52.5, 52.4, 52.3, 51.2 (2 carbons), 45.1, 44.6, 42.1, 41.9, 41.82, 41.76, 40.8 (2 carbons), 38.6, 38.4, 37.8 (2 carbons), 33.0, 32.8, 30.7, 30.5, 26.0 (2 carbons), 24.94, 24.91, 23.8, 23.7. IR (ATR, thin film): 2928, 2854, 2816, 2360 (weak), 2279 (weak), 1697, 1638, 1612, 1442, 1341, 1329, 1222, 1213, 1170, 1096, 1086, 995, 777 cm^{-1}. HRMS (ESI+) *m/z* calc'd for $C_{22}H_{30}NO_5$ $[M+H]^+$: 388.2119, found 388.2125. This compound is unambiguously characterized by single crystal X-ray crystallography.

Photocycloadduct 2.52. White solid. Mp (decomposition) >256–260 °C (not completely melted; morphology of the solid begins to change at ~110 °C and decomposition begins to occur at ~175–180 °C as evident by a color change from colorless to yellow and steadily darkens with temperature increase). This compound exists as a 2.8:1 mixture of rotamers in C_6D_6 at 25 °C. The rotameric signals do not fully coalesce at temperatures up to 50 °C. NMR characterization of the rotameric mixture at 25 °C is presented. ^{1}H NMR (600 MHz, C_6D_6, 25 °C, mixture of rotamers) δ 5.44 (s, 1H), 5.42 (s, 0.35H), 4.87 (s, 0.6H), 4.53 (s, 1.6H), 3.69 (d, *J* = 13.6 Hz, 1.6H), 3.52 (s, 1.6H), 3.43 (s, 4.7H), 3.36–3.31 (m, 2H), 3.23 (dd, *J* = 13.0, 6.8 Hz, 0.5H), 3.01 (s, 7H), 2.92 (s, 5H), 2.90 (s, 1.6H), 2.87–2.83 (m, 2H), 2.81 (d, *J* = 17.2 Hz, 1.6H), 2.64 (dd, *J* = 10.8, 6.1 Hz, 2H), 2.57 (dd, *J* = 9.6, 4.5 Hz, 0.6H), 2.31 (d, *J* = 17.7 Hz, 0.5H), 2.25 (d, *J* = 17.3 Hz, 1.6H), 2.07 (dd, *J* = 12.9, 6.3 Hz, 2H), 1.78–1.75 (m, 0.5H), 1.67 (dd, *J* = 14.6, 7.8 Hz, 1.6H), 1.63–1.57 (m, 8H), 1.48–1.42 (6H), 1.26 (dd, *J* = 13.8, 5.3 Hz, 2H), 1.05–0.94 (m, 2H); ^{13}C NMR (151 MHz, C_6D_6, mixture of rotamers) δ 195.8, 178.9, 156.1, 155.9 (minor), 101.63, 101.60 (minor), 77.3, 77.1 (minor), 61.3 (minor), 61.1, 56.4, 55.05, 55.04, 54.96 (minor), 52.80 (minor), 52.77¬, 52.4, 52.3 (minor), 51.38 (minor), 51.37¬, 46.45, 46.43 (minor), 45.0, 44.6 (minor), 42.3 (minor), 42.2, 41.03 (minor), 41.01, 38.63 (minor), 38.60, 34.8 (weak, br.), 33.1 (minor), 32.8, 30.7 (minor), 30.6, 26.6, 26.4 (minor), 26.2, 23.8; not all of the signals representative of the minor rotamer were observed. IR (ATR, thin film): 2922, 2887, 2852, 2817, 1687, 1640, 1606, 1591, 1440, 1362, 1337, 1331, 1247, 1216, 1196, 1185, 1111, 1066, 1077, 1035, 1018, 958, 778, 704 cm^{-1}. HRMS (ESI+) *m/z* calc'd for $C_{22}H_{29}NO_5Na$ $[M+Na]^+$: 410.1938, found 410.1937. This compound is unambiguously characterized by single crystal X-ray crystallography.

Photocycloadduct 2.54. White solid. This compound exists as a 2.4:1 mixture of rotamers in C_6D_6 at 25 °C. The rotameric signals do not fully coalesce at temperatures up to 50 °C. NMR characterization of the rotameric mixture at 25 °C is presented. ^{1}H NMR (900 MHz, C_6D_6, 25 °C, mixture of rotamers) δ 5.60 (s, 0.4H), 5.45 (s, 1H), 5.43 (s, 0.4H), 5.28 (s, 1H), 3.62 (d, *J* = 13.7 Hz, 1H), 3.55 (s, 1.4H), 3.49 (s, 3.7H), 3.44 (ddd, *J* = 13.5, 10.3, 3.0 Hz, 1.8H), 3.39 (dd, *J* = 14.2, 7.1 Hz, 1.6H), 3.36–3.22 (m, 2H), 3.14 (dd, *J* = 10.7, 8.1 Hz, 1.3H), 3.06 (s, 5H), 2.91 (s, 3.5H), 2.89 (s, 1.3H), 2.88–2.82 (m, 1.8H), 2.20 (ddd, *J* = 13.3, 9.3, 8.0 Hz, 1.4H), 2.18–2.15 (m, 0.4H) , 2.15–1.96 (m, 4H), 1.86 (d, *J* = 4.7 Hz, 0.5H), 1.68 (d, *J* = 5.0 Hz, 1H), 1.66–1.58 (m, 2H), 1.57–1.46 (m, 2H), 1.43–1.15 (m, 11H), 1.06–0.71 (m, 8H); ^{13}C NMR (226 MHz, C_6D_6, 25 °C, major rotamer) δ 200.0, 174.2, 156.3, 100.9, 81.1, 57.7, 55.9, 54.9, 52.5, 51.2, 50.3, 48.66, 46.5, 42.7, 41.2, 40.6, 34.8, 33.6, 30.1, 28.8, 25.8, 25.0; ^{13}C NMR (226 MHz, C_6D_6, 25 °C, minor rotamer) δ 200.0, 173.8, 156.2, 101.0, 81.2, 58.0, 56.0, 54.8, 52.3, 50.8, 50.4, 48.74, 45.0, 42.6, 41.3, 40.7, 34.8, 33.8, 30.3, 28.7, 25.8, 25.1. IR (ATR, neat): 2928, 2853, 2821, 1692, 1643, 1617, 1443, 1379, 1361, 1344, 1327, 1212, 1187, 1171, 1124, 1110, 1098, 1088, 1073, 993 cm^{-1}. HRMS (ESI+) *m/z* calc'd for $C_{22}H_{29}NO_5Na$ $[M+Na]^+$: 410.1938, found 410.1931. This compound is unambiguously characterized by single

crystal X-ray crystallography.

2.5.3 Photocycloaddition of arene 2.57

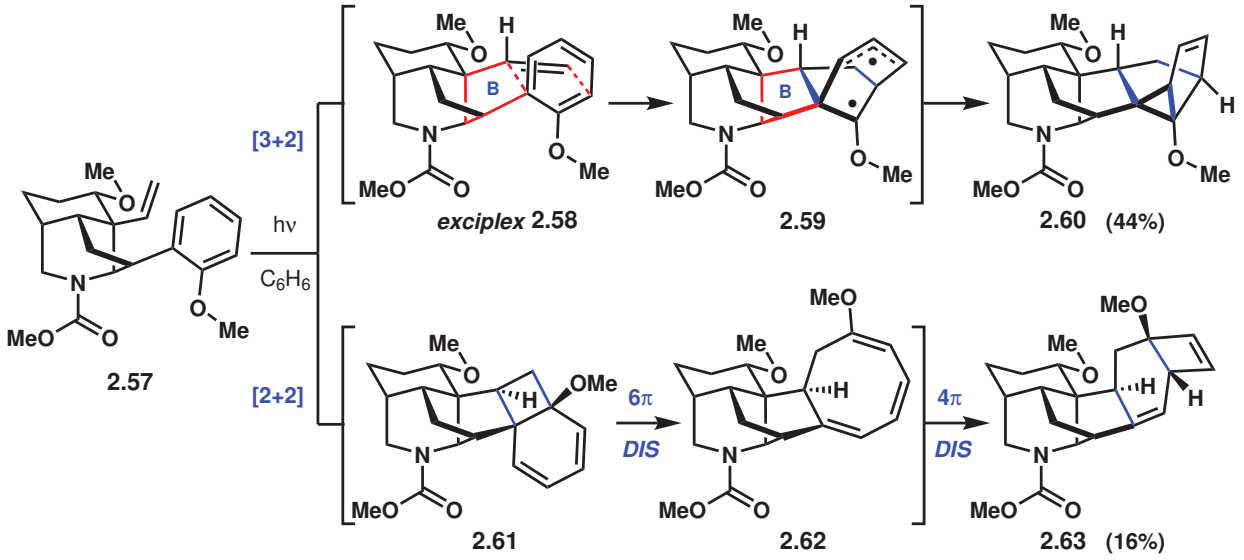

Vinyl arene **2.57** (50 mg, 0.13 mmol) was dissolved in C_6H_6 (7 mL) in a 10 mL quartz vial. The solution was degassed via freeze-pump-thaw cycles (3x). The quartz vial was then sealed and irradiated with UV-C light (254 nm) in a Rayonet photobox until complete conversion of the starting material was achieved as judged by ^{1}H NMR analysis of aliquots. Purification by gradient flash chromatography (eluting with 0:1 to 5:1 to 3:1 to 1:0 EtOAc:CH_2Cl_2) gave *meta*-π-arene photoadduct **2.60** (22 mg, 43%) and rearranged [2+2] photoadduct **2.63** (8 mg, 16%) as white crystalline solids.

We investigated the effect of solvent on the selectivity between **2.60** and **2.63** and found that the (3+2) pathway is generally favored except for when the reaction is performed in MeCN, in which case **2.60** and **2.63** are formed in near equal amounts (Table 2.1).

Photocycloadduct 2.60. Mp 94–95 °C. ^{1}H NMR (500 MHz, $CDCl_3$, major rotamer) δ 5.64 (dd, *J* = 5.7, 2.3 Hz, 1H), 5.57–5.51 (m, 1H), 4.95 (s, 1H), 3.90 (d, *J* = 13.7 Hz, 1H), 3.56 (s, 3H), 3.54–3.43 (m, 1H), 3.37 (s, 3H), 3.18 (d, *J* = 5.9, 2.7 Hz, 1H), 3.11 (s, 3H), 3.07 (dt, *J* = 10.7, 5.6 Hz, 1H), 2.90 (ddd, *J* = 12.1, 10.1, 5.7 Hz, 1H), 2.21 (d, *J* = 4.3 Hz, 1H), 1.82 (dq, *J* = 11.3, 6.3, 4.8 Hz, 1H), 1.74–1.54 (m, 5H), 1.56–1.33 (m, 3H), 1.20 (q, *J* = 14.0 Hz, 1H), 0.88 (s, 1H); ^{13}C NMR (125 MHz, $CDCl_3$, mixture of rotamers) δ 156.5, 131.9, 127.8, 92.8, 80.5, 60.3, 60.0, 56.5, 56.2, 55.3, 52.7, 51.2, 48.3, 48.2, 44.4, 44.0, 42.9, 41.9, 41.4, 40.2, 40.0, 37.6, 37.3, 33.4, 33.2, 31.9, 30.6, 30.4, 24.7. IR (ATR, thin film): 2929, 1697, 1447, 1092, 736 cm^{-1}; HRMS (ESI+) *m/z* calc'd for $C_{22}H_{30}NO_4$ $[M+H]^+$: 372.2169, found 372.2169. This compound is unambiguously characterized by single crystal X-ray crystallography.

Photocycloadduct 2.63. Mp 137–139 °C. ^{1}H NMR (500 MHz, C_6D_6, major rotamer): δ 5.96–5.94 (m, 1H), 5.79 (d, *J* = 2.5 Hz, 1H), 5.26 (dd, *J* = 6.3, 3.0 Hz, 1H), 4.56 (s, 1H), 3.72 (d, *J* = 13.7 Hz, 1H), 3.43 (s, 3H), 3.36 (d, *J* = 13.7 Hz, 1H), 3.30 (d, *J* = 6.3 Hz, 1H), 3.26 (s, 3H), 3.12–3.08 (m, 1H),

Table 2.1: The effect of solvent on photocycloaddition of **2.57**.

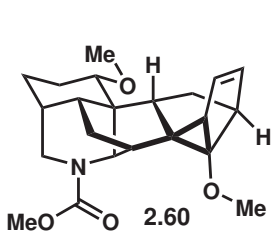

2.60

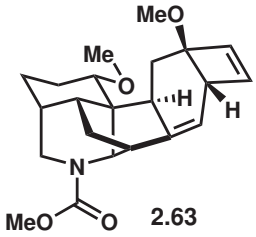

2.63

Solvent	2.60:2.63
C_6H_6	2.9:1
C_6H_{12}	4:1
MeOH	3.3:1
MeCN	1.1:1

3.07 (s, 3H), 2.92–2.90 (m, 1H), 2.56 (d, 1H), 1.96 (dd, J = 11.9, 4.4 Hz, 1H), 1.70–1.68 (m, 1H), 1.65–1.57 (m, 2H), 1.48–1.46 (m, 1H), 1.41–1.26 (m, 3H), 1.07–1.04 (m, 1H); ^{13}C NMR (150 MHz, C_6D_6) δ 155.6, 153.1, 136.9, 136.0, 110.5, 87.3, 76.9, 60.7, 56.5, 51.8, 51.0, 50.4, 48.5, 47.5, 45.0, 38.5, 36.9, 36.2, 32.5, 30.7, 30.2, 23.7; IR (ATR, thin film): 2930, 1697, 1447, 1335, 1095, 728 cm^{-1}. HRMS (ESI+) *m/z* calc'd for $C_{22}H_{30}NO_4$ $[M+H]^+$: 372.2169, found 372.2170. This compound is unambiguously characterized by single crystal X-ray crystallography.

2.6 References

1. Wilson, R. M.; Danishefsky, S. J. *J. Org. Chem.* **2007**, *72*, 4293–4305.
2. Corey, E. J.; Cheng, X.-M., *The Logic of Chemical Synthesis*; J. Wiley & Sons: New York, 1989.
3. Hendrickson, J. B. *J. Am. Chem. Soc.* **1977**, *99*, 5439–5450.
4. (a) Bertz, S. H. *J. Am. Chem. Soc.* **1982**, *104*, 5801–5803; (b) Bertz, S. H. *New J. Chem.* **2003**, *27*, 870–879; (c) Bertz, S. H.; Sommer, T. J. In *Org. Synth. Theory Appl. vol. 2*, Hudlicky, T., Ed.; JAI Press: Greenwich, CT, 1993, pp 67–92.
5. Wang, F. P.; Chen, Q. H.; Liu, X. Y. *Nat. Prod. Rep.* **2010**, *27*, 529–570.
6. (a) Pelletier, S. W.; Jacobs, W. A. *J. Am. Chem. Soc.* **1956**, *78*, 4144–4145; (b) Pelletier, S. W.; Parthasarathy, P. C. *Tetrahedron Lett.* **1963**, *4*, 205–208; (c) Masamune, S. *J. Am. Chem. Soc.* **1964**, *86*, 291–292; (d) Tahara, A.; Hirao, K. *Tetrahedron Lett.* **1966**, *7*, 1453–1459; (e) Nagata, W.; Sugasawa, T.; Narisada, M.; Wakabayashi, T.; Hayase, Y. *J. Am. Chem. Soc.* **1967**, *89*, 1483–1499; (f) Somei, M.; Okamoto, T. *Chem. Pharm. Bull.* **1970**, *18*, 2135–2138.
7. (a) Guthrie, R. W.; Valenta, Z.; Wiesner, K. *Tetrahedron Lett.* **1966**, *7*, 4645–4654; (b) Wiesner, K.; Tsai, T. Y.; Huber, K.; Bolton, S. E.; Vlahov, R. *J. Am. Chem. Soc.* **1974**, *96*, 4990–4992; (c) Wiesner, K. *Pure Appl. Chem.* **1979**, *51*, 689–703.
8. (a) Cherney, E. C.; Baran, P. S. *Isr. J. Chem.* **2011**, *51*, 391–405; (b) Hamlin, A. M.; Lapointe, D.; Owens, K.; Sarpong, R. *J. Org. Chem.* **2014**, *79*, 6783–6800.
9. Warren, S., *Organic Synthesis: The Disconnection Approach*; J. Wiley & Sons: Somerset, NJ, 1982.
10. (a) Davis, E. M.; Croteau, R. In *Top. Curr. Chem.* Springer Nature: 2000, pp 53–95; (b) Kaspera, R.; Croteau, R. Cytochrome P450 oxygenases of taxol biosynthesis., 2006.

11. Wang, F. P.; Liang, X. T. In *Alkaloids Chem. Biol.* Cordell, G. A., Ed.; Academic Press: San Diego, 2002; Vol. 59, pp 1–280.
12. (a) Ishihara, Y.; Baran, P. S. *Synlett* **2010**, 1733–1745; (b) Gaich, T.; Baran, P. S. *J. Org. Chem.* **2010**, *75*, 4657–4673.
13. (a) Johnson, W. S.; Semmelhack, M. F.; Sultanbawa, M. U.; Dolak, L. A. *J. Am. Chem. Soc.* **1968**, *90*, 2994–2996; (b) Fish, P. V.; Johnson, W. S. *J. Org. Chem.* **1994**, *59*, 2324–2335; (c) Ardkhean, R.; Caputo, D. F.; Morrow, S. M.; Shi, H.; Xiong, Y.; Anderson, E. A. *Chem. Soc. Rev.* **2016**, *45*, 1557–1569; (d) Baunach, M.; Franke, J.; Hertweck, C. *Angew. Chem.* **2015**, *127*, 2640–2664; (e) Baunach, M.; Franke, J.; Hertweck, C. *Angew. Chem., Int. Ed.* **2015**, *54*, 2604–2626.
14. (a) Wilde, N. C.; Isomura, M.; Mendoza, A.; Baran, P. S. *J. Am. Chem. Soc.* **2014**, *136*, 4909–4912; (b) McKerrall, S. J.; Jørgensen, L.; Kuttruff, C. A.; Ungeheuer, F.; Baran, P. S. *J. Am. Chem. Soc.* **2014**, *136*, 5799–5810; (c) Hung, K.; Condakes, M. L.; Novaes, L. F.; Harwood, S. J.; Morikawa, T.; Yang, Z.; Maimone, T. J. *J. Am. Chem. Soc.* **2019**, *141*, 3083–3099.
15. Fuchs, P. L. *Tetrahedron* **2001**, *57*, 6855–6875.
16. Corey, E. J.; Howe, W. J.; Orf, H. W.; Pensak, D. A.; Petersson, G. *J. Am. Chem. Soc.* **1975**, *97*, 6116–6124.
17. Marth, C. J.; Gallego, G. M.; Lee, J. C.; Lebold, T. P.; Kulyk, S.; Kou, K. G.; Qin, J.; Lilien, R.; Sarpong, R. *Nature* **2015**, *528*, 493–498.
18. Barone, R.; Chanon, M. *Tetrahedron* **2005**, *61*, 8916–8923.
19. Wender, P. A.; Miller, B. L. In *Org. Synth. Theory Appl. vol. 2*, Hudlicky, T., Ed.; JAI Press: Greenwich, CT, 1993, pp 27–66.
20. (a) Hamlin, A. M.; de Jesus Cortez, F.; Lapointe, D.; Sarpong, R. *Angew. Chem.* **2013**, *125*, 4954–4957; (b) Hamlin, A. M.; De Jesus Cortez, F.; Lapointe, D.; Sarpong, R. *Angew. Chem., Int. Ed.* **2013**, *52*, 4854–4857.
21. (a) Li, X.-H.; Zhu, M.; Wang, Z.-X.; Liu, X.-Y.; Song, H.; Zhang, D.; Wang, F.-P.; Qin, Y. *Angew. Chem.* **2016**, *128*, 15896–15900; (b) Li, X. H.; Zhu, M.; Wang, Z. X.; Liu, X. Y.; Song, H.; Zhang, D.; Wang, F. P.; Qin, Y. *Angew. Chem., Int. Ed.* **2016**, *55*, 15667–15671.
22. Liu, X. Y.; Qin, Y. *Nat. Prod. Rep.* **2017**, *34*, 1044–1050.
23. Zhou, S.; Guo, R.; Yang, P.; Li, A. *J. Am. Chem. Soc.* **2018**, *140*, 9025–9029.
24. (a) Liu, J.; Ma, D. *Angew. Chem., Int. Ed.* **2018**, *57*, 6676–6680; (b) Liu, J.; Ma, D. *Angew. Chem.* **2018**, *130*, 6786–6790.
25. Hoffmann, R. W. *Chem. Soc. Rev.* **2016**, *45*, 577–583.
26. (a) Cookson, R. C.; Trevett, M. E. *J. Chem. Soc.* **1956**, 3121–3129; (b) Wiesner, K.; Valenta, Z. In *Prog. Chem. Org. Nat. Prod.* Springer Vienna: Vienna, 1958, pp 26–89.
27. (a) Muratake, H.; Natsume, M. *Angew. Chem.* **2004**, *116*, 4746–4749; (b) Muratake, H.; Natsume, M. *Angew. Chem., Int. Ed.* **2004**, *43*, 4646–4649.
28. Peese, K. M.; Gin, D. Y. *Chem., A Eur. J.* **2008**, *14*, 1654–1665.
29. (a) Zhang, Q.; Zhang, Z.; Huang, Z.; Zhang, C.; Xi, S.; Zhang, M. *Angew. Chem.* **2018**, *130*, 949–953; (b) Zhang, Q.; Zhang, Z.; Huang, Z.; Zhang, C.; Xi, S.; Zhang, M. *Angew. Chem., Int. Ed.* **2018**, *57*, 937–941.
30. Kou, K. G.; Pflueger, J. J.; Kiho, T.; Morrill, L. C.; Fisher, E. L.; Clagg, K.; Lebold, T. P.; Kisunzu, J. K.; Sarpong, R. *J. Am. Chem. Soc.* **2018**, *140*, 8105–8109.

31. (a) Heathcock, C. H.; Davidsen, S. K.; Mills, S. G.; Sanner, M. A. *J. Org. Chem.* **1992**, *57*, 2531–2544; (b) Sheikh, Z.; Steel, R.; Tasker, A. S.; Johnson, A. P. *J. Chem. Soc., Chem. Commun.* **1994**, *6*, 763–764.
32. Kou, K. G.; Kulyk, S.; Marth, C. J.; Lee, J. C.; Doering, N. A.; Li, B. X.; Gallego, G. M.; Lebold, T. P.; Sarpong, R. *J. Am. Chem. Soc.* **2017**, *139*, 13882–13896.
33. Wang, F.-P.; Chen, Q.-H.; Liang, X.-T. In *Alkaloids Chem. Biol.* Cordell, G. A., Ed.; Academic Press: San Diego, 2009; Vol. 67, pp 1–78.
34. Wang, F.-P.; Chen, Q.-H. In *Alkaloids. Chem. Biol.* Cordell, G. A., Ed.; Academic Press: San Diego, 2010; Vol. 69, pp 1–577.
35. Stevens, M.; Peigneur, S.; Tytgat, J. *Front. Pharmacol.* **2011**, *2*, DOI: 10.3389/fphar.2011.00071.
36. Streit, U.; Bochet, C. G. *Beilstein J. Org. Chem.* **2011**, *7*, 525–542.
37. Avent, A. G.; Byrne, P. W.; Penkett, C. S. *Org. Lett.* **1999**, *1*, 2073–2075.
38. Wang, Q.; Chen, C. *Org. Lett.* **2008**, *10*, 1223–1226.
39. Adams, H.; Anderson, J. C.; Bell, R.; Neville Jones, D.; Peel, M. R.; Tomkinson, N. C. O. *J. Chem. Soc., Perkin Trans. 1* **1998**, 3967–3974.
40. Prabhakaran, J.; Lhermitte, H.; Das, J.; Sasi-Kumar, T. K.; Grierson, D. S. *Synlett* **2000**, *2000*, 0658–0662.
41. Lebold, T. P.; Gallego, G. M.; Marth, C. J.; Sarpong, R. *Org. Lett.* **2012**, *14*, 2110–2113.
42. Bandyopadhyaya, A. K.; Manion, B. D.; Benz, A.; Taylor, A.; Rath, N. P.; Evers, A. S.; Zorumski, C. F.; Mennerick, S.; Covey, D. F. *Bioorg. Med. Chem. Lett.* **2010**, *20*, 6680–6684.
43. Takaya, Y.; Ogasawara, M.; Hayashi, T. *Tetrahedron Lett.* **1999**, *40*, 6957–6961.
44. Lee, J.; Kim, M.; Chang, S.; Lee, H. Y. *Org. Lett.* **2009**, *11*, 5598–5601.
45. Steinbeck, C.; Han, Y.; Kuhn, S.; Horlacher, O.; Luttmann, E.; Willighagen, E. In *J. Chem. Inf. Comput. Sci.* 2003; Vol. 43, pp 493–500.
46. Coates, R. M.; Bertram, E. F. *J. Org. Chem.* **1971**, *36*, 3722–3729.
47. Adams, M. R.; Bu'Lock, J. D. *J. Chem. Soc., Chem. Commun.* **1975**, 389–391.
48. Lupi, A.; Patamia, M.; Grgurina, I.; Bettolo, R. M.; Di Leo, O.; Gioia, P.; Autnaroli, S. *Helv. Chim. Acta* **1984**, *67*, 2261–2263.
49. Wenkert, E. *Chem. Ind.* **1955**, 282–284.
50. Doering, W. E.; Farber, M. *J. Am. Chem. Soc.* **1949**, *71*, 1514.
51. Filippini, M. H.; Rodriguez, J. *Chem. Rev.* **1999**, *99*, 27–76.
52. Wiesner, K.; Tsai, T. Y. R.; Nambiar, K. P. *Can. J. Chem.* **1978**, *56*, 1451–1454.
53. Gottlieb, H. E.; Kotlyar, V.; Nudelman, A. *J. Org. Chem.* **1997**, *62*, 7512–7515.
54. Kou, K. G.; Li, B. X.; Lee, J. C.; Gallego, G. M.; Lebold, T. P.; Dipasquale, A. G.; Sarpong, R. *J. Am. Chem. Soc.* **2016**, *138*, 10830–10833.
55. Marth, C. J. Development of a Unified Strategy to the C18-, C19-, and C20-Diterpenoid Alkaloids., PhD Dissertation, University of California, Berkeley, 2015.
56. Ley, S. V.; Murray, P. J.; Palmer, B. D. *Tetrahedron* **1985**, *41*, 4765–4769.

Appendix 2.A NMR Spectral Data for Chapter 2

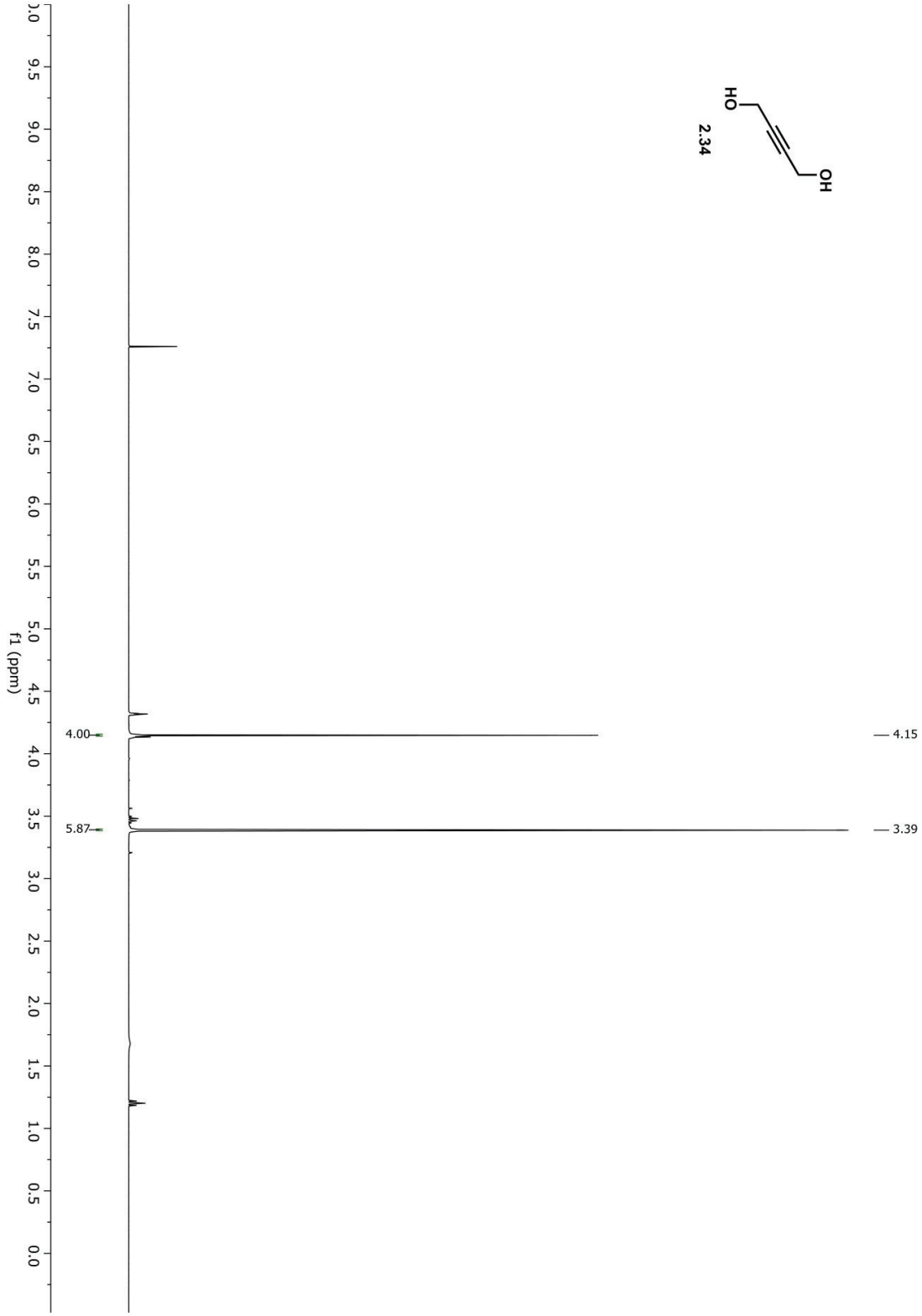

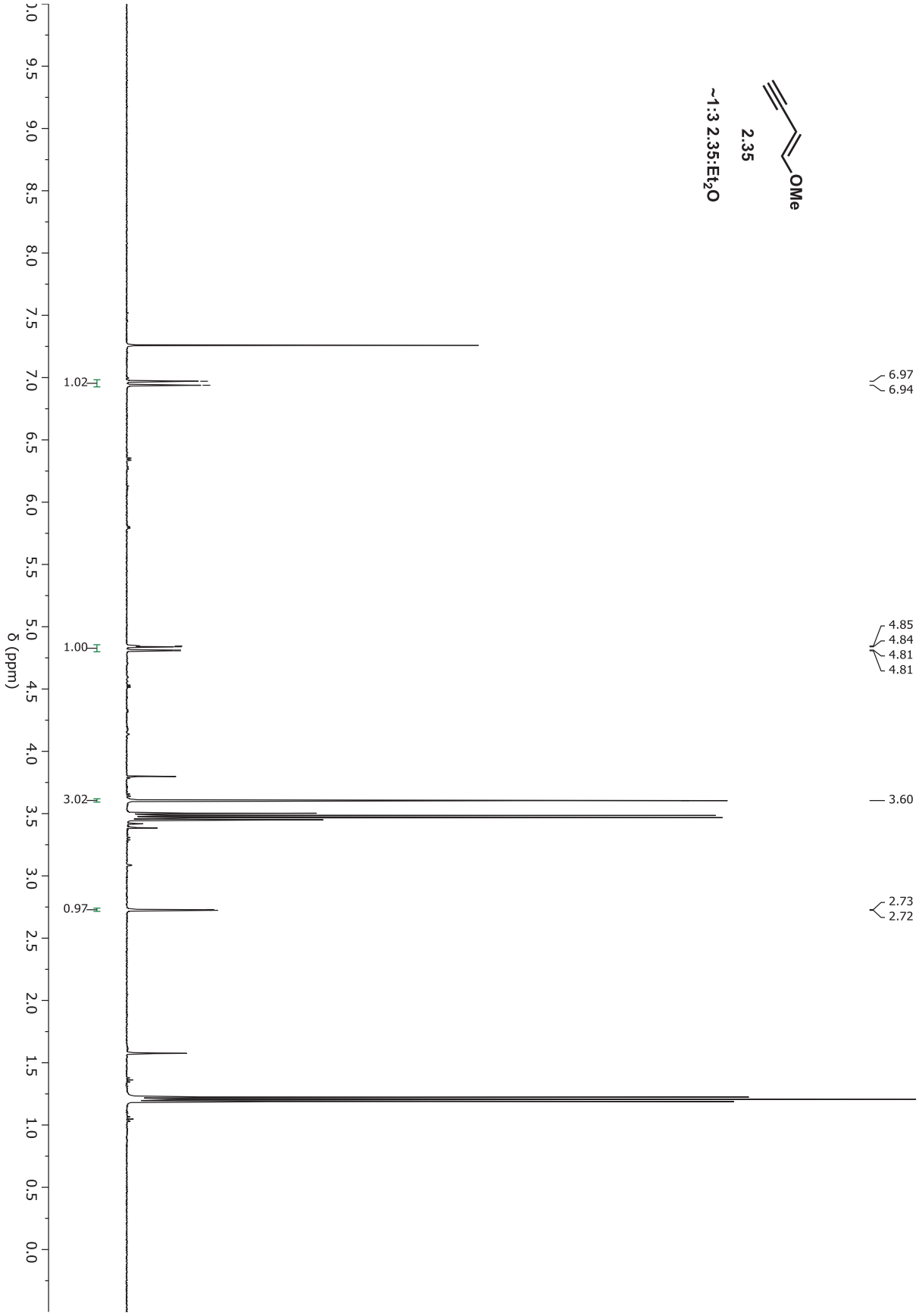
2.35
~1:3 2.35:Et2O
OMe
δ (ppm)
1.02
1.00
3.02
0.97
6.97
6.94
4.85
4.84
4.81
4.81
3.60
2.73
2.72

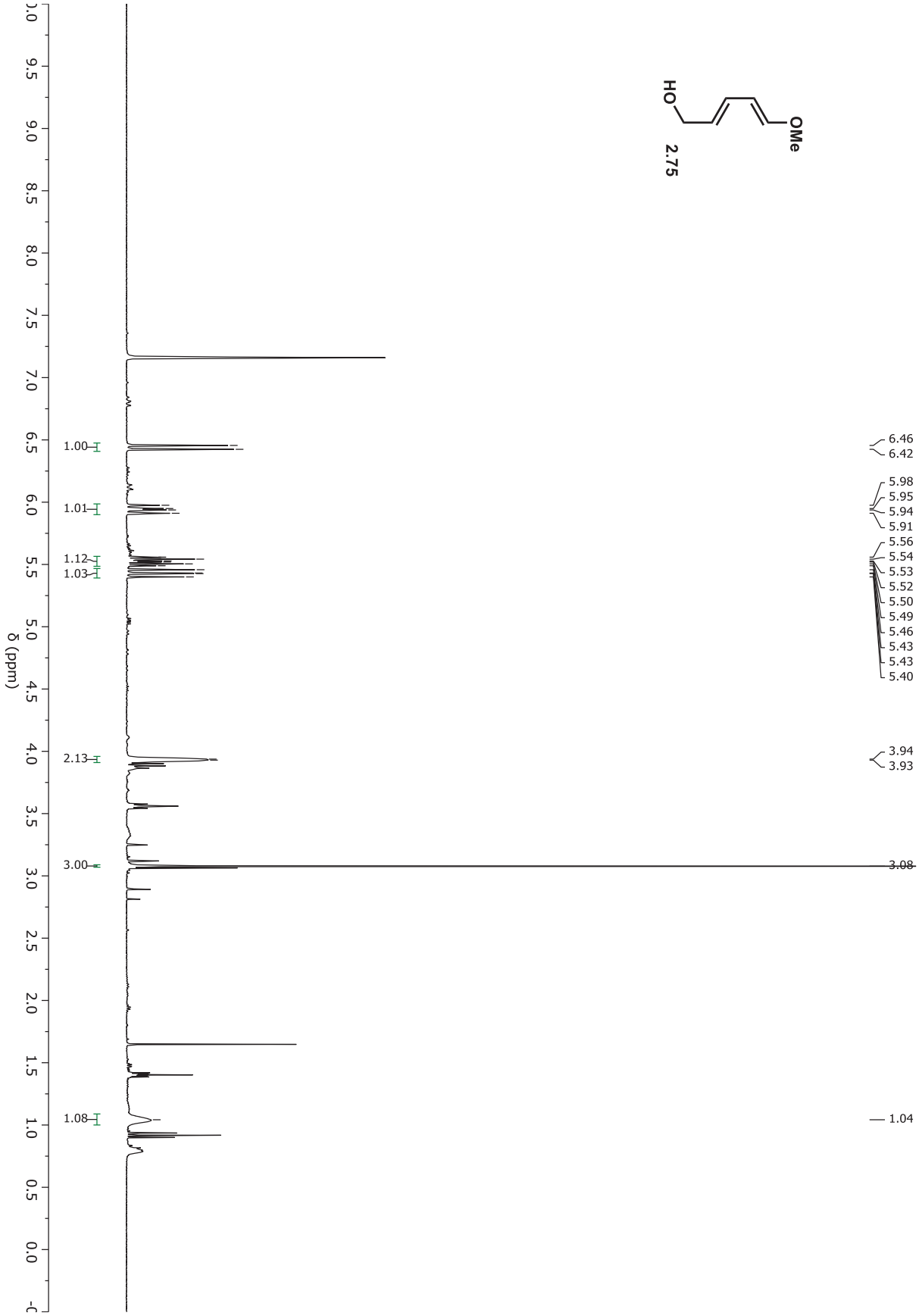
HO
2.75
OMe
δ (ppm)
1.00
1.01
1.12
1.03
2.13
3.00
1.08
6.46
6.42
5.98
5.95
5.94
5.91
5.56
5.54
5.53
5.52
5.50
5.49
5.46
5.43
5.43
5.40
3.94
3.93
3.08
1.04

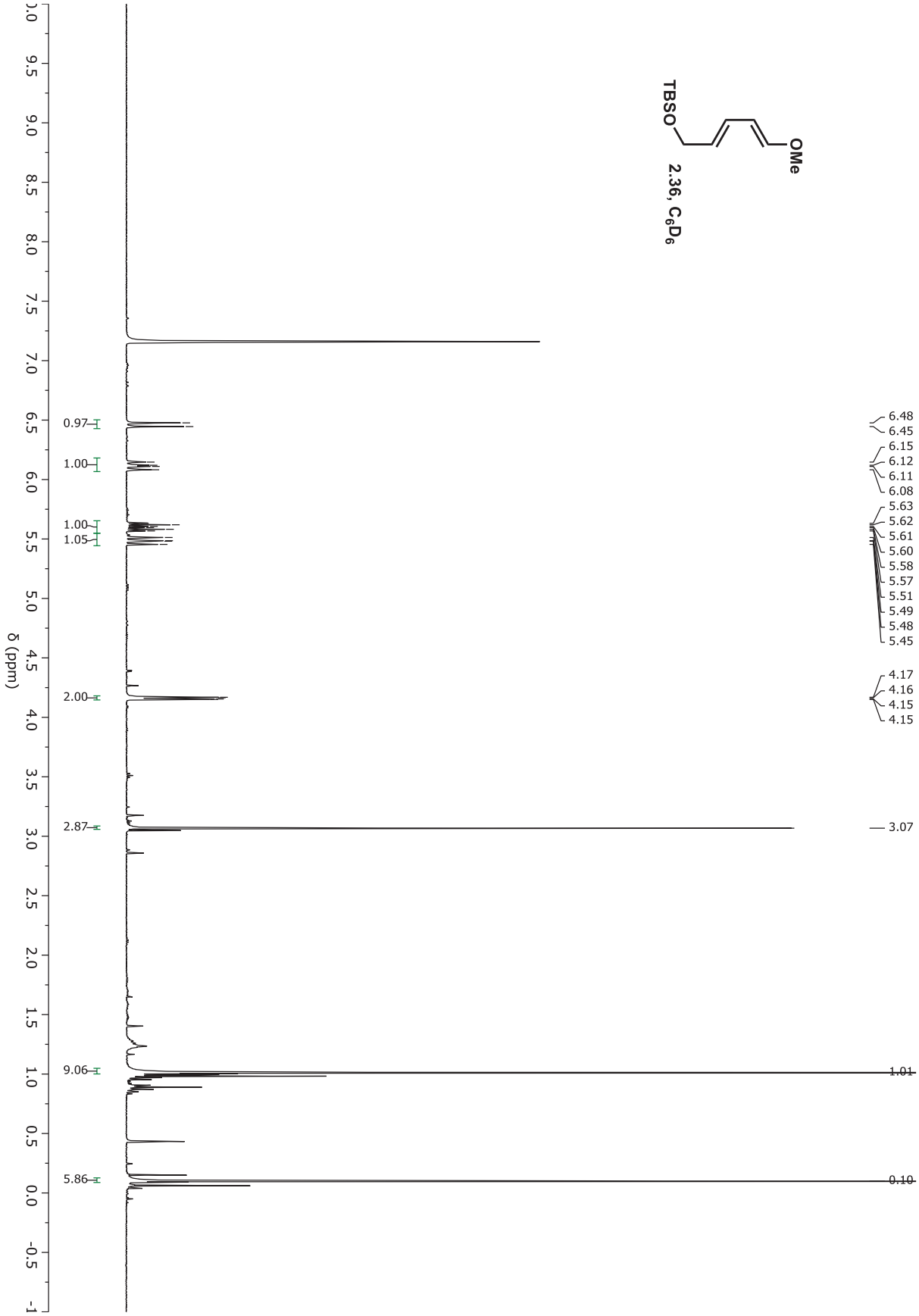
TBSO
OMe
2.36, C6D6
δ (ppm)
0.97
1.00
1.00
1.05
2.00
2.87
9.06
5.86
6.48
6.45
6.15
6.12
6.11
6.08
5.63
5.62
5.61
5.60
5.58
5.57
5.51
5.49
5.48
5.45
4.17
4.16
4.15
4.15
3.07
1.01
0.10

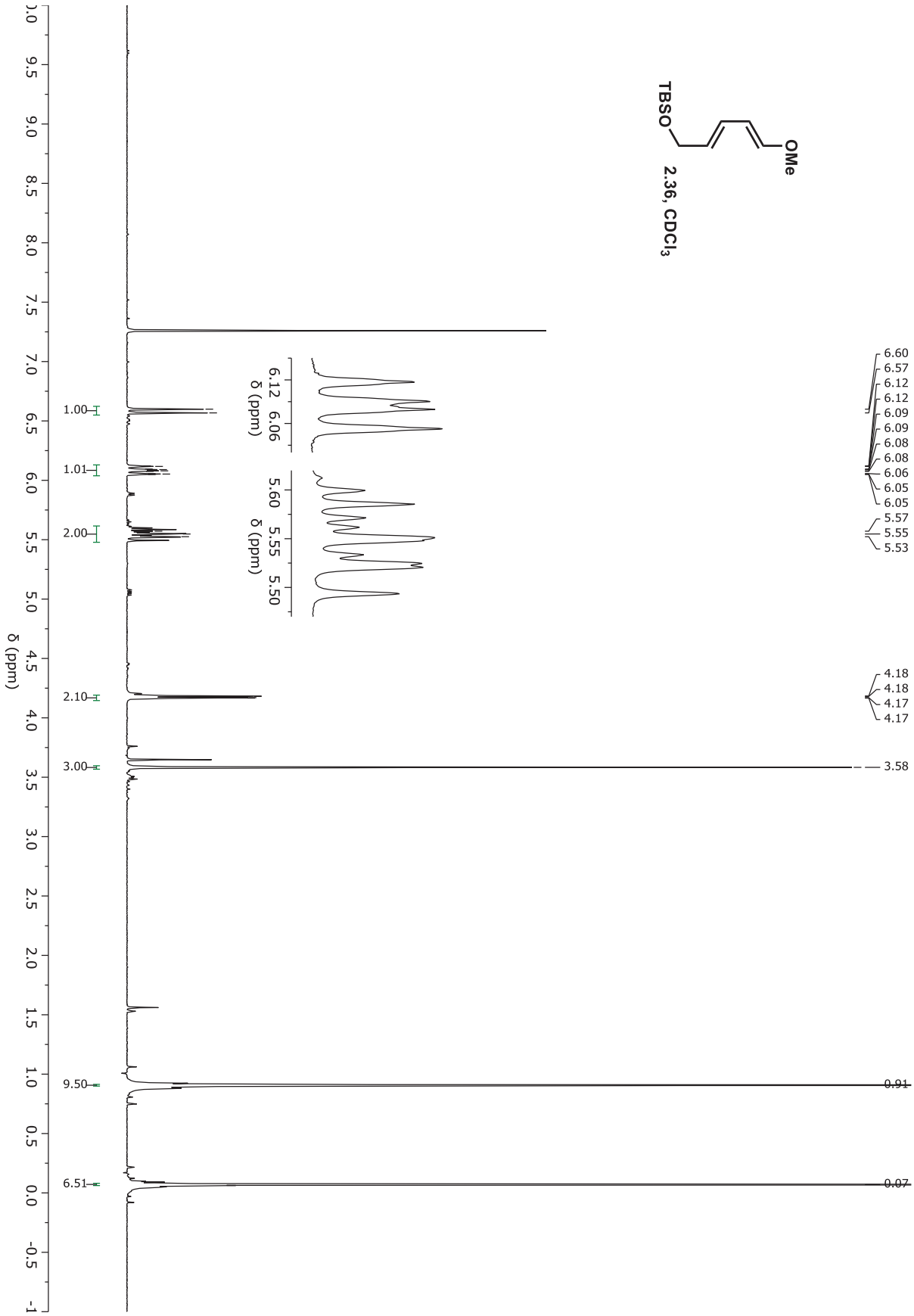
TBSO
OMe
2.36, CDCl3
δ (ppm)
6.12 6.06
5.60 5.55 5.50
6.60
6.57
6.12
6.12
6.09
6.09
6.08
6.08
6.06
6.05
6.05
5.57
5.55
5.53
4.18
4.18
4.17
4.17
3.58
0.91
0.07
1.00
1.01
2.00
2.10
3.00
9.50
6.51

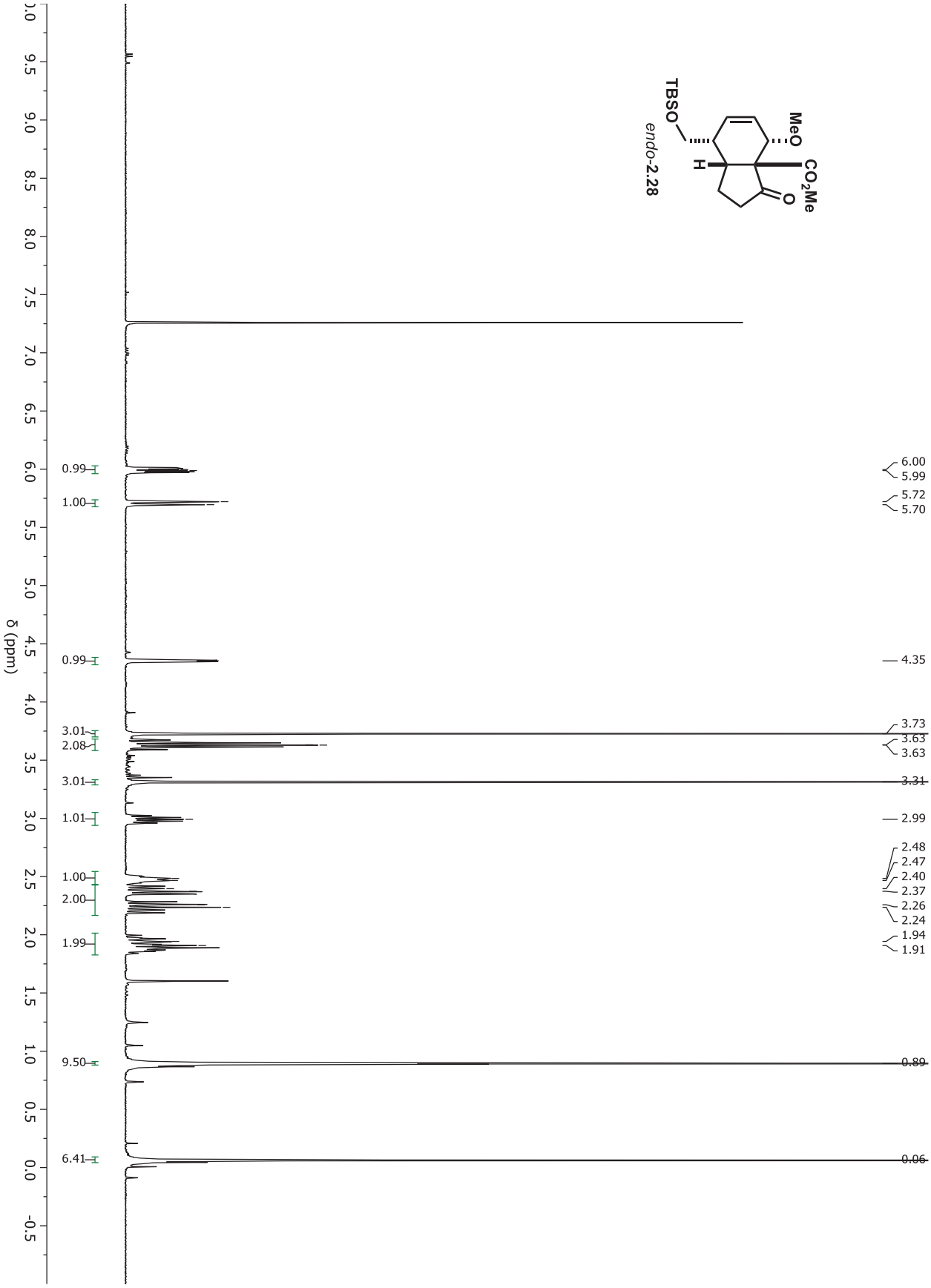
TBSO
MeO
CO2Me
H
O
endo-2.28
δ (ppm)
0.99
1.00
0.99
3.01
2.08
3.01
1.01
1.00
2.00
1.99
9.50
6.41
6.00
5.99
5.72
5.70
4.35
3.73
3.63
3.63
3.31
2.99
2.48
2.47
2.40
2.37
2.26
2.24
1.94
1.91
0.89
0.06

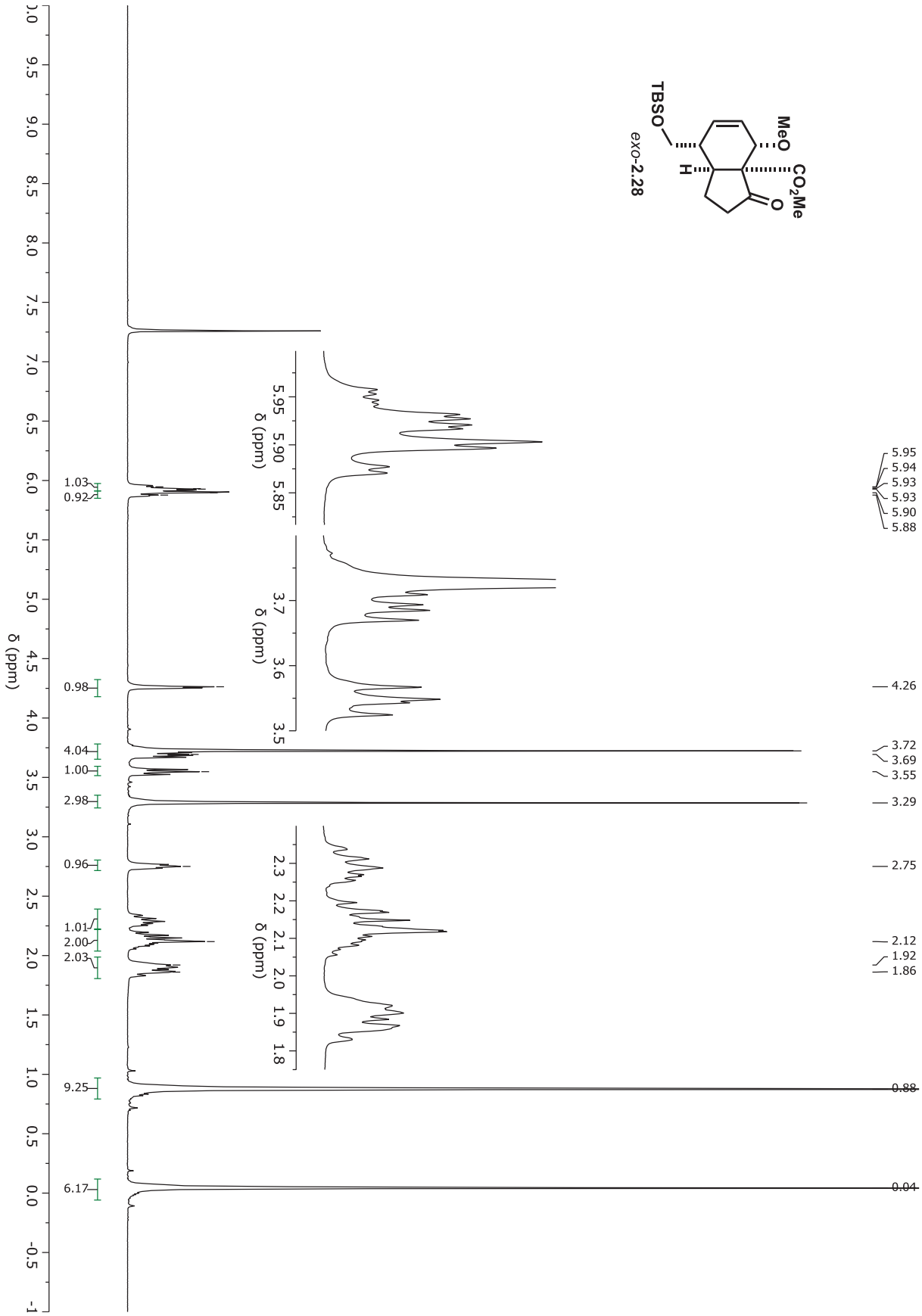
TBSO
H
MeO
CO2Me
O
exo-2.28
δ (ppm)
1.03
0.92
0.98
4.04
1.00
2.98
0.96
1.01
2.00
2.03
9.25
6.17
5.95
5.94
5.93
5.93
5.90
5.88
4.26
3.72
3.69
3.55
3.29
2.75
2.12
1.92
1.86
0.88
0.04

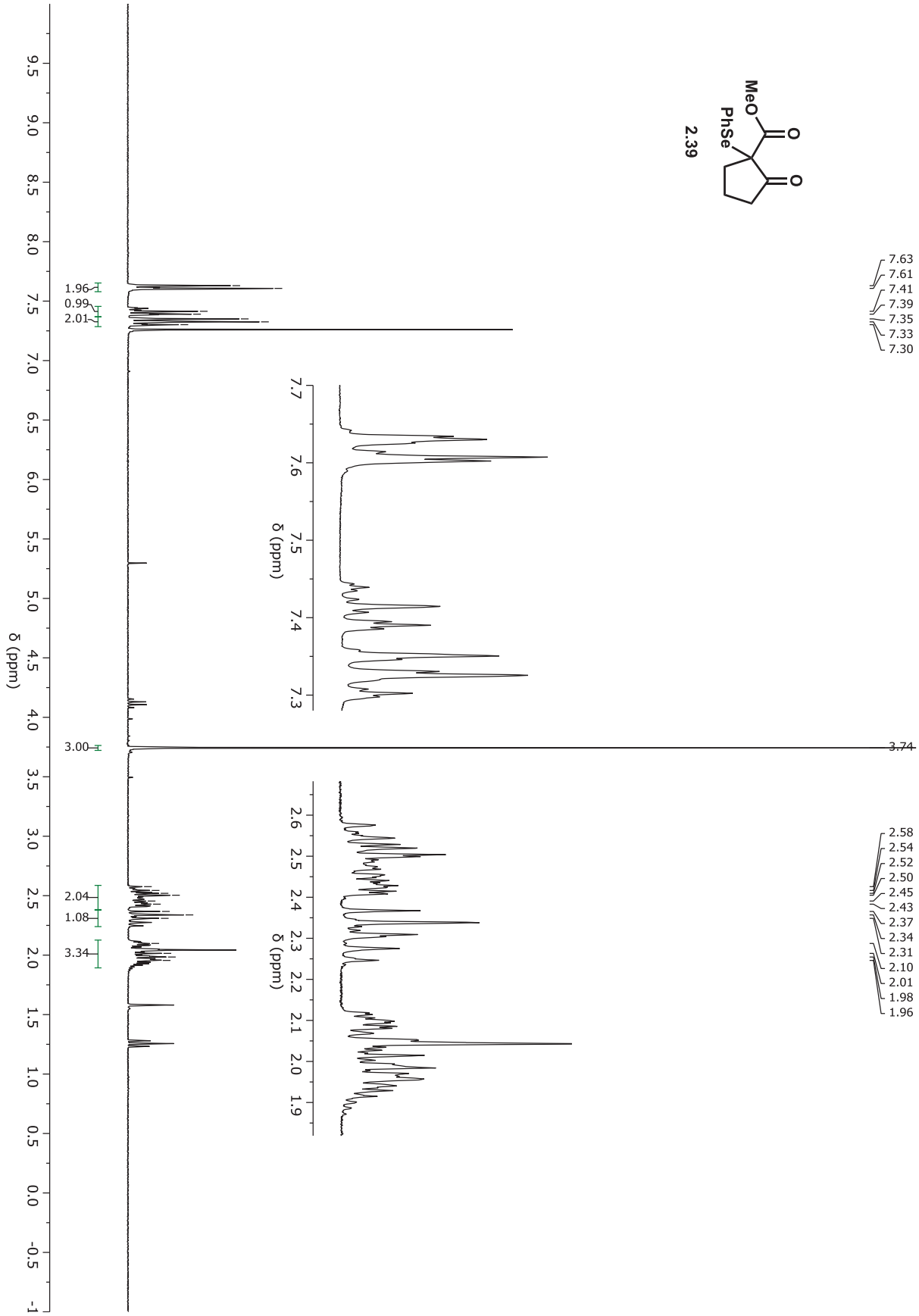
MeO
PhSe
O
O
2.39
δ (ppm)
9.5
9.0
8.5
8.0
7.5
7.0
6.5
6.0
5.5
5.0
4.5
4.0
3.5
3.0
2.5
2.0
1.5
1.0
0.5
0.0
-0.5
-1
1.96
0.99
2.01
3.00
2.04
1.08
3.34
7.7
7.6
7.5
7.4
7.3
2.6
2.5
2.4
2.3
2.2
2.1
2.0
1.9
7.63
7.61
7.41
7.39
7.35
7.33
7.30
3.74
2.58
2.54
2.52
2.50
2.45
2.43
2.37
2.34
2.31
2.10
2.01
1.98
1.96

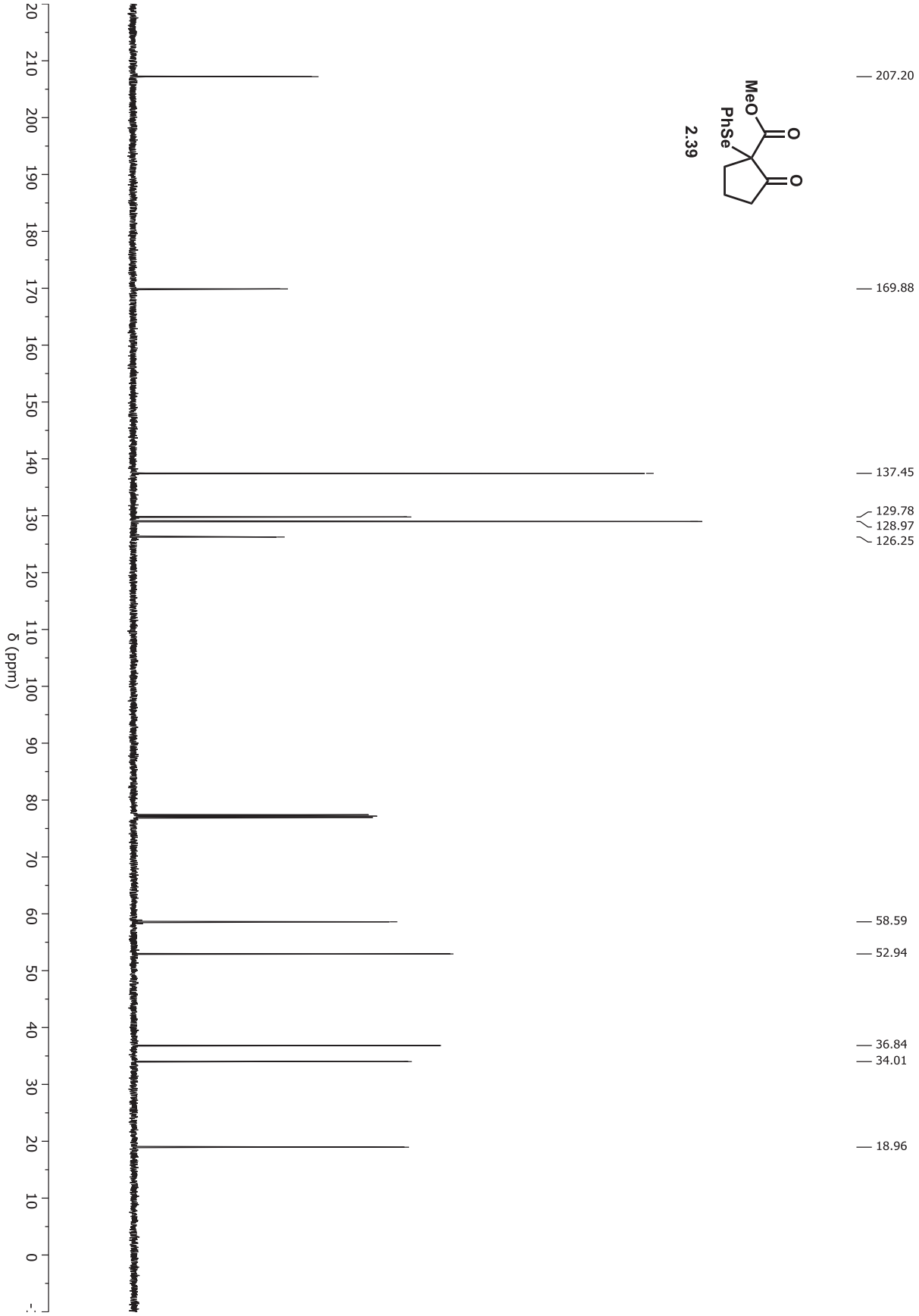
MeO
PhSe
O
O
2.39
207.20
169.88
137.45
129.78
128.97
126.25
58.59
52.94
36.84
34.01
18.96
δ (ppm)

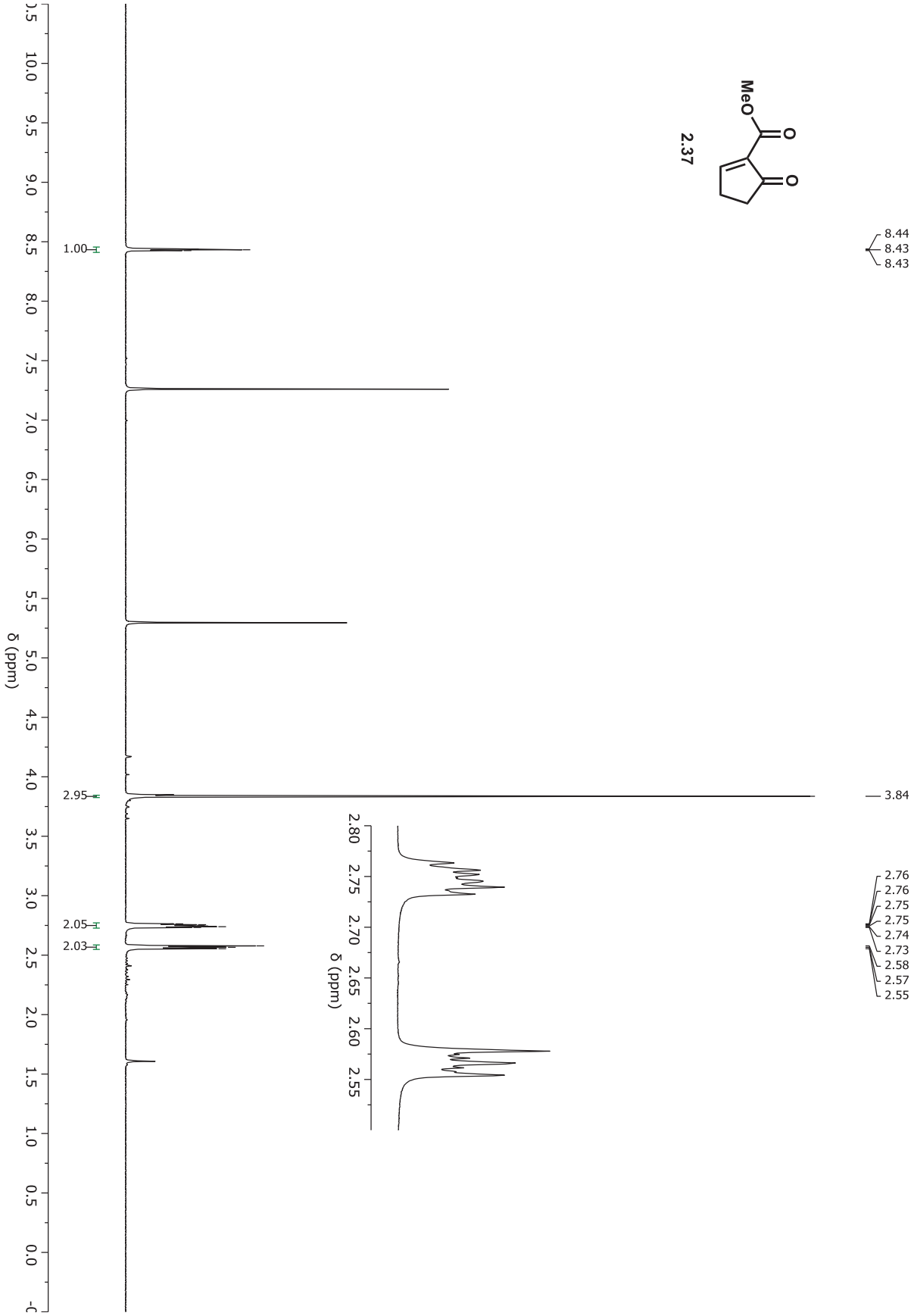
MeO
O
O
2.37
8.44
8.43
8.43
3.84
2.76
2.76
2.75
2.75
2.74
2.73
2.58
2.57
2.55
1.00
2.95
2.05
2.03
δ (ppm)
δ (ppm)

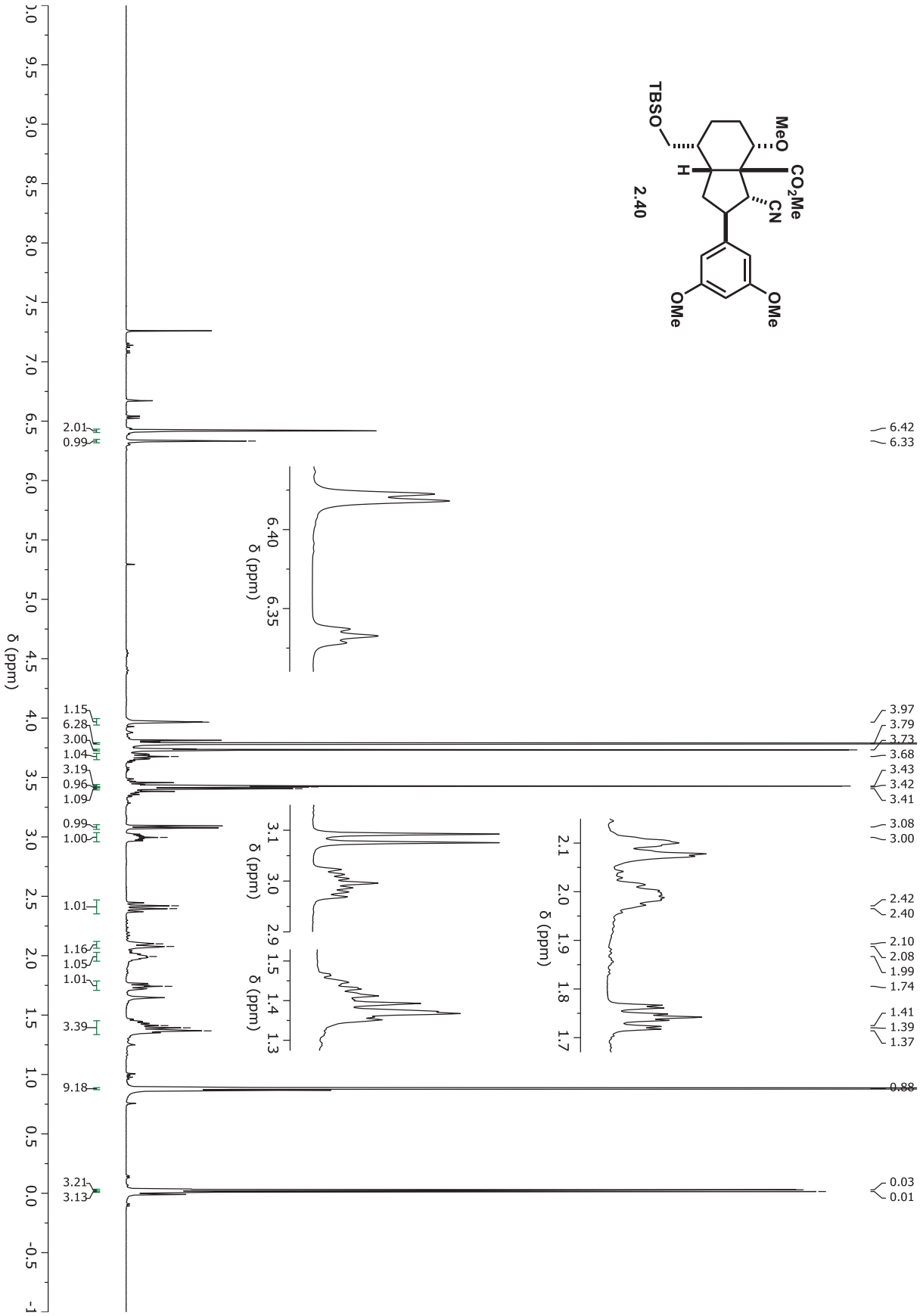
TBSO
H
MeO
CO2Me
CN
OMe
OMe
2.40
δ (ppm)
6.42
6.33
3.97
3.79
3.73
3.68
3.43
3.42
3.41
3.08
3.00
2.42
2.40
2.10
2.08
1.99
1.74
1.41
1.39
1.37
0.88
0.03
0.01
2.01
0.99
1.15
6.28
3.00
1.04
3.19
0.96
1.09
0.99
1.00
1.01
1.16
1.05
1.01
3.39
9.18
3.21
3.13

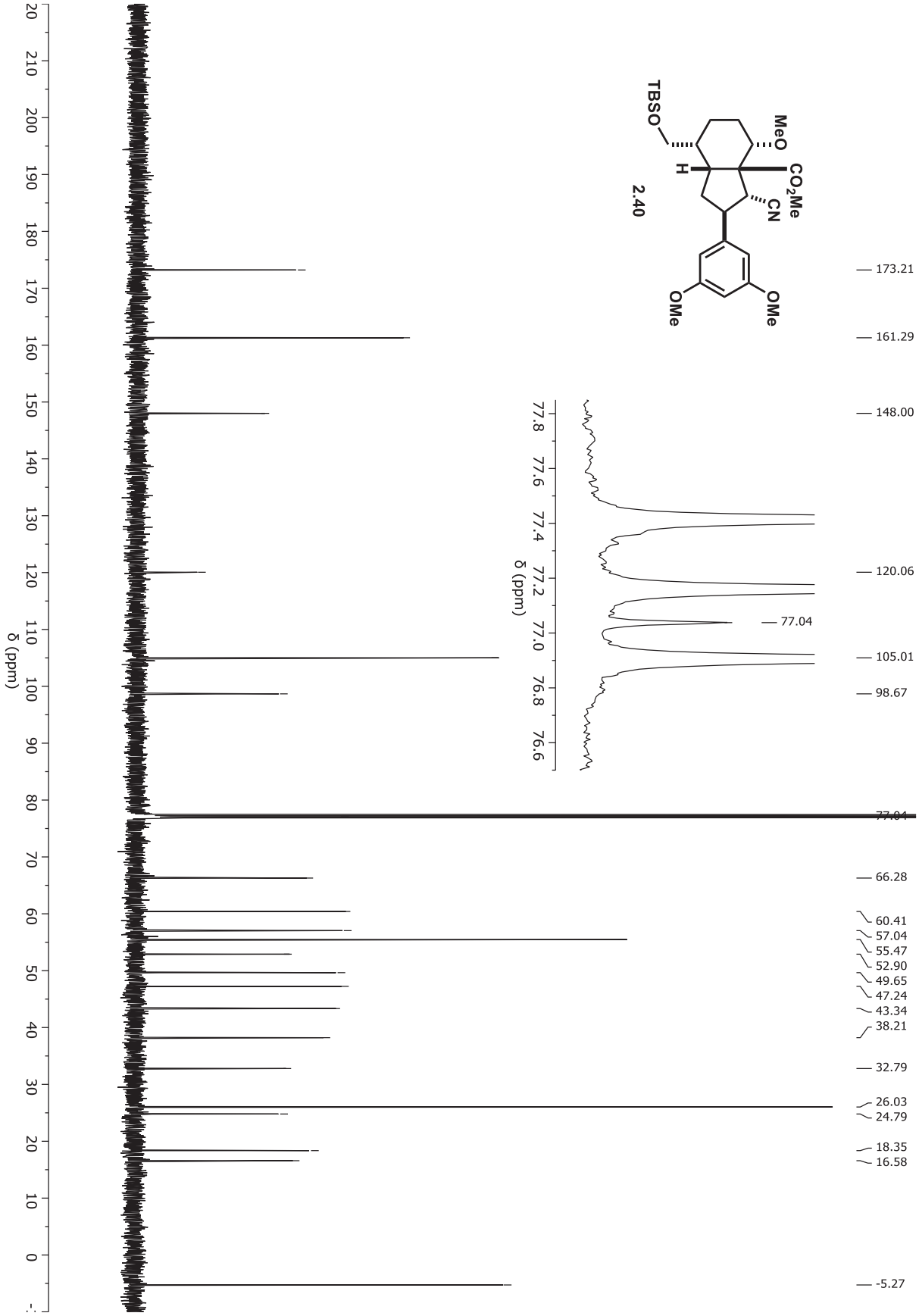
TBSO
MeO
H
CO2Me
CN
OMe
OMe
2.40
δ (ppm)
173.21
161.29
148.00
120.06
77.04
105.01
98.67
66.28
60.41
57.04
55.47
52.90
49.65
47.24
43.34
38.21
32.79
26.03
24.79
18.35
16.58
-5.27

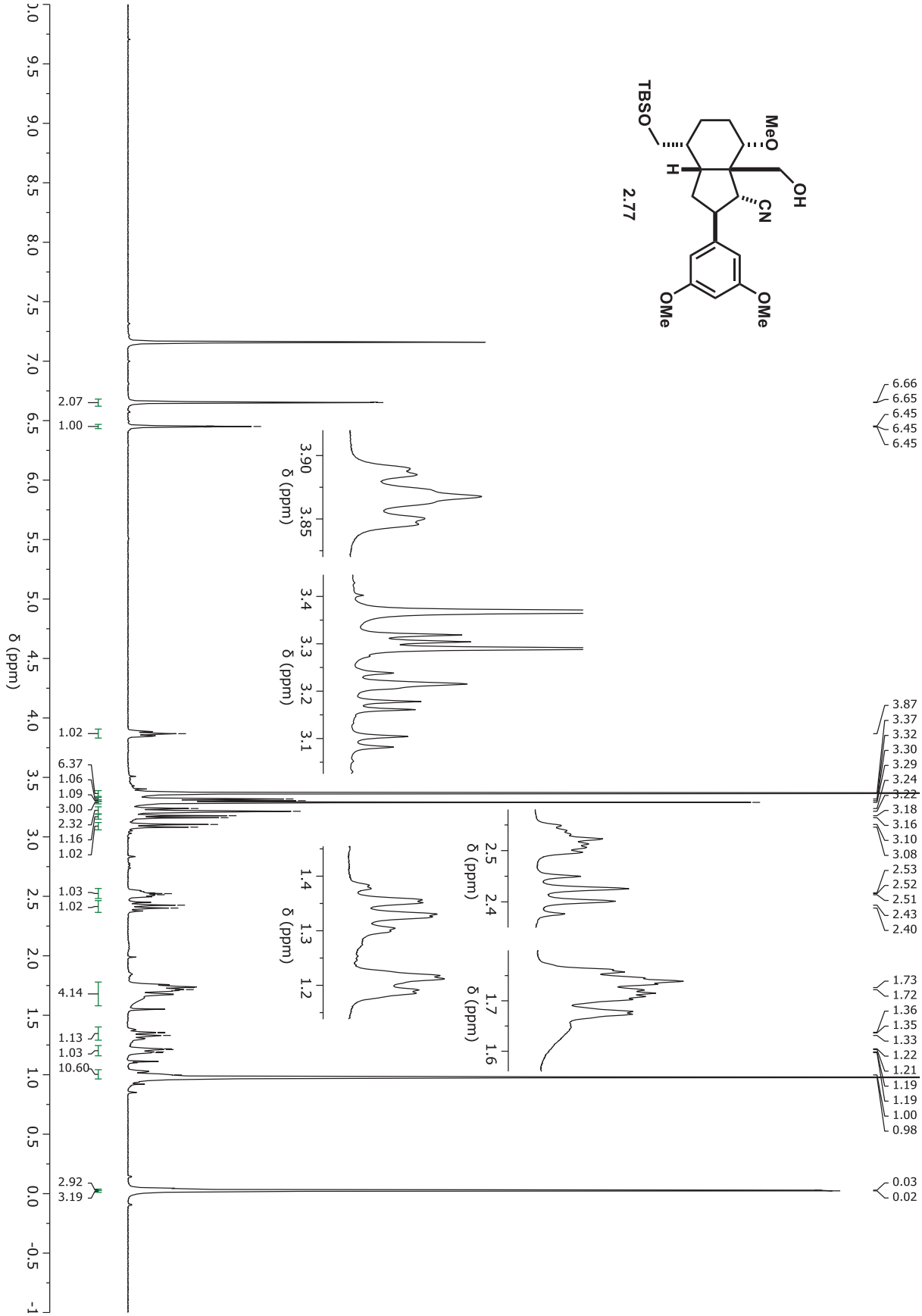
TBSO
MeO
H
CN
OH
OMe
OMe
2.77
δ (ppm)

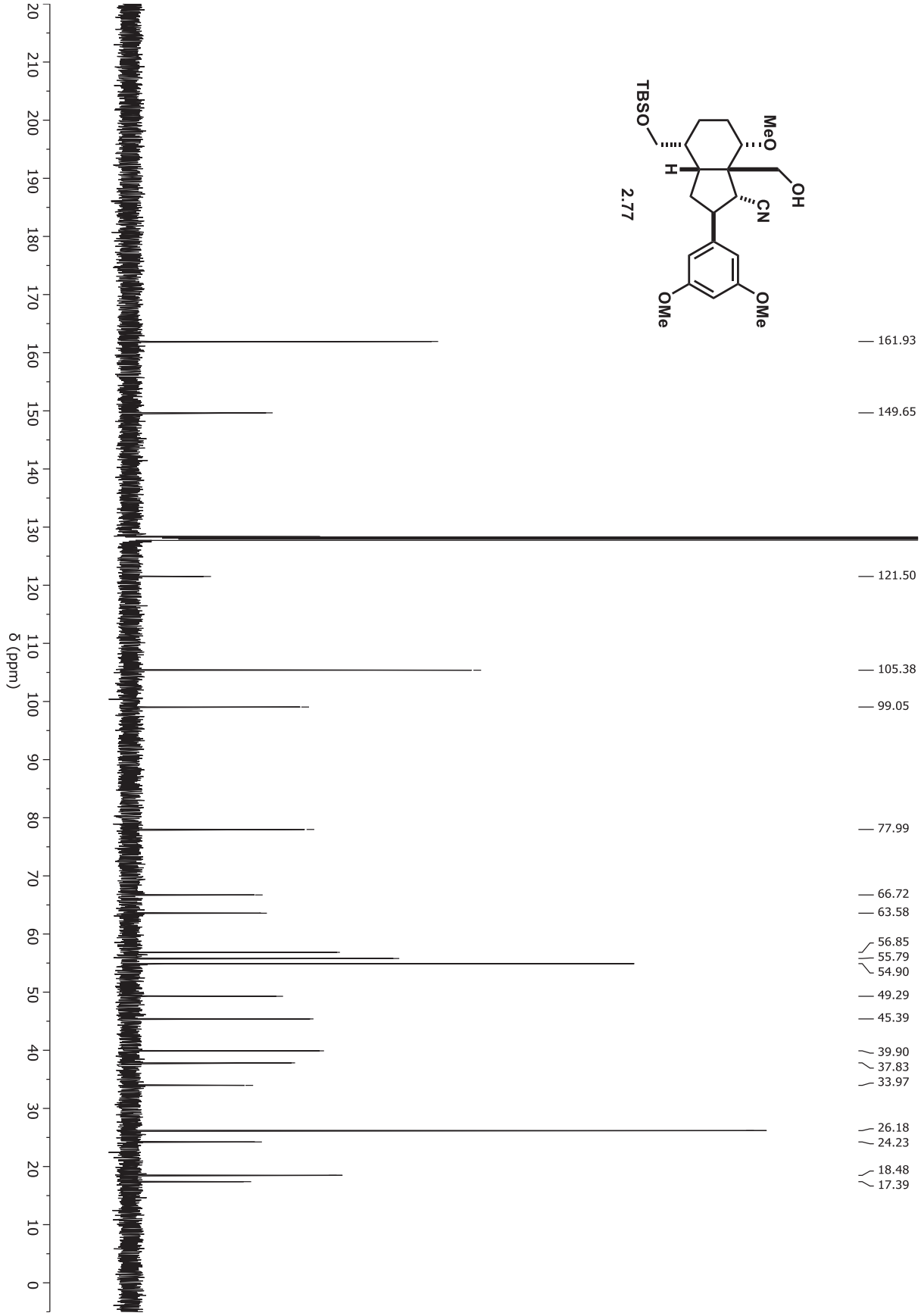
TBSO
MeO
H
OH
CN
OMe
OMe
2.77
δ (ppm)
161.93
149.65
121.50
105.38
99.05
77.99
66.72
63.58
56.85
55.79
54.90
49.29
45.39
39.90
37.83
33.97
26.18
24.23
18.48
17.39

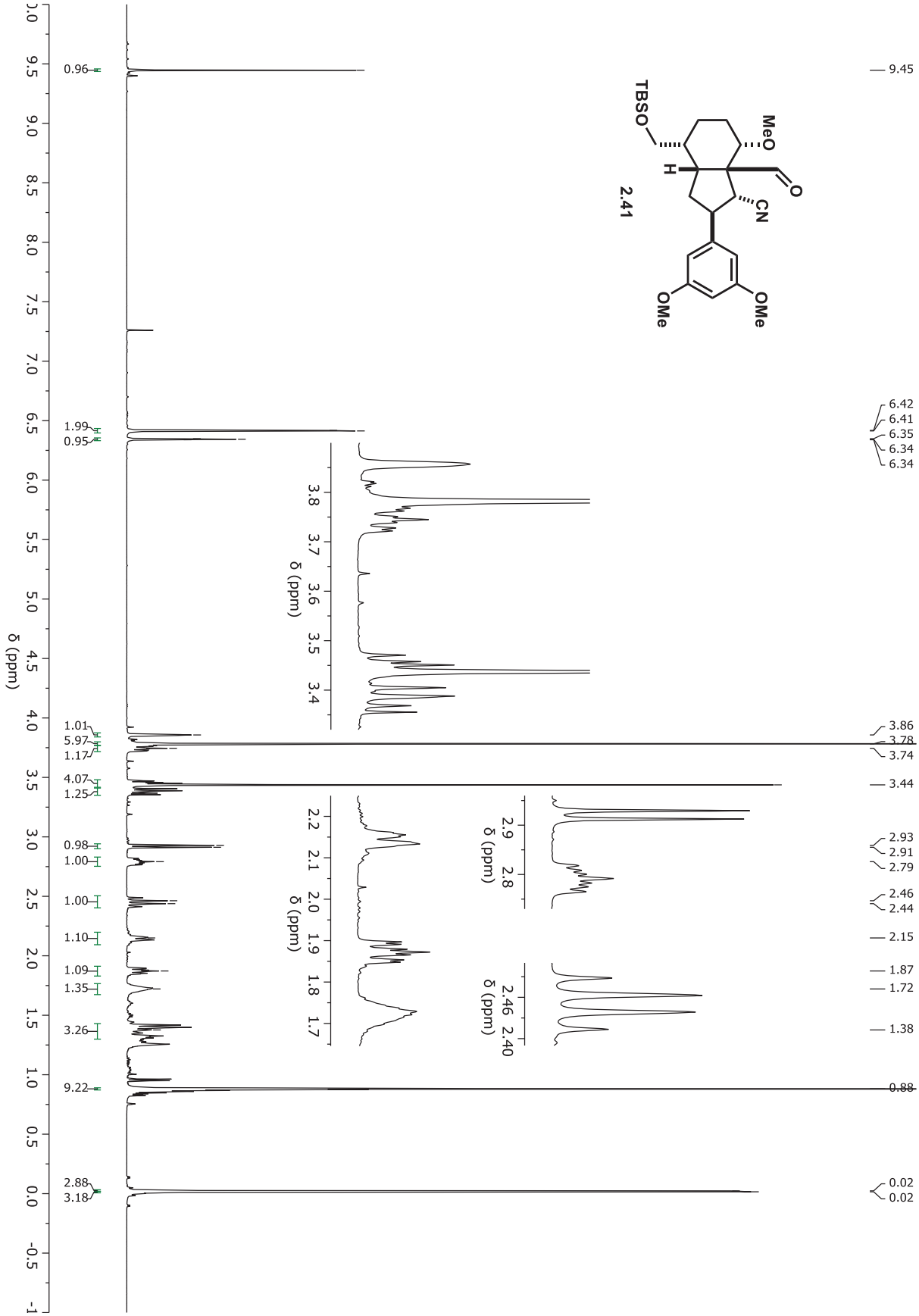
TBSO
MeO
H
O
CN
OMe
OMe
2.41
δ (ppm)

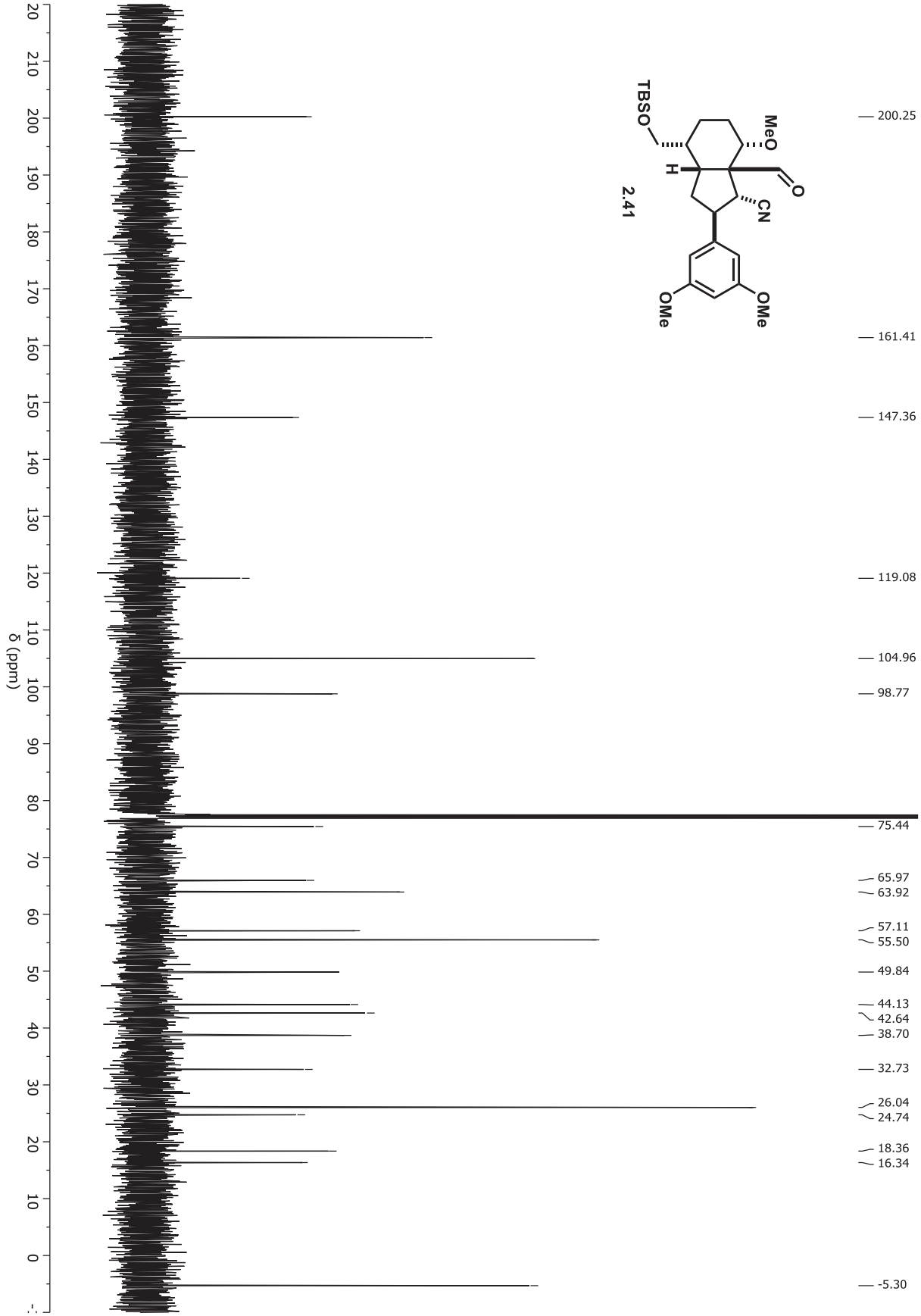
TBSO
MeO
H
O
CN
OMe
OMe
2.41
δ (ppm)
200.25
161.41
147.36
119.08
104.96
98.77
75.44
65.97
63.92
57.11
55.50
49.84
44.13
42.64
38.70
32.73
26.04
24.74
18.36
16.34
-5.30

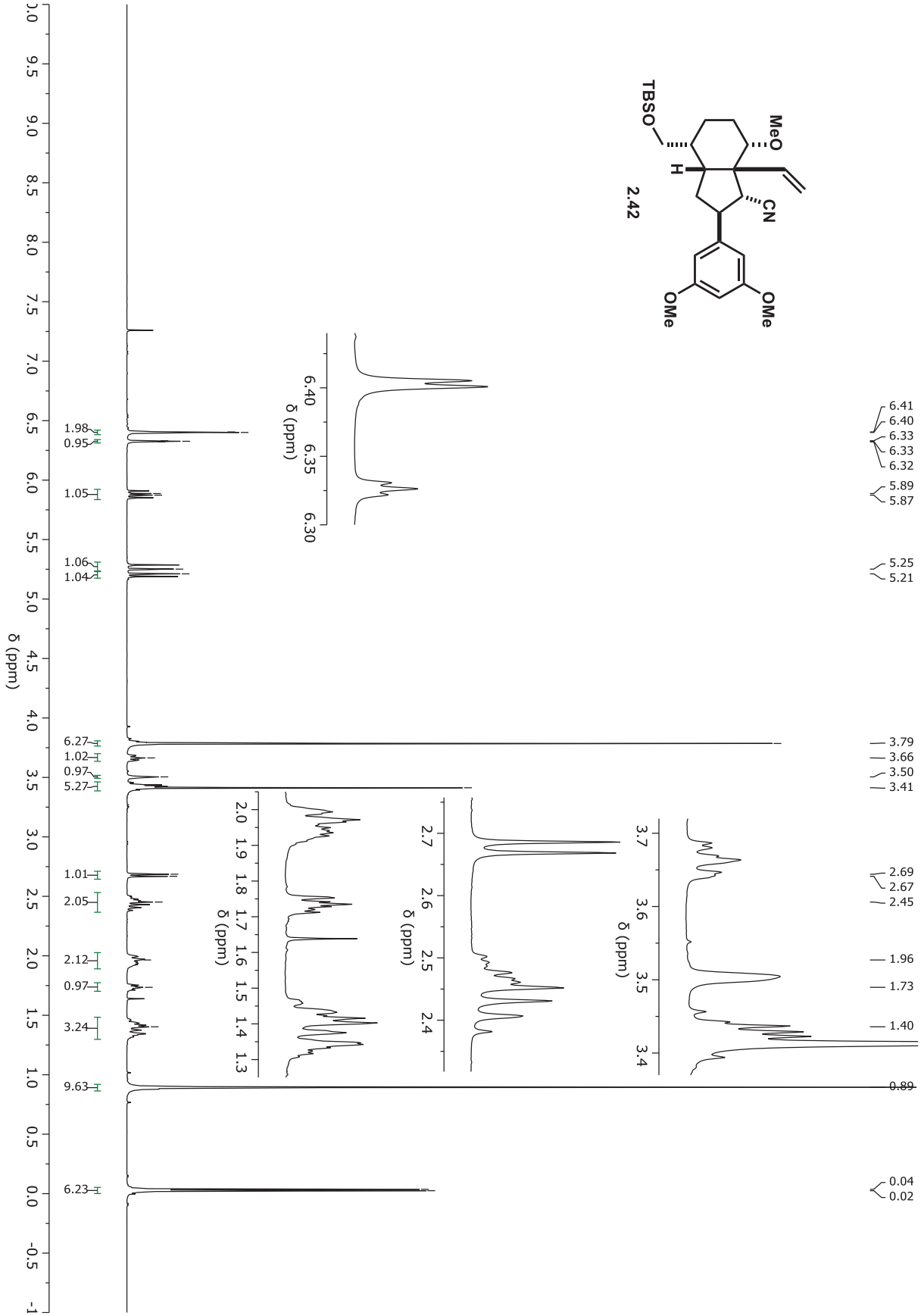
TBSO
MeO
H
CN
OMe
OMe
2.42
δ (ppm)
6.41
6.40
6.33
6.33
6.32
5.89
5.87
5.25
5.21
3.79
3.66
3.50
3.41
2.69
2.67
2.45
1.96
1.73
1.40
0.89
0.04
0.02
1.98
0.95
1.05
1.06
1.04
6.27
1.02
0.97
5.27
1.01
2.05
2.12
0.97
3.24
9.63
6.23

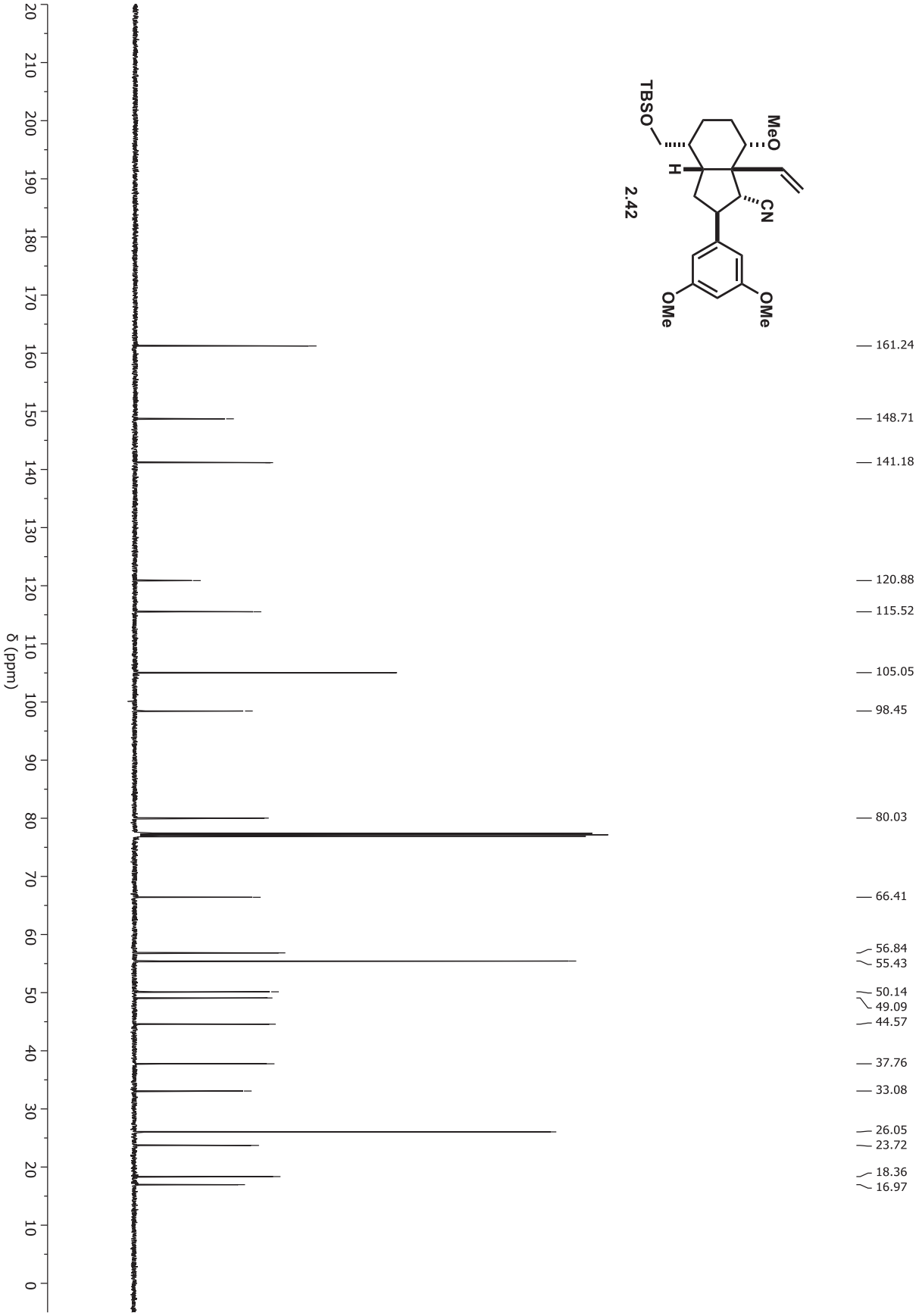
TBSO
MeO
H
CN
OMe
OMe
2.42
δ (ppm)
161.24
148.71
141.18
120.88
115.52
105.05
98.45
80.03
66.41
56.84
55.43
50.14
49.09
44.57
37.76
33.08
26.05
23.72
18.36
16.97

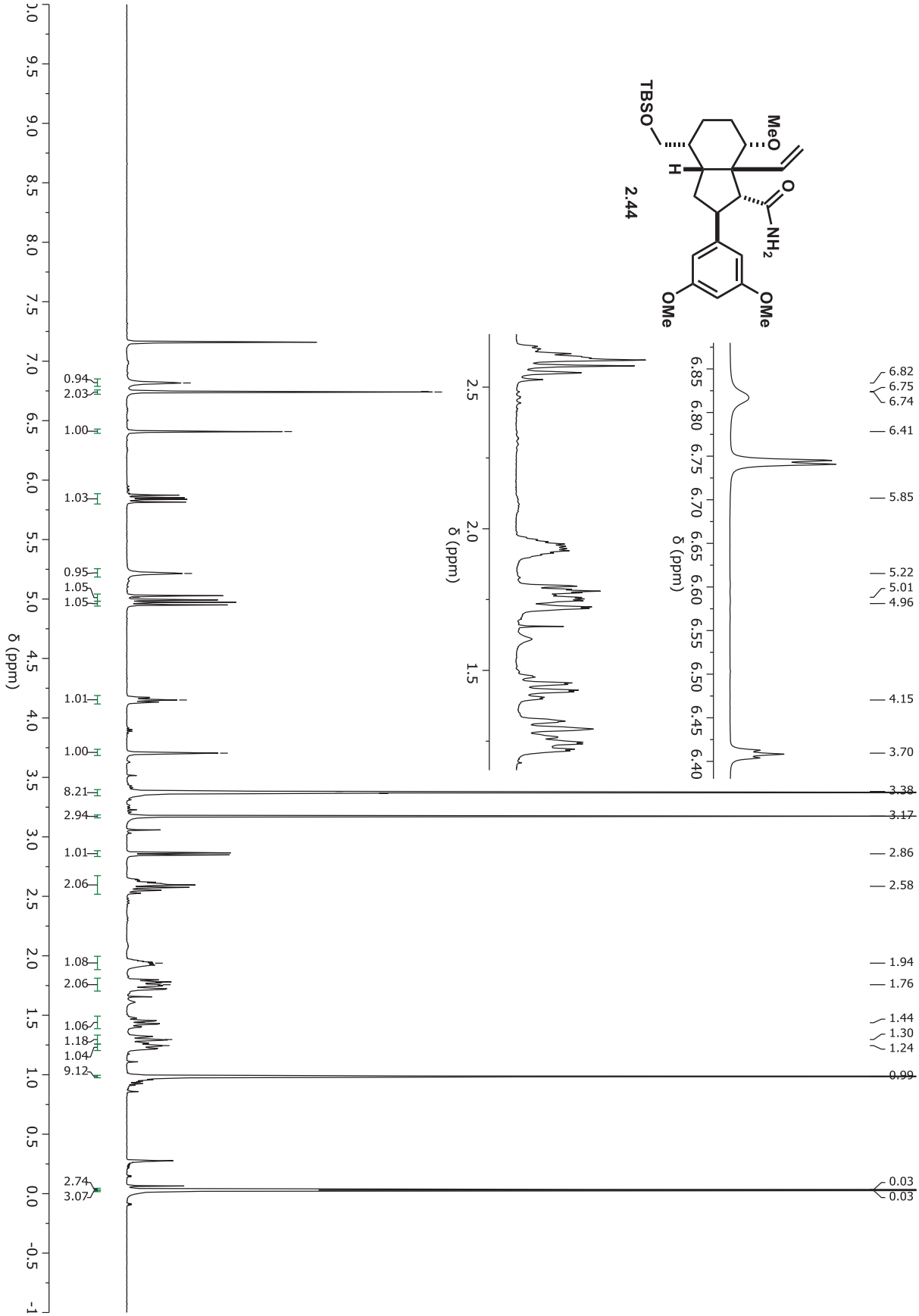
TBSO
MeO
H
O
NH2
OMe
OMe
2.44
δ (ppm)
0.94
2.03
1.00
1.03
0.95
1.05
1.05
1.01
1.00
8.21
2.94
1.01
2.06
1.08
2.06
1.06
1.18
1.04
9.12
2.74
3.07
6.82
6.75
6.74
6.41
5.85
5.22
5.01
4.96
4.15
3.70
3.38
3.17
2.86
2.58
1.94
1.76
1.44
1.30
1.24
0.99
0.03
0.03

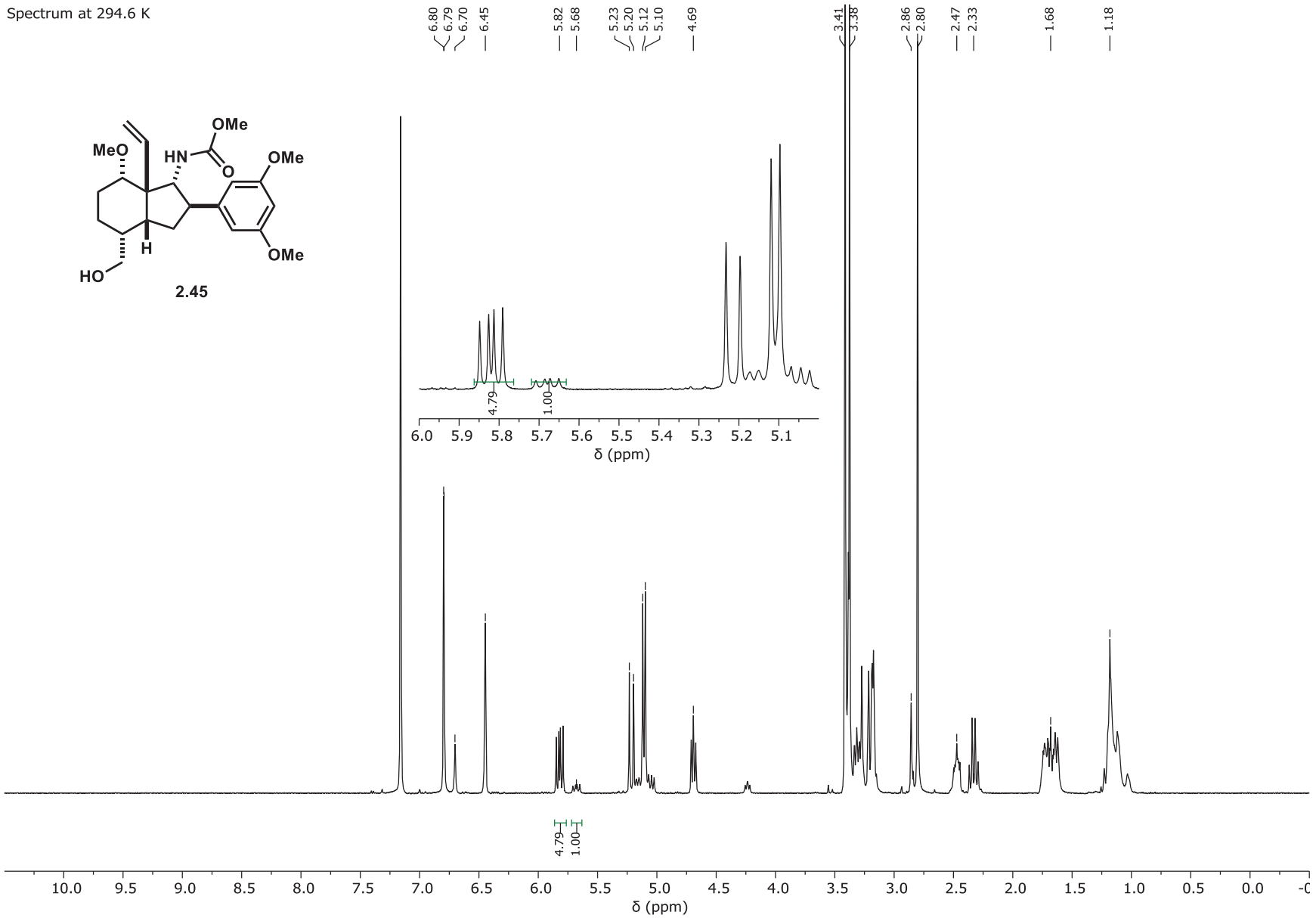
Spectrum at 294.6 K
6.80
6.79
6.70
6.45
5.82
5.68
5.23
5.20
5.12
5.10
4.69
3.41
3.38
2.86
2.80
2.47
2.33
1.68
1.18
MeO
HN
OMe
O
OMe
H
OMe
HO
2.45
4.79
1.00
6.0 5.9 5.8 5.7 5.6 5.5 5.4 5.3 5.2 5.1
δ (ppm)
4.79
1.00
10.0 9.5 9.0 8.5 8.0 7.5 7.0 6.5 6.0 5.5 5.0 4.5 4.0 3.5 3.0 2.5 2.0 1.5 1.0 0.5 0.0
δ (ppm)

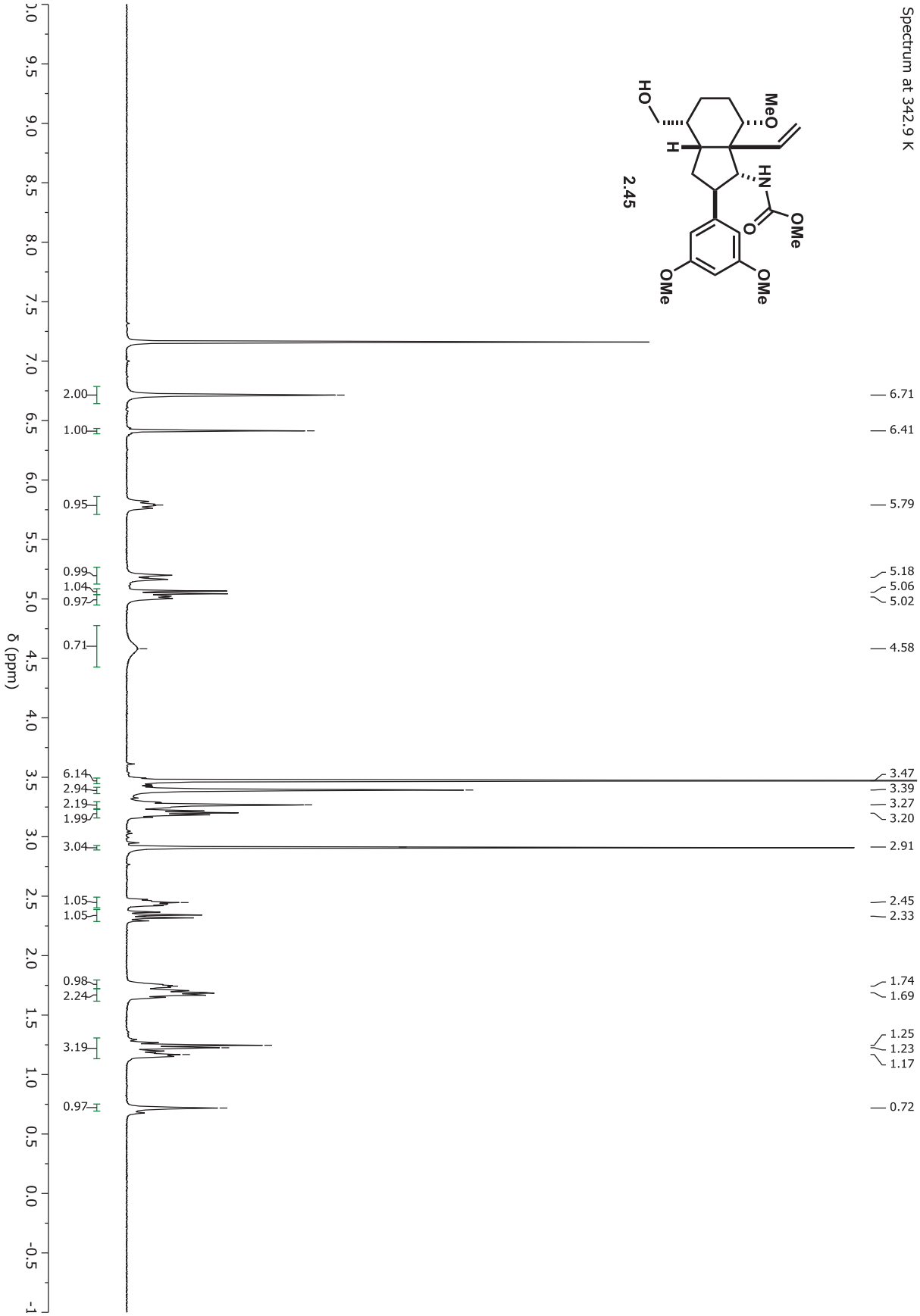
Spectrum at 342.9 K
2.45
HO
MeO
H
HN
O
OMe
OMe
OMe
δ (ppm)
2.00
1.00
0.95
0.99
1.04
0.97
0.71
6.14
2.94
2.19
1.99
3.04
1.05
1.05
0.98
2.24
3.19
0.97
6.71
6.41
5.79
5.18
5.06
5.02
4.58
3.47
3.39
3.27
3.20
2.91
2.45
2.33
1.74
1.69
1.25
1.23
1.17
0.72

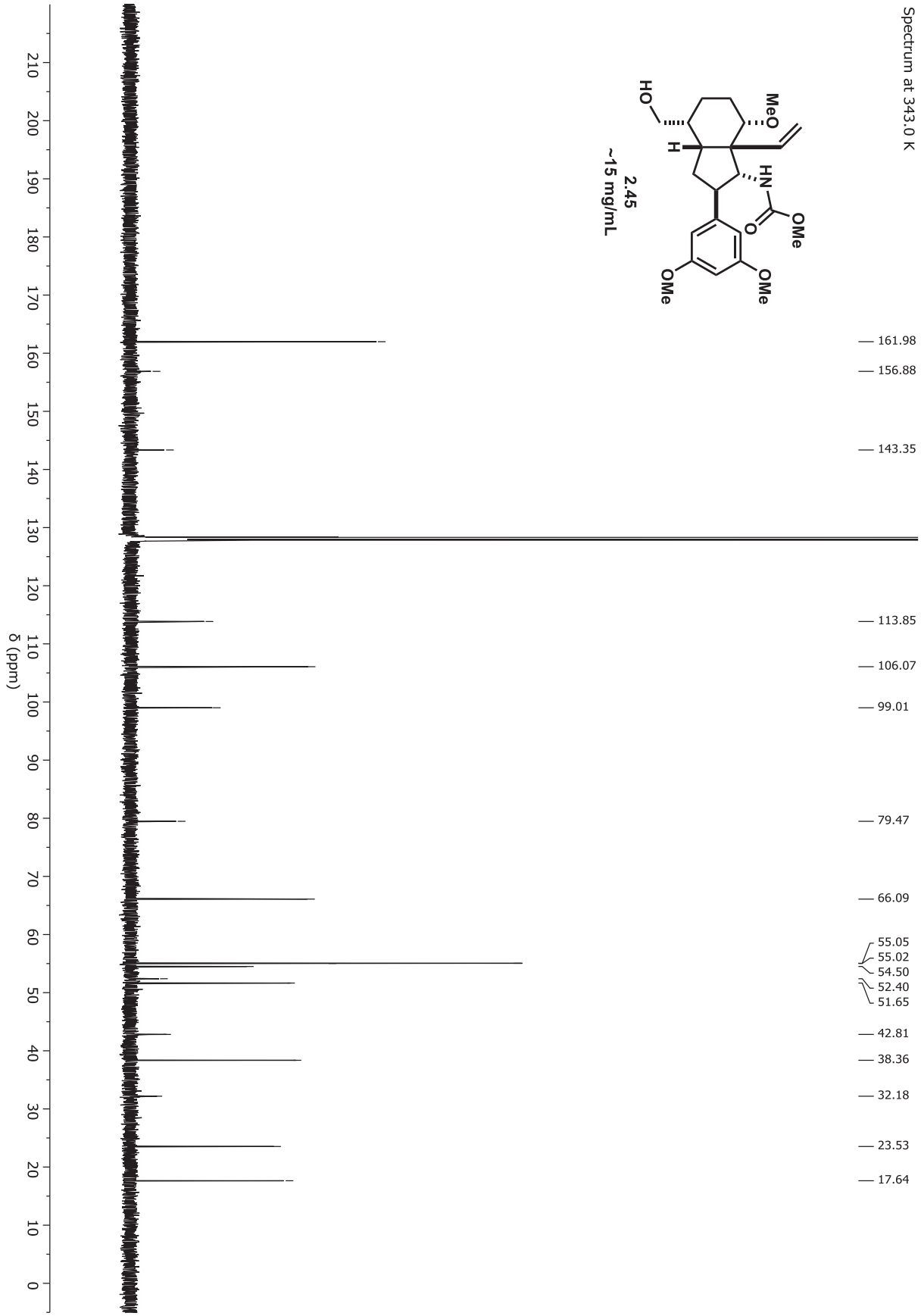
Spectrum at 343.0 K
2.45
~15 mg/mL
HO
MeO
H
HN
O
OMe
OMe
OMe
δ (ppm)
210
200
190
180
170
160
150
140
130
120
110
100
90
80
70
60
50
40
30
20
10
0
161.98
156.88
143.35
113.85
106.07
99.01
79.47
66.09
55.05
55.02
54.50
52.40
51.65
42.81
38.36
32.18
23.53
17.64

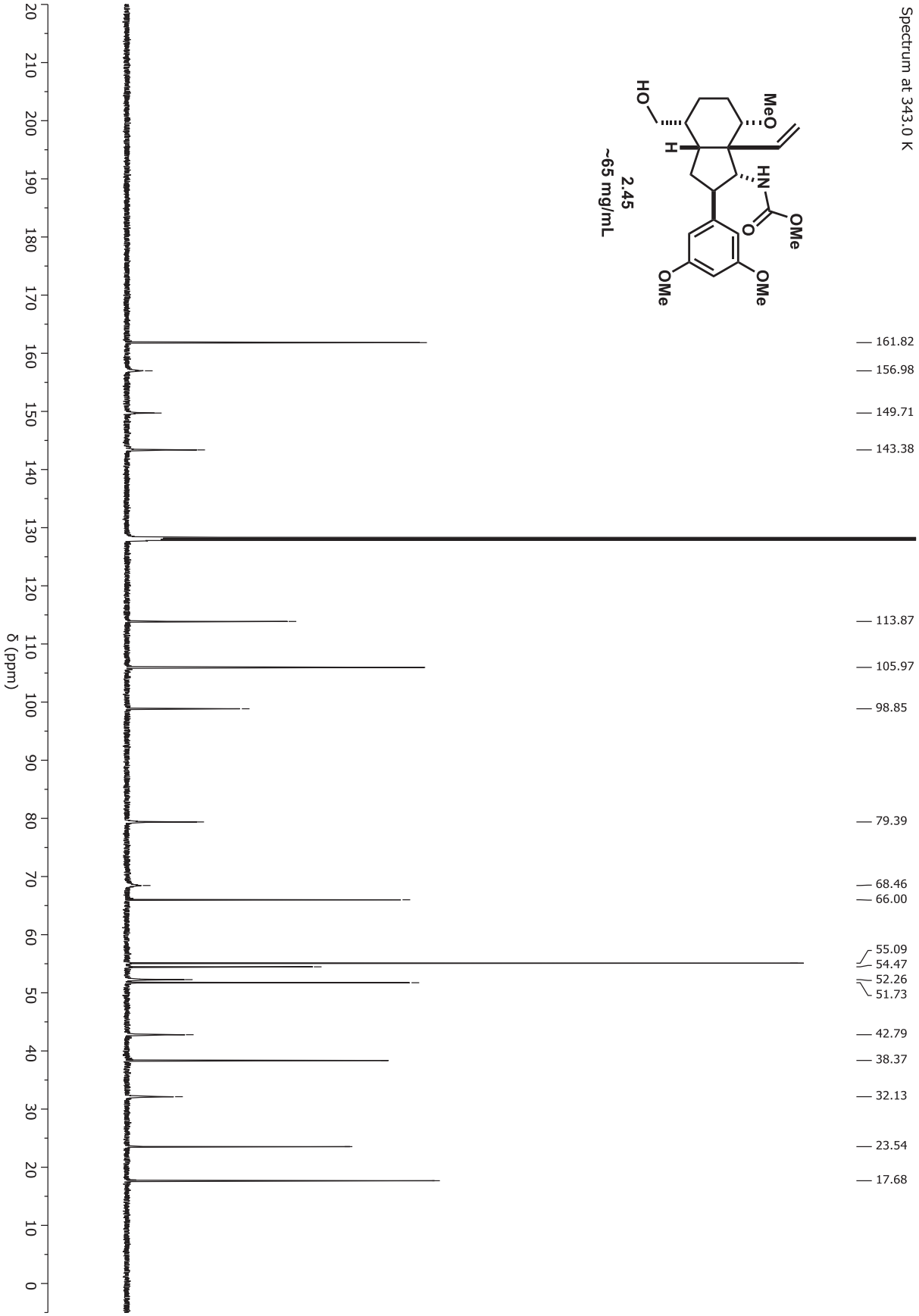
Spectrum at 343.0 K
2.45
~65 mg/mL
HO
MeO
H
HN
O
OMe
OMe
OMe
δ (ppm)
161.82
156.98
149.71
143.38
113.87
105.97
98.85
79.39
68.46
66.00
55.09
54.47
52.26
51.73
42.79
38.37
32.13
23.54
17.68

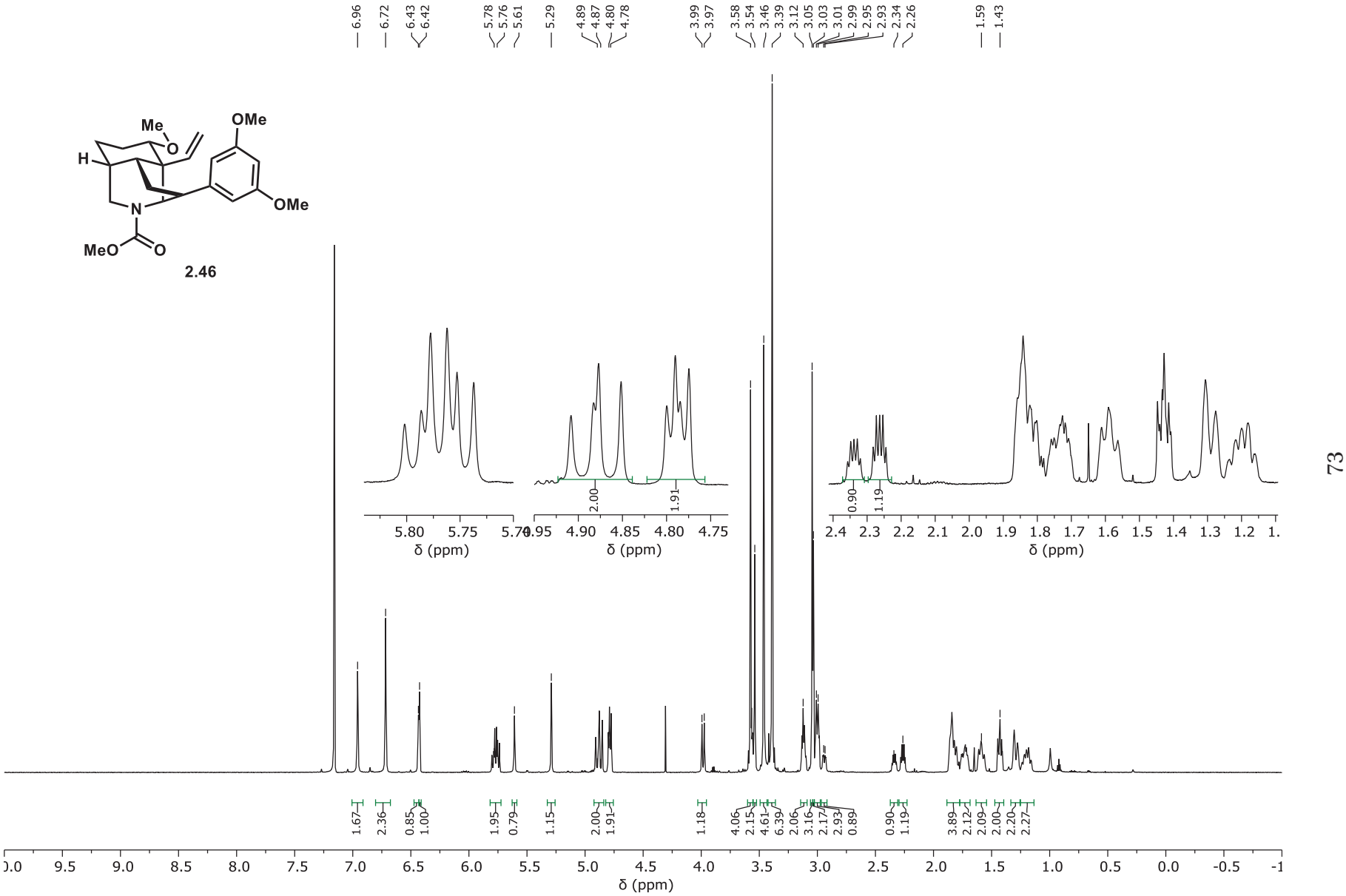
6.96
6.72
6.43
6.42
5.78
5.76
5.61
5.29
4.89
4.87
4.80
4.78
3.99
3.97
3.58
3.54
3.46
3.39
3.12
3.05
3.03
3.01
2.99
2.95
2.93
2.34
2.26
1.59
1.43
Me
O
OMe
H
OMe
N
MeO
O
2.46
δ (ppm)
δ (ppm)
δ (ppm)
δ (ppm)

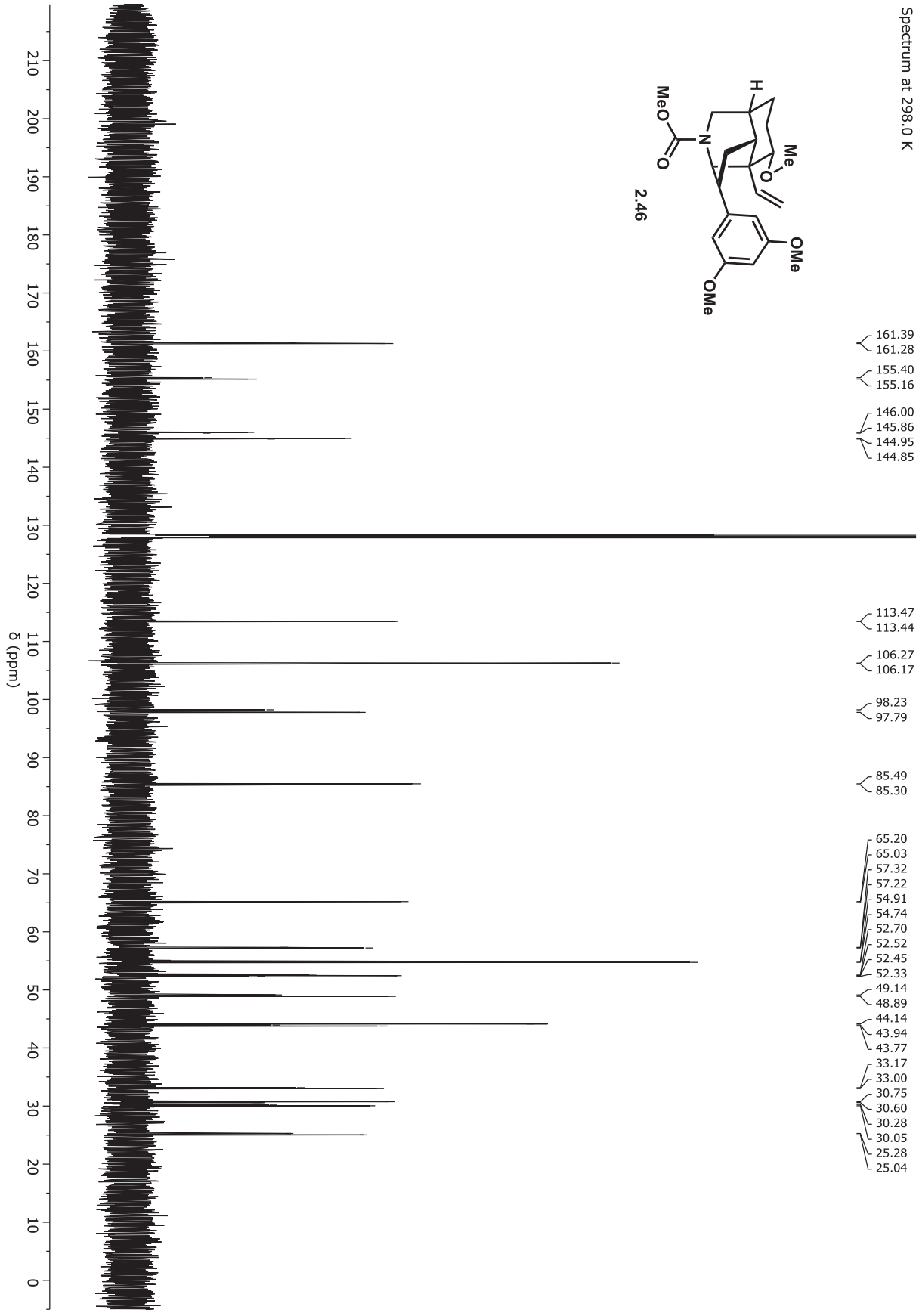
Spectrum at 298.0 K
MeO
O
N
H
Me
O
OMe
OMe
2.46
161.39
161.28
155.40
155.16
146.00
145.86
144.95
144.85
113.47
113.44
106.27
106.17
98.23
97.79
85.49
85.30
65.20
65.03
57.32
57.22
54.91
54.74
52.70
52.52
52.45
52.33
49.14
48.89
44.14
43.94
43.77
33.17
33.00
30.75
30.60
30.28
30.05
25.28
25.04
δ (ppm)
210
200
190
180
170
160
150
140
130
120
110
100
90
80
70
60
50
40
30
20
10
0

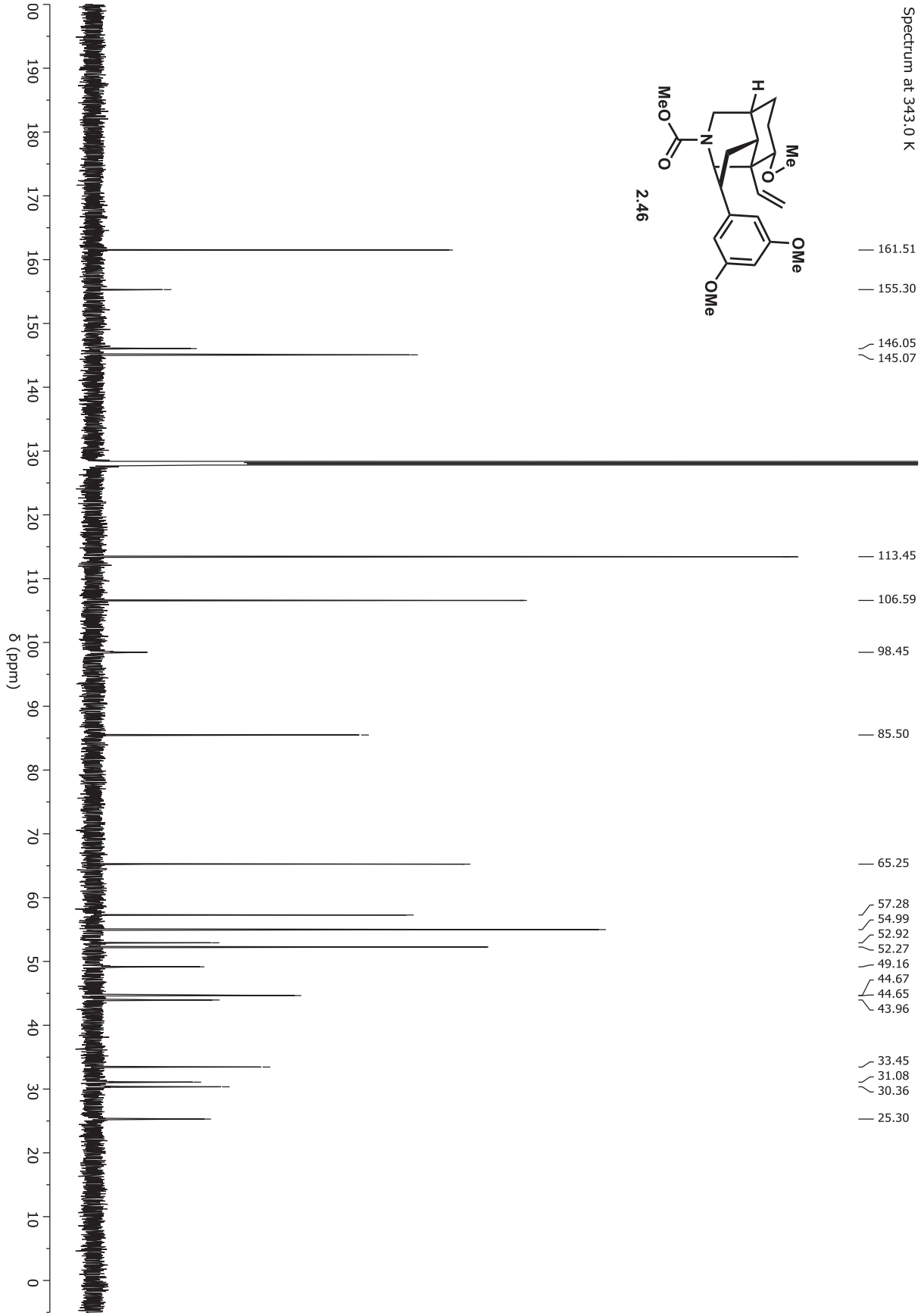
Spectrum at 343.0 K
2.46
MeO
O
N
H
Me
O
OMe
OMe
161.51
155.30
146.05
145.07
113.45
106.59
98.45
85.50
65.25
57.28
54.99
52.92
52.27
49.16
44.67
44.65
43.96
33.45
31.08
30.36
25.30
δ (ppm)

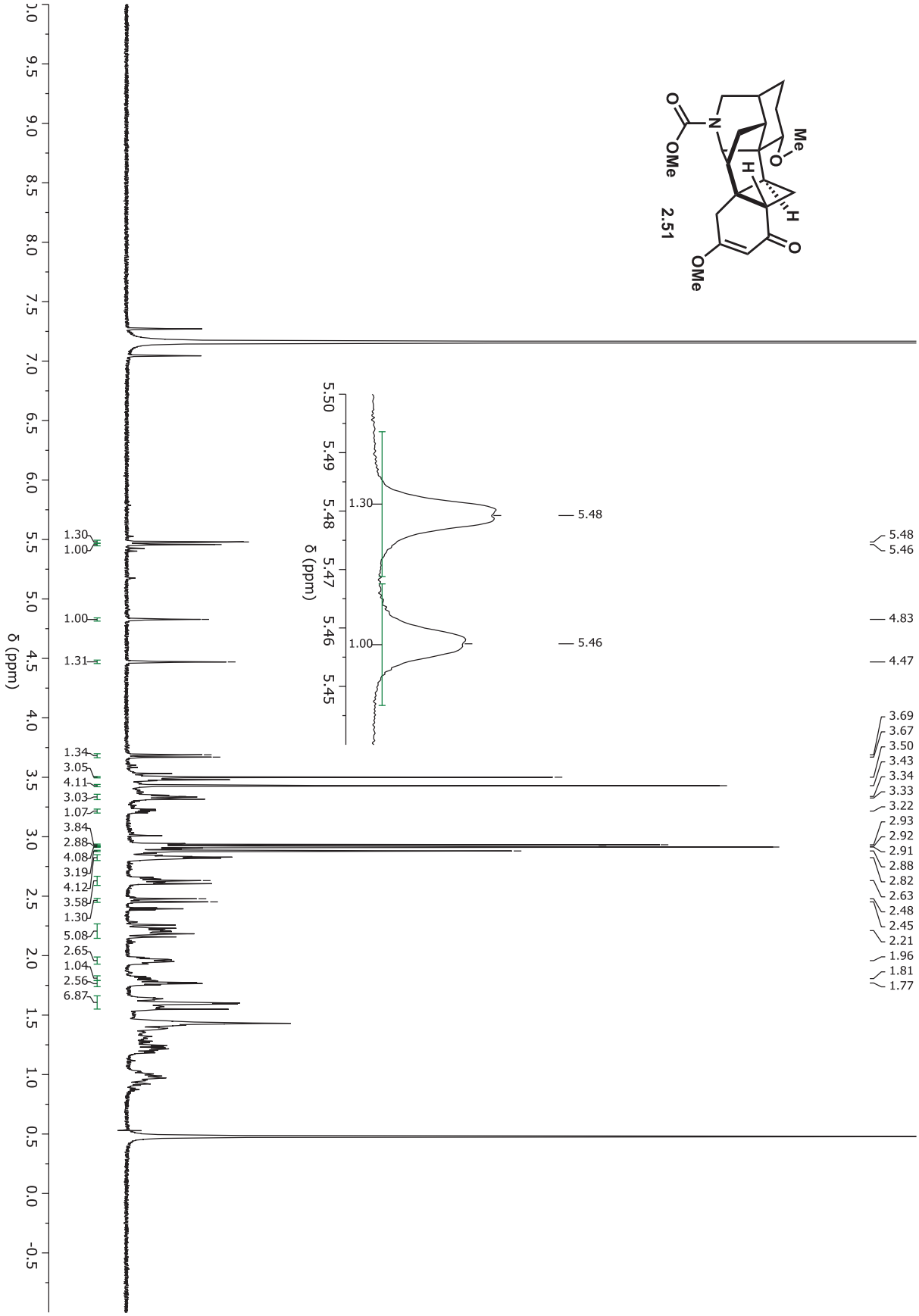
2.51
δ (ppm)
1.30
1.00
1.31
1.34
3.05
4.11
3.03
1.07
3.84
2.88
4.08
3.19
4.12
3.58
1.30
5.08
2.65
1.04
2.56
6.87
5.48
5.46
4.83
4.47
3.69
3.67
3.50
3.43
3.34
3.33
3.22
2.93
2.92
2.91
2.88
2.82
2.63
2.48
2.45
2.21
1.96
1.81
1.77

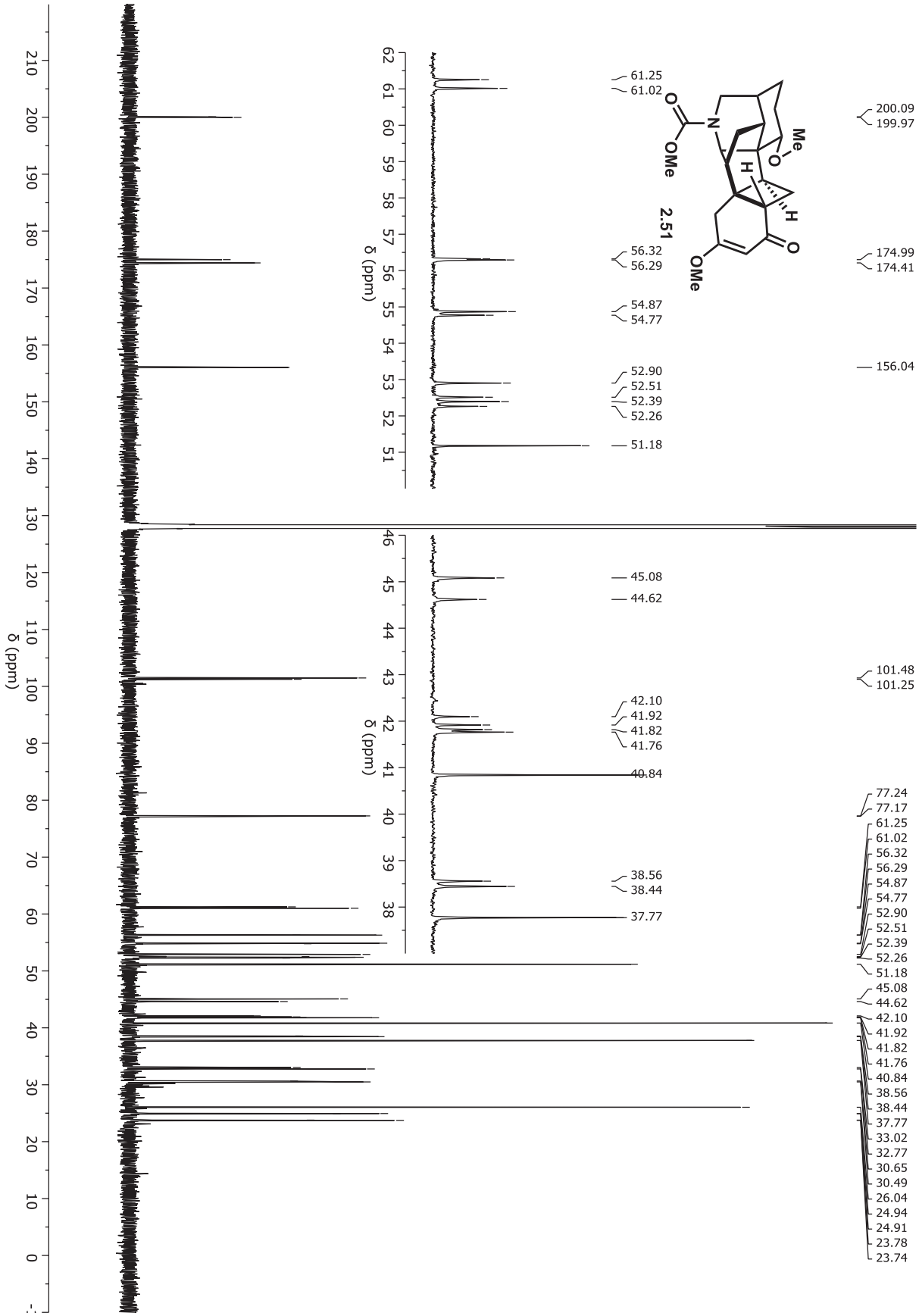
61.25
61.02
56.32
56.29
54.87
54.77
52.90
52.51
52.39
52.26
51.18
45.08
44.62
42.10
41.92
41.82
41.76
40.84
38.56
38.44
37.77
200.09
199.97
174.99
174.41
156.04
101.48
101.25
77.24
77.17
61.25
61.02
56.32
56.29
54.87
54.77
52.90
52.51
52.39
52.26
51.18
45.08
44.62
42.10
41.92
41.82
41.76
40.84
38.56
38.44
37.77
33.02
32.77
30.65
30.49
26.04
24.94
24.91
23.78
23.74
δ (ppm)
δ (ppm)
δ (ppm)
2.51
OMe
OMe
N
O
O
Me
H
H
O
O

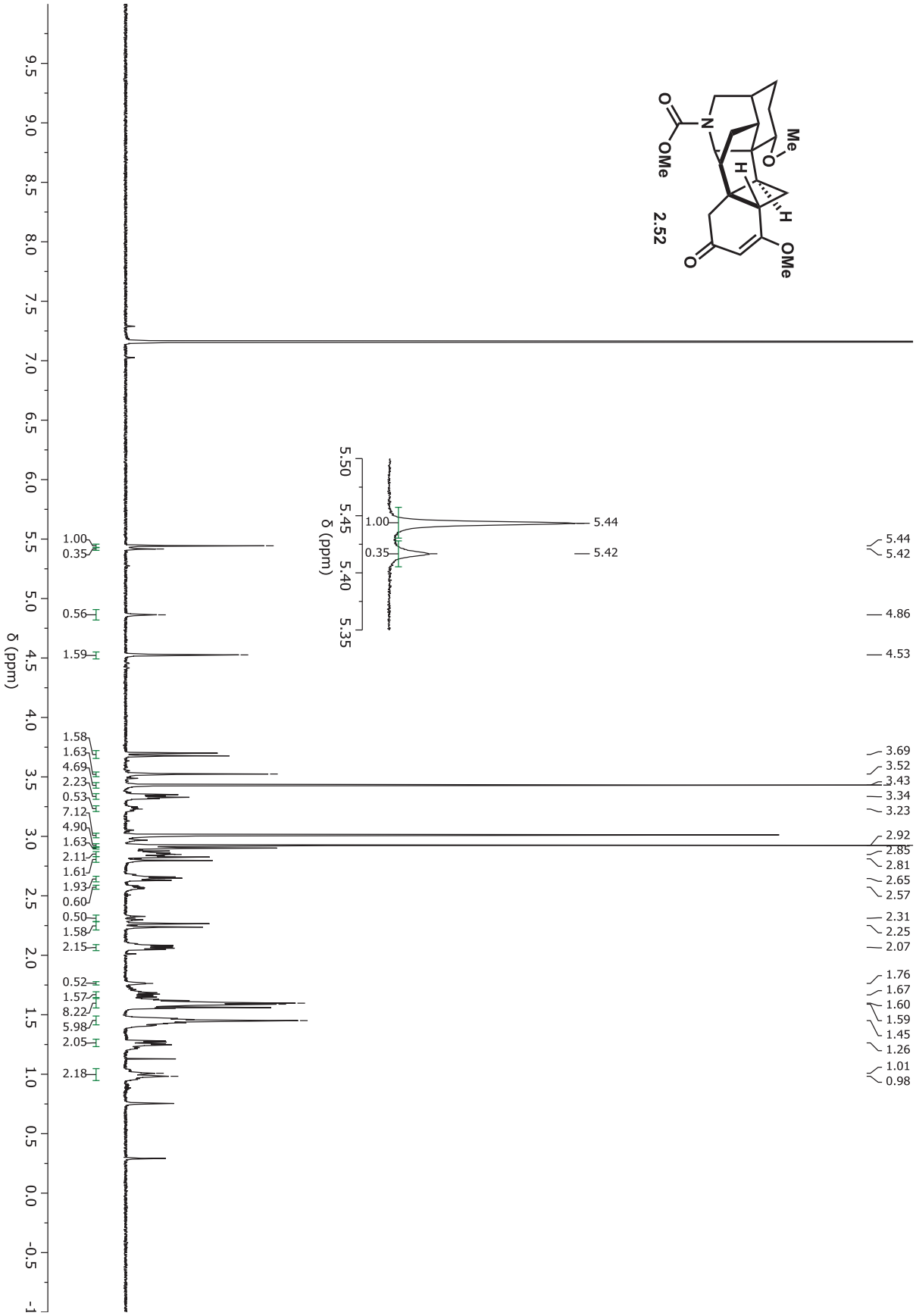
δ (ppm)
9.5
9.0
8.5
8.0
7.5
7.0
6.5
6.0
5.5
5.0
4.5
4.0
3.5
3.0
2.5
2.0
1.5
1.0
0.5
0.0
-0.5
-1
1.00
0.35
0.56
1.59
1.58
1.63
4.69
2.23
0.53
7.12
4.90
1.63
2.11
1.61
1.93
0.60
0.50
1.58
2.15
0.52
1.57
8.22
5.98
2.05
2.18
5.44
5.42
4.86
4.53
3.69
3.52
3.43
3.34
3.23
2.92
2.85
2.81
2.65
2.57
2.31
2.25
2.07
1.76
1.67
1.60
1.59
1.45
1.26
1.01
0.98
5.50
5.45
5.40
5.35
δ (ppm)
1.00
0.35
5.44
5.42
O
N
OMe
O
Me
H
H
OMe
O
2.52

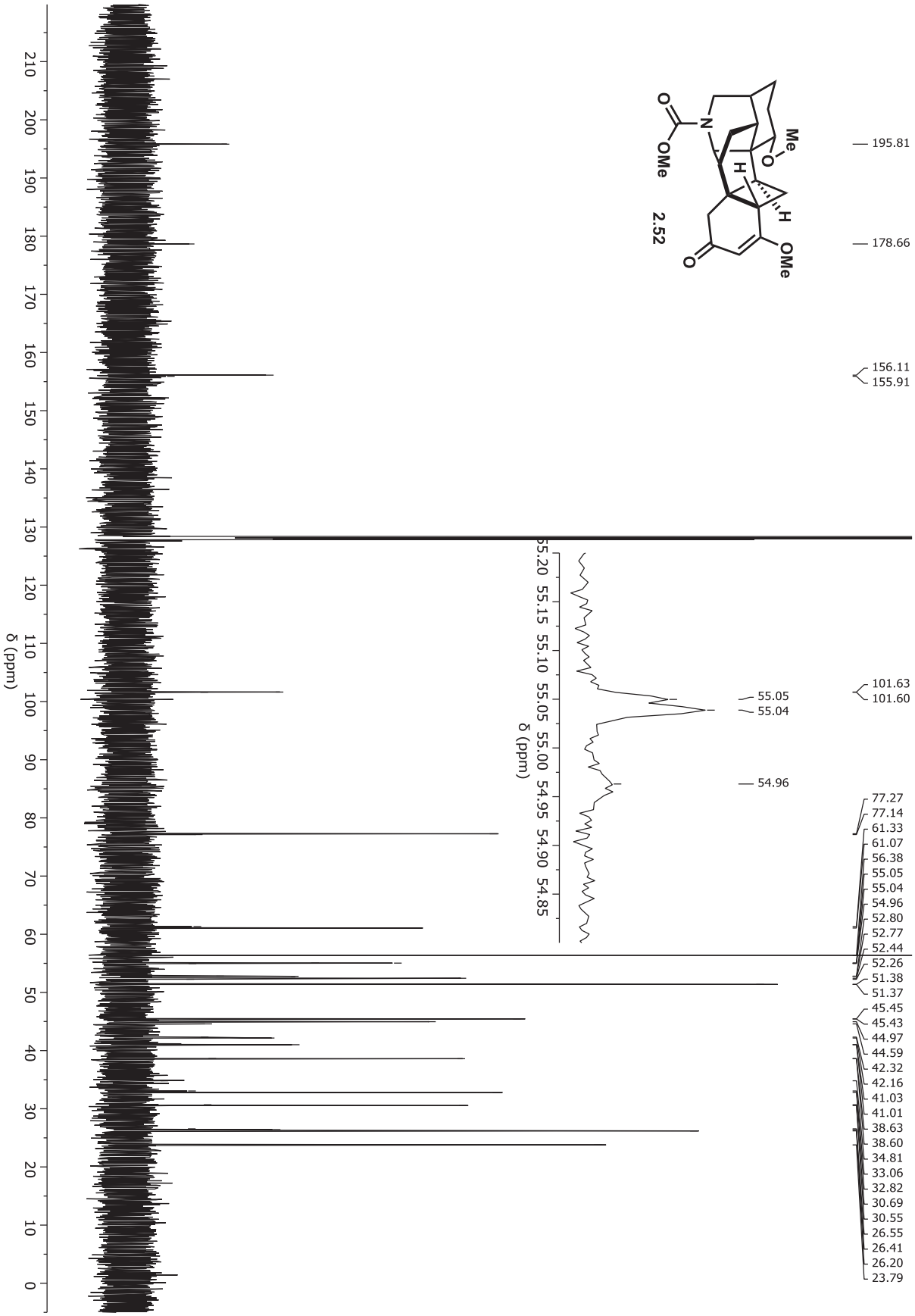
O
N
OMe
O
Me
O
H
H
OMe
O
2.52
δ (ppm)
195.81
178.66
156.11
155.91
101.63
101.60
55.05
55.04
54.96
77.27
77.14
61.33
61.07
56.38
55.05
55.04
54.96
52.80
52.77
52.44
52.26
51.38
51.37
45.45
45.43
44.97
44.59
42.32
42.16
41.03
41.01
38.63
38.60
34.81
33.06
32.82
30.69
30.55
26.55
26.41
26.20
23.79

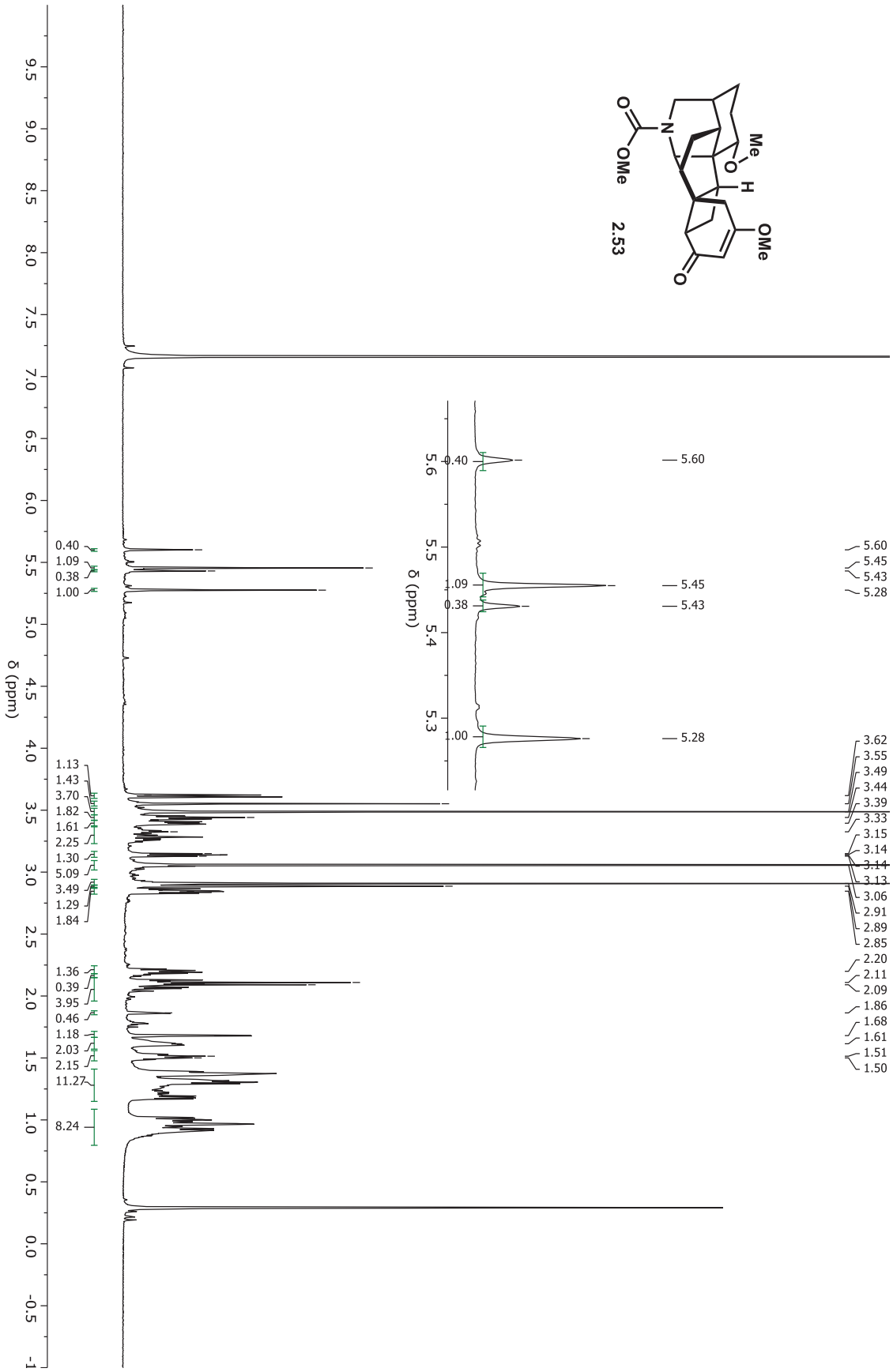
2.53
δ (ppm)
0.40
1.09
0.38
1.00
1.13
1.43
3.70
1.82
1.61
2.25
1.30
5.09
3.49
1.29
1.84
1.36
0.39
3.95
0.46
1.18
2.03
2.15
11.27
8.24
5.60
5.45
5.43
5.28
3.62
3.55
3.49
3.44
3.39
3.33
3.15
3.14
3.14
3.13
3.06
2.91
2.89
2.85
2.20
2.11
2.09
1.86
1.68
1.61
1.51
1.50

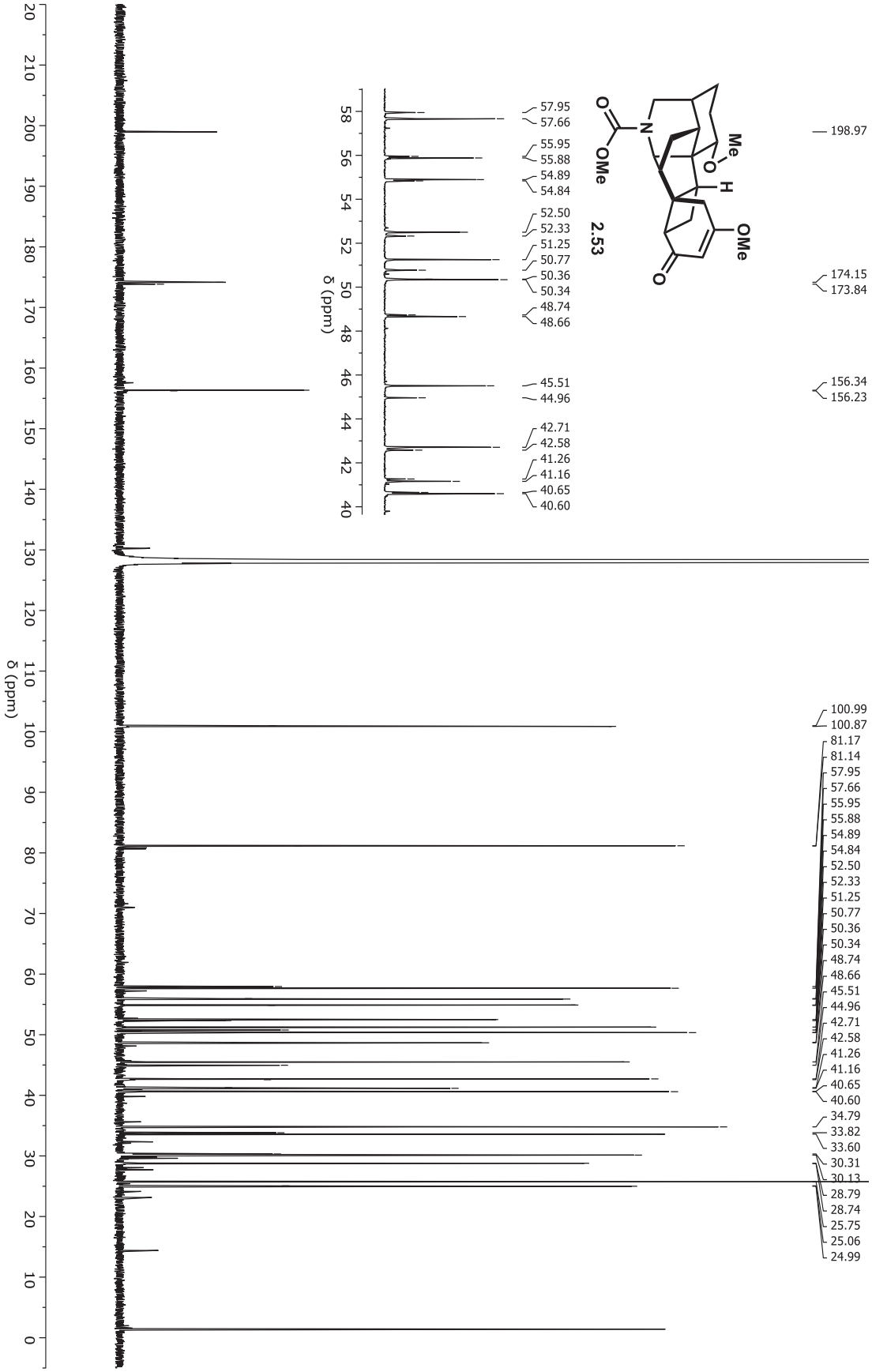
δ (ppm)
198.97
174.15
173.84
156.34
156.23
100.99
100.87
81.17
81.14
57.95
57.66
55.95
55.88
54.89
54.84
52.50
52.33
51.25
50.77
50.36
50.34
48.74
48.66
45.51
44.96
42.71
42.58
41.26
41.16
40.65
40.60
34.79
33.82
33.60
30.31
30.13
28.79
28.74
25.75
25.06
24.99
2.53
OMe
Me
OMe
O
H
N
O
O

Appendix 2.B X-Ray crystallography data for Chapter 2

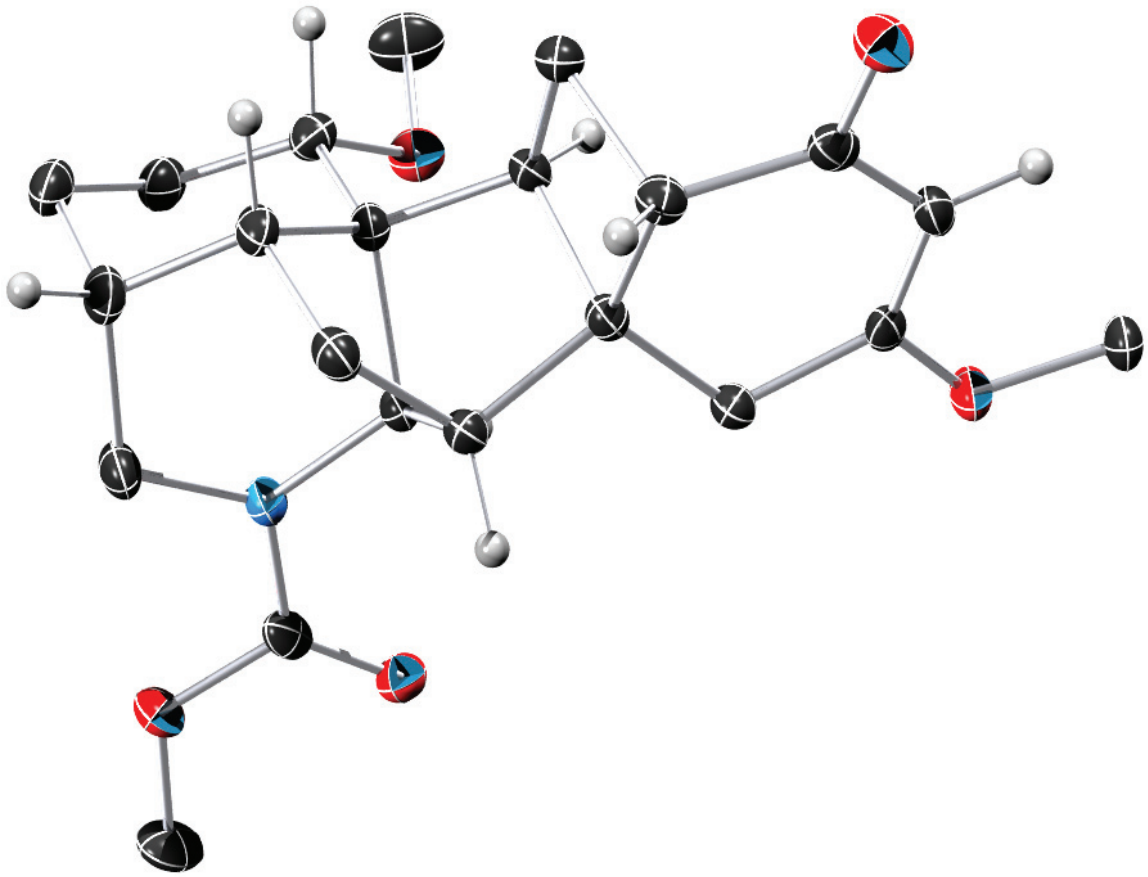

Figure 2.11: POV-Ray/ORTEP rendering of photocycloadduct **2.51** with ellipsoids at 50% probability. Only tertiary and vinylic hydrogens are shown for clarity.

Table 2.2: Crystal data and structure refinement for **2.51**.

Cambridge Crystallographic Data Center	1563394	
Empirical formula	C22 H29 N O5	
Formula weight	387.46	
Temperature	100(2) K	
Wavelength	0.71073 Å	
Crystal system	Triclinic	
Space group	P -1	
Unit cell dimensions	a = 7.8766(6) Å	α = 97.716(4)°
	b = 8.5007(7) Å	β = 92.753(4)°
	c = 14.5992(12) Å	γ = 101.587(4)°
Volume	946.09(13) $Å^3$	
Z	2	
Density (calculated)	1.360 Mg/m^3	
Absorption coefficient	0.096 mm^{-1}	
F(000)	416	
Crystal size	0.130 x 0.100 x 0.080 mm^3	
Theta range for data collection	1.412 to 25.380°	
Index ranges	-9<=h<=9, -10<=k<=10, -17<=l<=17	
Reflections collected	6705	
Independent reflections	6705 [R(int) = ?]	
Completeness to theta = 25.000°	99.3%	
Absorption correction	Semi-empirical from equivalents	
Max. and min. transmission	0.745 and 0.696	
Refinement method	Full-matrix least-squares on F^2	
Data / restraints / parameters	6705 / 0 / 257	
Goodness-of-fit on F^2	1.143	
Final R indices [I>2sigma(I)]	R1 = 0.0403, wR2 = 0.1112	
R indices (all data)	R1 = 0.0470, wR2 = 0.1139	
Extinction coefficient	n/a	
Largest diff. peak and hole	0.216 and -0.232 $e.Å^{-3}$	

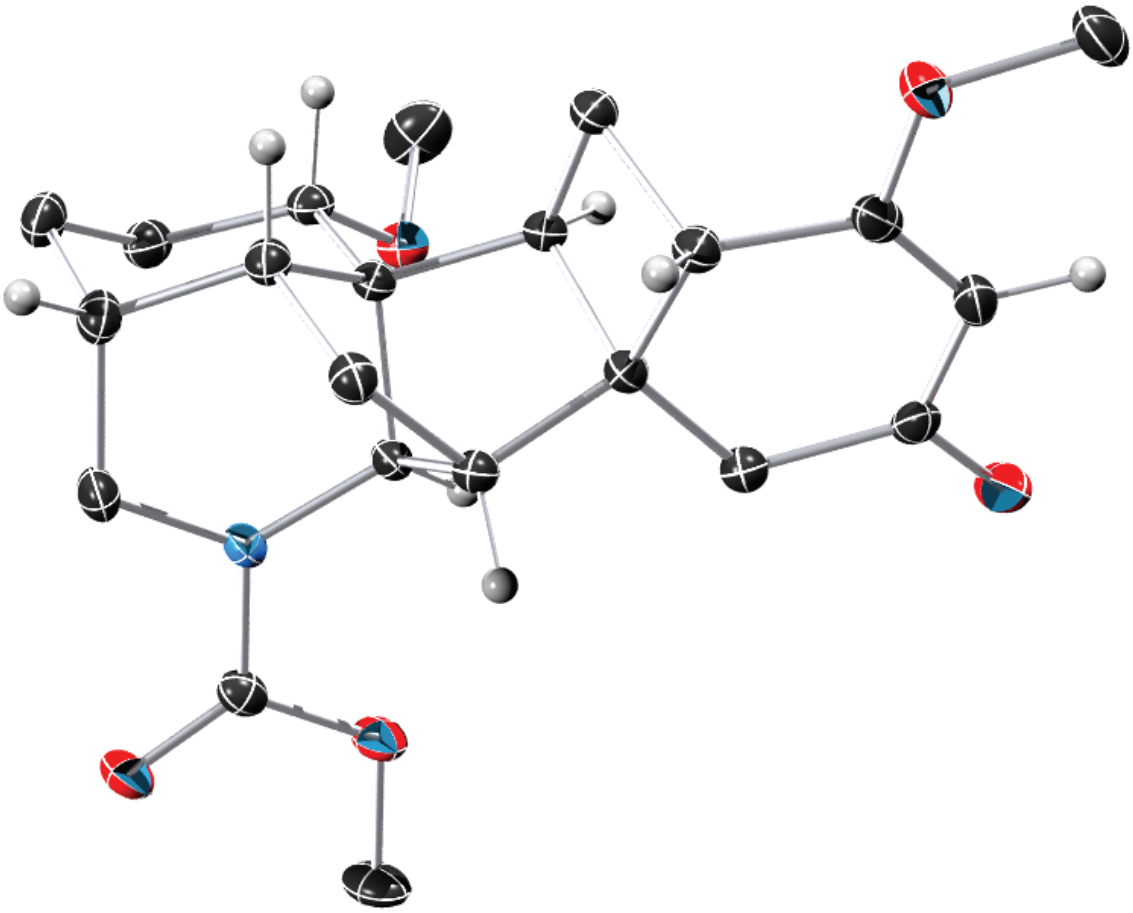

Figure 2.12: POV-Ray/ORTEP rendering of photocycloadduct **2.52** with ellipsoids at 50% probability. This compound crystallized as a dimer. Its monomeric form is depicted, with only tertiary and vinylic hydrogens are shown for clarity.

Table 2.3: Crystal data and structure refinement for **2.52**.

Cambridge Crystallographic Data Center	1563395
Empirical formula	C44 H58 N2 O10
Formula weight	774.92
Temperature	100(2) K
Wavelength	1.54178 Å
Crystal system	Triclinic
Space group	P -1
Unit cell dimensions	a = 8.7054(3) Å α = 79.4130(10)°
	b = 9.5129(3) Å β = 88.0490(10)°
	c = 11.7668(4) Å γ = 78.9590(10)°
Volume	940.13(5) $Å^3$
Z	1
Density (calculated)	1.369 Mg/m^3
Absorption coefficient	0.785 mm^{-1}
F(000)	416
Crystal size	0.110 x 0.060 x 0.050 mm^3
Theta range for data collection	3.822 to 68.215°
Index ranges	-7<=h<=10, -11<=k<=11, -14<=l<=14
Reflections collected	16301
Independent reflections	3363 [R(int) = 0.0240]
Completeness to theta = 67.000°	98.0%
Absorption correction	Semi-empirical from equivalents
Max. and min. transmission	0.817 and 0.763
Refinement method	Full-matrix least-squares on F^2
Data / restraints / parameters	3363 / 0 / 256
Goodness-of-fit on F^2	1.043
Final R indices [I>2sigma(I)]	R1 = 0.0360, wR2 = 0.0939
R indices (all data)	R1 = 0.0372, wR2 = 0.0950
Extinction coefficient	n/a
Largest diff. peak and hole	0.284 and -0.255 $e.Å^{-3}$

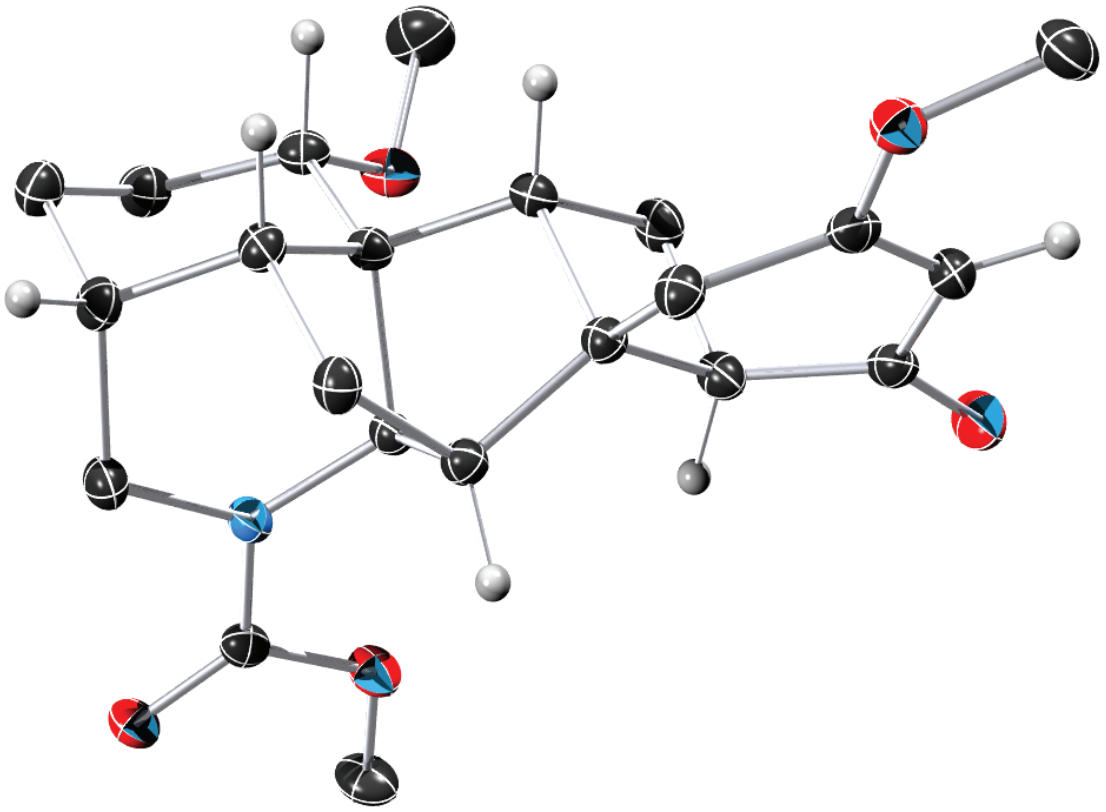

Figure 2.13: POV-Ray/ORTEP rendering of photocycloadduct **2.54** with ellipsoids at 50% probability. Only tertiary and vinylic hydrogens are shown for clarity.

Table 2.4: Crystal data and structure refinement for **2.54**.

Cambridge Crystallographic Data Center	1563396
Empirical formula	C22 H29 N O5
Formula weight	387.46
Temperature	100(2) K
Wavelength	1.54178 Å
Crystal system	Monoclinic
Space group	P 21/c
Unit cell dimensions	a = 11.9228(11) Å α = 90°
	b = 18.5020(17) Å β = 94.417(3)°
	c = 8.6469(8) Å γ = 90°
Volume	1901.8(3) $Å^3$
Z	4
Density (calculated)	1.353 Mg/m^3
Absorption coefficient	0.776 mm^{-1}
F(000)	832
Crystal size	0.100 x 0.080 x 0.080 mm^3
Theta range for data collection	3.718 to 68.303°
Index ranges	-14<=h<=14, -22<=k<=22, -10<=l<=6
Reflections collected	27979
Independent reflections	3431 [R(int) = 0.0257]
Completeness to theta = 67.000°	98.3%
Absorption correction	Semi-empirical from equivalents
Max. and min. transmission	0.753 and 0.704
Refinement method	Full-matrix least-squares on F^2
Data / restraints / parameters	3431 / 0 / 256
Goodness-of-fit on F^2	1.031
Final R indices [I>2sigma(I)]	R1 = 0.0348, wR2 = 0.0897
R indices (all data)	R1 = 0.0359, wR2 = 0.0907
Extinction coefficient	n/a
Largest diff. peak and hole	0.274 and -0.209 $e.Å^{-3}$

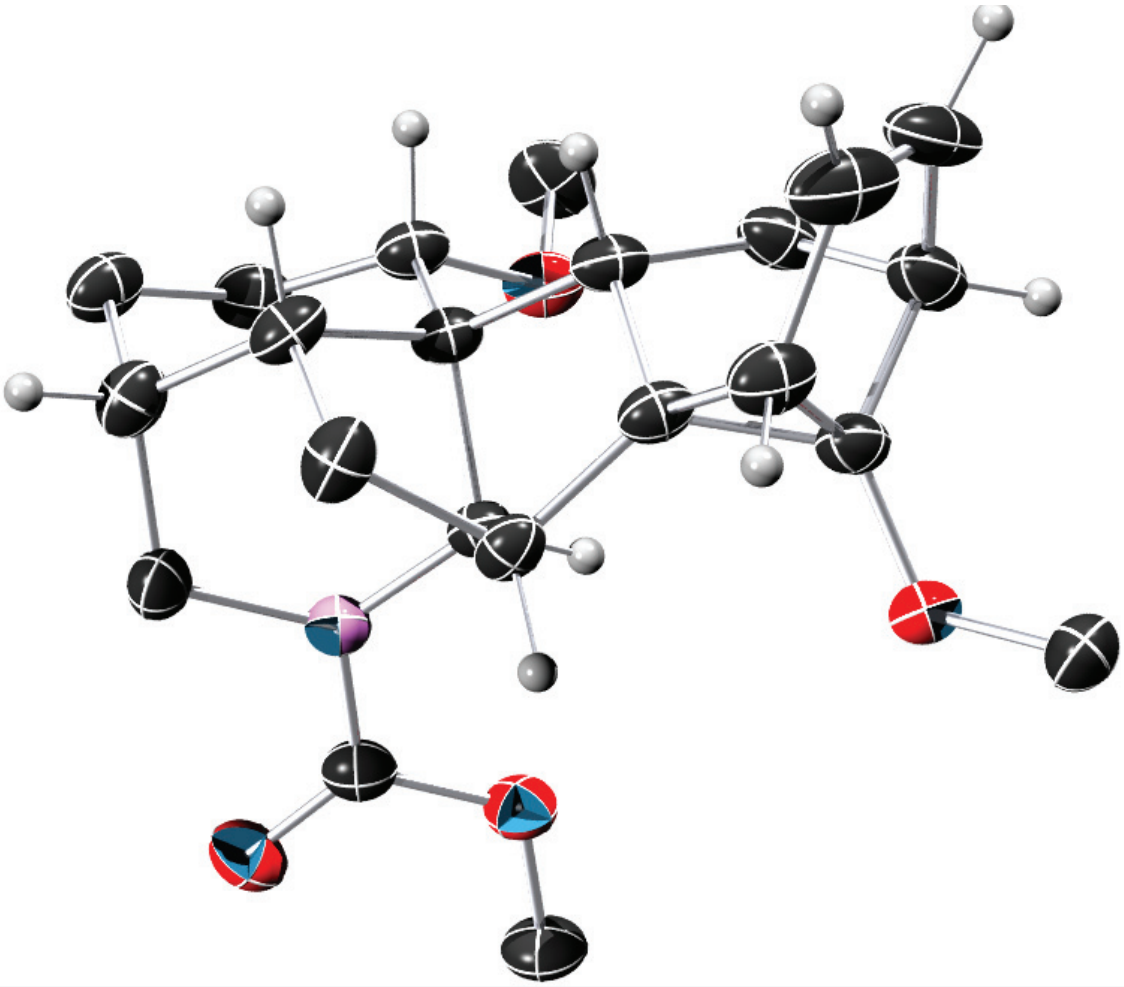

Figure 2.14: POV-Ray/ORTEP rendering of photocycloadduct **2.60** with ellipsoids at 50% probability. Only tertiary and vinylic hydrogens are shown for clarity.

Table 2.5: Crystal data and structure refinement for **2.60**.

Cambridge Crystallographic Data Center	1563404
Empirical formula	C22 H29 N O4
Formula weight	371.46
Temperature	100(2) K
Wavelength	1.54178 Å
Crystal system	Triclinic
Space group	P -1
Unit cell dimensions	a = 10.1894(4) Å α = 69.530(2)°
	b = 14.3413(5) Å β = 89.570(2)°
	c = 14.4462(5) Å γ = 78.333(2)°
Volume	1932.25(12) $Å^3$
Z	4
Density (calculated)	1.277 Mg/m^3
Absorption coefficient	0.701 mm^{-1}
F(000)	800
Crystal size	0.040 x 0.030 x 0.020 mm^3
Theta range for data collection	3.273 to 68.333°
Index ranges	-12<=h<=12, -13<=k<=16, -17<=l<=17
Reflections collected	45657
Independent reflections	6938 [R(int) = 0.0425]
Completeness to theta = 67.000°	98.6%
Absorption correction	Semi-empirical from equivalents
Max. and min. transmission	0.929 and 0.818
Refinement method	Full-matrix least-squares on F^2
Data / restraints / parameters	6938 / 0 / 493
Goodness-of-fit on F^2	1.041
Final R indices [I>2sigma(I)]	R1 = 0.0682, wR2 = 0.1896
R indices (all data)	R1 = 0.0865, wR2 = 0.2049
Extinction coefficient	n/a
Largest diff. peak and hole	0.437 and -0.247 $e.Å^{-3}$

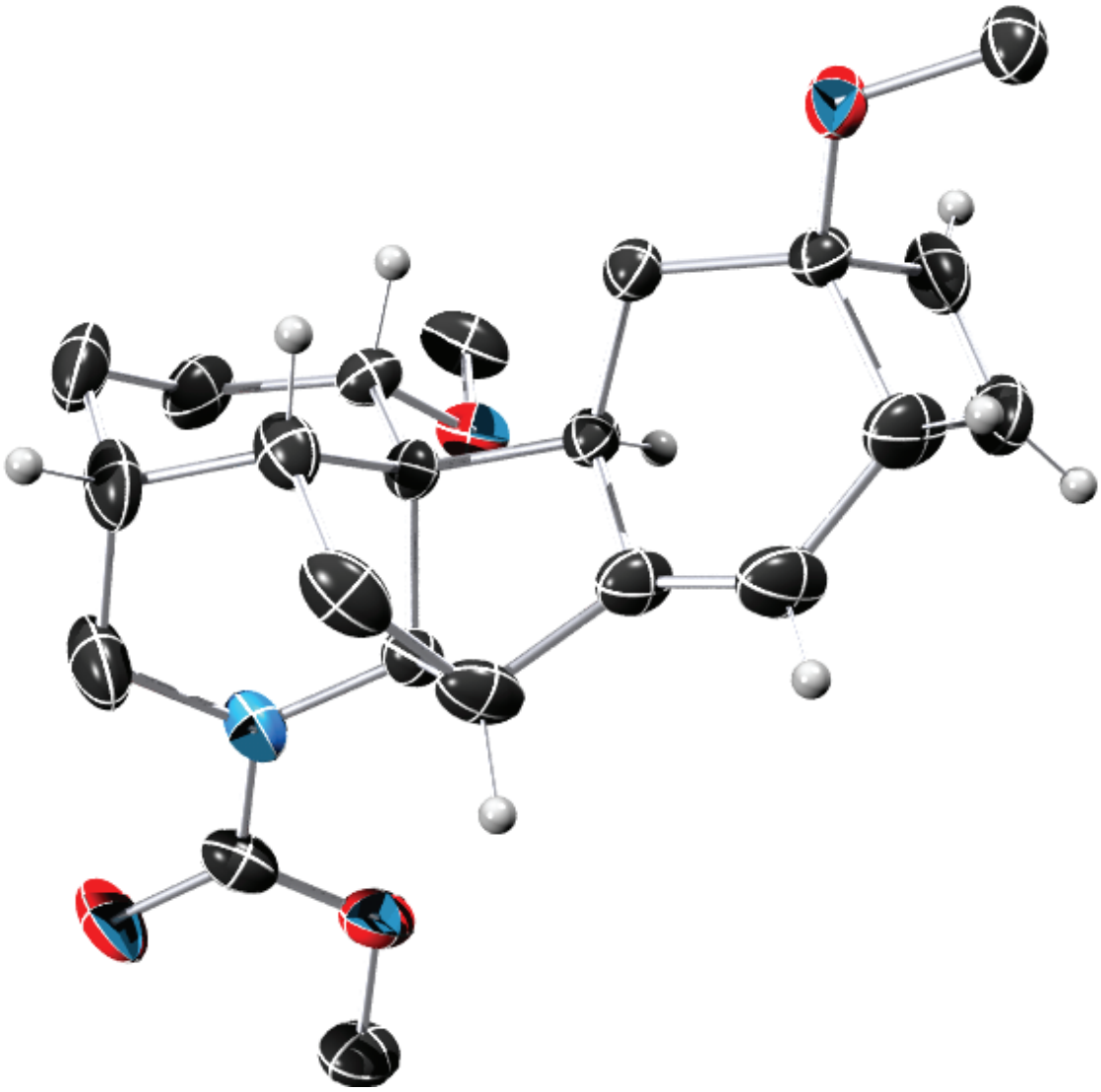

Figure 2.15: POV-Ray/ORTEP rendering of photocycloadduct **2.63** with ellipsoids at 50% probability. Only tertiary and vinylic hydrogens are shown for clarity.

Table 2.6: Crystal data and structure refinement for **2.63**.

Cambridge Crystallographic Data Center	1563397
Empirical formula	C22 H29 N O4
Formula weight	371.46
Temperature	100(2) K
Wavelength	1.54178 Å
Crystal system	Orthorhombic
Space group	P b c a
Unit cell dimensions	a = 7.0860(5) Å α = 90°
	b = 16.5585(10) Å β = 90°
	c = 32.2302(2) Å γ = 90°
Volume	3781.7(4) $Å^3$
Z	8
Density (calculated)	1.305 Mg/m^3
Absorption coefficient	0.716 mm^{-1}
F(000)	1600
Crystal size	0.040 x 0.030 x 0.010 mm^3
Theta range for data collection	2.742 to 68.524°
Index ranges	-8<=h<=8, -19<=k<=19, -38<=l<=37
Reflections collected	54271
Independent reflections	3470 [R(int) = 0.0651]
Completeness to theta = 67.000°	100.0%
Absorption correction	Semi-empirical from equivalents
Max. and min. transmission	0.929 and 0.824
Refinement method	Full-matrix least-squares on F^2
Data / restraints / parameters	3470 / 0 / 247
Goodness-of-fit on F^2	1.032
Final R indices [I>2sigma(I)]	R1 = 0.0784, wR2 = 0.2156
R indices (all data)	R1 = 0.0937, wR2 = 0.2289
Extinction coefficient	n/a
Largest diff. peak and hole	0.476 and -0.304 $e.Å^{-3}$

Chapter 3

Synthesis of analogs of aconitine-type diterpenoid alkaloids*

Aconitine (**1.3**, Figure 3.1) and lappaconitine (**1.5**) elicit contrasting effects upon interaction with human voltage-gated sodium (Na_V) channels; aconitine exposure induces persistent activation of neurons leading to cardiac arrest, whereas lappaconitine leads to blockage of acute

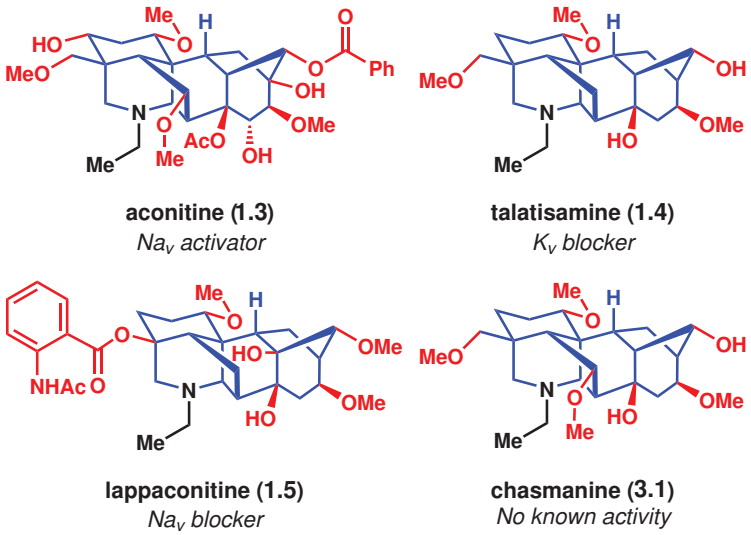

Figure 3.1: Selected examples of diterpenoid alkaloids.

pain signals.[2,3] These two related diterpenoid alkaloids exemplify the disparate effects of this class of natural products on voltage-gated ion channels.[4–7] Given that voltage-gated sodium (Na_V), calcium (Ca_V), and potassium (K_V) channels regulate biophysical responses across the nervous, circulatory, and muscular systems, the ability to selectively target voltage-gated sodium ion channels would have significant implications for the treatment of epilepsy, chronic pain, and myriad other channelopathies.[8]

*Reproduced in part with permission from Doering, N. A.; Kou, K. G. M.; Norseeda, K.; Lee, J. C.; Marth, C. J.; Gallego, G. M.; Sarpong R. *J. Org. Chem.* **2018**, *83*, 12911–12920.[1] Copyright 2018 American Chemical Society.

Diterpenoid alkaloids have long been recognized for their utility in combating channelopathies, appearing in traditional Chinese medicine as treatments for pain and cardiovascular disease.[7] Today, lappaconitine (**1.5**) is approved and marketed in China and Russia for pain relief and arrhythmia treatment,[9] effects which likely stem from lappaconitine blocking Na_V channels.[10] On the other hand, aconitine (**1.3**) is a highly toxic Na_V channel activator reported to be lethal to humans in doses as low as 1–2 mg.[11] Talatisamine (**1.4**) is a known K_V channel blocker,[12] whereas chasmanine (**3.1**) has no known ion channel activity.[5] This modulation of sodium channels by aconitine and lappaconitine is of interest to the pharmaceutical industry due to the possibility of harnessing this interaction to develop non-opioid pain drugs.[13,14]

3.1 Diterpenoid alkaloid modulation of sodium channels

3.1.1 Structure and function of sodium channels

Voltage-gated sodium (Na_V) channels are responsible for initiating action potentials in nerve, muscle, and other excitable cells, opening and closing in response to changes in the voltage gradient across the cell membrane.[15,16] To fulfill this role, Na_V channels activate rapidly upon sensing a sufficient decrease in membrane potential (depolarization), allowing Na^+ to flow into the cell, then inactivate within 1–2 ms, traits which are crucial for fast unidirectional signal propagation (Figure 3.2).[17,18] Electrical signaling then terminates through activation of K_V channels, which carry K^+ out of the cell to re-establish the original charge gradient across the membrane (repolarization). This leads to temporary hyperpolarization of the cell, which causes Na_V channels to return to their closed state prior to restoration of the resting potential.[18,19]

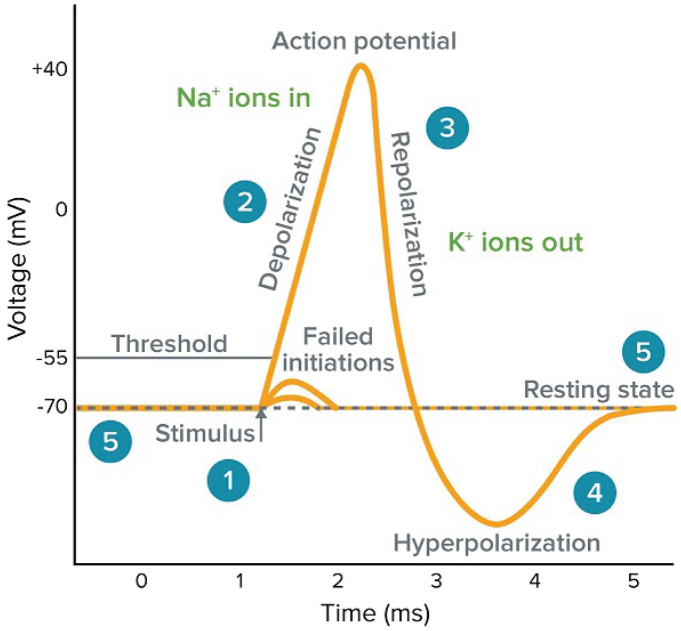

Figure 3.2: Graphical representation of the stages of an action potential. Figure reproduced from Molecular Devices, LLC.[20]

Each Na_V channel consists of a variable α subunit co-expressed with β subunits that are be-

lieved to play a role in the localization of the proteins within excitable cells, as well as modulate the kinetics and voltage-dependence of channel activation and inactivation.[16] As $Na_V\beta$ associations with α subunits are promiscuous[21] and it has been shown that only the α subunit must be encoded in order to express functional Na_V channels,[22–24] the remainder of this discussion will focus on the different sodium channel α subunits, which are expressed at different levels in various excitable tissues.[25] This sodium channel family consists of nine voltage-gated isoforms (Na_V channels), and one that is instead involved in salt sensing[26] (Na_X). $Na_V1.1$–$Na_V1.3$ and $Na_V1.6$ are the dominant sodium channels in the central nervous system. $Na_V1.4$ dominates in skeletal muscle while $Na_V1.5$ is the primary sodium channel in the heart. $Na_V1.7$–$Na_V1.9$ are predominantly located in the peripheral nervous system. $Na_V1.7$, in particular, has been identified as a promising pain target since it has been genetically validated in humans; loss-of-function mutations cause congenital insensitivity to pain without otherwise causing cognitive or motor disfunction,[27,28] whereas gain-of-function mutations are associated with hypersensitivity to pain.[29,30]

Na_V channels, like voltage-gated calcium (Ca_V) and potassium (K_V) channels, consist of 24 transmembrane segments that are split into four homologous domains (D1–D4) and, together, form a central ion-conducting pore and four voltage-sensing domains (Figure 3.3).[18,19] Within each of these domains, four transmembrane α-helices (S1–S4) constitute a voltage sensor and the remaining two (S5–S6) contribute to the central pore. Mutagenesis studies have shown that local anaesthetics bind to—and consequently block—the central pore of Na_V channels through amino acid residues in the S6 segments of D1, 3 and 4.[31–35] Large or hydrophilic drugs must access this site by entering the channel through the intracellular end of the pore. As such, these drugs may only bind to an open channel. Interestingly, there are also four fenestrations, or "pore portals", each controlled by a single residue (F203 in Na_VAb,[36†] F1764 in rat $Na_V1.2$[31]), that lead sideways through the lipid phase of the membrane, providing a way for hydrophobic drugs to bind the resting state of the channel.[36]

There exist at least six additional sites at which small molecule and peptide toxins bind to Na_V channels.[37] Site 1 sits at the extracellular end of the pore, with bound ligands directly blocking Na^+ from entering the channel. Site 2, situated near the local anaesthetic binding site, consists of residues (in S6 of D1/D4) deep within the pore. Its ligands include lipophilic toxins, such as batrachotoxin and veratridine, which bind to the open state of the channel and induce persistent activation. Studies on rat $Na_V1.4$ channels have shown I433, N434, L437, F1579, and N1584 to be key residues in this receptor, residue-to-lysine mutants thereof causing maximal disruption of toxin binding.[38,39] Sites 3 and 6, located at the extracellular end of the D4 voltage-sensor, typically bind toxins that reduce the rate of inactivation of an open channel. In contrast, site 4 (on the extracellular end of the D2 voltage-sensor) binds toxins that alter the threshold required for Na_V activation. Similarly, site 5, a relatively large region consisting of portions of S5 from D1 and S6 from D4, is known to bind small molecules, such as brevetoxin and the ciguatoxins, that impede activation by shifting the activation threshold of a channel to less polarized potentials.

Aconitine and other related diterpenoid alkaloids are believed to bind at site 2. Previous studies on aconitine have shown it to be a Na_V channel activator.[7,40] However, these studies largely

[†] Na_VAb is a bacterial voltage-gated sodium channel from *Arcobacter butzleri*. This channel functions similarly to its human counterparts, but is a homotetramer rather than a pseudotetramer.

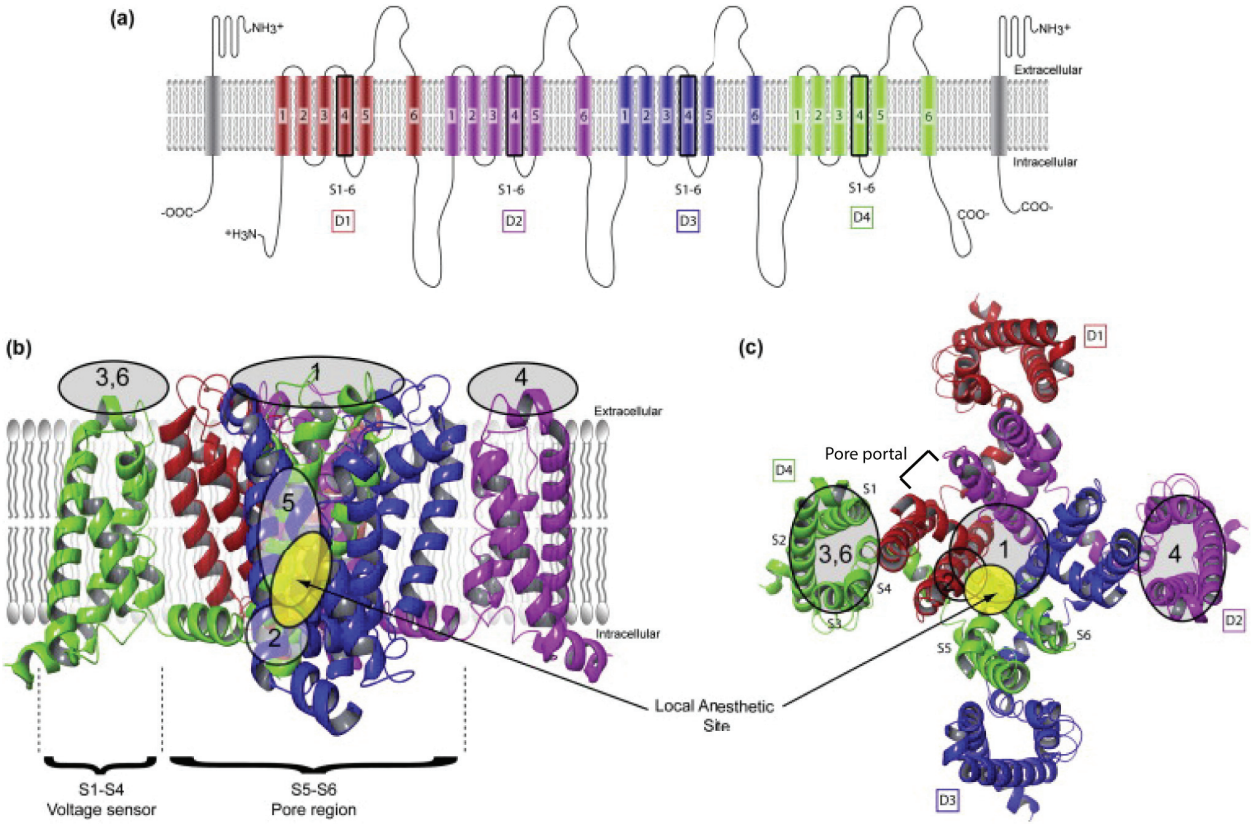

Figure 3.3: (a) Na_V channel structural topology. Domains D1–D4 are represented in different colors while β subunits are shown in gray. Transmembrane segments (S1–S6) are labelled together with connecting loops. (b) Side view of voltage-gated Na_VAb channel with highlighted toxin binding sites (1–6) and local anesthetic binding site (c) Top view. Figure adapted from Bagal et al.[37]

predate the ability to selectively study individual isoforms of sodium channels. As such, further studies would be needed in order to determine the specific effects of aconitine on different isoforms. Early studies on lappaconitine were similarly hindered and, once lappaconitine entered the clinic as an analgesic, subsequent studies largely focused on its pharmacokinetics and its efficacy as a combination therapy with opioid drugs.[41] Interested in a side-by-side comparison of the activity of diterpenoid alkaloids on specific Na_V isoforms, we began a collaboration with Dr. David Hackos in the neuroscience department at Genentech.

3.1.2 Electrophysiology studies with aconitine and lappaconitine

We began by investigating the effect of aconitine on activation of human $Na_V1.7$ channels. In this study, we looked at wild-type (WT) channels, as well as two single-point mutants. The first mutation, F1737K, is analogous to one that has been previously shown to disrupt binding to site 2 in rat $Na_V1.4$ channels.[39] The second mutation, I848T, is a mutation that causes inherited erythromelalgia in humans.[29]

To understand whether aconitine modifies the activation of the $Na_V1.7$ channel, we used a holding voltage of –80 mV, a short 30 msec pre-pulse to –120 mV, and a 200 msec pulse to voltages ranging from –80 mV to +60 mV in steps of 5 mV at a rate of once per 500 msec. A graphical representation of a voltage protocol and the trace showing the resultant current across the cell membrane is shown in Figure 3.4. Sodium flow through an open channel registers as negative

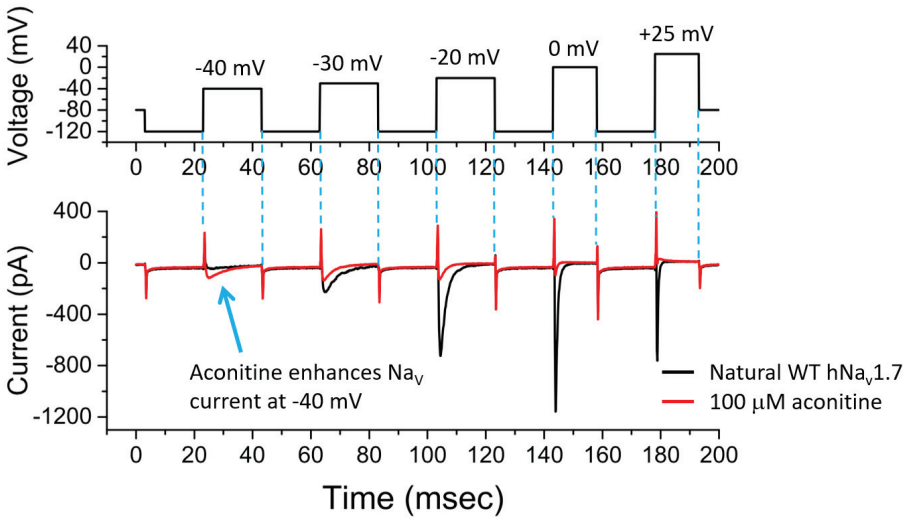

Figure 3.4: A graphical representation of a voltage protocol (top) and the corresponding traces observed (bottom) when WT $Na_V1.7$ channels were exposed to either a vehicle (black) or 100 µM aconitine solution (red).

current. The amplitude of this current correlates to the number of channels through which Na^+ is flowing. Comparing the traces for cells in 0 vs 100 µM aconitine solution, one sees that aconitine enhances current at –40 mV, indicating that it causes channels to open at more negative (hyperpolarized) voltages than they would naturally. The minima of the peaks from activation traces were plotted as a function of voltage to give an activation IV curve (Figure 3.5). Current for each trace was normalized based on the maximum current amplitude, as measured upon perfusion with the vehicle solution containing 0.1% DMSO (see 0 µM traces), to account for

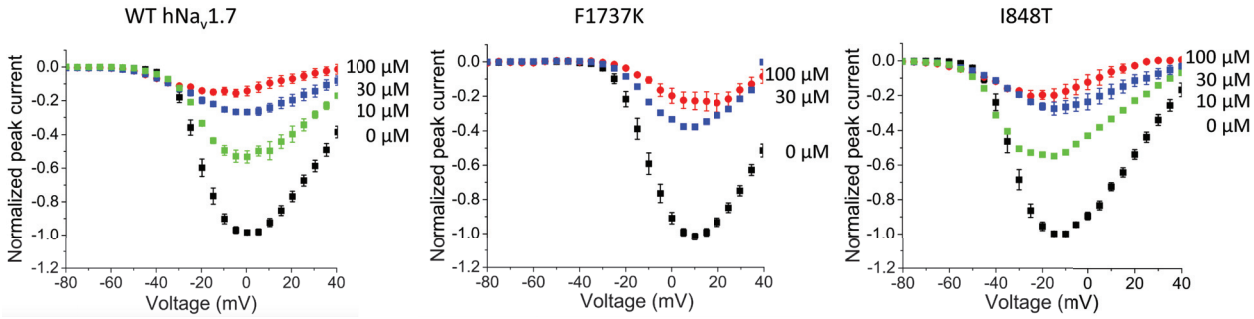

Figure 3.5: Dose-dependence of aconitine effect on WT (left), F1737K (center), and I848T (right) channels. Curves are shown for cells perfused with vehicle (black) or solutions of aconitine in 10 (green), 30 (blue), or 100 (red) µM concentrations.

differences in the number of channels expressed by the patched cell.

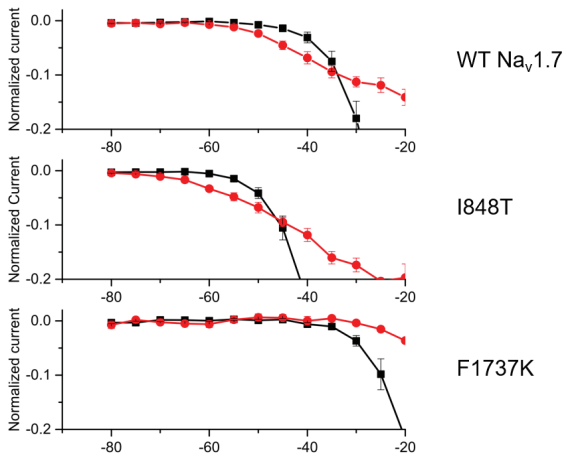

Figure 3.6: Enhancing effects of aconitine at hyperpolarized potentials. Curves in red represent cells perfused with 100 μM aconitine. Curves in black represent those perfused with the vehicle.

In this way, we obtained a curve showing the measured voltage-dependence of activation of the $Na_V1.7$ channels. Comparing results using a variety of concentrations of aconitine, we saw that aconitine exhibits a dose-dependent blocking effect on WT $Na_V1.7$. Similar extents of block were observed with both the F1737K and I848T mutant channels. Looking more closely at the effect of aconitine near the resting potential of the cells (ca. –60 mV for cells expressing each of the three channels), we saw why aconitine is considered to activate Na_V channels (Figure 3.6): it shifted the voltage-dependence of activation in WT channels by –15 mV, effectively lowering the threshold required to trigger an action potential (see Figure 3.2). This shift in the voltage-dependence was ablated in the F1737K mutant, indicating that F1737 is likely involved in the binding of aconitine to site 2. However, the fact that aconitine still blocked the mutant channels indicated that there are additional residues involved. This is consistent with previous studies on another site 2 ligand, veratridine, which similarly retained its ability to block—but not otherwise alter the behavior of—Na_V channels with this mutation.[39]

It should be noted that the F1737K mutation itself shifts the voltage-dependence of the channel by +10 mV without altering the shape of the activation IV curve. The I848T mutation also shifts the voltage-dependence of the channel. This shift of –10 mV relative to the WT channels is the reason why this mutation causes an extreme pain disorder in the people who have it.[30] Aconitine further shifted the voltage-dependence of these channels by –15 mV, as in the WT channels. This additive effect means that non-zero current is measured at the resting potential of the cells and is why transgenic mice expressing human $Na_V1.7$ (I848T) are used to test potential therapeutics for pain. Injection of aconitine into the paw of these mice elicits a strong pain response, which can be measured by counting how many times the mouse flinches in 5 min. In contrast, mice expressing WT human $Na_V1.7$ do not experience pain upon aconitine injection.

To measure steady-state inactivation of the channels, we started at a holding voltage of –120 mV to bring the channels fully to the closed state. We then pulsed to 0 mV while reducing the holding voltage from –120 mV to +30 mV in steps of 5 mV at a rate of once per 5 sec. As with activation, aconitine shifted the voltage-dependence of WT channel inactivation by –15 mV (Figure 3.7). A similar shift toward hyperpolarized potentials was observed with I848T mutant channels, but not with F1737K channels. We then investigated the effect of lappaconitine on human $Na_V1.7$ channels. In doing so, we found that lappaconitine blocks WT channels (Figure 3.8). However, unlike aconitine, lappaconitine does not shift the voltage-dependence of activation. This blocking effect is knocked out in F1737K channels.

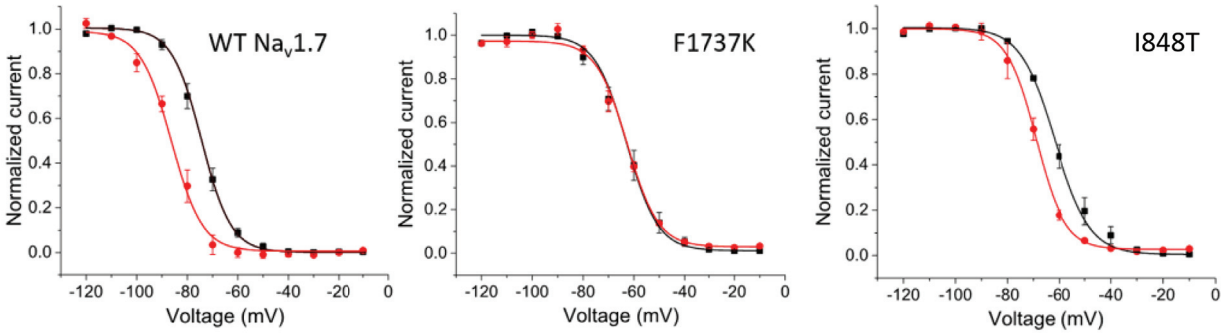

Figure 3.7: Effect of aconitine on steady-state inactivation of WT (left), F1737K (center), and I848T (right) channels. Curves in red represent cells perfused with 100 µM aconitine. Curves in black represent those perfused with the vehicle.

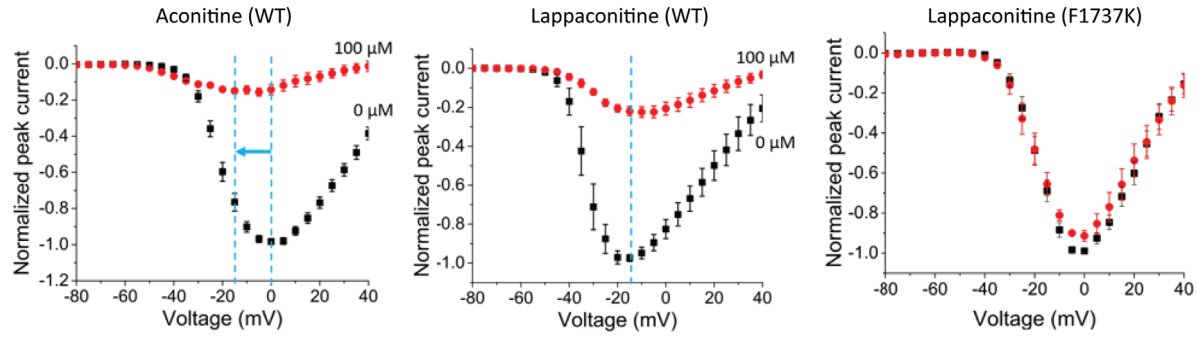

Figure 3.8: Comparison of aconitine effect on WT channels (left) to that of lappaconitine on WT (center) and F1737K (right) channels. Curves in red represent cells perfused with 100 µM of additive. Curves in black represent those perfused with the vehicle.

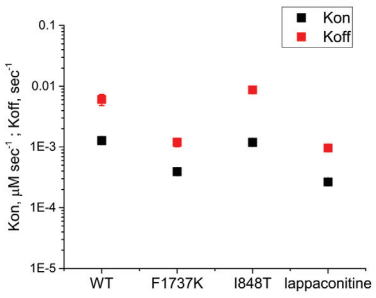

Figure 3.9: Comparison of the affinities and kinetics of Na$_V$1.7 binding by aconitine and lappaconitine.

Finally, we compared the kinetics of binding for aconitine and lappaconitine and found that, while aconitine and lappaconitine have similar affinity (~3–6 µM) for the WT channels, binding of lappaconitine is slower than that of aconitine (Figure 3.9). Interestingly, we observed that binding of aconitine to the F1737K mutant channels was also slower than to the WT channels. Aconitine's binding affinity for Na$_V$1.7 was not significantly altered by either the F1737K or I848T mutations.

Overall, we found that both aconitine and lappaconitine blocked Na$_V$ channels. However, aconitine additionally shifted the voltage-dependence of both activation and steady-state inactivation of the channels, where lappaconitine did not. In both cases, we found the on- and off-rates of the molecules to be very slow. This may be due to the steric bulk of the diterpenoid alkaloids, as has been postulated for another site 2 binder, batrachotoxin. Another study has since been published by Gan and Gao, corroborating the major findings of this work.[42] In that work, the authors found that pre-incubation of cells with a solution of lappaconitine en-

hanced lowered the measured IC_{50} for blocking, suggesting that our observed results may not have captured the full potential for diterpenoid alkaloids as sodium channel modulators. Still, these studies highlighted the differences in the biological activity of these structurally related molecules.

3.1.3 Structure–activity relationships of aconitine-type alkaloids

The pronounced impact of changes to the periphery of these pseudoalkaloids have made the structural origin of their biological activity a matter of interest for over a century. Among the first to explore the structure–activity relationships (SAR) of the diterpenoid alkaloids were Cash and Dunstan, who compared aconitine to two hydrolyzed derivatives, aconine and 14-*O*-benzoylaconine.[43] More recently, Tursunkhodzhaeva and co-workers probed these relationships with a larger set of isolated diterpenoid alkaloids and their derivatives.[44,45] This approach led to the identification of some key substituents on aconitine-type and lappaconitine-type natural products that imbue them with certain biological activities, but this study was limited by its inability to systematically vary the peripheral substituents. Not all combinations of substitution patterns are present in the known diterpenoid alkaloids and derivatization has been limited to hydrolysis of amides and to acylation—or, in one case, methylation—of free hydroxy groups. Furthermore, lack of site selectivity for acylation in the presence of multiple hydroxy groups has limited the synthesis of derivatives.

3.2 Analog design and retrosynthesis

Our lab has developed strategies to access several C_{18}-, C_{19}-, and C_{20}-diterpenoid alkaloids (see Section 2.2).[46–48] While these efforts yielded enough material for preliminary biological assays, the syntheses are relatively long and opportunities for wide-ranging introduction of oxygenation have been limited. In order to overcome these challenges, we explored a synthesis approach to aconitine-type analogs that should be more amenable to systematic variation of oxygenation patterns.

In designing these analogs, we generated a set of key considerations on the basis of which structural features are conserved and which are varied across this family of natural products (Figure 3.10). Previous SAR studies have indicated that variation in hydroxylation along the D

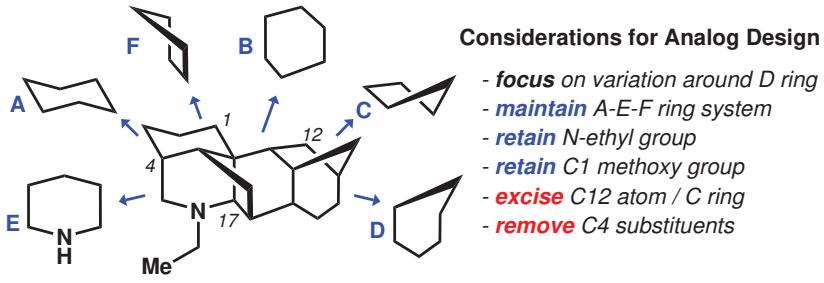

Figure 3.10: Ring labeling and analog design considerations.

ring has a drastic impact on the biological activity of aconitine-type diterpenoid alkaloids.[44,45]

The primary emphasis of our design strategy thus focuses on varying the substitution pattern around this ring, while maintaining selected features common to the aconitine-type natural products. To this end, our analogs were designed to retain the A–E–F ring carbon framework, which—unlike the [3.2.1] bicycle comprised by the C and D rings—is conserved across the majority of the atisane-derived alkaloids. The *N*-ethyl group and the C1 methoxy group are also highly conserved within this family and thus maintained in our designs for analogs. C4 substituents, however, differ greatly between aconitine- and lappaconitine-type diterpenoid alkaloids. To facilitate a thorough exploration of the importance of the D ring substitution patterns, the C4 substituents were excluded from our present study, although these C4 substituents may be incorporated at a later stage using previously established strategies.[48] Additionally, diterpenoid alkaloids bearing a [2.2.2] bicycle as their CD ring system, a change which significantly alters the conformation of the D ring compared to that of the aconitine system, are also known to modulate ion channels.[49] Therefore, our initial studies aimed to excise C12 as this structural simplification would allow more rapid access to natural product-inspired analogs that probe the tolerability of the binding site to modulations in polarity, shape and spatial orientation in the D ring.

On the basis of these considerations, we targeted analogs, such as pentacycle **3.2** and spirocycle **3.3** (Scheme 3.1). Each of these designed targets could ultimately arise from aldehyde **3.4**

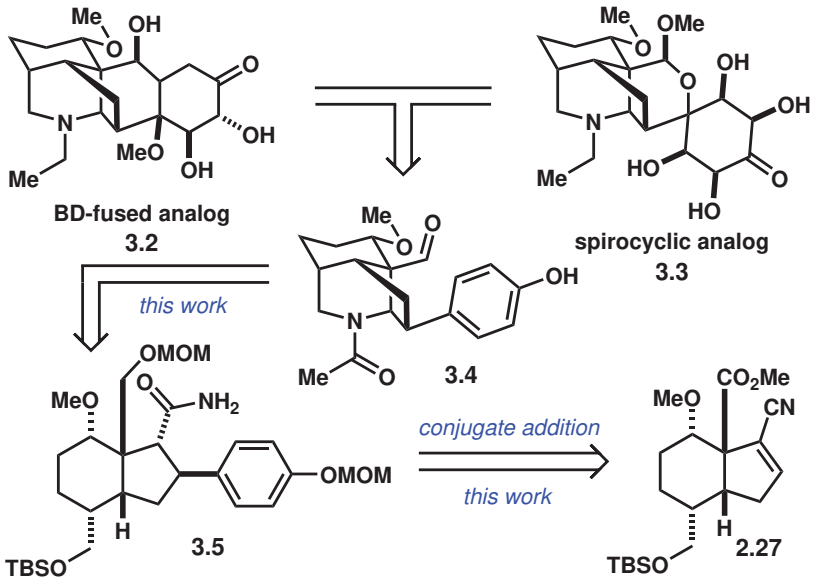

Scheme 3.1: Retrosynthesis of two classes of aconitine analogs.

through oxidative dearomatization strategies. Aldehyde **3.4**, in turn, could be taken back to primary amide **3.5**, which itself could be derived from known vinyl nitrile **2.27**.[46] In the forward sense, this route would begin with a conjugate addition of aryl nucleophiles into **2.27**. Additional analogs could be accessed through variation of the nucleophile in this step, resulting in differing oxygenation patterns on the aryl ring prior to oxidative dearomatization.

3.3 Oxygenation pattern variation through conjugate addition

Our initial approach toward these simplified analog scaffolds was to effect a Hayashi-type[50] Rh-catalyzed conjugate addition of boronate esters into vinyl nitrile **2.27**, following previously successful protocols from our laboratories.[46,48] However, this reaction proved to be sensitive to the electronics and substitution patterns of the arene nucleophiles. We thus set out to find an alternative method to effect this conjugate addition.

While the Rh-catalyzed method worked well for the two previously published substrates (Table 3.1, **3.6a** and **3.6b**), the same was not true when the boronate derived from MOM-protected *p*-bromophenol was used (see **3.6d**, Method A). In the latter case, low conversion (67% recovery of nitrile **2.27**) was observed. To address the poor reactivity of many substituted aryl boronate esters in the Rh(I)-catalyzed conjugate addition, we investigated an organocuprate-based strategy using copper(I) iodide and Grignard reagents (Method B). While the conditions that were initially selected followed related precedent involving addition of alkyl cuprates into simple—and often highly activated—vinyl nitriles,[51] high yields using structurally complex vinyl nitrile **2.27** were only realized after extensive optimization.

3.3.1 Development of copper-mediated conjugate addition

Precedent for this transformation was largely limited to conjugate additions into sterically unencumbered vinyl nitriles, many of which were activated by adjacent electron withdrawing groups.[51] Knowing that our substrate lacked such activating substituents, we decided to first remove the ester group of **2.27** (through reduction to the aldehyde and subsequent Wittig olefination using $Ph_3P{=}CH_2$), leaving the vinyl nitrile itself as the only electrophilic group on the molecule. Treatment of this compound with either aryl Grignard or Gilman reagents proved ineffective, both returning only starting material. Reductive Heck coupling was equally unsuccessful. However, Normant reagents—formed through the combination of Cu(I) salts with Grignard reagents—were featured in a report from Liu and co-workers for 1,4-addition into unsaturated cyclic α-cyanoketones.[52] Despite the lack of precedent for using these reagents on substrates lacking a carbonyl, these reagents seemed to add into more sterically encumbered substrates than other cuprates.

Preliminary studies showed that bromoanisoles could be added into our nitrile in a conjugate fashion using 5 equiv of a 1:1 CuCl:aryl Grignard reagent in THF.[53] However, no conversion was achieved with more sterically encumbered arenes, even upon heating of the reaction mixture at reflux. Gratifyingly, these successes also translated to the ester-containing vinyl nitrile (**2.27**).[54] Building on this initial hit, we screened Cu(I) salts, reaction temperature, and equivalents of both the copper and the Grignard reagents. Of the salts tested, CuCl and CuI gave the best results. CuI was chosen for use in further studies due to the greater stability of the reagent under ambient conditions. The ratio of copper and Grignard reagent used to form the Normant reagents also proved to be particularly important. Normant reagents exist as complex aggregates of the formula $Cu_xMg_yR_{(x+2y)}$ in THF solution, the ratio x:y varying not only with the ratio of CuI:RMgBr added, but also with temperature and time (the complexes being ill-defined above –50 °C).[55,56] Thus, temperature can have a significant impact on the nature of the Nor-

Table 3.1: Scope and comparison of Rh-catalyzed and Cu-mediated methods for conjugate addition.

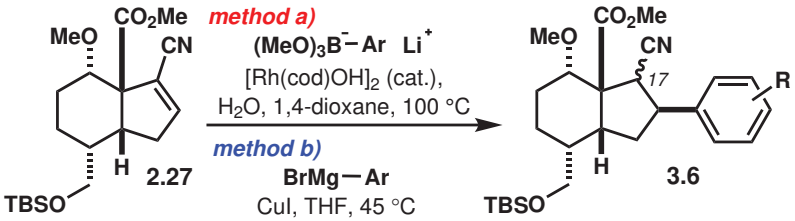

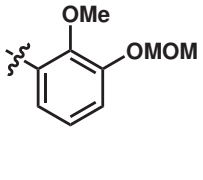

3.6a
a) 71% α-CN, 8% β-CN
b) <5% α-CN

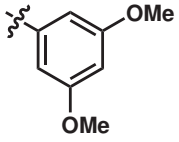

3.6b
a) 51% α-CN, 9% β-CN
b) 58% α-CN, 18% β-CN

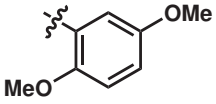

3.6c
b) 52% α-CN, 30% β-CN

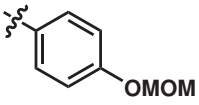

3.6d
a) 17% α-CN, 6% β-CN
b) 66% α-CN, 24% β-CN

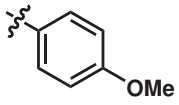

3.6e
a) 68% α-CN, 2% β-CN
b) 59% α-CN, 29% β-CN

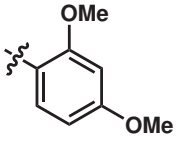

3.6f
b) 65% α-CN, 28% β-CN

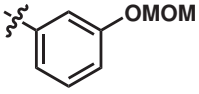

3.6g
b) 68% α-CN, 30% β-CN

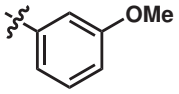

3.6h
b) 70% α-CN, 22% β-CN

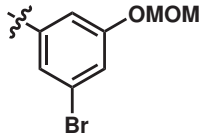

3.6i
b) 35% α-CN, 14% β-CN

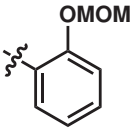

3.6j
b) 53% α-CN, 23% β-CN

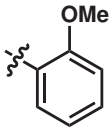

3.6k
b) 42% α-CN, 15% β-CN

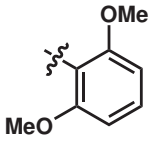

3.6l
b) 83% α-CN

mant reagent under the reaction conditions. The mutability of these aggregates is also likely why, upon further optimization, we found that reaction outcomes depended upon the temperature at which the reaction was run but not upon the temperature at which the Normant reagent was formed.

For most substrates, the ideal CuI:RMgBr ratio was 2:1, which is more in line with Gilman reagents than precedent for Normant reagents. However, the original 1:1 ratio was preferred for the least sterically demanding substrates (see **3.6b**, **3.6e**), suggesting that the size of the aryl group may influence the form of the active reagent. Further insight into this matter was complicated by the fact that the reaction mixtures were heterogeneous. As such, the ratio of

copper:arene in solution was unknown. Matters were further complicated by the fact that reactions using 1:1 CuI:RMgBr became homogeneous overnight with Cu(0) being plated onto the walls of the reaction vessel. Reactions using a 2:1 ratio also slowly became homogeneous, but did not generate visible Cu(0). Nevertheless, we were able to empirically determine that a 2:1 ratio was optimal for most substrates. Heating to 45 °C and addition of 2 equiv of copper were required in order to achieve full conversion of all substrates in 16 h. Substrates for which a 1:1 ratio of CuI:RMgBr was superior required an additional 3 equiv of copper, but could be run at room temperature (yields were ~10% lower than at 45 °C).

3.3.2 Comparison of rhodium and copper conjugate addition methods

Ultimately, our Cu-mediated conjugate addition method proceeded under milder conditions than the Rh-catalyzed approach and gave the desired product (**3.6d**) with improved efficiency over the Rh-catalyzed conjugate addition conditions (see **3.6d**, Method A). While a mixture of diastereomers were obtained (2.8:1 d.r. at C17), the same had also been true with the Rh-catalyzed method and the undesired β-isomer could be readily epimerized using base to the desired α-isomer (see Scheme 3.2). Notably, this Cu-mediated method also gave more consistent results with sets of related substrates than the Rh-catalyzed protocol did. For example, when the aryl boronate of *p*-bromoanisole was added into nitrile **2.27**, tricycle **3.6e** was obtained in 70% yield. However, when the analogous MOM-protected phenol was used, conversion was low and, even upon optimization, **3.6d** was only obtained in 24% yield. In contrast, results with methoxy- and OMOM-substituted arenes were much more consistent with the new protocol (see also **3.6g** vs **3.6h**).

In order to facilitate syntheses of analogs related to **3.2** and **3.3** with a variety of substitution patterns, we explored a series of Cu-mediated conjugate additions using various oxygenated arenes. The reaction proved to be robust, tolerating a variety of substitution patterns, including sterically hindered *o*-substituted arenes (**3.6j**, **3.6k**). While the use of *o*,*m*-disubstituted arenes (**3.6a**) resulted in low conversion, the reaction proceeded in good to excellent yield when other doubly oxygenated arenes with at least one *o*-substituent were used (**3.6c**, **3.6f**, **3.6l**). The conjugate addition also accommodated various phenols masked as MOM ethers (**3.6d**, **3.6g**, **3.6j**). Additionally, the method worked in the presence of a dibromoarene (see **3.6i**), allowing one of the bromine atoms to be preserved as a functional handle for further derivatization.

3.4 Advancement toward designed analogs

The tricycles synthesized using these optimized conditions for conjugate addition (see Table 3.1 for scope) could then be elaborated to the caged scaffold conserved between the bioactive diterpenoid alkaloids. Starting from vinyl nitrile **2.27**, conjugate addition of the cuprate derived from arylmagnesium bromide **3.7** afforded **3.6d** as a mixture of diastereomers, which were separated by flash column chromatography (Scheme 3.2). The minor β-CN product (β-**3.6d**) was converted to the desired α-CN diastereomer (α-**3.6d**) under basic conditions. The structure of nitrile β-**3.6d** and the configuration of the two newly installed stereocenters relative to the rest of the hydrindane system were unambiguously confirmed by X-ray crystallography (Figure 3.11).

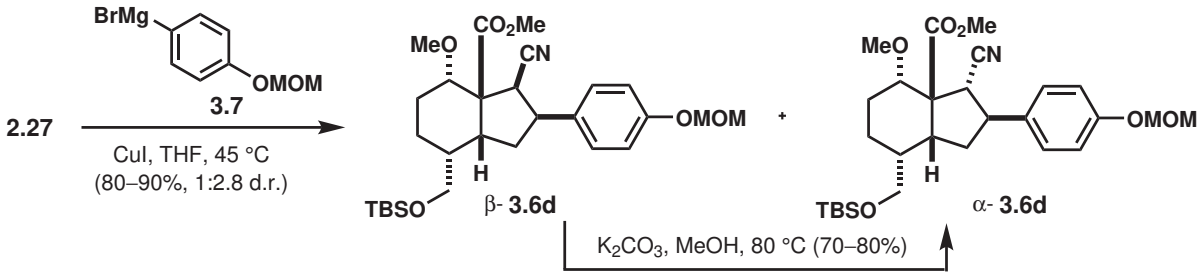

Scheme 3.2: Epimerization to obtain desired α-CN diastereomer of tricycle **3.6d**.

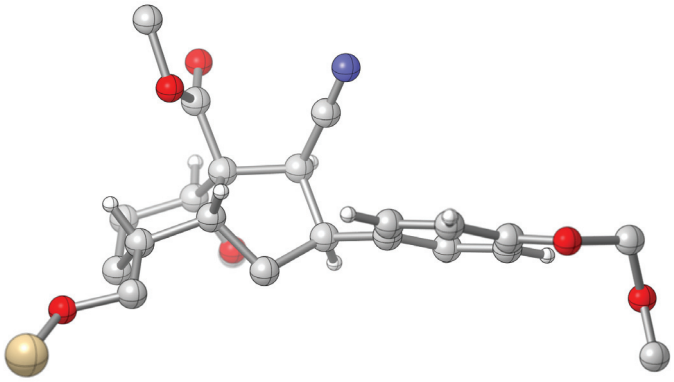

Figure 3.11: X-ray structure of minor conjugate addition product β-**3.6d** visualized with CYLview. Substituents on the silicon atom have been omitted for clarity.

3.4.1 First-generation approach to designed analogs

In a first generation approach to the designed analogs, α-**3.6d** was first hydrated to primary amide **3.8** under anhydrous conditions using acetaldoxime as a water equivalent in a protocol adapted from Chang and Lee (Scheme 3.3).[57] This amide then underwent Hofmann rearrangement in MeOH to give a methyl carbamate. Treatment with TBAF cleaved the silyl ether to give alcohol **3.9**, which could be mesylated and subsequently cyclized under basic conditions to afford caged piperidine **3.10**.

At this stage, the goal was to selectively reduce the methyl ester moiety of **3.10** in the presence of the methyl carbamate. However, no selective reduction was observed upon treatment with a wide variety of hydride sources. Presumably, the steric hindrance of the neopentyl ester prevented addition of any hydride source that was not also sufficiently active to also reduce the carbamate. Still, synthesis of both classes of designed analogs would involve reduction of the carbamate to a tertiary amine at a later stage. Therefore, we decided to instead reduce both the carbamate and ester groups at this stage. This was achieved through treatment of piperidine **3.10** with DIBAL in THF to give aminoalcohol **3.11**. If this reduction was instead run in PhMe, then the MOM ether was also cleaved to reveal phenol **3.12**. From there, intramolecular oxidative dearomatization of **3.12** was achieved using $PhI(OAc)_2$, giving dienone **3.13** and thereby completing the targeted spirocyclic analog scaffold (Scheme 3.4). Looking to further oxygenate this scaffold, we attempted a variety of epoxidation conditions, but observed decomposition of

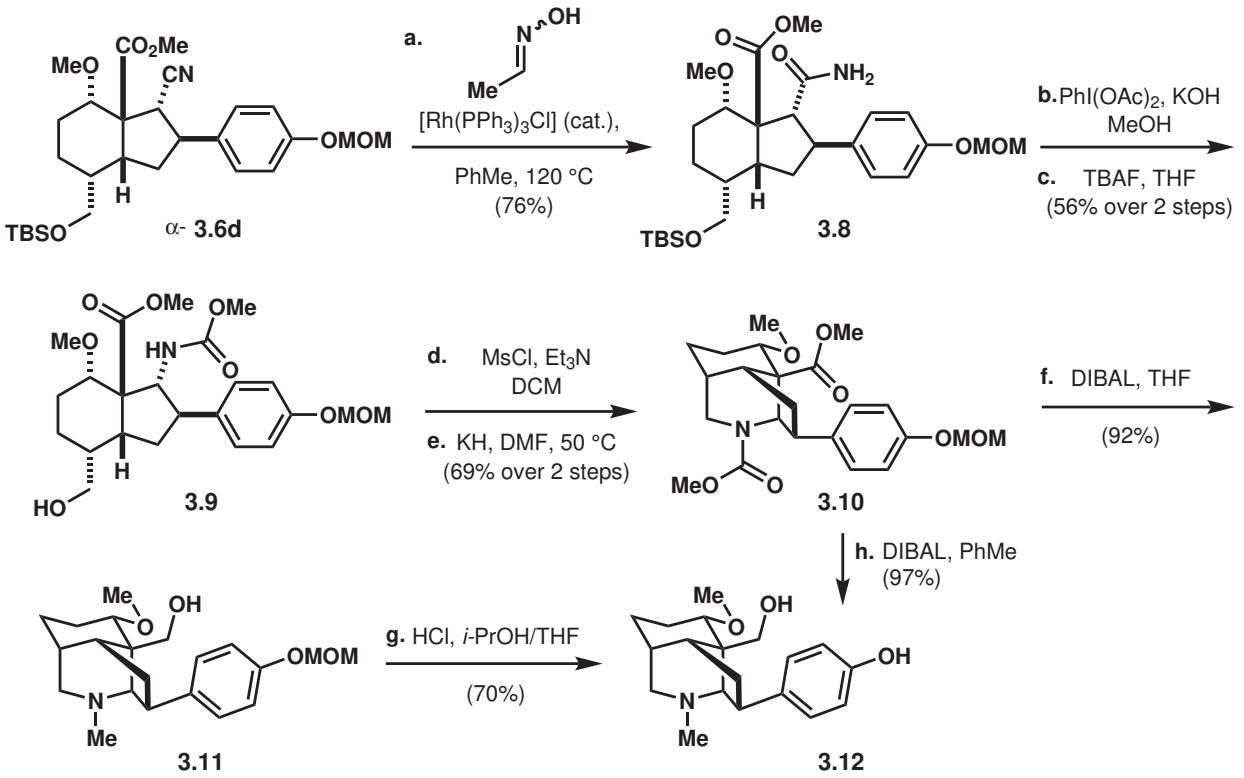

Scheme 3.3: Advancement of tricycle α-**3.6d** to spirocyclization substrate.

the dienone in all cases. Looking instead at dihydroxylation using a mixture of $RuCl_3$, $CeCl_3$, and $NaIO_4$, no conversion was achieved despite extended reaction times.

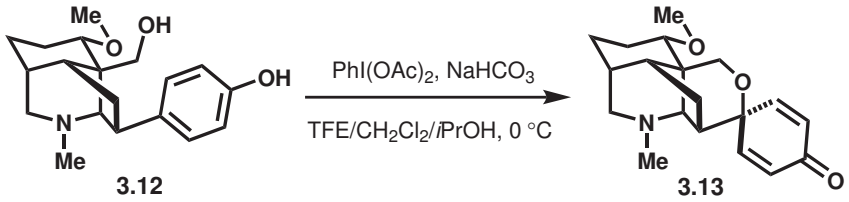

Scheme 3.4: Formation of targeted spirocyclic analog scaffold.

Given the lack of promise in this direction, we instead turned our attention to oxidation of diol **3.12** to the corresponding aldehyde prior to oxidative dearomatization. Only starting material was recovered under Ley oxidation conditions and the diol decomposed under Parikh–Doering conditions. Treatment with Dess–Martin periodinane (DMP) led to oxidation of the phenol ring, giving an *o*-quinone product that decomposed rapidly upon attempted isolation.

However, DMP oxidation of aminoalcohol **3.11** could be accomplished under basic conditions, the MOM ether preventing oxidation of the product (**3.16**) to the undesired *o*-quinone (Scheme 3.5). Aldehyde **3.16** was then treated with dilute HCl to reveal the phenol, setting the stage for oxidative dearomatization to form spirocycle **3.17**. Unfortunately, this product was unstable upon isolation, seeming to undergo fragmentation to lose the methoxy group. The acid sensitivity of these tertiary amine products was shown explicitly through titration of TFA into a solution of

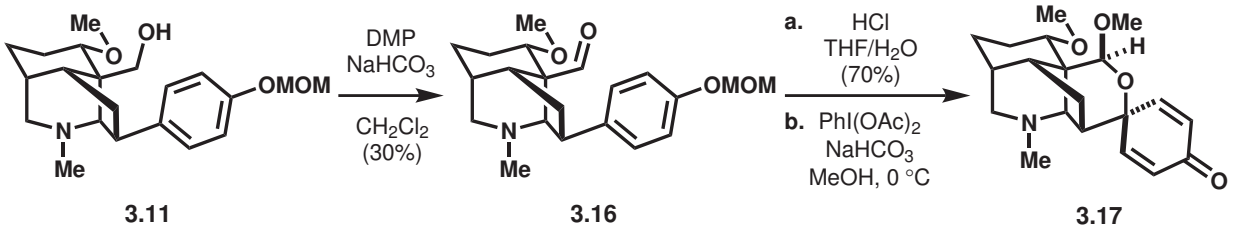

3.11 3.16 3.17

Scheme 3.5: Elaboration of tertiary amine toward spirocyclic scaffold.

diol **3.12** in a series of NMR experiments. In the case of **3.12**, water was generated as aliquots of TFA were added, suggesting a Grob fragmentation of the piperidine ring (Scheme 3.6). This instability precluded further attempts to functionalize these spirocycles.

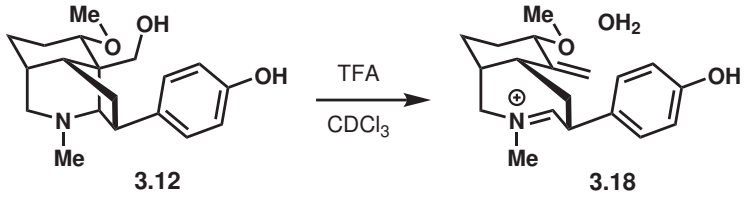

3.12 3.18

Scheme 3.6: Grob fragmentation of piperidine **3.12** upon treatment with TFA.

While additional oxygenation patterns could theoretically be achieved through variation of the arene used in the Cu-mediated conjugate addition, it would be preferable to be able to diversify these analogs at a late stage. As the tertiary amine was believed to be the main impediment to such late-stage functionalization, we rerouted to avoid generating a basic nitrogen until the very end of the synthesis.

3.4.2 Alternate route to spirocyclic analogs

As the reduction of the neopentyl ester **3.10** had proved challenging, we decided to attempt this reduction prior to piperidine formation, reasoning that it should be more sterically accessible in the hydrindane scaffold. A synthesis of aldehyde **3.4** (Scheme 3.7) is illustrative of our revised approach to the common aldehyde intermediates required to generate aconitine-type analogs. In this alternate route, the ester moiety of α-**3.6d** was reduced with Red-Al and the resultant alcohol was protected as a MOM ether to give **3.19**. This allowed us to retain the hydroxy group as a functional handle, in contrast to our previous syntheses, where the primary alcohol was converted to a terminal olefin.[46–48] The nitrile group was then hydrated under anhydrous conditions to afford primary amide **3.5**. A Hofmann rearrangement of this amide in H_2O/MeCN afforded primary amine **3.23**. Stirring rate turned out to be extremely important in this reaction. Insufficient stirring allowed the aqueous and organic layers to separate partially, giving rise to a urea side product (**3.25**) that we believed to arise from trapping of the isocyanate intermediate (**3.22**) by the amine product instead of by water or hydroxide (Scheme 3.8). Urea **3.25** formation could be avoided by pre-forming isocyanate **3.22** in MeCN and sonicating the resultant solution before adding aqueous KOH. In combination with either rapid stirring or the

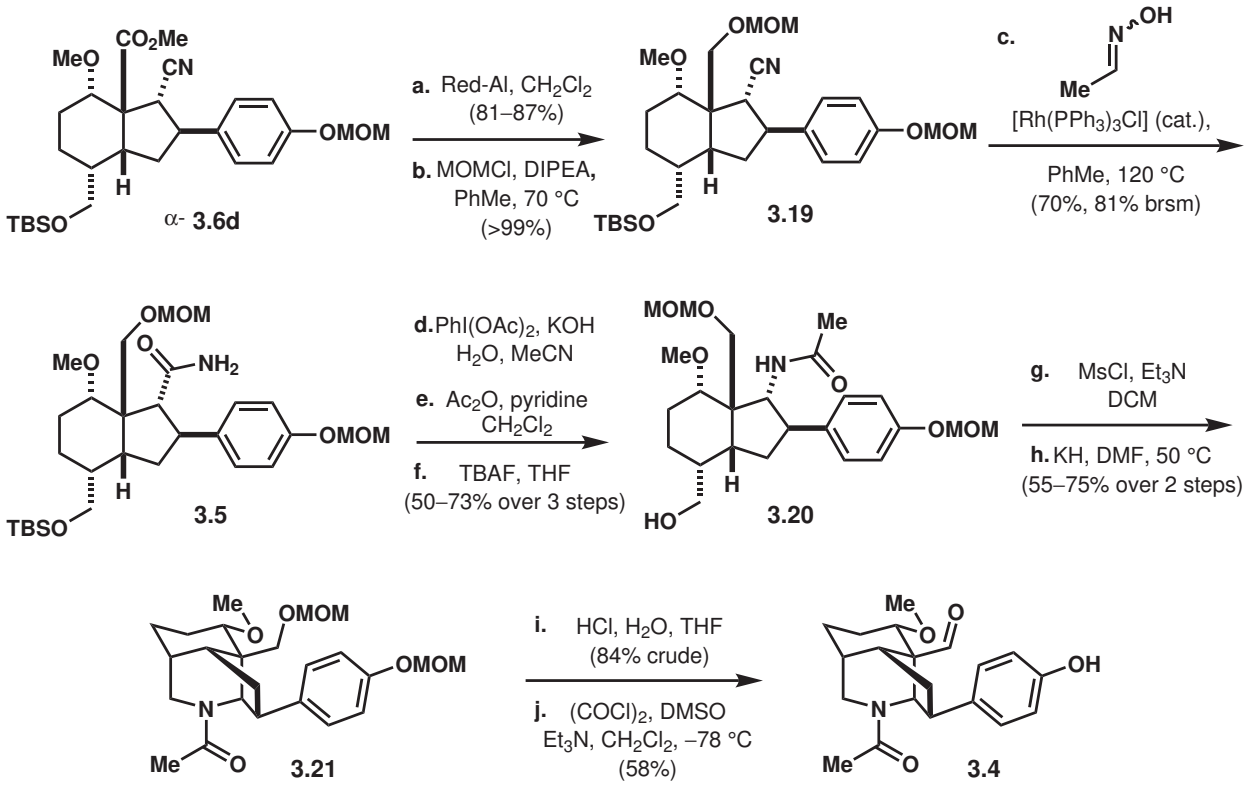

Scheme 3.7: Formation of caged piperidine skeleton.

use of a vortexer, this strategy fully shut down the urea-forming side reaction, enabling us to obtain amine **3.23** in consistently high yield.

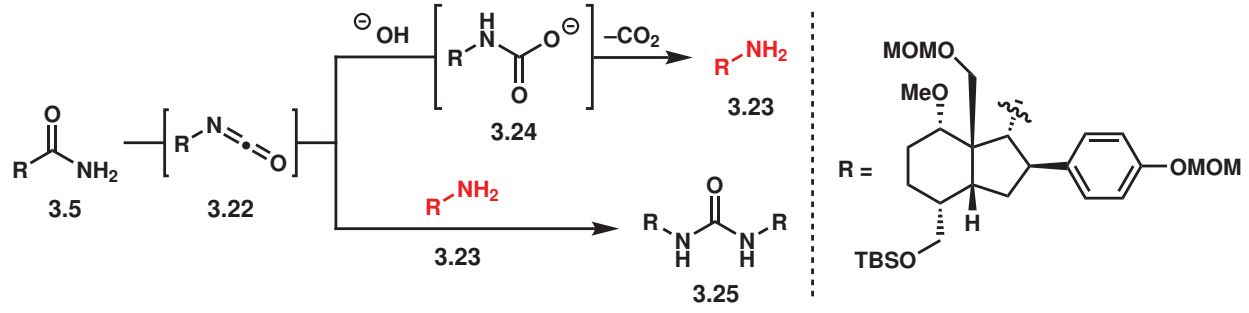

Scheme 3.8: Hofmann rearrangement of amide **3.5**.

This primary amine was subsequently acetylated to form an acetamide. In previous syntheses, a methyl carbamate had instead been installed on related substrates at this stage. This necessitated late-stage conversion of that carbamate into an acetamide. Strategies to do so required hydrolysis and decarboxylation, which generally required harsh reaction conditions. We surmised that the severe conditions for these steps would likely be problematic in the current synthesis due to the presence of free hydroxy groups in our late-stage intermediates. Given that we would eventually require an acetamide—that would ultimately be reduced to the ethylamine present in our designed analogs—we decided to convert amide **3.5** directly to an acetamide.

Following acetylation, TBAF-mediated cleavage of the TBS group gave alcohol **3.20**. Mesylation of the primary hydroxy group in **3.20** set the stage for cyclization to form piperidine **3.21** under basic conditions, completing the caged left-hand side of the molecule. The two MOM groups on **3.21** were then cleaved and the newly revealed primary hydroxy group of diol **3.29** was oxidized under Swern conditions to give aldehyde **3.4**.

Careful control of the amount of $(COCl)_2$ was necessary in the Swern oxidation as superstoichiometric quantities were required to achieve full conversion of alcohol **3.29**, but the use of excess $(COCl)_2$ also led to formation of a side product. NMR spectral data for this compound are consistent with thiol **3.28**, which we hypothesized would come from reaction of the phenol moiety in aldehyde **3.4** with excess $(COCl)_2$ (Scheme 3.9). Exploration of alternative oxida-

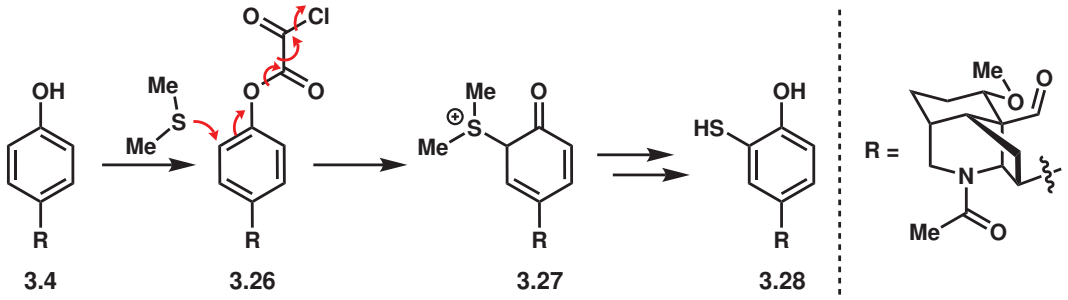

Scheme 3.9: Side reaction in Swern oxidation to form aldehyde **3.4**.

tion reactions was not fruitful, with no oxidation observed under Ley or Parikh–Doering conditions. A similar lack of reactivity was observed under Stahl oxidation conditions using *N*-oxyl-9-azabicyclo[3.3.1]nonane (ABNO), *N*-methylimidazole, catalytic Cu(I)$(MeCN)_4OTf$, and 4,4'-dimethoxy-2,2'-bipyridine (MeO-bpy) under air in MeCN at 50 °C. However, when catalyst loading was increased to 190 mol % and 2,2'-bipyridine was used in place of MeO-bpy, the desired aldehyde was obtained in 58% yield. While this result did present a viable option for oxidation of **3.29**, we chose to continue with the Swern conditions given the high catalyst loading required to achieve a comparable outcome in the Stahl oxidation. Treatment with Dess–Martin periodinane did oxidize diol **3.29** to give an aldehyde, but also oxidized phenol moiety to the corresponding *o*-quinone.

The exploration of various cyclization modes of key intermediates diol **3.29** and aldehyde **3.4** to the aconitine-type analogs was then undertaken. While diol **3.29** did seem to undergo intramolecular oxidative dearomatization to form dienone **3.30**, the compound proved unstable upon work-up (Scheme 3.10). It did, however, persist under the basic spirocyclization conditions, so we attempted further oxygenation of this scaffold to give analogs such as dihydroxylated spirocycle **3.31** or epoxide **3.32**. Low conversion was observed using H_2O_2 under a variety of basic conditions. The same was true for reactions with *t*-butylhydroperoxide and base in a variety of solvents. Attempts to increase reactivity through addition of Ti(O*i*-Pr)$_4$ and tartrate salts did not improve conversion. Use of pyrrolidine and H_2O_2 under neutral conditions led instead to decomposition of the dienone. Similarly, use of trityl hydroperoxide activated by premixing with MeLi did not yield anything recognizable. Attempts at dihydroxylation of dienone **3.30** were equally unproductive. Treatment with AD mix α or β in aqueous *t*-butanol led to slow

decomposition of the starting material, while treatment with OsO_4, with and without added citric acid, under a variety of conditions led to complete decomposition within a few hours.

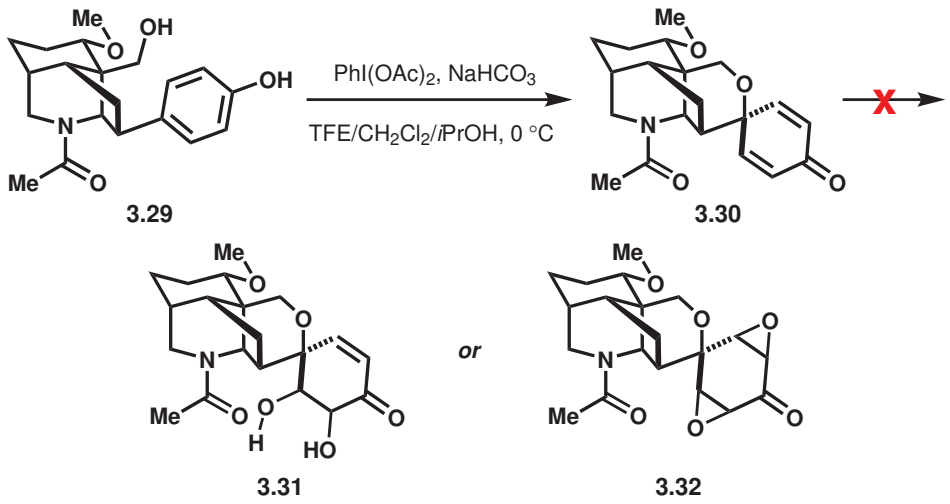

3.29 3.30 3.31 3.32

Scheme 3.10: Oxidative dearomatization of diol **3.29** to build spirocyclic scaffold.

Preliminary studies with aldehyde **3.4** toward the spirocyclic analogs were much more promising, and the desired dienone scaffold (**3.33**) was formed through oxidative dearomatization with $PhI(OAc)_2$ in the presence of methanol (Scheme 3.11).[‡] This dienone, lacking a basic amine,

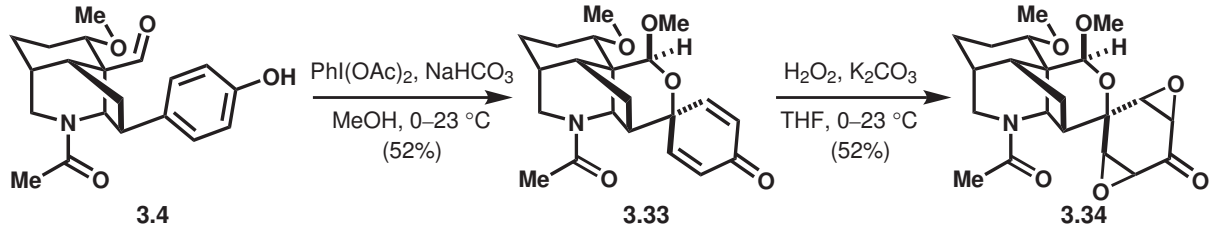

3.4 3.33 3.34

Scheme 3.11: Oxidative dearomatization of aldehyde **3.4** to build spirocyclic scaffold.

proved amenable to further oxygenation, as exemplified by epoxidation to give spirocycle **3.34**. As such, oxygenation patterns can now be set either through the conjugate addition or at a later stage. Intermolecular oxidative dearomatization, followed by intramolecular addition of the aldehyde carbon into the resultant dienone in an umpolung fashion, would give the BD-fused analogs (**3.2**).

3.5 Experimental contributors

Patch-clamp electrophysiology studies were carried out by Nicolle A. Doering (N. A. D.), under the direction of Dr. David Hackos. Cell preparation was initially done by Evera Wang, and later by N. A. D. Initial conjugate addition studies were conducted by Dr. Jack C. Lee, Dr. Gary M. Gallego, and Dr. Christopher J. Marth, who then jointly optimized the rhodium conjugate addition

[‡]Stereochemistry at the acetal carbon was determined by nOe correlations, most notably between the acetal proton and the methinyl proton adjacent to the amide moiety. See Appendix 3.A for details.

with Dr. Kevin G. M. Kou (K. G. M. K.). N. A. D. carried out optimization of the copper conjugate addition. Scale up of nitrile **2.27** during exploration of substrate scope was conducted by Krissada Norseeda (K. N.). K. G. M. K. developed the Swern oxidation to give aldehyde **3.4**. Oxidative dearomatization to give spirocycle **3.33** was explored concurrently by K. G. M. K. and N. A. D., who conducted all other experiments toward the designed analogs.

3.6 Materials and methods

Solvents and reagents. Unless noted below, commercial reagents were purchased from Sigma Aldrich, Acros Organics, Chem-Impex, Combi-blocks, TCI, and/or Alfa Aesar, and used without additional purification. Solvents were purchased from Fisher Scientific, Acros Organics, Alfa Aesar, and Sigma Aldrich. Tetrahydrofuran (THF), diethyl ether (Et_2O), acetonitrile (CH_3CN), benzene, methanol (MeOH), and triethylamine (Et_3N) were sparged with argon and dried by passing through alumina columns using argon in a Glass Contour solvent purification system. Dichloromethane (CH_2Cl_2) was freshly distilled over calcium hydride under a N_2 atmosphere prior to each use. DMSO and toluene (PhMe) were distilled over calcium hydride under a N_2 atmosphere, degassed via freeze–pump–thaw (3 cycles), and stored over 4 Å molecular sieves in a Schlenk flask under N_2. Dimethylformamide (DMF), acetone, *n*-BuLi solution, LiHMDS solution, Red-Al solution, Grignard solutions, and pyridine were purchased in Aldrich SureSeal, Acros AcroSeal, or Alfa Aesar ChemSeal bottling, and used directly. 1,4-Dioxane was purchased in AcroSeal bottling (99.5%, anhydrous, stabilized, over 4 Å molecular sieves) and additionally sparged with N_2 prior to use. $B(OMe)_3$ was distilled over calcium hydride, degassed via freeze-pump-thaw (3 cycles), and stored under N_2 in a Schlenk flask.

Reaction setup, progress monitoring, and product purification. Unless otherwise noted in the experimental procedures, reactions were carried out in flame or oven-dried glassware under a positive pressure of N_2 in anhydrous solvents using standard Schlenk techniques. Reaction temperatures above rt (22–23 °C) were controlled by an IKA temperature modulator and monitored using liquid-in-glass thermometers. Reaction progresses were monitored using a combination of LC–MS analysis (via a Shimadzu LCMS-2020 (UFLC) equipped with the LC-20AD solvent delivery system, a SPD-20AV prominence UV/Vis detector (SPD-M20A Photo Diode Array), and a Thermo Scientific Hypersil GOLD HPLC column (5 µm particle size, 4.6 x 50 mm)), and thin-layer chromatography (TLC) on Silicycle Siliaplates (glass backed, extra hard layer, 60 Å, 250 µm thickness, F254 indicator). Visualization of the developed plates was performed under UV-light (254 nm) irradiation, and then gently heated with $KMnO_4$, *p*-anisaldehyde, or ceric ammonium molybdate stains. Purification and isolation of products were performed via silica gel chromatography (both column and preparative thin-layer chromatography). Flash column chromatography was performed with either glass columns using Silicycle silica gel (40–63 µm particle size) or with a Yamazen Smart Flash EPCLC W-Prep 2XY (dual channel) automated flash chromatography system on prefilled, premium, universal columns using ACS grade solvents. Organic solutions were concentrated under reduced pressure on a Heidolph temperature-controlled rotary evaporator equipped with a dry ice/isopropanol condenser or a Büchi temperature-controlled rotary evaporator equipped with an Ecodyst Ecochyll system.

Analytical instrumentation. NMR spectral data were obtained using deuterated solvents were obtained from Cambridge Isotope Laboratories, Inc. ^{1}H NMR and ^{13}C NMR data were recorded

on Bruker AVB-400, AVQ-400, AV-500, DRX-500, AV-600, AV-700, or CRYO-900 MHz spectrometers using $CDCl_3$, C_6D_6, or D_2O solvents, typically at 20–23 °C. Variable temperature (VT) experiments, typically between 60–70 °C (in C_6D_6), were performed for compounds that exist as rotamers at rt. Chemical shifts (δ) are reported in ppm relative to the residual solvent signal (δ 7.26 for ^{1}H NMR, δ 77.16 for ^{13}C NMR in $CDCl_3$, δ 7.16 for ^{1}H NMR and δ 128.06 for ^{13}C NMR in C_6D_6).[58] When ^{13}C signals appear weak and/or broad (with poor signal/noise ratios), especially for variable temperature (VT) experiments, HSQC spectra are acquired to confirm signal authenticity. Data for ^{1}H NMR spectroscopy are reported as follows; chemical shift (δ ppm), multiplicity (s = singlet, bs = broad singlet, d = doublet, t = triplet, q = quartet, m = multiplet, dd = doublet of doublets, dt = doublet of triplets), coupling constant (Hz), integration. Data for ^{13}C NMR spectroscopy are reported in terms of chemical shift (δ ppm). ^{13}C NMR chemical shifts are reported to one decimal place; a second decimal place is included when two closely spaced, but distinct, signals resonate within 0.1 ppm of each other.

IR spectroscopic data were recorded on a Bruker ALPHA FT-IR spectrophotometer using a diamond attenuated total reflectance (ATR) accessory. Samples are loaded onto the diamond surface either neat or as a solution in organic solvent and the data acquired after the solvent had evaporated.

Mass spectral data were obtained from: 1) the QB3/Chemistry Mass Spectrometry Facility at the University of California, Berkeley, on a Finnigan/Thermo LTQ-FT instrument (ESI), and the data acquired and processed using the Xcalibur software, and 2) the Catalysis Facility of Lawrence Berkeley National Laboratory (supported by the Director, Office of Science, of the US Department of Energy, grant no. DE-AC02-05CH11231) using a PerkinElmer AxION 2 TOF-MS.

X-Ray data were collected on a Bruker APEX-II CCD diffractometer with Mo-Kα radiation (λ = 0.71073 Å) or a MicroStar-H X8 APEX-II diffractometer with Cu-Kα radiation (λ = 1.54178 Å) (supported by an NIH Shared Instrumentation Grant S10-RR027172). CYLview (Legault, C. Y., Université de Sherbrooke, 2009) was used for graphic rendering.

Electrophysiological characterization of diterpenoid alkaloid activity. $Na_V1.7$ voltage-clamp recordings were obtained from HEK293 heterologously expressing human $Na_V1.7$. The wild-type channels were stably expressed. For mutant $Na_V1.7$ channels, cells were transfected 15–20 hours prior to recording using Lipofectamine LTX (Life Technologies) following the manufacturer's protocol. GFP was co-transfected to aid in the identification of transfected cells.

Whole-cell patch clamp recordings were obtained using a Molecular Devices Axopatch 2008 patch clamp amplifier. The recording pipet intracellular solution contained (in mM): 120 CsF, 10 NaCl, 2 $MgCl_2$, 10 HEPES, adjusted to pH 7.2 with CsOH. The extracellular recording solution contained (in mM): 155 NaCl, 3 KCl, 1 $MgCl_2$, 1.5 $CaCl_2$, 10 HEPES, adjusted to pH 7.4 with NaOH. To this extracellular solution was added DMSO solution containing 0–100 mM aconitine or lappaconitine hydrobromide, such that the overall solution was 1% v/v DMSO. Currents were recorded at 20 kHz sampling frequency and filtered at 5 kHz. Series resistance compensation was applied at 60–80%

Activation and inactivation properties were studied for each $Na_V1.7$ channel in solutions containing lappaconitine and aconitine. To measure activation, we used a holding voltage of –100 mV, a short 30 msec pre-pulse to –120 mV, and a 50 msec pulse to voltages ranging from –80 mV

to +60 mV in steps of 5 mV at a rate of once per 3 sec. P/4 leak subtraction was used to reduce leak currents. The peaks of the resulting Na_V currents were measured. Conductance was calculated using the equation $G = I / (V - V_{Na})$, normalized, and plotted as a function of voltage. To measure inactivation, we used a holding voltage of –120 mV to bring the channels fully to the closed state. We then pulsed to 0 mV while reducing the holding voltage from –120 mV to +30 mV in steps of 5 mV at a rate of once per 5 sec. The peaks of the resulting Na_V currents were measured, normalized, and plotted as a function of voltage. To quantify these biophysical properties, we fit the activation and inactivation curves to the following Boltzmann equations:

$$G/G_{max} = 1 - \frac{1}{1 + e^{(V - V_{1/2})/sf}} \qquad (activation)$$

$$I/I_{max} = \frac{1}{1 + e^{(V - V_{1/2})/sf}} \qquad (inactivation)$$

$V_{1/2}$ is the voltage where half-maximal peak conductance (or current) was observed and *sf* is the slope factor.

3.7 Experimental details

3.7.1 Synthesis of aryl bromides for conjugate additions in Table 3.1

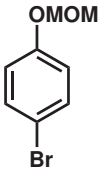

3.35

1-Bromo-4-(methoxymethoxy)benzene (3.35). 4-Bromophenol (25.2 g, 145 mmol, 1.0 equiv) and K_2CO_3 (30.2 g, 218 mmol, 1.5 equiv) were dissolved in acetone (200 mL, 0.67 M) at room temperature. To this stirring suspension was added MOMCl (16.5 mL, 218 mmol, 1.5 equiv) dropwise over 5 min. The reaction mixture was then heated in an oil bath at 60 °C for 20 h. The reaction mixture was then cooled to room temperature and concentrated *in vacuo* to remove acetone. The resultant wet solid was dissolved in water (75 mL), then extracted with Et_2O (3 x 75 mL). The combined organic extracts were washed with brine (25 mL), dried over $MgSO_4$, and concentrated *in vacuo*. Purification by flash column chromatography (eluting with 0–10% EtOAc in hexanes) gave 1-bromo-4-(methoxymethoxy)benzene as a colorless oil (26.3 g, 121 mmol, 83%). ^{1}H NMR (400 MHz, $CDCl_3$) δ 7.38 (m, 2H), 6.92 (m, 2H), 5.15 (s, 2H), 3.47 (s, 3H). Spectroscopic data for this compound were identical to those previously reported.[59]

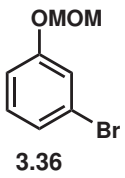

3.36

1-Bromo-3-(methoxymethoxy)benzene (3.36). 3-Bromophenol (1.37 g, 8.00 mmol, 1.0 equiv) and K_2CO_3 (1.66 g, 12.0 mmol, 1.5 equiv) were dissolved in acetone (12.0 mL, 0.67 M) at room temperature. To this stirring suspension was added MOMCl (0.91 mL, 12.0 mmol, 1.5 equiv) dropwise over 5 min. The reaction mixture was then heated in an oil bath at 60 °C for 16 h. The reaction mixture was then cooled to room temperature and concentrated *in vacuo* to remove acetone. The resultant wet solid was dissolved in water (10 mL), then extracted with Et_2O (3 × 10 mL). The combined organic extracts were washed with brine (5 mL), dried over $MgSO_4$, and concentrated *in vacuo*. Purification by flash column chromatography (eluting with 0–7% EtOAc in hexanes) gave 1-bromo-3-(methoxymethoxy)benzene as a colorless oil (879 mg, 4.05 mmol, 51%). ^{1}H NMR (600 MHz, $CDCl_3$) δ 7.22 (t, J = 1.7 Hz, 1H), 7.18–7.08 (m, 2H), 6.97 (dt, J = 6.6, 2.5

Hz, 1H), 5.16 (s, 2H), 3.47 (s, 3H). Spectroscopic data for this compound were identical to those previously reported.[60]

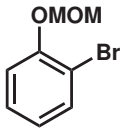

3.37

1-Bromo-2-(methoxymethoxy)benzene (3.37). 2-Bromophenol (1.38 g, 8.00 mmol, 1.0 equiv) and K_2CO_3 (1.67 g, 12.0 mmol, 1.5 equiv) were dissolved in acetone (12.0 mL, 0.67 M) at room temperature. To this stirring suspension was added MOMCl (0.91 mL, 12.0 mmol, 1.5 equiv) dropwise over 5 min. The reaction mixture was then heated in an oil bath at 60 °C for 16 h. The reaction mixture was then cooled to room temperature and concentrated *in vacuo* to remove acetone. The resultant wet solid was dissolved in water (10 mL), then extracted with Et_2O (3 x 10 mL). The combined organic extracts were washed with brine (5 mL), dried over $MgSO_4$, and concentrated *in vacuo*. Purification by flash column chromatography (eluting with 0–7% EtOAc in hexanes) gave 1-bromo-2-(methoxymethoxy)benzene as a colorless oil (1.13 g, 5.21 mmol, 65%). ^{1}H NMR (600 MHz, $CDCl_3$) δ 7.55 (dd, *J* = 7.9, 1.6 Hz, 1H), 7.25 (td, *J* = 7.6, 1.6 Hz, 1H), 7.15 (dd, *J* = 8.3, 1.5 Hz, 1H), 6.89 (td, *J* = 7.6, 1.5 Hz, 1H), 5.25 (s, 2H), 3.53 (s, 3H). Spectroscopic data for this compound were identical to those previously reported.[61]

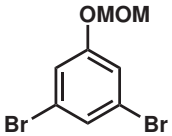

3.38

1,3-Dibromo-5-(methoxymethoxy)benzene (3.38). 3,5-Dibromophenol (1.37 g, 5.44 mmol, 1.0 equiv) and K_2CO_3 (1.18 g, 8.16 mmol, 1.5 equiv) were dissolved in acetone (8.0 mL, 0.67 M) at room temperature. To this stirring suspension was added MOMCl (0.41 mL, 8.16 mmol, 1.5 equiv) dropwise over 5 min. The reaction mixture was then heated in an oil bath at 60 °C for 16 h. The reaction mixture was then cooled to room temperature and concentrated *in vacuo* to remove acetone. The resultant wet solid was dissolved in water (5 mL), then extracted with Et_2O (3 x 5 mL). The combined organic extracts were washed with brine (5 mL), dried over $MgSO_4$, and concentrated *in vacuo*. Purification by flash column chromatography (eluting with 0–7% EtOAc in hexanes) gave 1,3-dibromo-5-(methoxymethoxy)benzene as a colorless oil (1.17 g, 3.95 mmol, 73%). ^{1}H NMR (600 MHz, $CDCl_3$) δ 7.30 (t, *J* = 1.6 Hz, 1H), 7.15 (d, *J* = 1.6 Hz, 2H), 5.14 (s, 2H), 3.47 (s, 3H). Spectroscopic data for this compound were identical to those previously reported.[62]

3.7.2 Copper-mediated conjugate additions

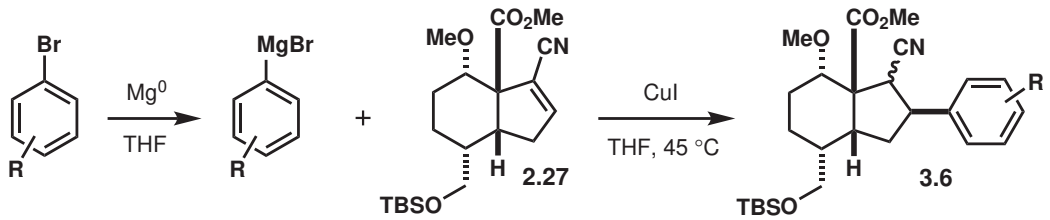

General procedure for copper conjugate additions using aryl bromides (method 1). Aryl bromide (0.527 mmol, 4.0 equiv) and magnesium (14.0 mg, 0.580 mmol, 4.4 equiv) were dissolved in THF (1 mL, 0.53 M with respect to aryl bromide) and heated in an oil bath at 50 °C for 45 min or until the magnesium turnings had mostly dissolved. The reaction mixture was then allowed

to cool to room temperature and then placed in an ice/water bath. The solution was then transferred via syringe to a chilled vial containing copper(I) iodide (50.0 mg, 0.263 mmol, 2.0 equiv) and stirred vigorously in the ice bath for 25 min. At this point, vinyl nitrile **2.27** (50.0 mg, 0.132 mmol, 1.0 equiv) was added as a solution in THF (0.5 mL, 0.26 M). The reaction mixture was removed from the ice bath, sealed with a Teflon cap, and heated in an oil bath at 45 °C and held at this temperature for 20 h. The reaction mixture was then allowed to cool to room temperature, quenched with MeOH (0.25 mL), diluted with NH_4Cl (saturated aqueous, 5 mL), and extracted with EtOAc (3 x 5 mL). The combined organic extracts were washed with brine (3 x 2 mL), dried over Na_2SO_4, and concentrated *in vacuo*.

General procedure for copper conjugate additions using commercially available Grignard reagents (method 2). Grignard reagent solution (0.527 mmol, 4.0 equiv) was diluted to 0.53 M in THF in a sealed 1 dram vial under N_2 and cooled in an ice/water bath. The solution was then transferred via syringe to a chilled vial containing copper(I) iodide (50.0 mg, 0.263 mmol, 2.0 equiv) and stirred vigorously in the ice bath for 25 min. At this point, vinyl nitrile **2.27** (50.0 mg, 0.132 mmol, 1.0 equiv) was added as a solution in THF (0.5 mL, 0.26 M). The reaction mixture was removed from the ice bath, sealed with a Teflon cap, and heated in an oil bath at 45 °C for 20 h. The reaction mixture was then allowed to cool to room temperature, quenched with MeOH (0.25 mL), diluted with NH_4Cl (saturated aqueous, 5 mL), and extracted with EtOAc (3 x 5 mL). The combined organic extracts were washed with brine (3 x 2 mL), dried over Na_2SO_4, and concentrated *in vacuo*.

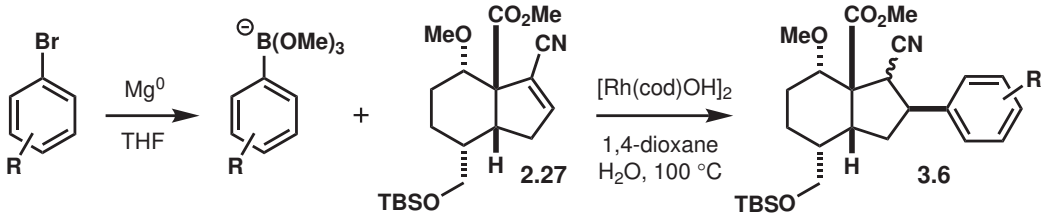

General procedure for rhodium conjugate additions Aryl bromide (3 equiv) was dissolved in Et_2O (0.45 M) under N_2 in a 250 mL Schlenk flask. The solution was cooled to –78 °C and a solution of *n*-BuLi (1.65 M in hexanes, 3.1 equiv) was added. The resulting mixture was maintained at –78 °C for 10 min, then stirred at rt for 30 min. The turbid mixture was then cooled to –40 °C and $B(OMe)_3$ (3 equiv) was added. The cold bath was subsequently removed and the reaction mixture was stirred at rt for 2.5 h, at which time the solvent was carefully evaporated *in vacuo* using a Schlenk manifold to give the boronate ester as a white foam. The Schlenk flask was brought into a nitrogen-filled glovebox and the boronate ester was dissolved in 1,4-dioxane (0.30 M). $[Rh(cod)OH]_2$ (0.06 equiv) and vinyl nitrile **2.27** (1.0 equiv) were subsequently added. The mixture was stirred at ambient glovebox temperature (~30 °C) for 2 h until a homogeneous solution was achieved, at which time H_2O (3.3 equiv) was added and the reaction mixture heated to 100 °C for 24 h. The reaction was cooled to rt, filtered over Celite, and concentrated *in vacuo*. With a 99:1 CH_2Cl_2/Et_2O mixture, purification by flash column chromatography eluting with 0–100% of this solvent mixture as the strong eluent and hexanes as the weak eluent, then flushing the column with 9:1 CH_2Cl_2/Et_2O gave a mixture of products and starting material **2.27**. This mixture can be additionally purified via a second cycle of flash column chromatography (eluting with 0–15% EtOAc in hexanes). This procedure has been previously

reported by us.[46,48]

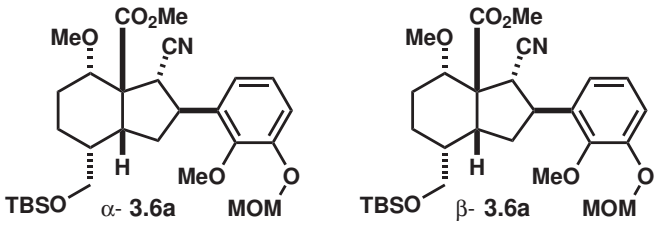

2-Methoxy-3-OMOM tricycle (3.6a). Prepared according to method 1. Purification by flash column chromatography (eluting with 60–100% CH_2Cl_2/hexanes, then 1–5% Et_2O/CH_2Cl_2) provided α-**3.6a** as a colorless oil in <5% yield. When instead prepared according to the rhodium method, α-**3.6a** (3.07 g, 5.60 mmol, 71%) and β-**3.6a** (359 mg, 0.632 mmol, 8%) were obtained from 3.00 g (7.90 mmol) of nitrile **2.27**.

α-**3.6a**. Isolated as a colorless oil. ^{1}H NMR (600 MHz, $CDCl_3$) δ 7.03 (dd, J = 8.1, 1.2 Hz, 1H), 6.97 (t, J = 7.9 Hz, 1H), 6.88 (dd, J = 7.7, 1.1 Hz, 1H), 5.2–5.18 (m, 2H), 4.04 (ddd, J = 11.6, 8.7, 2.9 Hz, 1H), 3.98 (s, 1 H), 3.94 (s, 3H), 3.74 (s, 3H), 3.52 (s, 3H), 3.44 (s, 3H), 3.40 (dd, J = 7.4, 2.3 Hz, 2H), 3.25 (d, J = 8.4 Hz, 1H), 3.11 (ddd, J = 13.3, 9.0, 4.9 Hz, 1H), 2.40 (q, J = 12.5 Hz, 1H), 2.09 (ddd, J = 13.8, 4.9, 2.2 Hz, 1H), 2.00 (dtt, J = 11.8, 7.4, 4.5 Hz, 1H), 1.63 (ddd, J = 12.3, 9.1, 3.0 Hz, 1H), 1.47–1.32 (m, 3H), 0.88 (s, 9H), 0.02 (s, 3H), –0.01 (s, 3H). Spectroscopic data for this compound were identical to those previously reported.[46]

β-**3.6a**. Isolated as a colorless oil. ^{1}H NMR (600 MHz, $CDCl_3$) δ 7.05–7.02 (m, 3H), 5.22 (d, J = 6.6 Hz, 1H), 5.19 (d, J = 6.6 Hz, 1H), 4.26 (ddd, J = 11.2, 9.7, 3.0 Hz, 1H), 3.93 (tt, J = 2.1, 0.9 Hz, 1H), 3.89 (s, 3H), 3.76 (s, 3H), 3.72 (d, J = 9.7 Hz, 1H), 3.50 (s, 3H), 3.48 (d, J = 7.5 Hz, 2H), 3.40 (s, 3H), 3.22 (ddd, J = 13.6, 8.8, 5.0 Hz, 1H), 2.28 (td, J = 13.2, 11.3 Hz, 1H), 2.16 (dtd, J = 15.0, 7.4, 5.1 Hz, 1H), 2.07 (dq, J = 14.5, 3.2 Hz, 1H), 1.89 (ddd, J = 12.3, 8.8, 3.0 Hz, 1H), 1.37–1.30 (m, 2H), 1.20 (dddd, J = 17.0, 9.4, 5.6, 2.0 Hz, 1H), 0.92 (s, 9H), 0.07 (s, 3H), 0.06 (s, 3H); ^{13}C NMR (151 MHz, $CDCl_3$) δ 172.8, 150.0, 148.0, 136.6, 124.1, 121.5, 119.2, 115.7, 95.3, 79.7, 66.5, 62.9, 61.0, 57.4, 56.4, 52.9, 44.3, 41.2, 38.2, 38.0, 31.0, 26.0, 25.5, 18.4, 16.4, –5.25, –5.28; IR (thin film) 2930, 2237, 1740 cm^{-1}; HRMS (ESI) m/z $[M + Na]^+$ calc'd for $C_{29}H_{45}NaNO_7Si$ 570.2858, found 570.2867.

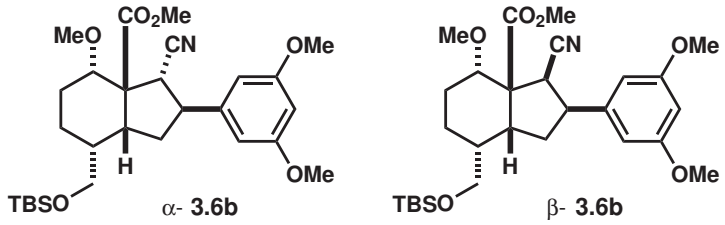

3,5-Dimethoxy tricycle (3.6b). Prepared according to method 1. Run with modified equivalents of reagents (6.0 equiv of Grignard solution, 5.0 equiv of CuI). Purification by flash column chromatography (eluting with 60–100% CH_2Cl_2/hexanes, then 1–5% Et_2O/CH_2Cl_2) provided α-**3.6b** (37.1 mg, 0.0717 mmol, 58%) and β-**3.6b** (11.6 mg, 0.0224 mmol, 18%). When instead prepared according to the rhodium method, α-**3.6b** (1.80 g, 3.74 mmol, 51%) and β-**3.6b** (309 mg, 0.597 mmol, 9%) were obtained from 2.60 g (6.85 mmol) of nitrile **2.27**.

α-**3.6b**. Isolated as a colorless oil. ^{1}H NMR (500 MHz, $CDCl_3$) δ 6.42 (d, J = 2.2 Hz, 2H), 6.33 (t, J = 2.2 Hz, 1H), 3.97 (bs, 1H), 3.79 (s, 6H), 3.73 (s, 3H), 3.68 (ddd, J = 11.4, 8.4, 2.8 Hz, 1H), 3.43 (s, 3H), 3.42 (s, 1H), 3.41 (s, 1H), 3.08 (d, J = 8.4 Hz, 1H), 3.00 (ddd, J = 13.6, 8.9, 4.8 Hz, 1H), 2.41 (q, J = 12.6 Hz, 1H), 2.12–2.06 (m, 1H), 2.02–1.95 (m, 1H), 1.74 (ddd, J = 12.4, 9.0, 2.9 Hz, 1H), 1.50–1.27 (m, 3H), 0.88 (s, 9H), 0.03 (s, 3H), 0.01 (s, 3H). Spectroscopic data for this compound were identical to those previously reported.[48]

β-**3.6b**. Isolated as a pale yellow oil. ^{1}H NMR (600 MHz, $CDCl_3$) δ 6.43 (d, J = 2.2 Hz, 2H), 6.34 (t, J = 2.2 Hz, 1H), 3.92 (s, 1H), 3.82–3.77 (m, 1H), 3.78 (s, 6H), 3.78 (s, 3H), 3.64 (d, J = 9.7 Hz, 1H), 3.49 (dd, J = 9.8, 7.4 Hz, 1H), 3.43 (dd, J = 9.9, 7.3 Hz, 1H), 3.37 (s, 3H), 3.22 (ddd, J = 13.6, 8.9, 5.3 Hz, 1H), 2.28 (td, J = 13.0, 11.5 Hz, 1H), 2.15 (tdd, J = 12.0, 7.3, 4.7 Hz, 1H), 2.07 (dq, J = 14.4, 3.0 Hz, 1H), 1.86 (ddd, J = 12.5, 9.0, 3.1 Hz, 1H), 1.41–1.34 (m, 1H), 1.31 (qd, J = 13.1, 2.9 Hz, 1H), 1.19 (dddd, J = 14.9, 13.3, 3.7, 1.8 Hz, 1H), 0.90 (s, 9H), 0.06 (s, 3H), 0.04 (s, 3H); ^{13}C NMR (151 MHz, $CDCl_3$) δ172.7, 160.9, 145.0, 119.2, 106.7, 99.1, 79.6, 66.6, 63.1, 57.3, 55.4, 53.0, 46.1, 44.8, 41.4, 38.1, 32.3, 26.1, 25.4, 18.4, 16.4, –5.2; IR (thin film) 2950, 2930, 2900, 2856, 2237, 1738, 1596, 1460, 1250, 1205, 1153, 1105, 1085, 835, 775 cm^{-1}; HRMS (ESI) m/z [M + Na]$^+$ calc'd for $C_{28}H_{43}O_6NNaSi$ 540.2752, found 540.2743.

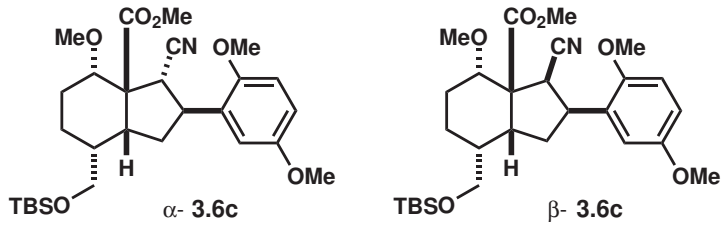

2,5-Dimethoxy tricycle (3.6c). Prepared according to method 1. Purification by flash column chromatography (eluting with 60–100% CH_2Cl_2/hexanes, then 1–5% Et_2O/CH_2Cl_2) provided α-**3.6c** and β-**3.6c** in 93% combined yield.

α-**3.6c**. Isolated as a colorless oil (44.3 mg, 0.0856 mmol, 28%). ^{1}H NMR (600 MHz, $CDCl_3$) δ 6.78 (d, J = 8.8 Hz, 1H), 6.77 (d, J = 3.0 Hz, 1H), 6.73 (dd, J = 8.8, 3.0 Hz, 1H), 3.97 (q, J = 1.8 Hz, 1H), 3.87 (ddd, J = 11.9, 8.7, 3.2 Hz, 1H), 3.79 (s, 3H), 3.76 (s, 3H), 3.74 (s, 3H), 3.44 (s, 3H), 3.42 (d, J = 8.7 Hz, 1H), 3.41–3.38 (m, 2H), 3.16 (ddd, J = 13.3, 9.1, 4.9 Hz, 1H), 2.31 (q, J = 12.3 Hz, 1H), 2.09 (dq, J = 14.0, 3.0 Hz, 1H), 1.96 (tt, J = 11.5, 3.8 Hz, 1H), 1.71 (ddd, J = 12.4, 9.1, 3.3 Hz, 1H), 1.47–1.32 (m, 3H), 0.88 (s, 9H), 0.02 (s, 3H), 0.01 (s, 3H); ^{13}C NMR (151 MHz, $CDCl_3$) δ 173.6, 153.7, 151.5, 133.5, 120.6, 116.0, 112.2, 111.9, 77.2, 66.6, 60.6, 57.0, 55.9, 55.9, 52.8, 46.1, 44.0, 42.7, 38.4, 32.1, 26.1, 25.0, 18.4, 16.8, –5.3; IR (thin film) 2950, 2931, 2896, 2856, 2237, 1728, 1501, 1248, 1223, 1101, 1080, 1048, 835, 775 cm^{-1}; HRMS (ESI) m/z [M + Na]$^+$ calc'd for $C_{28}H_{43}O_6NNaSi$ 540.2752, found 540.2749.

β-**3.6c**. Isolated as a colorless oil (19.3 mg, 0.0372 mmol, 65%). ^{1}H NMR (600 MHz, $CDCl_3$) δ 6.87 (d, J = 3.0 Hz, 1H), 6.78 (d, J = 8.8 Hz, 1H), 6.74 (dd, J = 8.8, 2.9 Hz, 1H), 4.12 (ddd, J = 11.4, 9.9, 2.9 Hz, 1H), 3.91 (p, J = 1.5 Hz, 1H), 3.80 (s, 3H), 3.79–3.75 (m, 1H), 3.76 (s, 3H), 3.75 (s, 3H), 3.54 (dd, J = 9.9, 7.0 Hz, 1H), 3.45 (dd, J = 9.9, 7.5 Hz, 1H), 3.39 (s, 3H), 3.17 (ddd, J = 13.5, 8.4, 4.9 Hz, 1H), 2.21 (td, J = 13.1, 11.2 Hz, 1H), 2.12 (tdd, J = 12.0, 7.3, 4.8 Hz, 1H), 2.07 (dq, J = 14.7, 3.3 Hz, 1H), 1.93 (ddd, J = 12.3, 8.7, 3.1 Hz, 1H), 1.42–1.29 (m, 2H), 1.19 (tdd, J = 14.7, 4.2, 2.0 Hz, 1H), 0.91 (s, 9H), 0.07 (s, 3H), 0.07 (s, 3H); ^{13}C NMR (151 MHz, $CDCl_3$) δ 172.9, 153.7, 151.8,

131.9, 119.4, 115.0, 111.9, 111.2, 79.8, 66.8, 62.9, 57.5, 56.0, 55.9, 52.9, 43.8, 41.1, 39.4, 38.2, 29.7, 26.1, 25.6, 18.5, 16.6, –5.2; IR (thin film) 2952, 2928, 2855, 2234, 1739, 1591, 1496, 1250, 1219, 1106, 1087, 1054, 837, 776 cm^{-1}; HRMS (ESI) *m/z* $[M + Na]^+$ calc'd for $C_{28}H_{43}O_6NNaSi$ 540.2752, found 540.2747.

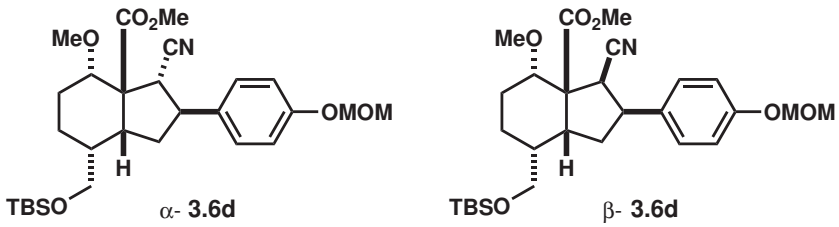

4-OMOM tricycle (3.6d). Prepared according to method 1. Purification by flash column chromatography (eluting with 60–100% CH_2Cl_2/hexanes, then 1–5% Et_2O/CH_2Cl_2) provided *α*-**3.6d** (1.10 g, 2.13 mmol, 66%) and *β*-**3.6d** (394 mg, 0.761 mmol, 24%) from 1.23 g (3.24 mmol) of nitrile **2.27**. When instead prepared according to the rhodium method, *α*-**3.6d** (62.4 mg, 0.121 mmol, 17%) and *β*-**3.6d** (20.7 mg, 40.0 µmol, 6%) were obtained from 250. mg (0.659 mmol) of nitrile **2.27**.

α-**3.6d**. Isolated as a colorless oil. ^{1}H NMR (500 MHz, $CDCl_3$) δ 7.20–7.17 (m, 2H), 7.00–6.96 (m, 2H), 5.21–4.93 (m, 2H), 3.97 (bs, 1H), 3.73 (s, 3H), 3.70 (ddd, *J* = 11.4, 8.3, 2.7 Hz, 1H), 3.47 (s, 3H), 3.45–3.37 (m, 2H), 3.43 (s, 3H), 3.03 (ddd, *J* = 13.5, 9.1, 4.5 Hz, 1H), 3.02 (d, *J* = 8.4 Hz, 1H), 2.43 (td, *J* = 13.1, 11.5 Hz, 1H), 2.09 (dq, *J* = 12.9, 2.7 Hz, 1H), 2.00 (dtd, *J* = 10.7, 6.2, 3.5 Hz, 1H), 1.72 (ddd, *J* = 12.4, 9.0, 2.9 Hz, 1H), 1.47–1.32 (m, 3H), 0.89 (s, 9H), 0.03 (s, 3H), 0.01 (s, 3H); ^{13}C NMR (126 MHz, $CDCl_3$) δ 173.3, 156.2, 139.1, 128.0, 120.1, 116.8, 94.6, 77.1, 66.2, 60.4, 57.1, 56.1, 52.9, 48.7, 47.8, 43.4, 38.2, 33.1, 26.0, 24.8, 18.4, 16.6, –5.26, –5.29; IR (thin film) 2951, 2929, 2897, 2856, 2240, 1731, 1511, 1462, 1237, 1079, 1005, 815, 776 cm^{-1}; HRMS (ESI) *m/z* $[M + Na]^+$ calc'd for $C_{28}H_{43}O_6NNaSi$ 540.2752, found 540.2757.

β-**3.6d**. Isolated as a colorless oil, which slowly solidified overnight at rt. ^{1}H NMR (600 MHz, $CDCl_3$) δ 7.19 (d, *J* = 8.4 Hz, 2H), 6.98 (d, *J* = 8.8 Hz, 2H), 5.16 (qd, *J* = 6.8, 1.2 Hz, 2H), 3.92 (bs, 1H), 3.83–3.76 (m, 1H), 3.78 (s, 3H), 3.64 (d, *J* = 9.7 Hz, 1H), 3.49–3.41 (m, 2H), 3.74 (s, 3H) 3.37 (s, 3H), 3.25 (ddd, *J* = 13.6, 8.8, 5.4 Hz, 1H), 2.32 (q, *J* = 12.8 Hz, 1H), 2.15 (qd, *J* = 12.1, 6.7 Hz, 1H), 2.07 (dt, *J* = 14.6, 3.4 Hz, 1H), 1.82 (ddd, *J* = 12.4, 8.8, 2.8 Hz, 1H), 1.39–1.16 (m, 3H), 0.91 (s, 9H), 0.06 (s, 3H), 0.04 (s, 3H); ^{13}C NMR (151 MHz, $CDCl_3$) δ 172.8, 156.4, 136.4, 129.5, 119.3, 116.3, 94.6, 79.6, 66.5, 63.1, 57.3, 56.1, 53.0, 45.1, 44.9, 41.4, 38.0, 32.9, 26.1, 25.4, 18.4, 16.4, -5.22, -5.24; IR (thin film) 2951, 2929, 2856, 2233, 1739, 1512, 1462, 1248, 1153, 1103, 1006, 836, 776 cm^{-1}; HRMS (ESI) *m/z* $[M + Na]^+$ calc'd for $C_{28}H_{43}O_6NNaSi$ 540.2752, found 540.2756. This compound is unambiguously characterized by single crystal X-ray crystallography.

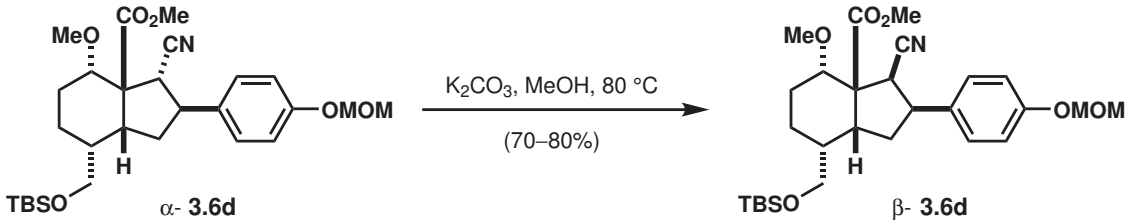

α-**3.6d** from β-**3.6d**. β-**3.6d** (366.9 mg, 0.709 mmol, 1.0 equiv) and K_2CO_3 (147.0 mg, 1.06 mmol, 1.5 equiv) were dissolved in MeOH (7.0 mL, 0.1 M) and heated in an oil bath at 80 °C for 1 h. The reaction mixture was allowed to cool to room temperature, at which time it was quenched with NH_4Cl (saturated aqueous, 5 mL), concentrated *in vacuo* to remove MeOH, and then extracted with CH_2Cl_2 (3 x 4 mL). The combined organic extracts were washed with brine (2 mL), dried over Na_2SO_4, and concentrated *in vacuo* to give a yellow oil. Purification by flash column chromatography (eluting with 5–35% EtOAc/hexanes) provided α-**3.6d** as a colorless oil (321.2 mg, 0.620 mmol, 88%).

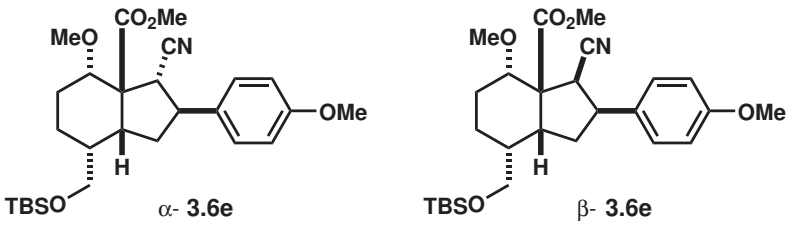

4-Methoxy tricycle (3.6e). Prepared according to method 2. Run with modified equivalents of reagents (6.0 equiv of Grignard solution, 5.0 equiv of CuI). Purification by flash column chromatography (eluting with 60–100% CH_2Cl_2/hexanes, then 1–5% Et_2O/CH_2Cl_2) provided α-**3.6e** (37.7 mg, 0.0773 mmol, 59%) and β-**3.6e** (18.7 mg, 0.0383 mmol, 29%). When instead prepared according to the rhodium method, α-**3.6e** (176 mg, 0.361 mmol, 68%) and β-**3.6e** (35.3 mg, 72.3 µmol, 2%) were obtained from 200. mg (0.527 mmol) of nitrile **2.27**.

α-**3.6e**. Isolated as a colorless oil. ^{1}H NMR (500 MHz, $CDCl_3$) δ 7.22 (d, J = 8.7 Hz, 2H), 6.87 (d, J = 8.6 Hz, 2H), 4.00 (bs, 1H), 3.81 (s, 3H), 3.76 (s, 3H), 3.72 (ddd, J = 11.3, 8.4, 2.9 Hz, 1H), 3.46 (s, 3H), 3.49–3.39 (m, 2H), 3.07 (ddd, J = 13.3, 8.7, 4.8 Hz, 1H), 3.05 (d, J = 8.4 Hz, 1H), 2.47 (td, J = 12.9, 11.7 Hz, 1H), 2.12 (dq, J = 12.7, 2.6 Hz, 1H), 2.03 (qd, J = 7.2, 2.7 Hz, 1H), 1.75 (ddd, J = 12.2, 8.9, 2.9 Hz, 1H), 1.52–1.31 (m, 3H), 0.93 (s, 9H), 0.06 (s, 3H), 0.04 (s, 3H).; ^{13}C NMR (126 MHz, $CDCl_3$) δ 173.3, 158.5, 137.8, 127.9, 120.1, 114.3, 77.0, 66.1, 57.0, 55.4, 52.8, 48.6, 47.8, 43.3, 38.1, 33.1, 26.0, 24.8, 18.3, 16.5, –5.3, –5.4; IR (thin film) 2948, 2928, 2855, 2238, 1736, 1612, 1514, 1435, 1250, 1106, 1077, 834, 809, 778 cm^{-1}; HRMS (ESI) *m/z* [M + Na]$^+$ calc'd for $C_{27}H_{41}O_5NNaSi$ 510.2646, found 510.2648.

β-**3.6e**. Isolated as a pale yellow oil. ^{1}H NMR (500 MHz, $CDCl_3$) δ 7.23–7.13 (m, 2H), 6.92–6.67 (m, 2H), 3.91 (bs, 1H), 3.83–3.75 (m, 1H), 3.79 (s, 3H), 3.78 (s, 3H), 3.64 (d, J = 9.7 Hz, 1H), 3.46 (d, J = 7.4 Hz, 2H), 3.37 (s, 3H), 3.26 (ddd, J = 13.6, 8.8, 4.9 Hz, 1H), 2.33 (td, J = 13.1, 11.0 Hz, 1H), 2.15 (tdd, J = 12.3, 7.4, 4.9 Hz, 1H), 2.07 (dq, J = 14.9, 3.4 Hz, 1H), 1.82 (ddd, J = 12.3, 8.8, 3.0 Hz, 1H), 1.38–1.24 (m, 2H), 1.19 (dddd, J = 14.4, 12.2, 4.8, 2.0 Hz, 1H), 0.92 (s, 9H), 0.06 (s, 3H), 0.04 (s, 3H); ^{13}C NMR (151 MHz, $CDCl_3$) δ 172.8, 158.6, 135.1, 129.4, 119.4, 114.0, 79.6, 66.5, 63.1, 57.3, 55.3, 53.0, 45.03, 44.98, 41.4, 38.0, 32.9, 26.1, 25.4, 18.4, 16.4, –5.22, –5.24; IR (thin film) 2950, 2930, 2899, 2856, 2234, 1738, 1612, 1514, 1462, 1249, 1179, 1102, 1085, 835, 775 cm^{-1}; HRMS (ESI) *m/z* [M + Na]$^+$ calc'd for $C_{27}H_{41}O_5NNaSi$ 510.2646, found 510.2645.

2,4-Dimethoxy tricycle (3.6f). Prepared according to method 1. Purification by flash column chromatography (eluting with 60–10% CH_2Cl_2/hexanes, then 1–5% Et_2O/CH_2Cl_2) provided α-**3.6f** and β-**3.6f** in 82% combined yield.

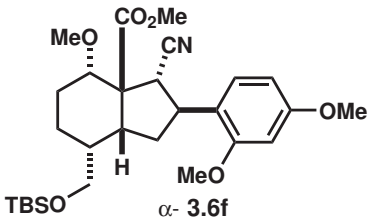

α- **3.6f**

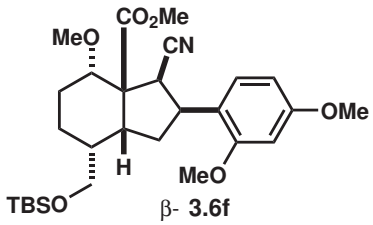

β- **3.6f**

α-**3.6f**. Isolated as a colorless oil (35.3 mg, 0.0682 mmol, 52%). ^{1}H NMR (600 MHz, $CDCl_3$) δ 7.08 (d, *J* = 8.3 Hz, 1H), 6.44 (d, *J* = 2.4 Hz, 1H), 6.40 (dd, *J* = 8.3, 2.4 Hz, 1H), 3.97 (bs, 1H), 3.84 (td, *J* = 8.6, 4.3 Hz, 1H), 3.81 (s, 3H), 3.79 (s, 3H), 3.73 (s, 3H), 3.43 (s, 3H), 3.40 (d, *J* = 7.4 Hz, 2H), 3.35 (d, *J* = 8.5 Hz, 1H), 3.16 (ddd, *J* = 13.3, 9.0, 5.0 Hz, 1H), 2.29 (q, *J* = 12.3 Hz, 1H), 2.08 (ddd, *J* = 12.4, 5.2, 2.2 Hz, 1H), 1.96 (tdd, *J* = 11.7, 7.5, 4.7 Hz, 1H), 1.70 (ddd, *J* = 12.3, 9.0, 3.2 Hz, 1H), 1.46–1.28 (m, 3H), 0.88 (s, 9H), 0.03 (s, 3H), 0.01 (s, 3H); ^{13}C NMR (151 MHz, $CDCl_3$) δ 173.7, 160.1, 158.2, 129.8, 124.9, 120.8, 104.1, 99.2, 77.3, 66.5, 60.5, 57.0, 55.5, 55.3, 52.7, 45.6, 44.2, 42.6, 38.4, 31.9, 26.1, 25.0, 18.4, 16.8, –5.3; IR (thin film) 2950, 2930, 2892, 2856, 2237, 1730, 1613, 1507, 1463, 1257, 1209, 1102, 1083, 1038, 836, 776 cm^{-1}; HRMS (ESI) *m/z* [M + Na]$^{+}$ calc'd for $C_{28}H_{43}O_6NNaSi$ 540.2752, found 540.2762.

β-**3.6f**. Isolated as a colorless oil (20.7 mg, 0.0400 mmol, 30%). ^{1}H NMR (600 MHz, $CDCl_3$) δ 7.20 (d, *J* = 8.3 Hz, 1H), 6.46 (dd, *J* = 8.3, 2.4 Hz, 1H), 6.44 (d, *J* = 2.4 Hz, 1H), 4.05 (ddd, *J* = 11.8, 9.8, 2.8 Hz, 1H), 3.90 (p, *J* = 1.4 Hz, 1H), 3.82 (s, 3H), 3.79 (s, 3H), 3.75 (s, 3H), 3.74 (d, *J* = 9.8 Hz, 1H), 3.53–3.44 (m, 2H), 3.38 (s, 3H), 3.21 (ddd, *J* = 13.5, 8.4, 5.6 Hz, 1H), 2.22 (td, *J* = 13.1, 11.1 Hz, 1H), 2.12 (ddd, *J* = 14.4, 7.1, 1.9 Hz, 1H), 2.06 (dq, *J* = 14.5, 3.2 Hz, 1H), 1.93 (ddd, *J* = 12.8, 8.5, 2.8 Hz, 1H), 1.36–1.31 (m, 2H), 1.18 (dtd, *J* = 16.9, 6.0, 1.9 Hz, 1H), 0.93 (s, 9H), 0.08 (s, 3H), 0.07 (s, 3H); ^{13}C NMR (151 MHz, $CDCl_3$) δ 173.0, 159.9, 158.4, 128.2, 123.3, 119.7, 104.2, 98.7, 79.8, 66.7, 62.8, 57.5, 55.5, 55.4, 52.9, 43.9, 41.1, 38.5, 38.1, 29.9, 26.1, 25.6, 18.5, 16.6, –5.2; IR (thin film) 2952, 2933, 2904, 2856, 2238, 1739, 1613, 1587, 1464, 1290, 1252, 1103, 1085, 836, 776 cm^{-1}; HRMS (ESI) *m/z* [M + Na]$^{+}$ calc'd for $C_{28}H_{43}O_6NNaSi$ 540.2752, found 540.2748.

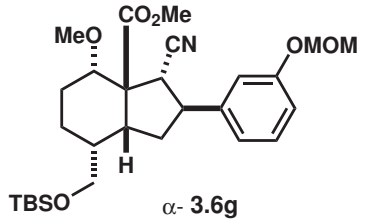

α- **3.6g**

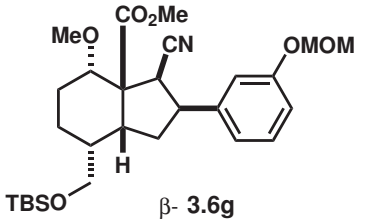

β- **3.6g**

3-OMOM tricycle (3.6g). Prepared according to method 1. Purification by flash column chromatography (eluting with 60–100% CH_2Cl_2/hexanes, then 1–5% Et_2O/CH_2Cl_2) provided *α*-**3.6g** and *β*-**3.6g** in 98% combined yield.

α-**3.6g**. Isolated as a colorless oil (46.2 mg, 0.0892 mmol, 68%). ^{1}H NMR (600 MHz, $CDCl_3$) δ 7.25–7.21 (m, 1H), 6.92 (s, 2H), 6.91 (d, *J* = 2.1 Hz, 1H), 5.19 (d, *J* = 6.8 Hz, 1H), 5.15 (d, *J* = 6.8 Hz, 1H), 3.97 (p, *J* = 1.3 Hz, 1H), 3.74 (s, 3H), 3.71 (ddd, *J* = 11.4, 8.4, 2.9 Hz, 1H), 3.48 (s, 3H), 3.45–3.38 (m, 2H), 3.43 (s, 3H), 3.08 (d, *J* = 8.4 Hz, 1H), 3.03 (ddd, *J* = 13.6, 9.0, 4.9 Hz, 1H), 2.44 (td, *J* = 13.0, 11.5 Hz, 1H), 2.09 (dq, *J* = 13.8, 2.4 Hz, 1H), 2.00 (dtd, *J* = 16.1, 7.4, 4.9 Hz, 1H), 1.74 (ddd, *J* = 12.3, 9.0, 2.8 Hz, 1H), 1.49–1.30 (m, 3H), 0.89 (s, 9H), 0.03 (s, 3H), 0.01 (s, 3H); ^{13}C NMR

(151 MHz, $CDCl_3$) δ 173.3, 157.8, 147.3, 130.2, 120.2, 112.0, 115.5, 114.3, 94.6, 77.1, 66.2, 60.5, 57.1, 56.2, 52.9, 49.3, 47.4, 43.4, 38.2, 33.0, 26.0, 24.8, 18.3, 16.6, –5.27, –5.30; IR (thin film) 2953, 2929, 2897, 2855, 2240, 1731, 1584, 1462, 1452, 1249, 1150, 1078, 1020, 981, 834, 774 cm^{-1}; HRMS (ESI) *m/z* $[M + Na]^+$ calc'd for $C_{28}H_{43}O_6NNaSi$ 540.2752, found 540.2749.

β-**3.6g**. Isolated as a colorless oil (20.8 mg, 0.0402 mmol, 30%). ^1H NMR (600 MHz, $CDCl_3$) δ 7.25–7.21 (m, 1H), 6.95 (dt, *J* = 7.7, 1.2 Hz, 1H), 6.92 (ddd, *J* = 5.2, 2.7, 1.7 Hz, 2H), 5.17 (s, 2H), 3.92 (t, *J* = 2.5 Hz, 1H), 3.81 (ddd, *J* = 11.8, 9.9, 2.9 Hz, 1H), 3.78 (s, 3H), 3.66 (d, *J* = 9.7 Hz, 1H), 3.50–3.43 (m, 2H), 3.48 (s, 3H), 3.37 (s, 3H), 3.24 (ddd, *J* = 13.6, 9.1, 5.2 Hz, 1H), 2.31 (td, *J* = 13.1, 11.0 Hz, 1H), 2.15 (dtd, *J* = 12.0, 7.3, 3.7 Hz, 1H), 2.07 (dq, *J* = 14.5, 3.3 Hz, 1H), 1.86 (ddd, *J* = 12.4, 8.9, 3.0 Hz, 1H), 1.40–1.28 (m, 2H), 1.19 (dddd, *J* = 14.9, 13.1, 4.2, 2.0 Hz, 1H), 0.91 (s, 9H), 0.06 (s, 3H), 0.04 (s, 3H); ^{13}C NMR (151 MHz, $CDCl_3$) δ 172.7, 157.4, 144.6, 129.7, 121.8, 119.1, 116.8, 114.8, 94.7, 79.6, 66.5, 63.1, 57.3, 56.1, 53.0, 45.8, 44.8, 41.5, 38.1, 32.5, 26.1, 25.4, 18.4, 16.4, –5.23, –5.24; IR (thin film) 2951, 2928, 2898, 2856, 2238, 1739, 1609, 1585, 1462, 1249, 1151, 1080, 1025, 1009, 835, 775, 729 cm^{-1}; HRMS (ESI) *m/z* $[M + Na]^+$ calc'd for $C_{28}H_{43}O_6NNaSi$ 540.2752, found 540.2752.

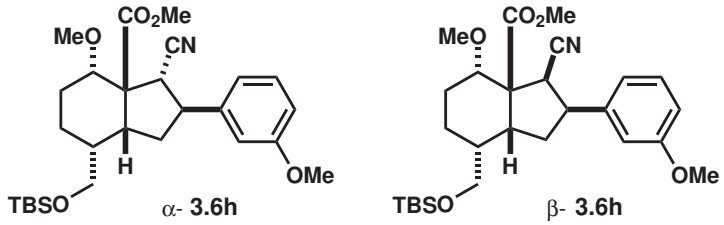

3-Methoxy tricycle (3.6h). Prepared according to method 2. Purification by flash column chromatography (eluting with 60–100% CH_2Cl_2/hexanes, then 1–5% Et_2O/CH_2Cl_2) provided *α*-**3.6h** and *β*-**3.6h** in 92% combined yield from 1.26 mmol of nitrile **2.27**.

α-**3.6h**. Isolated as a colorless oil (430 mg, 0.882 mmol, 70%). ^1H NMR (600 MHz, $CDCl_3$) δ 7.24 (t, *J* = 7.9 Hz, 1H), 6.87 (dt, *J* = 7.6, 1.2 Hz, 1H), 6.81 (t, *J* = 2.1 Hz, 1H), 6.77 (ddd, *J* = 8.2, 2.6, 0.9 Hz, 1H), 3.97 (bs, 1H), 3.81 (s, 3H), 3.73 (s, 3H), 3.71 (ddd, *J* = 11.3, 8.4, 2.9 Hz, 1H), 3.43 (s, 3H), 3.47–3.37 (m, 2H), 3.08 (d, *J* = 8.3 Hz, 1H), 3.03 (ddd, *J* = 13.6, 8.9, 4.8 Hz, 1H), 2.44 (td, *J* = 13.1, 11.6 Hz, 1H), 2.09 (dq, *J* = 14.1, 3.1 Hz, 1H), 2.00 (dtd, *J* = 16.0, 7.5, 4.9 Hz, 1H), 1.76 (ddd, *J* = 12.3, 9.0, 2.8 Hz, 1H), 1.48–1.33 (m, 3H), 0.89 (s, 9H), 0.03 (s, 3H), 0.01 (s, 3H); ^{13}C NMR (151 MHz, $CDCl_3$) δ 173.3, 160.1, 147.3, 130.1, 120.0, 119.1, 113.0, 112.2, 77.1, 66.3, 60.5, 57.1, 55.4, 52.9, 49.4, 47.5, 43.4, 38.2, 33.0, 26.0, 24.8, 18.4, 16.6, –5.26, –5.28; IR (thin film) 2951, 2929, 2897, 2857, 2239, 1732, 1600, 1463, 1255, 1119, 1084, 1051, 837, 777 cm^{-1}; HRMS (ESI) *m/z* $[M + Na]^+$ calc'd for $C_{27}H_{41}O_5NNaSi$ 510.2646, found 510.2647.

β-**3.6h**. Isolated as a colorless oil (132 mg, 0.271 mmol, 22%). ^1H NMR (600 MHz, $CDCl_3$) δ 7.24 (d, *J* = 7.9 Hz, 1H), 6.88 (dt, *J* = 7.5, 1.2 Hz, 1H), 6.80 (t, *J* = 2.1 Hz, 1H), 6.78 (ddd, *J* = 8.2, 2.6, 0.9 Hz, 1H), 3.92 (bs, 1H), 3.85–3.78 (m, 1H), 3.80 (s, 3H), 3.78 (s, 3H), 3.66 (d, *J* = 9.8 Hz, 1H), 3.46 (qd, *J* = 9.9, 7.4 Hz, 2H), 3.37 (s, 3H), 3.25 (ddd, *J* = 13.6, 8.9, 5.0 Hz, 1H), 2.31 (td, *J* = 13.1, 11.0 Hz, 1H), 2.15 (tdd, *J* = 12.3, 7.6, 4.9 Hz, 1H), 2.08 (dq, *J* = 14.1, 2.9 Hz, 1H), 1.87 (ddd, *J* = 12.4, 8.8, 3.0 Hz, 1H), 1.39–1.35 (m, 1H), 1.31 (qd, *J* = 12.9, 3.0 Hz, 1H), 1.20 (dddd, *J* = 14.8, 12.8, 4.0, 2.0 Hz, 1H), 0.91 (s, 9H), 0.06 (s, 3H), 0.04 (s, 3H); ^{13}C NMR (151 MHz, $CDCl_3$) δ 172.7, 159.7, 144.5, 129.6, 120.7, 119.2, 114.6, 112.4, 79.6, 66.6, 63.1, 57.3, 55.3, 53.0, 45.9, 44.8, 41.5, 38.1, 32.5, 26.1,

25.4, 18.4, 16.4, –5.2; IR (thin film) 2951, 2930, 2856, 2359, 1737, 1602, 1462, 1422, 1257, 1230, 1105, 1086, 1053, 837, 813, 803,778 cm^{-1}; HRMS (ESI) *m/z* $[M + Na]^+$ calc'd for $C_{27}H_{41}O_5NNaSi$ 510.2646, found 510.2639.

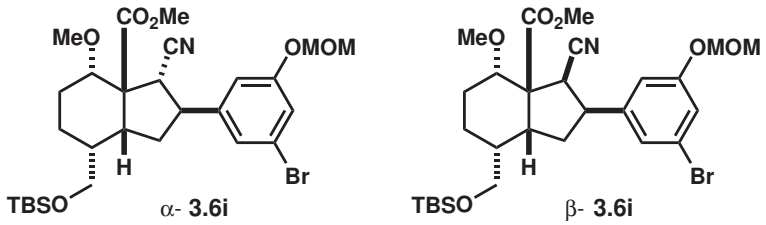

3-Bromo-5-OMOM tricycle (3.6i). Prepared according to method 1. Purification by flash column chromatography (eluting with 60–100% CH_2Cl_2/hexanes, then 1–5% Et_2O/CH_2Cl_2) provided **3.6i** (39.8 mg, 0.0667 mmol) as an inseparable mixture of diastereomers (2.3:1 α:β-**3.6i**) in 49% combined yield. NMR data reported separately for each isomer. IR (thin film) 2953, 2930, 2895, 2857, 2241, 1732, 1602, 1568, 1462, 1451, 1437, 1256, 1152, 1083, 1026, 1007, 838, 776 cm^{-1}; HRMS (APCI) *m/z* $[M + H]^+$ calc'd for $C_{28}H_{43}{}^{81}BrNO_6Si$ 598.2017, found 598.2020.

α-**3.6i**. ^{1}H NMR (600 MHz, $CDCl_3$) δ 7.10 (dd, *J* = 2.3, 1.7 Hz, 1H), 7.04 (t, *J* = 1.6 Hz, 1H), 6.85 (t, *J* = 1.9 Hz, 1H), 5.17 (d, *J* = 6.9 Hz, 1H), 5.12 (d, *J* = 6.9 Hz, 1H), 3.98–3.95 (m, 1H), 3.75 (s, 3H), 3.67 (ddd, *J* = 11.5, 8.5, 3.0 Hz, 1H), 3.47 (s, 3H), 3.47–3.44 (m, 1H), 3.42 (s, 3H), 3.40–3.33 (m, 1H), 3.04 (d, *J* = 8.5 Hz, 1H), 3.00 (ddd, *J* = 13.3, 8.9, 4.9 Hz, 1H), 2.48–2.37 (m, 1H), 2.09 (dq, *J* = 13.8, 3.0 Hz, 1H), 2.03–1.98 (m, 1H), 1.71 (ddd, *J* = 12.4, 9.0, 2.9 Hz, 1H), 1.48–1.41 (m, 1H), 1.34 (tt, *J* = 10.7, 3.5 Hz, 2H), 0.90 (s, 9H), 0.04 (s, 3H), 0.02 (s, 3H); ^{13}C NMR (151 MHz, $CDCl_3$) δ 173.1, 158.4, 148.8, 123.1, 120.2, 119.7, 117.8, 114.7, 94.6, 77.0, 66.1, 60.4, 57.1, 56.3, 53.0, 49.1, 47.2, 43.2, 38.1, 32.9, 26.1, 24.8, 18.4, 16.5, –5.25, –5.28.

β-**3.6i**. ^{1}H NMR (600 MHz, $CDCl_3$) δ 7.23 (tdd, *J* = 7.3, 2.0, 0.8 Hz, 1H), 6.92 (s, 1H), 6.91 (d, *J* = 2.4 Hz, 1H), 5.20 (d, *J* = 6.8 Hz, 1H), 5.15 (d, *J* = 6.8 Hz, 1H), 3.98–3.95 (m, 1H), 3.74 (s, 3H), 3.71 (ddd, *J* = 11.5, 8.6, 3.0 Hz, 1H), 3.48 (s, 3H), 3.47–3.44 (m, 1H), 3.43 (s, 3H), 3.40–3.33 (m, 1H), 3.08 (d, *J* = 8.3 Hz, 1H), 3.00 (ddd, *J* = 13.3, 8.9, 4.9 Hz, 1H), 2.48–2.37 (m, 1H), 2.09 (dq, *J* = 13.8, 3.0 Hz, 1H), 2.03–1.98 (m, 1H), 1.74 (ddd, *J* = 12.4, 9.0, 2.9 Hz, 1H), 1.48–1.41 (m, 1H), 1.37 (tt, *J* = 10.7, 3.5 Hz, 2H), 0.89 (s, 9H), 0.03 (s, 3H), 0.01 (s, 3H); ^{13}C NMR (151 MHz, $CDCl_3$) δ 173.3, 157.8, 147.4, 130.2, 123.4, 120.0, 115.5, 114.3, 94.6, 77.1, 66.2, 60.5, 57.1, 56.2, 52.9, 49.3, 47.4, 43.4, 38.2, 33.1, 26.0, 24.8, 18.4, 16.6, –5.26, –5.29.

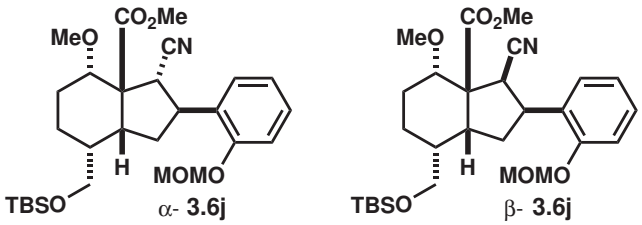

2-OMOM tricycle (3.6j). Prepared according to method 1. Purification by flash column chromatography (eluting with 60–100% CH_2Cl_2/hexanes, then 1–5% Et_2O/CH_2Cl_2) provided α-**3.6j** and β-**3.6j** in 76% combined yield.

α-**3.6j**. Isolated as a colorless oil (36.3 mg, 0.0701 mmol, 53%). ^{1}H NMR (600 MHz, $CDCl_3$) δ 7.22 (dd, *J* = 7.6, 1.7 Hz, 1H), 7.19 (ddd, *J* = 8.2, 7.3, 1.7 Hz, 1H), 7.11 (dd, *J* = 8.3, 1.2 Hz, 1H), 6.95 (td, *J* = 7.4, 1.2 Hz, 1H), 5.25 (d, *J* = 6.9 Hz, 1H), 5.23 (d, *J* = 6.9 Hz, 1H), 4.01 (ddd, *J* = 11.6, 8.6, 3.0 Hz, 1H), 3.99 (dd, *J* = 3.2, 1.6 Hz, 1H), 3.72 (s, 3H), 3.50 (s, 3H), 3.45 (s, 3H), 3.42 (d, *J* = 7.3 Hz, 2H), 3.30 (d, *J* = 8.4 Hz, 1H), 3.15 (ddd, *J* = 13.4, 8.8, 4.9 Hz, 1H), 2.38 (q, *J* = 12.4 Hz, 1H), 2.13–2.07 (m, 1H), 1.98 (dq, *J* = 12.1, 5.9 Hz, 1H), 1.76 (ddd, *J* = 12.2, 8.9, 3.0 Hz, 1H), 1.48–1.32 (m, 3H), 0.89 (s, 9H), 0.03 (s, 3H), 0.02 (s, 3H); ^{13}C NMR (151 MHz, $CDCl_3$) δ 173.6, 155.0, 133.2, 128.8, 128.3, 122.1, 120.5, 114.2, 94.4, 77.2, 66.6, 60.6, 57.0, 56.3, 52.8, 44.79, 44.76, 43.0, 38.4, 32.0, 26.0, 25.0, 18.4, 16.8, –5.2, –5.3; IR (thin film) 2952, 2929, 2895, 2856, 2239, 1728, 1492, 1471, 1249, 1077, 1000, 835, 775, 753 cm^{-1}; HRMS (ESI) *m/z* [M + Na]$^+$ calc'd for $C_{28}H_{43}O_6NNaSi$ 540.2752, found 540.2748.

β-**3.6j**. Isolated as a colorless oil (15.5 mg, 0.0299 mmol, 23%). ^{1}H NMR (600 MHz, $CDCl_3$) δ 7.33 (dd, *J* = 7.7, 1.6 Hz, 1H), 7.21 (ddd, *J* = 8.2, 7.4, 1.7 Hz, 1H), 7.10 (dd, *J* = 8.3, 1.2 Hz, 1H), 7.00 (td, *J* = 7.5, 1.2 Hz, 1H), 5.25 (d, *J* = 6.6 Hz, 1H), 5.20 (d, *J* = 6.6 Hz, 1H), 4.17 (td, *J* = 11.2, 2.7 Hz, 1H), 3.93 (p, *J* = 1.3 Hz, 1H), 3.78 (d, *J* = 9.8 Hz, 1H), 3.75 (s, 3H), 3.52 (s, 3H), 3.54–3.47 (m, 2H), 3.40 (s, 3H), 3.23 (ddd, *J* = 13.5, 8.5, 4.9 Hz, 1H), 2.26 (td, *J* = 13.2, 11.1 Hz, 1H), 2.18–2.09 (m, 1H), 2.08 (dq, *J* = 14.4, 3.1 Hz, 1H), 1.99 (ddd, *J* = 12.1, 8.4, 2.7 Hz, 1H), 1.39–1.30 (m, 2H), 1.20 (ddd, *J* = 17.1, 10.4, 4.3 Hz, 1H), 0.93 (s, 9H), 0.08 (s, 3H), 0.07 (s, 3H); ^{13}C NMR (151 MHz, $CDCl_3$) δ 172.9, 155.4, 131.4, 128.4, 127.8, 122.0, 119.4, 114.0, 95.0, 79.8, 66.7, 62.9, 57.4, 56.3, 52.9, 43.7, 41.3, 38.9, 38.1, 29.9, 26.1, 25.5, 18.5, 16.6, –5.18, –5.20; IR (thin film) 2951, 2928, 2896, 2855, 2236, 1739, 1492, 1457, 1249, 1231, 1082, 1003, 836, 776, 754 cm^{-1}; HRMS (ESI) *m/z* [M + Na]$^+$ calc'd for $C_{28}H_{43}O_6NNaSi$ 540.2752, found 540.2746.

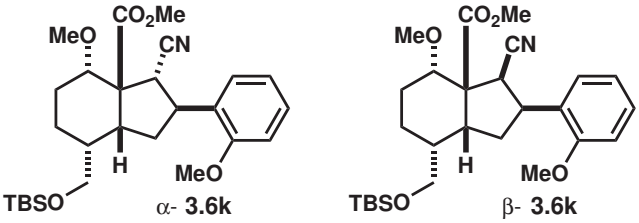

2-Methoxy tricycle (3.6k). Prepared according to method 2. Purification by flash column chromatography (eluting with 60–100% CH_2Cl_2/hexanes, then 1–5% Et_2O/CH_2Cl_2) provided α-**3.6k** and β-**3.6k** in 57% combined yield from 200 mg (0.527 mmol) of nitrile **2.27**.

α-**3.6k**. Isolated as a colorless oil (110. mg, 0.223 mmol, 42%). ^{1}H NMR (600 MHz, $CDCl_3$) δ 7.22 (td, *J* = 7.6, 1.7 Hz, 1H), 7.19 (dd, *J* = 7.6, 1.6 Hz, 1H), 6.89 (td, *J* = 7.5, 1.0 Hz, 1H), 6.86 (d, *J* = 8.2 Hz, 1H), 3.97 (t, *J* = 2.1 Hz, 1H), 3.92 (ddd, *J* = 11.7, 8.5, 3.1 Hz, 1H), 3.84 (s, 3H), 3.73 (s, 3H), 3.44 (s, 3H), 3.41 (dd, *J* = 7.4, 1.3 Hz, 2H), 3.38 (d, *J* = 8.5 Hz, 1H), 3.18 (ddd, *J* = 13.3, 8.9, 4.9 Hz, 1H), 2.32 (q, *J* = 12.3 Hz, 1H), 2.09 (dq, *J* = 12.4, 2.5 Hz, 1H), 1.97 (dtt, *J* = 11.8, 7.6, 4.5 Hz, 1H), 1.75 (ddd, *J* = 12.3, 9.0, 3.2 Hz, 1H), 1.46–1.31 (m, 3H), 0.88 (s, 9H), 0.03 (s, 3H), 0.01 (s, 3H); ^{13}C NMR (151 MHz, $CDCl_3$) δ 173.7, 157.3, 132.4, 129.3, 128.3, 120.8, 120.7, 111.0, 77.3, 66.5, 60.6, 57.0, 55.3, 52.8, 45.7, 44.1, 42.7, 38.3, 31.8, 26.0, 25.0, 18.4, 16.8, –5.2; IR (thin film) 2951, 2930, 2856, 2239, 1730, 1601, 1494, 1462, 1247, 1102, 1082, 837, 776, 753 cm^{-1}; HRMS (ESI) *m/z* [M + Na]$^+$ calc'd for $C_{27}H_{41}O_5NNaSi$ 510.2646, found 510.2653.

β-**3.6k**. Isolated as a colorless oil (37.7 mg, 0.0773 mmol, 15%). ^{1}H NMR (600 MHz, $CDCl_3$) δ

7.31 (dd, *J* = 7.7, 1.6 Hz, 1H), 7.23 (ddd, *J* = 8.2, 7.4, 1.7 Hz, 1H), 6.95 (td, *J* = 7.5, 1.1 Hz, 1H), 6.87 (dd, *J* = 8.2, 1.1 Hz, 1H), 4.13 (ddd, *J* = 11.4, 9.7, 2.7 Hz, 1H), 3.92 (t, *J* = 2.9 Hz, 1H), 3.85 (s, 3H), 3.78 (d, *J* = 9.7 Hz, 1H), 3.75 (s, 3H), 3.54–3.46 (m, 2H), 3.40 (s, 3H), 3.23 (ddd, *J* = 13.5, 8.5, 4.9 Hz, 1H), 2.24 (td, *J* = 13.1, 11.0 Hz, 1H), 2.13 (dt, *J* = 14.0, 7.4 Hz, 1H), 2.07 (dq, *J* = 14.5, 3.3 Hz, 1H), 1.99 (ddd, *J* = 12.2, 8.5, 2.8 Hz, 1H), 1.37–1.30 (m, 2H), 1.23–1.15 (m, 1H), 0.93 (s, 9H), 0.08 (s, 3H), 0.07 (s, 3H); ^{13}C NMR (151 MHz, $CDCl_3$) δ 172.8, 157.3, 130.6, 128.1, 127.5, 120.5, 119.3, 110.3, 79.6, 66.5, 62.6, 57.3, 55.3, 52.7, 43.5, 41.0, 38.8, 37.9, 29.5, 25.9, 25.4, 18.3, 16.4, –5.38, –5.39; IR (thin film) 2950, 2930, 2857, 2235, 1740, 1494, 1463, 1244, 1103, 1086, 1056, 1033, 837, 776, 752 cm^{-1}; HRMS (ESI) *m/z* [M + Na]$^+$ calc'd for $C_{27}H_{41}O_5NNaSi$ 510.2646, found 510.2641.

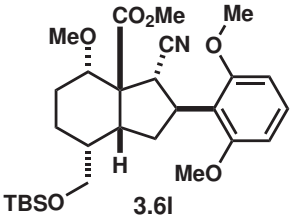

3.6l

2,6-Dimethoxy tricycle (3.6l). Prepared according to method 1. Purification by flash column chromatography (eluting with 60–100% CH_2Cl_2/hexanes, then 1–5% Et_2O/CH_2Cl_2) provided α-**3.6l** as a single diastereomer (52.4 mg, 0.101 mmol, 83%). ^{1}H NMR (600 MHz, $CDCl_3$) δ 7.16 (t, *J* = 8.3 Hz, 1H), 6.54 (d, *J* = 8.3 Hz, 2H), 4.48 (ddd, *J* = 11.9, 10.2, 3.5 Hz, 1H), 3.90 (t, *J* = 2.5 Hz, 1H), 3.80 (s, 6H), 3.79 (s, 3H), 3.56–3.43 (m, 3H), 3.40 (s, 3H), 3.35 (dd, *J* = 9.9, 7.9 Hz, 1H), 2.14–1.98 (m, 3H), 1.91 (ddd, *J* = 12.2, 9.2, 3.5 Hz, 1H), 1.40 (dq, *J* = 11.6, 3.6 Hz, 1H), 1.32 (qd, *J* = 13.1, 3.0 Hz, 1H), 1.18 (tdd, *J* = 13.5, 3.8, 1.9 Hz, 1H), 0.89 (s, 9H), 0.04 (s, 3H), 0.03 (s, 3H); ^{13}C NMR (151 MHz, $CDCl_3$) δ 173.1, 158.9, 128.3, 120.30, 118.5, 104.3, 80.2, 67.2, 63.5, 57.5, 55.7, 52.8, 43.1, 40.9, 38.6, 34.8, 31.0, 26.1, 25.8, 18.5, 16.9, –5.17, –5.22; IR (thin film) 2951, 2931, 2895, 2856, 2237, 1739, 1594, 1474, 1594, 1474, 1249, 1102, 838, 775 cm^{-1}; HRMS (ESI) *m/z* [M + Na]$^+$ calc'd for $C_{28}H_{43}O_6NNaSi$ 540.2752, found 540.2746.

3.7.3 First-generation approach to designed analogs

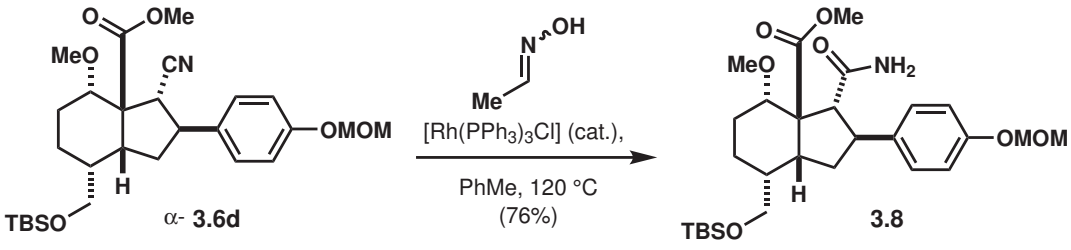

Amide 3.8. Nitrile **2.27** (66 mg, 0.13 mmol) and $Rh(PPh_3)_3Cl$ (11 mg, 13 μmol) were added to a vial and taken into a glovebox. Toluene (60 μL) was added, followed by acetaldoxime (0.20 mL, 3.2 mmol). The reaction mixture was heated to 120 °C for 14.5 h, then cooled to room temperature and diluted with EtOAc to prevent solid formation. The crude reaction mixture was immediately purified by flash column chromatography (1–70% EtOAc in hexanes) to afford 52 mg of amide **3.8** as a clear oil (97 μmol, 76% yield). ^{1}H NMR (600 MHz, $CDCl_3$) δ 7.25 (d, *J*

= 8.6 Hz, 2H), 6.97 (d, *J* = 8.6 Hz, 2H), 5.96 (bs, 1H), 5.44 (bs, 1H), 5.17–5.12 (m, 2H), 4.10–4.08 (m, 1H), 3.82–3.71 (m, 1H), 3.75 (s, 3H), 3.47 (s, 3H), 3.40–3.31 (m, 3H), 3.24 (s, 3H), 3.03 (ddd, *J* = 13.3, 8.7, 4.6 Hz, 1H), 2.41 (q, *J* = 12.5 Hz, 1H), 2.07–2.00 (m, 1H), 1.83 (dt, *J* = 12.1, 7.9 Hz, 1H), 1.57–1.46 (m, 1H), 1.56 (ddd, *J* = 12.4, 8.9, 3.0 Hz, 1H), 1.43–1.30 (m, 2H), 0.88 (s, 9H), 0.01 (s, 3H), –0.01 (s, 3H); ^{13}C NMR (151 MHz, $CDCl_3$) δ 176.2, 173.7, 155.8, 141.7, 128.2, 116.8, 94.7, 66.4, 62.9, 60.0, 56.6, 56.0, 52.7, 45.2, 44.2, 38.7, 34.8, 34.0, 26.0, 25.1, 18.3, 17.0, –5.29, –5.31; IR (ATR, thin film) 2950, 2928, 2895, 2856, 1726, 1672, 1608, 1510 cm^{-1}; HRMS (ESI) *m/z* [M + H]$^+$ calc'd for $C_{28}H_{46}O_7NSi$ 536.3038, found 536.3036.

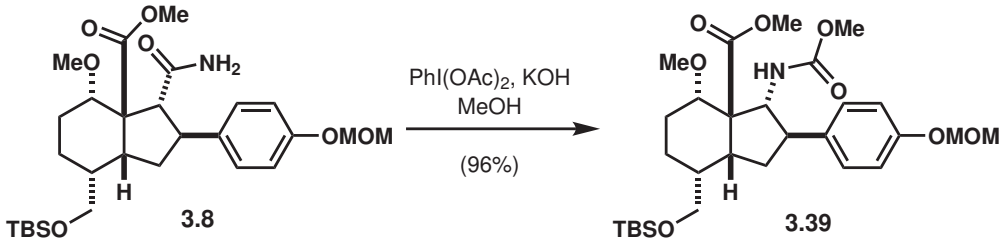

Carbamate 3.39. Amide **3.8** (0.10 g, 0.19 mmol) and KOH (40 mg, 0.66 mmol) were suspended in MeOH (1.9 mL). The mixture was stirred until only fine KOH particulates were visible, then cooled in an ice/water bath before $PhI(OAc)_2$ (81 mg, 0.25 mmol) was added. The reaction mixture was stirred in the cold bath for 1 h, then at room temperature for 1.5 h. The reaction mixture was concentrated *in vacuo* to remove MeOH, reconstituted in water, and extracted with CH_2Cl_2. The combined organic extracts were washed with brine, dried over Na_2SO_4, filtered, and concentrated *in vacuo* to afford 1.0 g of carbamate **3.39** as a clear oil (0.19 mmol, 96% yield), which was used without purification. ^{1}H NMR (500 MHz, $CDCl_3$) δ 7.16 (d, *J* = 8.0 Hz, 2H), 6.95 (d, *J* = 8.1 Hz, 2H), 5.14 (s, 2H), 4.99 (d, *J* = 10.1 Hz, 1H), 4.41 (t, *J* = 9.3 Hz, 1H), 4.04 (s, 1H), 3.70 (s, 3H), 3.56 (s, 3H), 3.47 (s, 3H), 3.45–3.37 (m, 2H), 3.36 (s, 3H), 3.18 (t, *J* = 8.9 Hz, 1H), 3.07 (q, *J* = 13.3, 11.3 Hz, 1H), 2.33 (q, *J* = 12.6 Hz, 1H), 2.13 (d, *J* = 9.5 Hz, 1H), 1.77 (bs, 1H), 1.51 (t, *J* = 11.0 Hz, 1H), 1.39–1.23 (m, 3H), 0.89 (s, 9H), 0.02 (s, 3H), 0.00 (s, 3H); ^{13}C NMR (126 MHz, $CDCl_3$, 323 K) δ 174.7, 156.6, 156.0, 140.2, 128.2, 116.7, 94.9, 67.8, 66.2, 59.4, 56.0, 55.8, 52.5, 52.1, 51.1, 41.5, 38.9, 32.0, 26.1, 24.6, 18.4, 17.1, –5.23, –5.24;* IR (ATR, thin film) 2952, 2937, 2929, 2856, 1728, 1511, 1463 cm^{-1}; HRMS (ESI) *m/z* [M + Na]$^+$ calc'd for $C_{29}H_{47}O_8NNaSi$ 588.2963, found 588.2965. *^{13}C NMR spectrum taken at 323 K in order to allow rotamers to converge.

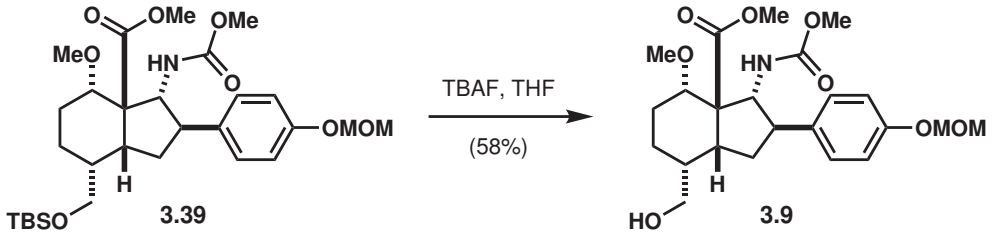

Alcohol 3.9. Carbamate **3.39** (0.11 g, 0.19 mmol) was dissolved in THF (1.9 mL) at room temperature. A 1.0 M solution of TBAF in THF (0.28 mL, 0.28 mmol) was added dropwise and the reaction mixture was stirred for 11 h. The reaction mixture was concentrated *in vacuo* to remove THF, then reconstituted in EtOAc. The crude mixture was then washed with water and with brine, then dried over Na_2SO_4, filtered and concentrated *in vacuo*. The concentrate was

purified by flash column chromatography (34–55% EtOAc in hexanes) to afford 54 mg of alcohol **3.9** as a white foam (0.12 mmol, 58% yield). ^{1}H NMR (600 MHz, $CDCl_3$) δ 7.15 (d, *J* = 8.3 Hz, 2H), 6.94 (d, *J* = 8.3 Hz, 2H), 5.12 (s, 2H), 4.99 (d, *J* = 10.1 Hz, 1H), 4.42 (t, *J* = 9.3 Hz, 1H), 4.05 (bs, 1H), 3.69 (s, 3H), 3.55 (s, 3H), 3.45 (s, 3H), 3.44–3.38 (m, 2H), 3.35 (s, 3H), 3.13 (dt, *J* = 18.1, 8.6 Hz, 2H), 2.33 (q, *J* = 12.4 Hz, 1H), 2.13 (d, *J* = 13.1 Hz, 1H), 1.79 (bs, 1H), 1.52 (t, *J* = 10.3 Hz, 1H), 1.41–1.20 (m, 4H); ^{13}C NMR (126 MHz, C_6D_6) δ 174.5, 156.8, 140.3, 128.4, 117.2, 100.5, 95.0, 76.7, 66.0, 59.8, 55.5, 55.3, 52.2, 51.8, 51.5, 41.8, 39.3, 32.3, 30.2, 24.9, 17.4;* IR (ATR, thin film) 3600–3200, 3195, 2950, 2929, 1723, 1511 cm^{-1}; HRMS (ESI) *m/z* [M + H]$^+$ calc'd for $C_{23}H_{34}NO_8$ 452.2279, found 452.2276. *^{13}C NMR spectrum taken at 343 K in C_6D_6 in order to allow rotamers to converge.

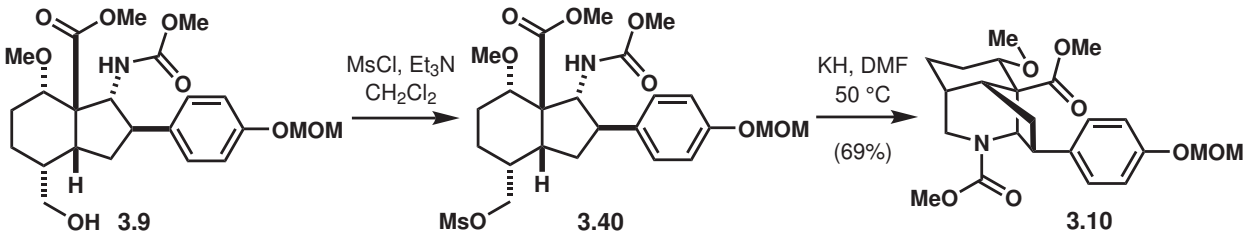

Piperidine 3.10. To a solution of alcohol **3.9** (74.4 mg, 0.160 mmol) in CH_2Cl_2 (1.6 mL, 0.1 M) was added Et_3N (0.11 mL, 0.820 mmol, 5 equiv). MsCl (19 μL, 0.250 mmol, 1.5 equiv) was added dropwise via syringe. The reaction mixture was stirred at room temperature for 3.25 h, then quenched with NH_4Cl (saturated aqueous, 0.5 mL). The aqueous layer was extracted with CH_2Cl_2 (3 x 1 mL). Then, the combined organic extracts were washed with brine (0.5 mL), dried over Na_2SO_4, filtered, and concentrated *in vacuo* to give mesylate **3.40** as a pale yellow foam (81.8 mg, 0.154 mmol, 94% yield), which was advanced without further purification. ^{1}H NMR (400 MHz, C_6D_6) δ 7.22 (d, *J* = 8.5 Hz, 2H), 7.06 (d, *J* = 8.2 Hz, 2H), 4.93 (dt, *J* = 18.6, 10.0 Hz, 2H), 4.83 (s, 2H), 4.07 (bs, 1H), 3.75 (dd, *J* = 9.4, 7.4 Hz, 1H), 3.68 (dd, *J* = 9.6, 6.9 Hz, 1H), 3.55 (s, 3H), 3.32 (s, 3H), 3.26 (ddd, *J* = 13.3, 4.7, 4.3 Hz, 1H), 3.22–3.15 (m, 1H), 3.12 (s, 3H), 2.76 (s, 3H), 2.15 (s, 3H), 1.99–1.88 (m, 1H), 1.75–1.68 (m, 1H), 1.42 (ddd, *J* = 12.3, 9.2, 3.1 Hz, 1H), 1.16–1.03 (m, 3H).

To a solution of mesylate **3.40** (131.8 mg, 0.249 mmol) in DMF (2.5 mL, 0.1 M) was added KH (dried by washing with 3 x 1 mL hexanes, 25.4 mg, 0.473 mmol, 2.5 equiv). The reaction mixture was stirred at room temperature for 32 h, at which point TLC analysis showed remaining starting material. An additional portion of KH (10.0 mg, 0.249 mmol, 1 equiv) was added and the reaction allowed to stir for 2 h. The reaction was quenched with H_2O (1 mL), then poured into a 9:1 H_2O:brine mixture and extracted with EtOAc (3 x 5 mL). The combined organic extracts were dried with Na_2SO_4, filtered, and concentrated *in vacuo* to give piperidine **3.10** as a clear oil (74.3 mg, 0.171 mmol, 69% yield). ^{1}H NMR (600 MHz, C_6D_6) δ 7.08 (d, *J* = 8.6 Hz, 2H), 7.05 (d, *J* = 8.7 Hz, 2H), 4.87–4.83 (m, 2H), 4.58 (d, *J* = 14.4 Hz, 1H), 4.31 (s, 1H), 4.23 (s, 2H), 3.64 (dd, *J* = 10.4, 7.5 Hz, 1H), 3.39 (d, *J* = 9.7 Hz, 1H), 3.13 (s, 3H), 3.09 (s, 3H), 3.04 (s, 3H), 2.84–2.78 (m, 1H), 2.29 (s, 3H), 2.26 (t, *J* = 5.0 Hz, 1H), 2.18 (dt, *J* = 13.3, 6.6 Hz, 1H), 1.80 (dt, *J* = 12.1, 6.0 Hz, 1H), 1.70 (dd, *J* = 13.6, 9.8 Hz, 1H), 1.67–1.61 (m, 1H), 1.30–1.23 (m, 1H); IR (thin film) 3472, 2950, 1698, 1601, 1511, 1466, 1236, 1151, 1080, 978, 837, 776 cm^{-1}; HRMS (ESI) *m/z* [M + Na]$^+$ calc'd for $C_{23}H_{31}NaNO_7$ 456.1993, found 456.1995.

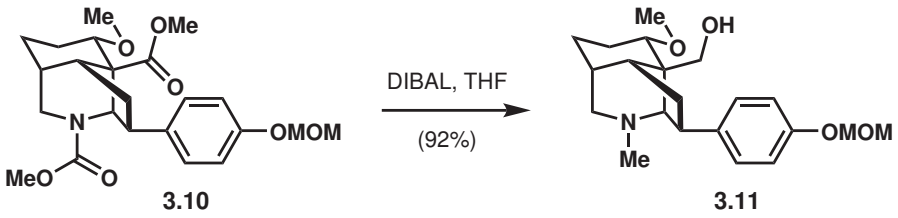

Alcohol 3.11. To a vial containing ester **3.10** (226.4 mg, 0.522 mmol) was added THF (5.20 mL) at room temperature in a glovebox. Solution was cooled in freezer at –30 °C. To the cold ester solution was added a 1.0 M solution of DIBAL in PhMe (3.20 mL, 2.87 mmol, 5.5 equiv). The reaction mixture was stored in the freezer for 10 min, then allowed to stir at ambient temperature (~30 °C) for 43 h. The reaction mixture was removed from the glovebox and quenched with an aqueous solution of Rochelle's salt (20 wt %, 2.0 mL). The quenched mixture was allowed to stir at room temperature under air for 12 h, then extracted with a 2:1 mixture of $CHCl_3$:EtOH (3 x 3 mL). The crude mixture was then washed brine (1.0 mL), dried over Na_2SO_4, filtered and concentrated *in vacuo*. The concentrate was purified by flash column chromatography (eluting with 10% MeOH in CH_2Cl_2 with 0.1% saturated aqueous NH_4OH) to afford 174 mg of alcohol **3.11** as a clear oil (0.481 mmol, 92% yield). ^{1}H NMR (600 MHz, C_6D_6) δ 7.28 (d, *J* = 7.7 Hz, 2H), 7.15 (d, *J* = 7.7 Hz, 2H), 4.89 (s, 2H), 3.83 (s, 1H), 3.50 (d, *J* = 10.5, 1H), 3.48 (d, *J* = 11.0, 1H), 3.20–3.16 (m, 2H), 3.16 (s, 3H), 3.11 (s, 3H), 2.53 (dtd, *J* = 14.1, 11.1, 5.4 Hz, 1H), 2.24 (d, *J* = 11.6 Hz, 1H), 2.15 (ddd, *J* = 11.8, 5.1, 2.0 Hz, 1H), 2.09 (s, 3H), 2.04 (dt, *J* = 13.0, 6.4 Hz, 1H), 1.85–1.79 (m, 1H), 1.65–1.56 (m, 3H), 1.35–1.25 (m, 2H); ^{13}C NMR (126 MHz, C_6D_6) δ 155.8, 139.5, 128.4, 116.4, 94.6, 84.3, 68.7, 67.5, 55.8, 55.5, 53.3, 52.4, 42.6, 42.3, 36.8, 34.8, 34.1, 30.3, 26.0. IR (thin film) 3426, 2925, 2892, 2826, 2782, 1509, 1444, 1234, 1180, 1077, 1002, 859, 839, 651, 556 cm^{-1}; HRMS (ESI) *m/z* $[M + H]^+$ calc'd for $C_{21}H_{32}NO_4$ 362.2326, found 362.2324.

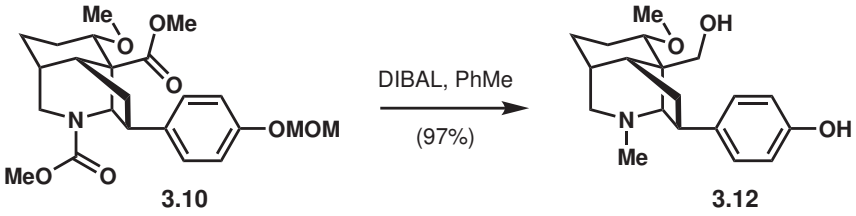

Diol 3.12. Piperidine **3.10** (512 mg, 1.18 mmol) was dissolved in PhMe (2.60 mL) at room temperature, then cooled to –30 °C in a glovebox freezer. A 0.90 M solution of DIBAL in PhMe (9.20 mL, 8.26 mmol, 7.0 equiv) was added dropwise. The reaction mixture was stored at –30 °C for 10 min, then allowed to warm to room temperature over 10 h. At this point, the reaction mixture contained ~2:1 MOM ether **3.11** and desired product ??. The reaction mixture was then removed from the glovebox and heated in an oil bath at 30 °C for 8 h, at which point it was cooled to room temperature and quenched with an aqueous solution of Rochelle's salt (20 wt %, 3.0 mL). The quenched mixture was allowed to stir at room temperature under air for 12 h, then extracted with a 2:1 mixture of $CHCl_3$:EtOH (3 x 3 mL). The crude mixture was then washed brine (2 mL), dried over Na_2SO_4, filtered and concentrated *in vacuo*. The concentrate was purified by flash column chromatography (eluting with 10% MeOH in CH_2Cl_2 with 0.1% saturated aqueous NH_4OH) to afford 364 mg of diol **3.12** as a flat white powder (1.15 mmol, 97% yield). ^{1}H NMR (600 MHz, $CDCl_3$) δ 7.15 (d, *J* = 8.2 Hz, 2H), 6.60 (d, *J* = 8.5 Hz, 2H), 4.31 (d, *J* = 9.1

Hz, 1H)*, 3.77 (s, 1H), 3.64 (dd, *J* = 10.9, 6.7 Hz, 1H), 3.42 (s, 3H), 3.42–3.38 (m, 1H), 3.32–3.28 (m, 1H), 3.28 (d, *J* = 11.1 Hz, 1H), 2.49 (d, *J* = 11.8 Hz, 1H), 2.49–2.42 (m, 1H), 2.41 (dd, *J* = 12.3, 4.6 Hz, 1H), 2.26 (s, 3H), 2.15 (dt, *J* = 13.1, 6.3 Hz, 1H), 2.02 (dt, *J* = 16.4, 6.5 Hz, 1H), 1.87–1.81 (m, 2H), 1.73 (t, *J* = 5.1 Hz, 1H), 1.66 (t, *J* = 3.7 Hz, 1H), 1.49 (t, *J* = 13.8 Hz, 1H); ^{13}C NMR (226 MHz, $CDCl_3$) δ 154.3, 136.3, 127.2, 115.2, 87.4, 77.3, 69.8, 68.3, 56.2, 53.3, 51.5, 43.0, 42.8, 36.5, 34.6, 33.5, 30.1, 25.8; IR (thin film) 3491, 3181, 2930, 2920, 2874, 1882, 1613, 1512, 1300, 1071, 941, 839, 820, 718, 525 cm^{-1}; HRMS (ESI) *m/z* [M + H]$^+$ calc'd for $C_{19}H_{28}NO_3$ 318.2064, found 318.2064. *Signal corresponds to the aliphatic hydroxy group based on HSQC correlations.

3.7.4 Synthesis of dienone 3.33 from ester α-3.6d

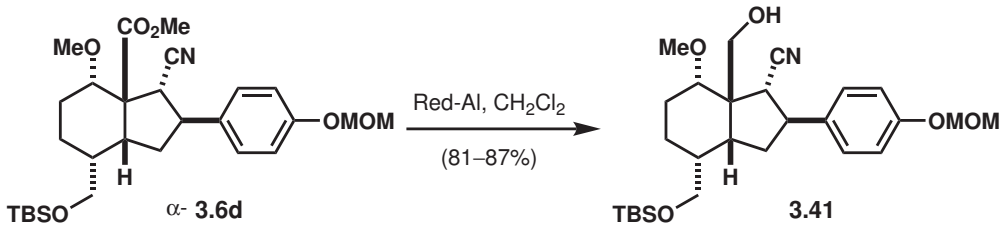

Alcohol 3.41. Ester *α*-**3.6d** (1.732 g, 3.34 mmol, 1.0 equiv) was dissolved in CH_2Cl_2 (33 mL, 0.1 M) and cooled in an ice/water bath. Red-Al solution (3.4 mL, 11.7 mmol, 3.5 equiv, 70 wt % in PhMe) was added dropwise over 5 min. The reaction mixture was stirred in the bath for 1 h, then allowed to warm gradually to room temperature over 2.25 h. The reaction mixture was then diluted with THF (25 mL), at which point it was cooled in an ice/water bath again and quenched by the serial addition of H_2O (88 μL), NaOH (2.0 M aqueous, 88 μL), and H_2O (3 x 88 μL). The reaction mixture was allowed to warm gradually to room temperature over 12 h, then filtered over a plug of Celite, which was rinsed with THF (25 mL), then EtOAc (50 mL). The combined organic filtrates were concentrated *in vacuo* to give a colorless oil. Purification by flash column chromatography (eluting with 17–37% EtOAc/hexanes) provided alcohol **3.41** as a clear gum (1.365 g, 2.79 mmol, 83%). ^{1}H NMR (700 MHz, C_6D_6) δ 7.21 (dd, *J* = 8.2, 1.2 Hz, 2H), 7.05 (dd, *J* = 8.7, 1.0 Hz, 2H), 4.86 (qd, *J* = 6.9, 1.0 Hz, 2H), 3.80 (ddd, *J* = 11.4, 8.4, 2.7 Hz, 1H), 3.33 (dd, *J* = 14.8, 7.0 Hz, 1H), 3.32 (dd, *J* = 14.8, 7.0 Hz, 1H), 3.28 (s, 3H), 3.24 (d, *J* = 11.1 Hz, 1H), 3.20 (s, 1H), 3.15 (s, 3H), 3.06 (d, *J* = 8.5 Hz, 1H), 2.52 (ddd, *J* = 13.4, 8.6, 4.7 Hz, 1H), 2.39 (q, *J* = 12.4 Hz, 1H), 1.79–1.71 (m, 2H), 1.70 (dq, *J* = 14.8, 3.1 Hz, 1H), 1.63 (ddd, *J* = 12.2, 8.7, 2.7 Hz, 1H), 1.34 (qd, *J* = 13.4, 3.4 Hz, 1H), 1.22 (dd, *J* = 13.3, 3.5 Hz, 1H), 1.01 (tt, *J* = 12.9, 2.3 Hz, 1H), 0.97 (s, 9H), 0.03 (s, 3H), 0.01 (s, 3H); ^{13}C NMR (176 MHz, C_6D_6) δ 156.7, 140.5, 128.3, 121.5, 117.0, 94.5, 78.0, 66.8, 63.5, 56.9, 55.8, 55.5, 48.2, 45.8, 39.7, 37.8, 34.3, 26.1, 24.3, 18.5, 17.4, –5.3; IR (thin film) 3474, 2952, 2929, 2890, 2857, 2234, 1511, 1250, 1088, 1007, 836, 776 cm^{-1}; HRMS (ESI) *m/z* [M + Na]$^+$ calc'd for $C_{27}H_{43}NNaO_5Si$ 512.2803, found 512.2806.

MOM ether 3.19. Alcohol **3.41** (2.60 g, 5.30 mmol, 1.0 equiv) was dissolved in PhMe (26 mL, 0.2 M) in a round-bottomed flask. DIPEA (3.70 mL, 21.2 mmol, 4.0 equiv) was added to the stirring mixture, followed by MOMCl (1.60 mL, 21.2 mmol, 4.0 equiv). The flask was fitted with a reflux condenser and heated in an oil bath at 70 °C for 12 h. The reaction mixture was then allowed to cool to room temperature, at which point it was quenched by the addition of $NaHCO_3$

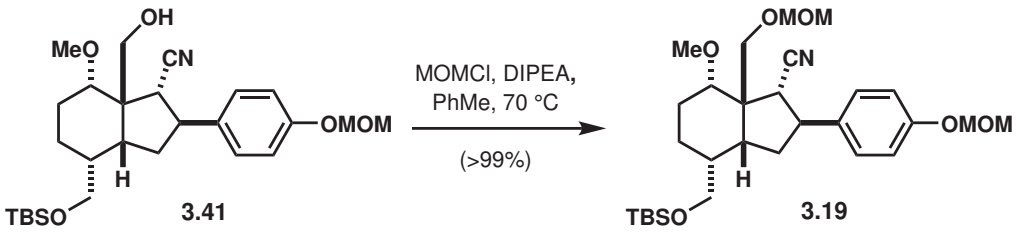

(saturated aqueous, 20 mL) and extracted with EtOAc (3 x 10 mL). The combined organic extracts were washed with brine (10 mL), dried over Na_2SO_4, filtered, and concentrated *in vacuo* to provide MOM ether **3.19** as an orange oil (2.84 g, 5.30 mmol, >99% crude yield), which was advanced without further purification. ^{1}H NMR (500 MHz, C_6D_6) δ 7.22 (d, *J* = 8.7 Hz, 2H), 7.05 (d, *J* = 8.7 Hz, 2H), 4.91–4.69 (m, 2H), 4.30 (bs, 2H), 3.83 (ddd, *J* = 11.4, 8.4, 2.7 Hz, 1H), 3.34–3.29 (m, 1H), 3.30 (s, 3H), 3.31–3.25 (m, 3H), 3.21 (d, *J* = 9.9 Hz, 1H), 3.13 (s, 3H), 3.12 (s, 1H), 3.10 (s, 3H), 2.57 (ddd, *J* = 13.4, 8.6, 4.8 Hz, 1H), 2.39 (q, *J* = 12.3 Hz, 1H), 1.76 (qt, *J* = 7.3, 3.6 Hz, 1H), 1.71–1.63 (m, 1H), 1.66 (t, *J* = 3.7 Hz, 1H), 1.33 (qd, *J* = 13.0, 2.4 Hz, 1H), 1.14 (dd, *J* = 13.4, 3.5 Hz, 1H), 1.08–0.97 (m, 1H), 0.95 (s, 9H), 0.01 (s, 3H), –0.01 (s, 3H); ^{13}C NMR (126 MHz, C_6D_6) δ 156.7, 140.5, 128.2, 120.9, 117.0, 96.5, 94.4, 78.0, 68.9, 66.5, 57.0, 55.5, 55.1, 54.4, 48.3, 46.8, 40.6, 37.8, 34.0, 26.1, 24.2, 18.4, 17.3, –5.3; IR (thin film) 2950, 2929, 2889, 2856, 2235, 1732, 1610, 1511, 1151, 1080, 1039, 833, 774 cm^{-1}; HRMS (ESI) *m/z* [M + Na]$^+$ calc'd for $C_{29}H_{47}NNaO_6Si$ 556.3065, found 556.3077.

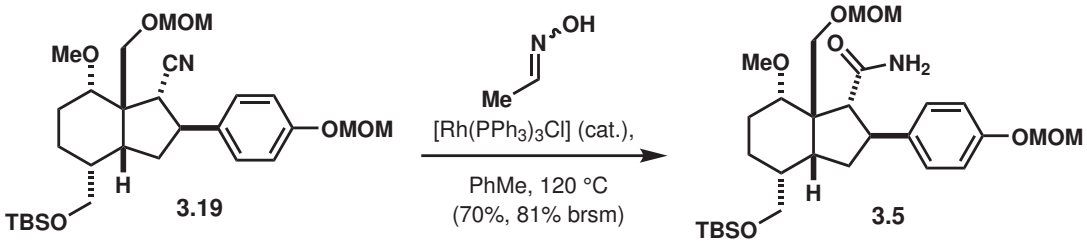

Amide 3.5. MOM ether **3.19** (1.34 g, 2.51 mmol, 1.0 equiv) and $Rh(PPh_3)_3Cl$ (234.5 mg, 0.251 mmol, 10 mol %) were dissolved in PhMe (5.0 mL, 0.5 M) in a round-bottomed flask. Acetaldoxime (3.8 mL, 62.8 mmol, 25 equiv) was sparged with N_2 for 15 min, then added to the flask, which was then fitted with a reflux condenser. The reaction mixture was heated to 120 °C and held at this temperature for 14 h, at which point it was allowed to cool to room temperature, mixed with silica (10 mL), and concentrated carefully *in vacuo*. This mixture was then loaded directly onto a column for purification. Purification by flash column chromatography (eluting with 1–70% EtOAc/hexanes) provided amide **3.5** as an amorphous white solid (974 mg, 1.77 mmol, 70% over 2 steps, 81% based on recovered 12). ^{1}H NMR (500 MHz, C_6D_6) δ 7.40 (d, *J* = 8.6 Hz, 2H), 7.09 (d, *J* = 8.5 Hz, 2H), 6.15 (bs, 1H), 6.13 (s, 1H), 4.86 (s, 2H), 4.37 (d, *J* = 6.4 Hz, 1H), 4.32 (d, *J* = 6.5 Hz, 1H), 4.16 (ddd, *J* = 10.7, 8.0, 2.3 Hz, 1H), 3.89 (d, *J* = 9.5 Hz, 1H), 3.66 (t, *J* = 2.9 Hz, 1H), 3.44 (d, *J* = 9.6 Hz, 1H), 3.43–3.36 (m, 1H), 3.40 (t, *J* = 7.1 Hz, 1H), 3.19 (s, 3H), 3.18 (s, 1H), 3.13 (s, 3H), 3.09 (s, 3H), 2.62 (ddd, *J* = 13.0, 8.2, 4.8 Hz, 1H), 2.52 (q, *J* = 12.1 Hz, 1H), 1.91 (ddq, *J* = 15.8, 7.1, 4.1 Hz, 1H), 1.77 (dq, *J* = 14.1, 2.9 Hz, 1H), 1.66 (ddd, *J* = 11.6, 6.9, 2.4 Hz, 1H), 1.47 (qd, *J* = 13.1, 3.4 Hz, 1H), 1.27 (ddd, *J* = 12.8, 6.4, 2.8 Hz, 1H), 1.16 (tt, *J* = 13.5, 2.7 Hz, 1H), 0.98 (s, 9H), 0.04 (s, 3H), 0.02 (s, 3H); ^{13}C NMR (126 MHz, C_6D_6) δ 174.8, 156.2, 143.6, 128.6, 117.0, 96.6, 94.5, 77.4, 71.6, 66.9, 61.4, 56.6, 55.5, 55.2, 53.5, 45.4, 42.3, 38.2, 34.0, 26.2, 24.3, 18.5,

17.8, –5.27, –5.29; IR (thin film) 3500–3300, 2950, 2930, 2889, 2821, 1673, 1510, 1153, 1089, 836, 776 cm^{-1}; HRMS (ESI) *m/z* $[M + H]^+$ calc'd for $C_{29}H_{50}NO_7Si$ 552.3351, found 552.3360.

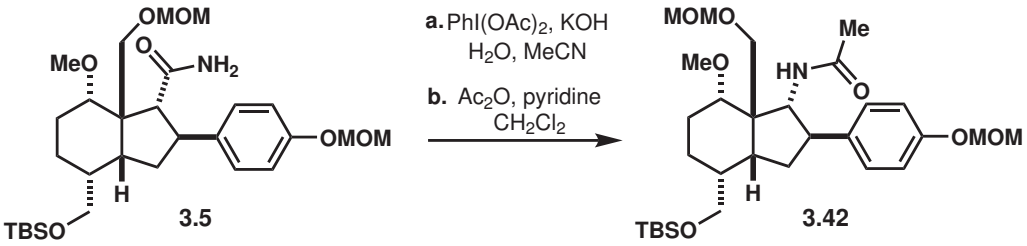

Acetamide 3.42. Amide **3.5** (719 mg, 1.30 mmol, 1.0 equiv) was dissolved in MeCN (8.7 mL, 0.15 M) in a round-bottomed flask open to air. $PhI(OAc)_2$ (548 mg, 1.70 mmol, 1.3 equiv) was added and the reaction mixture was stirred vigorously for 5 min, at which point KOH (365 mg, 6.51 mmol, 5.0 equiv) was added as a solution in H_2O (4.3 mL, 0.30 M with respect to amide **3.5**). The reaction mixture was capped loosely and stirred at room temperature for 6 h. The resulting pink-orange solution was diluted with H_2O (5 mL) and concentrated *in vacuo* to remove the MeCN. The aqueous material was extracted with EtOAc (3 x 10 mL); then the combined organic extracts were washed with brine (5 mL), dried over Na_2SO_4, filtered, and concentrated *in vacuo*. The corresponding primary amine (**3.23**) was obtained as a pink oil, which was then azeotropically dried with benzene (3 x 5 mL) and advanced without further purification. ^{1}H NMR (500 MHz, C_6D_6) δ 7.30 (d, *J* = 8.1 Hz, 2H), 7.11 (d, *J* = 8.0 Hz, 2H), 4.91 (s, 2H), 4.43 (s, 2H), 3.52 (d, *J* = 9.4 Hz, 1H), 3.46 (d, *J* = 7.4 Hz, 1H), 3.41 (dd, *J* = 9.6, 7.3 Hz, 1H), 3.33–3.28 (m, 2H), 3.26 (s, 1H), 3.16 (s, 3H), 3.15 (s, 3H), 3.08 (ddd, *J* = 9.4, 7.5, 2.7 Hz, 1H), 3.01 (s, 3H), 2.54 (ddd, *J* = 13.3, 8.6, 4.8 Hz, 1H), 2.40 (q, *J* = 12.2 Hz, 1H), 1.91 (dq, *J* = 9.0, 4.2 Hz, 1H), 1.79 (dt, *J* = 14.2, 3.2 Hz, 1H), 1.65–1.59 (m, 1H), 1.48–1.37 (m, 3H), 1.31 (dd, *J* = 13.1, 3.6 Hz, 1H), 1.22 (t, *J* = 13.9 Hz, 1H), 0.97 (s, 9H), 0.04 (s, 3H), 0.03 (s, 3H).

Crude amine **3.23** (700 mg) was dissolved in CH_2Cl_2 (13 mL, 0.1 M), then cooled in an ice/water bath. Pyridine (0.53 mL, 6.58 mmol, 5.0 equiv) was added, followed by Ac_2O (0.37 mL, 3.91 mmol, 3.0 equiv). Each addition was performed dropwise over 5 min by syringe. The reaction mixture was allowed to warm gradually to room temperature over 16 h, at which time it was quenched with $NaHCO_3$ (10 mL) and extracted with CH_2Cl_2 (3 x 10 mL). The combined organic extracts were dried over Na_2SO_4, filtered, and concentrated *in vacuo* to give the corresponding acetamide as an orange oil, which was advanced without further purification. ^{1}H NMR (600 MHz, C_6D_6) δ 7.39 (d, *J* = 8.6 Hz, 2H), 7.11 (d, *J* = 8.7 Hz, 2H), 5.40 (d, *J* = 10.0 Hz, 1H), 5.19 (dd, *J* = 10.1, 8.6 Hz, 1H), 4.84 (s, 2H), 4.66 (d, *J* = 6.4 Hz, 1H), 3.47 (dd, *J* = 9.7, 6.7 Hz, 1H), 3.43–3.38 (m, 2H), 3.34 (s, 3H), 3.19–3.14 (m, 2H), 3.12 (s, 3H), 2.85 (s, 3H), 2.82 (bs, 1H), 2.77 (ddd, *J* = 13.3, 8.8, 4.7 Hz, 1H), 2.40 (q, *J* = 12.4 Hz, 1H), 1.96 (tt, *J* = 9.7, 6.0 Hz, 1H), 1.73 (dq, *J* = 15.1, 3.2 Hz, 1H), 1.61 (ddd, *J* = 12.4, 9.1, 3.2 Hz, 1H), 1.60 (s, 3H), 1.43–1.33 (m, 2H), 1.14 (dtd, *J* = 13.8, 6.8, 3.5 Hz, 1H), 0.99 (s, 9H), 0.06 (s, 3H), 0.05 (s, 3H); ^{13}C NMR (126 MHz, C_6D_6) δ 168.3, 156.4, 141.0, 128.4, 116.8, 97.8, 94.6, 78.3, 69.5, 66.7, 62.4, 55.4, 55.3, 55.2, 52.5, 50.7, 38.20, 38.18, 33.1, 26.2, 24.0, 23.3, 18.5, 17.8, –5.21, –5.24; IR (thin film) 2929, 2889, 2856, 2824, 1655, 1510, 1233, 1151, 1080, 1047, 985, 835, 775 cm^{-1}; HRMS (ESI) *m/z* $[M + H]^+$ calc'd for $C_{30}H_{52}NO_7Si$ 566.3508, found 566.3511.

Urea 3.25. As discussed in the text, when stirring rate was insufficient in the Hofmann rear-

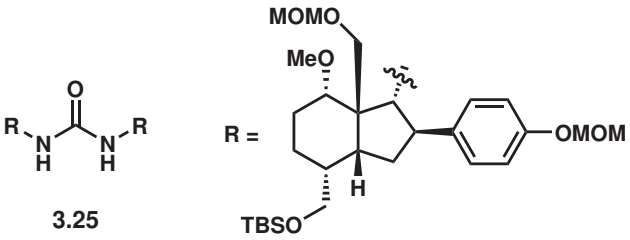

rangement of amide **3.5** in MeCN/H_2O, a urea side product was formed. This product could be separated following the acetylation step.

Beginning with Amide **3.5** (1.06 g, 1.92 mmol, 1.0 equiv) was dissolved in MeCN (12.8 mL, 0.15 M) in a round-bottomed flask open to air. $PhI(OAc)_2$ (804 mg, 2.49 mmol, 1.3 equiv) was added and the reaction mixture was stirred for 5 min, at which point KOH (538 mg, 9.59 mmol, 5.0 equiv) was added as a solution in H_2O (6.4 mL, 0.30 M with respect to amide **3.5**). The reaction mixture was capped loosely and stirred at room temperature for 14 h. The resulting pink-orange solution was diluted with H_2O (5 mL) and concentrated *in vacuo* to remove the MeCN. The aqueous material was extracted with EtOAc (3 x 10 mL); then the combined organic extracts were washed with brine (5 mL), dried over Na_2SO_4, filtered, and concentrated *in vacuo*. The crude mixture was then dissolved in CH_2Cl_2 (19 mL, 0.1 M), then cooled in an ice/water bath. Pyridine (0.77 mL, 9.59 mmol, 5.0 equiv) was added, followed by Ac_2O (0.54 mL, 5.75 mmol, 3.0 equiv). Each addition was performed dropwise over 5 min by syringe. The reaction mixture was allowed to warm gradually to room temperature over 3 days, at which time it was quenched with $NaHCO_3$ (10 mL) and extracted with CH_2Cl_2 (3 x 10 mL). The combined organic extracts were dried over Na_2SO_4, filtered, and concentrated *in vacuo*. Purification by flash column chromatography (eluting with 30–65% EtOAc/hexanes) provided urea **3.25** (649 mg, 0.605 mmol, 63% yield) as a white foam, along with desired acetamide **3.42** (275 mg, 0.486 mmol, 25% yield over 2 steps). ^{1}H NMR (500 MHz, C_6D_6, 343 K)* δ 7.35 (d, *J* = 8.4 Hz, 2H), 7.31 (d, *J* = 8.6 Hz, 2H), 7.06 (d, *J* = 7.0 Hz, 2H), 7.05 (d, *J* = 7.1 Hz, 2H), 4.93 (d, *J* = 2.0 Hz, 2H), 4.91 (d, *J* = 6.5 Hz, 1H), 4.89 (d, *J* = 6.5 Hz, 1H), 4.78–4.72 (m, 2H), 4.66 (d, *J* = 6.2 Hz, 1H), 4.65 (bs, 1H), 4.63 (d, *J* = 6.2 Hz, 1H), 4.57 (d, *J* = 6.2 Hz, 1H), 4.51 (bs, 1H), 4.47 (d, *J* = 11.6 Hz, 1H), 3.50–3.36 (m, 7H), 3.33 (s, 3H), 3.28 (s, 3H), 3.25 (d, *J* = 9.7 Hz, 1H), 3.22 (s, 3H), 3.20 (s, 3H), 3.19–3.15 (m, 2H), 3.05 (s, 3H), 3.03 (s, 1H), 2.96 (s, 3H), 2.69 (dddd, *J* = 23.5, 13.2, 8.9, 4.8 Hz, 2H), 2.62 (s, 1H), 2.34 (qd, *J* = 12.5, 4.7 Hz, 2H), 1.94 (dtd, *J* = 12.1, 7.4, 3.4 Hz, 2H), 1.81 (d, *J* = 14.2 Hz, 1H), 1.77 (d, *J* = 14.2 Hz, 1H), 1.66 (ddd, *J* = 12.4, 8.8, 3.2 Hz, 1H), 1.59 (ddd, *J* = 12.4, 8.8, 3.2 Hz, 1H), 1.43–1.20 (m, 5H), 1.15 (t, *J* = 14.0 Hz, 1H), 0.960 (s, 9H), 0.957 (s, 9H), 0.05 (s, 3H), 0.042 (s, 3H), 0.039 (s, 3H), 0.03 (s, 3H); ^{13}C NMR (126 MHz, C_6D_6, 343 K) δ 157.8, 157.5, 156.53, 156.48, 141.8, 141.7, 128.6, 128.5, 117.2, 117.1, 97.8, 97.7, 95.20, 95.15, 78.3, 78.1, 70.0, 68.9, 66.84, 66.81, 64.9, 64.7, 55.53, 55.50, 55.4, 55.3, 55.2, 55.1, 52.53, 52.53, 51.2, 50.8, 38.6, 38.5, 38.4, 37.9, 32.6, 31.8, 26.2, 24.3, 24.2, 18.5, 17.87, 17.85, –5.20, –5.21; IR (neat) 3416, 2929, 2887, 2856, 2824, 1659, 1510, 1233, 1151, 1079, 1044, 833, 774, 666 cm^{-1}; HRMS (ESI) *m/z* [M + Na]$^+$ calc'd for $C_{57}H_{96}NaN_2O_{13}Si_2$ 1095.6343, found 1095.6343. *Rotameric mixture (~1:1 ratio of rotamers at 343 K); both sets of peaks reported.

Alcohol 3.20. Crude acetamide **3.42** (740 mg, 1.31 mmol, 1.0 equiv) was dissolved in THF (13 mL, 0.1 M) in a round-bottomed flask open to air. TBAF solution (2.6 mL, 2.62 mmol, 2.0 equiv,

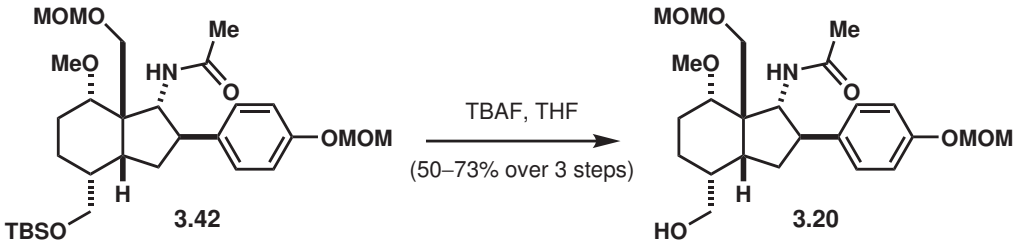

1 M in THF) was added and the reaction mixture stirred for 15 h. The crude reaction mixture was concentrated *in vacuo* to give a brown oil. Purification by flash column chromatography (eluting with 5–55% acetone/CH_2Cl_2) provided alcohol **3.20** (445 mg, 0.985 mmol, 75% over 3 steps) as a white gum. ^{1}H NMR (500 MHz, C_6D_6, 343 K)* δ 7.33 (d, *J* = 8.4 Hz, 2H), 7.06 (d, *J* = 8.1 Hz, 2H), 5.42 (d, *J* = 10.1 Hz, 1H), 5.09 (t, *J* = 9.4 Hz, 1H), 4.88 (s, 2H), 4.76 (d, *J* = 6.5 Hz, 1H), 4.66 (d, *J* = 6.2 Hz, 1H), 3.42 (dd, *J* = 16.5, 10.0 Hz, 2H), 3.33 (s, 3H), 3.29 (d, *J* = 7.6 Hz, 1H), 3.24 (t, *J* = 8.5 Hz, 1H), 3.16 (s, 3H), 2.94 (bs, 1H), 2.91 (s, 3H), 2.69–2.57 (m, 1H), 2.33 (q, *J* = 12.6 Hz, 1H), 1.75 (d, *J* = 15.5 Hz, 1H), 1.62 (s, 3H), 1.56 (t, *J* = 10.7 Hz, 1H), 1.36–1.26 (m, 2H), 1.20 (t, *J* = 12.6 Hz, 1H), 1.06–0.95 (m, 1H); ^{13}C NMR (126 MHz, C_6D_6, 343 K) δ 168.2, 156.5, 140.9, 128.4, 117.1, 98.0, 95.0, 78.4, 70.4, 66.3, 62.6, 55.5, 55.4, 55.1, 52.5, 50.8, 38.7, 38.4, 33.0, 24.2, 23.2, 17.7; IR (thin film) 3375, 2932, 2889, 2824, 1651, 1509, 1232, 1150, 1044, 919, 830 cm^{-1}; HRMS (ESI) *m/z* $[M + Na]^+$ calc'd for $C_{24}H_{37}NNaO_7$ 474.2462, found 474.2451. *^{1}H NMR peaks did not fully coalesce at 343 K, so peaks are reported for major rotamer at that temperature.

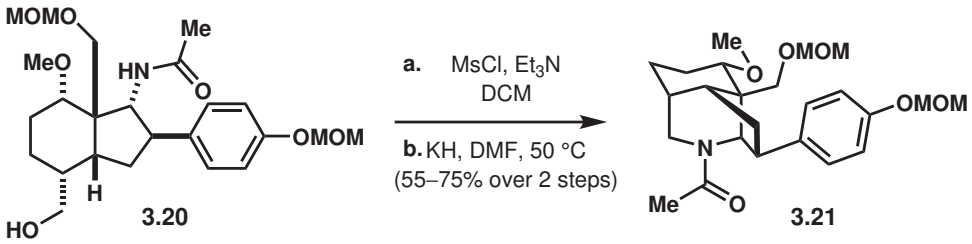

Piperidine 3.21. Alcohol **3.20** (445 mg, 0.984 mmol, 1.0 equiv) was dissolved in CH_2Cl_2 (10. mL, 0.1 M). Et_3N (0.69 mL, 4.92 mmol, 5.0 equiv) was added via syringe, followed by MsCl (120 µL, 1.48 mmol, 1.5 equiv). The reaction mixture was stirred at room temperature for 3.5 h, then quenched by the addition of brine (10 mL). The solution was extracted with CH_2Cl_2 (3 x 10 mL) and the combined organic extracts were dried over Na_2SO_4, filtered, and concentrated *in vacuo* to give the corresponding mesylate (**3.43**) as a pale brown foam (530 mg), which was advanced without further purification. ^{1}H NMR (500 MHz, C_6D_6) δ 7.30 (d, *J* = 8.2 Hz, 2H), 7.08 (d, *J* = 8.2 Hz, 2H), 5.46 (d, *J* = 10.0 Hz, 1H), 5.07 (t, *J* = 9.4 Hz, 1H), 4.86 (s, 2H), 4.78 (d, *J* = 6.5 Hz, 1H), 4.63 (d, *J* = 6.4 Hz, 1H), 3.80 (t, *J* = 8.2 Hz, 1H), 3.76 (t, *J* = 8.7 Hz, 1H), 3.31 (s, 3H), 3.13 (s, 3H), 2.83 (s, 3H), 2.75 (bs, 1H), 2.56 (td, *J* = 8.8, 4.2 Hz, 1H), 2.24 (s, 3H), 2.19 (d, *J* = 12.5 Hz, 1H), 1.96 (bs, 1H), 1.61 (s, 3H), 1.40 (t, *J* = 11.1 Hz, 1H), 1.24 (q, *J* = 12.5 Hz, 1H), 1.18 (t, *J* = 11.3 Hz, 1H), 1.01 (t, *J* = 14.7 Hz, 1H), 0.90–0.75 (m, 1H).

Mesylate **3.43** (530 mg, 0.984 mmol, 1.0 equiv) was dissolved in DMF (10. mL, 0.1 M). KH (59.2 mg, 1.48 mmol, 1.5 equiv) was added and the reaction mixture was heated in an oil bath at 50 °C for 15 h. At this point, conversion was judged to be incomplete (by TLC and LC–MS analysis) and additional KH (39.0 mg, 0.984 mmol, 1.0 equiv) was added after allowing the reaction mix-

ture to cool to room temperature. The reaction mixture was returned to the oil bath and heated at 50 °C for 2 h. The reaction mixture was cooled to room temperature, diluted with brine (10 mL) and H_2O (90 mL), and extracted with EtOAc (3 x 25 mL). The combined organic extracts were washed with brine (5 mL), dried over Na_2SO_4, filtered, and concentrated *in vacuo* to give a yellow oil. Purification by flash column chromatography (eluting with 45–70% acetone/CH_2Cl_2) provided piperidine **3.21** (366 mg, 0.844 mmol, 86% over 2 steps) as a white gum. ^{1}H NMR (500 MHz, C_6D_6, 343 K) δ 7.09–6.97 (m, 4H), 4.87 (d, *J* = 1.1 Hz, 2H), 4.54 (d, *J* = 14.3 Hz, 1H), 4.29 (s, 1H), 4.29–4.22 (m, 1H), 4.23 (s, 1H), 3.62 (dd, *J* = 10.2, 7.5 Hz, 1H), 3.36 (d, *J* = 9.7 Hz, 1H), 3.14 (dd, *J* = 17.0, 7.9 Hz, 1H), 3.14 (s, 3H), 3.08 (s, 3H), 3.05 (s, 3H), 3.02 (d, *J* = 9.7 Hz, 1H), 2.82 (dd, *J* = 14.5, 4.6 Hz, 1H), 2.27 (s, 3H), 2.26 (bs, 1H), 2.18 (dt, *J* = 13.2, 6.5 Hz, 1H), 1.84–1.78 (m, 1H), 1.73 (dd, *J* = 13.4, 9.8 Hz, 1H), 1.69–1.63 (m, 1H), 1.65–1.58 (m, 1H), 1.38 (t, *J* = 4.1 Hz, 1H), 1.26 (td, *J* = 14.1, 5.5 Hz, 1H); ^{13}C NMR (126 MHz, C_6D_6, 343 K) δ 167.2, 156.3, 137.5, 127.5, 116.9, 97.0, 95.0, 77.4, 66.5, 64.8, 56.6, 55.6, 55.1, 53.0, 47.5, 42.1, 41.1, 33.5, 33.0, 30.1, 24.3, 22.1; IR (thin film) 2923, 2897, 2863, 2818, 1631, 1511, 1422, 1016, 916, 513 cm^{-1}; HRMS (ESI) *m/z* [M + Na]$^+$ calc'd for $C_{24}H_{35}NNaO_6$ 456.2357, found 456.2346.

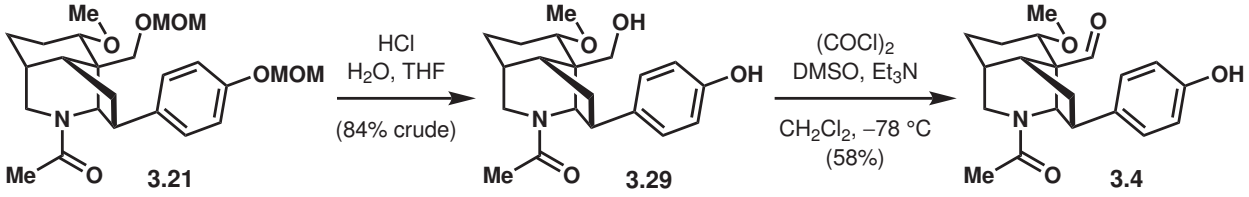

Aldehyde 3.4. Piperidine **3.21** (79.0 mg, 0.182 mmol, 1.0 equiv) was dissolved in THF (1.4 mL, 75 mM) in a round-bottomed flask left open to air. A 6 N aqueous HCl solution (0.84 mL, 5.0 mmol, 28 equiv) was added and the reaction mixture was stirred at room temperature for 28 h, at which point it was concentrated *in vacuo* to remove THF. The aqueous phase was diluted with brine (5 mL) and extracted with CH_2Cl_2 (3 x 5 mL). The combined organic extracts were dried over Na_2SO_4, filtered, and concentrated *in vacuo* to give diol **3.29** an amorphous white solid (52 mg, 0.151 mmol, 84% crude yield), which was advanced without further purification. IR (thin film) 3288, 2966, 2930, 2818, 1609, 1515, 1452, 1264, 1105, 830 cm^{-1}; HRMS (ESI) *m/z* [M + Na]$^+$ calc'd for $C_{20}H_{27}NNaO_4$ 368.1832, found 368.1825.

Diol **3.29** (52.0 mg, 0.151 mmol, 1.0 equiv) was suspended in CH_2Cl_2 (4.0 mL, 37 mM). DMSO (75 µL, 1.05 mmol, 7.0 equiv) was added and the resulting suspension was cooled in a dry ice/acetone bath at –78 °C. Oxalyl chloride (26 µL, 0.303 mmol, 2.0 equiv) was added dropwise and the reaction mixture was maintained at –78 °C for 75 min. Et_3N (210 µL, 1.51 mmol, 10. equiv) was then added via syringe and the solution was maintained at –78 °C for 45 min. The light yellow solution was removed from the bath and stirred at room temperature for 1 h, at which point it was quenched with NH_4Cl (saturated aqueous, 15 mL) and brine (5 mL). Upon extraction with CH_2Cl_2 (3 x 5 mL), the combined organic extracts were dried over Na_2SO_4, filtered, and concentrated *in vacuo*. Purification by flash column chromatography (eluting with 0–40% acetone/CH_2Cl_2) provided aldehyde **3.4** (30.0 mg, 0.0874 mmol, 58%) as a colorless oil. ^{1}H NMR (700 MHz, C_6D_6)* δ 9.37 (s, 1H), 7.00 (d, *J* = 8.1 Hz, 2H), 6.82 (d, *J* = 8.4 Hz, 2H),4.93 (bs, 1H), 4.32 (d, *J* = 14.3 Hz, 1H), 3.53 (dd, *J* = 10.3, 6.8 Hz, 1H), 3.42 (dd, *J* = 9.9, 6.1 Hz, 1H), 3.21 (d, *J* = 1.5 Hz, 3H), 3.06 (dd, *J* = 14.4, 5.3 Hz, 1H), 2.56 (t, *J* = 4.9 Hz, 1H), 2.33 (d, *J* = 1.4 Hz, 3H), 2.21 (dt, *J* = 13.1, 6.3 Hz, 1H), 2.03 (td, *J* = 6.5, 3.4 Hz, 1H), 1.98 (dd, *J* = 14.3, 9.6 Hz, 1H), 1.92–1.89 (m,

1H), 1.86 (q, *J* = 5.2 Hz, 1H), 1.56–1.50 (m, 1H), 1.47 (qd, *J* = 12.3, 4.9 Hz, 1H); ^{13}C NMR (176 MHz, C_6D_6) δ 206.9, 169.1, 154.9, 131.5, 128.8, 115.9, 80.4, 65.2, 62.2, 56.5, 47.6, 41.7, 41.4, 32.5, 30.8, 29.1, 24.1, 22.4; IR (thin film) 3252, 2958, 2934, 2856, 2358, 1717, 1613, 1591, 1514, 1450, 1260, 1090, 1027, 799 cm^{-1}; HRMS (ESI) *m/z* [M + H]$^+$ calc'd for $C_{20}H_{26}NO_4$ 344.1856, found 344.1855. *Rotameric mixture (3:1 ratio of rotamers at 298 K); peaks reported for major rotamer.

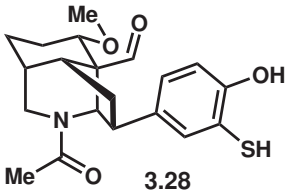

3.28

Thiol 3.28. When excess oxalyl chloride was employed in the Swern oxidation to give aldehyde **3.4**, thiol **3.28** was also isolated from the reaction mixture. In the experiment described above, thiol **3.28** was obtained as a clear oil (13 mg, 35 μmmol, 21% yield). ^{1}H NMR (500 MHz, $CDCl_3$) δ 9.35 (s, 1H), 6.97 (dd, *J* = 8.2, 2.6 Hz, 1H), 6.88–6.83 (m, 2H), 4.90 (s, 1H), 4.32 (d, *J* = 14.2 Hz, 1H), 3.54–3.49 (m, 1H), 4.32 (d, *J* = 14.2 Hz, 1H), 3.54–3.48 (m, 1H), 3.42 (dd, *J* = 9.8, 6.4 Hz, 1H), 3.21 (s, 3H), 3.05 (dd, *J* = 14.1, 5.1 Hz, 1H), 2.56 (t, *J* = 5.1 Hz, 1H), 2.32 (s, 3H), 2.06–1.83 (m, 8H), 1.57–1.43 (m, 2H); ^{13}C NMR (126 MHz, $CDCl_3$) δ 206.6, 168.9, 154.0, 131.6, 129.7, 128.8, 128.2, 117.3, 80.4, 65.3, 62.1, 56.4, 47.6, 41.6, 41.3, 32.4, 30.7, 29.1, 24.0, 22.5.

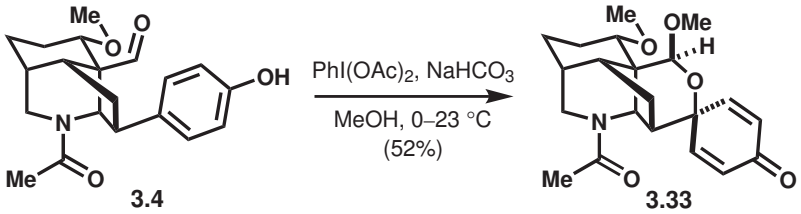

3.4 **3.33**

Dienone 3.33. Aldehyde **3.4** (23.0 mg, 0.0670 mmol, 1.0 equiv) and $NaHCO_3$ (23.4 mg, 0.279 mmol, 4.0 equiv) were suspended in MeOH (3.0 mL, 22 mM), then sonicated until dissolution was nearly complete. The mixture was cooled in an ice/water bath at 0 °C before $PhI(OAc)_2$ (22.6 mg, 0.0702 mmol, 1.04 equiv) was added. The reaction mixture was allowed to warm gradually to room temperature over 3.5 h, at which point H_2O (0.5 mL) was added and the mixture concentrated *in vacuo* to remove MeOH. The resulting residue was diluted with H_2O (1.0 mL) and extracted with EtOAc (3 x 1 mL). The combined organic extracts were washed with brine (0.5 mL), dried over Na_2SO_4, filtered, and concentrated *in vacuo*. Purification by preparatory TLC (eluting with 20–50% acetone/CH_2Cl_2) provided dienone **3.33** (13.0 mg, 0.0348 mmol, 52%) as a colorless oil. ^{1}H NMR (600 MHz, C_6D_6)* δ 6.62 (dd, *J* = 10.4, 3.2 Hz, 1H), 6.56 (dd, *J* = 10.4, 3.2 Hz, 1H), 6.03 (dd, *J* = 10.4, 2.0 Hz, 1H), 5.98 (dd, *J* = 10.4, 2.0 Hz, 1H), 4.90 (s, 1H), 4.21 (d, *J* = 14.4 Hz, 1H), 4.16 (s, 1H), 3.27 (dd, *J* = 10.9, 7.0 Hz, 1H), 3.21 (s, 3H), 3.00 (s, 3H), 2.68 (dd, *J* = 13.7, 6.2 Hz, 1H), 2.14 (dd, *J* = 7.2, 4.7 Hz, 1H), 2.01 (s, 3H), 2.00–1.95 (m, 1H), 1.68–1.61 (m, 1H), 1.50 (dq, *J* = 13.3, 2.9 Hz, 1H), 1.40–1.33 (m, 2H), 1.23 (dt, *J* = 7.5, 3.3 Hz, 1H), 1.10 (t, *J* = 8.5 Hz, 2H); ^{13}C NMR (126 MHz, C_6D_6) δ 183.7, 168.2, 148.9, 147.6, 128.6, 128.5, 103.8, 78.4, 74.9, 58.1, 56.8, 56.3, 52.5, 48.9, 41.3, 37.6, 32.5, 29.6, 29.4, 24.1, 22.4; IR (thin film) 2932, 2828, 1720, 1671, 1629, 1450, 1378, 1251, 1194, 1135, 1090, 948 cm^{-1}; HRMS (ESI) *m/z* [M + H]$^+$ calc'd for $C_{21}H_{28}NO_5$

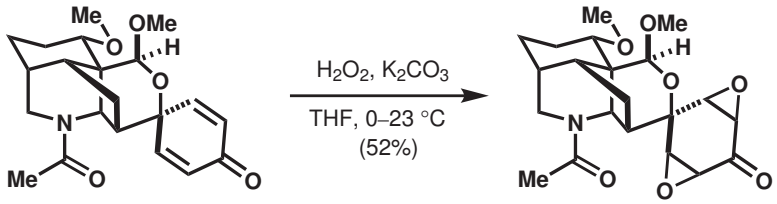

3.33 **3.34**

374.1962, found 374.1942. *Rotameric mixture (4:1 ratio of rotamers at 298 K); peaks reported for major rotamer.

Diepoxide 3.34. Dienone **3.33** (12.4 mg, 330 μmmol) was dissolved in THF (230. μL) under air. To this solution was added H_2O (200. μL, 70 mM overall), which was then cooled in an ice/water bath. A 35% w/w aqueous solution of H_2O_2 (31.5 μL, 0.330 mmol, 10. equiv) was added, followed by K_2CO_3 (37.0 mg, 0.270 mmol, 8.2 equiv). The reaction mixture, which turned yellow upon the addition of K_2CO_3, was stirred cold for 3.5 h. After stirring for an additional 1 h at room temperature, the reaction was quenched by the addition of NH_4Cl (saturated aqueous, 0.2 mL). The crude mixture was then extracted with EtOAc (3 x 1 mL), then washed with brine, dried over Na_2SO_4, filtered, and concentrated *in vacuo* to give diepoxide **3.34** (172 μmmol, 52% yield). ^{1}H NMR (700 MHz, $CDCl_3$)* δ 5.36 (s, 1H), 5.07 (d, *J* = 12.6 Hz, 2H), 4.49 (s, 1H), 4.17 (t, *J* = 4.0 Hz, 1H), 4.14 (d, *J* = 14.4 Hz, 1H), 3.83 (t, *J* = 3.9 Hz, 1H), 3.75 (t, *J* = 3.9 Hz, 1H), 3.72 (t, *J* = 4.0 Hz, 1H), 3.55 (d, *J* = 4.8 Hz, 4H), 3.44 (dd, *J* = 4.0, 2.7 Hz, 1H), 3.41 (ddd, *J* = 7.1, 3.9, 2.5 Hz, 2H), 3.37 (d, *J* = 12.6 Hz, 1H), 3.36 (s, 3H), 3.34 (s, 3H), 3.32–3.27 (m, 1H), 2.97 (dd, *J* = 14.1, 5.4 Hz, 1H), 2.47–2.36 (m, 4H), 2.22 (t, *J* = 7.7 Hz, 1H), 2.17 (d, *J* = 8.1 Hz, 1H), 2.14 (s, 3H), 2.08 (s, 3H), 2.03 (d, *J* = 7.5 Hz, 1H), 2.03–1.97 (m, 1H), 1.93–1.82 (m, 5H), 1.75 (dd, *J* = 14.3, 8.6 Hz, 1H), 1.60–1.54 (m, 1H), 1.50–1.46 (m, 2H), 1.30–1.26 (m, 8H); ^{13}C NMR (176 MHz, $CDCl_3$)* δ 199.6, 198.6, 170.6, 169.3, 105.9, 105.4, 79.1, 78.9, 74.4, 74.4, 63.0, 62.9, 61.8, 61.6, 57.8, 57.21, 57.15, 57.1, 56.8, 55.94, 55.88, 55.6, 55.4, 52.6, 52.5, 51.8, 45.9, 44.4, 44.0, 41.1, 37.9, 37.8, 32.8, 32.3, 29.8, 29.1, 28.1, 27.7, 23.98, 23.96, 22.9, 22.6; HRMS (ESI) *m/z* $[M + Na]^+$ calc'd for $C_{21}H_{27}NNaO_7$ 428.1680, found 428.1699. *Rotameric mixture (~1:1 ratio of rotamers at 298 K); both sets of peaks reported. It is also possible that this was an inseparable of diastereomers. However, we found this unlikely since all other compounds containing the acetamide group displayed rotamers.

3.8 References

1. Doering, N. A.; Kou, K. G. M.; Norseeda, K.; Lee, J. C.; Marth, C. J.; Gallego, G. M.; Sarpong, R. *J. Org. Chem.* **2018**, *83*, 12911–12920.
2. Wang, F. P.; Chen, Q. H.; Liu, X. Y. *Nat. Prod. Rep.* **2010**, *27*, 529–570.
3. Wang, X. W.; Xie, H. *Drugs Future* **1999**, *24*, 877–882.
4. Wang, F.-P.; Chen, Q.-H.; Liang, X.-T. In *Alkaloids Chem. Biol.* Cordell, G. A., Ed.; Academic Press: San Diego, 2009; Vol. 67, pp 1–78.
5. Wang, F.-P.; Chen, Q.-H. In *Alkaloids. Chem. Biol.* Cordell, G. A., Ed.; Academic Press: San Diego, 2010; Vol. 69, pp 1–577.
6. Wang, F. P.; Liang, X. T. In *Alkaloids Chem. Biol.* Cordell, G. A., Ed.; Academic Press: San Diego, 2002; Vol. 59, pp 1–280.
7. Ameri, A. *Prog. Neurobiol.* **1998**, *56*, 211–235.

8. Conte Camerino, D.; Tricarico, D.; Desaphy, J. F. *Neurotherapeutics* **2007**, *4*, 184–198.
9. Vakhitova, Y. V.; Farafontova, E. I.; Khisamutdinova, R. Y.; Yunusov, V. M.; Tsypysheva, I. P.; Yunusov, M. S. *Russ. J. Bioorganic Chem.* **2013**, *39*, 92–101.
10. Wright, S. N. *Mol. Pharmacol.* **2001**, *59*, 183–192.
11. Fujita, Y.; Terui, K.; Fujita, M.; Kakizaki, A.; Sato, N.; Oikawa, K.; Aoki, H.; Takahashi, K.; Endo, S. *J. Anal. Toxicol.* **2007**, *31*, 132–137.
12. Song, M. K.; Liu, H.; Jiang, H. L.; Yue, J. M.; Hu, G. Y.; Chen, H. Z. *Neuroscience* **2008**, *155*, 469–475.
13. Vetter, I.; Deuis, J. R.; Mueller, A.; Israel, M. R.; Starobova, H.; Zhang, A.; Rash, L. D.; Mobli, M. *Pharmacol. Ther.* **2017**, *172*, 73–100.
14. Kingwell, K. *Nat. Rev. Drug Discov.* **2019**, *18*, 321–323.
15. (a) Hodgkin, A. L.; Huxley, A. F. *J. Physiol.* **1952**, *117*, 500–544; (b) Hodgkin, A. L.; Huxley, A. F. *J. Physiol.* **1952**, *116*, 497–506; (c) Hodgkin, A. L.; Huxley, A. F. *J. Physiol.* **1952**, *116*, 449–472; (d) Hodgkin, A. L.; Huxley, A. F. *J. Physiol.* **1952**, *116*, 473–496.
16. Catterall, W. A. *J. Physiol.* **2012**, *590*, 2577–2589.
17. Hille, B., *Ion Channels of Excitable Membranes*, 3rd; Sinauer Associates Inc.: Sunderland, MA, 2001.
18. Catterall, W. A. *Annu. Rev. Biochem.* **1995**, *64*, 493–531.
19. Catterall, W. A.; Perez-Reyes, E.; Snutch, T. P.; Striessnig, J. *Pharmacol. Rev.* **2005**, *57*, 411–425.
20. Molecular Devices. What is an action potential? https://www.moleculardevices.com/applications/patch-clamp-electrophysiology (accessed March 9, 2020).
21. Brackenbury, W. J.; Isom, L. L. *Front. Pharmacol.* **2011**, *2*, 53.
22. Noda, M. et al. *Nature* **1984**, *312*, 121–127.
23. Noda, M.; Ikeda, T.; Suzuki, H.; Takeshima, H.; Takahashi, T.; Kuno, M.; Numa, S. *Nature* **1986**, *322*, 826–828.
24. Goldin, A. L.; Snutch, T.; Lubbert, H.; Dowsett, A.; Marshall, J.; Auld, V.; Downey, W.; Fritz, L. C.; Lester, H. A.; Dunn, R. *Proc. Natl. Acad. Sci. U. S. A.* **1986**, *83*, 7503–7507.
25. Goldin, A. L. *Annu. Rev. Physiol.* **2001**, *63*, 871–894.
26. Watanabe, E.; Fujikawa, A.; Matsunaga, H.; Yasoshima, Y.; Sako, N.; Yamamoto, T.; Saegusa, C.; Noda, M. *J. Neurosci.* **2000**, *20*, 7743–7751.
27. Cox, J. J. et al. *Nature* **2006**, *444*, 894–898.
28. Goldberg, Y. P. et al. *Clin. Genet.* **2007**, *71*, 311–319.
29. Fertleman, C. R.; Baker, M. D.; Parker, K. A.; Moffatt, S.; Elmslie, F. V.; Abrahamsen, B.; Ostman, J.; Klugbauer, N.; Wood, J. N.; Gardiner, R. M.; Rees, M. *Neuron* **2006**, *52*, 767–774.
30. Yang, Y.; Wang, Y.; Li, S.; Xu, Z.; Li, H.; Ma, L.; Fan, J.; Bu, D.; Liu, B.; Fan, Z.; Wu, G.; Jin, J.; Ding, B.; Zhu, X.; Shen, Y. *J. Med. Genet.* **2004**, *41*, 171–174.
31. Ragsdale, D. S.; McPhee, J. C.; Scheuer, T.; Catterall, W. A. *Science (80-.).* **1994**, *265*, 1724–1728.
32. Ragsdale, D. S.; Mcphee, J. C.; Scheuer, T.; Catterall, W. A. *Proc. Natl. Acad. Sci. U. S. A.* **1996**, *93*, 9270–9275.
33. Wang, G. K.; Quan, C.; Wang, S. Y. *Pflugers Arch. Eur. J. Physiol.* **1998**, *435*, 293–302.
34. Yarov-Yarovoy, V.; Brown, J.; Sharp, E. M.; Clare, J. J.; Scheuer, T.; Catterall, W. A. *J. Biol. Chem.* **2001**, *276*, 20–27.

35. Yarov-Yarovoy, V.; McPhee, J. C.; Idsvoog, D.; Pate, C.; Scheuer, T.; Catterall, W. A. *J. Biol. Chem.* **2002**, *277*, 35393–35401.
36. Payandeh, J.; Scheuer, T.; Zheng, N.; Catterall, W. A. *Nature* **2011**, *475*, 353–359.
37. Bagal, S. K.; Chapman, M. L.; Marron, B. E.; Prime, R.; Storer, R. I.; Swain, N. A. *Bioorg. Med. Chem. Lett.* **2014**, *24*, 3690–3699.
38. Wang, S. Y.; Wang, G. K. *Proc. Natl. Acad. Sci. U. S. A.* **1998**, *95*, 2653–2658.
39. Wang, G.; Quan, C.; Seaver, M.; Wang, S.-Y. *Pflügers Arch. - Eur. J. Physiol.* **2000**, *439*, 705–713.
40. Nyirimigabo, E.; Xu, Y.; Li, Y.; Wang, Y.; Agyemang, K.; Zhang, Y. *J. Pharm. Pharmacol.* **2015**, *67*, 1–19.
41. (a) Yu, J. Z.; Zhang, B. J.; Jiang, X. T. *Acad. J. Second Mil. Med. Univ.* **2005**, *26*, 822–824; (b) Chen, M. G.; Wang, Q. H.; Lin, Y. B. *Chin. J. Integr. Tradit. West Med.* **1996**, *3*, 257–260; (c) Ono, M.; Satoh, T. *Res. Commun. Chem. Pathol. Pharmacol.* **1989**, *63*, 13–25; (d) Ono, M.; Satoh, T. *Jpn. J. Pharmacol.* **1992**, *58*, 251–257; (e) Ameri, A. *Brain Res.* **1997**, *769*, 36–43.
42. Li, Y.-F.; Zheng, Y.-M.; Yu, Y.; Gan, Y.; Gao, Z.-B. *Acta Pharmacol. Sin.* **2018**, *40*, 451–459.
43. Cash, J. T.; Dunstan, W. R. *Philos. Trans. R. Soc. B Biol. Sci.* **1898**, *190*, 239–393.
44. Tursunkhodzhaeva, F. M.; Dzhakhangirov, F. N.; Salimov, B. T. *Chem. Nat. Compd.* **2016**, *52*, 1–4.
45. Dzhakhangirov, F. N.; Tursunkhodzhaeva, F. M.; Sultankhodzhaev, M. N.; Salimov, B. T. *Chem. Nat. Compd.* **2013**, *49*, 702–706.
46. Marth, C. J.; Gallego, G. M.; Lee, J. C.; Lebold, T. P.; Kulyk, S.; Kou, K. G.; Qin, J.; Lilien, R.; Sarpong, R. *Nature* **2015**, *528*, 493–498.
47. Kou, K. G.; Li, B. X.; Lee, J. C.; Gallego, G. M.; Lebold, T. P.; Dipasquale, A. G.; Sarpong, R. *J. Am. Chem. Soc.* **2016**, *138*, 10830–10833.
48. Kou, K. G.; Kulyk, S.; Marth, C. J.; Lee, J. C.; Doering, N. A.; Li, B. X.; Gallego, G. M.; Lebold, T. P.; Sarpong, R. *J. Am. Chem. Soc.* **2017**, *139*, 13882–13896.
49. Jin, S. S.; Guo, Q.; Xu, J.; Yu, P.; Liu, J. H.; Tang, Y. Q. *Chin. J. Nat. Med.* **2015**, *13*, 361–367.
50. Takaya, Y.; Ogasawara, M.; Hayashi, T. *Tetrahedron Lett.* **1999**, *40*, 6957–6961.
51. (a) Fleming, F. F.; Gudipati, S. *Org. Lett.* **2006**, *8*, 1557–1559; (b) Majetich, G.; Casares, A. M.; Chapman, D.; Behnke, M. *Tetrahedron Lett.* **1983**, *24*, 1909–1912; (c) Fleming, F. F.; Wang, Q. *Chem. Rev.* **2003**, *103*, 2035–2078.
52. Kung, L. R.; Tu, C. H.; Shia, K. S.; Liu, H. J. *Chem. Commun.* **2003**, *3*, 2490–2491.
53. Marth, C. J. Development of a Unified Strategy to the C18-, C19-, and C20-Diterpenoid Alkaloids., PhD Dissertation, University of California, Berkeley, 2015.
54. Gallego, G. M. Enantioselective Hydroarylation of Unactivated Ketones with Aryl Pinacolboronic Esters and A Hydrindanone-Based Approach Toward Natural Products., PhD Dissertation, University of California, Berkeley, 2013.
55. Ashby, E. C.; Smith, R. S.; Goel, A. B. *J. Organomet. Chem.* **1981**, *215*, C1–C5.
56. Ashby, E. C.; Goellb, A. B. *J. Org. Chem.* **1983**, *48*, 2125–2130.
57. Lee, J.; Kim, M.; Chang, S.; Lee, H. Y. *Org. Lett.* **2009**, *11*, 5598–5601.
58. Gottlieb, H. E.; Kotlyar, V.; Nudelman, A. *J. Org. Chem.* **1997**, *62*, 7512–7515.
59. Gu, W.; She, X.; Pan, X.; Yang, T. K. *Tetrahedron: Asymmetry* **1998**, *9*, 1377–1380.
60. Neufeind, S.; Hülsken, N.; Neudörfl, J. M.; Schlörer, N.; Schmalz, H. G. *Chem., A Eur. J.* **2011**, *17*, 2633–2641.

61. Deguchi, J.; Sasaki, T.; Hirasawa, Y.; Kaneda, T.; Kusumawati, I.; Shirota, O.; Morita, H. *Tetrahedron Lett.* **2014**, *55*, 1362–1365.
62. Komatsu, H.; Oi, W.; Naritani, K.; Takaishi, K.; Uchiyama, M.; Muranaka, A.; Maeda, H. *Chem., A Eur. J.* **2013**, *19*, 6956–6960.

Appendix 3.A NMR spectral data for Chapter 3

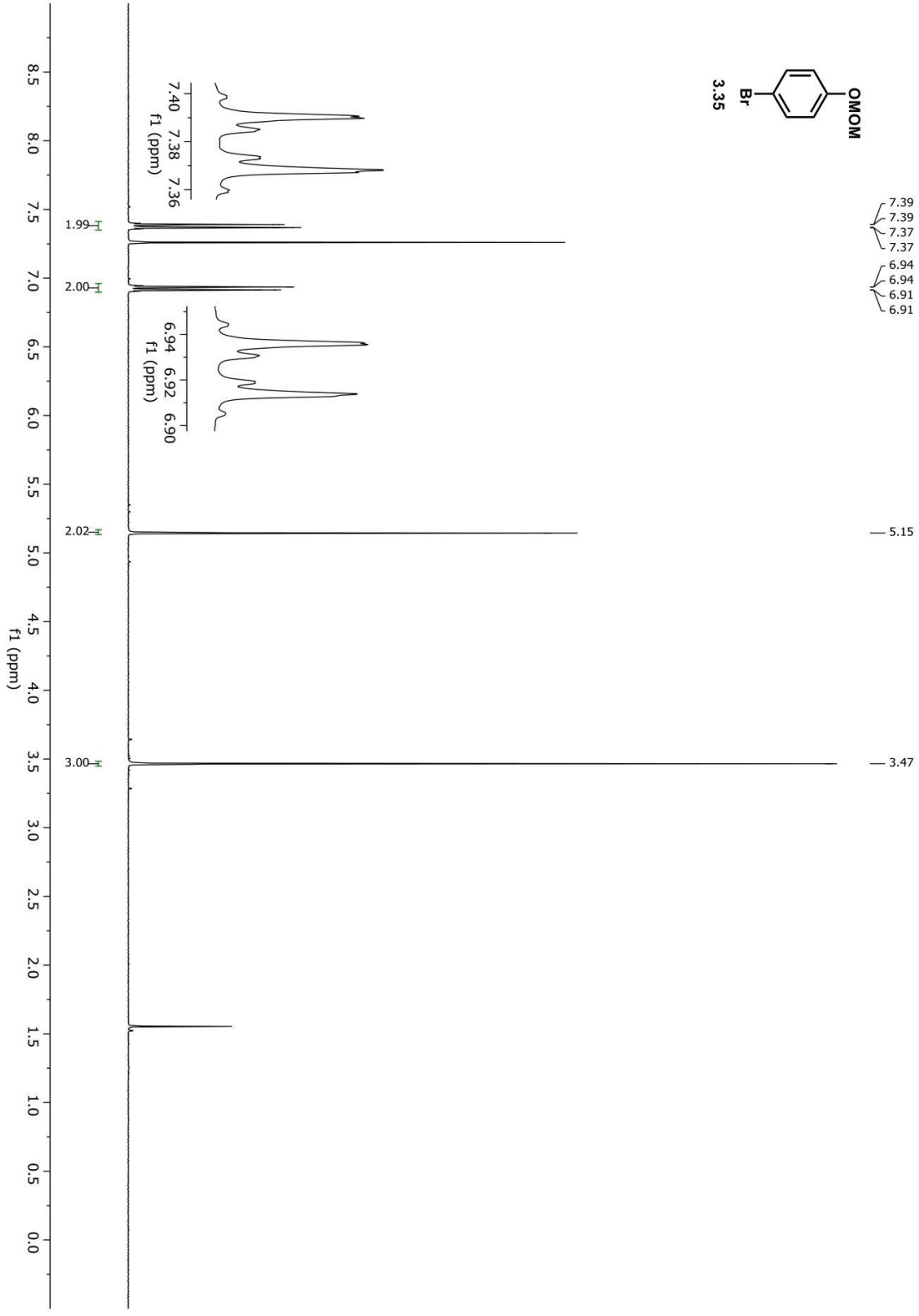

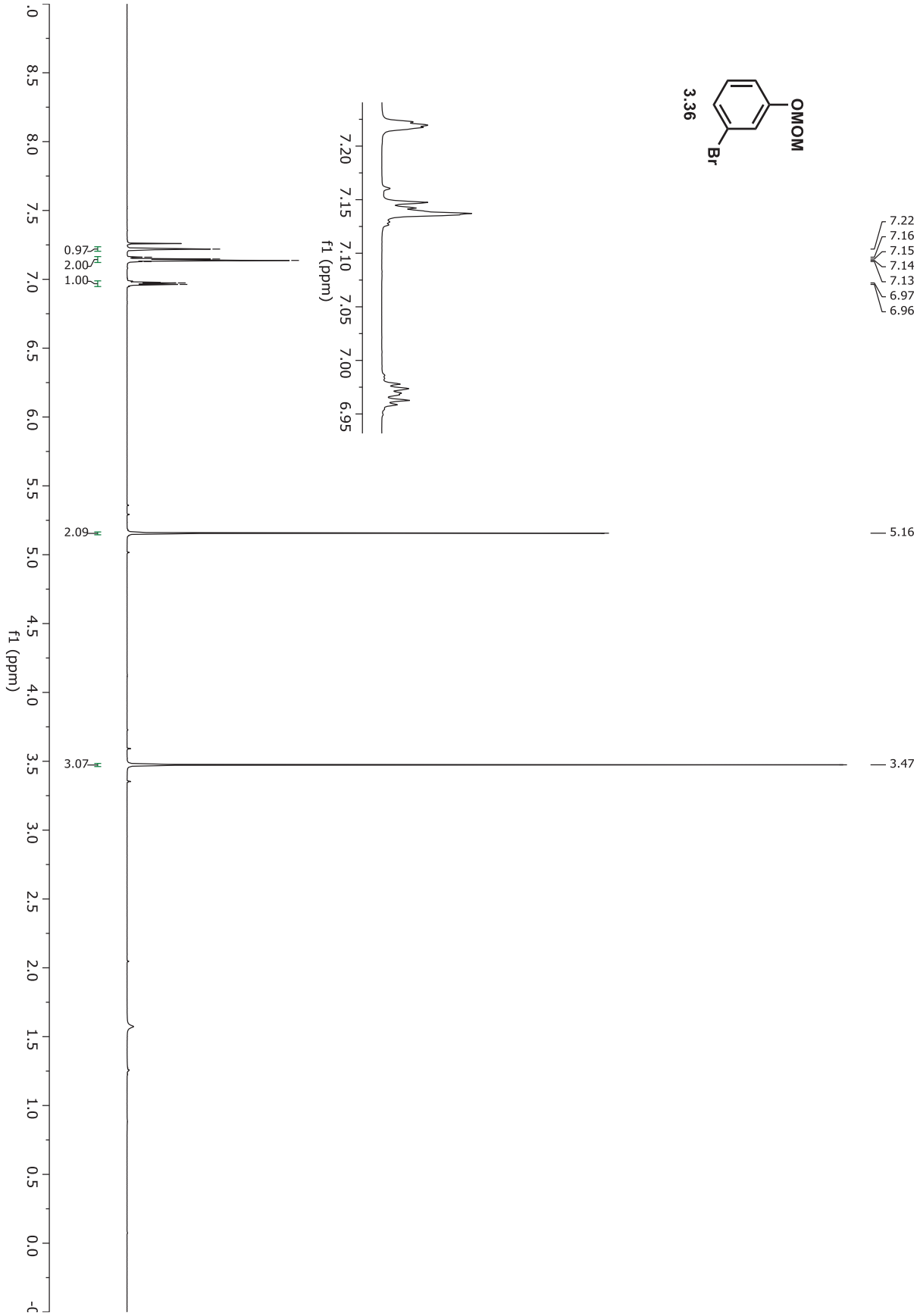
3.36
OMOM
Br
7.22
7.16
7.15
7.14
7.13
6.97
6.96
5.16
3.47
0.97
2.00
1.00
2.09
3.07
f1 (ppm)
7.20
7.15
7.10
7.05
7.00
6.95
f1 (ppm)

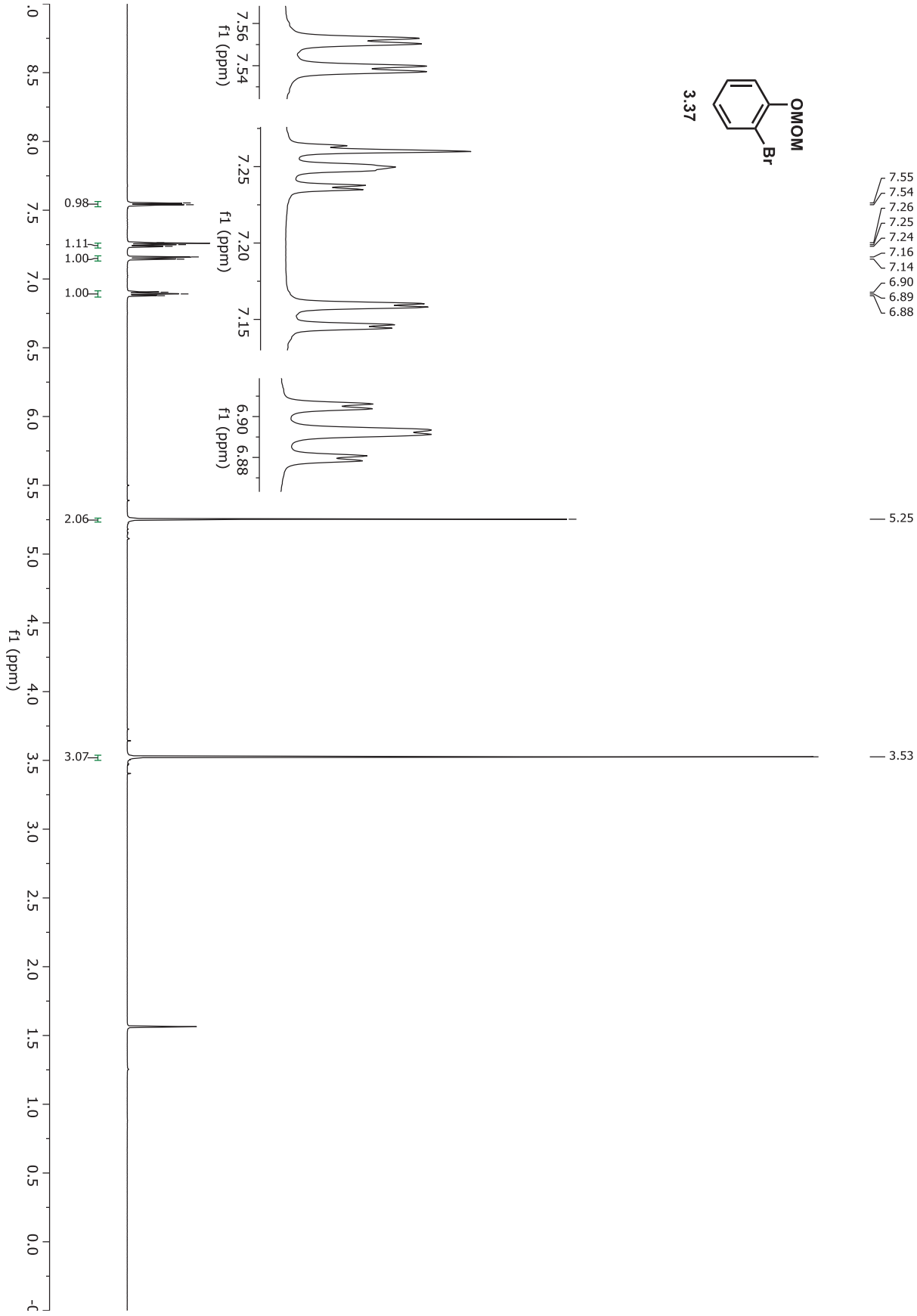
OMOM
Br
3.37
7.55
7.54
7.26
7.25
7.24
7.16
7.14
6.90
6.89
6.88
5.25
3.53
0.98
1.11
1.00
1.00
2.06
3.07
f1 (ppm)

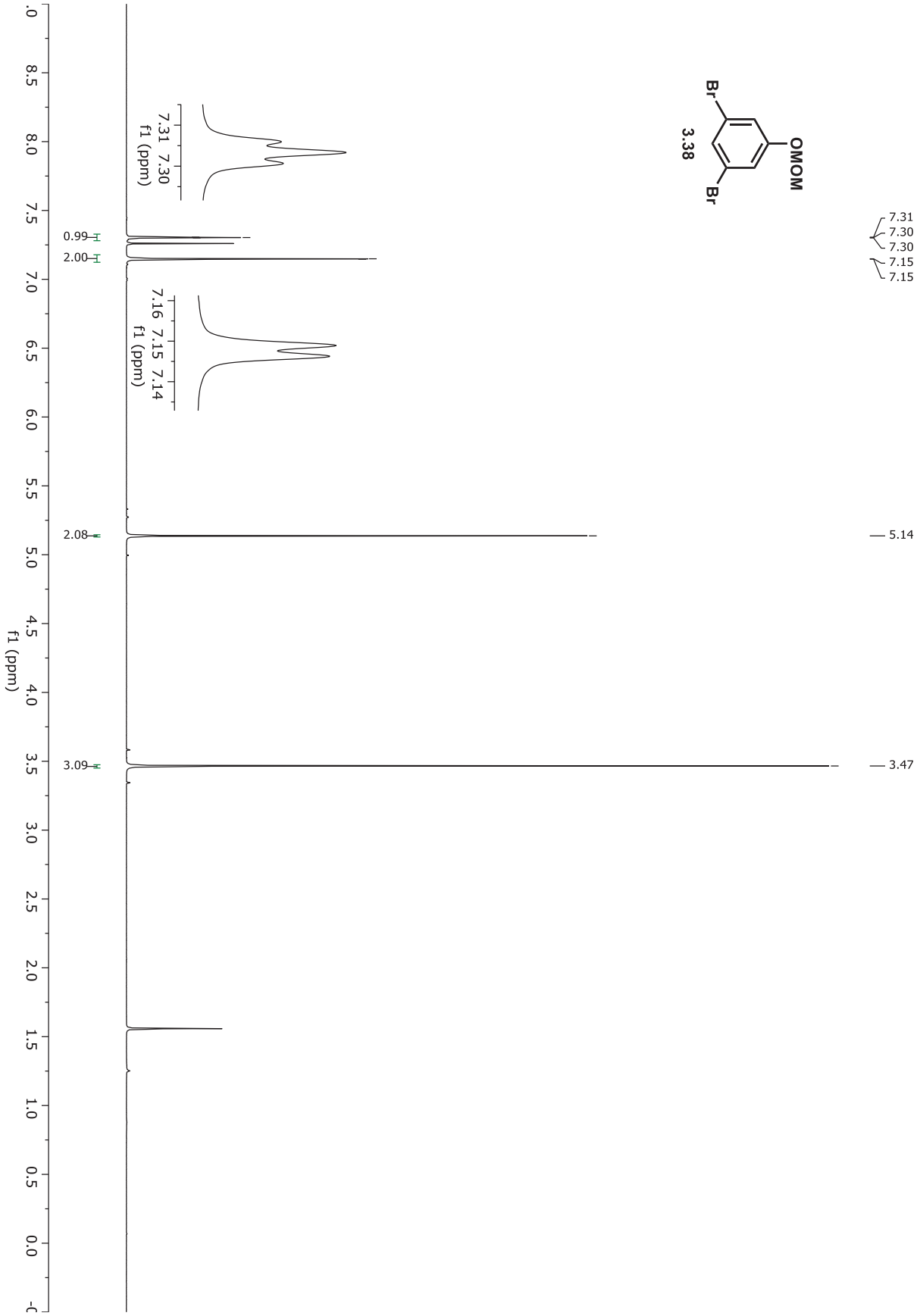
3.38
Br
Br
OMOM
7.31
7.30
7.30
7.15
7.15
5.14
3.47
0.99
2.00
2.08
3.09
7.31 7.30
f1 (ppm)
7.16 7.15 7.14
f1 (ppm)
f1 (ppm)

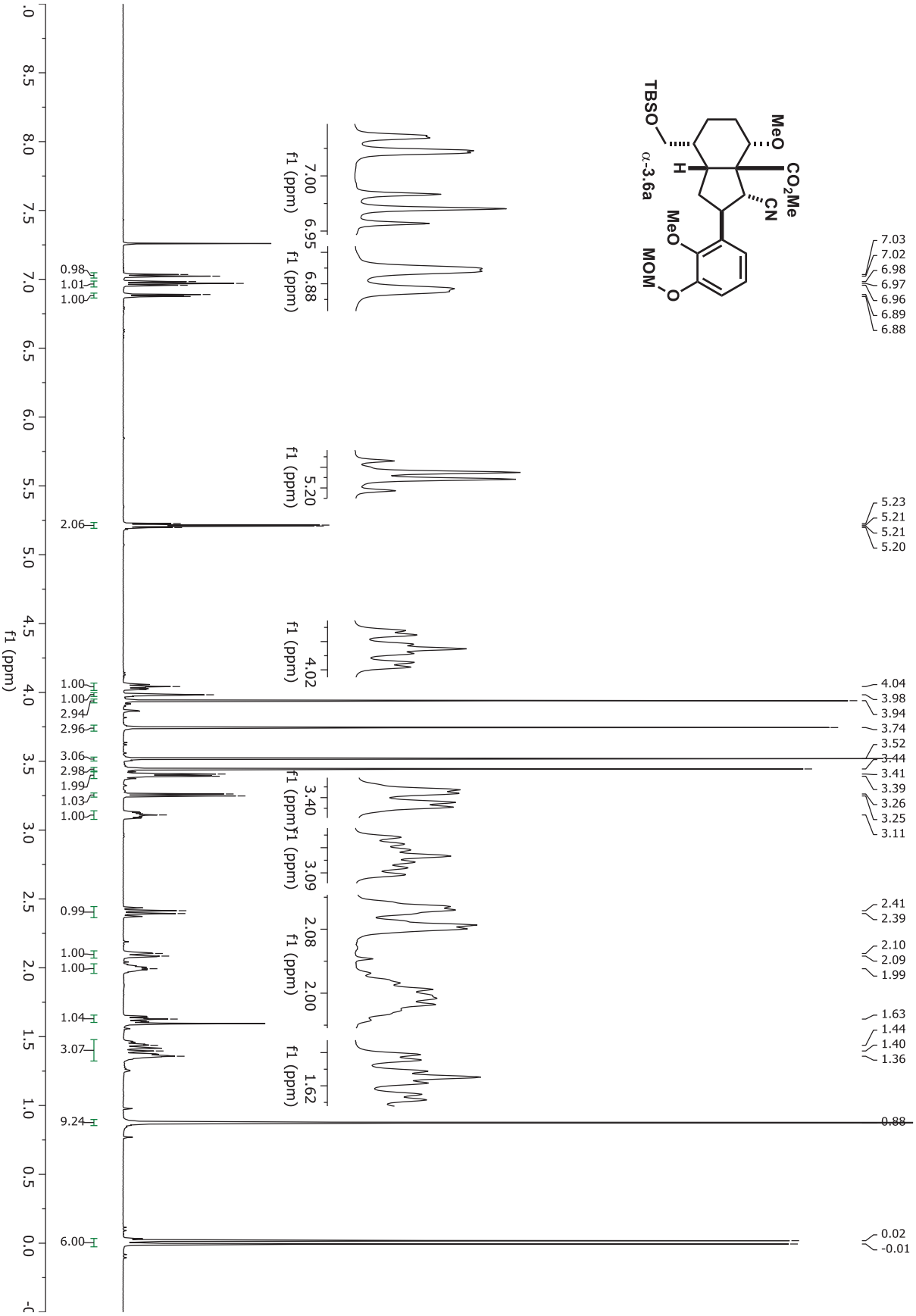
TBSO
MeO
CO2Me
CN
H
α-3.6a
MeO
MOM
O
f1 (ppm)

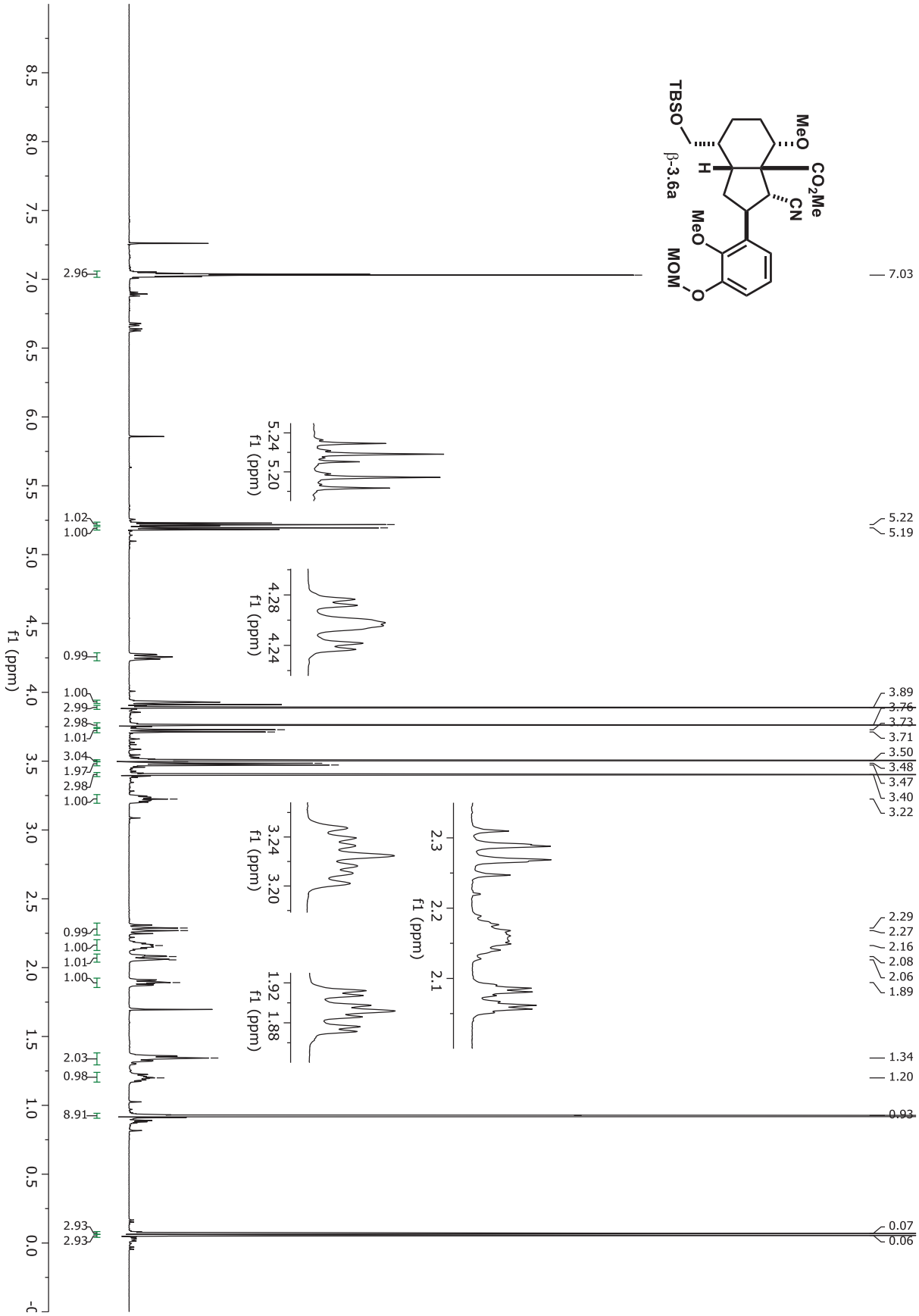
TBSO
β-3.6a
H
MeO
CO2Me
CN
MeO
MOM
O
f1 (ppm)
5.24 5.20
4.28 4.24
3.24 3.20
2.3 2.2 2.1
1.92 1.88
2.96
1.02
1.00
0.99
1.00
2.99
2.98
1.01
3.04
1.97
2.98
1.00
0.99
1.00
1.01
1.00
2.03
0.98
8.91
2.93
2.93
7.03
5.22
5.19
3.89
3.76
3.73
3.71
3.50
3.48
3.47
3.40
3.22
2.29
2.27
2.16
2.08
2.06
1.89
1.34
1.20
0.93
0.07
0.06

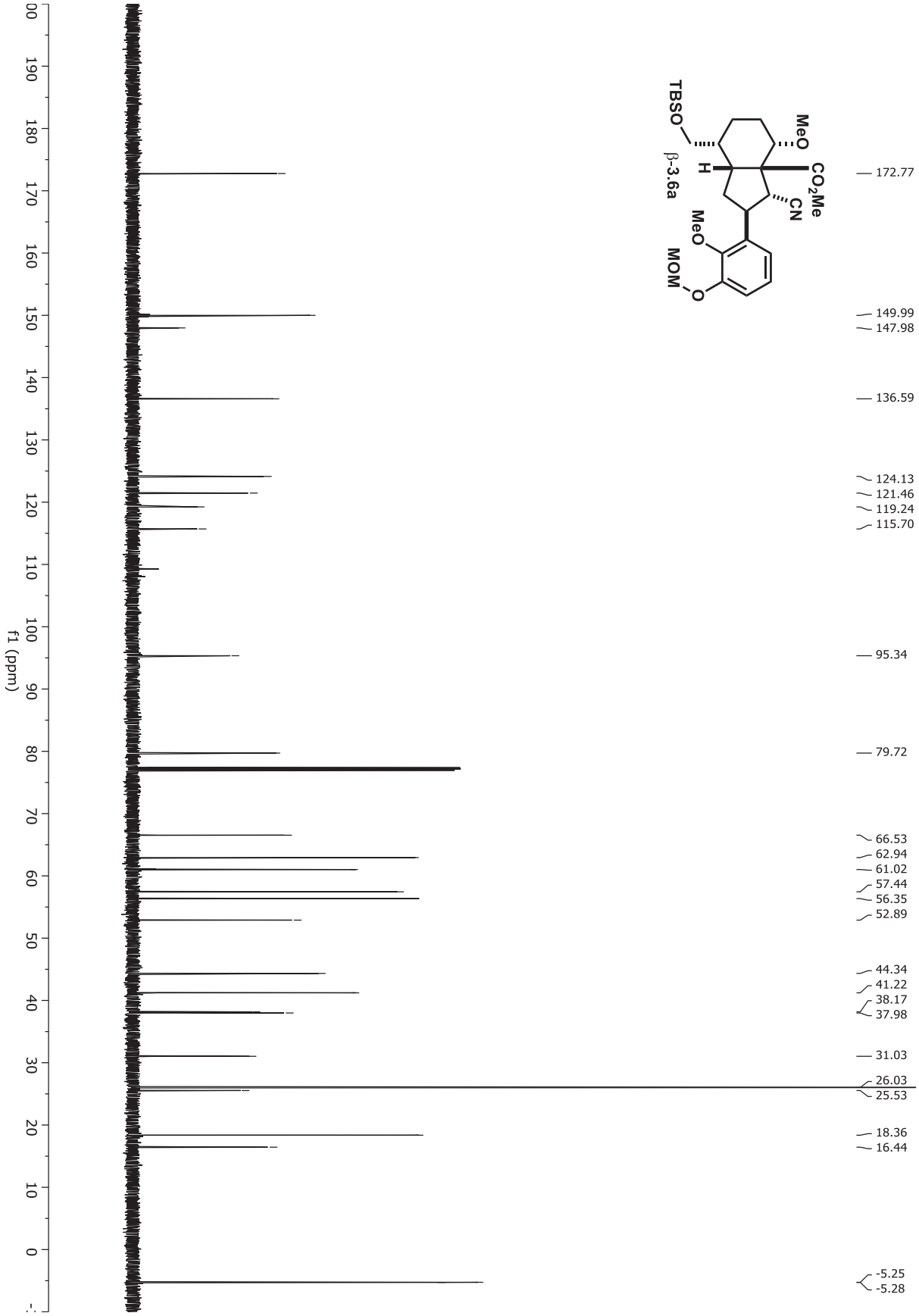
TBSO
MeO
CO2Me
CN
H
β-3.6a
MeO
MOM
O
172.77
149.99
147.98
136.59
124.13
121.46
119.24
115.70
95.34
79.72
66.53
62.94
61.02
57.44
56.35
52.89
44.34
41.22
38.17
37.98
31.03
26.03
25.53
18.36
16.44
-5.25
-5.28
f1 (ppm)

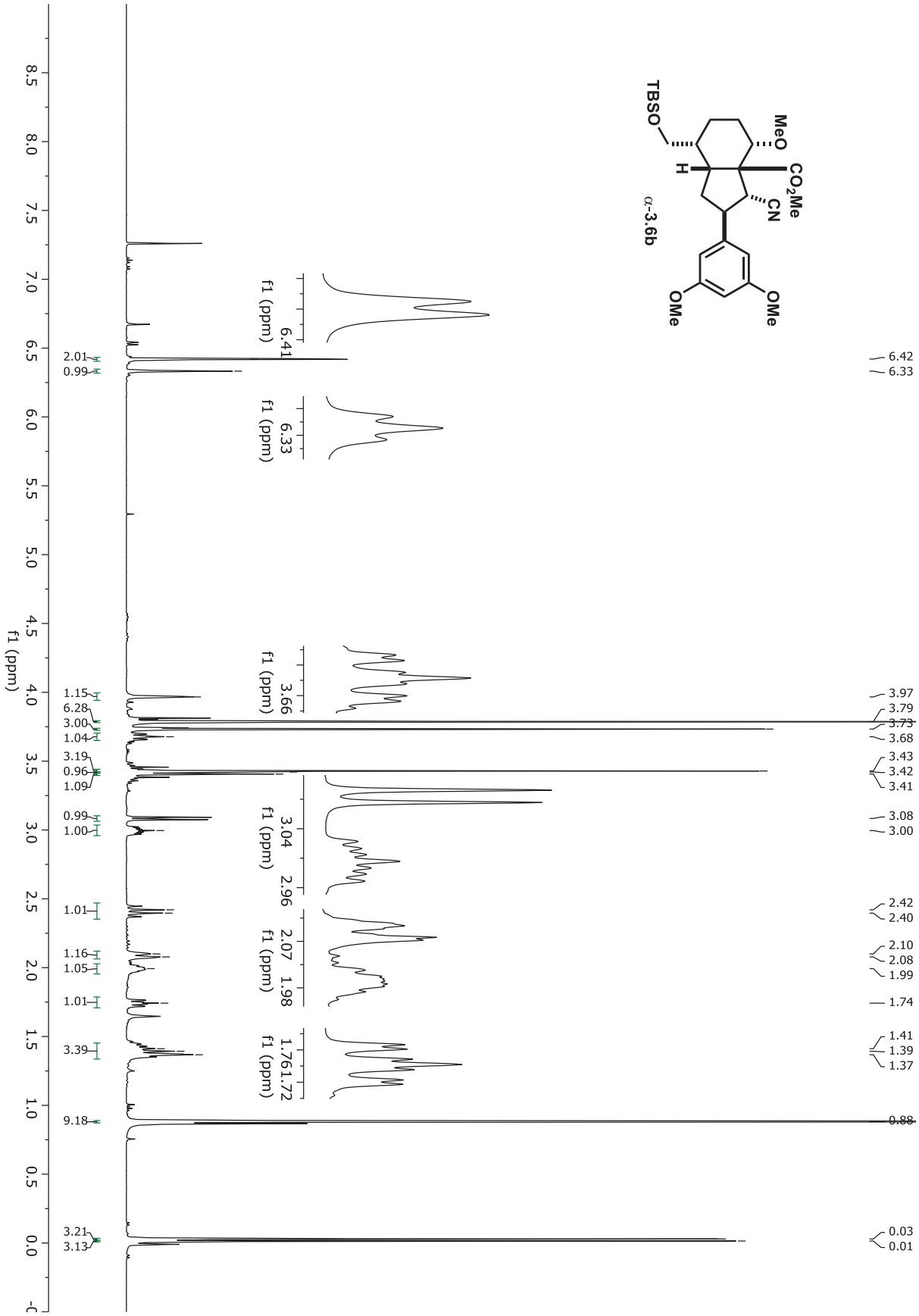
TBSO
MeO
H
CO2Me
CN
OMe
OMe
α-3.6b
f1 (ppm)

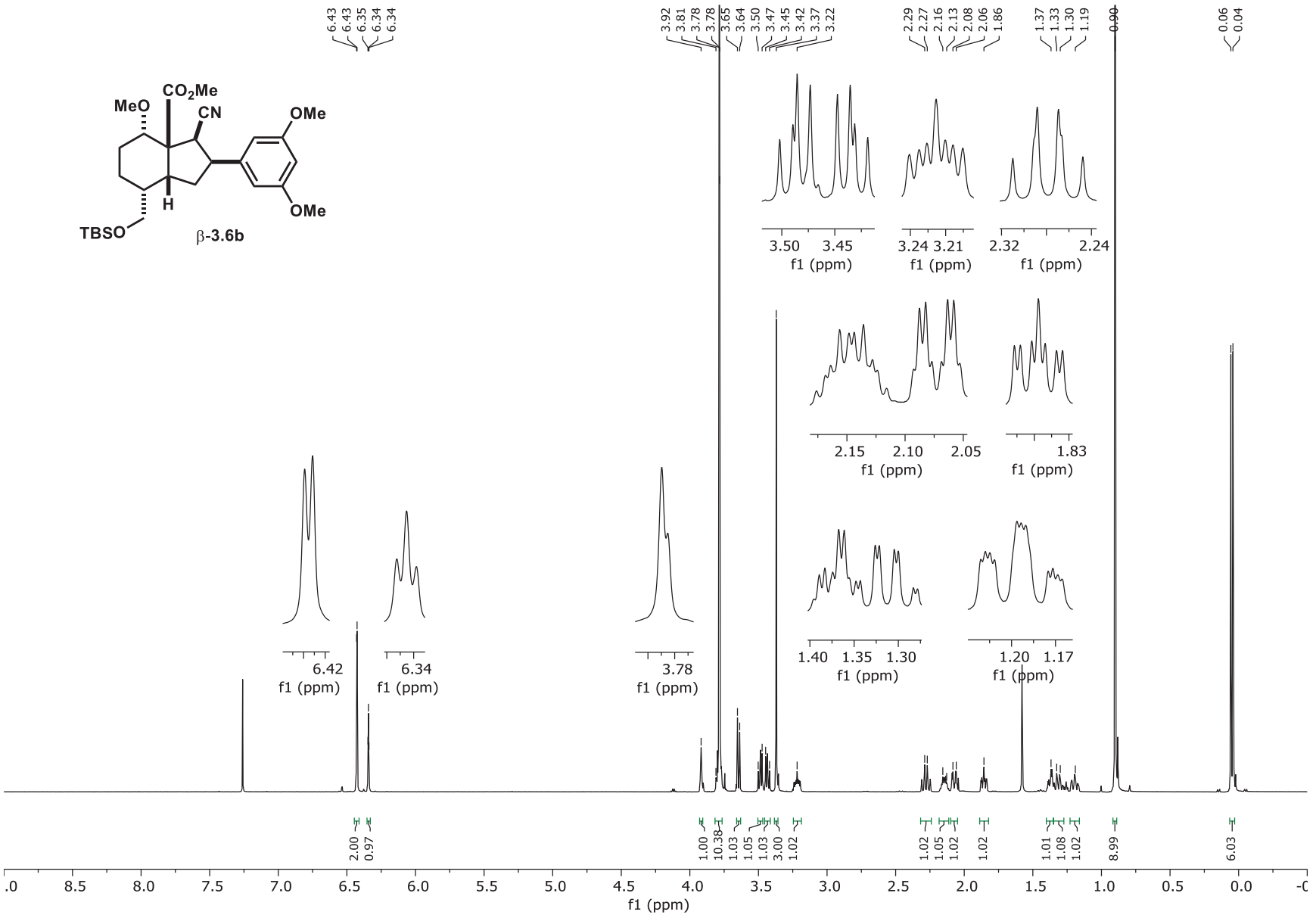
β-3.6b
f1 (ppm)

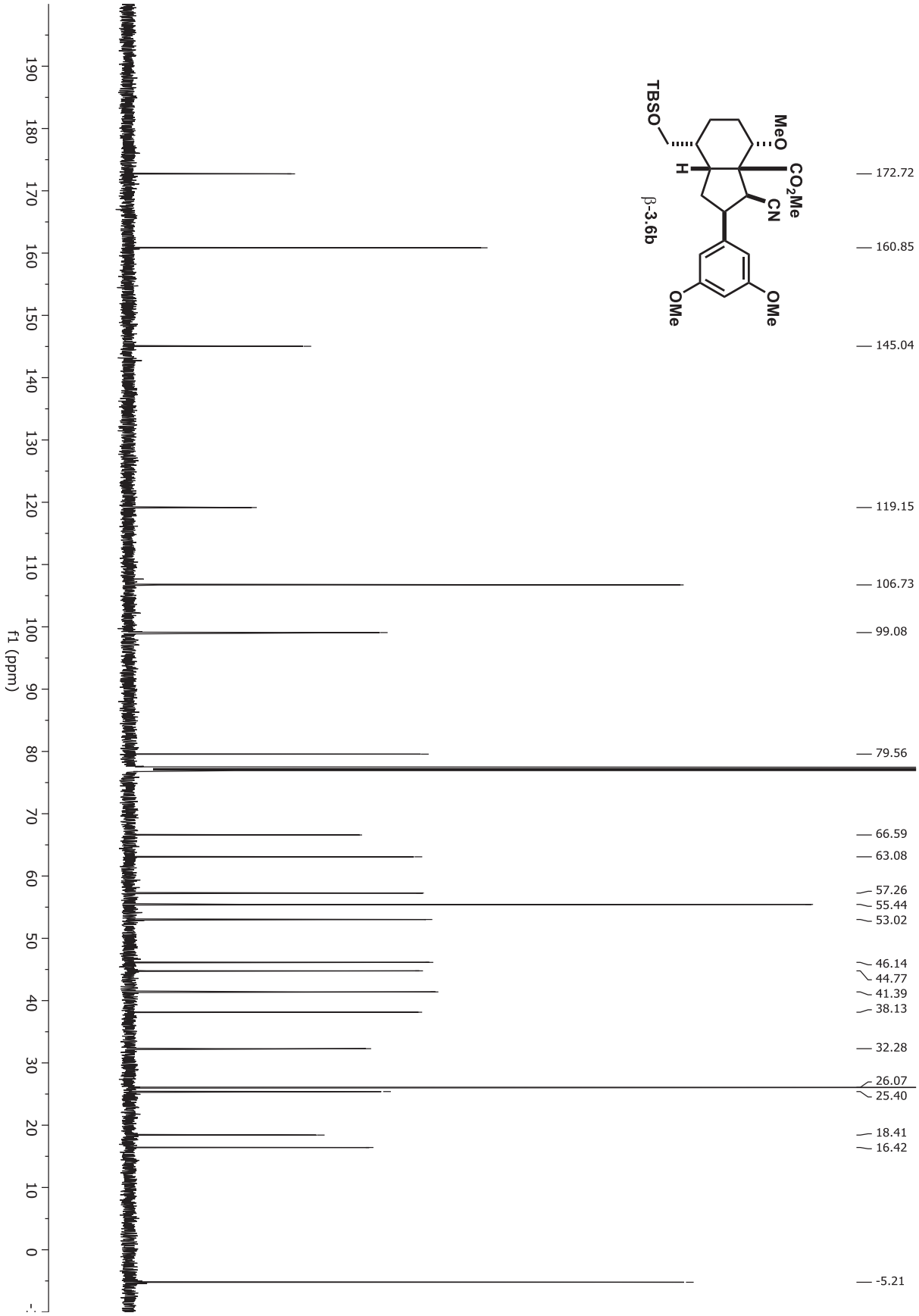
TBSO
MeO
H
CO2Me
CN
OMe
OMe
β-3.6b
f1 (ppm)
190
180
170
160
150
140
130
120
110
100
90
80
70
60
50
40
30
20
10
0
172.72
160.85
145.04
119.15
106.73
99.08
79.56
66.59
63.08
57.26
55.44
53.02
46.14
44.77
41.39
38.13
32.28
26.07
25.40
18.41
16.42
-5.21

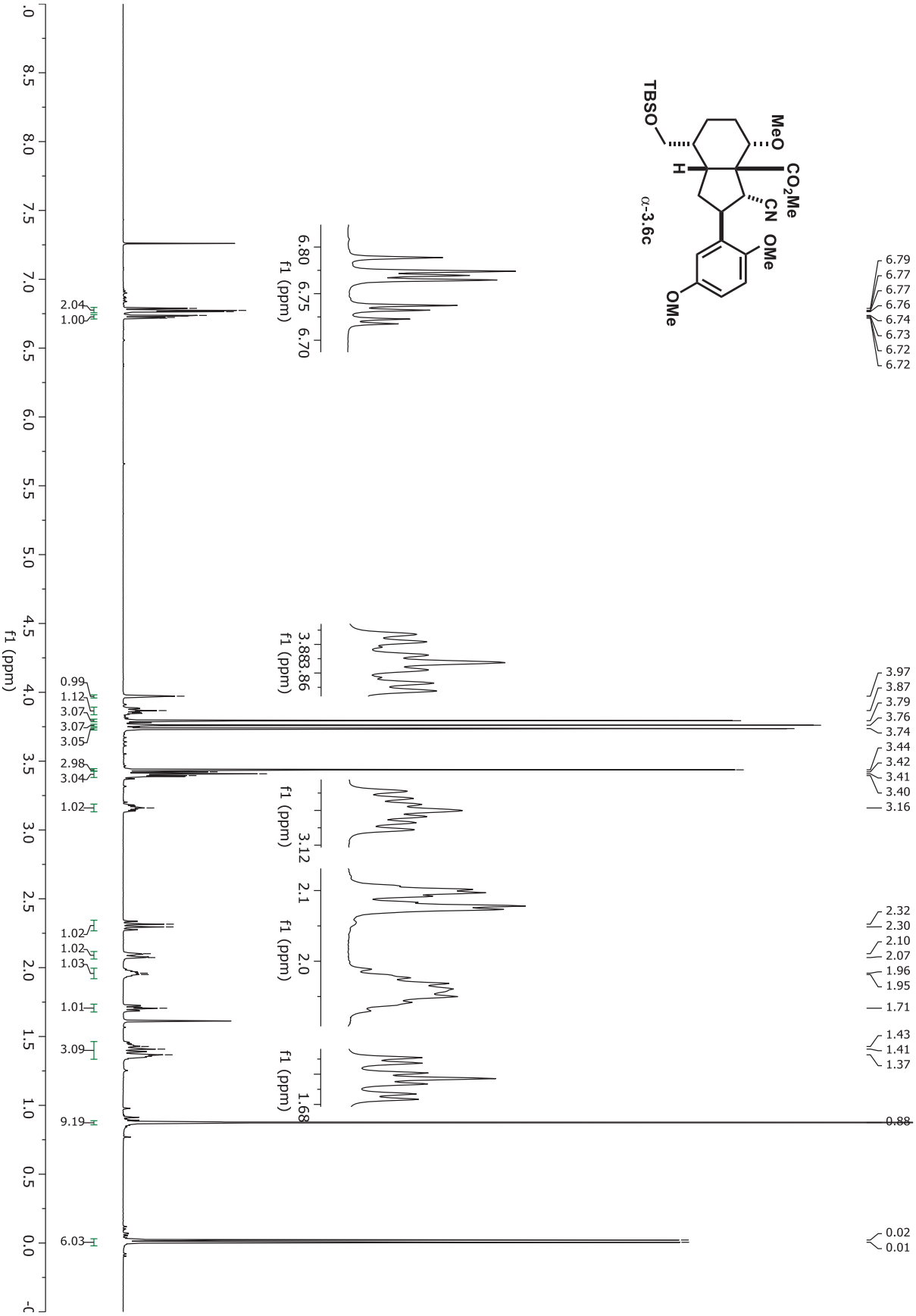
TBSO
MeO
H
CO2Me
CN
OMe
OMe
α-3.6c
f1 (ppm)

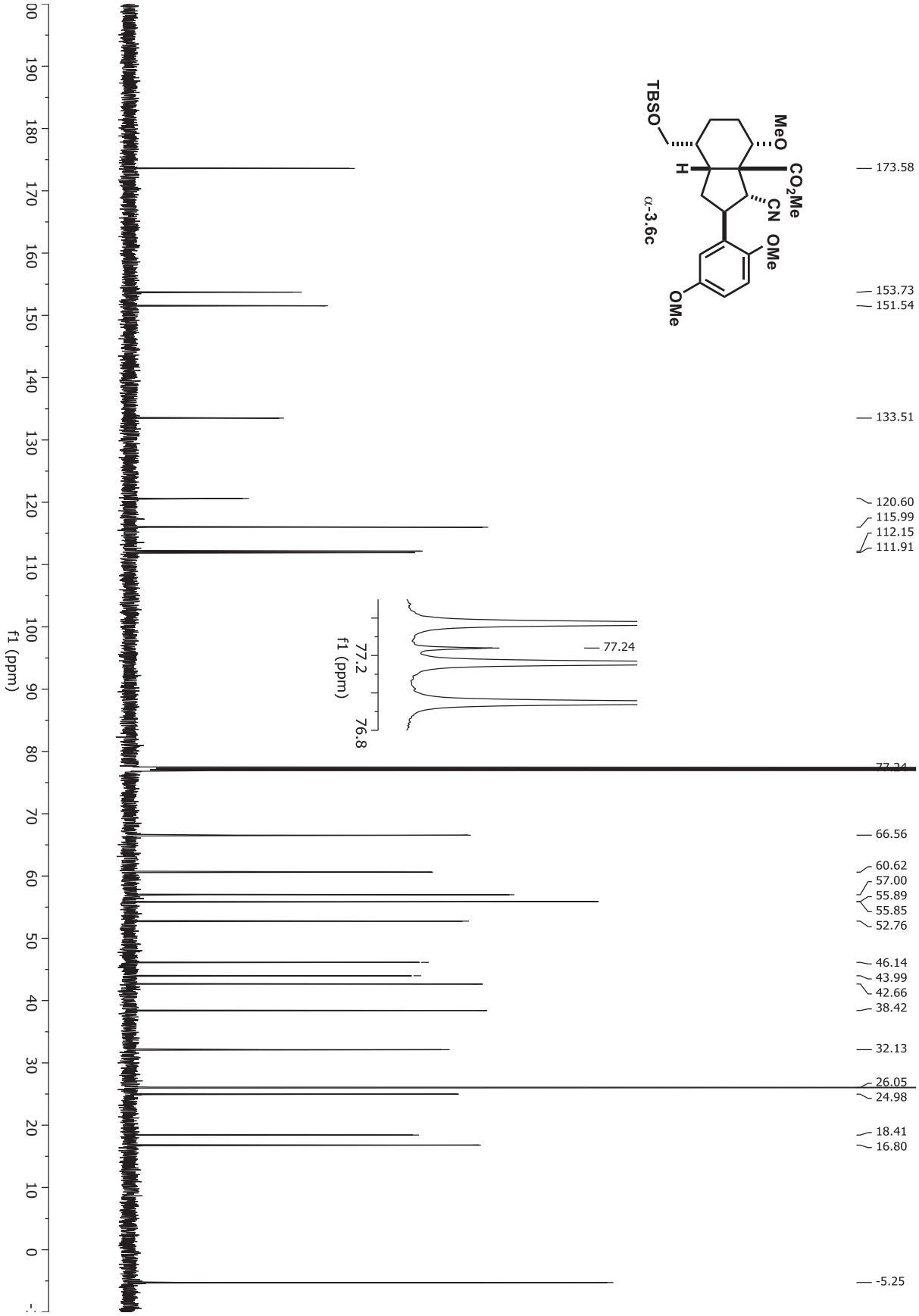
TBSO
MeO
H
CO2Me
CN
OMe
OMe
α-3.6c
173.58
153.73
151.54
133.51
120.60
115.99
112.15
111.91
77.24
66.56
60.62
57.00
55.89
55.85
52.76
46.14
43.99
42.66
38.42
32.13
26.05
24.98
18.41
16.80
-5.25
f1 (ppm)
77.2
76.8

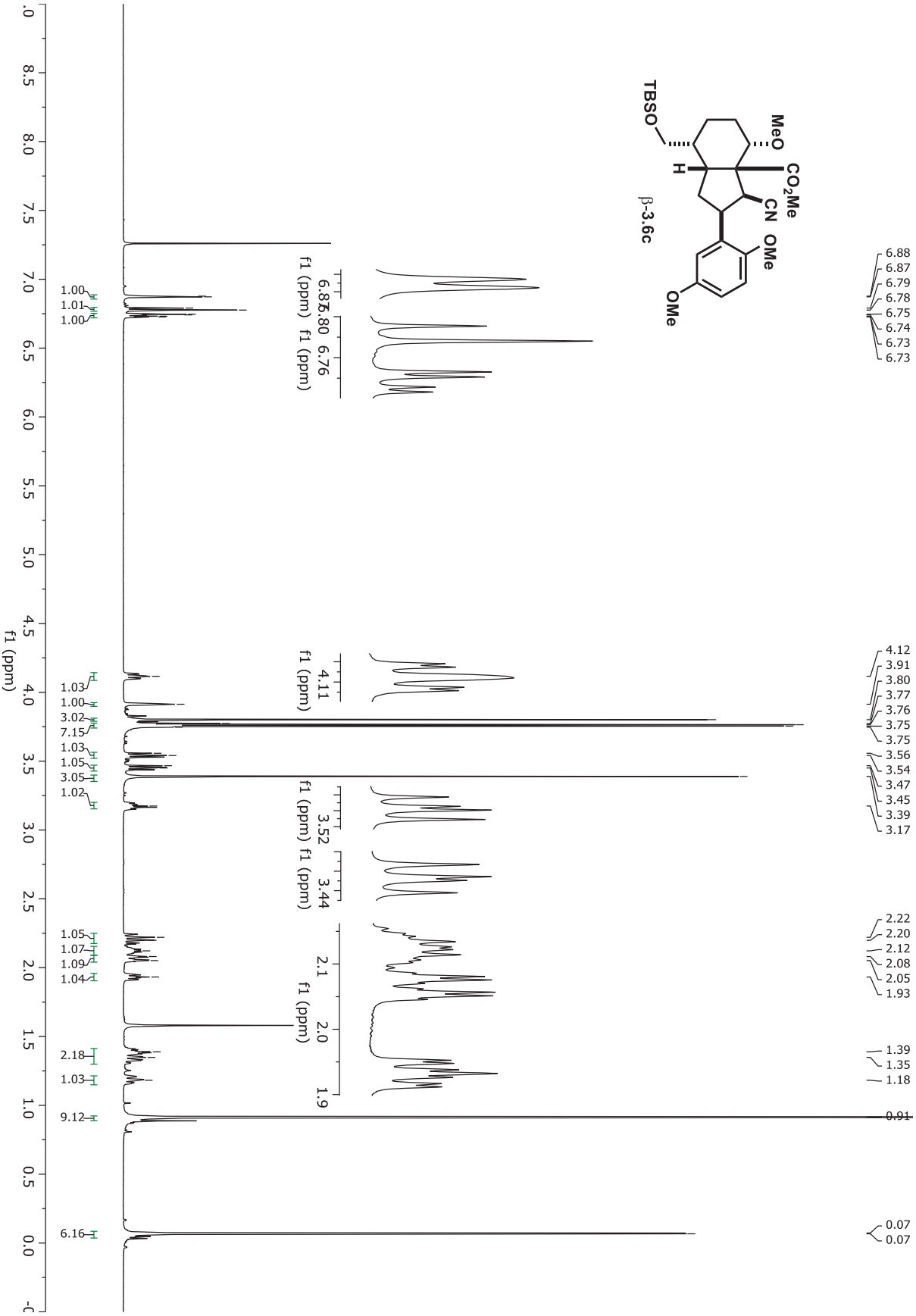
TBSO
MeO
H
CO2Me
CN
OMe
OMe
β-3.6c
f1 (ppm)

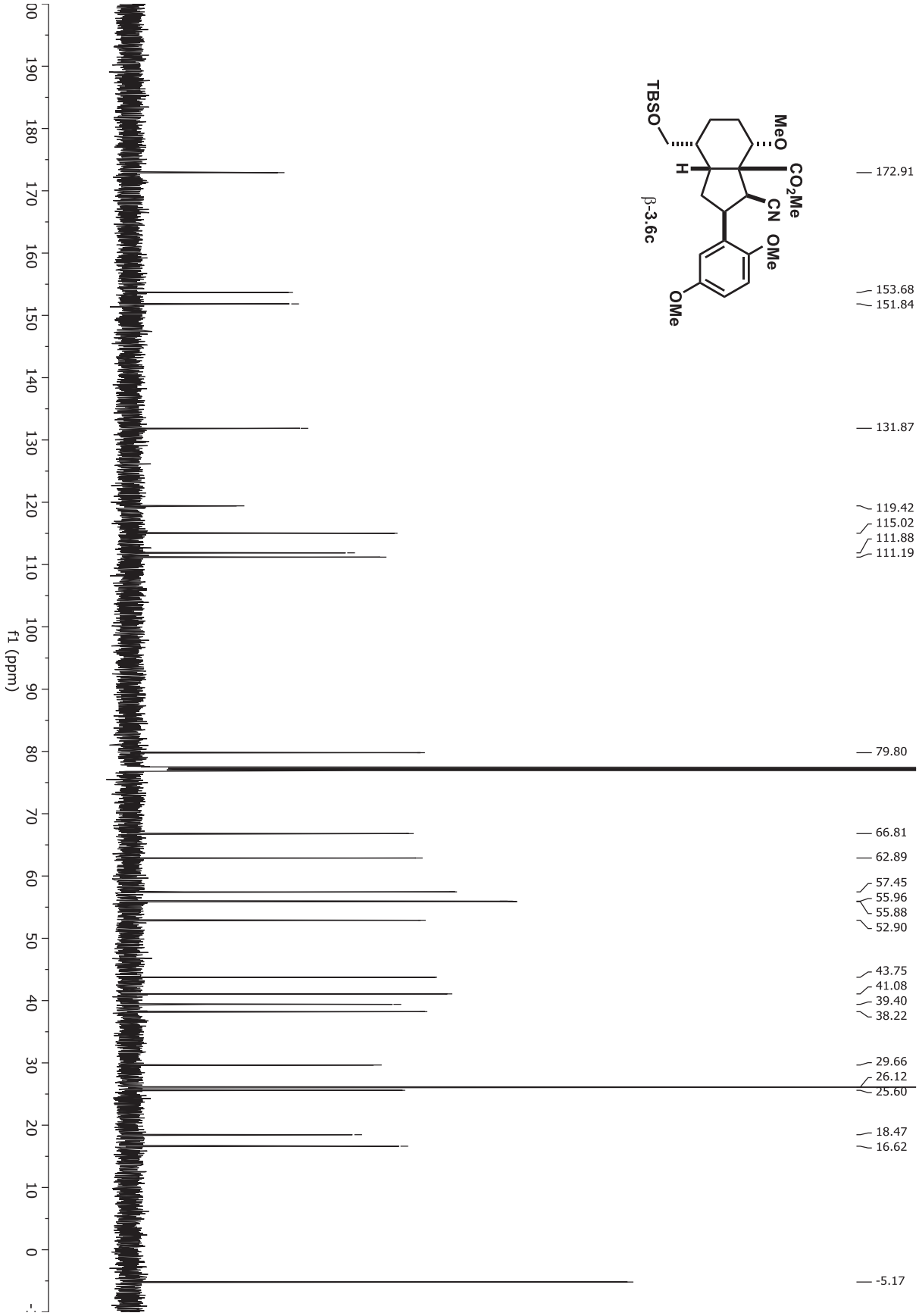
TBSO
MeO
H
CO2Me
CN
OMe
OMe
β-3.6c
172.91
153.68
151.84
131.87
119.42
115.02
111.88
111.19
79.80
66.81
62.89
57.45
55.96
55.88
52.90
43.75
41.08
39.40
38.22
29.66
26.12
25.60
18.47
16.62
-5.17
f1 (ppm)

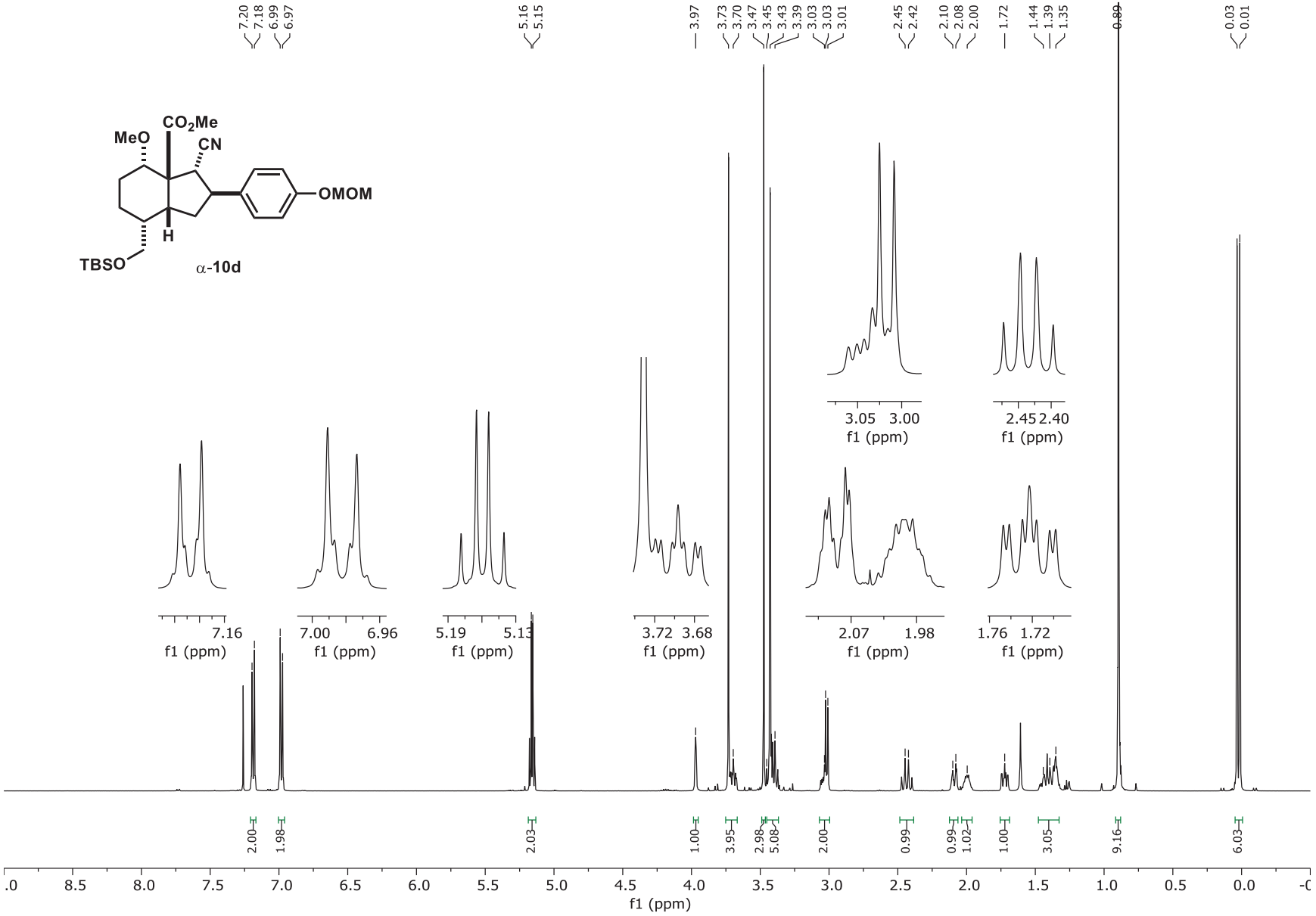
CO2Me
MeO
CN
OMOM
H
TBSO
α-10d
7.20
7.18
6.99
6.97
5.16
5.15
3.97
3.73
3.70
3.47
3.45
3.43
3.39
3.03
3.03
3.01
2.45
2.42
2.10
2.08
2.00
1.72
1.44
1.39
1.35
0.89
0.03
0.01
f1 (ppm)

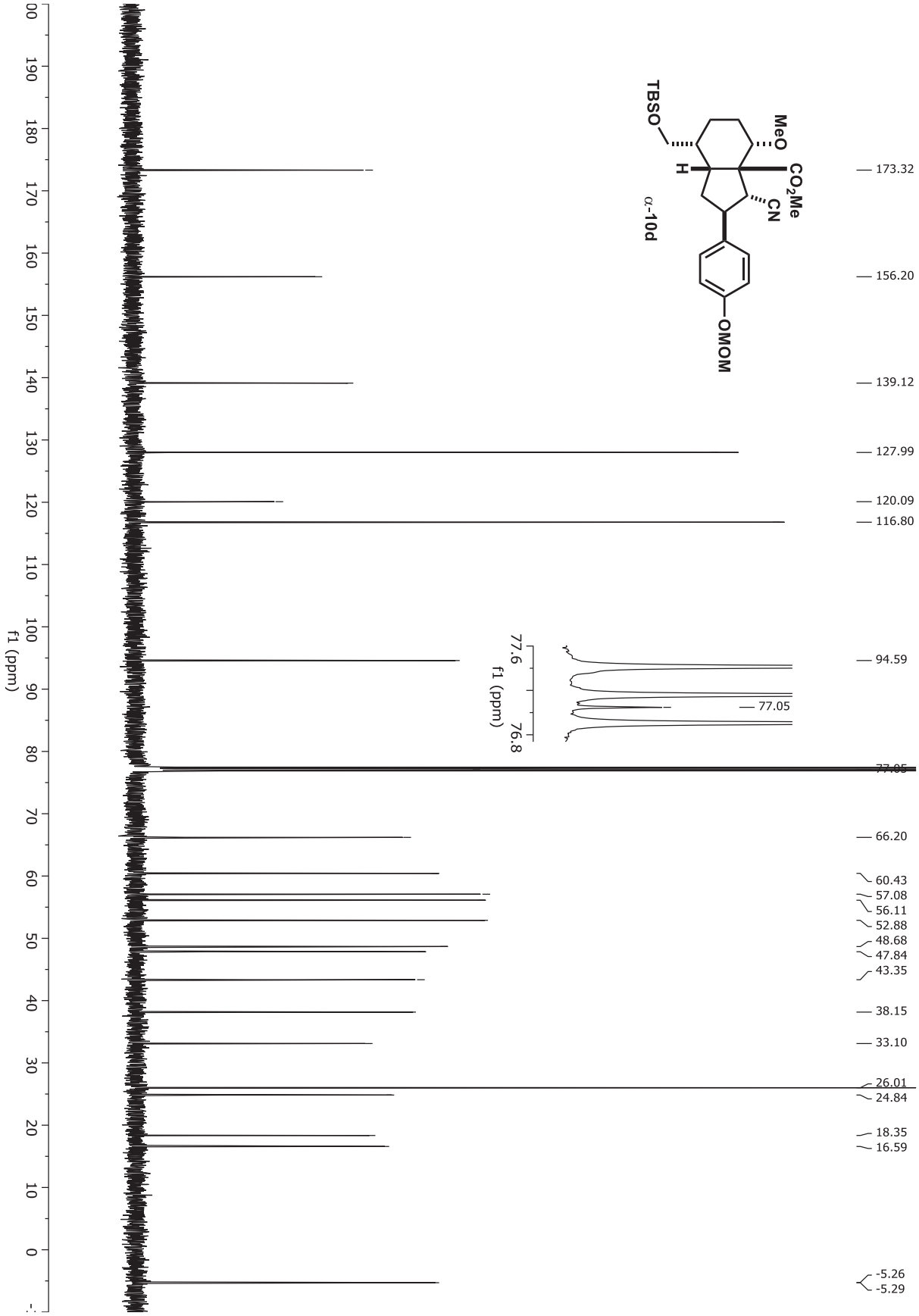
TBSO
MeO
H
CO2Me
CN
OMOM
α-10d
173.32
156.20
139.12
127.99
120.09
116.80
94.59
77.05
66.20
60.43
57.08
56.11
52.88
48.68
47.84
43.35
38.15
33.10
26.01
24.84
18.35
16.59
-5.26
-5.29
f1 (ppm)
77.6
76.8

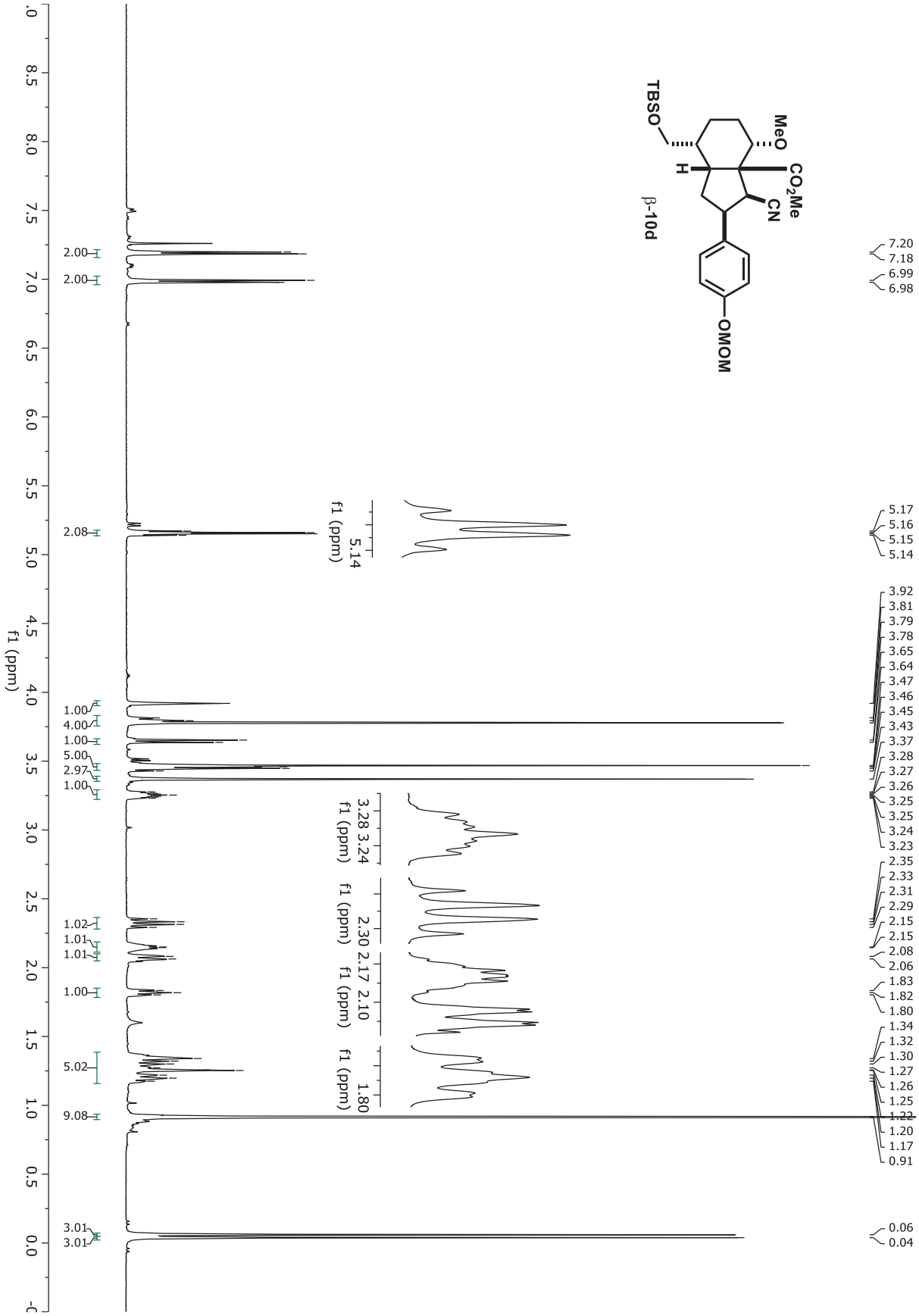
TBSO
MeO
CO2Me
CN
H
OMOM
β-10d
f1 (ppm)

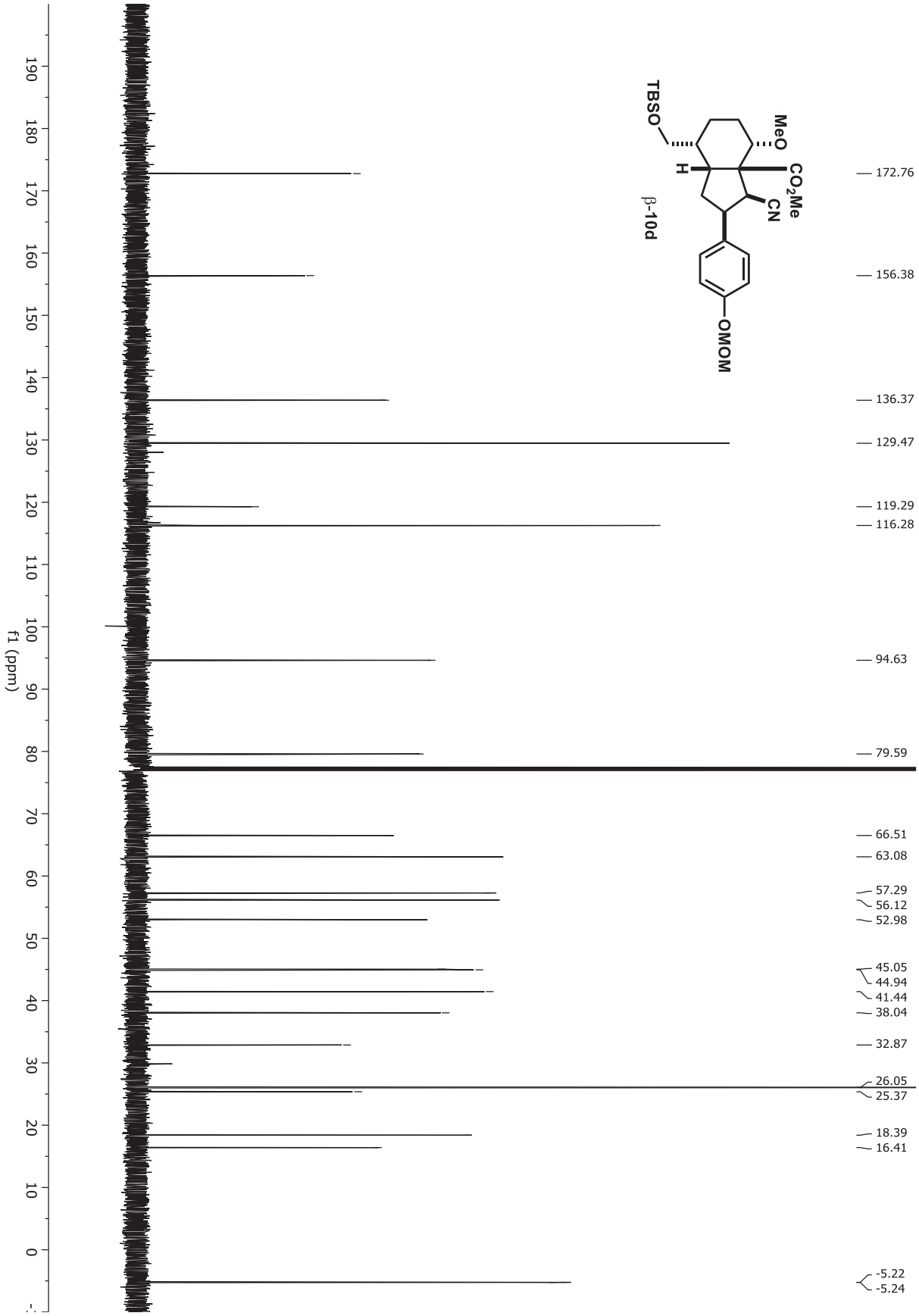
TBSO
MeO
H
CO2Me
CN
OMOM
β-10d
172.76
156.38
136.37
129.47
119.29
116.28
94.63
79.59
66.51
63.08
57.29
56.12
52.98
45.05
44.94
41.44
38.04
32.87
26.05
25.37
18.39
16.41
-5.22
-5.24
f1 (ppm)

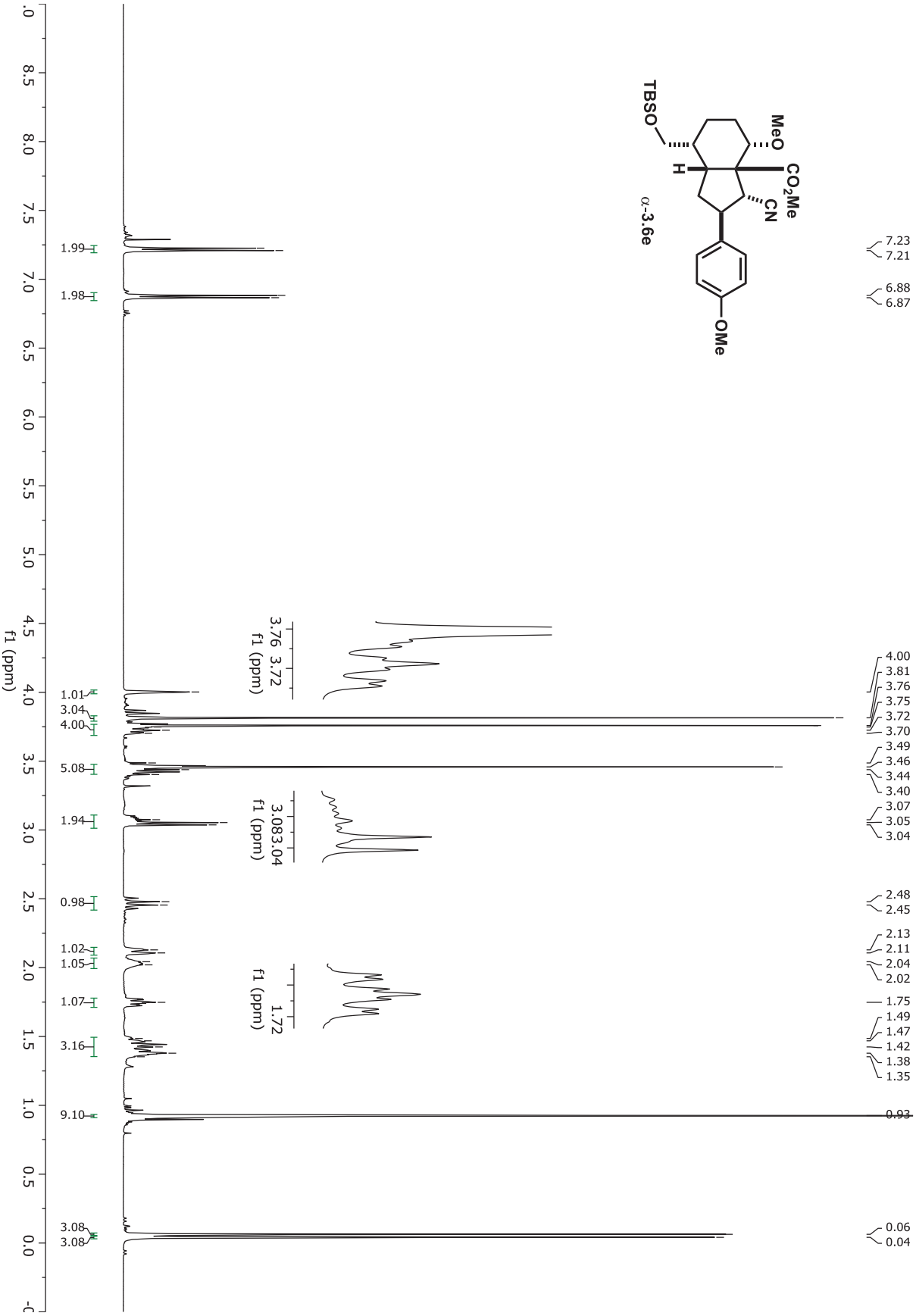
TBSO
MeO
CO2Me
CN
H
OMe
α-3.6e
f1 (ppm)

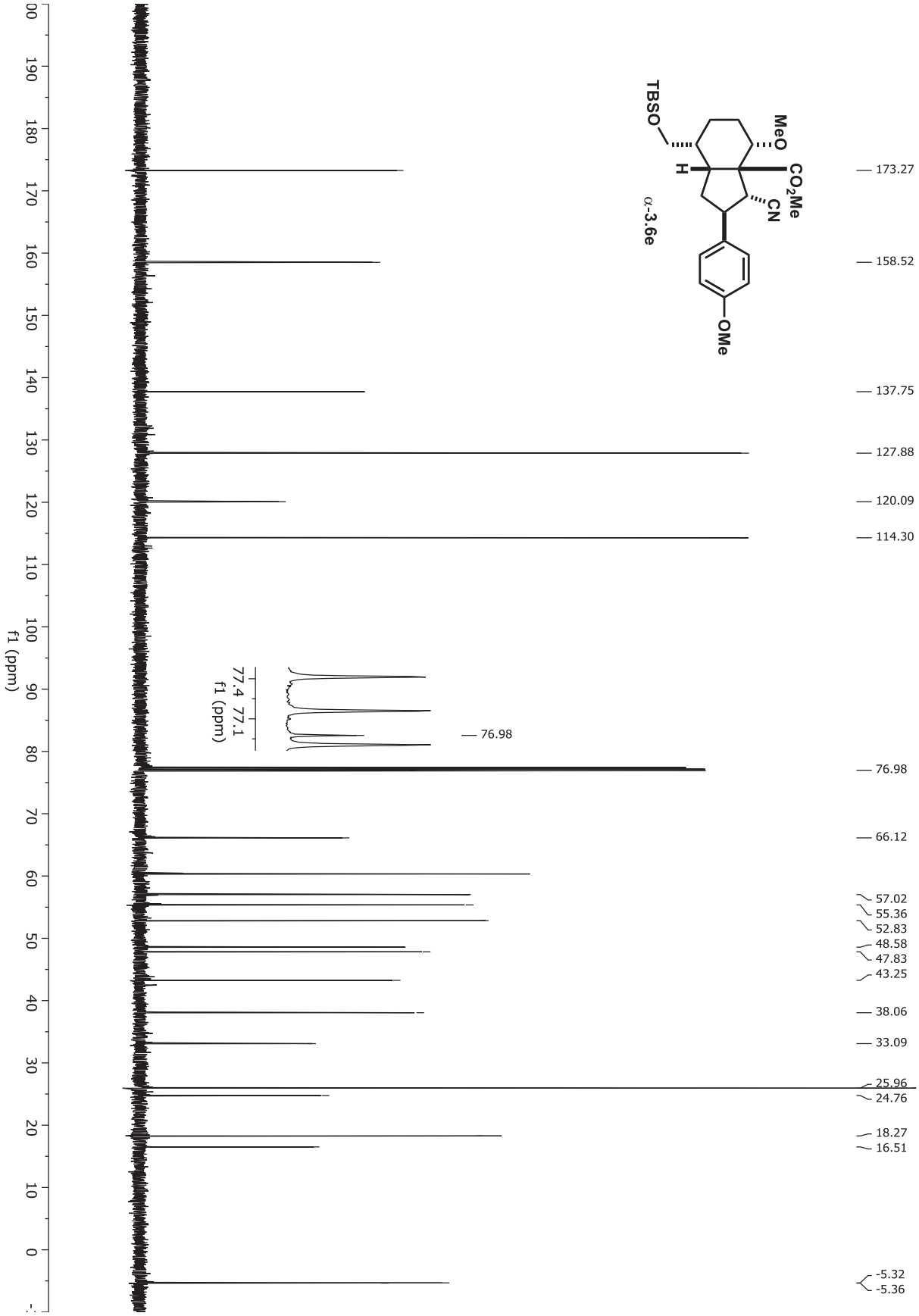
TBSO
MeO
H
CO2Me
CN
OMe
α-3.6e
173.27
158.52
137.75
127.88
120.09
114.30
76.98
66.12
57.02
55.36
52.83
48.58
47.83
43.25
38.06
33.09
25.96
24.76
18.27
16.51
-5.32
-5.36
77.4 77.1
f1 (ppm)
f1 (ppm)

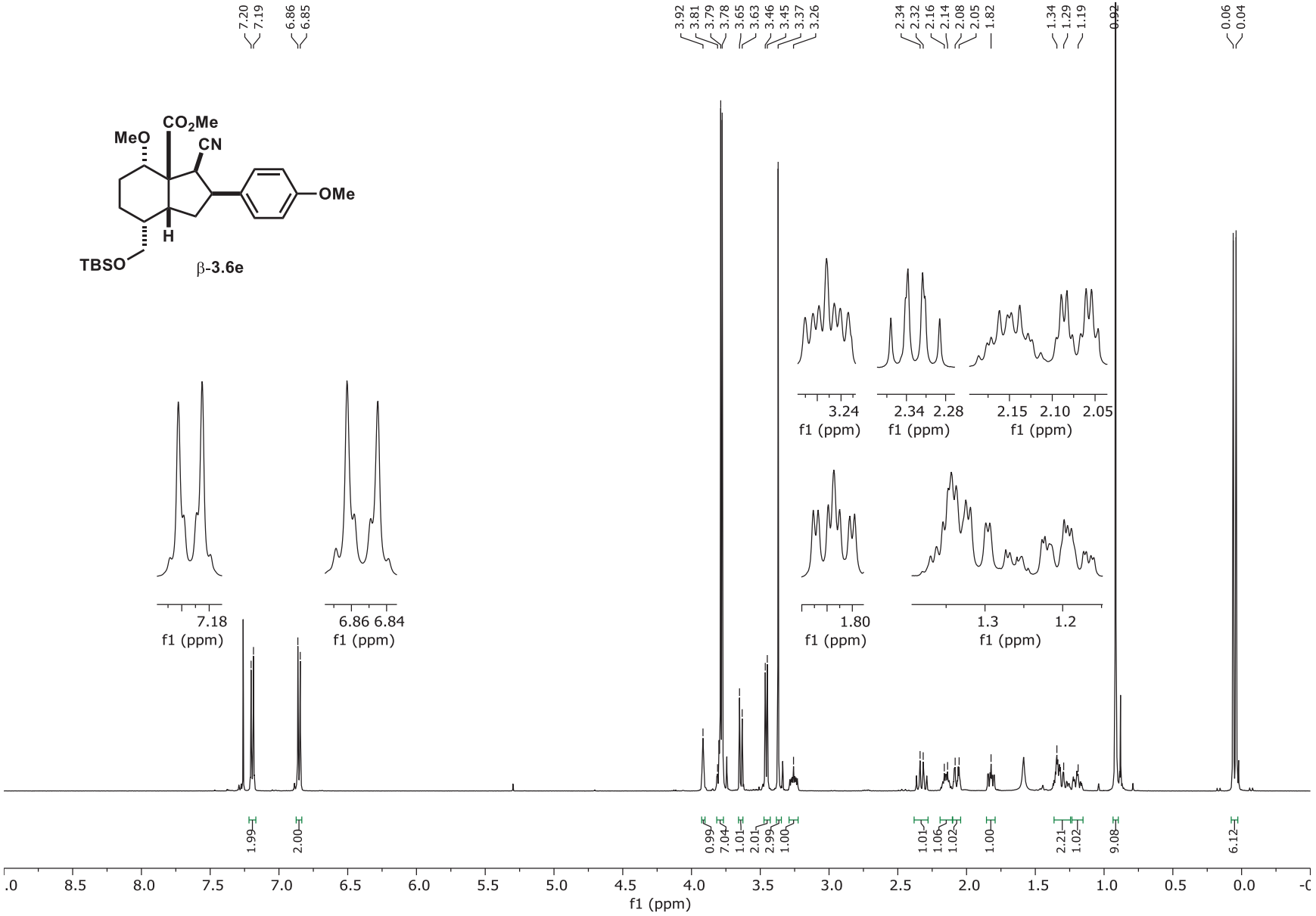
7.20
7.19
6.86
6.85
3.92
3.81
3.79
3.78
3.65
3.63
3.46
3.45
3.37
3.26
2.34
2.32
2.16
2.14
2.08
2.05
1.82
1.34
1.29
1.19
0.92
0.06
0.04
CO2Me
MeO
CN
OMe
H
TBSO
β-3.6e
7.18
f1 (ppm)
6.86 6.84
f1 (ppm)
3.24
f1 (ppm)
2.34 2.28
f1 (ppm)
2.15 2.10 2.05
f1 (ppm)
1.80
f1 (ppm)
1.3
1.2
f1 (ppm)
1.99
2.00
0.99
7.04
1.01
2.01
2.99
1.00
1.01
1.06
1.02
1.00
2.21
1.02
9.08
6.12
f1 (ppm)

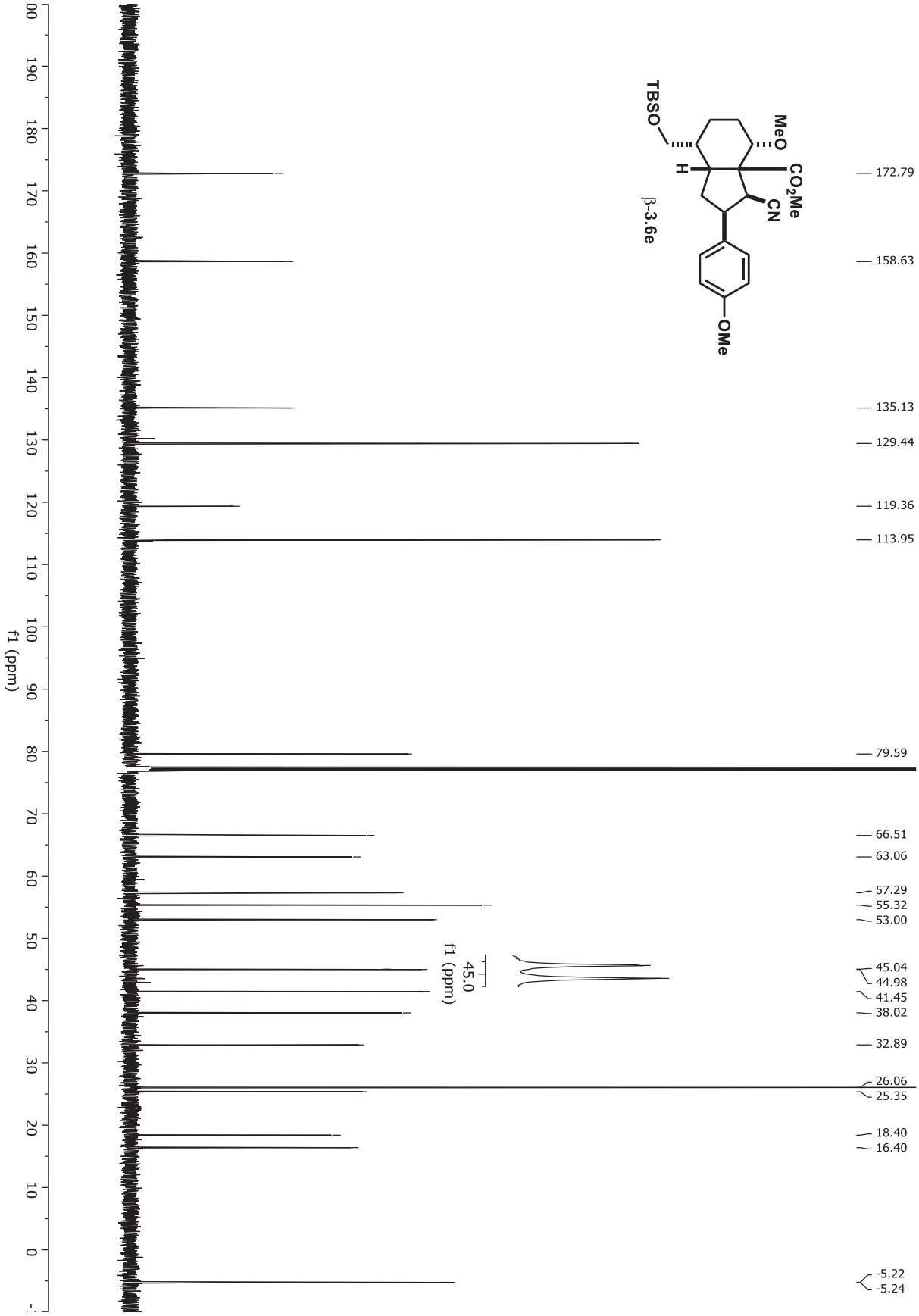
TBSO
MeO
H
CO2Me
CN
OMe
β-3.6e
172.79
158.63
135.13
129.44
119.36
113.95
79.59
66.51
63.06
57.29
55.32
53.00
45.04
44.98
41.45
38.02
32.89
26.06
25.35
18.40
16.40
-5.22
-5.24
45.0
f1 (ppm)
f1 (ppm)

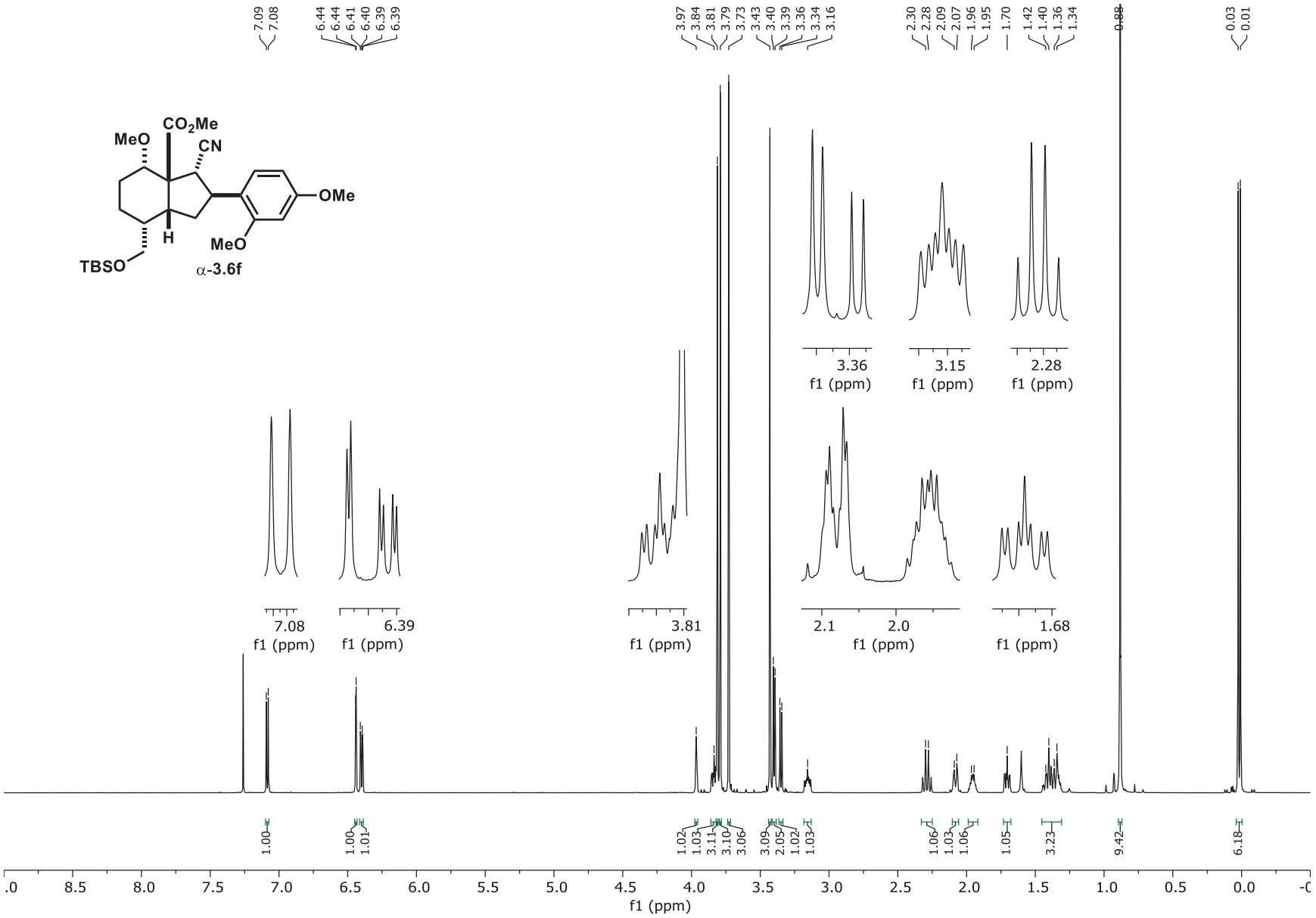
CO2Me
MeO
CN
OMe
H
MeO
TBSO
α-3.6f
7.09
7.08
6.44
6.44
6.41
6.40
6.39
6.39
3.97
3.84
3.81
3.79
3.73
3.43
3.40
3.39
3.36
3.34
3.16
2.30
2.28
2.09
2.07
1.96
1.95
1.70
1.42
1.40
1.36
1.34
0.88
0.03
0.01
7.08
f1 (ppm)
6.39
f1 (ppm)
3.81
f1 (ppm)
3.36
f1 (ppm)
3.15
f1 (ppm)
2.28
f1 (ppm)
2.1
2.0
f1 (ppm)
1.68
f1 (ppm)
1.00
1.00
1.01
1.02
1.03
3.11
3.10
3.06
3.09
2.05
1.02
1.03
1.06
1.03
1.06
1.05
3.23
9.42
6.18
f1 (ppm)

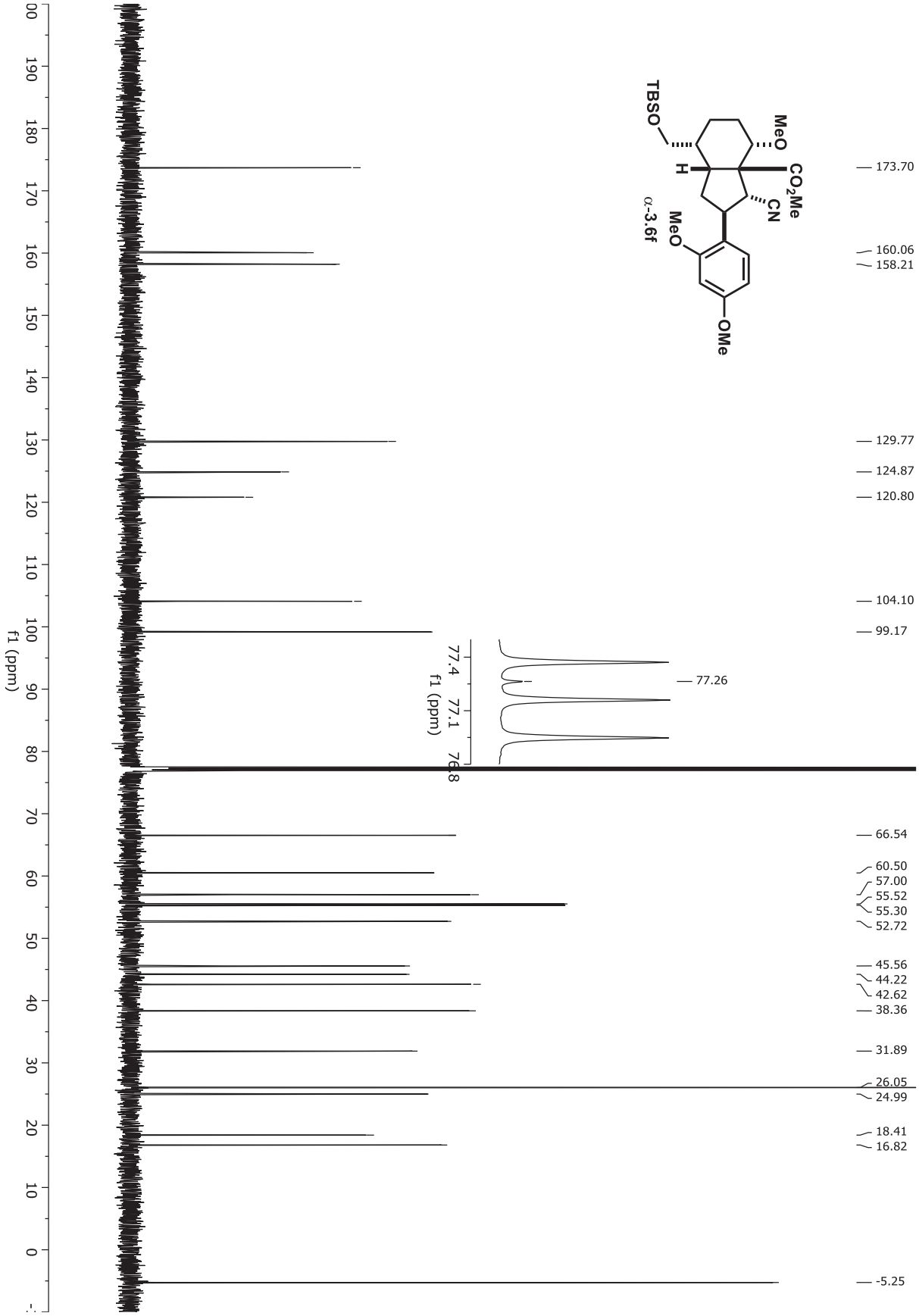
TBSO
MeO
H
CO2Me
CN
MeO
OMe
α-3.6f
173.70
160.06
158.21
129.77
124.87
120.80
104.10
99.17
77.26
66.54
60.50
57.00
55.52
55.30
52.72
45.56
44.22
42.62
38.36
31.89
26.05
24.99
18.41
16.82
-5.25
f1 (ppm)
77.4
77.1
76.8

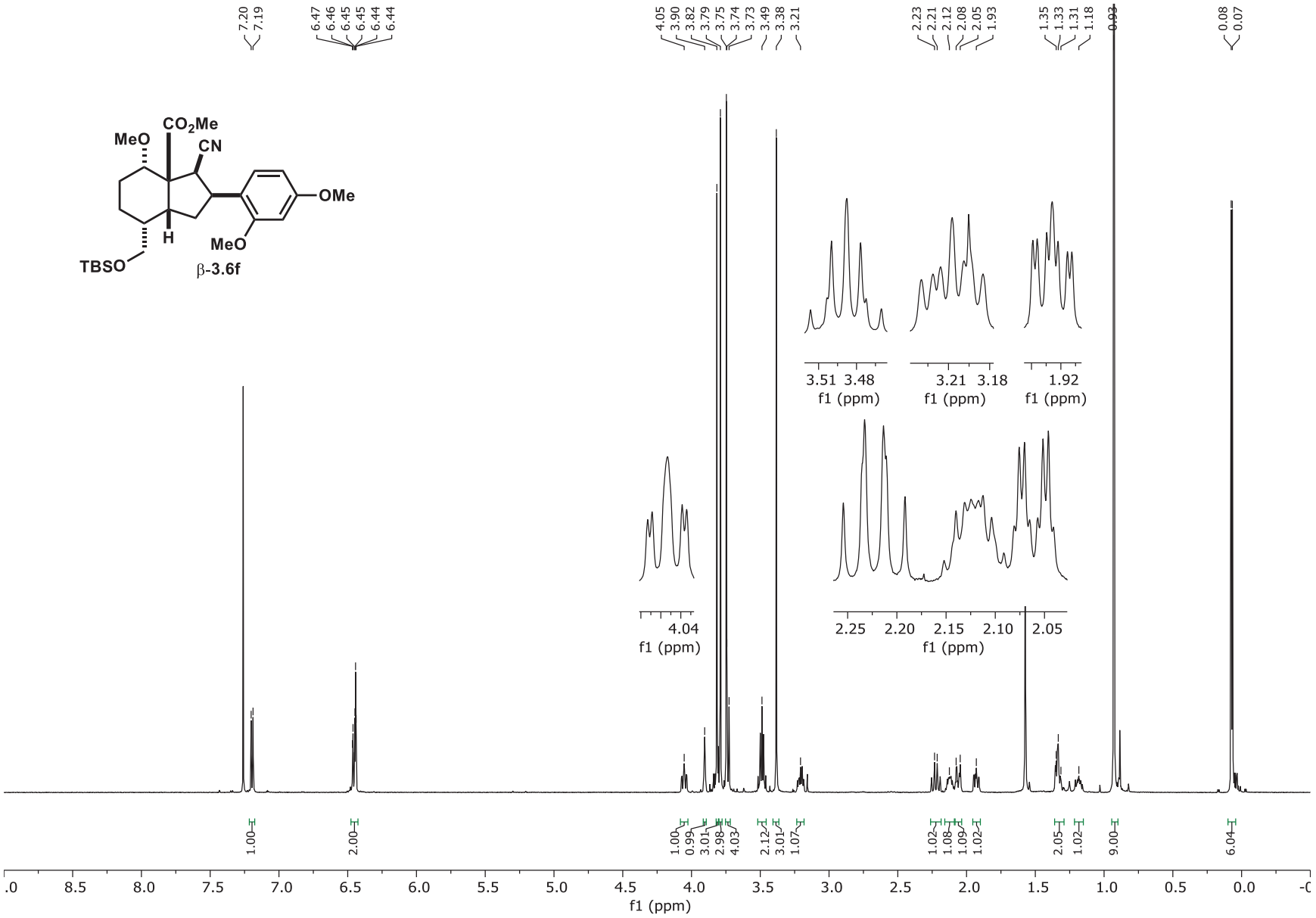
7.20
7.19
6.47
6.46
6.45
6.45
6.44
6.44
4.05
3.90
3.82
3.79
3.75
3.74
3.73
3.49
3.38
3.21
2.23
2.21
2.12
2.08
2.05
1.93
1.35
1.33
1.31
1.18
0.93
0.08
0.07
CO2Me
MeO
CN
OMe
H
MeO
TBSO
β-3.6f
3.51 3.48
f1 (ppm)
3.21 3.18
f1 (ppm)
1.92
f1 (ppm)
4.04
f1 (ppm)
2.25 2.20 2.15 2.10 2.05
f1 (ppm)
1.00
2.00
1.00
0.99
3.01
2.98
4.03
2.12
3.01
1.07
1.02
1.08
1.09
1.02
2.05
1.02
9.00
6.04
f1 (ppm)

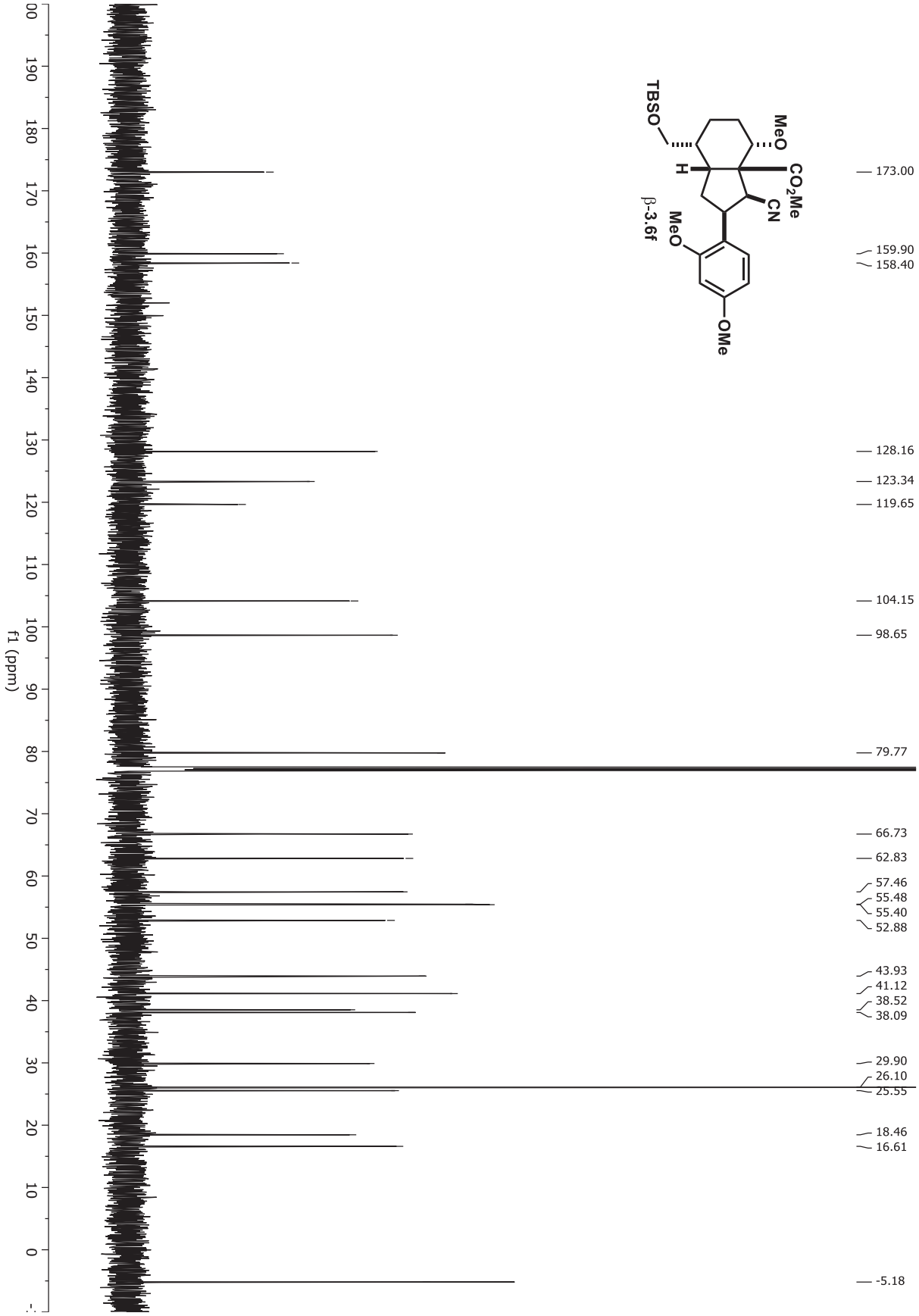
TBSO
MeO
H
CO2Me
CN
β-3.6f
MeO
OMe
f1 (ppm)
173.00
159.90
158.40
128.16
123.34
119.65
104.15
98.65
79.77
66.73
62.83
57.46
55.48
55.40
52.88
43.93
41.12
38.52
38.09
29.90
26.10
25.55
18.46
16.61
-5.18

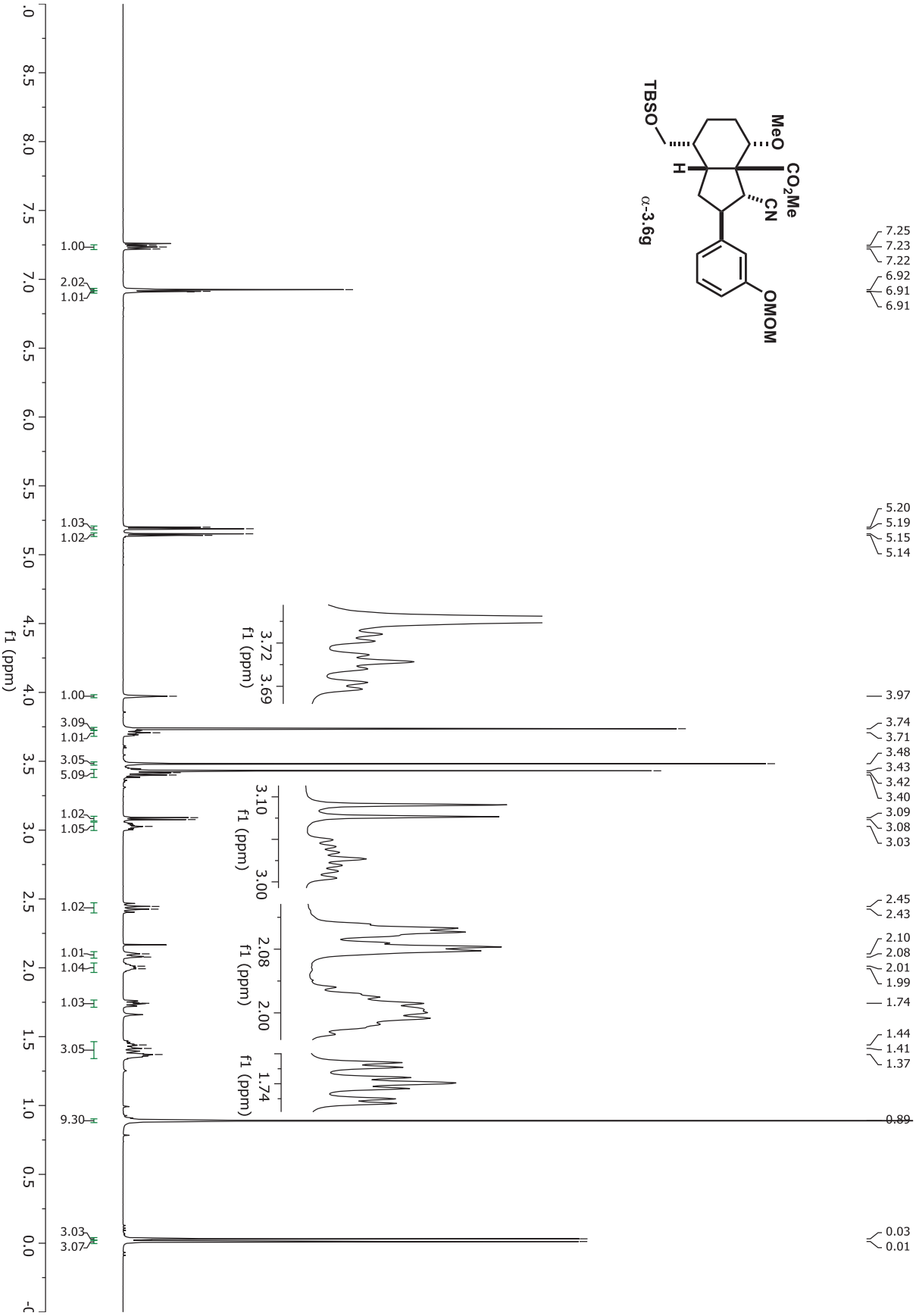
TBSO
MeO
H
CO2Me
CN
OMOM
α-3.6g
f1 (ppm)

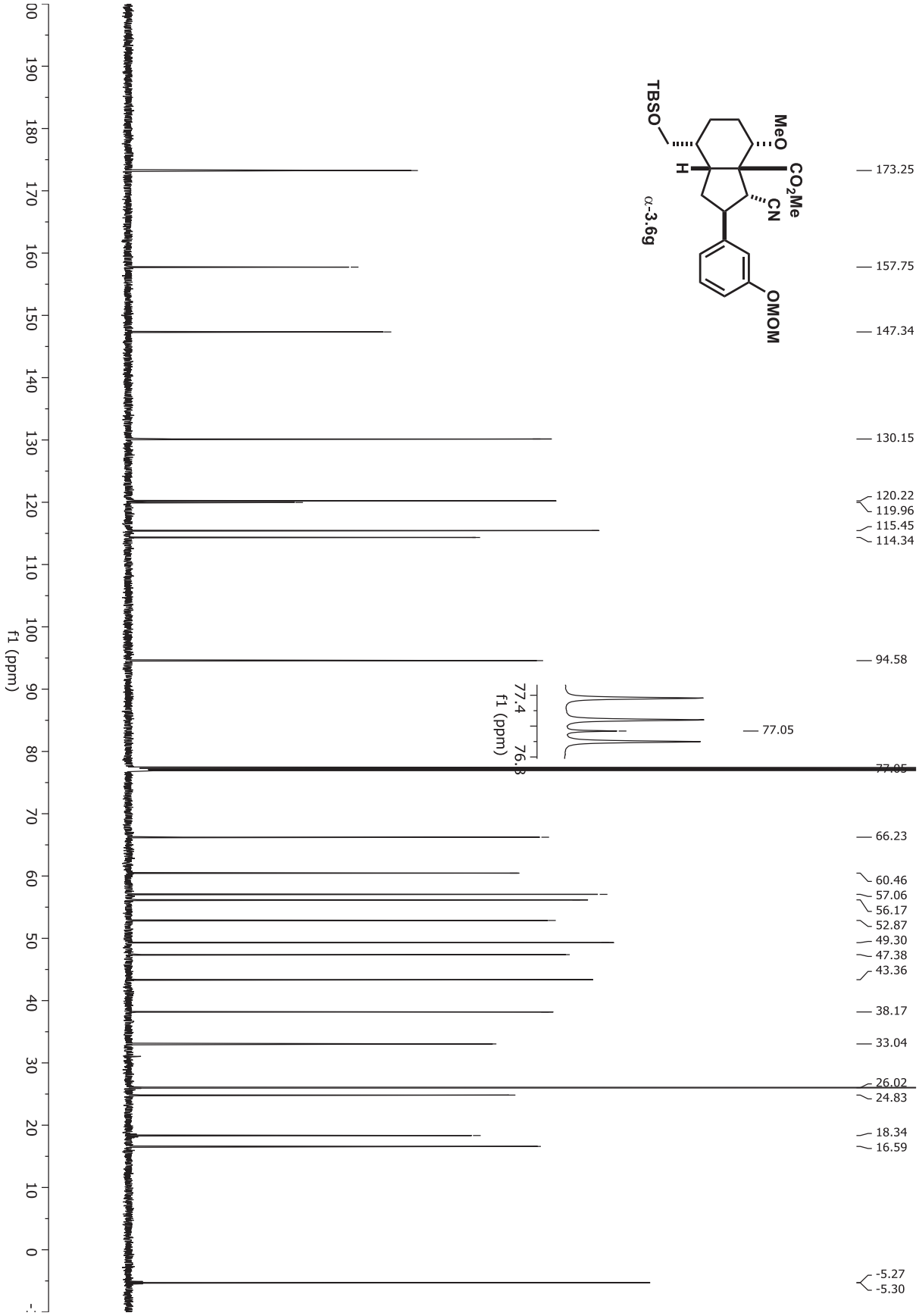
TBSO
MeO
H
CO2Me
CN
OMOM
α-3.6g
173.25
157.75
147.34
130.15
120.22
119.96
115.45
114.34
94.58
77.05
66.23
60.46
57.06
56.17
52.87
49.30
47.38
43.36
38.17
33.04
26.02
24.83
18.34
16.59
-5.27
-5.30
f1 (ppm)
77.4
76.8
f1 (ppm)

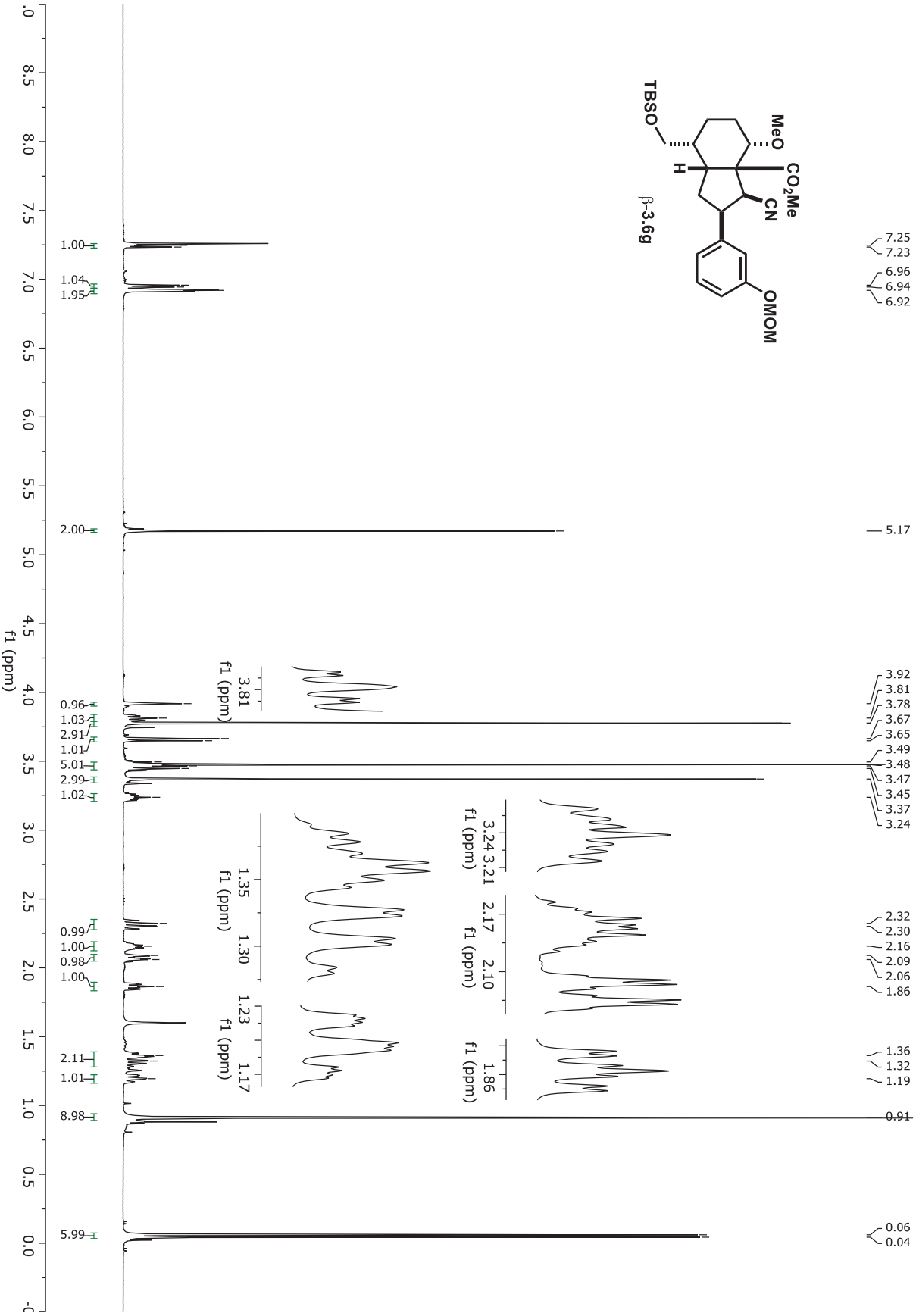
TBSO
MeO
CO2Me
CN
H
OMOM
β-3.6g
f1 (ppm)

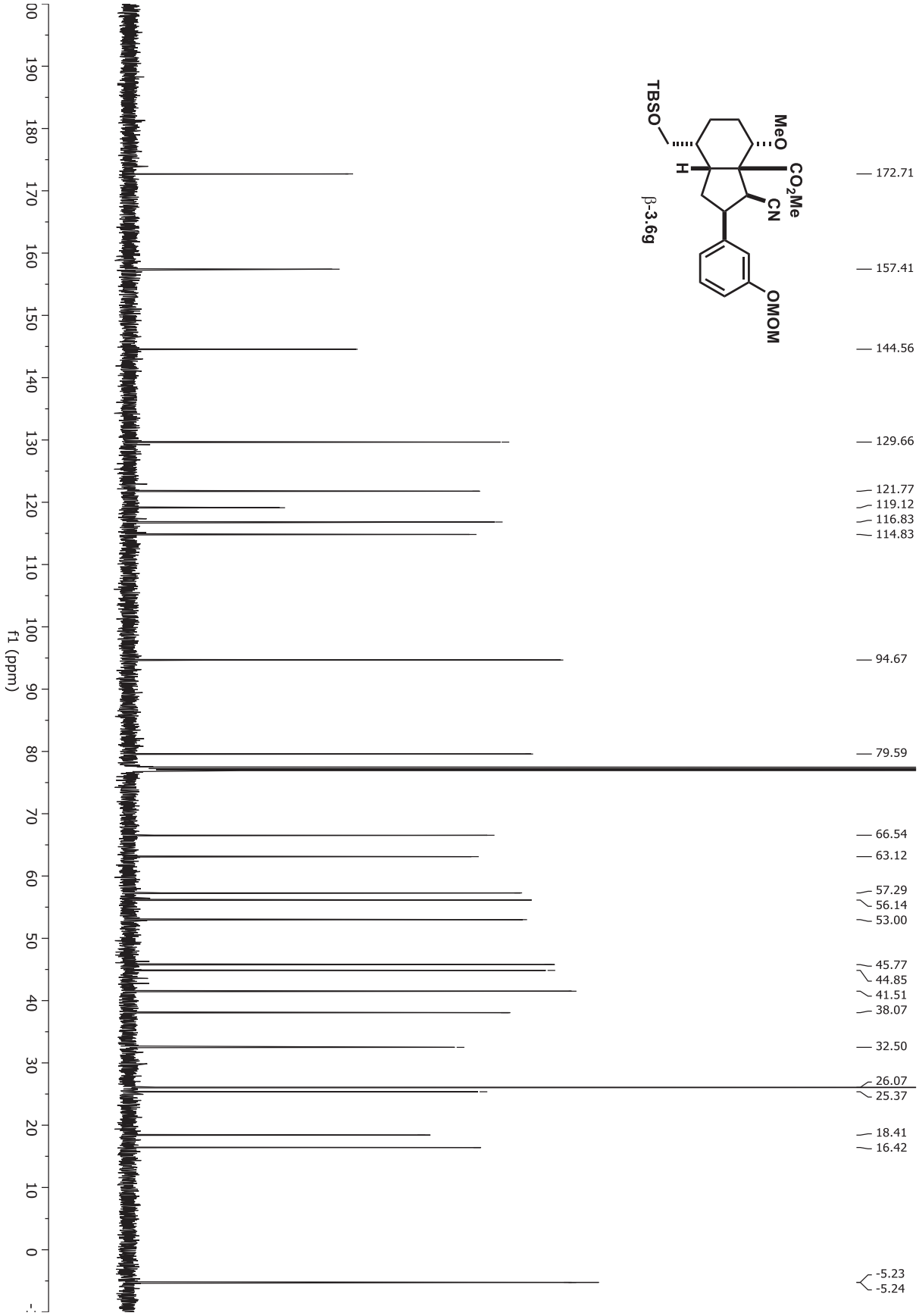
TBSO
MeO
H
CO2Me
CN
OMOM
β-3.6g
f1 (ppm)
200
190
180
170
160
150
140
130
120
110
100
90
80
70
60
50
40
30
20
10
0
-:
172.71
157.41
144.56
129.66
121.77
119.12
116.83
114.83
94.67
79.59
66.54
63.12
57.29
56.14
53.00
45.77
44.85
41.51
38.07
32.50
26.07
25.37
18.41
16.42
-5.23
-5.24

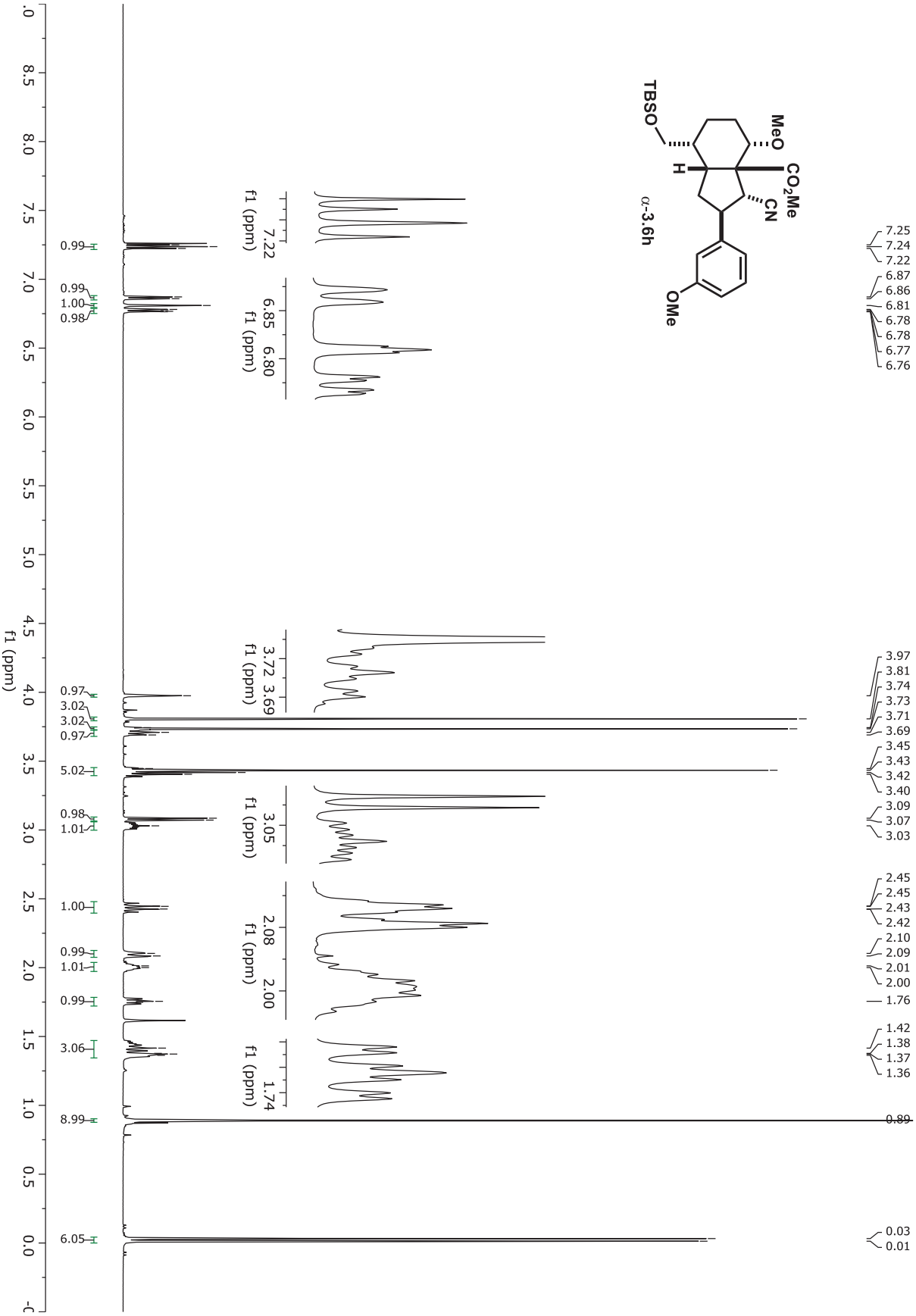
TBSO
MeO
CO2Me
CN
H
OMe
α-3.6h
f1 (ppm)

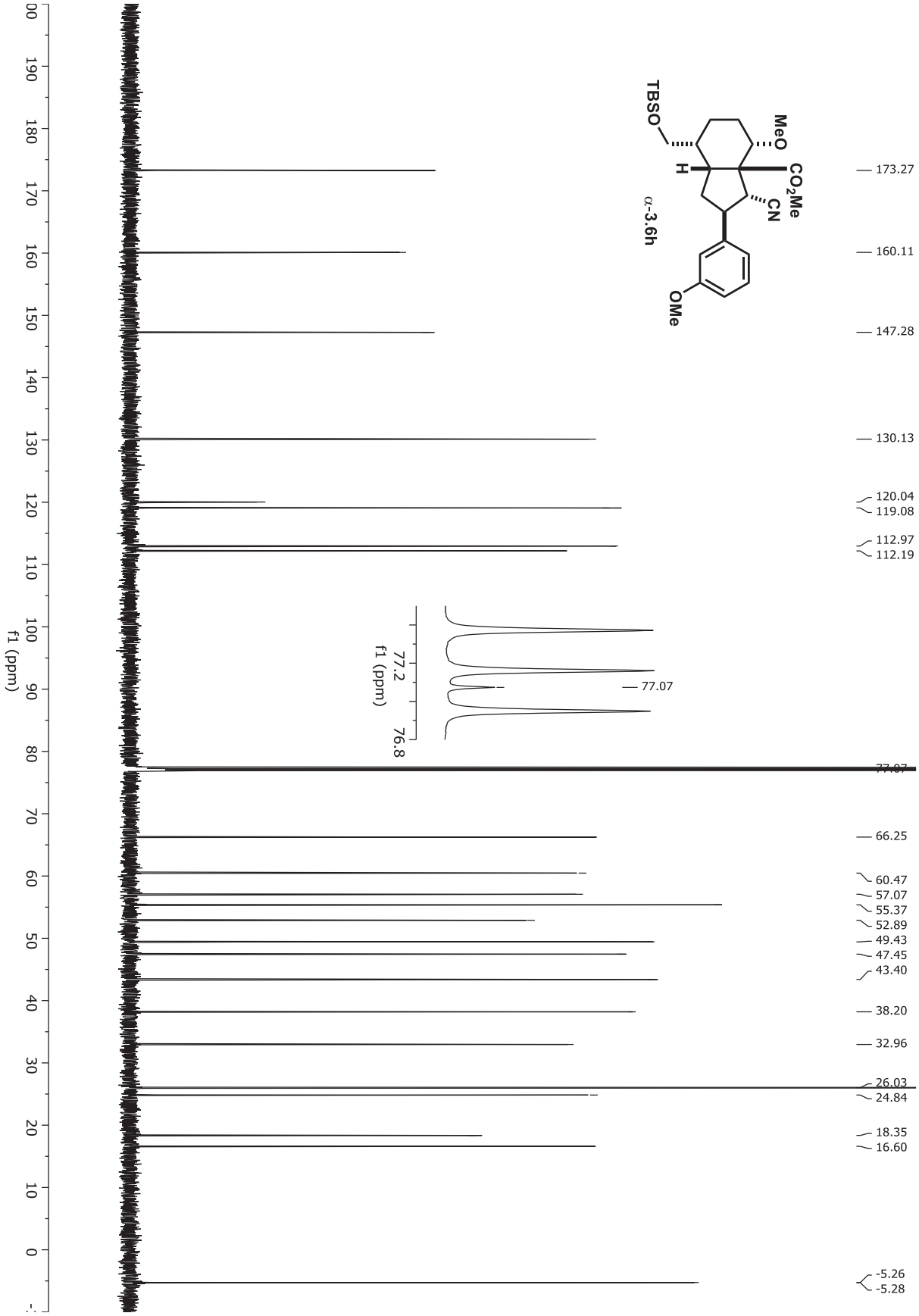
TBSO
MeO
H
CO2Me
CN
OMe
α-3.6h
173.27
160.11
147.28
130.13
120.04
119.08
112.97
112.19
77.07
66.25
60.47
57.07
55.37
52.89
49.43
47.45
43.40
38.20
32.96
26.03
24.84
18.35
16.60
-5.26
-5.28
f1 (ppm)

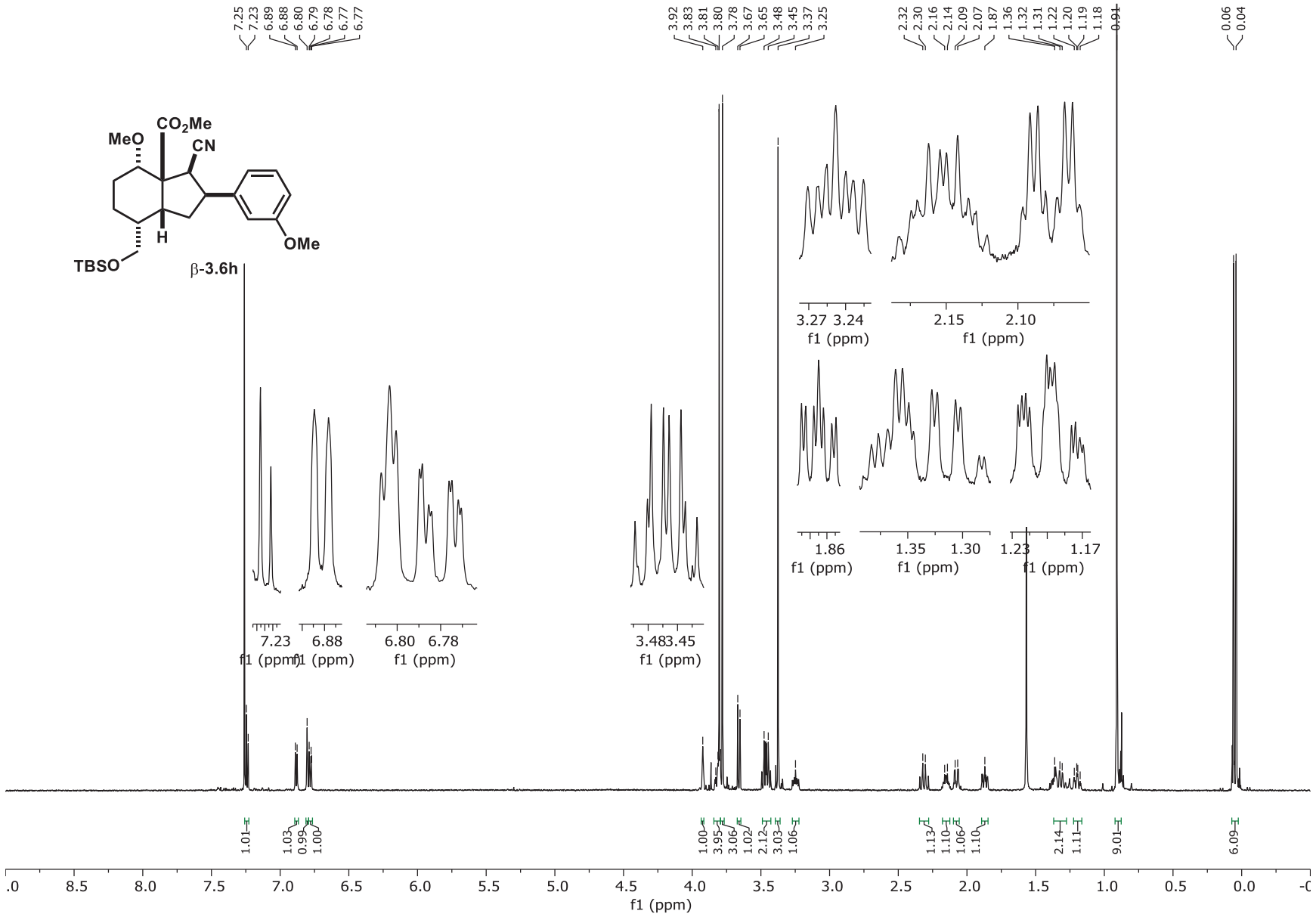
MeO
CO2Me
CN
H
OMe
TBSO
β-3.6h
7.25
7.23
6.89
6.88
6.80
6.79
6.78
6.77
6.77
3.92
3.83
3.81
3.80
3.78
3.67
3.65
3.48
3.45
3.37
3.25
2.32
2.30
2.16
2.14
2.09
2.07
1.87
1.36
1.32
1.31
1.22
1.20
1.19
1.18
0.91
0.06
0.04
7.23
6.88
6.80
6.78
3.48
3.45
3.27
3.24
2.15
2.10
1.86
1.35
1.30
1.23
1.17
f1 (ppm)
1.01
1.03
0.99
1.00
1.00
3.95
3.06
1.02
2.12
3.03
1.06
1.13
1.10
1.06
1.10
2.14
1.11
9.01
6.09
8.5
8.0
7.5
7.0
6.5
6.0
5.5
5.0
4.5
4.0
3.5
3.0
2.5
2.0
1.5
1.0
0.5
0.0

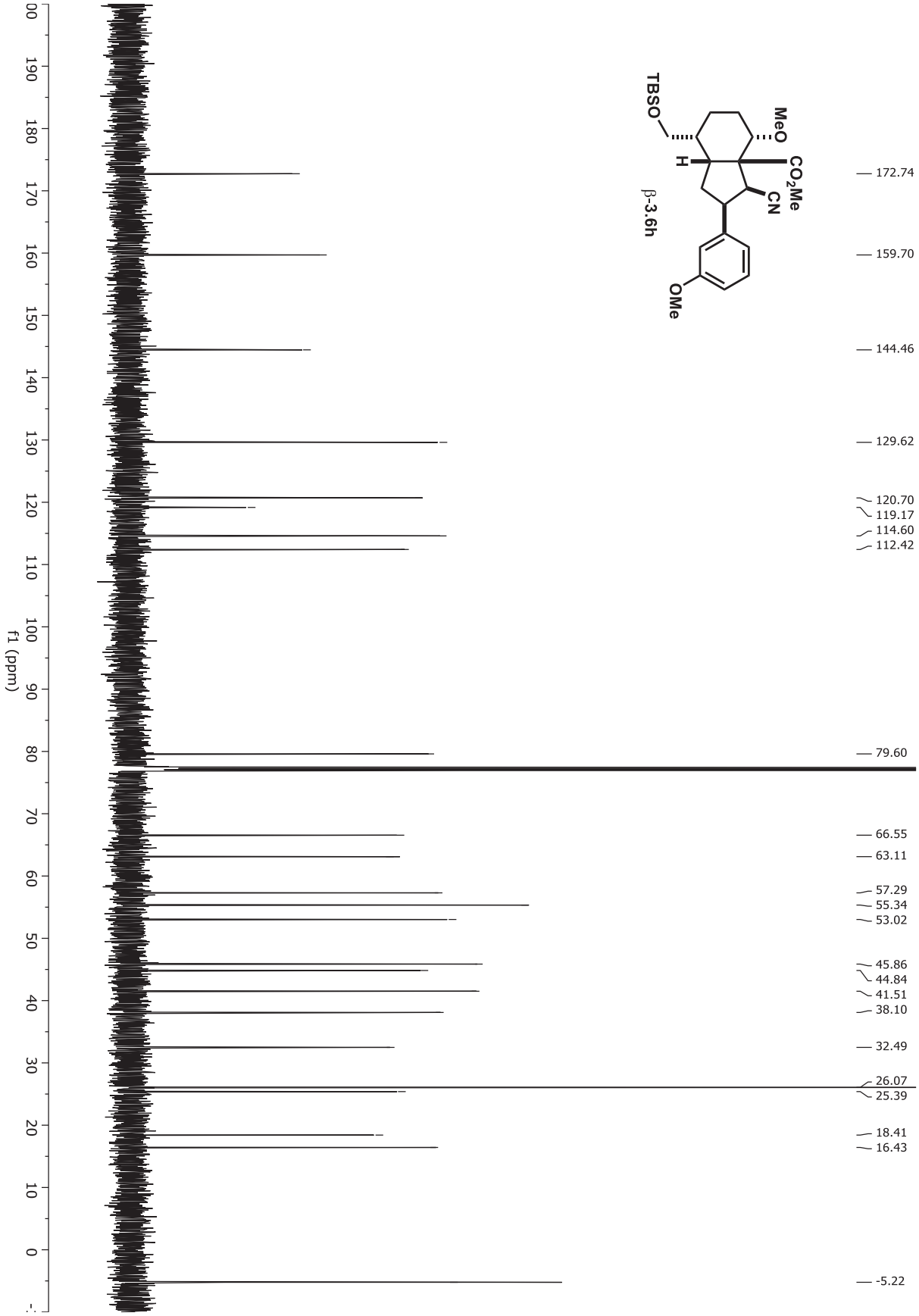
TBSO
MeO
H
CO2Me
CN
OMe
β-3.6h
172.74
159.70
144.46
129.62
120.70
119.17
114.60
112.42
79.60
66.55
63.11
57.29
55.34
53.02
45.86
44.84
41.51
38.10
32.49
26.07
25.39
18.41
16.43
-5.22
f1 (ppm)

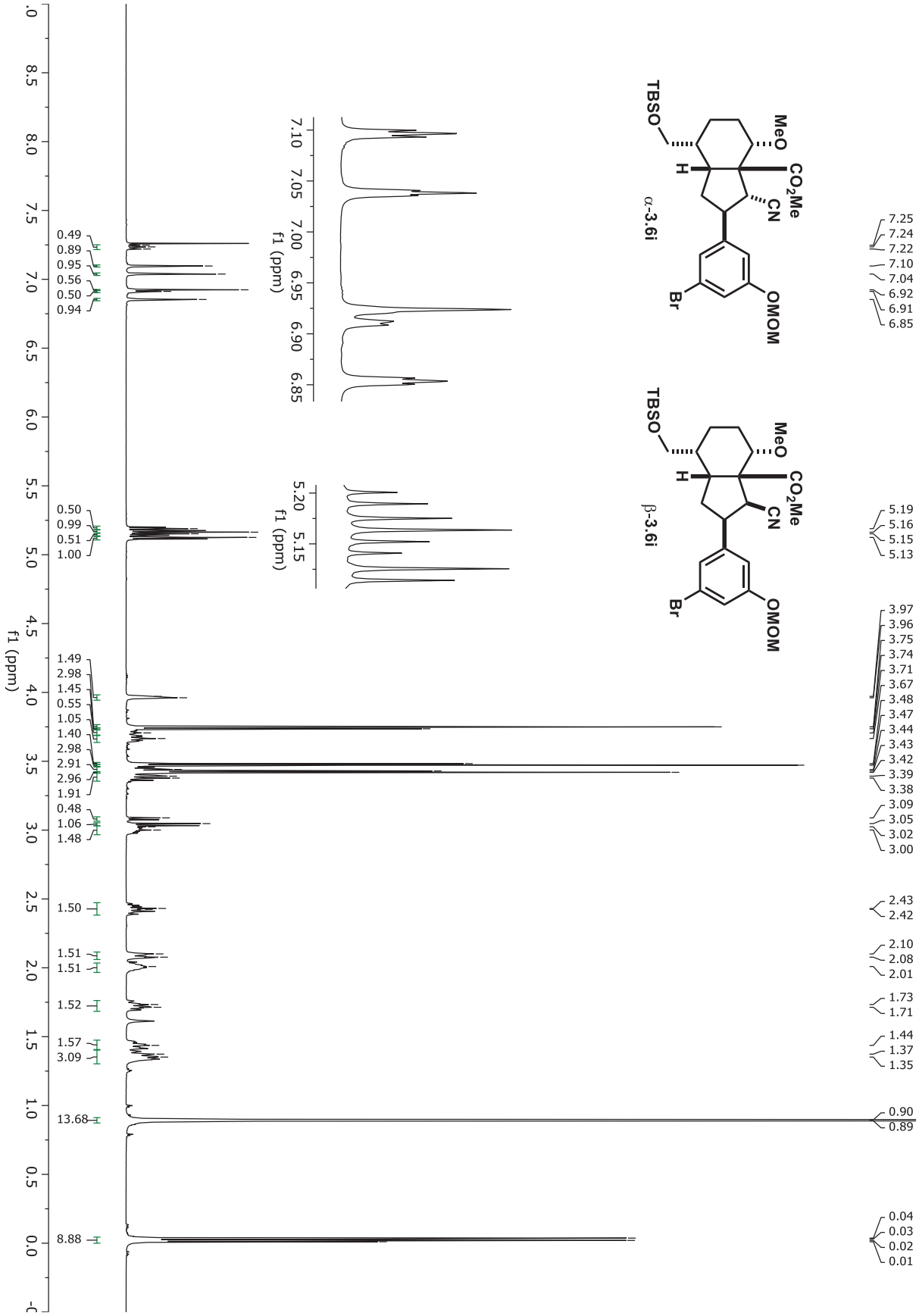
TBSO
MeO
H
CO2Me
CN
Br
OMOM
α-3.6i
β-3.6i
f1 (ppm)

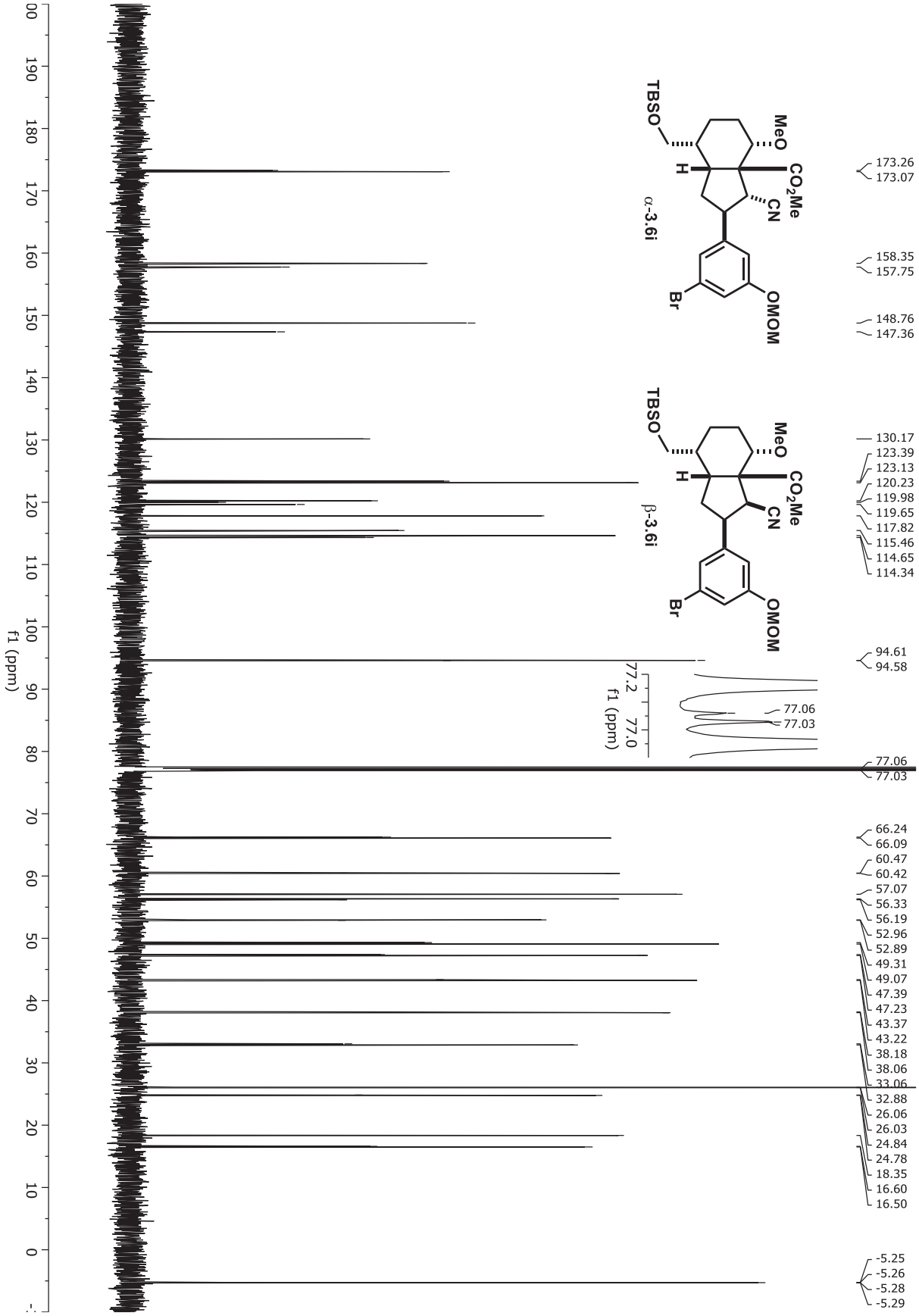
TBSO
MeO
H
CO2Me
CN
Br
OMOM
α-3.6i
β-3.6i
173.26
173.07
158.35
157.75
148.76
147.36
130.17
123.39
123.13
120.23
119.98
119.65
117.82
115.46
114.65
114.34
94.61
94.58
77.06
77.03
66.24
66.09
60.47
60.42
57.07
56.33
56.19
52.96
52.89
49.31
49.07
47.39
47.23
43.37
43.22
38.18
38.06
33.06
32.88
26.06
26.03
24.84
24.78
18.35
16.60
16.50
-5.25
-5.26
-5.28
-5.29
77.2
77.0
f1 (ppm)

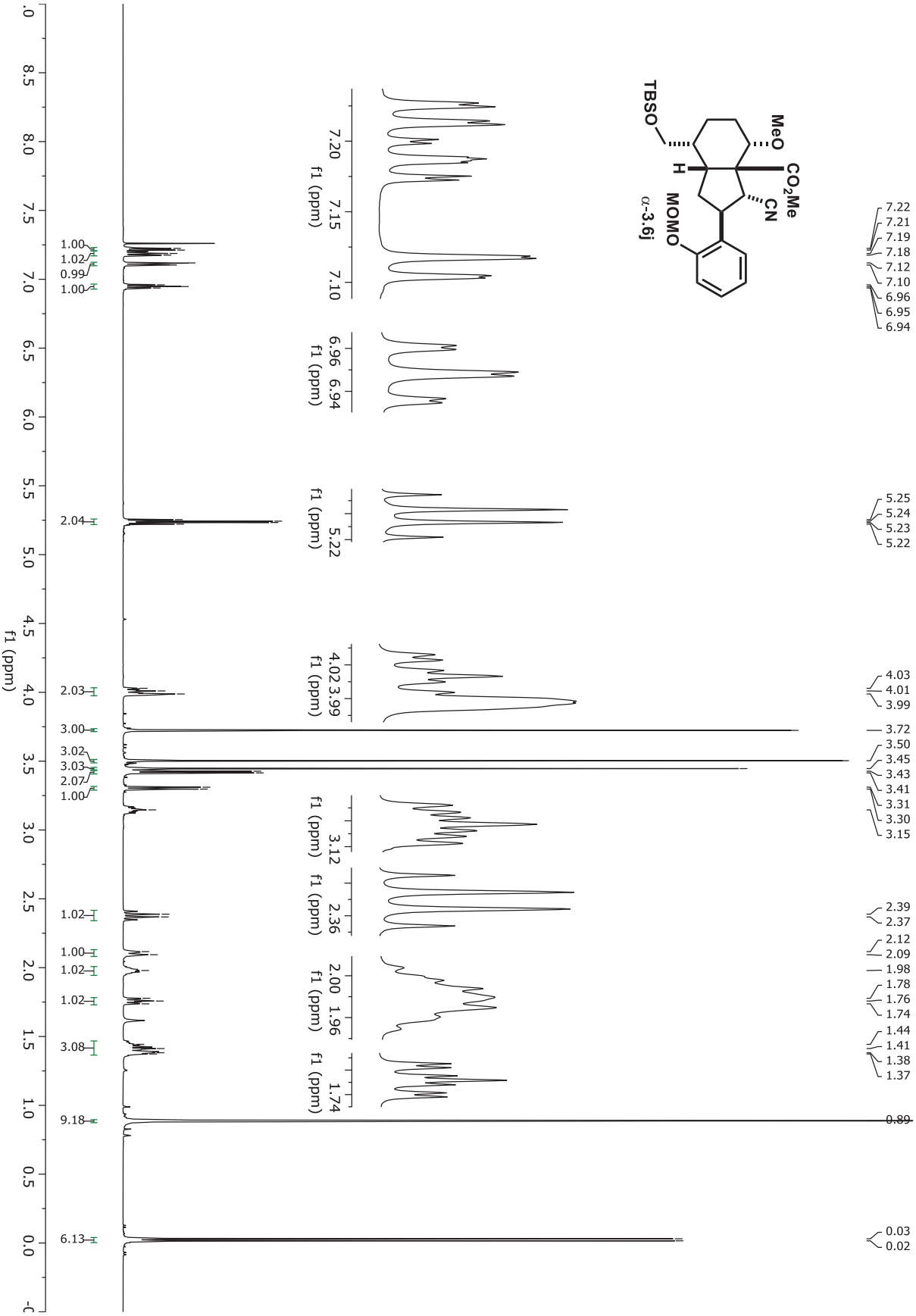
TBSO
MeO
CO2Me
CN
H
MOMO
α-3.6j
f1 (ppm)

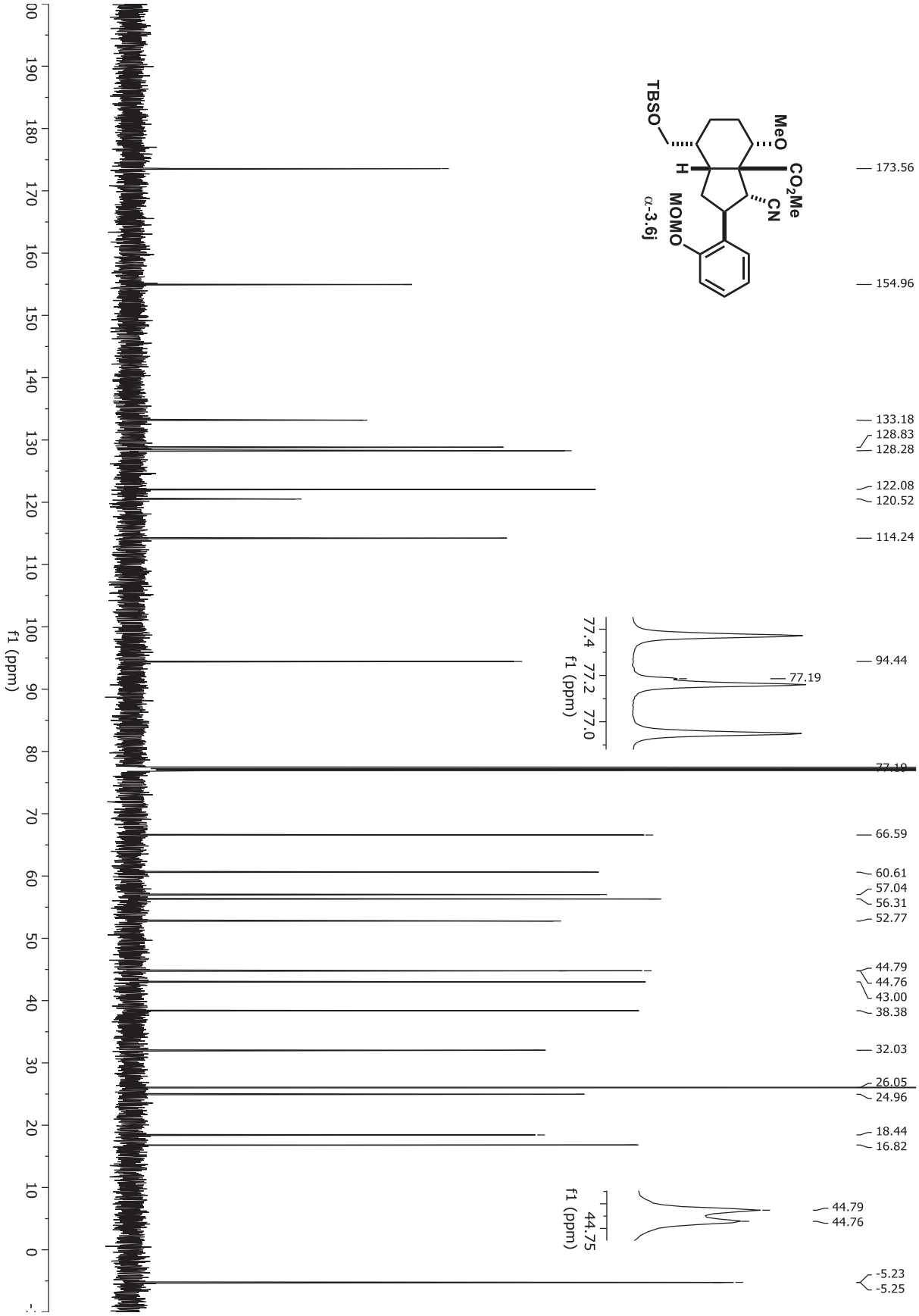
TBSO
MeO
H
CO2Me
CN
MOMO
α-3.6j
173.56
154.96
133.18
128.83
128.28
122.08
120.52
114.24
94.44
77.19
66.59
60.61
57.04
56.31
52.77
44.79
44.76
43.00
38.38
32.03
26.05
24.96
18.44
16.82
-5.23
-5.25
f1 (ppm)

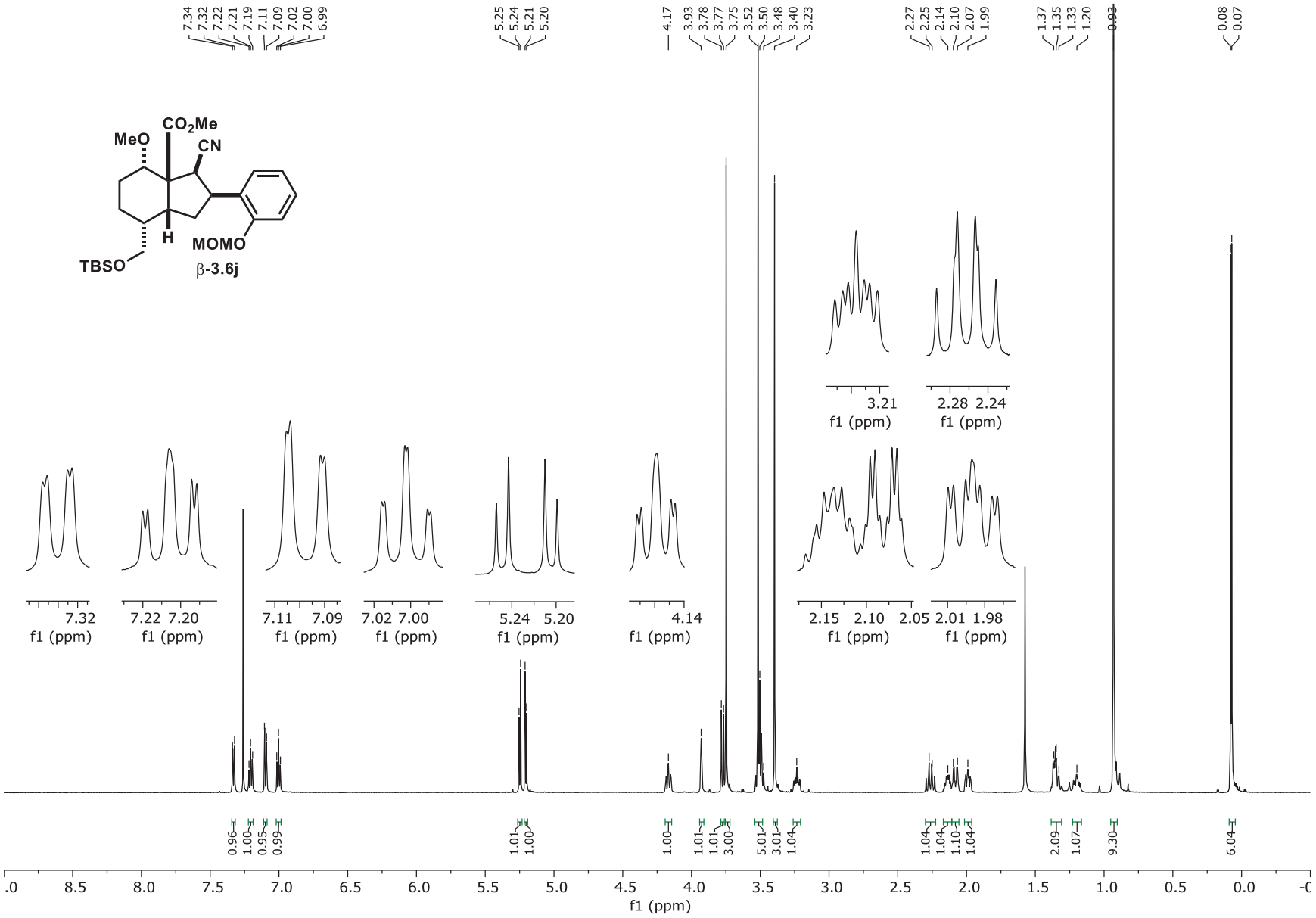
7.34
7.32
7.22
7.21
7.19
7.11
7.09
7.02
7.00
6.99
5.25
5.24
5.21
5.20
4.17
3.93
3.78
3.77
3.75
3.52
3.50
3.48
3.40
3.23
2.27
2.25
2.14
2.10
2.07
1.99
1.37
1.35
1.33
1.20
0.93
0.08
0.07
CO2Me
MeO
CN
H
MOMO
TBSO
β-3.6j
7.32
7.22 7.20
7.11 7.09
7.02 7.00
5.24 5.20
4.14
3.21
2.28 2.24
2.15 2.10 2.05
2.01 1.98
f1 (ppm)
0.96
1.00
0.95
0.99
1.01
1.00
1.00
1.01
1.01
3.00
5.01
3.01
1.04
1.04
1.04
1.10
1.04
2.09
1.07
9.30
6.04
f1 (ppm)

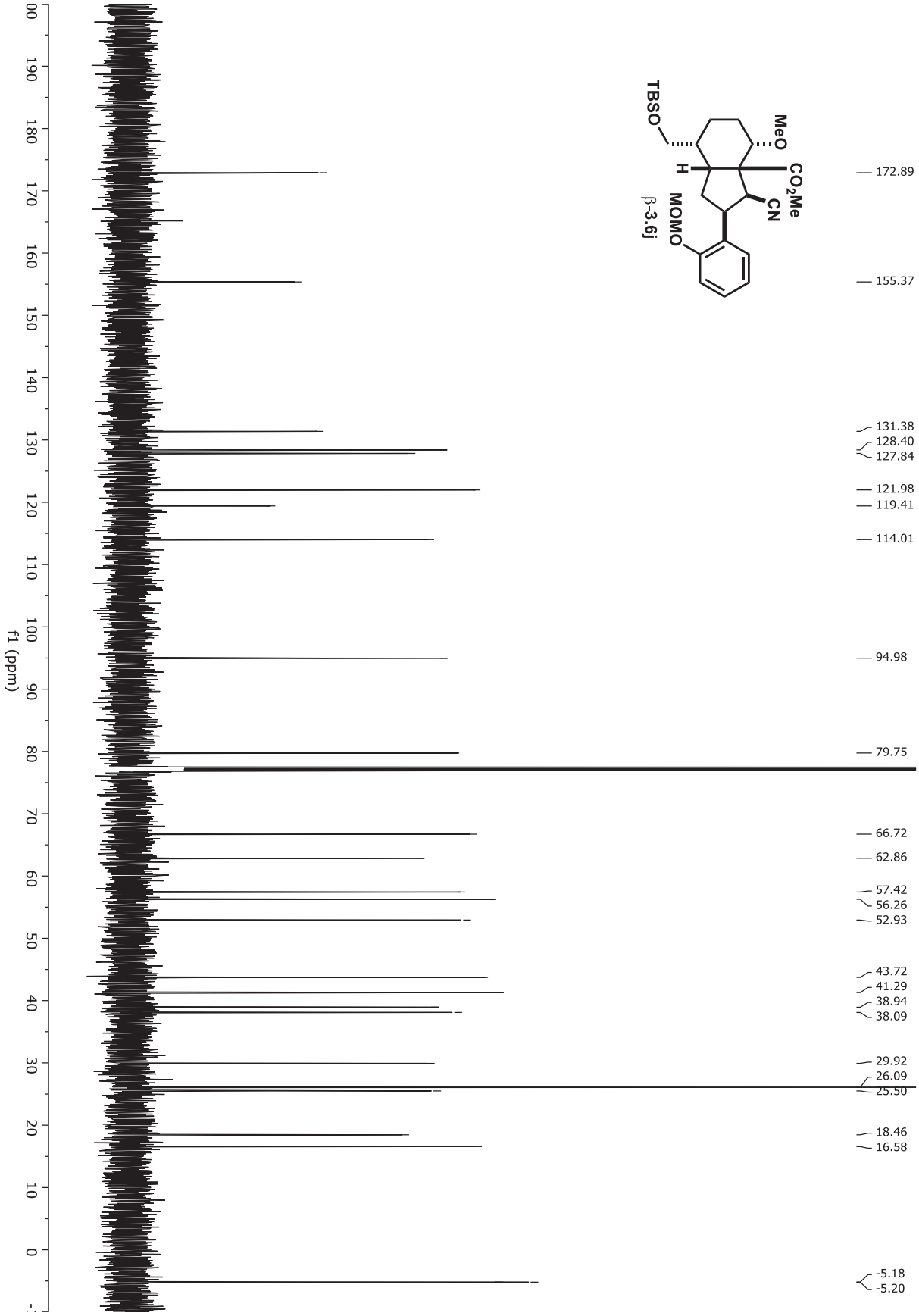
TBSO
MeO
H
CO2Me
CN
MOMO
β-3.6j
f1 (ppm)
172.89
155.37
131.38
128.40
127.84
121.98
119.41
114.01
94.98
79.75
66.72
62.86
57.42
56.26
52.93
43.72
41.29
38.94
38.09
29.92
26.09
25.50
18.46
16.58
-5.18
-5.20

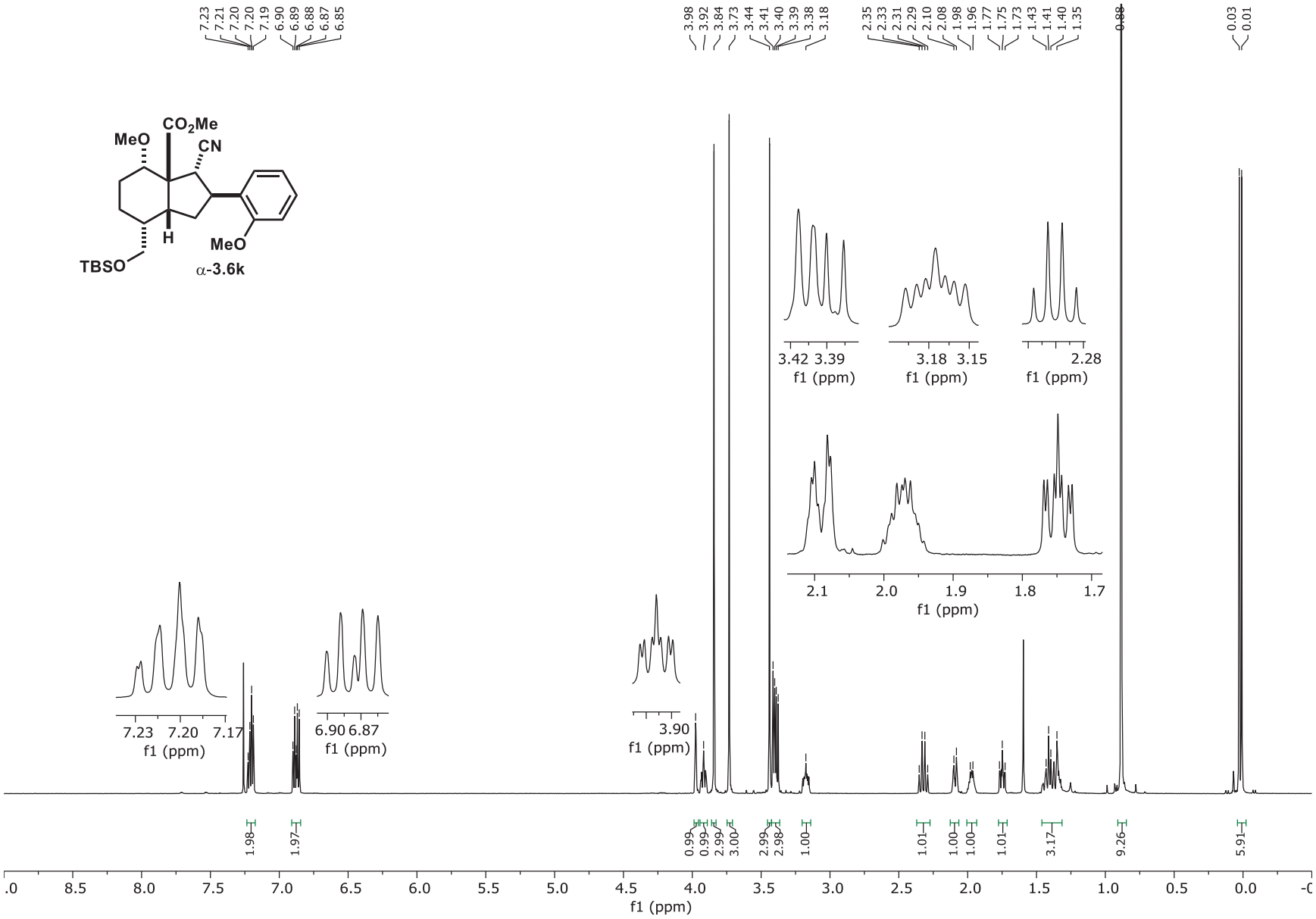
7.23 7.21 7.20 7.20 7.19 6.90 6.89 6.88 6.87 6.85
3.98 3.92 3.84 3.73 3.44 3.41 3.40 3.39 3.38 3.18
2.35 2.33 2.31 2.29 2.10 2.08 1.98 1.96 1.77 1.75 1.73 1.43 1.41 1.40 1.35
0.88
0.03 0.01
CO2Me
MeO
CN
H
MeO
TBSO
α-3.6k
3.42 3.39
f1 (ppm)
3.18 3.15
f1 (ppm)
2.28
f1 (ppm)
2.1 2.0 1.9 1.8 1.7
f1 (ppm)
7.23 7.20 7.17
f1 (ppm)
6.90 6.87
f1 (ppm)
3.90
f1 (ppm)
1.98 1.97 0.99 0.99 2.99 3.00 2.99 2.98 1.00 1.01 1.00 1.00 1.01 3.17 9.26 5.91
.0 8.5 8.0 7.5 7.0 6.5 6.0 5.5 5.0 4.5 4.0 3.5 3.0 2.5 2.0 1.5 1.0 0.5 0.0
f1 (ppm)

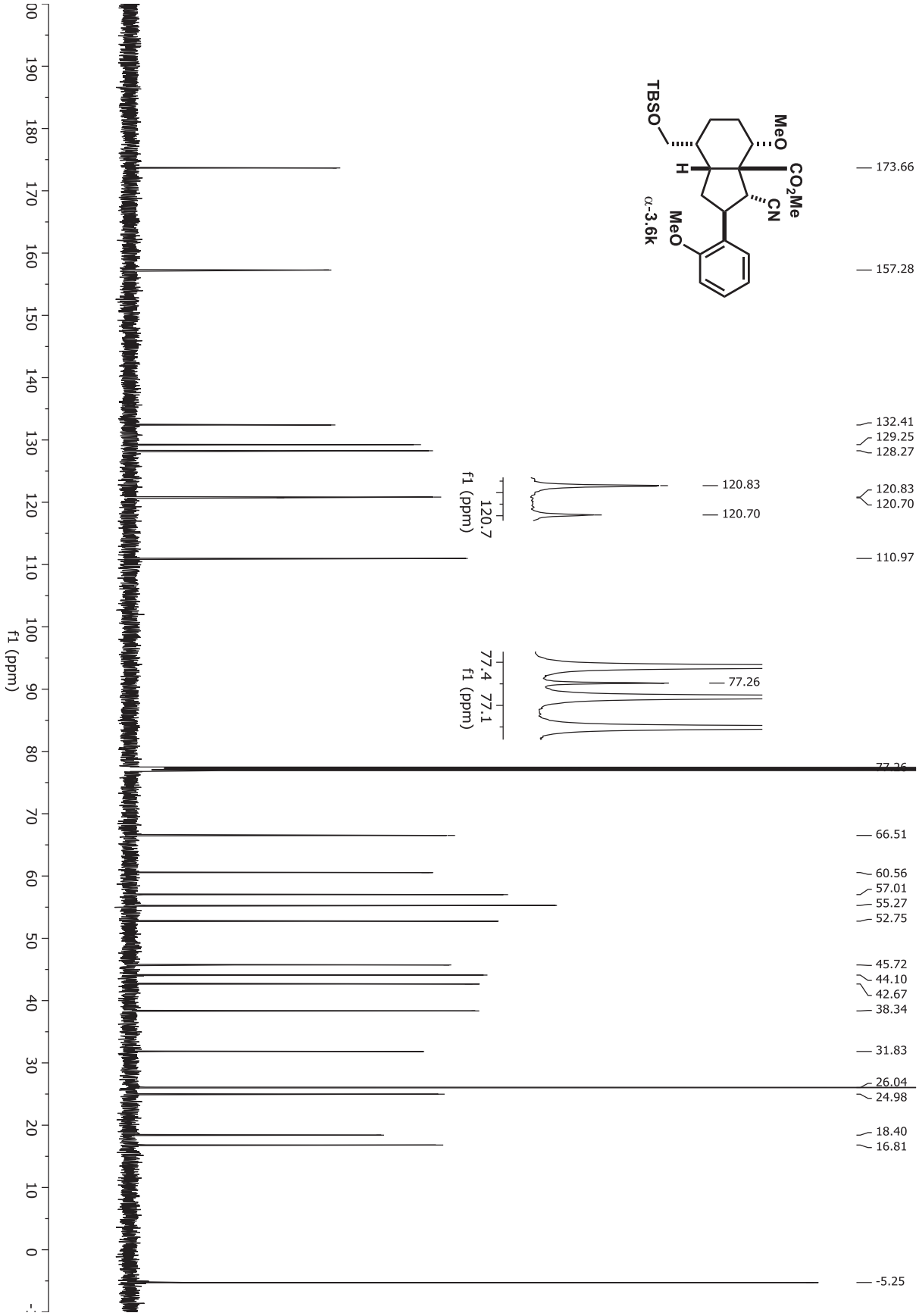
TBSO
MeO
H
CO2Me
CN
MeO
α-3.6k
173.66
157.28
132.41
129.25
128.27
120.83
120.70
110.97
77.26
66.51
60.56
57.01
55.27
52.75
45.72
44.10
42.67
38.34
31.83
26.04
24.98
18.40
16.81
-5.25
f1 (ppm)

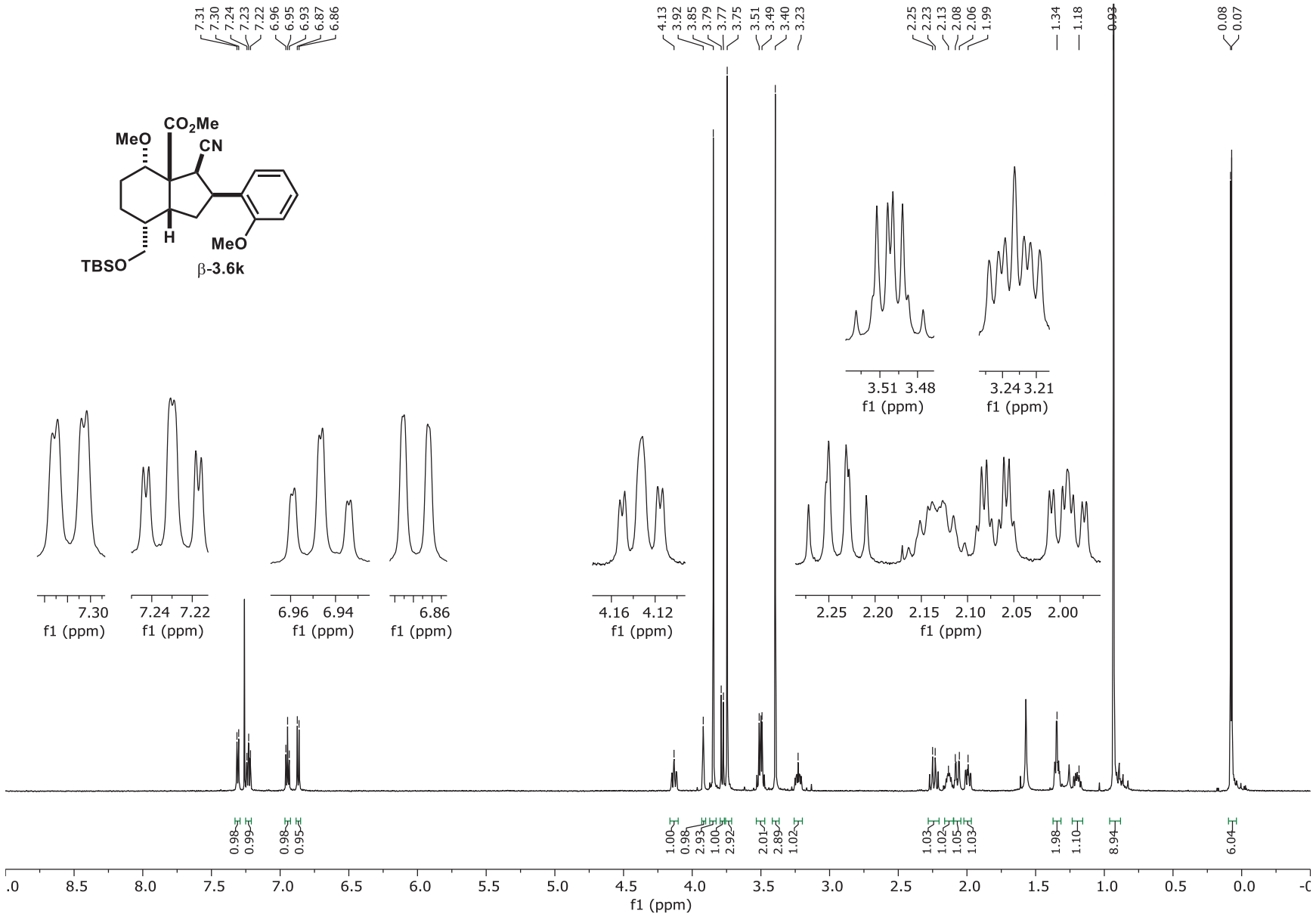
7.31
7.30
7.24
7.23
7.22
6.96
6.95
6.93
6.87
6.86
4.13
3.92
3.85
3.79
3.77
3.75
3.51
3.49
3.40
3.23
2.25
2.23
2.13
2.08
2.06
1.99
1.34
1.18
0.93
0.08
0.07
CO2Me
MeO
CN
H
MeO
TBSO
β-3.6k
7.30
f1 (ppm)
7.24 7.22
f1 (ppm)
6.96 6.94
f1 (ppm)
6.86
f1 (ppm)
4.16 4.12
f1 (ppm)
3.51 3.48
f1 (ppm)
3.24 3.21
f1 (ppm)
2.25 2.20 2.15 2.10 2.05 2.00
f1 (ppm)
0.98
0.99
0.98
0.95
1.00
0.98
2.93
1.00
2.92
2.01
2.89
1.02
1.03
1.02
1.05
1.03
1.98
1.10
8.94
6.04
f1 (ppm)

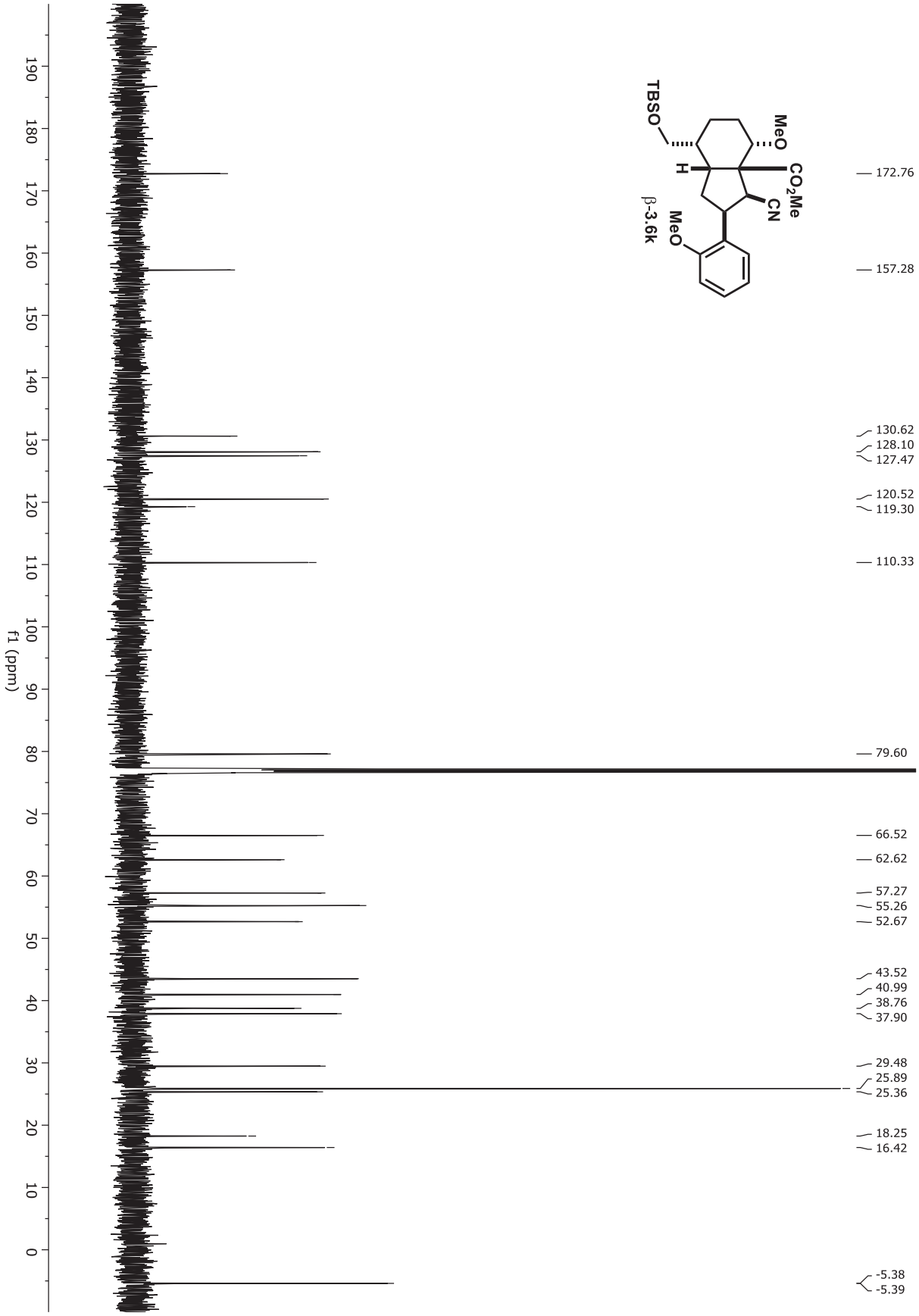
TBSO
MeO
H
CO2Me
CN
MeO
β-3.6k
f1 (ppm)
190
180
170
160
150
140
130
120
110
100
90
80
70
60
50
40
30
20
10
0
172.76
157.28
130.62
128.10
127.47
120.52
119.30
110.33
79.60
66.52
62.62
57.27
55.26
52.67
43.52
40.99
38.76
37.90
29.48
25.89
25.36
18.25
16.42
-5.38
-5.39

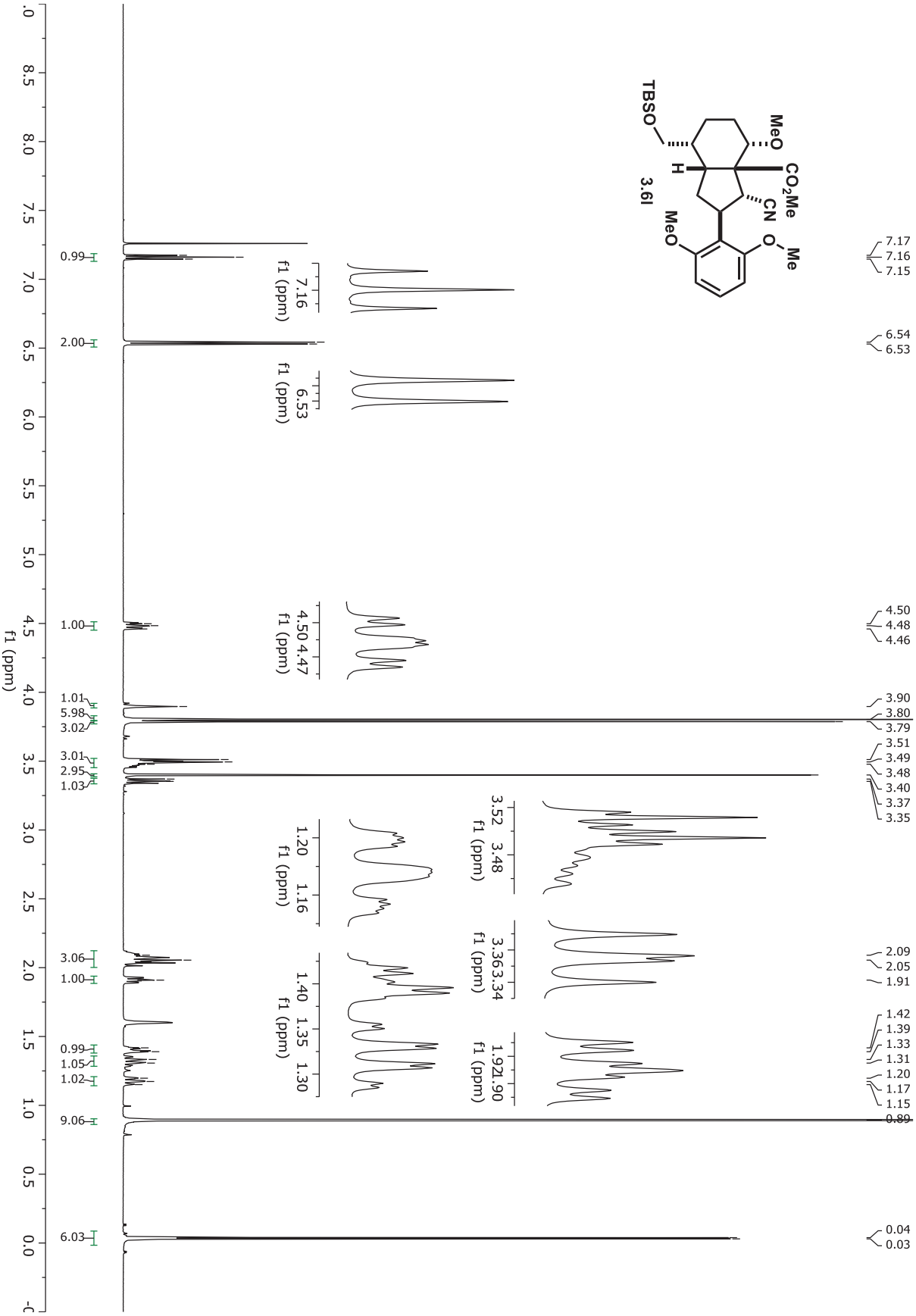
TBSO
MeO
H
CO2Me
CN
O
Me
MeO
3.6l
f1 (ppm)

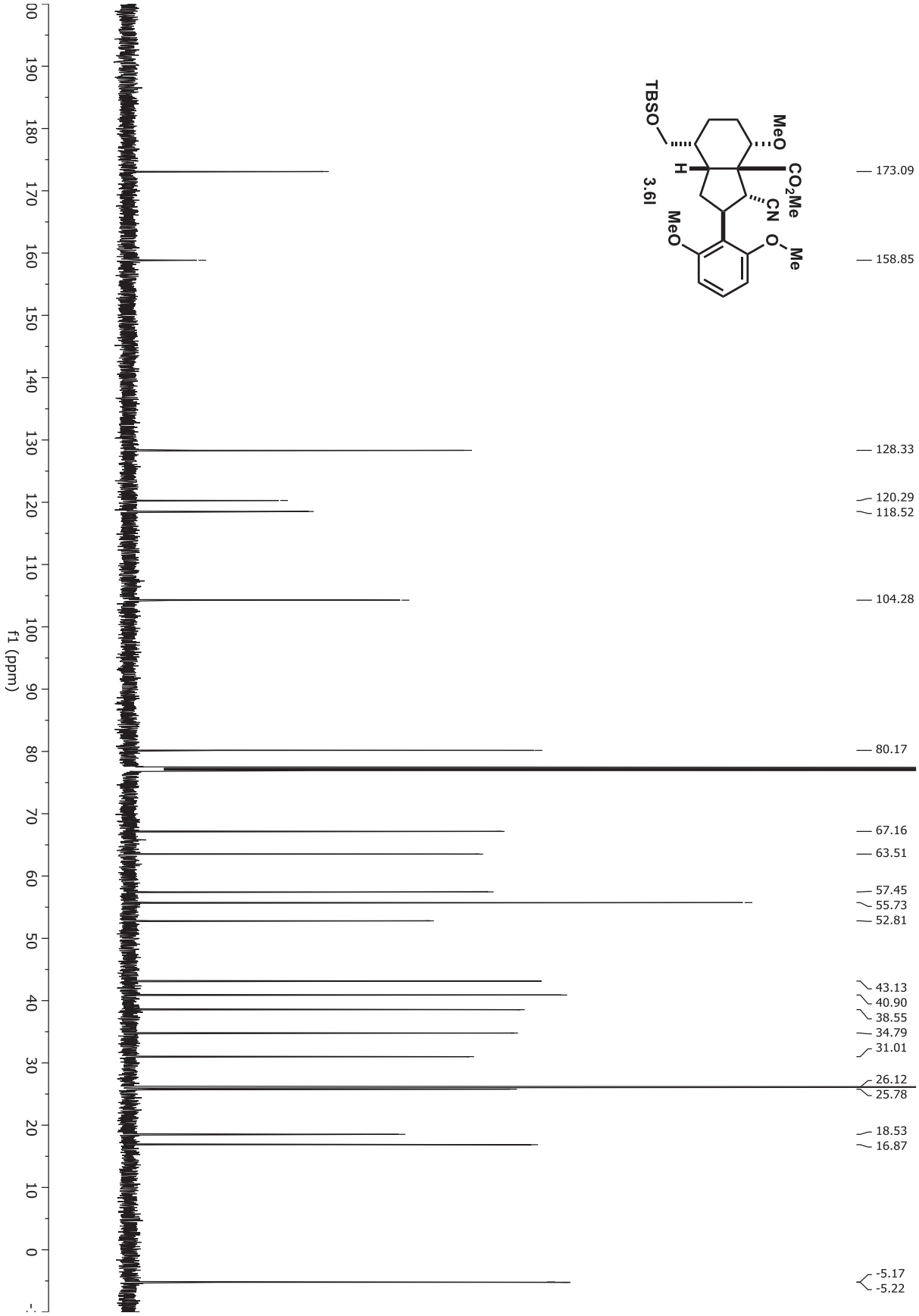
TBSO
MeO
H
CO2Me
CN
MeO
O
Me
3.6l
f1 (ppm)
173.09
158.85
128.33
120.29
118.52
104.28
80.17
67.16
63.51
57.45
55.73
52.81
43.13
40.90
38.55
34.79
31.01
26.12
25.78
18.53
16.87
-5.17
-5.22

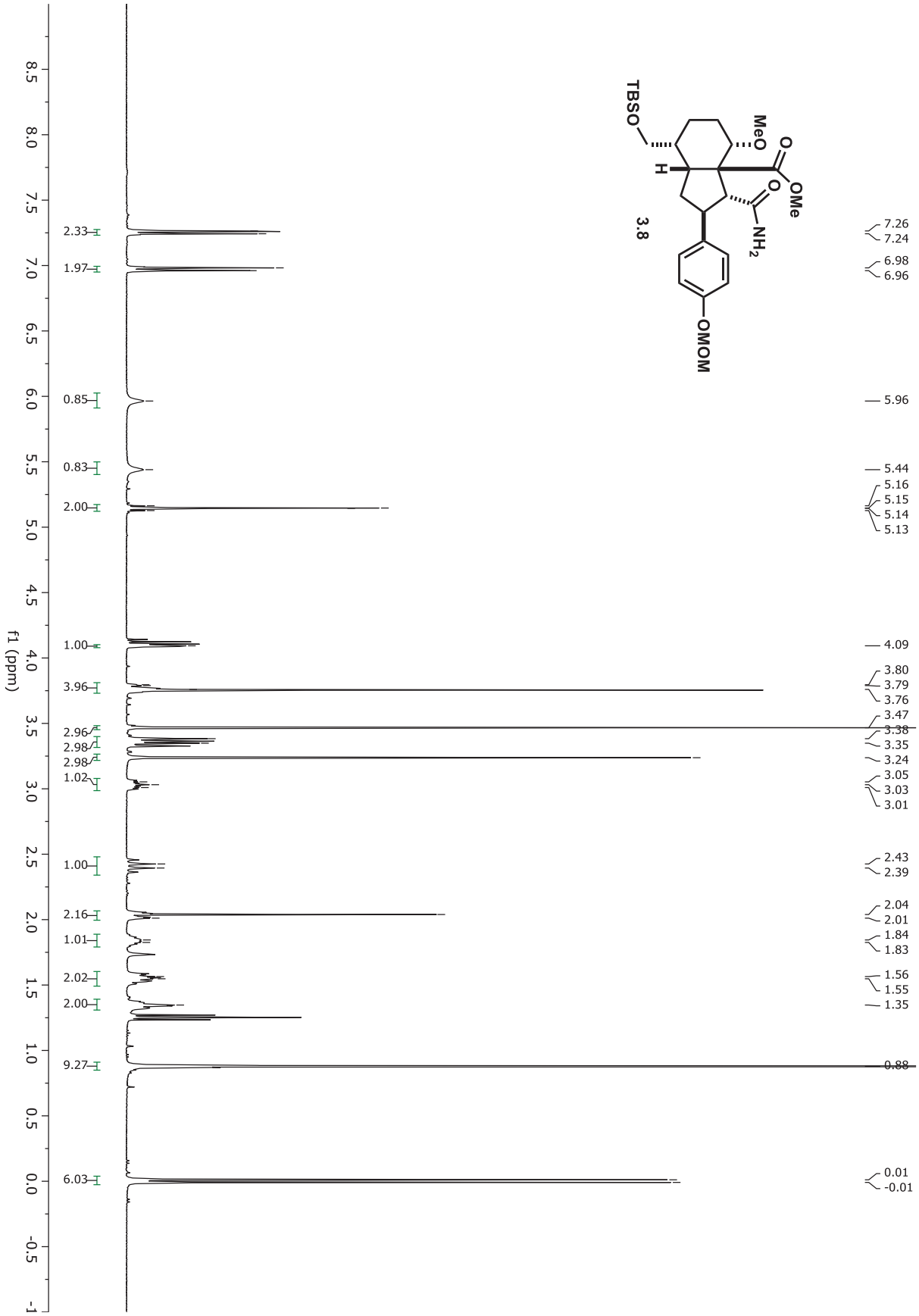
TBSO
H
MeO
O
O
OMe
O
NH2
OMOM
3.8
f1 (ppm)
8.5
8.0
7.5
7.0
6.5
6.0
5.5
5.0
4.5
4.0
3.5
3.0
2.5
2.0
1.5
1.0
0.5
0.0
-0.5
-1
2.33
1.97
0.85
0.83
2.00
1.00
3.96
2.96
2.98
2.98
1.02
1.00
2.16
1.01
2.02
2.00
9.27
6.03
7.26
7.24
6.98
6.96
5.96
5.44
5.16
5.15
5.14
5.13
4.09
3.80
3.79
3.76
3.47
3.38
3.35
3.24
3.05
3.03
3.01
2.43
2.39
2.04
2.01
1.84
1.83
1.56
1.55
1.35
0.88
0.01
-0.01

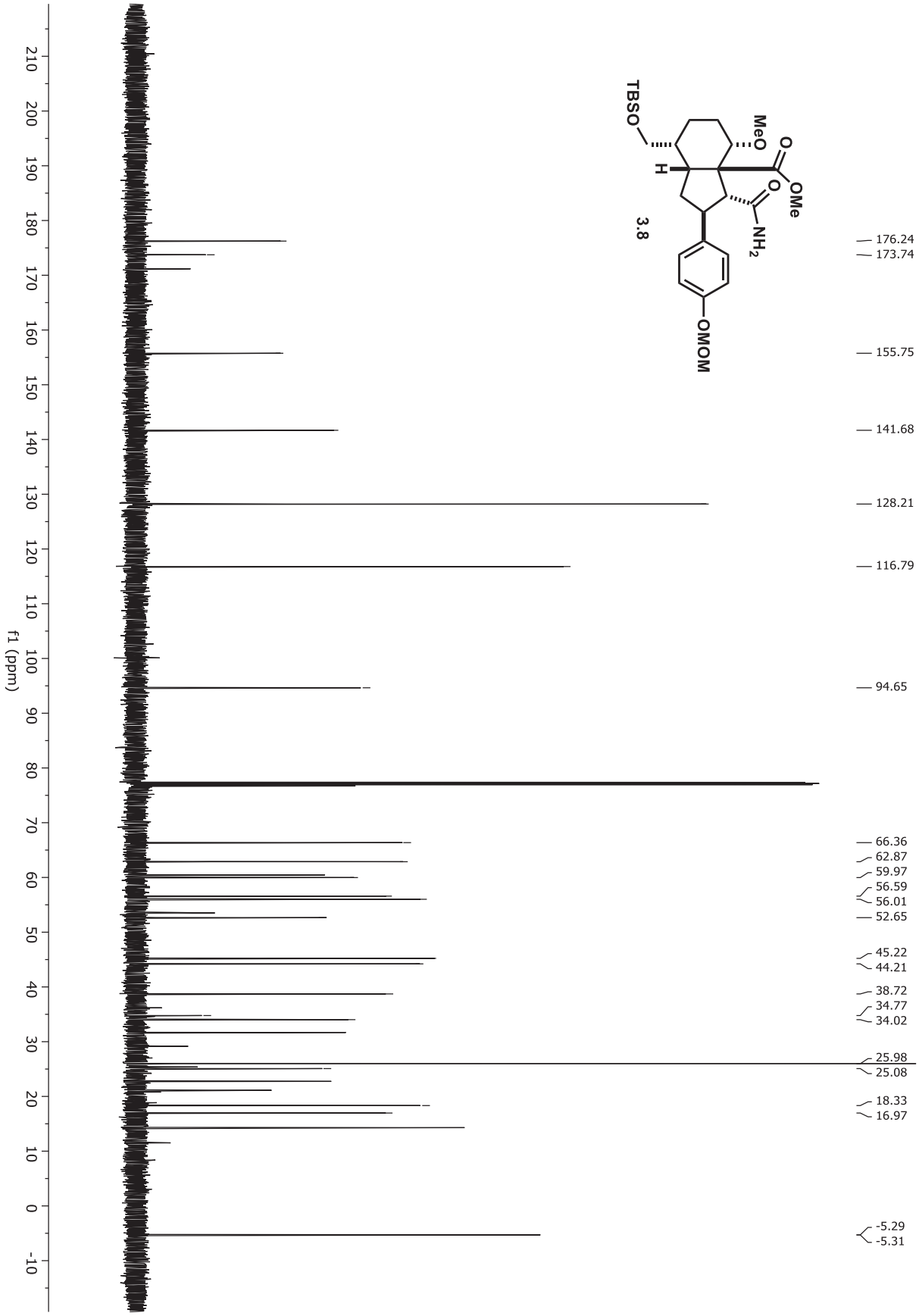
f1 (ppm)
210
200
190
180
170
160
150
140
130
120
110
100
90
80
70
60
50
40
30
20
10
0
-10
TBSO
H
MeO
O
O
OMe
O
NH2
OMOM
3.8
176.24
173.74
155.75
141.68
128.21
116.79
94.65
66.36
62.87
59.97
56.59
56.01
52.65
45.22
44.21
38.72
34.77
34.02
25.98
25.08
18.33
16.97
-5.29
-5.31

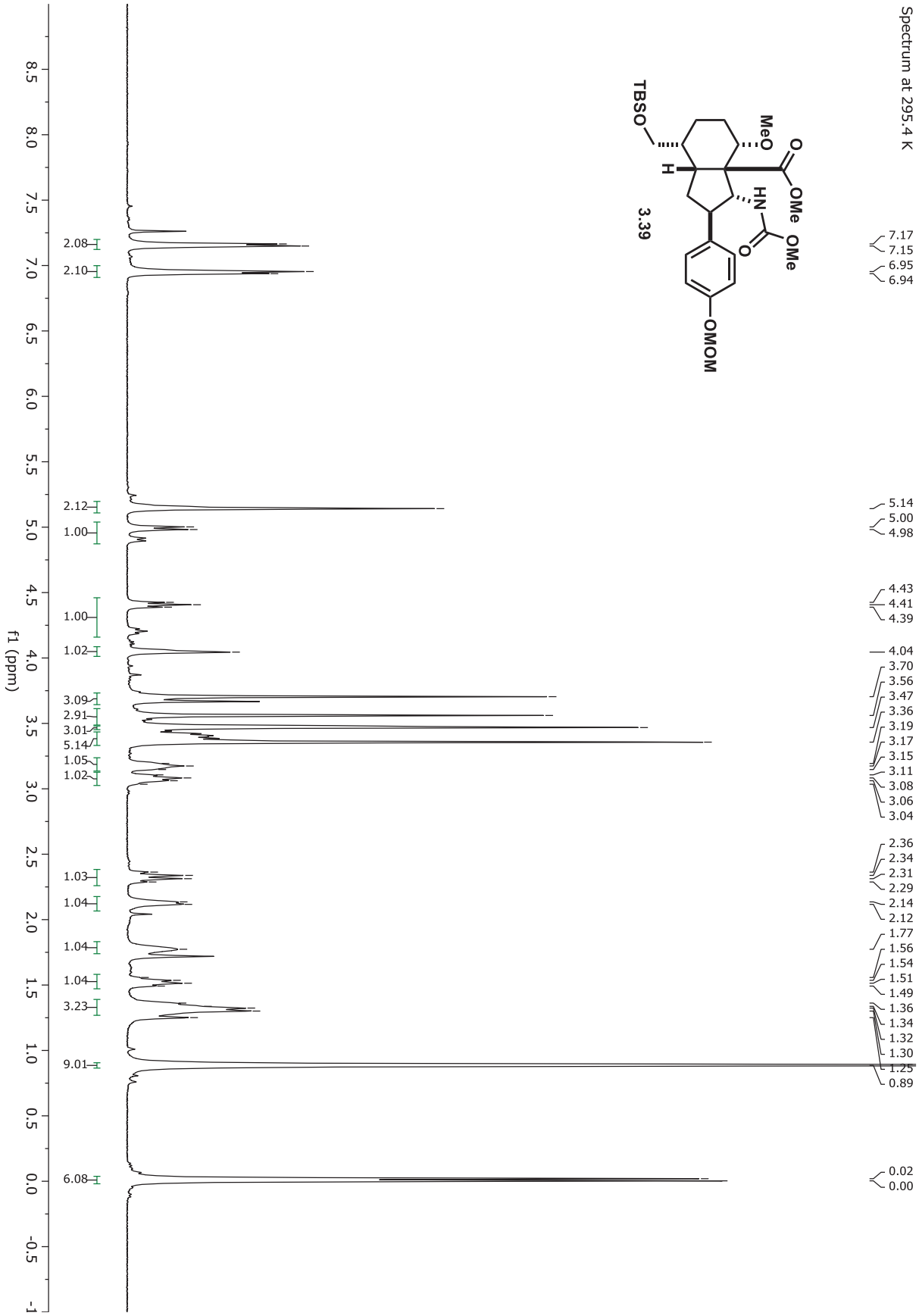
Spectrum at 295.4 K
TBSO
H
MeO
O
OMe
HN
O
OMe
OMOM
3.39
7.17
7.15
6.95
6.94
5.14
5.00
4.98
4.43
4.41
4.39
4.04
3.70
3.56
3.47
3.36
3.19
3.17
3.15
3.11
3.08
3.06
3.04
2.36
2.34
2.31
2.29
2.14
2.12
1.77
1.56
1.54
1.51
1.49
1.36
1.34
1.32
1.30
1.25
0.89
0.02
0.00
2.08
2.10
2.12
1.00
1.00
1.02
3.09
2.91
3.01
5.14
1.05
1.02
1.03
1.04
1.04
1.04
3.23
9.01
6.08
f1 (ppm)

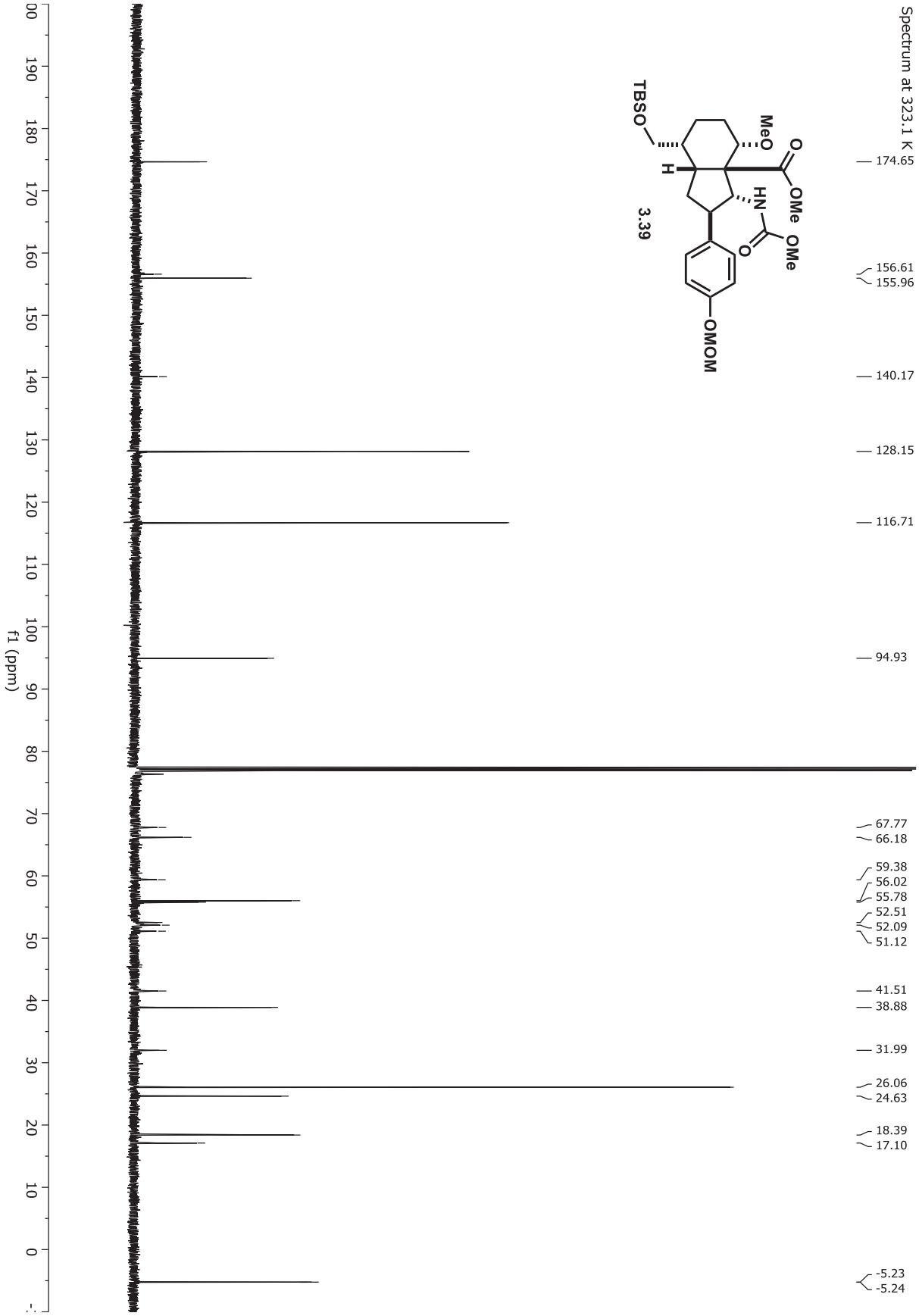
Spectrum at 323.1 K
174.65
156.61
155.96
140.17
128.15
116.71
94.93
67.77
66.18
59.38
56.02
55.78
52.51
52.09
51.12
41.51
38.88
31.99
26.06
24.63
18.39
17.10
-5.23
-5.24
f1 (ppm)
TBSO
H
MeO
O
OMe
HN
O
OMe
OMOM
3.39

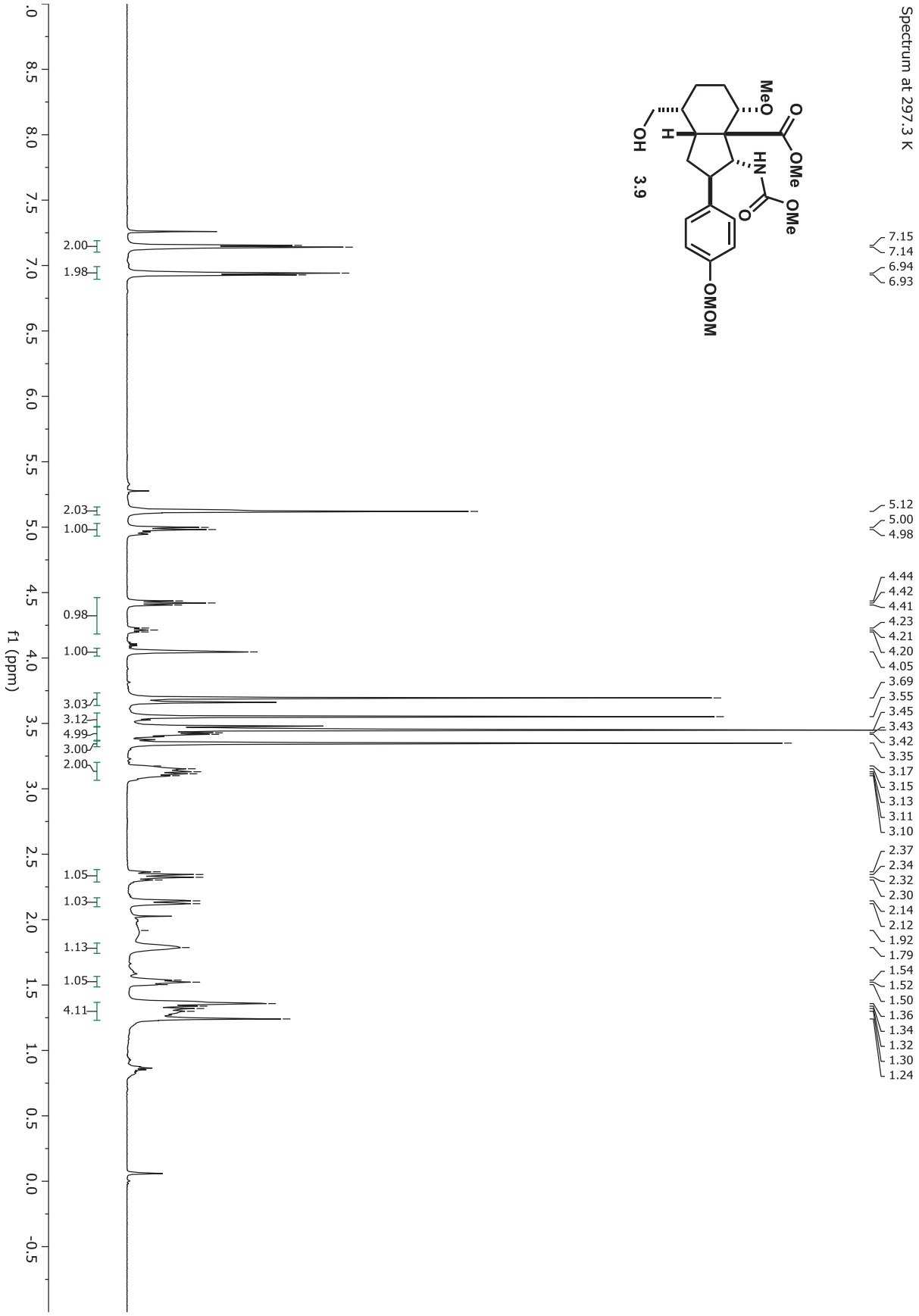
Spectrum at 297.3 K
f1 (ppm)
OMOM
OMe
OMe
MeO
HN
OH
H
3.9
7.15
7.14
6.94
6.93
5.12
5.00
4.98
4.44
4.42
4.41
4.23
4.21
4.20
4.05
3.69
3.55
3.45
3.43
3.42
3.35
3.17
3.15
3.13
3.11
3.10
2.37
2.34
2.32
2.30
2.14
2.12
1.92
1.79
1.54
1.52
1.50
1.36
1.34
1.32
1.30
1.24
2.00
1.98
2.03
1.00
0.98
1.00
3.03
3.12
4.99
3.00
2.00
1.05
1.03
1.13
1.05
4.11

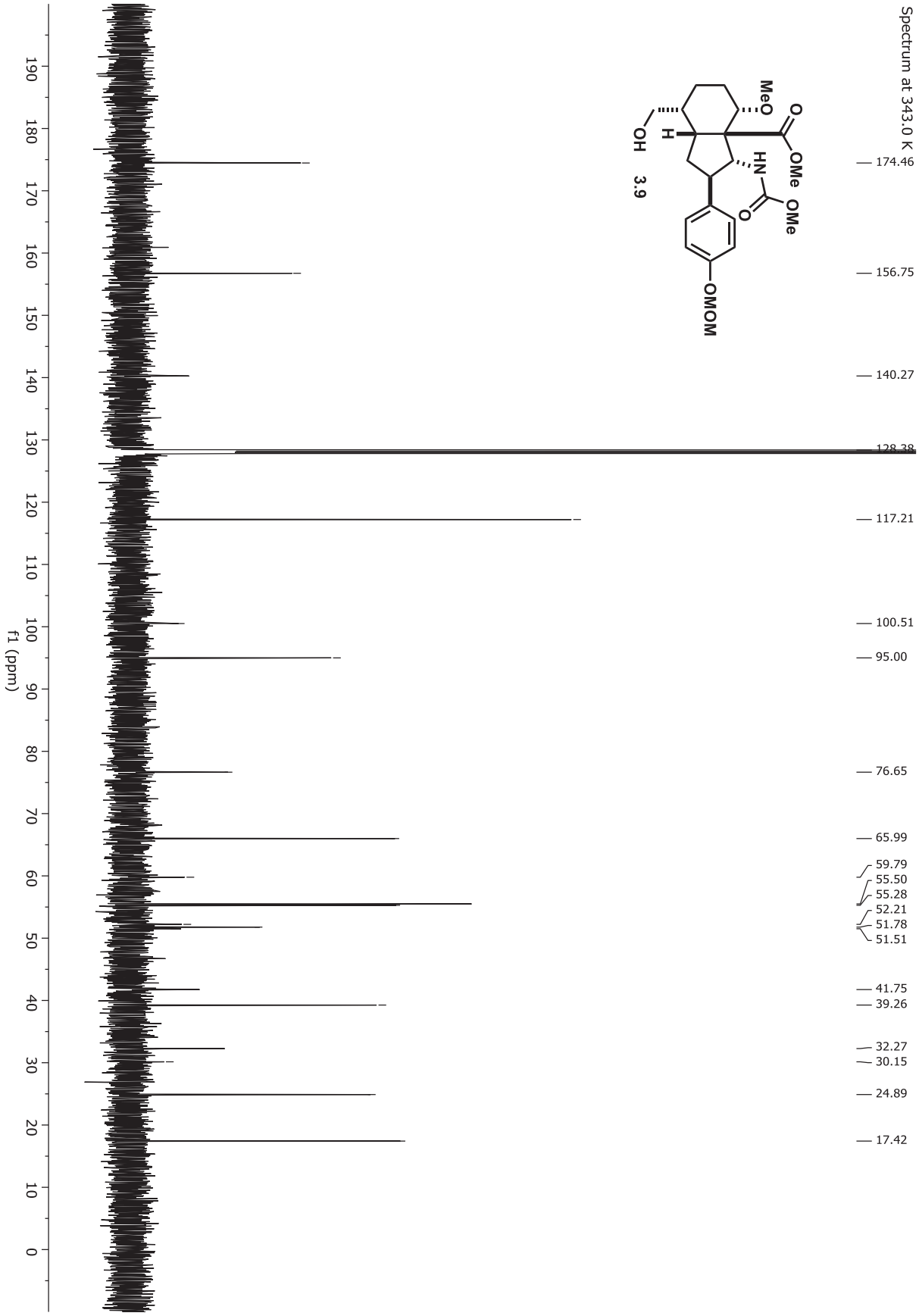
Spectrum at 343.0 K
174.46
156.75
140.27
128.38
117.21
100.51
95.00
76.65
65.99
59.79
55.50
55.28
52.21
51.78
51.51
41.75
39.26
32.27
30.15
24.89
17.42
f1 (ppm)
MeO
OMe
OMe
HN
OMOM
OH
3.9
H

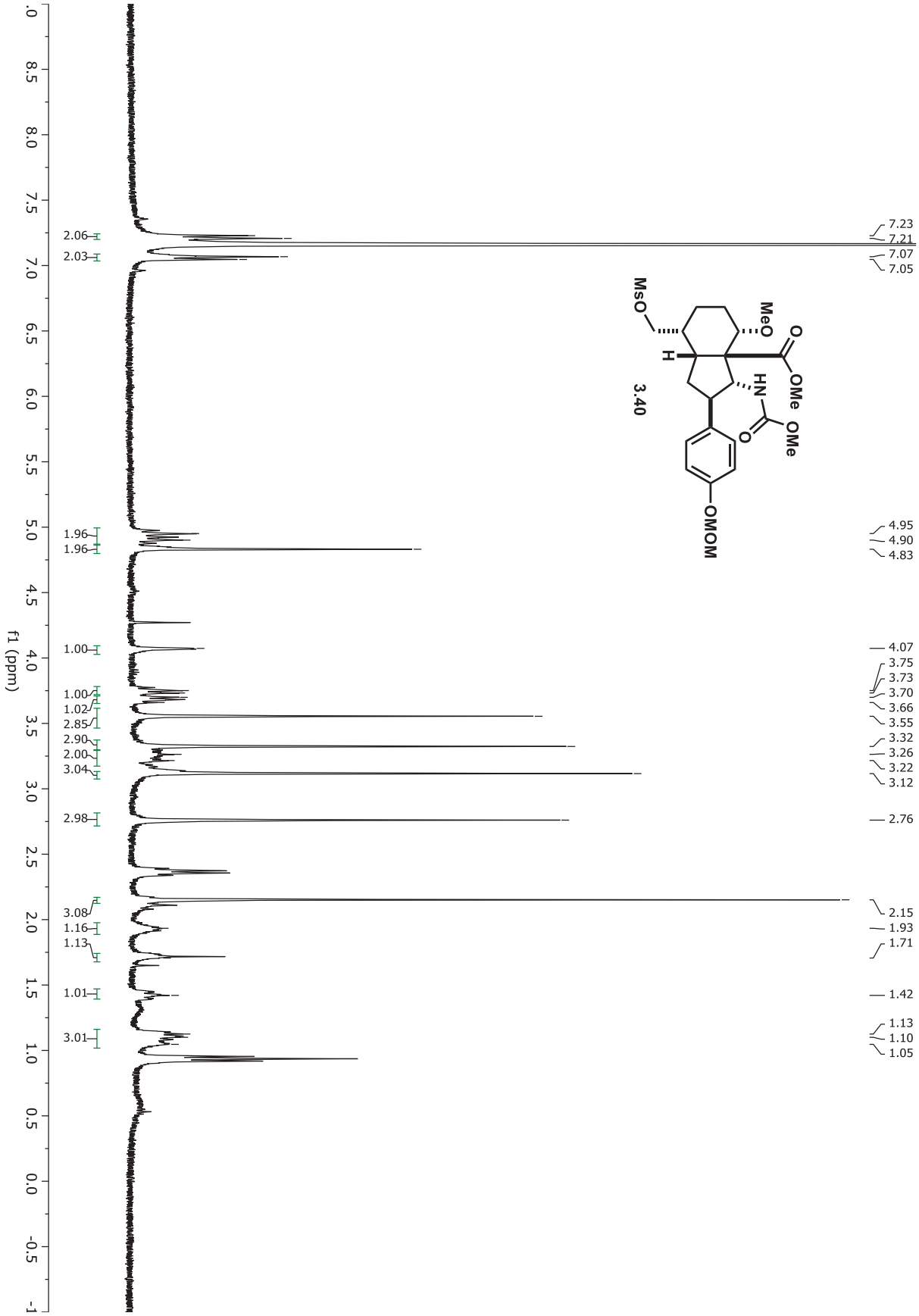
f1 (ppm)
.0
8.5
8.0
7.5
7.0
6.5
6.0
5.5
5.0
4.5
4.0
3.5
3.0
2.5
2.0
1.5
1.0
0.5
0.0
-0.5
-1
2.06
2.03
1.96
1.96
1.00
1.00
1.02
2.85
2.90
2.00
3.04
2.98
3.08
1.16
1.13
1.01
3.01
7.23
7.21
7.07
7.05
4.95
4.90
4.83
4.07
3.75
3.73
3.70
3.66
3.55
3.32
3.26
3.22
3.12
2.76
2.15
1.93
1.71
1.42
1.13
1.10
1.05
MsO
MeO
H
HN
O
OMe
OMe
OMOM
3.40

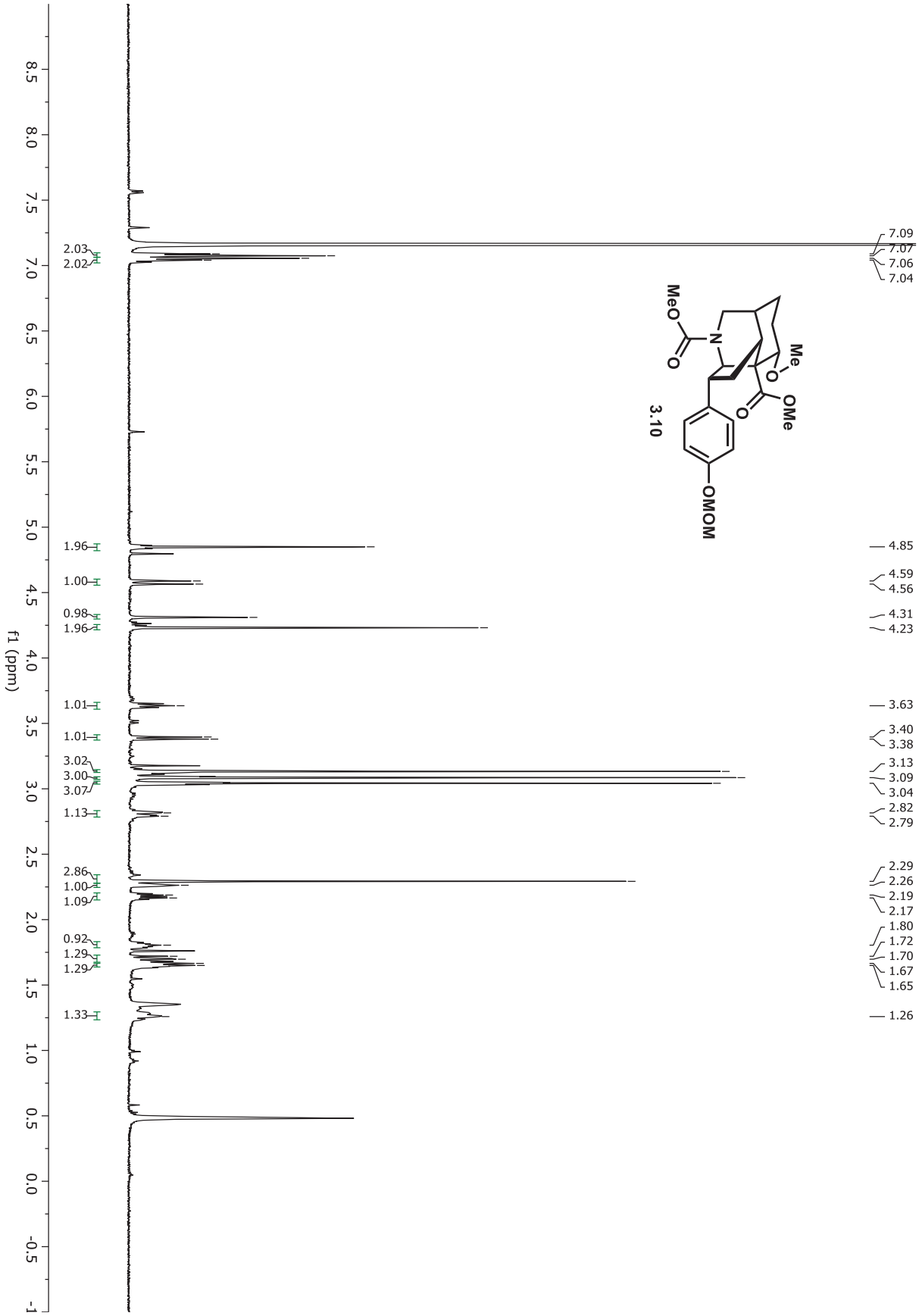
f1 (ppm)
8.5
8.0
7.5
7.0
6.5
6.0
5.5
5.0
4.5
4.0
3.5
3.0
2.5
2.0
1.5
1.0
0.5
0.0
-0.5
-1
2.03
2.02
1.96
1.00
0.98
1.96
1.01
1.01
3.02
3.00
3.07
1.13
2.86
1.00
1.09
0.92
1.29
1.29
1.33
7.09
7.07
7.06
7.04
4.85
4.59
4.56
4.31
4.23
3.63
3.40
3.38
3.13
3.09
3.04
2.82
2.79
2.29
2.26
2.19
2.17
1.80
1.72
1.70
1.67
1.65
1.26
MeO
O
N
Me
O
OMe
O
OMOM
3.10

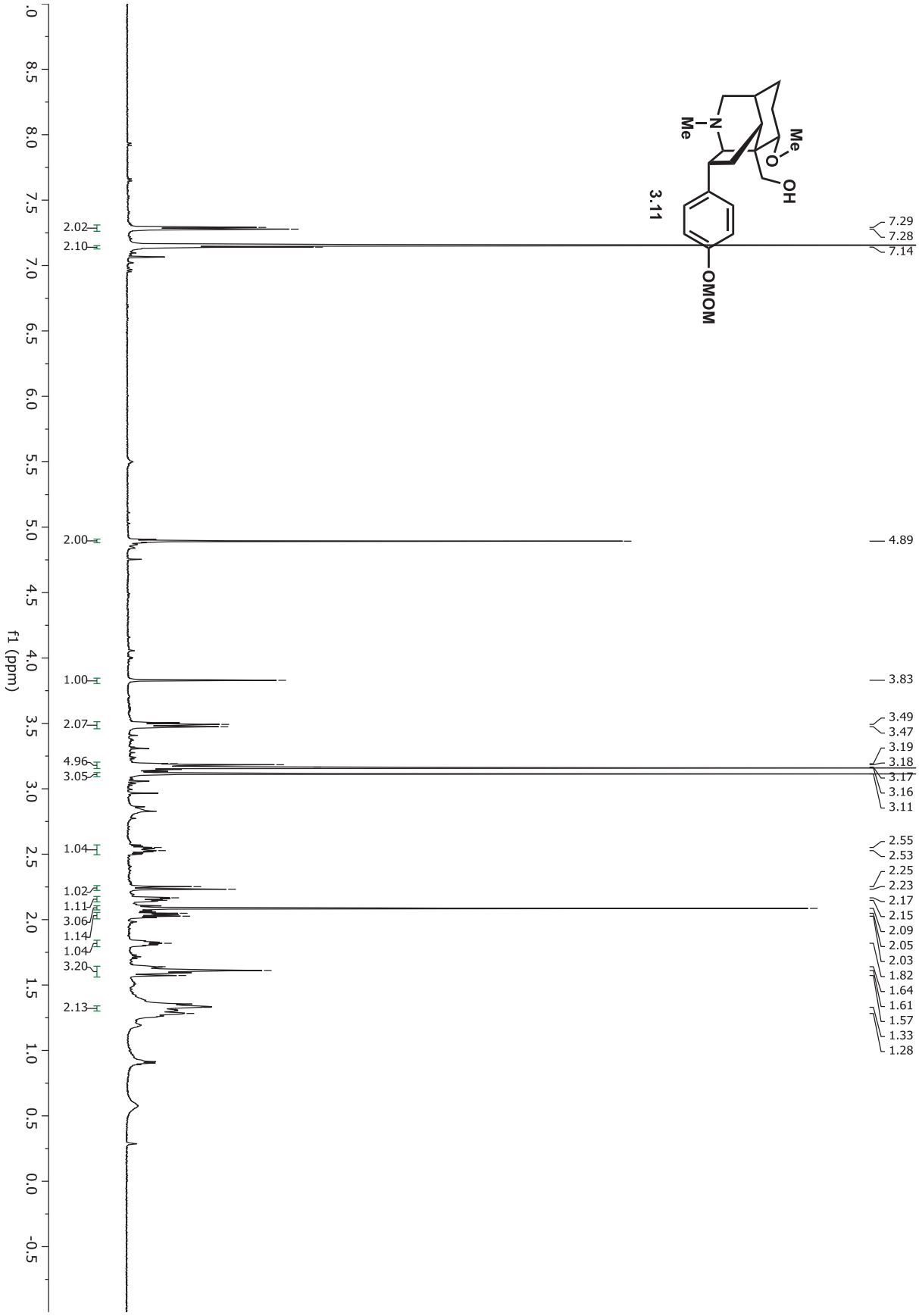
3.11
N
Me
Me
O
OH
OMOM
f1 (ppm)
2.02
2.10
2.00
1.00
2.07
4.96
3.05
1.04
1.02
1.11
3.06
1.14
1.04
3.20
2.13
7.29
7.28
7.14
4.89
3.83
3.49
3.47
3.19
3.18
3.17
3.16
3.11
2.55
2.53
2.25
2.23
2.17
2.15
2.09
2.05
2.03
1.82
1.64
1.61
1.57
1.33
1.28

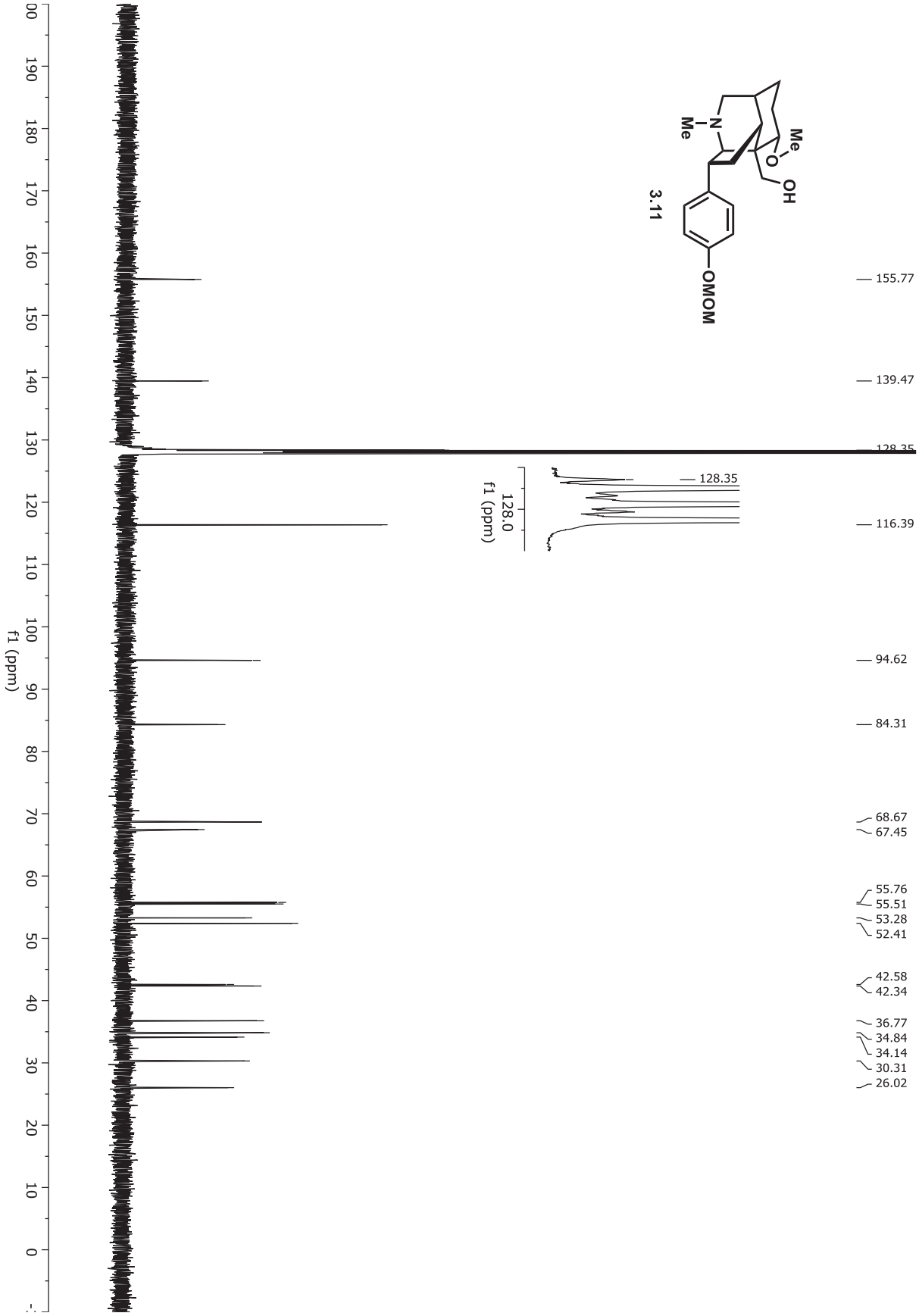
3.11
Me
N
Me
Me
O
OH
OMOM
155.77
139.47
128.35
116.39
94.62
84.31
68.67
67.45
55.76
55.51
53.28
52.41
42.58
42.34
36.77
34.84
34.14
30.31
26.02
128.35
128.0
f1 (ppm)
f1 (ppm)

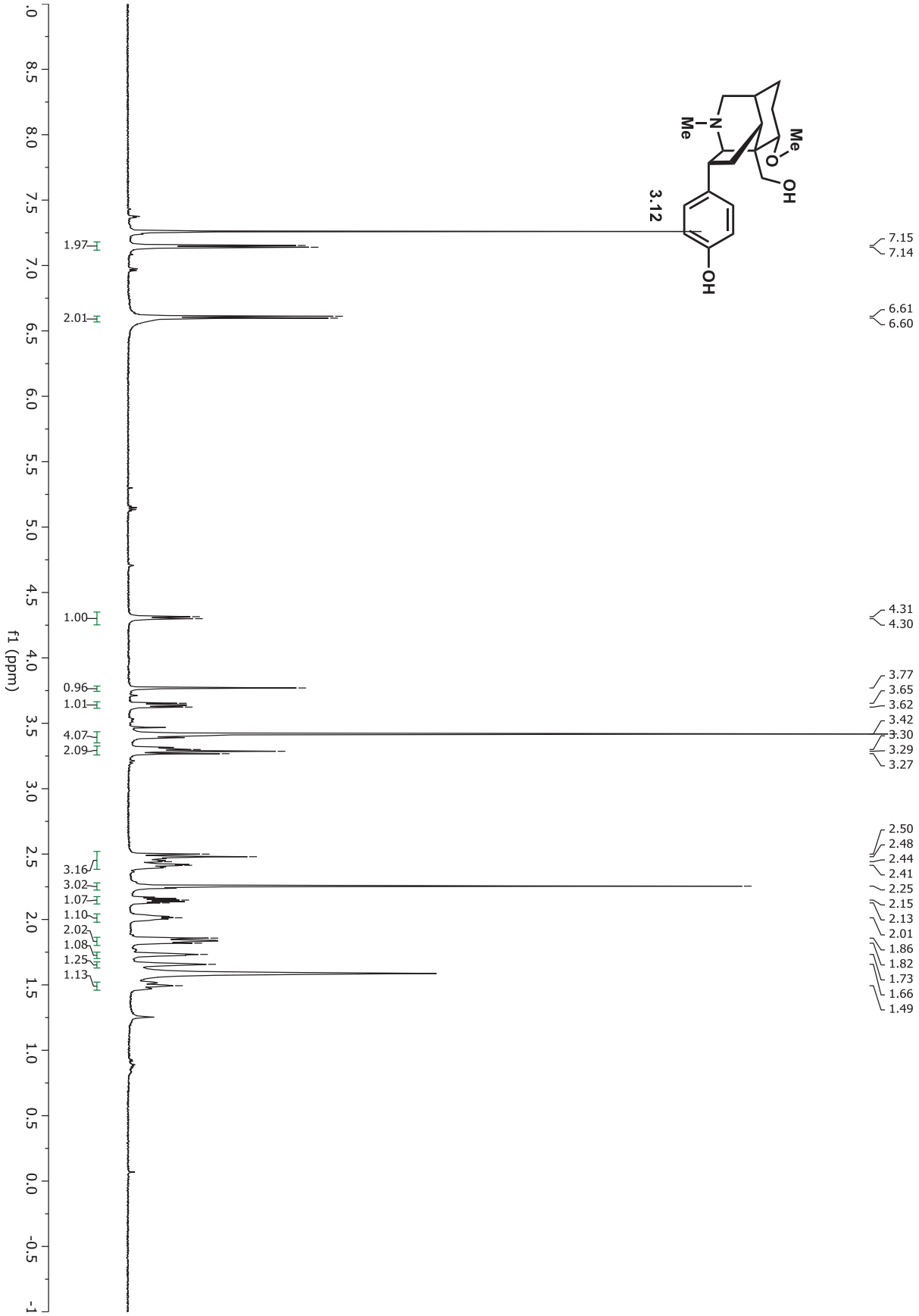
3.12
1.97
2.01
1.00
0.96
1.01
4.07
2.09
3.16
3.02
1.07
1.10
2.02
1.08
1.25
1.13
7.15
7.14
6.61
6.60
4.31
4.30
3.77
3.65
3.62
3.42
3.30
3.29
3.27
2.50
2.48
2.44
2.41
2.25
2.15
2.13
2.01
1.86
1.82
1.73
1.66
1.49
f1 (ppm)

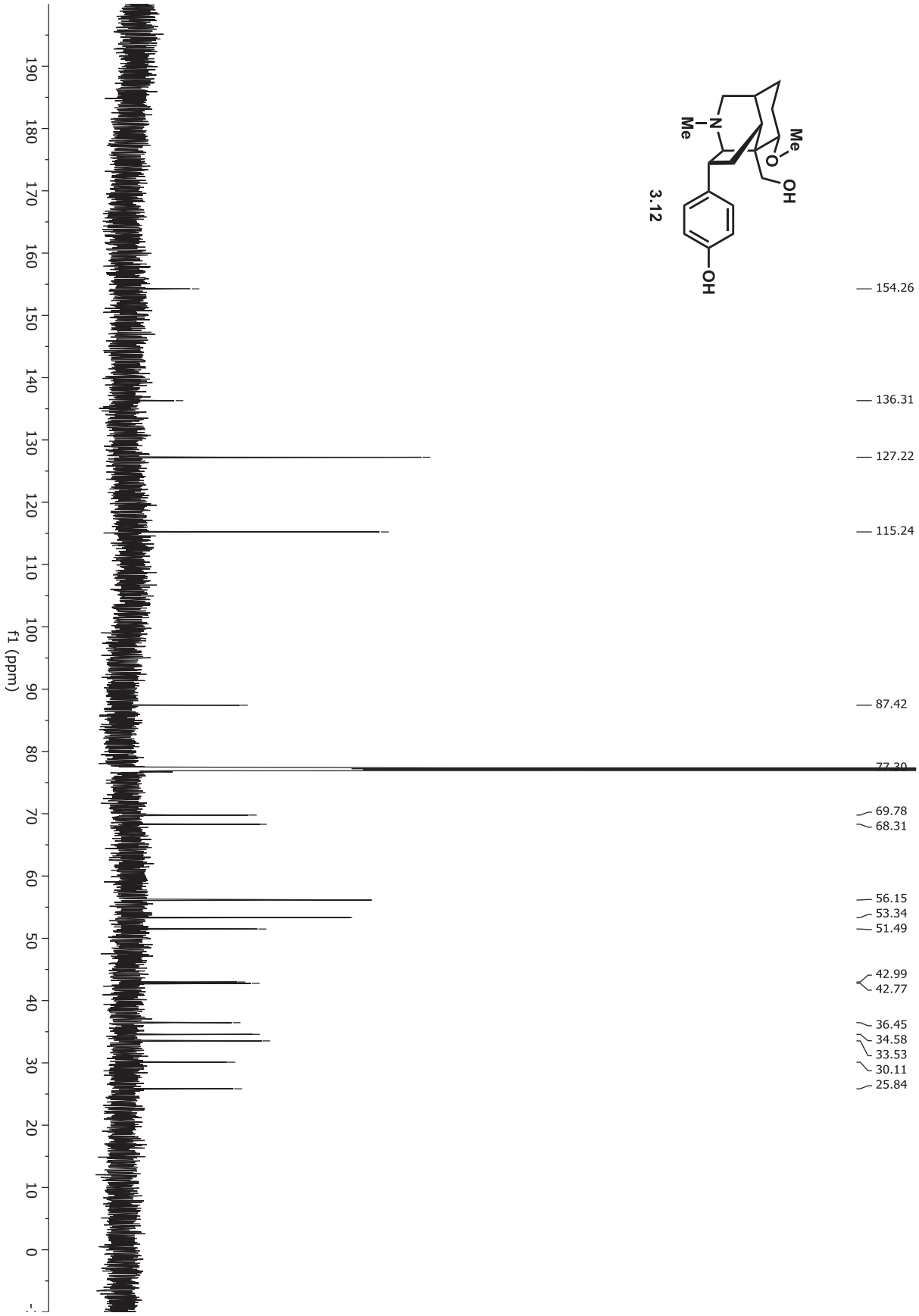
3.12
Me
N
Me
Me
O
OH
OH
154.26
136.31
127.22
115.24
87.42
77.30
69.78
68.31
56.15
53.34
51.49
42.99
42.77
36.45
34.58
33.53
30.11
25.84
f1 (ppm)

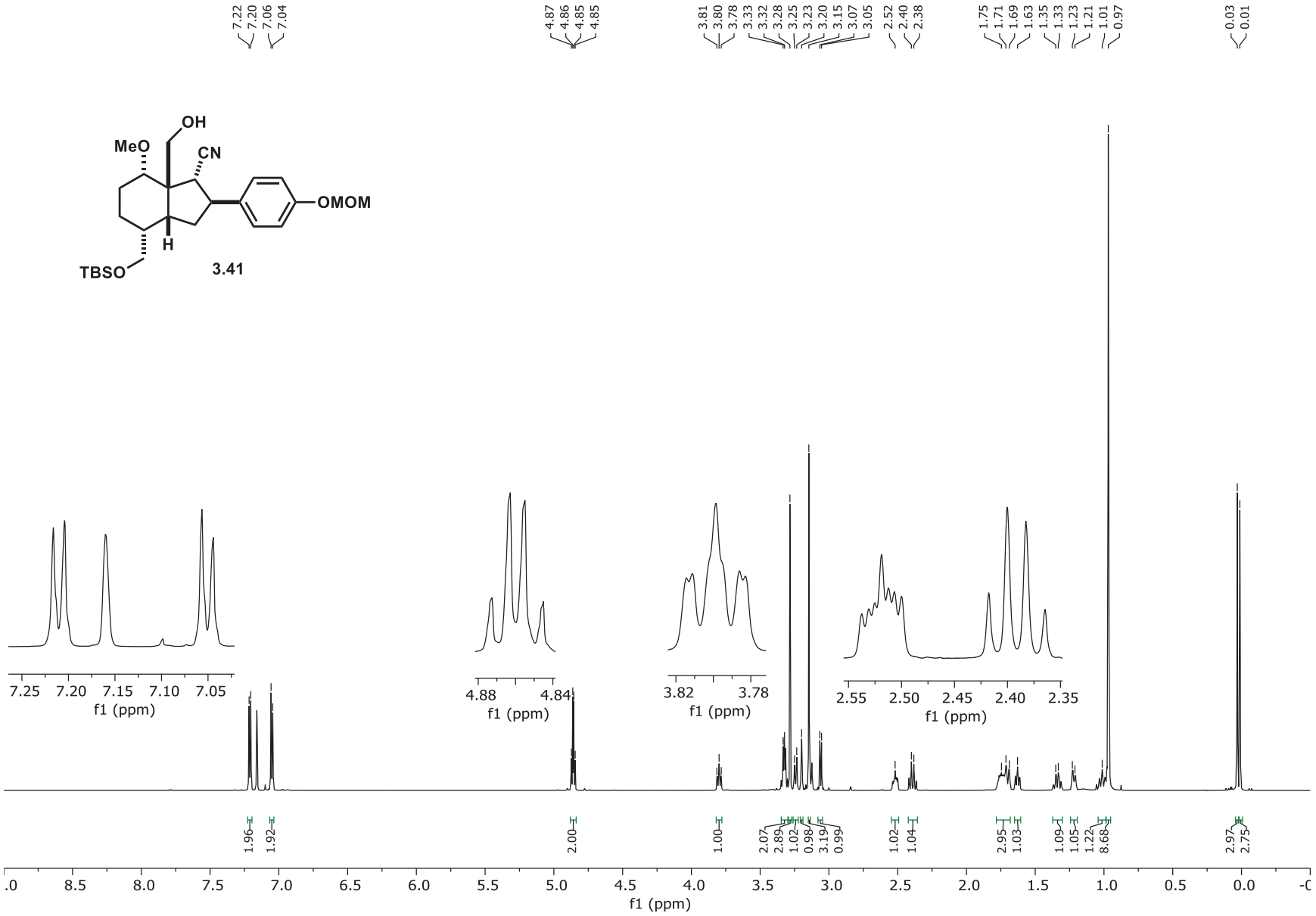
7.22
7.20
7.06
7.04
4.87
4.86
4.85
4.85
3.81
3.80
3.78
3.33
3.32
3.28
3.25
3.23
3.20
3.15
3.07
3.05
2.52
2.40
2.38
1.75
1.71
1.69
1.63
1.35
1.33
1.23
1.21
1.01
0.97
0.03
0.01
OH
MeO
CN
OMOM
H
TBSO
3.41
7.25 7.20 7.15 7.10 7.05
f1 (ppm)
4.88 4.84
f1 (ppm)
3.82 3.78
f1 (ppm)
2.55 2.50 2.45 2.40 2.35
f1 (ppm)
1.96
1.92
2.00
1.00
2.07
2.89
1.02
0.98
3.19
0.99
1.02
1.04
2.95
1.03
1.09
1.05
1.22
8.68
2.97
2.75
.0 8.5 8.0 7.5 7.0 6.5 6.0 5.5 5.0 4.5 4.0 3.5 3.0 2.5 2.0 1.5 1.0 0.5 0.0
f1 (ppm)

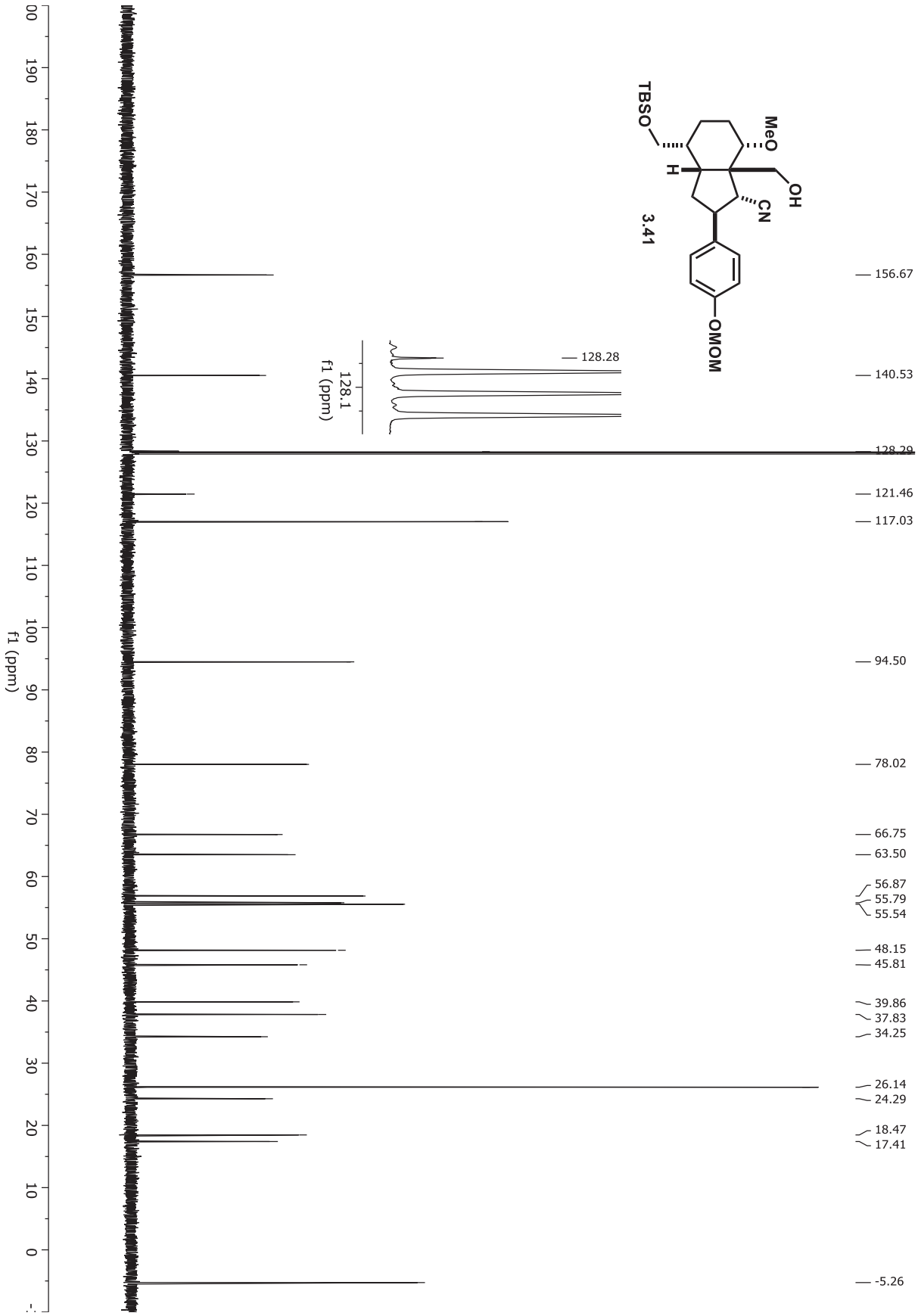
TBSO
MeO
H
CN
OH
OMOM
3.41
156.67
140.53
128.28
128.29
121.46
117.03
94.50
78.02
66.75
63.50
56.87
55.79
55.54
48.15
45.81
39.86
37.83
34.25
26.14
24.29
18.47
17.41
-5.26
128.1
f1 (ppm)
f1 (ppm)

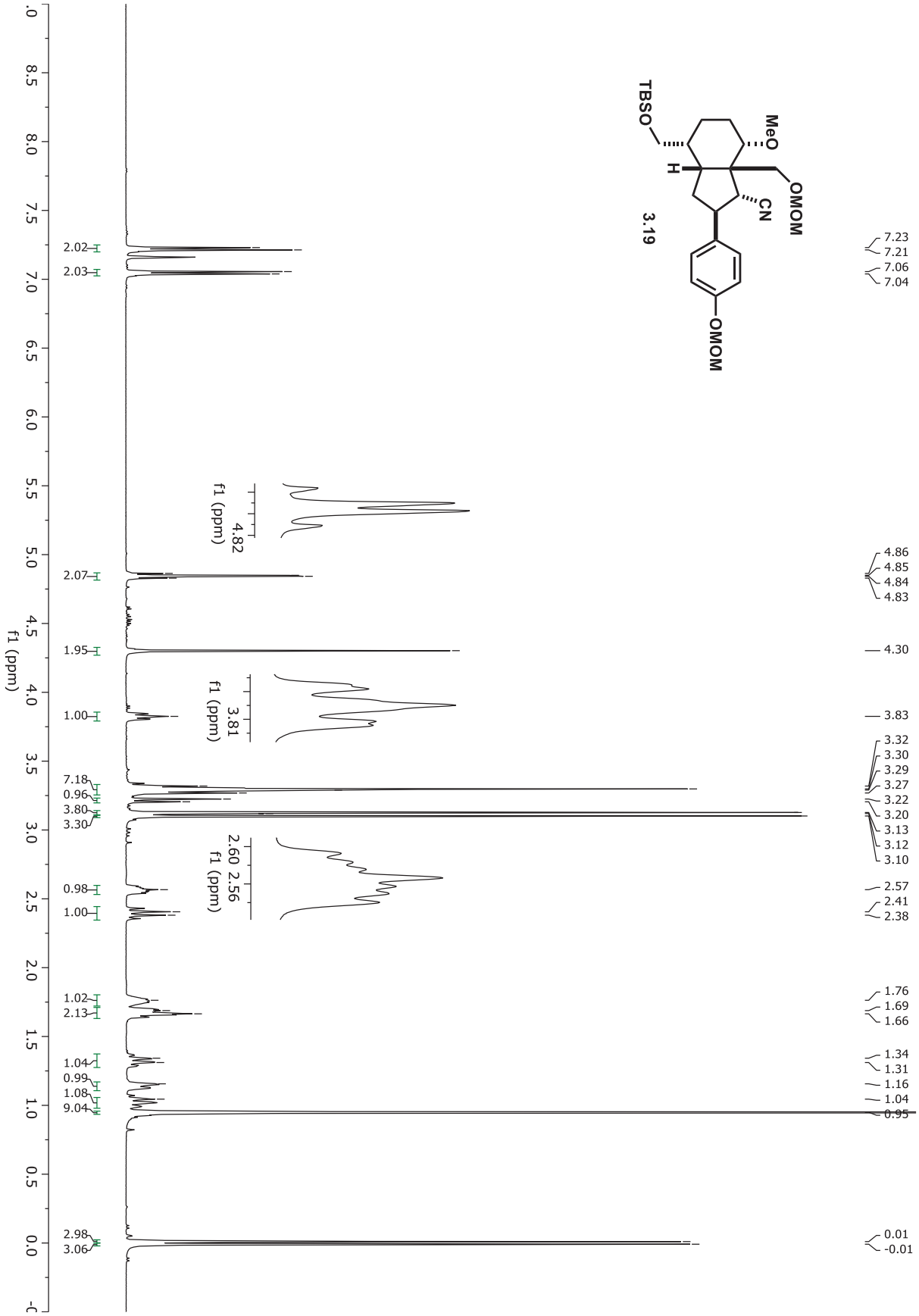
TBSO
MeO
H
CN
OMOM
OMOM
3.19
f1 (ppm)
4.82
3.81
2.60 2.56
2.02
2.03
2.07
1.95
1.00
7.18
0.96
3.80
3.30
0.98
1.00
1.02
2.13
1.04
0.99
1.08
9.04
2.98
3.06
7.23
7.21
7.06
7.04
4.86
4.85
4.84
4.83
4.30
3.83
3.32
3.30
3.29
3.27
3.22
3.20
3.13
3.12
3.10
2.57
2.41
2.38
1.76
1.69
1.66
1.34
1.31
1.16
1.04
0.95
0.01
-0.01

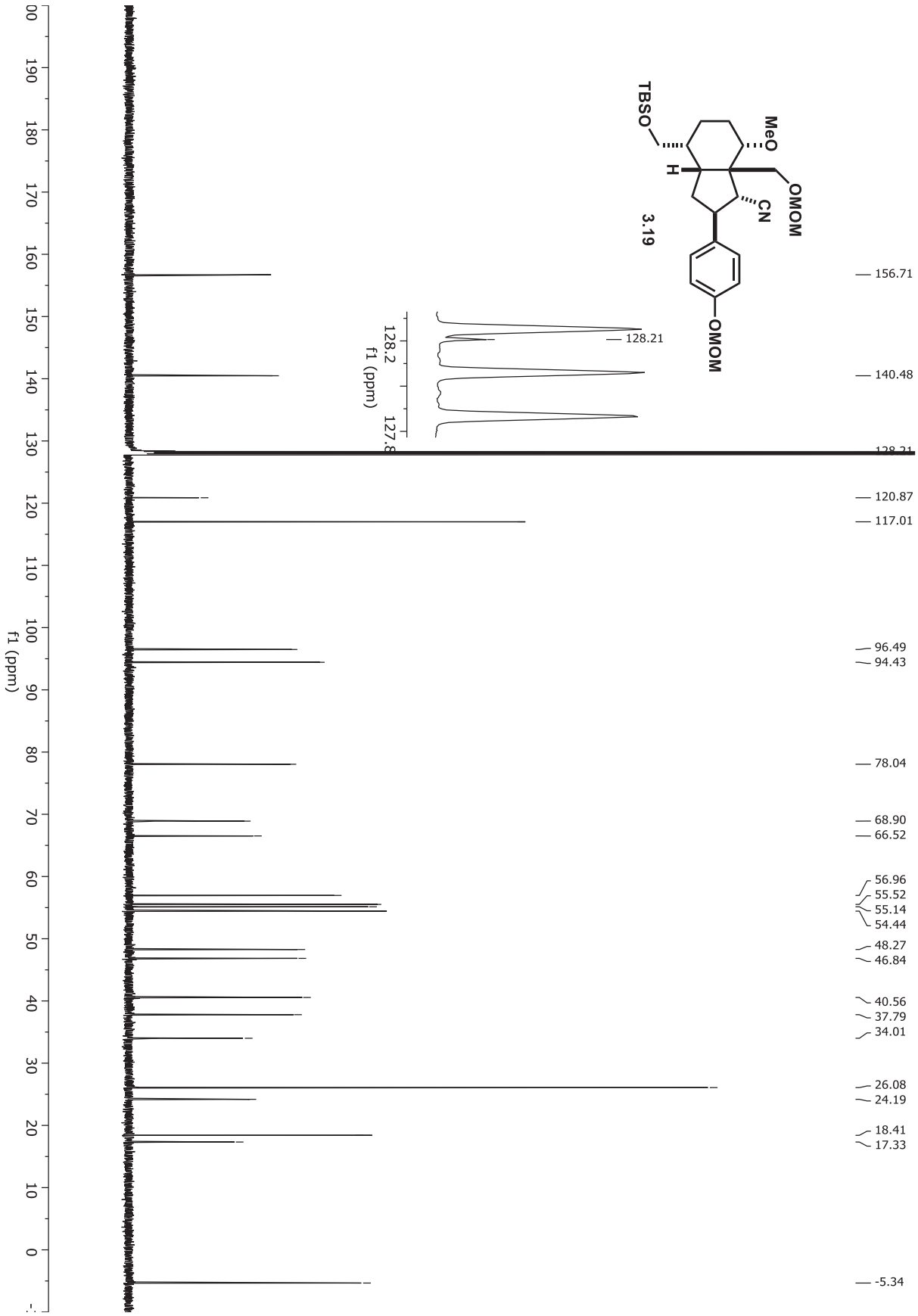
TBSO
H
MeO
CN
OMOM
OMOM
3.19
156.71
140.48
128.21
120.87
117.01
96.49
94.43
78.04
68.90
66.52
56.96
55.52
55.14
54.44
48.27
46.84
40.56
37.79
34.01
26.08
24.19
18.41
17.33
-5.34
f1 (ppm)
128.2
127.8
f1 (ppm)

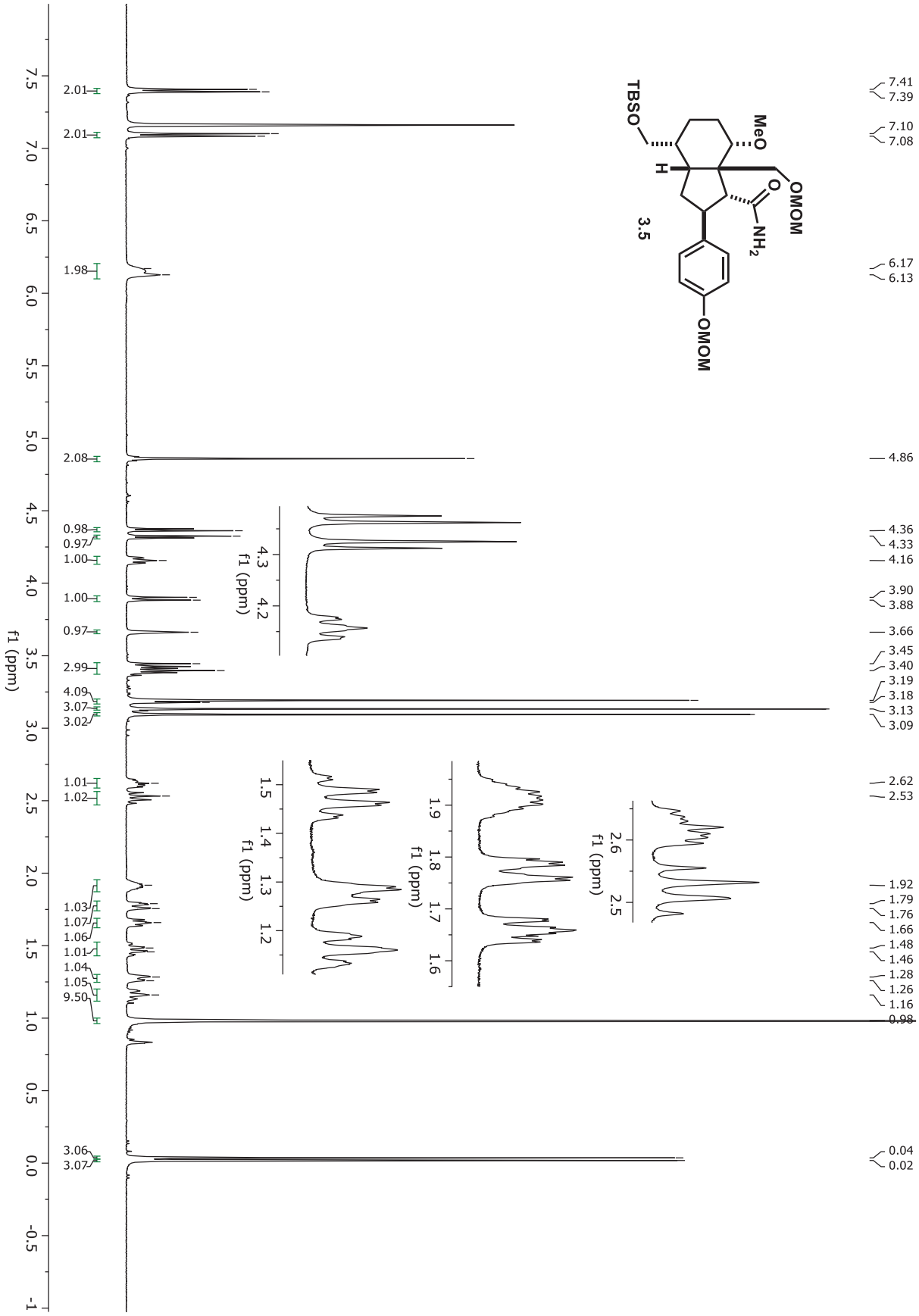
TBSO
MeO
OMOM
O
NH2
H
3.5
OMOM
f1 (ppm)

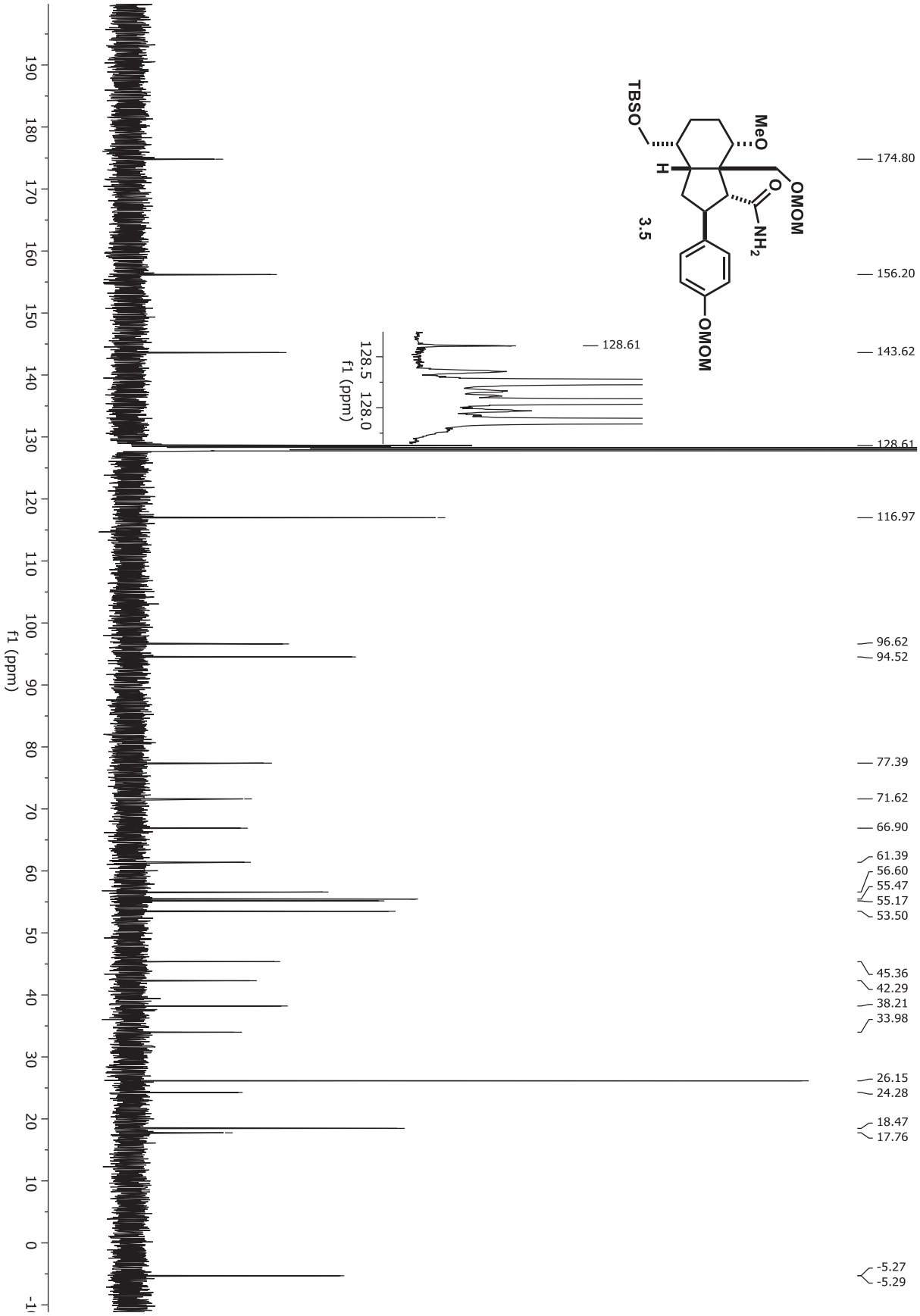
TBSO
H
MeO
O
OMOM
NH2
3.5
OMOM
f1 (ppm)
128.5 128.0
128.61
174.80
156.20
143.62
128.61
116.97
96.62
94.52
77.39
71.62
66.90
61.39
56.60
55.47
55.17
53.50
45.36
42.29
38.21
33.98
26.15
24.28
18.47
17.76
-5.27
-5.29
f1 (ppm)

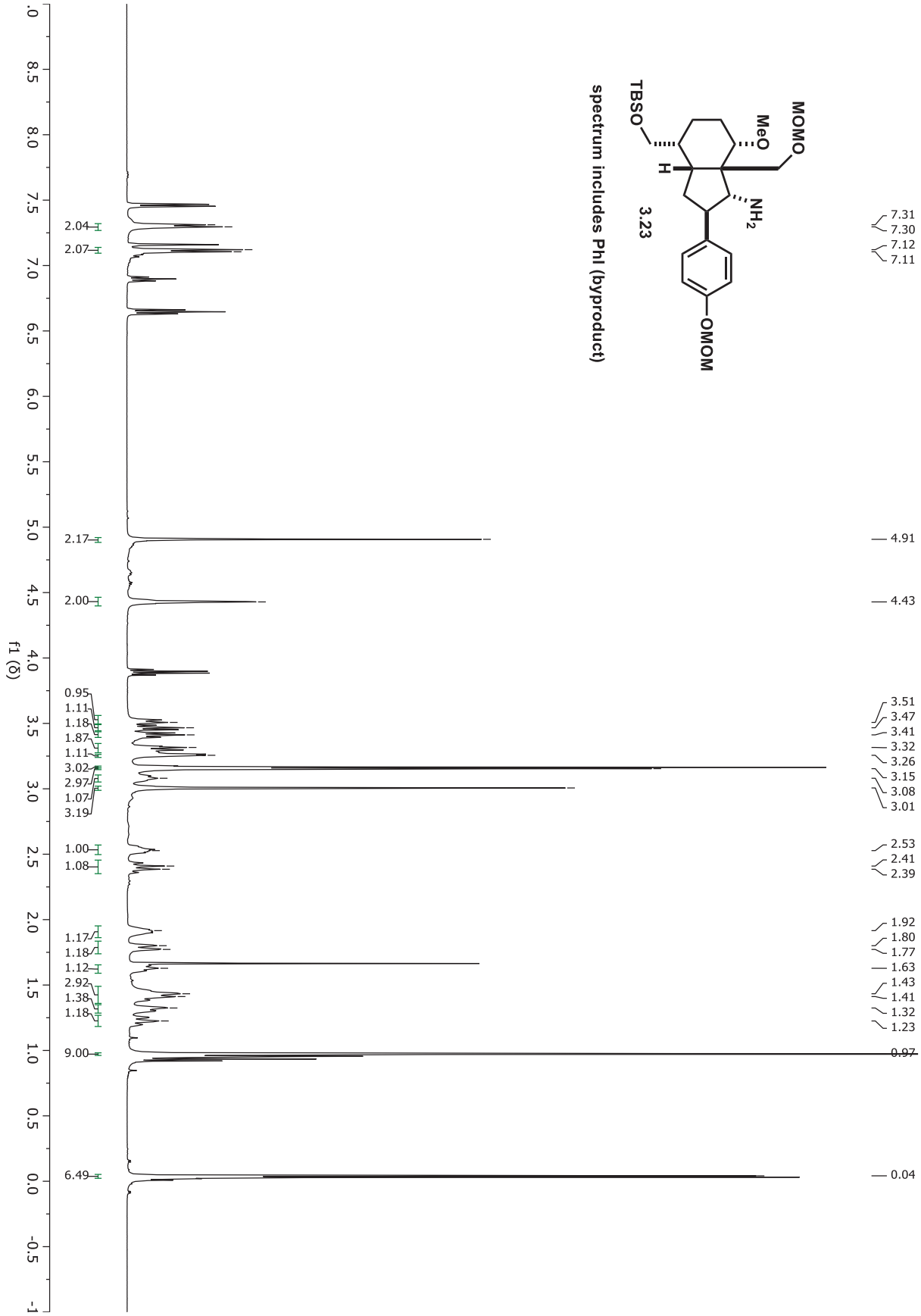
spectrum includes PhI (byproduct)
TBSO
MeO
MOMO
NH2
OMOM
H
3.23
f1 (δ)
2.04
2.07
2.17
2.00
0.95
1.11
1.18
1.87
1.11
3.02
2.97
1.07
3.19
1.00
1.08
1.17
1.18
1.12
2.92
1.38
1.18
9.00
6.49
7.31
7.30
7.12
7.11
4.91
4.43
3.51
3.47
3.41
3.32
3.26
3.15
3.08
3.01
2.53
2.41
2.39
1.92
1.80
1.77
1.63
1.43
1.41
1.32
1.23
0.97
0.04

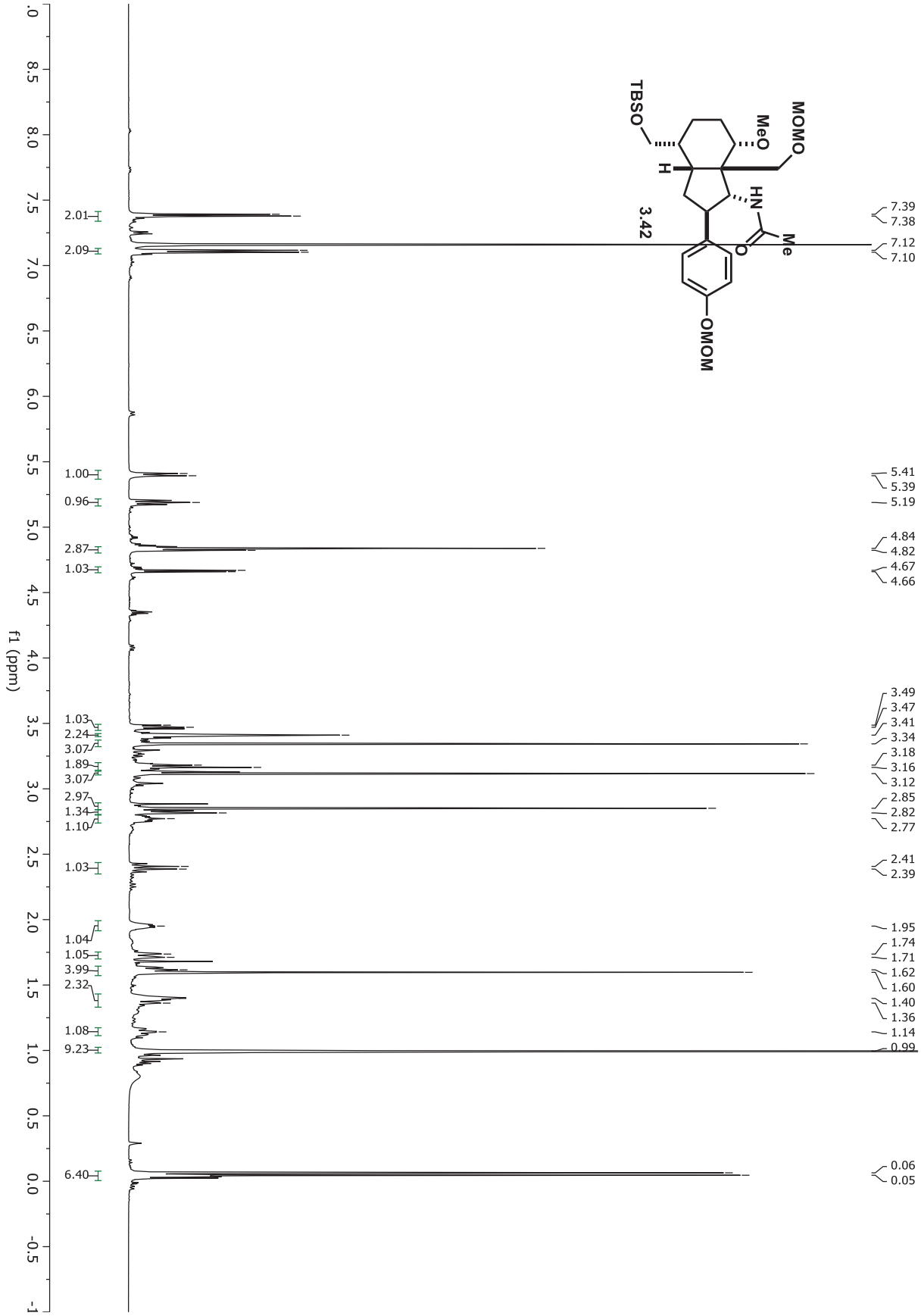
TBSO
MOMO
MeO
H
HN
Me
O
OMOM
3.42
f1 (ppm)
2.01
2.09
1.00
0.96
2.87
1.03
1.03
2.24
3.07
1.89
3.07
2.97
1.34
1.10
1.03
1.04
1.05
3.99
2.32
1.08
9.23
6.40
7.39
7.38
7.12
7.10
5.41
5.39
5.19
4.84
4.82
4.67
4.66
3.49
3.47
3.41
3.34
3.18
3.16
3.12
2.85
2.82
2.77
2.41
2.39
1.95
1.74
1.71
1.62
1.60
1.40
1.36
1.14
0.99
0.06
0.05

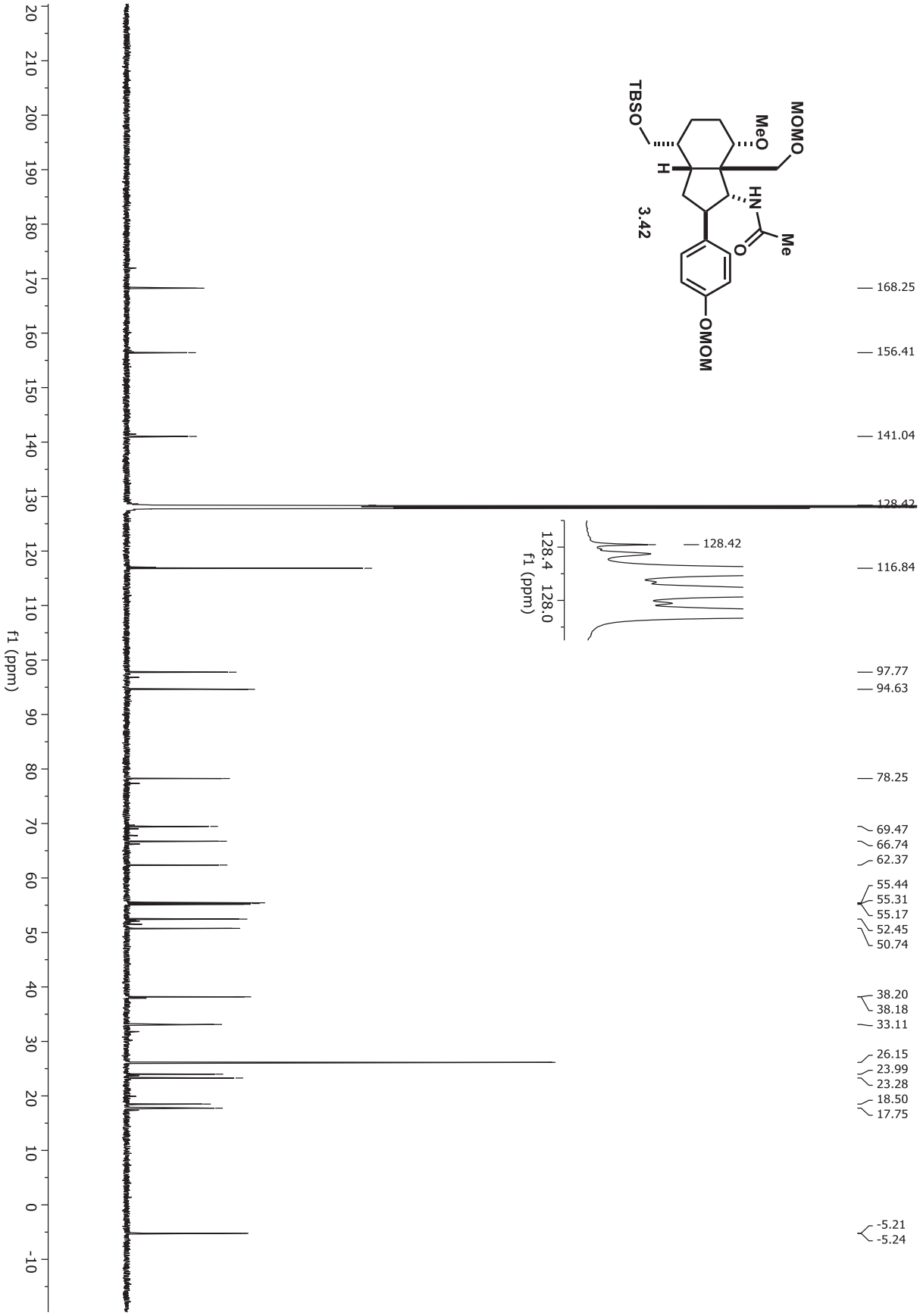
TBSO
H
MeO
MOMO
HN
Me
O
OMOM
3.42
168.25
156.41
141.04
128.42
116.84
97.77
94.63
78.25
69.47
66.74
62.37
55.44
55.31
55.17
52.45
50.74
38.20
38.18
33.11
26.15
23.99
23.28
18.50
17.75
-5.21
-5.24
f1 (ppm)

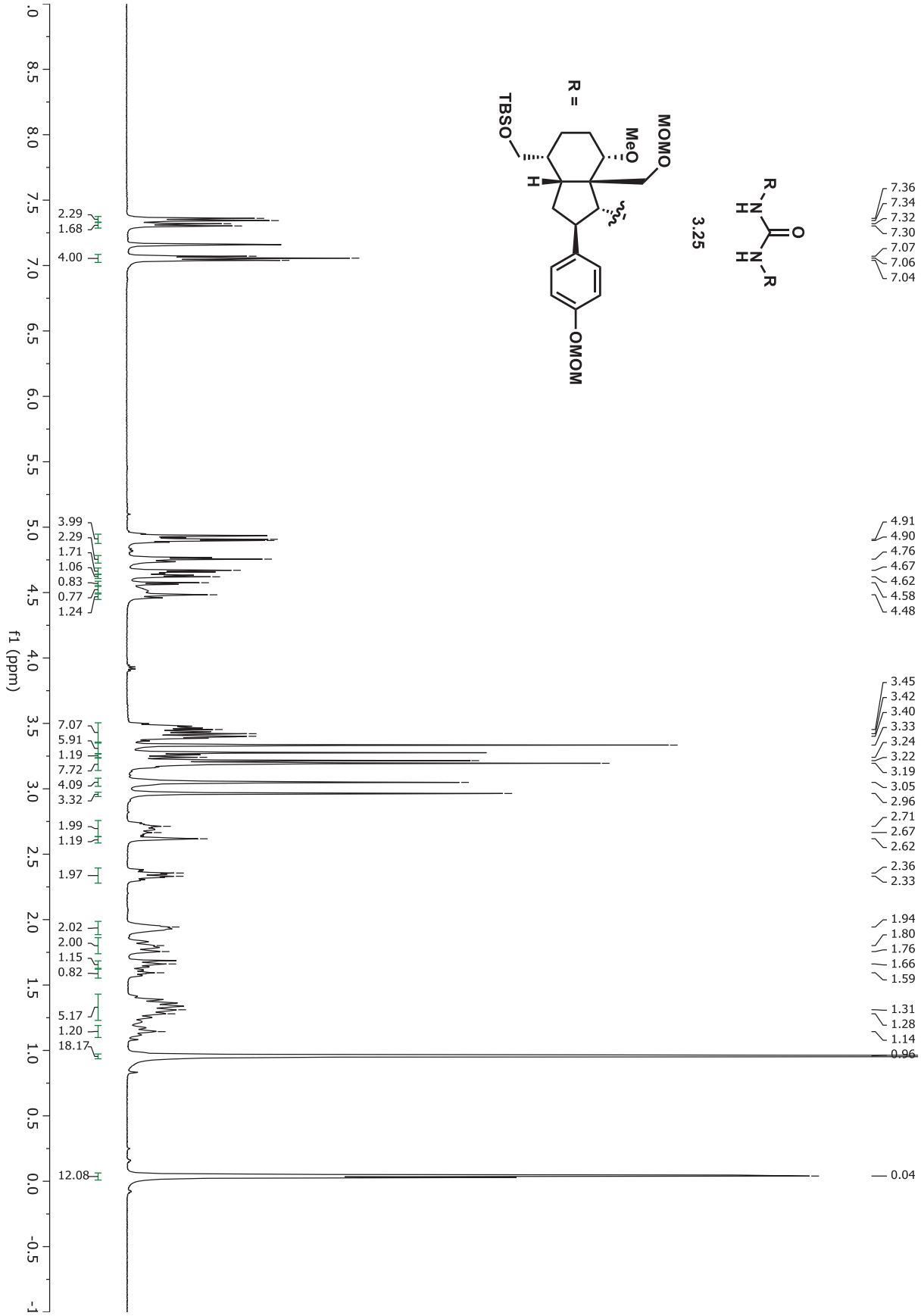
R =
TBSO
MeO
MOMO
OMOM
H
3.25
f1 (ppm)

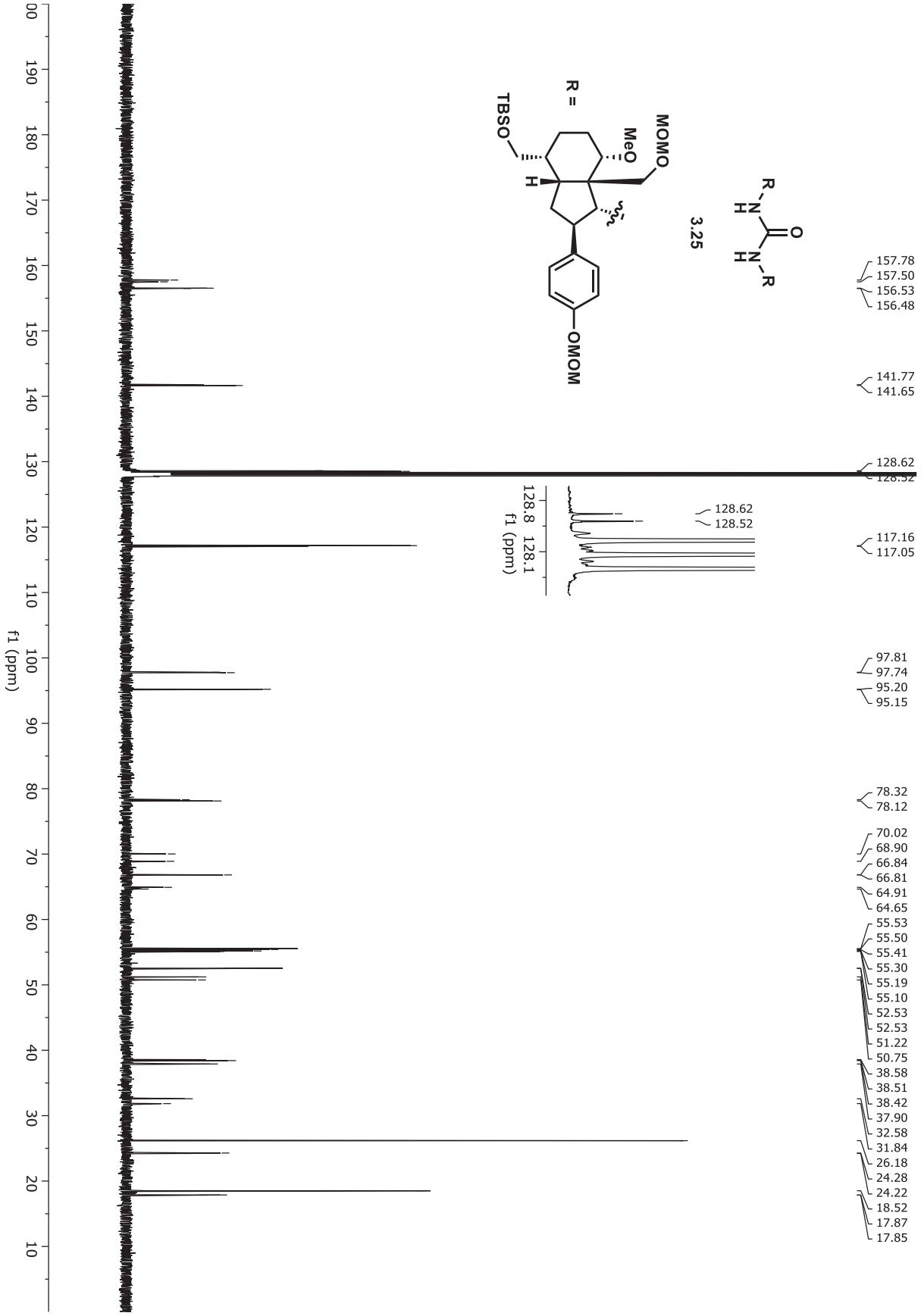
R =
TBSO
H
MeO
MOMO
OMOM
3.25
R
N
H
O
N
H
R
157.78
157.50
156.53
156.48
141.77
141.65
128.62
128.52
117.16
117.05
97.81
97.74
95.20
95.15
78.32
78.12
70.02
68.90
66.84
66.81
64.91
64.65
55.53
55.50
55.41
55.30
55.19
55.10
52.53
52.53
51.22
50.75
38.58
38.51
38.42
37.90
32.58
31.84
26.18
24.28
24.22
18.52
17.87
17.85
128.62
128.52
128.8
128.1
f1 (ppm)
f1 (ppm)

Spectrum at 298 K

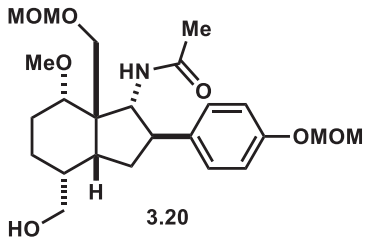

3.20

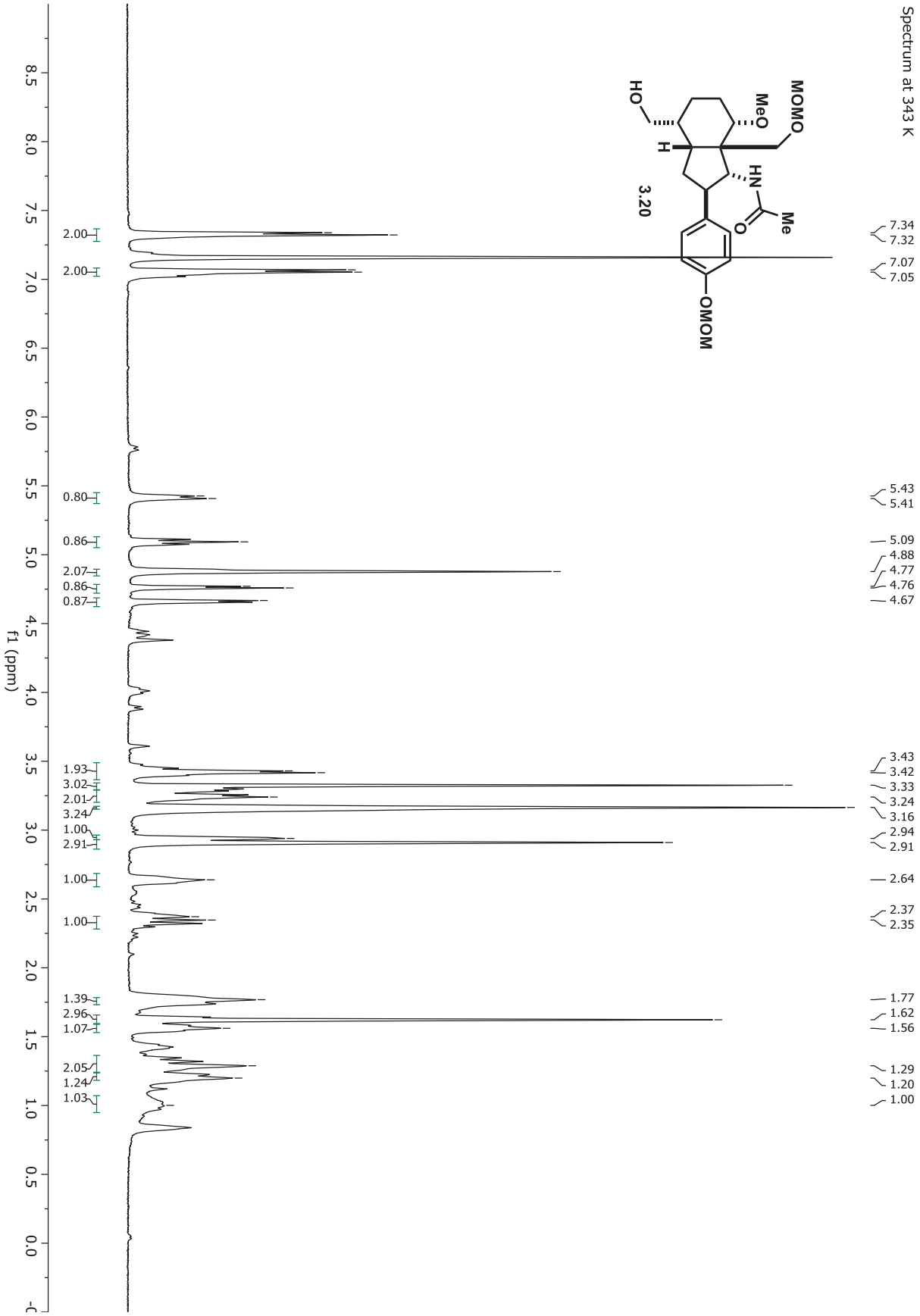
Spectrum at 343 K
f1 (ppm)
8.5
8.0
7.5
7.0
6.5
6.0
5.5
5.0
4.5
4.0
3.5
3.0
2.5
2.0
1.5
1.0
0.5
0.0
2.00
2.00
0.80
0.86
2.07
0.86
0.87
1.93
3.02
2.01
3.24
1.00
2.91
1.00
1.00
1.39
2.96
1.07
2.05
1.24
1.03
7.34
7.32
7.07
7.05
5.43
5.41
5.09
4.88
4.77
4.76
4.67
3.43
3.42
3.33
3.24
3.16
2.94
2.91
2.64
2.37
2.35
1.77
1.62
1.56
1.29
1.20
1.00
HO
H
MeO
MOMO
HN
Me
O
OMOM
3.20

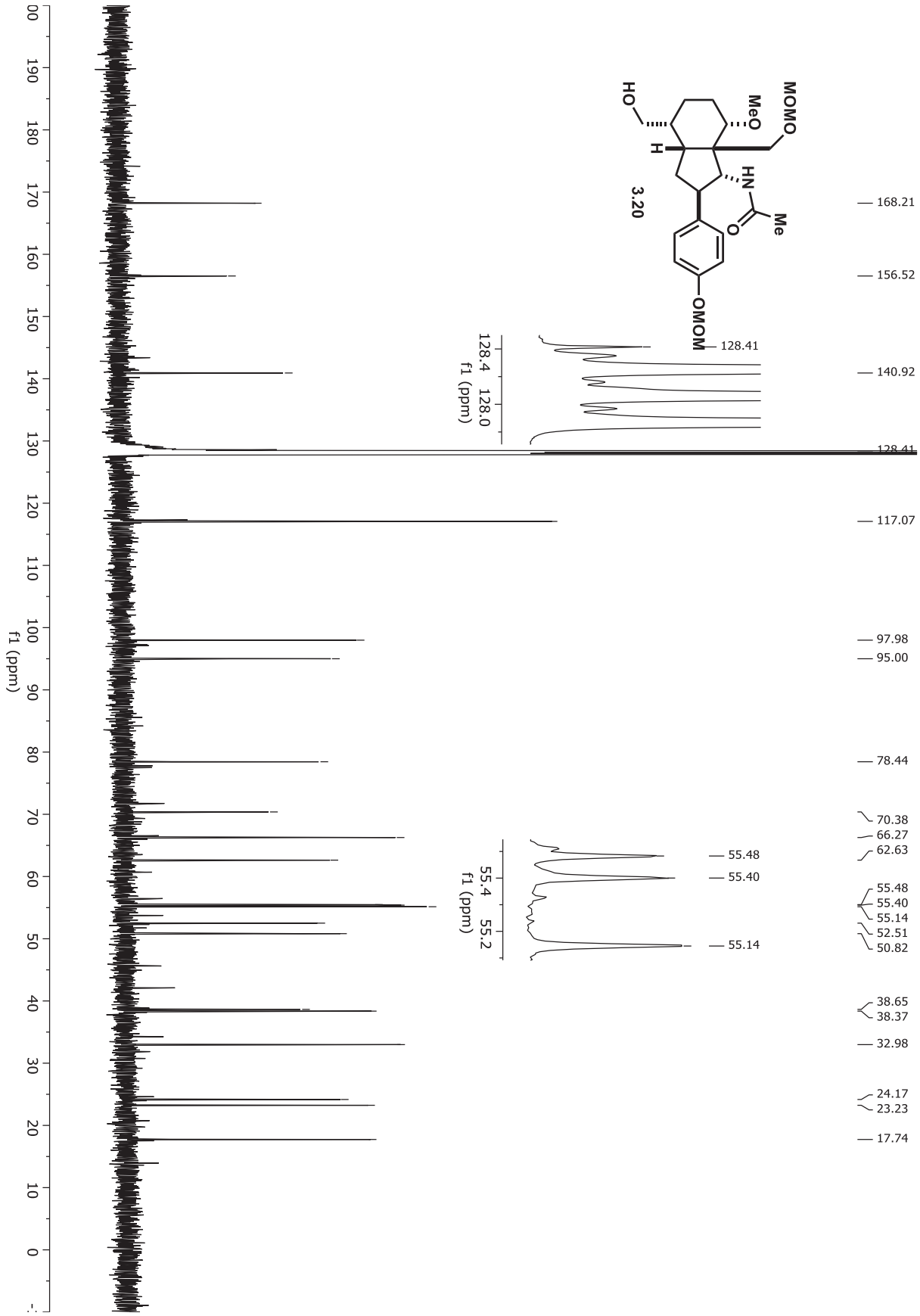
HO
MeO
MOMO
H
HN
Me
O
OMOM
3.20
168.21
156.52
128.41
140.92
128.41
117.07
97.98
95.00
78.44
70.38
66.27
62.63
55.48
55.40
55.14
52.51
50.82
38.65
38.37
32.98
24.17
23.23
17.74
f1 (ppm)

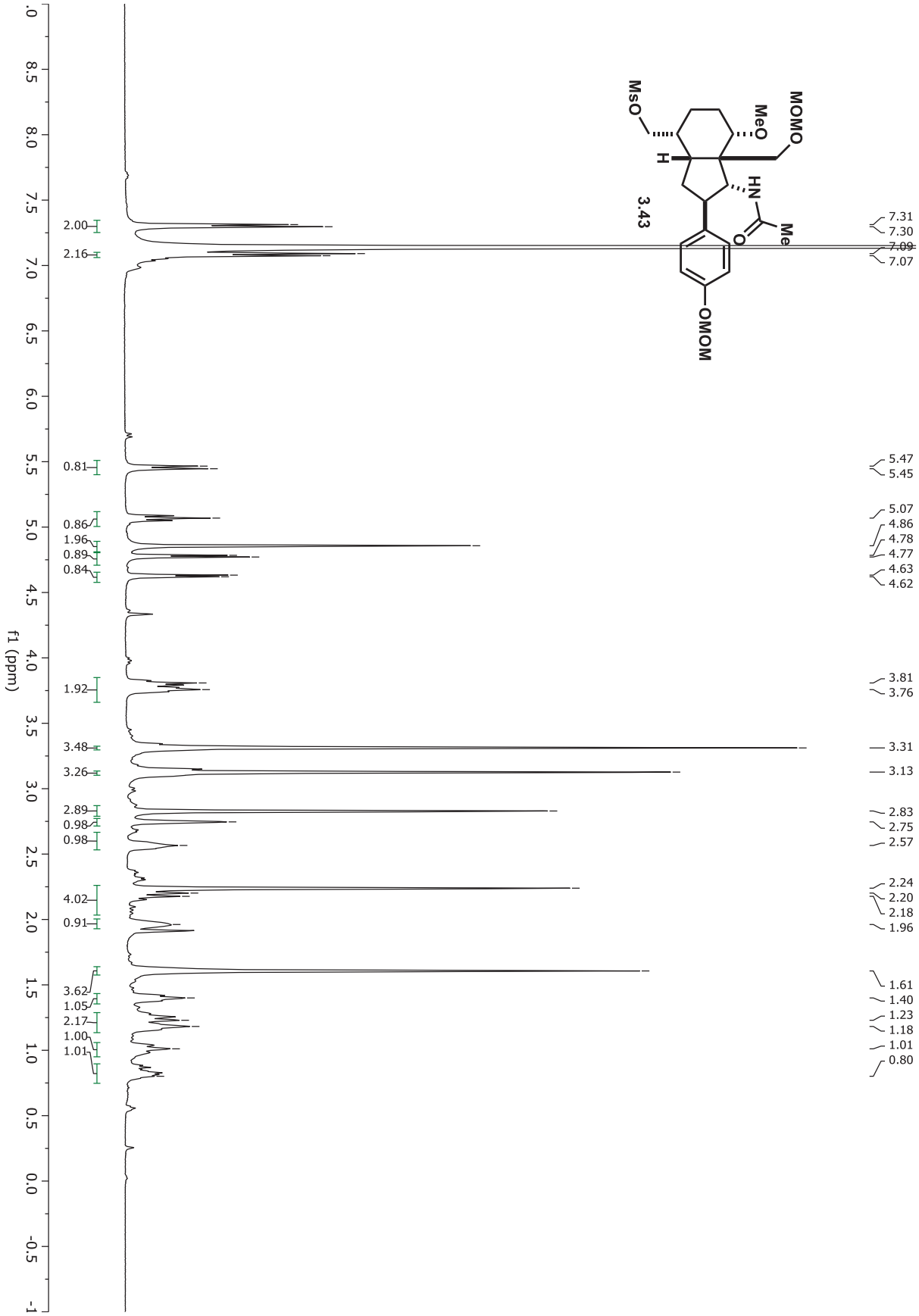
MsO
MeO
MOMO
H
HN
Me
O
OMOM
3.43
f1 (ppm)
2.00
2.16
0.81
0.86
1.96
0.89
0.84
1.92
3.48
3.26
2.89
0.98
0.98
4.02
0.91
3.62
1.05
2.17
1.00
1.01
7.31
7.30
7.09
7.07
5.47
5.45
5.07
4.86
4.78
4.77
4.63
4.62
3.81
3.76
3.31
3.13
2.83
2.75
2.57
2.24
2.20
2.18
1.96
1.61
1.40
1.23
1.18
1.01
0.80

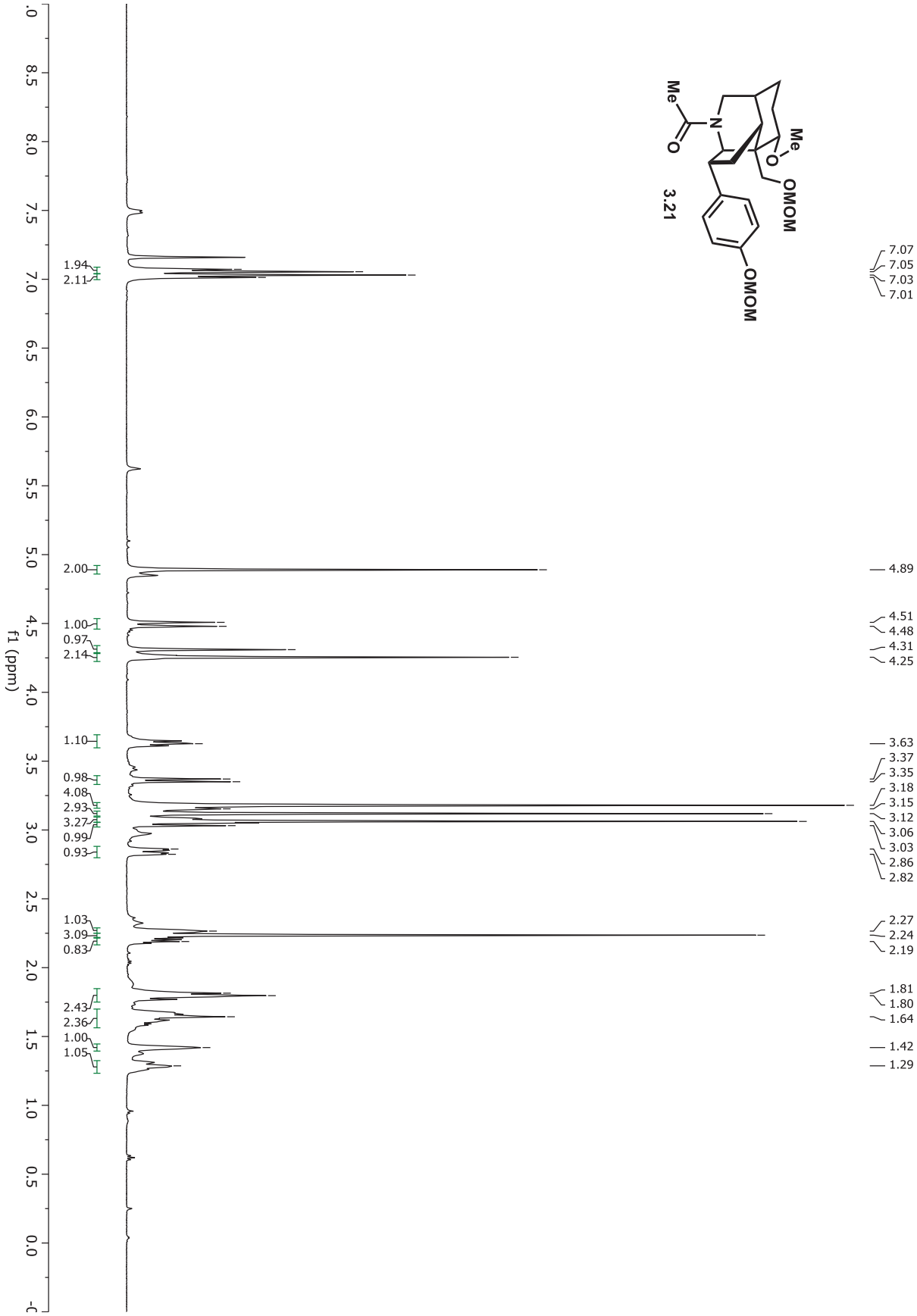
3.21
Me
N
O
Me
O
OMOM
OMOM
f1 (ppm)
1.94
2.11
2.00
1.00
0.97
2.14
1.10
0.98
4.08
2.93
3.27
0.99
0.93
1.03
3.09
0.83
2.43
2.36
1.00
1.05
7.07
7.05
7.03
7.01
4.89
4.51
4.48
4.31
4.25
3.63
3.37
3.35
3.18
3.15
3.12
3.06
3.03
2.86
2.82
2.27
2.24
2.19
1.81
1.80
1.64
1.42
1.29

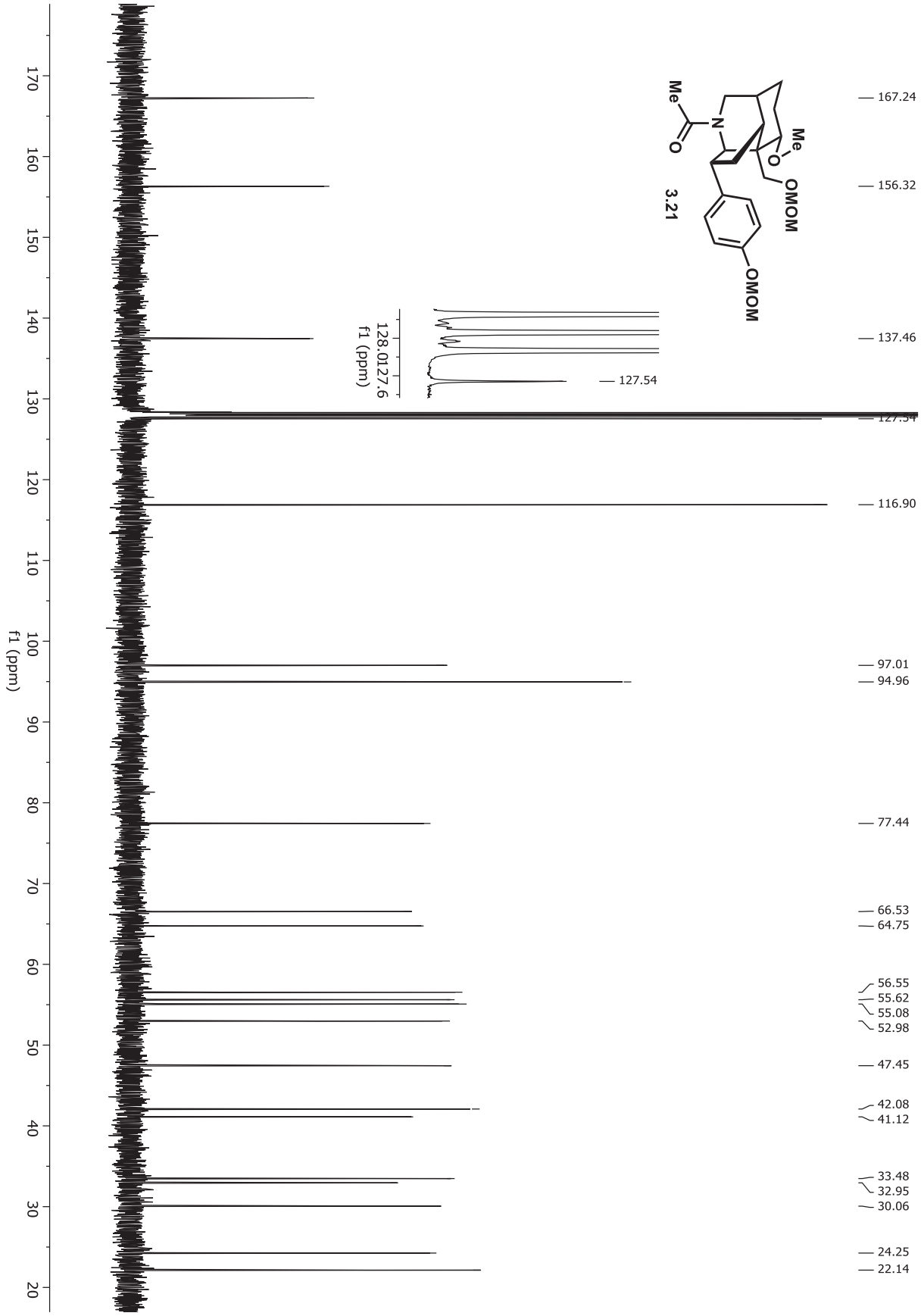
3.21
Me
N
O
Me
O
OMOM
OMOM
167.24
156.32
137.46
127.54
116.90
97.01
94.96
77.44
66.53
64.75
56.55
55.62
55.08
52.98
47.45
42.08
41.12
33.48
32.95
30.06
24.25
22.14
f1 (ppm)
128.0127.6
f1 (ppm)

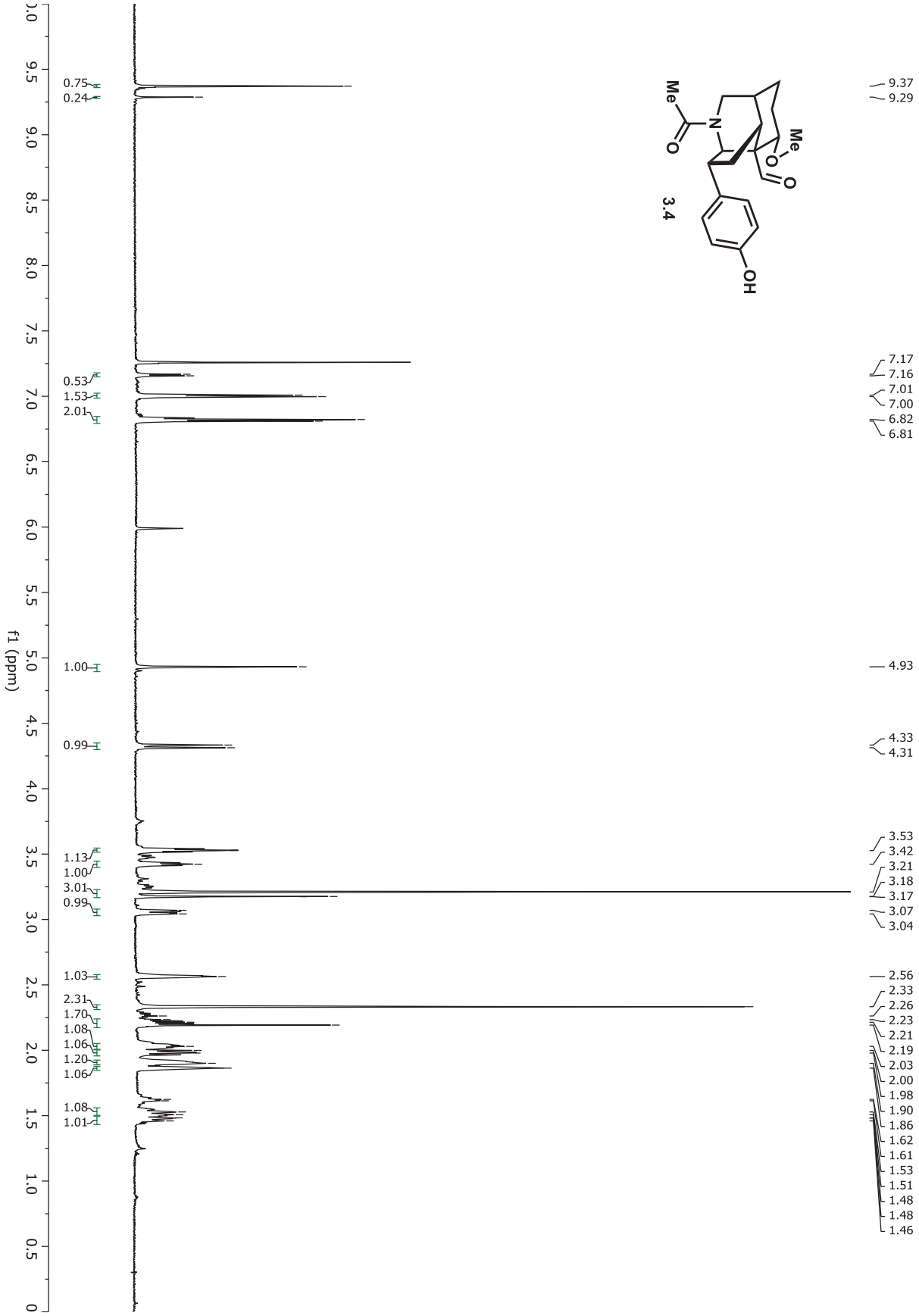
f1 (ppm)
10.0
9.5
9.0
8.5
8.0
7.5
7.0
6.5
6.0
5.5
5.0
4.5
4.0
3.5
3.0
2.5
2.0
1.5
1.0
0.5
0
0.75
0.24
0.53
1.53
2.01
1.00
0.99
1.13
1.00
3.01
0.99
1.03
2.31
1.70
1.08
1.06
1.20
1.06
1.08
1.01
Me
N
O
Me
O
O
OH
3.4
9.37
9.29
7.17
7.16
7.01
7.00
6.82
6.81
4.93
4.33
4.31
3.53
3.42
3.21
3.18
3.17
3.07
3.04
2.56
2.33
2.26
2.23
2.21
2.19
2.03
2.00
1.98
1.90
1.86
1.62
1.61
1.53
1.51
1.48
1.48
1.46

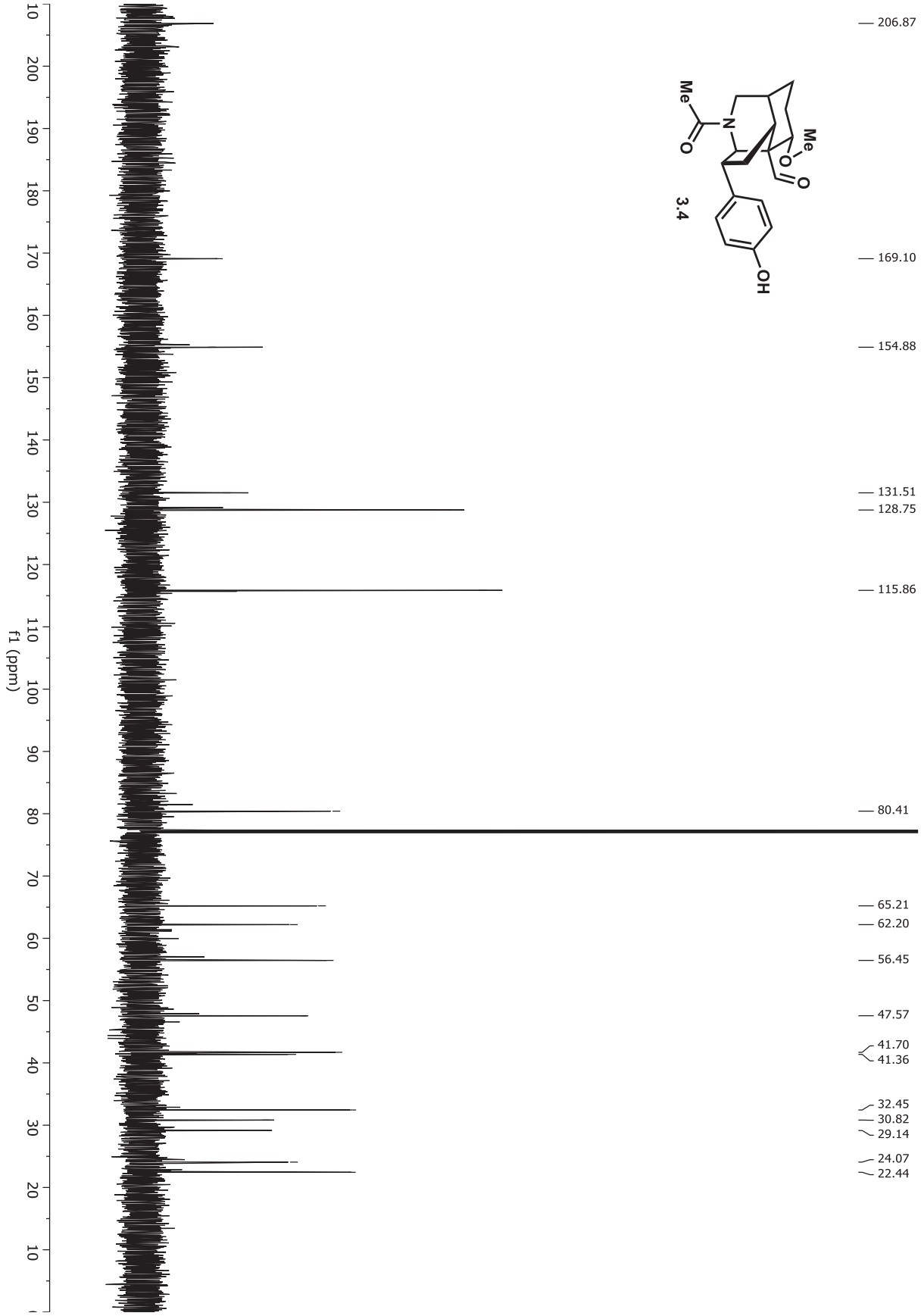
206.87
169.10
154.88
131.51
128.75
115.86
80.41
65.21
62.20
56.45
47.57
41.70
41.36
32.45
30.82
29.14
24.07
22.44
f1 (ppm)
Me
O
N
Me
O
O
OH
3.4

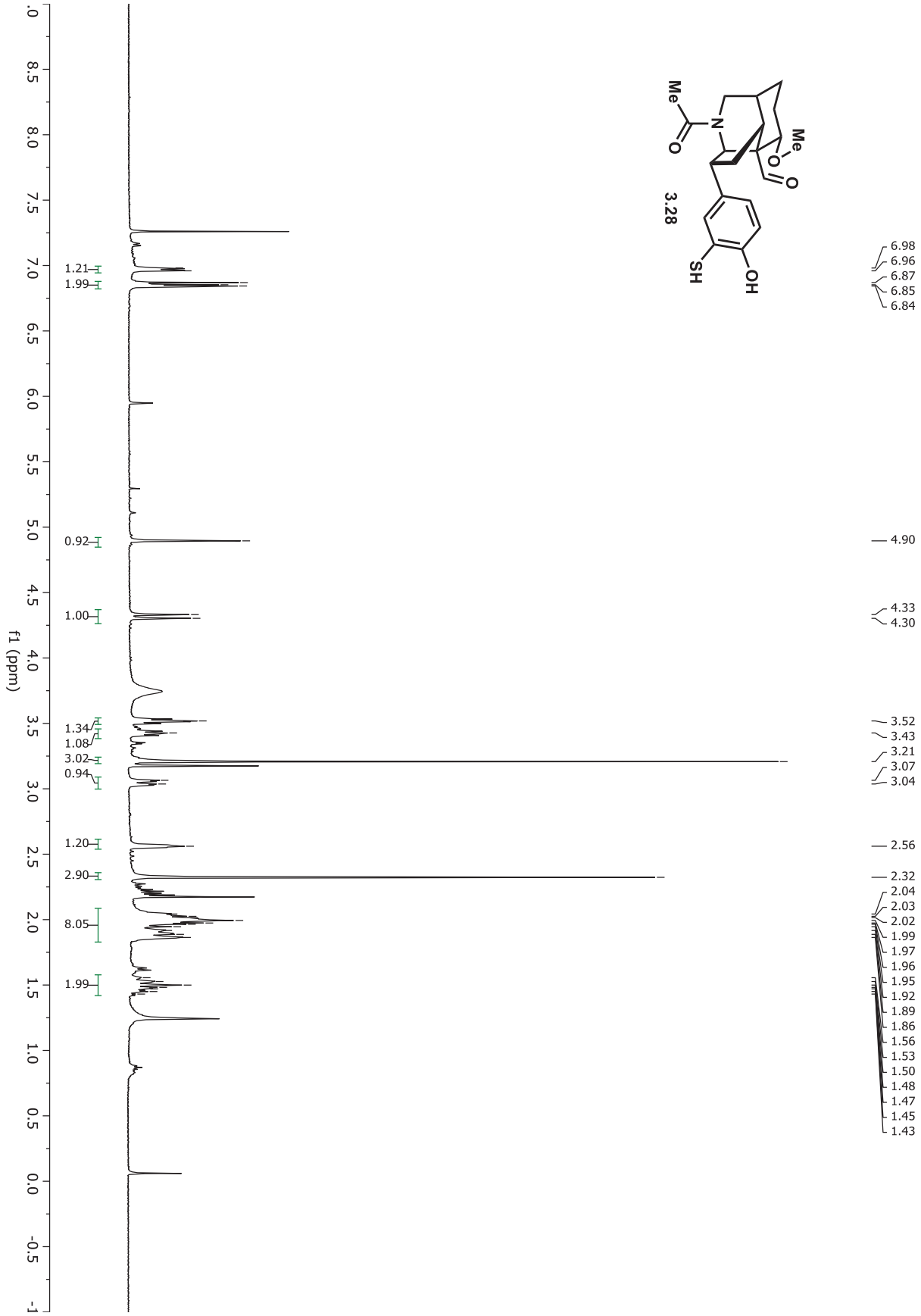
f1 (ppm)
1.21
1.99
0.92
1.00
1.34
1.08
3.02
0.94
1.20
2.90
8.05
1.99
3.28
Me
N
O
Me
O
O
SH
OH
6.98
6.96
6.87
6.85
6.84
4.90
4.33
4.30
3.52
3.43
3.21
3.07
3.04
2.56
2.32
2.04
2.03
2.02
1.99
1.97
1.96
1.95
1.92
1.89
1.86
1.56
1.53
1.50
1.48
1.47
1.45
1.43

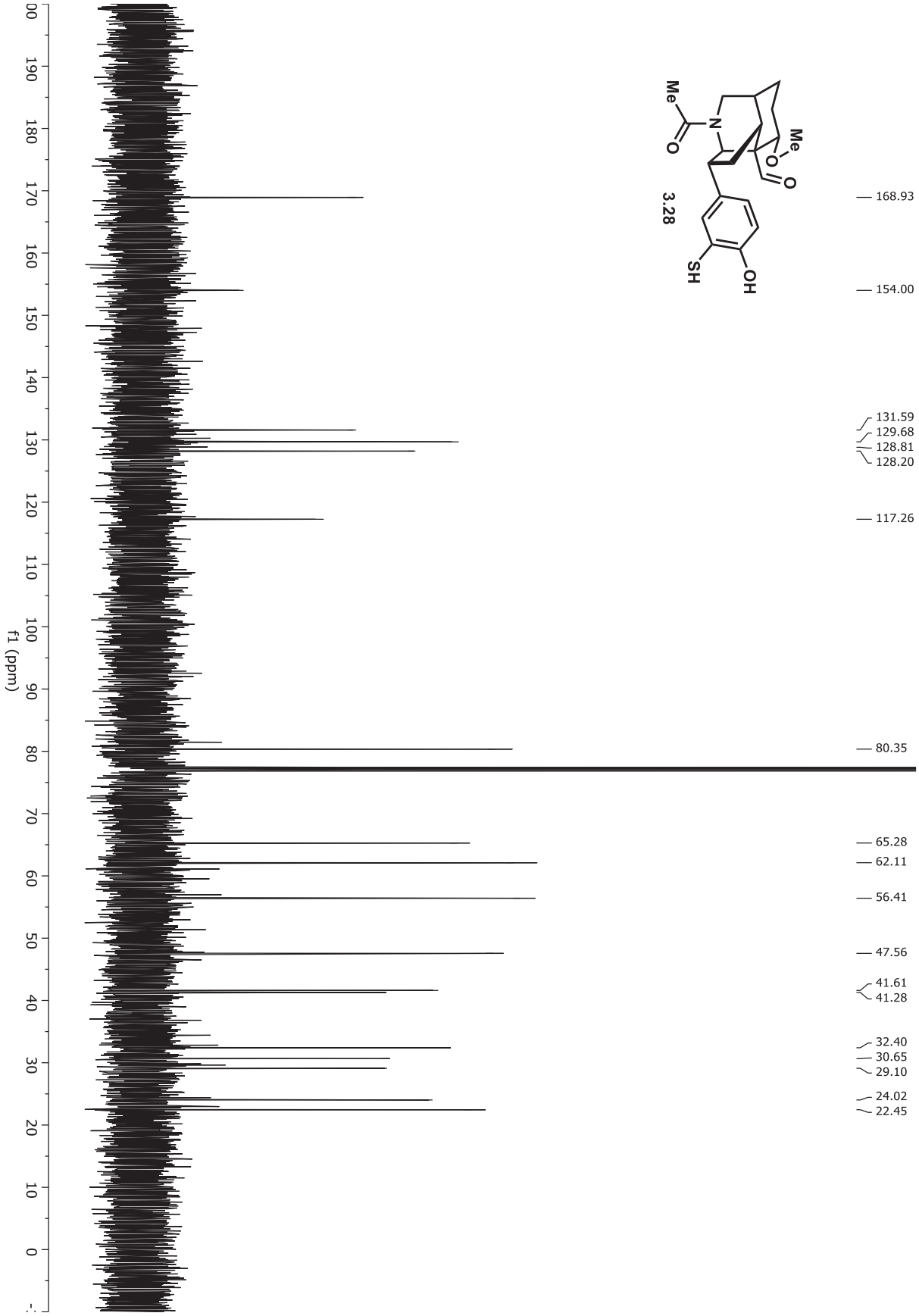
Me
N
O
Me
O
O
3.28
SH
OH
168.93
154.00
131.59
129.68
128.81
128.20
117.26
80.35
65.28
62.11
56.41
47.56
41.61
41.28
32.40
30.65
29.10
24.02
22.45
f1 (ppm)

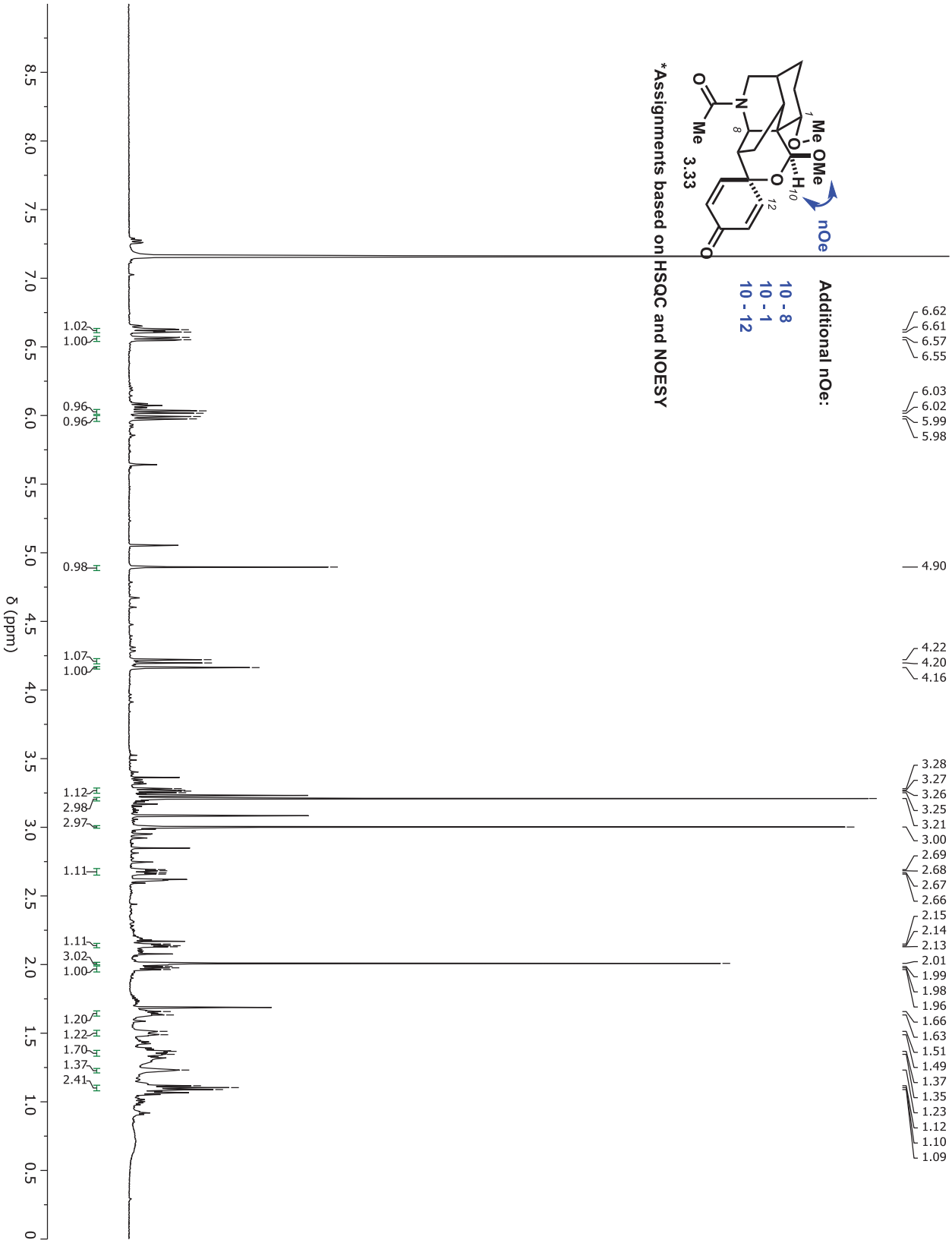
*Assignments based on HSQC and NOESY
Additional nOe:
10 - 8
10 - 1
10 - 12
nOe
Me OMe
Me
3.33
δ (ppm)
8.5
8.0
7.5
7.0
6.5
6.0
5.5
5.0
4.5
4.0
3.5
3.0
2.5
2.0
1.5
1.0
0.5
0
1.02
1.00
0.96
0.96
0.98
1.07
1.00
1.12
2.98
2.97
1.11
1.11
3.02
1.00
1.20
1.22
1.70
1.37
2.41
6.62
6.61
6.57
6.55
6.03
6.02
5.99
5.98
4.90
4.22
4.20
4.16
3.28
3.27
3.26
3.25
3.21
3.00
2.69
2.68
2.67
2.66
2.15
2.14
2.13
2.01
1.99
1.98
1.96
1.66
1.63
1.51
1.49
1.37
1.35
1.23
1.12
1.10
1.09

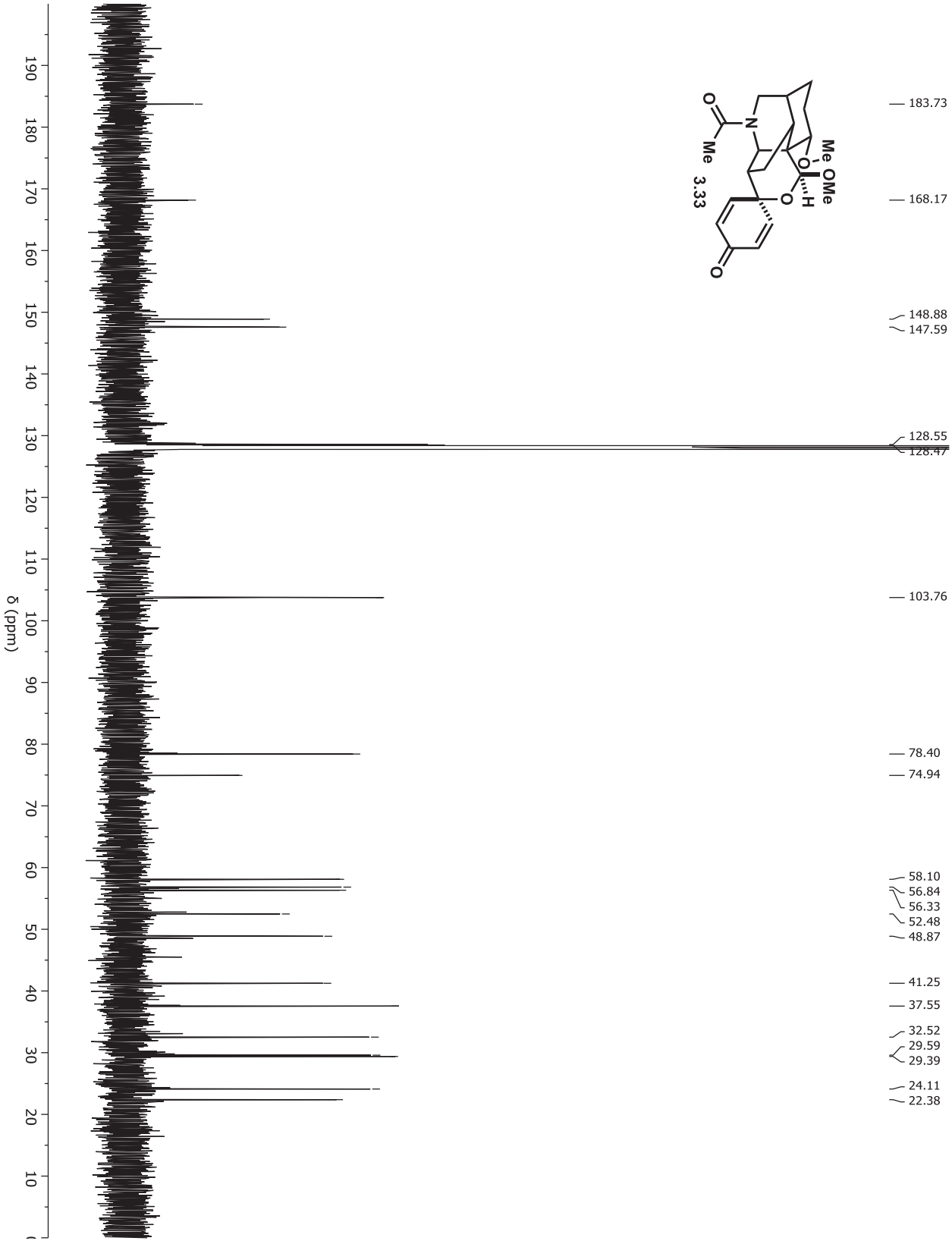
δ (ppm)
190
180
170
160
150
140
130
120
110
100
90
80
70
60
50
40
30
20
10
Me
3.33
Me OMe
183.73
168.17
148.88
147.59
128.55
128.47
103.76
78.40
74.94
58.10
56.84
56.33
52.48
48.87
41.25
37.55
32.52
29.59
29.39
24.11
22.38

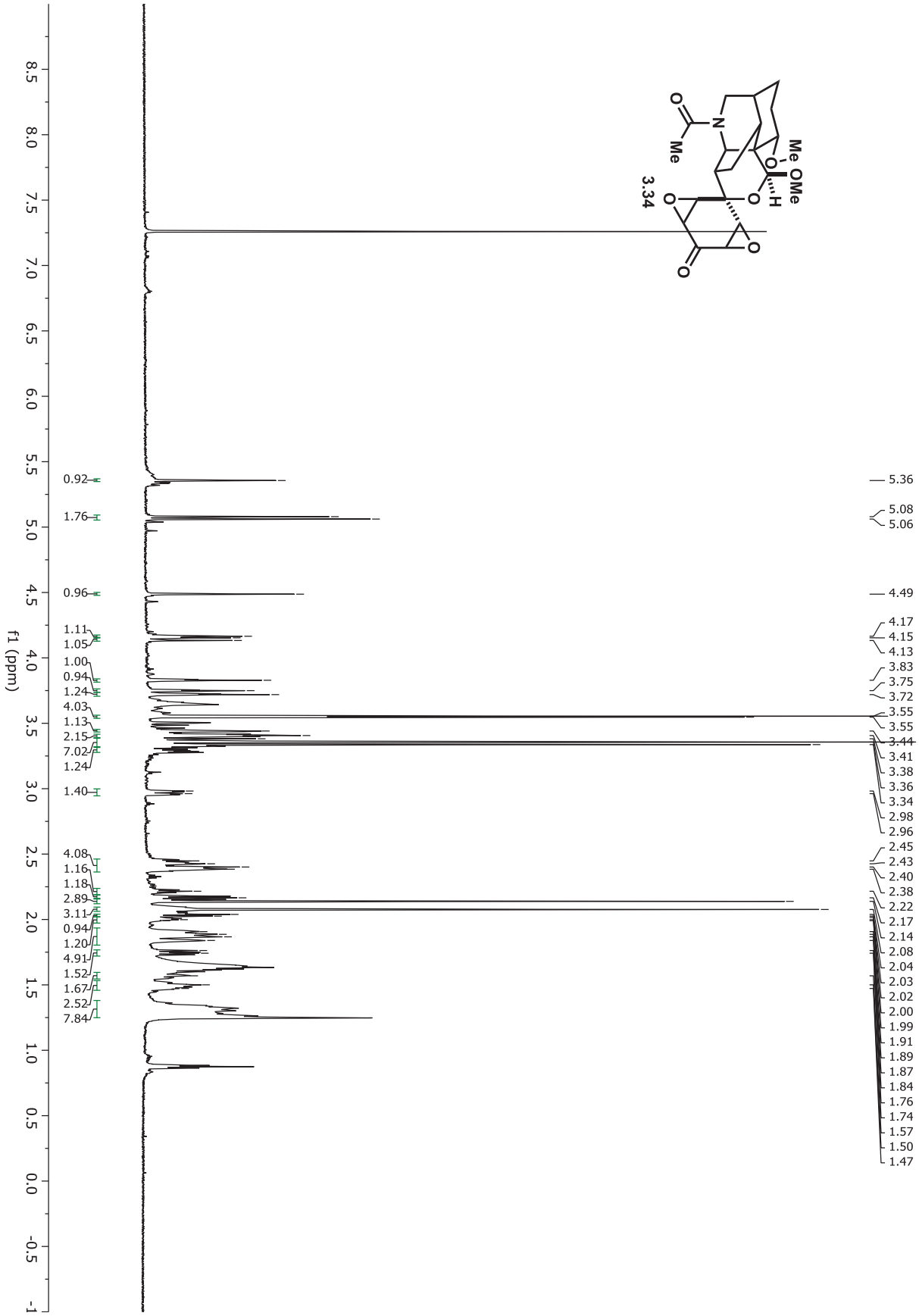
3.34
Me
OMe
H
f1 (ppm)
8.5
8.0
7.5
7.0
6.5
6.0
5.5
5.0
4.5
4.0
3.5
3.0
2.5
2.0
1.5
1.0
0.5
0.0
-0.5
-1
0.92
1.76
0.96
1.11
1.05
1.00
0.94
1.24
4.03
1.13
2.15
7.02
1.24
1.40
4.08
1.16
1.18
2.89
3.11
0.94
1.20
4.91
1.52
1.67
2.52
7.84
5.36
5.08
5.06
4.49
4.17
4.15
4.13
3.83
3.75
3.72
3.55
3.55
3.44
3.41
3.38
3.36
3.34
2.98
2.96
2.45
2.43
2.40
2.38
2.22
2.17
2.14
2.08
2.04
2.03
2.02
2.00
1.99
1.91
1.89
1.87
1.84
1.76
1.74
1.57
1.50
1.47

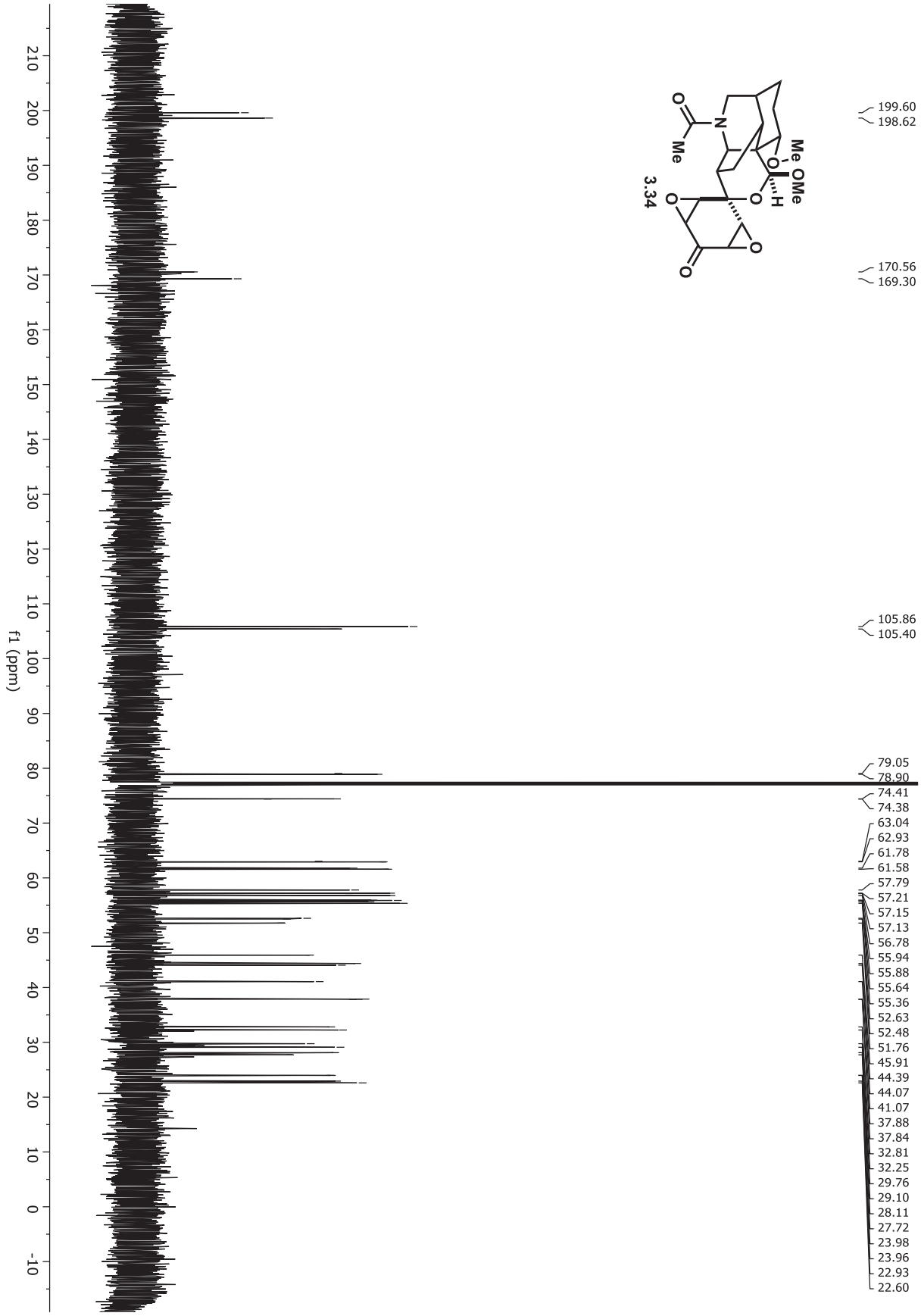
3.34
Me
Me OMe
H
199.60
198.62
170.56
169.30
105.86
105.40
79.05
78.90
74.41
74.38
63.04
62.93
61.78
61.58
57.79
57.21
57.15
57.13
56.78
55.94
55.88
55.64
55.36
52.63
52.48
51.76
45.91
44.39
44.07
41.07
37.88
37.84
32.81
32.25
29.76
29.10
28.11
27.72
23.98
23.96
22.93
22.60
f1 (ppm)

Appendix 3.B X-Ray crystallography data for Chapter 3

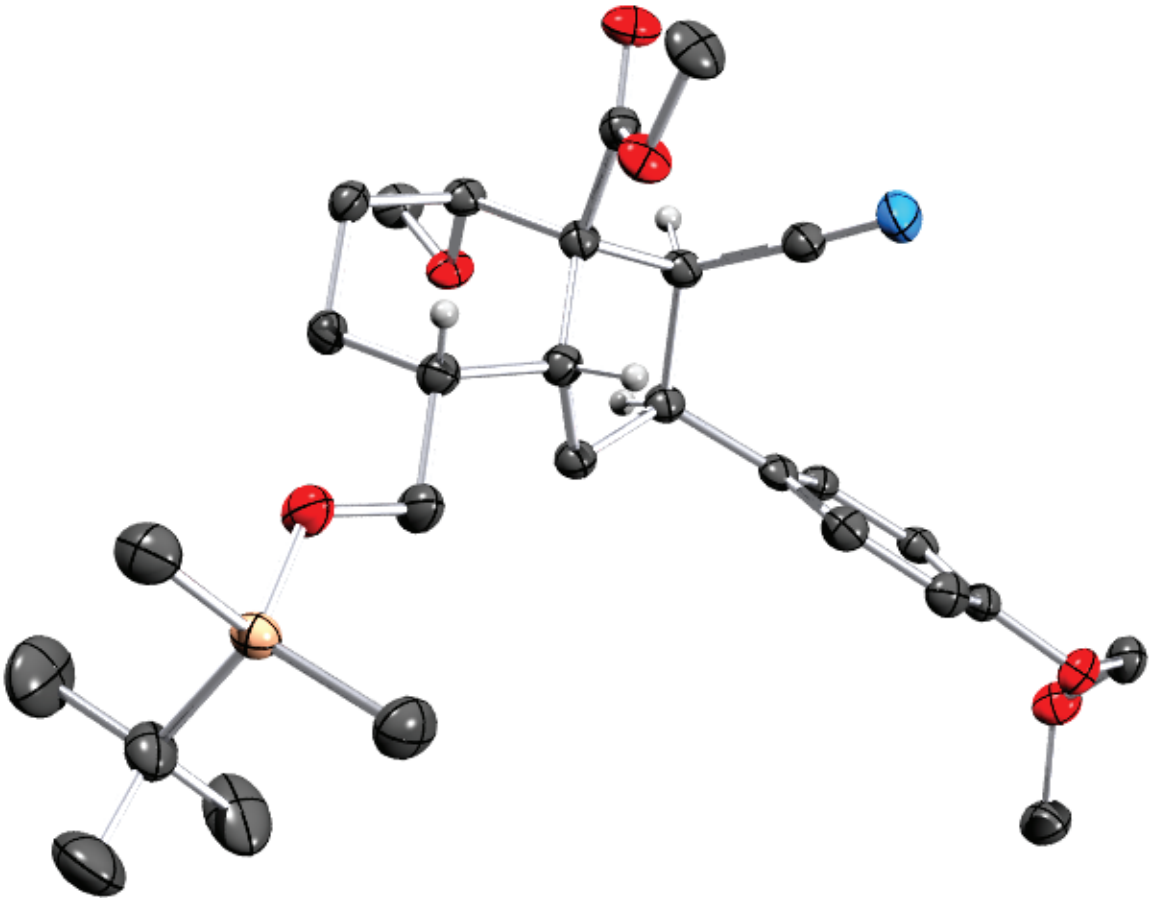

Figure 3.12: POV-Ray/ORTEP rendering of minor conjugate addition product β-**3.6d** with ellipsoids at 50% probability. Only tertiary and vinylic hydrogens are shown for clarity.

Table 3.2: Crystal data and structure refinement for tricycle β-**3.6d**.

Cambridge Crystallographic Data Center	1859315
Empirical formula	C28 H43 N O6 Si
Formula weight	517.72
Temperature	100(2) K
Wavelength	1.54178 Å
Crystal system	Monoclinic
Space group	P 21/c
Unit cell dimensions	a = 16.0538(5) Å α = 90°
	b = 15.9623(5) Å β = 93.733(2)°
	c = 11.2628(3) Å γ = 90°
Volume	2880.03(15) Å^3
Z	4
Density (calculated)	1.194 Mg/m^3
Absorption coefficient	1.043 mm^{-1}
F(000)	1120
Crystal size	0.060 x 0.040 x 0.020 mm^3
Theta range for data collection	2.758 to 68.357°
Index ranges	-19<=h<=19, -19<=k<=19, -11<=l<=13
Reflections collected	80807
Independent reflections	5282 [R(int) = 0.0457]
Completeness to theta = 67.000°	99.9%
Absorption correction	Semi-empirical from equivalents
Max. and min. transmission	0.929 and 0.782
Refinement method	Full-matrix least-squares on F^2
Data / restraints / parameters	5282 / 0 / 333
Goodness-of-fit on F^2	1.078
Final R indices [I>2sigma(I)]	R1 = 0.0519, wR2 = 0.1338
R indices (all data)	R1 = 0.0546, wR2 = 0.1362
Extinction coefficient	n/a
Largest diff. peak and hole	0.435 and -0.364 e.Å^{-3}

Chapter 4

Total synthesis of somaliensene A

4.1 Toward the total synthesis of somaliensene A through deoxygenation of a carvone-derived pinene scaffold

4.1.1 Introduction

Cyclic sesterterpenes somaliensene A (**4.1**) and B (**4.2**) were isolated by Liu et al. in 2018 from a culture of *E. coli* (engineered strain BW25113) heterologously expressing a potential terpene cyclase gene from *Streptomyces somaliensis*.[1] This gene (*stsC*) was identified as part of a larger gene cluster during a broader genome mining effort to discover novel diterpenes. Based on homology of the encoded enzyme with other terpene cyclases and a series of incubation experiments, **4.1** and **4.2** were proposed to arise from geranylfarnesyl pyrophosphate (**4.3**, Scheme 4.1). Liu proposed that **4.3** isomerizes to terminal alkene **4.4**, then ionizes and undergoes 1,6-cycliza-

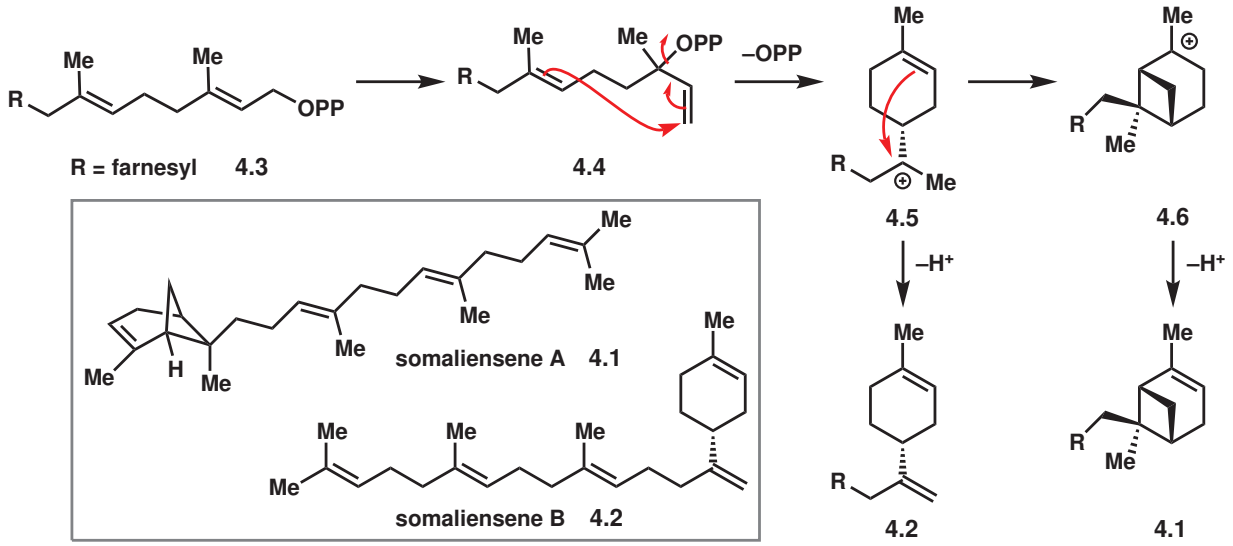

Scheme 4.1: Proposed biosynthesis of sesterterpenes somaliensene A (**4.1**) and B (**4.2**).

tion to give carbocation **4.5**. Loss of a proton from this intermediate gives somaliensene B (**4.2**). Carbocation **4.5** can instead cyclize to forge a [3.1.1] bicycle (**4.6**), which then loses a proton to afford somaliensene A (**4.1**).

That the somaliensenes are derived from geranylfarnesyl pyrophosphate is typical of sesterterpene natural products.[2,3] Less typical is the fact that the cyclase enzyme came from *Streptomyces*; prior to their isolation, only one of ~1000 characterized sesterterpenes had been isolated from a bacterial source.[1] The majority of reported sesterterpenes are derived from either marine sponges or terrestrial fungi. This rare class of terpenes features a host of structurally diverse scaffolds and remains largely unexplored. Early studies have shown that these compounds are often implicated in organism defense,[4,5] with potential applications as anti-inflammatory, antimicrobial, and anti-cancer agents.[6,7] Given that *Streptomyces* species are well known as sources of biologically active secondary natural products,[8] we were interested in synthesizing the somaliensenes and exploring the bioactivities of these unusual sesterterpenes.

Of particular interest to us was the more topologically complex somaliensene A (**4.1**), which we envisioned could be derived from an unnatural pinene oxide (**4.8**) through coupling with farnesyl bromide (**4.7**) in the forward sense (Scheme 4.2). Pinene oxide **4.8** could, in turn, be obtained through a key deoxygenation of known diol **4.9**, which can be synthesized from (*S*)-carvone (**4.10**).

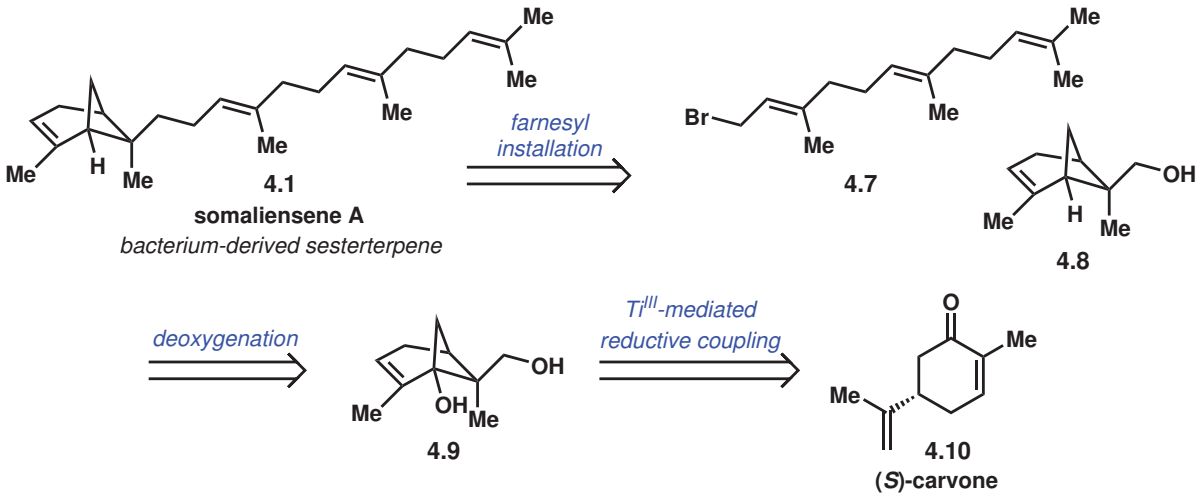

Scheme 4.2: Retrosynthesis of somaliensene A through deoxygenation of a pinene scaffold derived from (*S*)-carvone.

4.1.2 First generation route toward somaliensene A

The forward synthesis of somaliensene A began with epoxidation of (*S*)-carvone (**4.10**) to give epoxycarvone (**4.11**, 1:1 dr), which could then undergo titanium-mediated reductive cyclization to afford known diols **4.9** and **4.12** (Scheme 4.3).[9,10] With major diastereomer **4.9** in hand, we began to look at deoxygenation conditions.[11,12] We first attempted Barton–McCombie type deoxygenation of a cyclic thiocarbonate (**4.14**). However, we never obtained thiocarbonate **4.14**.

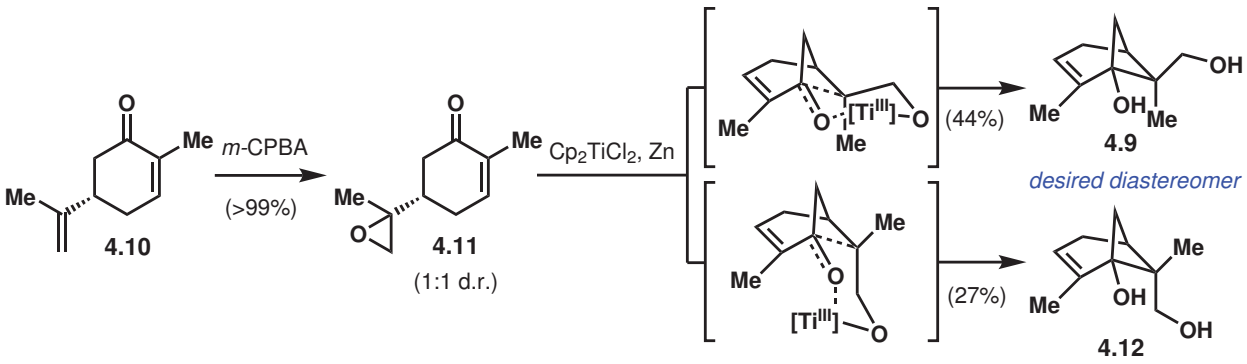

Scheme 4.3: Synthesis of diols **4.9** and **4.12** from (*S*)-carvone.

We instead observed regeneration of carvone (**4.10**), which we believe occurs through Grob fragmentation of intermediate **4.13** (Scheme 4.4).

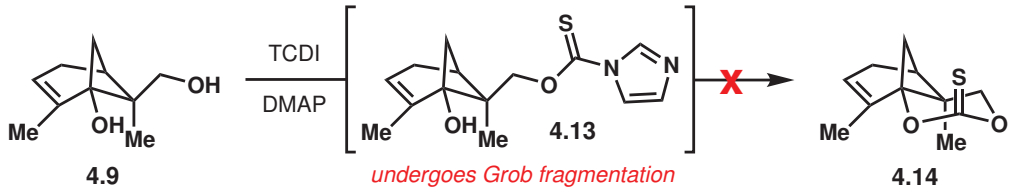

Scheme 4.4: Unsuccessful attempt to synthesize a cyclic thiocarbonate.

This fragmentation pathway could be shut down by protecting the primary hydroxy group of **4.9** as a silyl ether (**4.15**, Scheme 4.5). Exploration of alcohol **4.15** as a deoxygenation substrate was limited by its lack of reactivity, presumably due to steric constraints. As such, no conversion was observed when **4.15** was treated with TCDI, phenyl chlorodithioformate, acyl chlorides, PMBCl, or BOMCl, among others. This held true in a variety of solvent systems, even upon addition of different bases and/or heating to reflux. We were, however, able to make the methyl xanthate (**4.16**) of **4.15** by first treating with NaH and phase-transfer catalyst TBAI, then adding CS_2 and quenching with MeI. Still, full conversion to **4.16** was only achieved with superstoichiometric quantities of all reagents, which necessitated purification of this unstable product. Attempts to use the crude product in various deoxygenation reactions were unsuccessful.

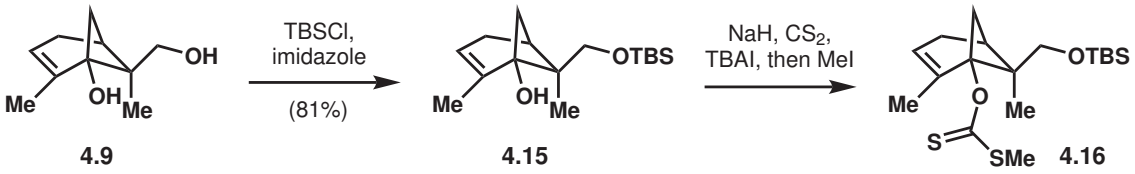

Scheme 4.5: Synthesis of Barton–McCombie deoxygenation substrate **4.16**.

It was also possible to acetylate alcohol **4.15** to give silyl ether **4.17**. Treatment with samarium iodide or with sodium and *t*-$BuNH_2$, known to effect deoxygenation of some esters,[13–15] led to decomposition of the starting material. We then looked at dissolving metal reduction of this substrate based on precedent showing that, upon single electron transfer to the ester, fragmentation of the resultant radical anion (**4.18**) to give a tertiary alkyl radical (**4.19**) can be

faster than a second single electron reduction (Scheme 4.6). However, in this case, we instead

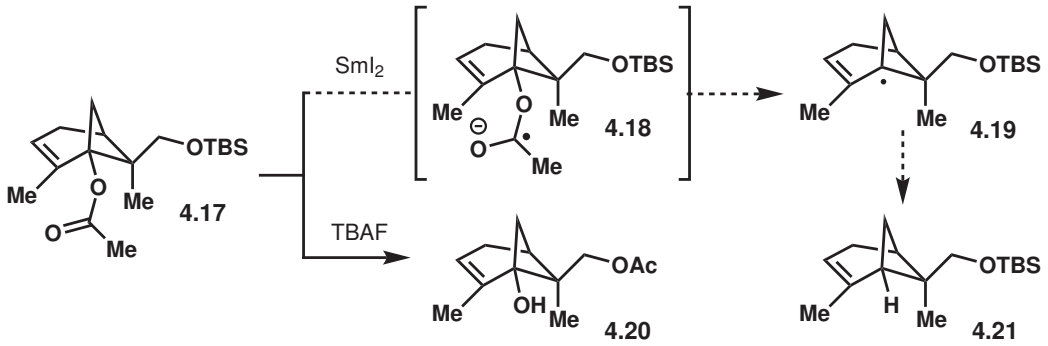

Scheme 4.6: Synthesis of Barton–McCombie deoxygenation substrate **4.16**.

observed formation of diol **4.9**, indicating that the second reduction was favored over fragmentation. Wondering if the silyl ether was interfering with this reaction, we treated **4.17** with TBAF to cleave the TBS group. The goal from there would be to install the farnesyl side chain prior to deoxygenation. However, while the silyl ether was cleaved successfully, the acetate group migrated to the primary hydroxy group, affording **4.20** as the major product.

Following up on this idea of installing the farnesyl side chain prior to deoxygenation, we attempted alkylation of **4.15** on the basis of the low migratory aptitude of alkyl groups. While removal of an alkyl ether later would be challenging, we were primarily interested in such compounds as a model system. Methylation of tertiary alcohol **4.15** to give ether **4.22** was possible but required use of both NaH and phase-transfer catalyst TBAI (Scheme 4.7). Upon treatment with TBAF to cleave the silyl ether, decomposition was observed. Given the instability of the TBS-cleavage product of methyl ether **4.22** relative to diol **4.9**, we next attempted farnesyl installation on **4.9** itself. Since installation of leaving groups on the primary alcohol had been shown to induce Grob fragmentation, we instead considered an oxidation–Wittig olefination approach, which would require selective hydrogenation of the newly formed alkene. However, while oxidation to aldehyde **4.23** could be achieved using PCC or DMP, retro-aldol processes were observed under acidic, basic, and neutral conditions to give complex mixtures of aldehyde-containing products.

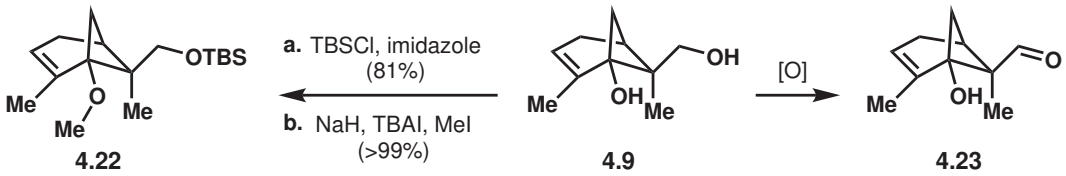

Scheme 4.7: Attempts to install farnesyl side chain prior to deoxygenation.

On the basis of this tendency toward fragmentation, we returned to the original strategy of effecting Barton–McCombie-type deoxygenation prior to farnesyl installation. Having found acetate **4.17** to be more stable than xanthate **4.16**, we began to investigate oxalate esters as substrates for deoxygenation, building on precedent from MacMillan and co-workers.[16] Formation of mixed oxalate ester **4.24** proceeded smoothly, the product stable on silica gel and showing

no signs of degradation upon standing in a vial at room temperature for weeks. We then treated oxalate ester **4.24** with AIBN and *n*-Bu_3SnH in hopes of obtaining deoxygenated bicycle **4.21** (Scheme 4.8). When 0.5 equiv of AIBN and superstoichiometric amounts of stannane were used, the major product was silyl ether **4.15**. We believe that this product is formed through formation of an acetal radical (**4.26**) that, rather than fragment to give the desired bridgehead radical (**4.19**), instead directly abstracts a hydrogen atom from *n*-Bu_3SnH to give acetal **4.25**. This acetal could then hydrolyze upon work-up to return precursor **4.15**. Use of a 1:2 ratio of AIBN:*n*-Bu_3SnH should then shut down this pathway, the initiation by AIBN consuming all of the *n*-Bu_3SnH, leaving only stannyl radicals to interact with oxalate ester **4.24**. Under these conditions, we instead observed deoxygenated stannane **4.27** as the major product.

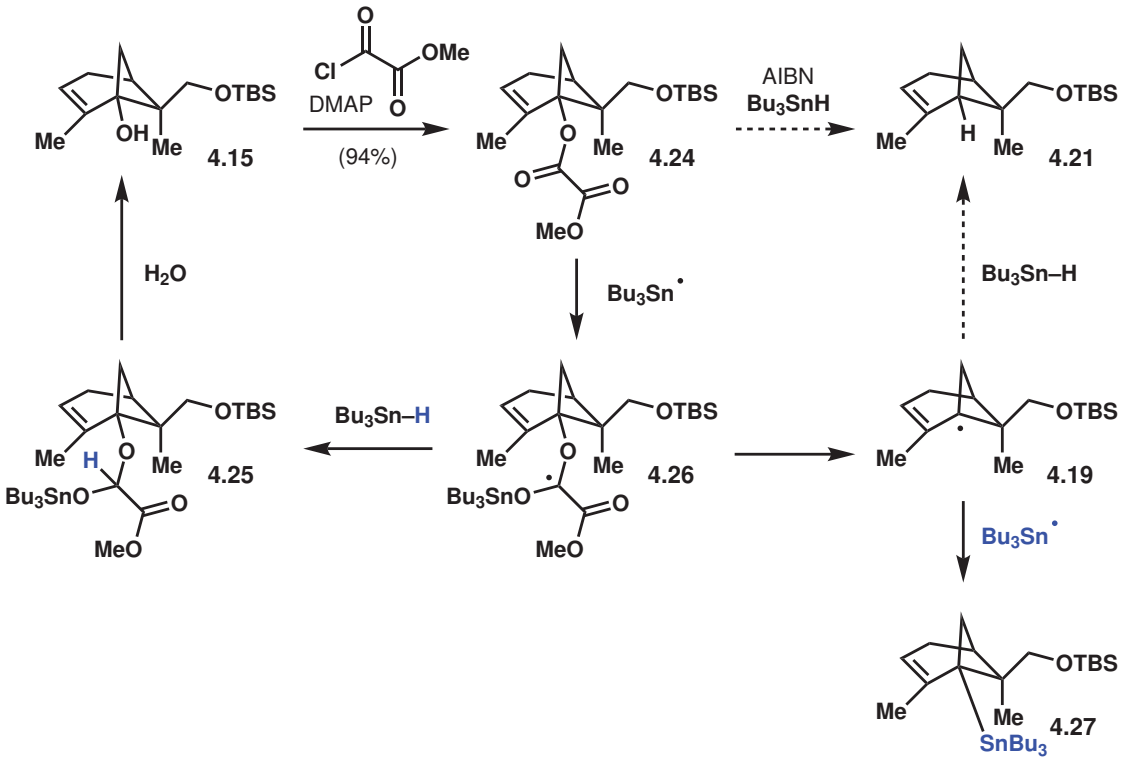

Scheme 4.8: Attempted Barton–McCombie deoxygenation of oxalate ester **4.24**.

Unfortunately, attempts to achieve proto-destannylation through treatment with various acids were unsuccessful. Treatment with *n*-BuLi to form the stannate (**4.28**), followed by addition of acid was similarly unsuccessful (Scheme 4.9). This transformation relies upon protonation of an intermediate (**4.29**) in which the C–Sn bond is already broken and thus requires an equi-

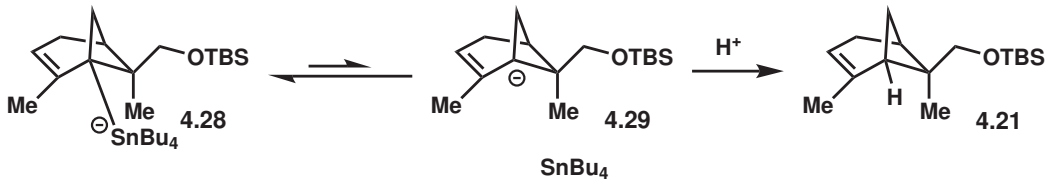

Scheme 4.9: Attempted proto-destanylation of stannane **4.27**.

librium to be established between carbanion **4.29** and stannate **4.28**. This does not seem to occur in our system. Still, as stannane **4.27** likely arises through an intermediate bridgehead radical (**4.19**), we turned our attention to other deoxygenation strategies that would intercept this intermediate radical.

4.1.3 Deoxygenation using iridium photocatalysis*

Radical decarboxylation under photocatalytic conditions has emerged as an entry into a wide variety of chemical transformations.[18–21] While the majority of the precedent in this field has involved mono-decarboxylation to break a C–C bond, there have also been reports of double decarboxylation of oxalic acid derivatives to instead break a C–O bond. Given our ability to access oxalate ester **4.24**, we were particularly interested in reports by Overman[22] and MacMillan[23] on iridium-catalyzed photoredox reactions using similar substrates (Scheme 4.10).

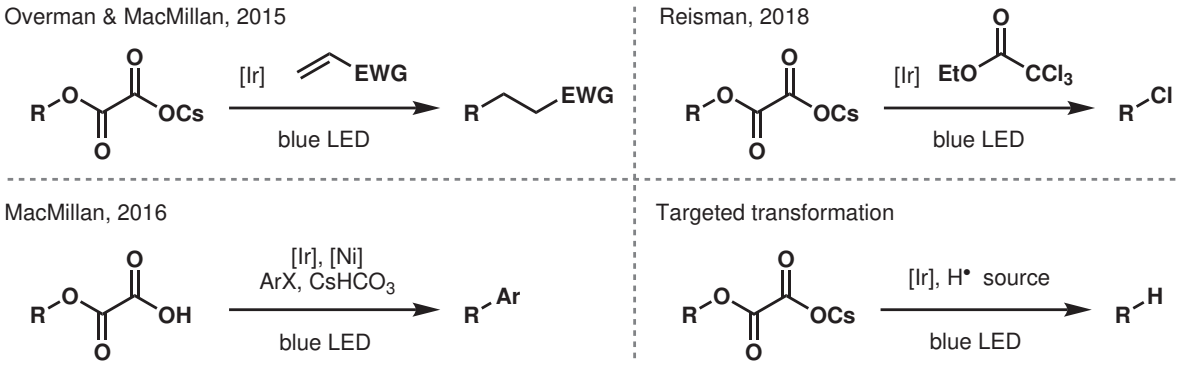

Scheme 4.10: Precedent for iridium photocatalysis using cesium oxalates by Overman,[22] MacMillan,[23] and Reisman.[24]

Looking to adapt this precedent to our desired deoxygenation, we first synthesized the cesium oxalate (**4.30**, Scheme 4.11). This could be achieved in two ways, proceeding through either the oxalic acid monoester (**4.31**) or the methyl ester (**4.24**). Both proceeded in nearly quantitative yield, the slightly lower yield of the methyl ester route being offset by an increase in purity of the material obtained since **4.24** could be purified by flash column chromatography, unlike acid **4.31** or cesium oxalate **4.30**.

Cesium oxalate **4.30** was treated with photocatalyst $Ir[dF(CF_3)ppy]_2(dtbby)PF_6$ and irradiated with blue light at ~30 °C in a fan-cooled photobox. Under these conditions, the cesium oxalate (**4.30**) was expected to undergo double decarboxylation to give a tertiary radical (**4.19**), which would then be trapped by a hydrogen atom source (Scheme 4.12). However, despite screening of a wide variety of hydrogen atom sources, the desired deoxygenated product (**4.21**) was never obtained. We instead observed formation of alcohol **4.15** and formate ester **4.33**. Formate **4.33** likely arose from mono-decarboxylation to give an acyl radical (**4.32**), which was then trapped with a hydrogen atom prior to a second decarboxylation event. That the second decarboxylation would be slow is in line with results from our attempted Barton–McCombie deoxygenation

*Adapted in part from Kim S. Mühlfenzl's thesis (unpublished).[17]

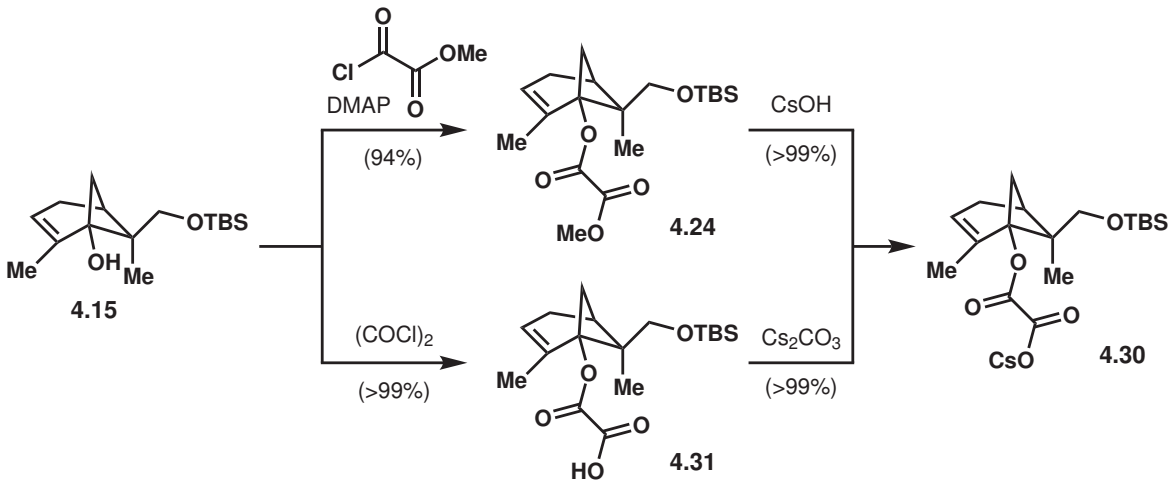

Scheme 4.11: Synthesis of cesium oxalate **4.30** from alcohol **4.15**.

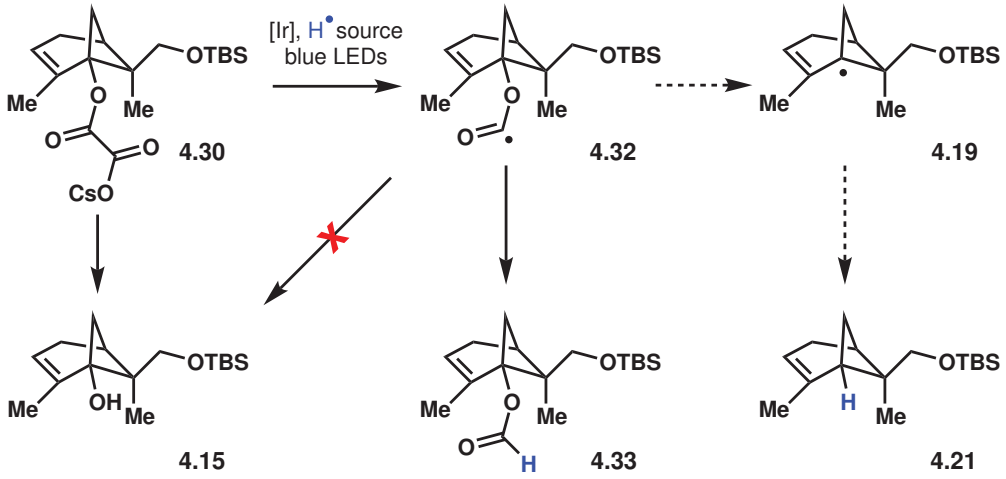

Scheme 4.12: Attempted deoxygenation of cesium oxalate **4.30** using iridium photocatalysis.

of methyl oxalate **4.24**, in which fragmentation of the acetal radical (**4.26**) to give the bridgehead radical (**4.19**) was slow. Alcohol **4.15** could arise from the same acyl radical (**4.32**) as formate **4.33** through loss of CO; however, DFT calculations showed that pathway to be unfavorable. Preliminary calculations indicated that loss of CO from **4.32**, while 3.90 kcal/mol downhill, is less favorable than loss of CO_2, which is 22.16 kcal/mol downhill.[†] While these differences in ground state energies may not be fully reflected in the transition states, it is nevertheless more likely that alcohol **4.15** arises through hydrolysis of the substrate, as observed by MacMillan and co-workers in a variety of solvents.[23]

Since loss of the second molecule of CO_2 was a significant challenge, we envisioned that con-

[†]DFT calculations were carried out in the gas phase at the B3LYP/6-31g(d) level of theory. The absolute energy of the acyl radical (**4.32**) was –1180.034171, the oxygen-centered radical that would result from loss of CO was –1066.716832, the bridgehead radical (**4.19**) was –991.479413, CO was –113.323561, and CO_2 was –188.590066. All absolute energies are given in Hartree/particle. No imaginary frequencies were found for any of the optimized structures.

ducting the reaction at a higher reaction temperature would favor the entropically-driven fragmentation. Therefore, the next reactions were carried out at 70 °C, using a transparent oil bath to ensure a constant temperature, as well as two blue LED lamps for irradiation. Unfortunately, formate **4.33** and alcohol **4.15** were again obtained as the only identifiable products. However, mass recovery was low, raising concerns about volatility of the products, especially if the TBS group did not remain intact. As such, we instead shifted our attention to the analogous TBDPS ether (**4.45**), which was heavier and more robust. However, the cesium oxalate of **4.45** (**4.78**, see section 4.5.1) ultimately gave similar results to the TBS ether (**4.15**) under the iridium photoredox conditions.

4.1.4 Deoxygenation using ruthenium photocatalysis[‡]

Given the lack of success with the iridium conditions, we began to investigate an alternative ruthenium-catalyzed photoreaction involving irradiation of alkyl *N*-phthalimidoyl oxalates. In 1991, Okada et al. reported a C–C bond formation through photo-induced decarboxylation of *N*-(acyloxy)phthalimides and subsequent Giese reaction with a variety of Michael acceptors.[25] Combining this idea with Barton's use of *N*-hydroxypyridine-2-thionyl oxalates to generate carbon-centered radicals from tertiary alcohols,[26,27] Overman et al. later developed a method utilizing alkyl *N*-phthalimidoyl oxalates to access tertiary alkyl radicals, thereby using tertiary alcohols as an entry point for Giese reactions (Scheme 4.13).[28,29] In this reaction,

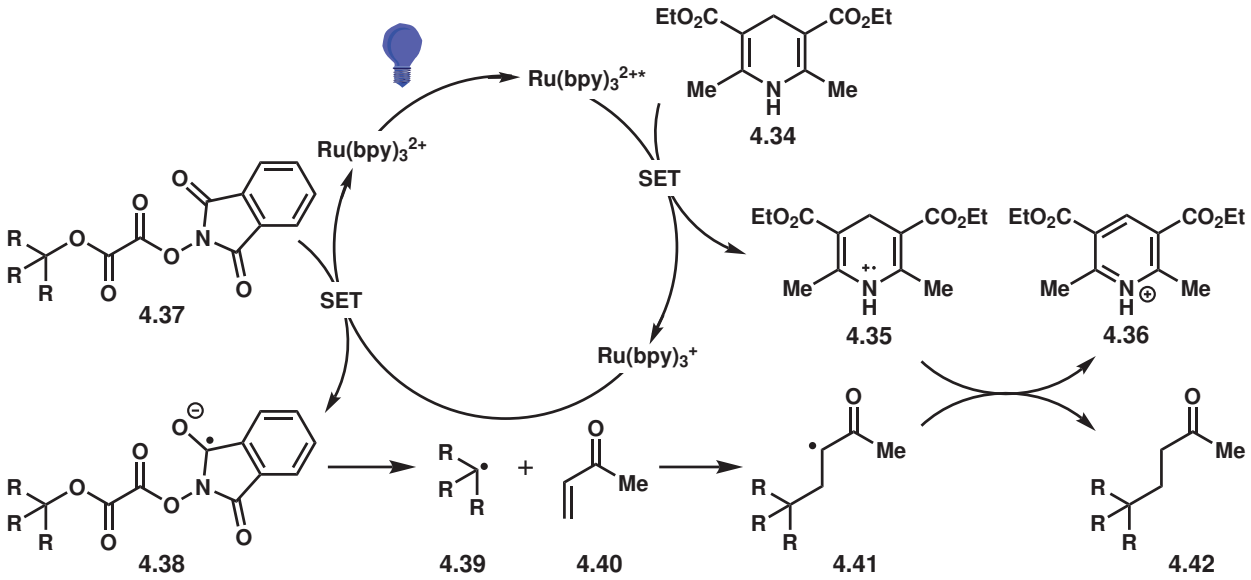

Scheme 4.13: Overman's coupling of *N*-phthalimidoyl oxalates with Michael acceptors.

$Ru(bpy)_3(PF_6)_2$ is excited with blue light and reduced by Hantzsch ester (**4.34**), the resulting ruthenium(I) complex then turns over by effecting single-electron transfer to the *N*-phthalimidoyl oxalate substrate (**4.37**). The newly generated radical anion (**4.38**) then fragments to give a tertiary alkyl radical (**4.39**). Upon coupling with a Michael acceptor (**4.40**), the resultant radical

[‡]Adapted in part from Kim S. Mühlfenzl's thesis (unpublished).[17]

(**4.41**) abstracts a hydrogen atom from the previously generated radical cation of Hantzsch ester (**4.35**). Yields improved upon addition of *i*-$Pr_2NEt \cdot HBF_4$. With these conditions, it became possible to construct a variety of sterically hindered quaternary carbon centers.

Looking to adapt this protocol to effect our desired deoxygenation, we first synthesized the photoredox-active *N*-phthalimidoyl oxalates of alcohols **4.15** and **4.45**. Treatment of *N*-hydroxyphthalimide (**4.43**) with oxalyl chloride gave *N*-phthalimidoyl oxalyl chloride (**4.44**) which could be further reacted with alcohols **4.15** and **4.45** to afford **4.46** and **4.47**, respectively (Scheme 4.14). Unsurprisingly, these products were sensitive to both air and moisture and, as such, had to be separately prepared immediately prior to each photoreaction.

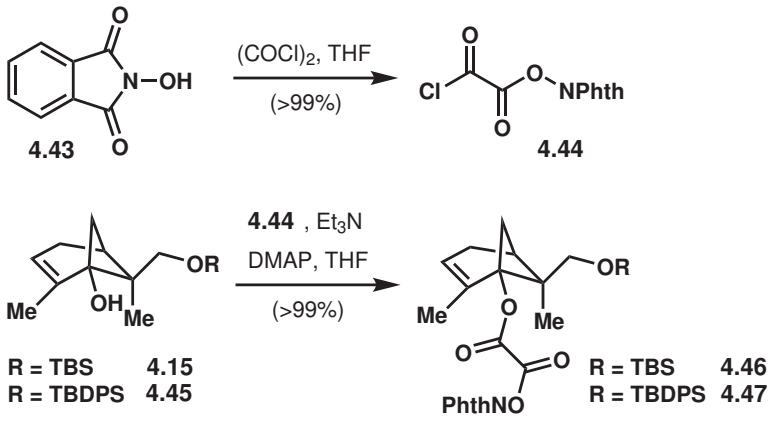

Scheme 4.14: Synthesis of *N*-phthalimidoyl oxalates **4.46** and **4.47**.

Preliminary reactions using TBDPS ether **4.47** were performed in 1:1 THF:CH_2Cl_2 in a Merck photobox equipped with a 450 nm LED array and a cooling fan (Table 4.1). Regardless of the hydrogen atom source used, the formate (**4.48**) was the major product. The best results were obtained with 1,4-cyclohexadiene, Hantzsch ester, or $(TMS)_3SiH$ (entries 1–3). Isolation of the formate (**4.48**) indicated that, as with our previous deoxygenation attempts, the second decarboxylation was slow relative to side reactions of the acyl radical (see Scheme 4.12). Trace amounts of the formate (**4.48**) were also detected when the reaction was run outside of the photobox and exposure to ambient light was minimized (entries 4–6). In this case, the majority of the material decomposed, indicating that background processes may be contributing to the low yields.

This challenge was not unique to our substrate: in Overman's original report,[28] formation of a bridgehead adamantyl radical was similarly challenging. Adamantyl oxalate **4.50** gave formate ester **4.51**, which presumably formed through Giese addition of the acyl radical into methyl vinyl ketone, as the major product rather than the desired **4.52** (Scheme 4.15).

As discussed in the previous section, the second decarboxylation should be entropically favorable and the fragmentation should therefore be increasingly favorable as the temperature is raised. We thus chose to attempt the reaction using a blue Kessil lamp instead of the photobox. The reaction vessel was placed about an inch away from the lamp. Upon switching to this broader spectrum blue LED, formate **4.48** remained the major product (Table 4.1, entries 7–9). However, the desired deoxygenated product (**4.49**) could also be isolated in 4% yield. As the na-

Table 4.1: Screening of light sources for a ruthenium-catalyzed photoredox reaction of *N*-phthalimidoyl oxalate **4.47**.

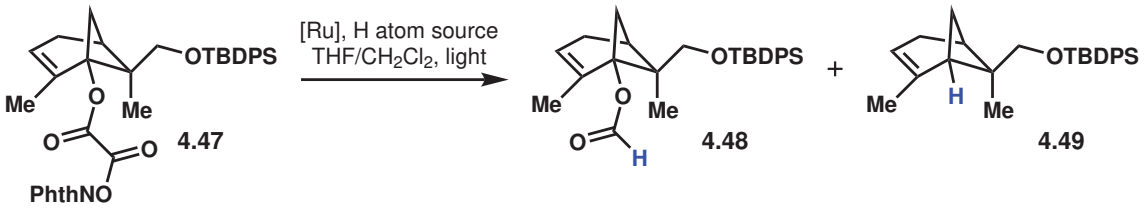

Entry[a]	H Atom Source	Light Source	Result
1	1,4-cyclohexadiene	450 nm	**4.48**
2	Hantzsch ester	450 nm	**4.48**
3	$(TMS)_3SiH$	450 nm	**4.48**
4	1,4-cyclohexadiene	–	trace **4.48**
5	Hantzsch ester	–	trace **4.48**
6	$(TMS)_3SiH$	–	trace **4.48**
7	1,4-cyclohexadiene	blue Kessil	**4.48** + **4.49** (6:1)[b], 4%[c]
8	Hantzsch ester	blue Kessil	**4.48** + **4.49** (7:1)[b], 4%[c]
9	$(TMS)_3SiH$	blue Kessil	**4.48** + **4.49** (7:1)[b], 4%[c]

[a]All reactions were run with 0.05 mmol of the H atom source, 1.5 equiv **4.47**, 1.5 mol % of $Ru(bpy)_3(PF_6)_2$ in 1:1 THF:CH_2Cl_2 (0.1 M) and irradiated for 13.5 h. [b]Determined by ^1H NMR analysis following filtration of the crude reaction mixture over a 1 cm SiO_2 plug. [c]Isolated yield of **4.49**.

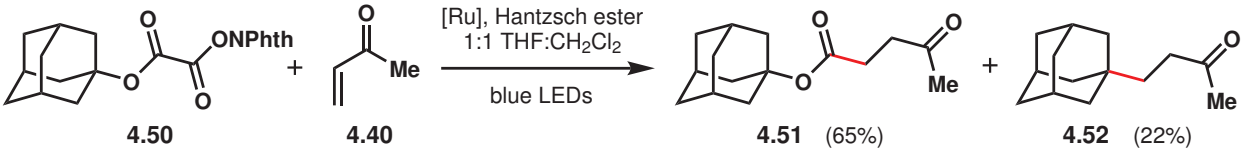

Scheme 4.15: Challenging fragmentation to form bridgehead adamantyl radical under Overman's Giese reaction conditions.

ture of the hydrogen atom source again had no impact on the outcome, we chose to run future reactions with Hantzsch ester, the most robust of the three reagents.

Having successfully obtained the desired silyloxypinene (**4.49**) for the first time, we set out to optimize this ruthenium-catalyzed deoxygenation reaction. Beginning with a solvent screen, we found that protic solvents, such as MeOH (entry 7) and DMF (entry 8), did not lead to any recognizable products (Table 4.2). Non-protic solvents (entries 1–6) led to mixtures of formate **4.48**, pinene **4.49**, and hydrolysis product **4.45**. In terms of the ratio of desired product (**4.49**) to byproducts (**4.45** and **4.48**), non-polar solvents outperformed more polar ones. Additionally, low boiling solvents afforded higher proportions of formate **4.48** than their high boiling counterparts. The best results were obtained with THF (entry 2), benzene (entry 5), and EtOAc (entry 6), which were thus selected for use in further optimization experiments.

Believing the heat generated by the Kessil lamp to be influencing reaction outcomes, we performed a series of experiments with two Kessil lamps. When the Kessil lamps were set up on

Table 4.2: Screening of solvents for the ruthenium-catalyzed photoredox reaction of *N*-phthalimidoyl oxalate **4.47**.

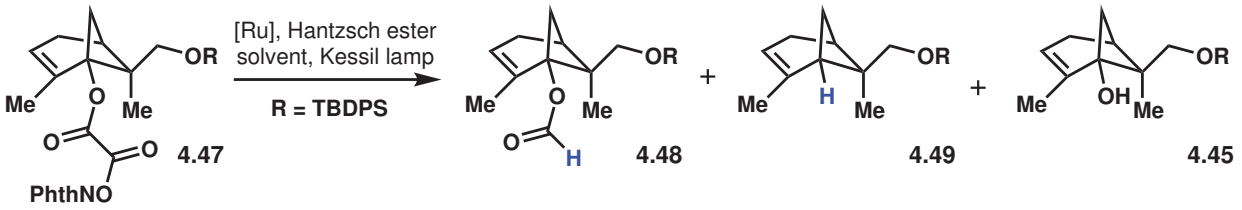

Entry[a]	Solvent	ε	Time	**4.48**:**4.49**:**4.45**
1	Et_2O	4.3	3.5 h	5.4:1.0:1.4
2	THF	7.6	3.5 h	2.1:1.0:0.7
3	CH_2Cl_2	9.1	3.5 h	10.9:1.0:1.2
4	MeCN	37.5	3.5 h	3.5:1.0:1.1
5	PhH	2.3	14.5 h	1.5:1.0:0.9
6	EtOAc	6.0	14.5 h	3.0:1.0:trace
7	MeOH	32.7	14.5 h	–
8	DMF	36.7	14.5 h	–

[a]All reactions were run with 0.03 mmol of **4.47**, 1.0 equiv Hantzsch ester, and 1.5 mol % of $Ru(bpy)_3(PF_6)_2$ in 0.1 M solvent and irradiated using a blue Kessil lamp.

opposite sides of the sealed reaction vessel, each about 1 inch from the vial, and no effort was made to trap the generated heat, the reaction mixtures reached ~40 °C and the deoxygenated product (**4.49**) was obtained in a ratio of 1:5.8–7.0 with formate **4.48** (Table 4.3, entries 1–3). The internal reaction temperature was ~65 °C when the entire set-up was wrapped in foil to trap the heat generated by the lamps. In this case, the ratio of **4.49** to **4.48** seemed to improve. Delaying the addition of the hydrogen atom source (entry 6) further increased the proportion of the desired product.

In order to ensure consistent reaction temperatures, a transparent oil bath was used for further reactions. Two test reactions were carried out at 65 °C to verify that sufficient light passed through the oil bath and similar results were obtained as when the heat from the lamps was trapped with aluminum foil. In the case of Hantzsch ester (entry 8), full consumption of oxalate **4.47** was observed and a 1.0:3.4 ratio of pinene **4.49** to formate **4.48** was obtained. In contrast, when using 1,4-cyclohexadiene (entry 7), the ratio was similar but conversion was low.

Scaling up the reaction in benzene and heating at 80 °C, we found that the ratios did not vary significantly with scale and that the desired product (**4.49**) could be isolated in 8–9% yield (Table 4.4, entries 1–4). Identical results were obtained when the reaction was instead run with TBS ether **4.46** (entry 5). In order to test whether trapped CO_2 could be inhibiting fragmentation of the acyl radical, we also ran this reaction under dynamic nitrogen instead of the typical sealed vial (entry 6). No improvement in ratio of desired product (**4.49**) to formate ester (**4.48**) was observed.

Given that the greatest improvements in yield had been obtained by increasing the temperature, we turned our attention to solvents with even higher boiling points, finding that yields

Table 4.3: Screening of reaction temperatures for the ruthenium-catalyzed photoredox reaction of *N*-phthalimidoyl oxalate **4.47**.

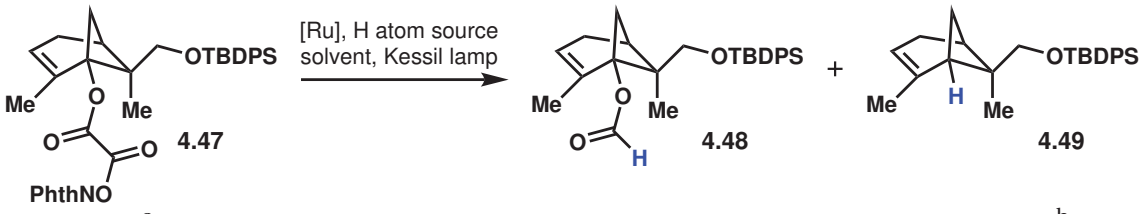

Entry[a]	Solvent	H Atom Source	Temperature Control	**4.48**:**4.49**[b]
1	EtOAc	Hantzsch ester	open air	5.8:1.0
2	THF	Hantzsch ester	open air	7.0:1.0
3	PhH	Hantzsch ester	open air	6.2:1.0
4	PhH	Hantzsch ester	foil-wrapped	8.5:1.0[d]
5	PhH	1,4-cyclohexadiene	foil-wrapped	3.1:1.0
6	PhH	1,4-cyclohexadiene[c]	foil-wrapped	2.1:1.0
7	PhH	1,4-cyclohexadiene	65 °C oil bath	2.7:1.0
8	PhH	Hantzsch ester	65 °C oil bath	3.4:1.0

[a]All reactions were run with 0.08 mmol of **4.47**, 1.0 equiv H atom source, and 1.5 mol % of $Ru(bpy)_3(PF_6)_2$ in 0.1 M solvent and irradiated with two blue Kessil lamps for 12–16 h. [b]Determined by ^{1}H NMR analysis after filtration through 1 cm SiO_2 plug. [c]H atom source added after 2 h. [d]Reaction mixture not filtered prior to ^{1}H NMR.

improved in both toluene (entry 7) and 5:1 dioxane:DMSO (entry 8). Notably, while the reaction in dioxane/DMSO—unlike reactions without DMSO—was homogeneous, the yield of **4.49** was still lower than in the less polar toluene. Increasing the amount of Hantzsch ester from 1.0 to 1.5 equiv (entry 10) led to a slight increase in the ratio of formate **4.48** to pinene **4.49**, but did not impact the isolated yield of **4.49**. Further optimization studies are planned using other high-boiling benzene derivatives, such as mesitylene. The possibility of delayed addition of the hydrogen atom source will also be revisited.

Table 4.4: Effect of scale on the ruthenium-catalyzed photoredox reaction of *N*-phthalimidoyl oxalate **4.47**.

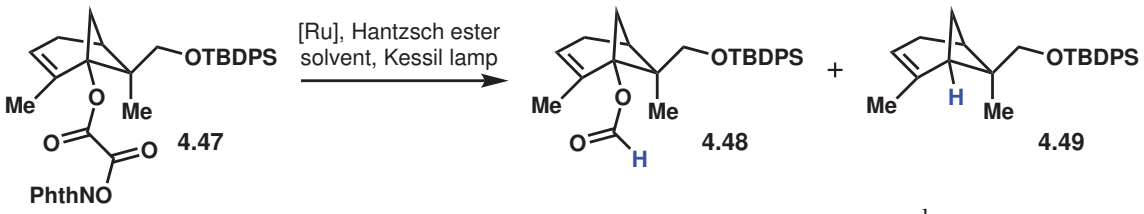

Entry[a]	Scale (mmol)	Solvent	Temperature	**4.48**:**4.49**[b]	Yield **4.49**
1	0.080	PhH	80 °C	2.9:1.0	n.d.
2	0.168	PhH	80 °C	2.8:1.0	9%
3	0.370	PhH	80 °C	2.1:1.0	9%
4	0.419	PhH	80 °C	3.9:1.0	8%
5[c]	0.461	PhH	80 °C	4.9:1.0	8%
6[d]	0.080	PhMe	80 °C	6.0:1.0	n.d.
7	0.110	PhMe	105 °C	1.9:1.0	14%
8	0.110	dioxane:DMSO (5:1)	105 °C	2.4:1.0	11%
9	0.414	PhMe	110 °C	1.1:1.0	15%
10[e]	0.458	PhMe	110 °C	1.6:1.0	15%

[a]All reactions were run with 1.0 equiv Hantzsch ester, and 1.5 mol % of $Ru(bpy)_3(PF_6)_2$ in 0.1 M solvent and irradiated with two blue Kessil lamps for 12–18 h. [b]Determined by ^{1}H NMR analysis after filtration through 1 cm SiO_2 plug. [c] TBS ether **4.46** used as substrate to give formate **4.33** and pinene **4.21**. [d]Reaction was run under dynamic nitrogen instead of in a sealed vial. [e]1.5 equiv of Hantzsch ester were used.

4.1.5 Advancement of deoxygenated pinene scaffold toward somaliensene A

With deoxygenation product **4.49** in hand, we turned our attention to the installation of the farnesyl side chain to complete the synthesis of somaliensene A. Deoxygenated bicycle **4.49** was treated with TASF to cleave the silyl group and give pinene oxide **4.8**, which was then converted to the corresponding tosylate (**4.53**, Scheme 4.16). The tosylate group was displaced with NaI

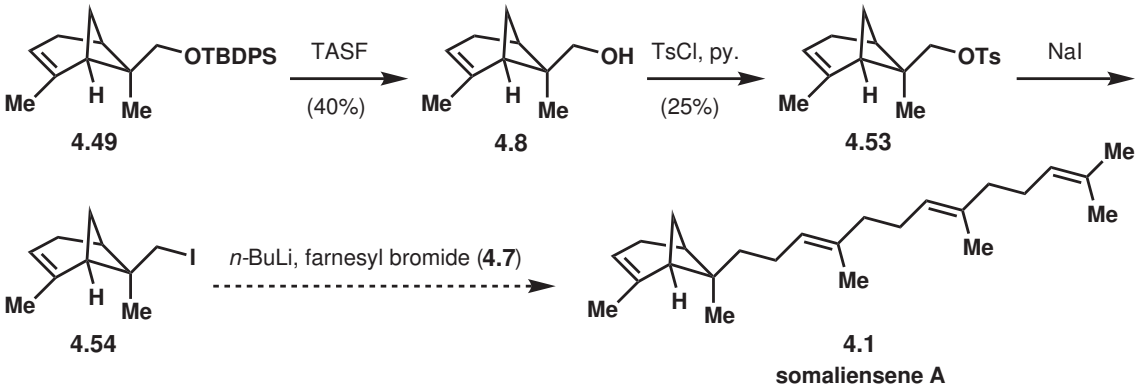

Scheme 4.16: Endgame for the synthesis of somaliensene A from deoxygenation product **4.49**.

to give iodide **4.54**, which we plan to treat with the lithiate of farnesyl bromide to complete the synthesis of somaliensene A. Studies into this final displacement will commence in our laboratory once the COVID-19 outbreak subsides and we are allowed to return to work.

4.2 Rearrangement of verbenone and advancement to chrysanthenol derivatives

While pursuing the total synthesis of somaliensene A through a deoxygenation strategy, we also became interested in the possibility of a complementary C–H functionalization strategy to the sesterterpene (Scheme 4.17). In this alternative retrosynthesis, somaliensene A (**4.1**) is still traced back to unnatural pinene oxide **4.8**, which is again proposed to arise from a more highly oxygenated precursor. However, to circumvent the low-yielding deoxygenation of diol **4.9** at a bridgehead position, we instead propose deoxygenation of the secondary hydroxy group of diol **4.55**, which could arise from *cis*-chrysanthenol (**4.56**) through a key C–H oxygenation. *cis*-Chrysanthenol could be obtained through rearrangement and reduction of (+)-verbenone (**4.57**).

The rearrangement of verbenone (**4.57**) to chrysanthenone (**4.60**) was first reported by Hurst and Whitaker,[30] who proposed that the carbonyl of verbenone was excited to give diradical **4.58**, which then fragmented to give **4.59** (Scheme 4.18). Recombination of the enol radical α to the carbonyl (position marked with a blue dot) with the tertiary radical would then give chrysanthenone (**4.60**). However, even upon optimization by Erman and co-workers, this transformation required long reaction times and led to mixtures of products.[31] Racemization of the product, believed to proceed through retro-[2+2] cycloaddition to give ketene **4.61**, was minimized

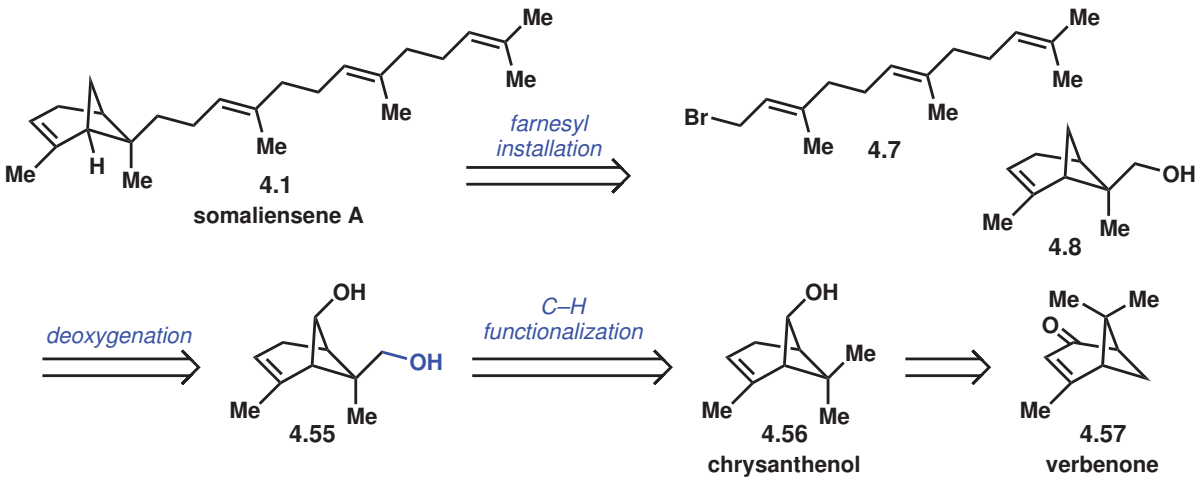

Scheme 4.17: Alternative strategy toward somaliensene A using key C–H functionalization.

when reaction temperatures were kept below 65 °C. However, in all cases, another rearranged [3.1.1] bicycle (**4.64**) was obtained as a side product.

Since irradiation of chrysanthenone (**4.60**) with an unfiltered mercury lamp was shown to produce **4.64**,[31a] we propose that bicycle **4.64** forms through Norrish I-type fragmentation of **4.60** to give allylic radical **4.63**. Recombination of the acyl radical with the opposite terminus of the allyl system (position marked with a red dot) would then give **4.64**. We thus postulated that irradiation with a longer wavelength of light would prevent excitation of the product ketone while still achieving excitation of the starting enone. Irradiating verbenone (**4.57**, ~60% ee) for 4 h using a 365 nm LED array in a fan-cooled photobox, we were able to achieve very good yields of chrysanthenone (**4.60**) without observing side product **4.64**. Additionally, we did not observe a reduction in optical rotation, even after an additional 12 h irradiation. While chysanthenone

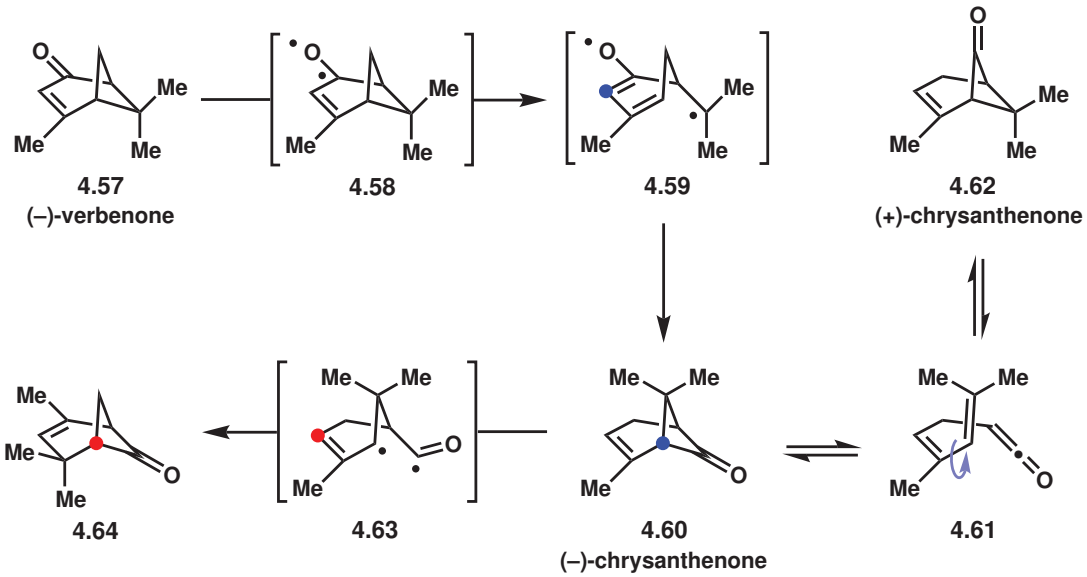

Scheme 4.18: Alternative strategy toward somaliensene A using key C–H functionalization.

(**4.60**) was not well suited to silica gel chromatography (~30% of the mass was lost on each column), it could be stored in a freezer for weeks without degrading.

Chrysanthenone (**4.60**) could be reduced with DIBAL in the same pot to give *cis*-chrysanthenol (**4.56**) as a single diastereomer (see Scheme 4.17). This one-step procedure could also be split into a two-step, one-pot protocol without any changes in the overall yield. Similar yields were also obtained when the reduction was carried out with $LiAlH_4$ or L-selectride in THF. Given the success of chrysanthenone reduction with sterically hindered hydride sources, we were curious as to whether other nucleophiles could be added into **4.60**, opening the door for application of this strategy to other natural products, such as xishacorene B (**4.65**, Scheme 4.19). If a carbon nucleophile, such as 1-propynylmagnesium bromide, were added into (–)-chrysanthenone, the resultant chrysanthenol derivative (**4.67**) could then undergo an oxy-Cope rearrangement to effect a net ring expansion and generate a [3.3.1] bicycle (**4.66**). From there conjugate addition of a vinyl group into the enone, directed C–H functionalization of the *gem*-dimethyl group, and removal of the carbonyl would give xishacorene B (**4.65**). C–H functionalization of chrysanthenol derivative **4.67** could also be envisioned prior to the oxy-Cope rearrangement (as in Scheme 4.17).

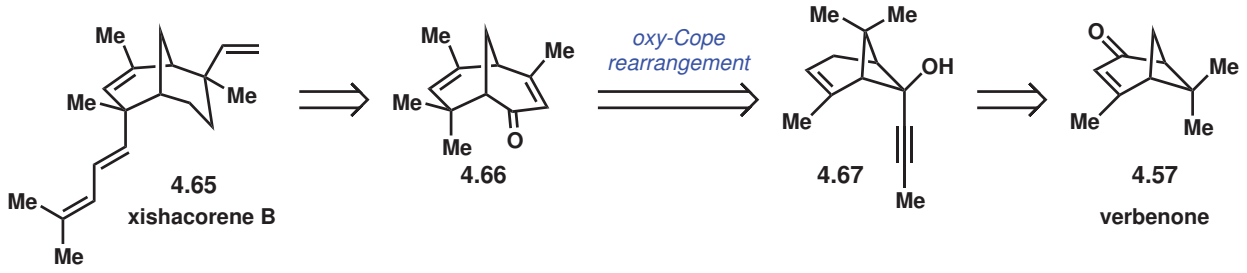

Scheme 4.19: Retrosynthesis of xishacorene B from verbenone.

This addition worked well with 1-propynyl or ethynylmagnesium bromide to give the desired adducts (**4.67** and **4.68**, respectively) in good yield (Scheme 4.20). However, initial attempts to effect an oxy-Cope rearrangement were unsuccessful with no observed [3.3.1] bicycle (**4.66**) formation. To test whether the geometry of alkynes **4.67** and **4.68** were impeding the rearrangement—a fully synchronous reaction would be unlikely, but a highly asynchronous, concerted process, or even a stepwise process proceeding through a diradical intermediate, could be operative—we next looked at the addition of vinylmagnesium bromide to give adduct **4.69**, which would be capable of pre-organizing to place the vinyl group under the trisubstituted olefin with which it would need to interact in an oxy-Cope rearrangement.

Here, 1,2-addition to form adduct **4.69** was again successful. However, with extended reaction time and/or increased temperature, the 1,2-addition product (**4.69**) underwent spontaneous rearrangement to a new [3.1.1] bicycle (**4.71**) analogous to ketone **4.64**. Intrigued by this unexpected rearrangement, we also explored a variety of other nucleophliles. In doing so, we found that 1,2-addition products with vinyl groups (*e.g.*, **4.69**) underwent this formal 1,3-alkyl shift, whereas aryl (**4.70**) and alkynyl products (**4.67** and **4.68**) did not, even upon heating to 65 °C for 24 h. Cyclopropylmagnesium bromide, on the other hand, did not add into chrysanthenone (**4.60**) even under forcing conditions. Instead, we observed rearrangement of the starting material. Believing this rearrangement was likely catalyzed by $MgBr_2$—which could be generated

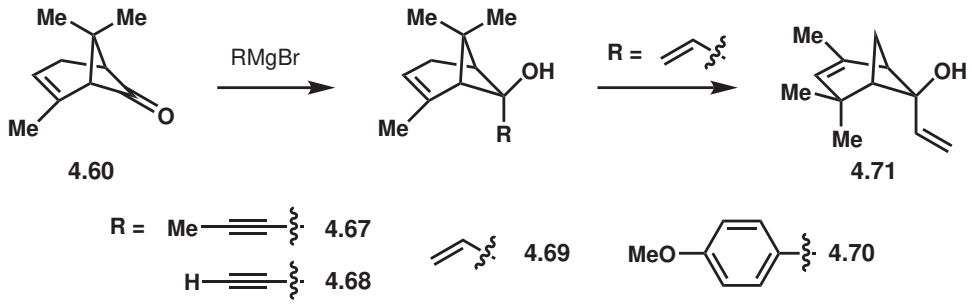

Scheme 4.20: Addition of Grignard reagents to chrysanthenone (**4.60**) and subsequent rearrangement of vinyl adduct **4.69** to give novel [3.1.1] bicycle **4.71**.

through Schlenk equilibration of the cyclopropylmagnesium bromide—we subjected chrysanthenone (**4.60**) to $MgBr_2$ directly at 65 °C and found that the starting material rearranged to the same product, known fused bicycle **4.74** (Scheme 4.21). Erman et al. proposed that this fused product (**4.74**) could arise through a Wagner–Meerwein shift (see bond highlighted in red) to give a non-classical carbocation (**4.73**), which would be further stabilized through interaction across the allyl group.[31c]

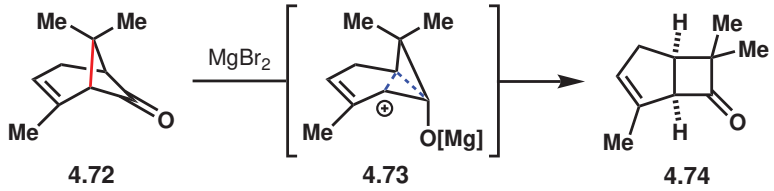

Scheme 4.21: $MgBr_2$-catalyzed rearrangement of chrysanthenone (**4.60**) to a known fused bicycle (**4.74**).

Curious about the divergent reactivity of various Grignard reagents with chrysanthenone (**4.60**), we began to probe the mechanistic origin of these differences. Preliminary DFT calculations show that the formal 1,3-alkyl shift (see **4.69** to **4.71**) is favored by 1–2.5 kcal/mol in all cases (Table 4.5). The substrate-dependent outcome of these reactions must then be under kinetic control. Additionally, the ratios of 1,2-addition to rearranged products were unchanged when the reactions were run in the dark, indicating that this process—unlike conversion of chrysanthenone to **4.64**—is likely thermally induced. Transition state studies and accompanying ex-

Table 4.5: Comparison of ground state energies of 1,2-addition products of chrysanthenone (**4.60**) and formal 1,3-alkyl shifted products. All calculations were carried out in the gas phase at the B3LYP/6-31g(d) level of theory. Absolute energies are given in Hartree/particle.

Substituent	$E_{rearranged}$	$E_{1,2\text{-addition}}$	$\Delta E_{rearrangement}$
H	–465.663993	–465.661190	–1.76 kcal/mol
1-Propyne	–581.094974	–581.092665	–1.45 kcal/mol
Ethyne	–541.793926	–541.791298	–1.65 kcal/mol
4-Methoxyphenyl	–811.128909	–811.127083	–1.15 kcal/mol
Vinyl	–543.025709	–543.022076	–2.28 kcal/mol

perimental work are ongoing in collaboration with Bohyun Park from the laboratory of Prof. Mu-Hyun Baik at KAIST.

4.3 Experimental contributors

Kim S. Mühlfenzl (K. S. M.) optimized conditions for deoxygenation using photoredox catalysis, following up on initial hits by Nicolle A. Doering (N. A. D.). N. A. D. ran all other experiments related to the synthesis of somaliensene A. N. A. D. optimized the conversion of verbenone (**4.57**) to chrysanthenone (**4.60**) and began to look at reductions of **4.60** for use in C–H functionalization reactions. In attempting Cope rearrangement to turn these chrysanthenol derivatives into [3.3.1] bicycles, Kerry E. Jones (K. E. J.) discovered that a rearranged product (**4.71**) was formed upon addition of vinylmagnesium bromide to **4.60**. This result was followed up on by both K. E. J. and N. A. D. to confirm the structure of **4.71**. K. E. J. then investigated conversion of **4.71** to a [3.3.1] bicycle while N. A. D. explored the scope of the chrysanthenol rearrangement. Preliminary computations were carried out by N. A. D. with more in-depth studies (not reported here) being conducted by Bohyun Park from KAIST.

4.4 Materials and methods

Solvents and reagents. Unless noted below, commercial reagents were purchased from Sigma Aldrich, Acros Organics, Chem-Impex, Combi-blocks, TCI, and/or Alfa Aesar, and used without additional purification. Solvents were purchased from Fisher Scientific, Acros Organics, Alfa Aesar, and Sigma Aldrich. Tetrahydrofuran (THF), toluene (PhMe), diethyl ether (Et_2O), acetonitrile (CH_3CN), benzene, methanol (MeOH), and triethylamine (Et_3N) were sparged with argon and dried by passing through alumina columns using argon in a Glass Contour solvent purification system. Dichloromethane (CH_2Cl_2) was freshly distilled over calcium hydride under a N_2 atmosphere prior to each use. Dimethylformamide (DMF), acetone, DIBAL solution, Grignard solutions, and pyridine were purchased in Aldrich SureSeal, Acros AcroSeal, or Alfa Aesar ChemSeal bottling, and used directly. 1,4-Dioxane was purchased in AcroSeal bottling (99.5%, anhydrous, stabilized, over 4 Å molecular sieves).

Reaction setup, progress monitoring, and product purification. Unless otherwise noted in the experimental procedures, reactions were carried out in flame or oven-dried glassware under a positive pressure of N_2 in anhydrous solvents using standard Schlenk techniques. Reaction temperatures above rt (22–23 °C) were controlled by an IKA temperature modulator and monitored using liquid-in-glass thermometers. Reaction progresses were monitored using a combination of LC–MS analysis (via a Shimadzu LCMS-2020 (UFLC) equipped with the LC-20AD solvent delivery system, a SPD-20AV prominence UV/Vis detector (SPD-M20A Photo Diode Array), and a Thermo Scientific Hypersil GOLD HPLC column (5 µm particle size, 4.6 x 50 mm)), and thin-layer chromatography (TLC) on Silicycle Siliaplates (glass backed, extra hard layer, 60 Å, 250 µm thickness, F254 indicator). Visualization of the developed plates was performed under UV-light (254 nm) irradiation, and then gently heated with $KMnO_4$, *p*-anisaldehyde, or ceric ammonium molybdate stains. Purification and isolation of products were performed via silica gel chromatography (both column and preparative thin-layer chromatography). Flash column chromatography was performed with either glass columns using Silicycle silica gel

(40–63 μm particle size) or with a Yamazen Smart Flash EPCLC W-Prep 2XY (dual channel) automated flash chromatography system on prefilled, premium, universal columns using ACS grade solvents. Organic solutions were concentrated under reduced pressure on a Heidolph temperature-controlled rotary evaporator equipped with a dry ice/isopropanol condenser or a Büchi temperature-controlled rotary evaporator equipped with an Ecodyst Ecochyll system.

Analytical instrumentation. NMR spectral data were obtained using deuterated solvents were obtained from Cambridge Isotope Laboratories, Inc. ^{1}H NMR and ^{13}C NMR data were recorded on Bruker AVB-400, AVQ-400, AV-500, NEO-500, AV-600, or AV-700 MHz spectrometers using $CDCl_3$ or C_6D_6. Chemical shifts (δ) are reported in ppm relative to the residual solvent signal (δ 7.26 for ^{1}H NMR, δ 77.16 for ^{13}C NMR in $CDCl_3$ and δ 7.16 for ^{1}H NMR, δ 128.06 for ^{13}C NMR in C_6D_6).[32] When ^{13}C signals appear weak and/or broad (with poor signal/noise ratios), HSQC spectra are acquired to confirm signal authenticity. Data for ^{1}H NMR spectroscopy are reported as follows; chemical shift (δ ppm), multiplicity (s = singlet, bs = broad singlet, d = doublet, t = triplet, q = quartet, m = multiplet, dd = doublet of doublets, dt = doublet of triplets), coupling constant (Hz), integration. Data for ^{13}C NMR spectroscopy are reported in terms of chemical shift (δ ppm). ^{13}C NMR chemical shifts are reported to one decimal place; a second decimal place is included when two closely spaced, but distinct, signals resonate within 0.1 ppm of each other.

IR spectroscopic data were recorded on a Bruker ALPHA FT-IR spectrophotometer using a diamond attenuated total reflectance (ATR) accessory. Samples are loaded onto the diamond surface either neat or as a solution in organic solvent and the data acquired after the solvent had evaporated.

Mass spectral data were obtained from the QB3/Chemistry Mass Spectrometry Facility at the University of California, Berkeley, on a Finnigan/Thermo LTQ-FT instrument (ESI), and the data acquired and processed using the Xcalibur software.

X-Ray data were collected on a Bruker APEX-II CCD diffractometer with Mo-Kα radiation (λ = 0.71073 Å) or a MicroStar-H X8 APEX-II diffractometer with Cu-Kα radiation (λ = 1.54178 Å) (supported by an NIH Shared Instrumentation Grant S10-RR027172). CYLview (Legault, C. Y., Université de Sherbrooke, 2009) was used for graphic rendering.

4.5 Experimental details

4.5.1 Total synthesis of somaliensene A

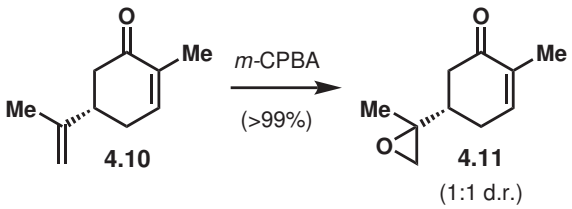

Epoxycarvone (4.11). *m*-Chloroperbenzoic acid (49.3 g, 231 mmol, 1.05 equiv) was added portionwise to a stirred and ice-cooled solution of (*S*)-carvone (33.0 g, 220 mmol) in CH_2Cl_2 (1200

ml). The mixture was stirred overnight at room temperature, and filtered through Celite. The Celite layer was washed with ether. The combined filtrate and washings were washed with $NaHCO_3$ (saturated aqueous) and brine, dried with magnesium sulfate, and concentrated *in vacuo* to give 36.5 g (>99%) of **4.11** in 1:1 dr. ^{1}H NMR (400 MHz, $CDCl_3$) δ 6.72 (qq, *J* = 3.9, 1.5 Hz, 2H), 2.70 (d, *J* = 4.4 Hz, 1H), 2.66 (d, *J* = 4.2 Hz, 1H), 2.58 (dd, *J* = 7.1, 4.5 Hz, 2H), 2.56–2.51 (m, 2H), 2.45–2.34 (m, 2H), 2.30–2.14 (m, 5H), 2.10–2.01 (m, 1H), 1.76 (dq, *J* = 2.8, 1.4 Hz, 6H), 1.32 (s, 3H), 1.30 (s, 3H); ^{13}C NMR (101 MHz, $CDCl_3$) δ 198.4, 198.3, 143.9, 143.7, 135.19, 135.15, 57.6, 57.5, 52.5, 52.2, 41.0, 40.6, 40.0, 39.6, 27.7, 27.5, 18.6, 18.2, 15.41, 15.40. The spectral data are consistent with those reported in the literature.[10]

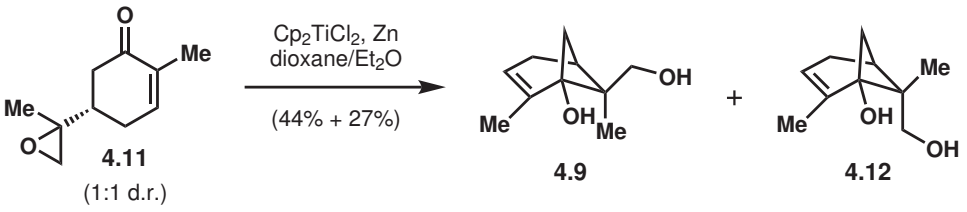

Diols 4.9 and 4.12. A 1 L flask was charged with Cp_2TiCl_2 (16.5 g, 66.2 mmol, 2.2 equiv) and zinc dust (13.0 g, 199 mmol, 6.6 equiv), equipped with an addition funnel, and placed under an inert nitrogen atmosphere. A mixture of Et_2O (120 mL, nitrogen sparged) and dioxane (120 mL, nitrogen sparged) was added to the flask and the heterogeneous mixture was stirred for 1 h, after which the color of the mixture had turned a deep green color. Meanwhile, the addition funnel was charged with epoxycarvone **4.11** (5.00 g, 30.1 mmol) as a solution in Et_2O (100 mL) and dioxane (100 mL) and sparged with nitrogen for 1 h. Then, the solution of epoxycarvone (**4.11**) was added dropwise into the deep green reaction mixture over the course of 2 h and the mixture was allowed to stir additional 18 h. The reaction mixture was quenched with NaH_2PO_4 (saturated aqueous, 250 mL), brine (50 mL), and EtOAc (50 mL) and allowed to stir open to air for 12 h, during which time the organic phase turned a clear orange color. The resulting mixture was filtered through a pad of Celite. The aqueous phase was extracted with EtOAc (2 x 30 mL), the combined organic phase was washed with brine, dried over $MgSO_4$, filtered and the solvents were removed *in vacuo*. The crude residue was purified by flash column chromatography (25–60% EtOAc/hexanes) to yield diol **4.9** (2.67 g, 53%) as white solid along with the undesired diastereomer, diol **4.12** (1.61 g, 32%) as a white solid. The spectroscopic data obtained are consistent with those previously reported in the literature.[9]

*Diol **4.9**.* ^{1}H NMR (300 MHz, $CDCl_3$) δ 5.24 (m, 1H), 4.31 (d, *J* = 11.0 Hz, 1H), 3.71 (d, *J* = 11.1 Hz, 1H), 2.41 (dd, *J* = 8.6, 7.0 Hz, 1H), 2.23–2.13 (m, 1H), 2.12–2.06 (m,1H), 1.91 (ddd, *J* = 7.1, 5.2, 2.4 Hz, 1H), 1.76 (q, *J* = 2.1 Hz, 3H), 1.67 (d, *J* = 8.6 Hz, 1H), 1.59 (bs, 2H), 1.07 (s, 3H).

*Diol **4.12**.* ^{1}H NMR (400 MHz, $CDCl_3$) δ 5.27 (s, 1H), 3.75 (d, *J* = 10.3 Hz, 1H), 3.40 (dd, *J* = 10.3, 1.8 Hz, 1H), 2.27 (dd, *J* = 8.2, 6.8 Hz, 1H), 2.22–2.05 (m, 3H), 1.81 (q, *J* = 2.1 Hz, 3H), 1.62 (d, *J* = 8.2 Hz, 1H), 1.34 (s, 3H).

Silyl ether 4.15. To a solution of diol **4.9** (639 mg, 3.80 mmol, 1.0 equiv) in CH_2Cl_2 (38.0 mL, 0.1 M) was added imidazole (1.03 g, 15.2 mmol, 4.0 equiv), followed by TBSCl (1.14 g, 7.60 mmol, 2.0 equiv) as solids in one portion. The resulting heterogeneous solution was stirred for 3 h at room temperature before being quenched by the addition of water (40 mL). The aqueous

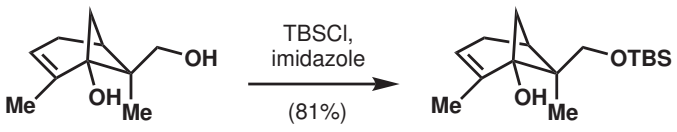

4.9 4.15

layer was extracted with CH_2Cl_2 (4 x 80 mL), dried over Na_2SO_4, filtered, and concentrated *in vacuo*. The crude material was purified by flash column chromatography (5% EtOAc/hexanes) to afford alcohol **4.15** (828 mg, 77%) as clear oil. ^{1}H NMR (500 MHz, $CDCl_3$) δ 5.17 (tt, *J* = 3.1, 1.6 Hz, 1H), 4.30 (s, 1H), 4.27 (d, *J* = 10.1 Hz, 1H), 3.72 (d, *J* = 10.1 Hz, 1H), 2.36 (dd, *J* = 8.6, 7.0 Hz, 1H), 2.13 (dq, *J* = 17.5, 2.6 Hz, 1H), 2.05 (dq, *J* = 17.5, 2.6 Hz, 1H), 1.91 (dq, *J* = 5.5, 2.7 Hz, 1H), 1.75 (q, *J* = 2.1 Hz, 3H), 1.67 (d, *J* = 8.6 Hz, 1H), 1.00 (s, 3H), 0.92 (s, 9H), 0.10 (d, *J* = 5.1 Hz, 6H); ^{13}C NMR (126 MHz, $CDCl_3$) δ 147.6, 116.6, 78.7, 70.9, 46.5, 40.8, 31.5, 30.6, 26.0, 18.3, 17.5, 14.9, –5.5; IR (thin film) 3488, 2953, 2928, 2883, 2857, 1471, 1254, 1156, 1088, 1066, 835, 777 cm^{-1}; HRMS (ESI) *m/z* $[M + H]^+$ calc'd for $C_{16}H_{31}O_2Si$ 283.2088, found 283.2087.

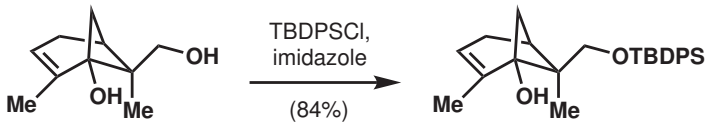

4.9 4.45

Silyl ether 4.45. To a solution of diol **4.9** (337 mg, 2.00 mmol, 1.0 equiv) in CH_2Cl_2 (20.0 mL, 0.1 M) was added imidazole (409 mg, 6.00 mmol, 3.0 equiv), followed by TBDPSCl (676 µL, 2.60 mmol, 1.3 equiv). The reaction mixture was stirred for 1.5 h at room temperature before being quenched by the addition of water (20 mL). The aqueous layer was extracted with CH_2Cl_2 (4 x 40 mL), dried over Na_2SO_4, filtered, and concentrated *in vacuo*. The crude material was purified by gradient flash column chromatography (2.5–5.0% EtOAc/hexanes) to afford alcohol **4.45** (683 mg, 84%) as colorless oil. ^{1}H NMR (500 MHz, $CDCl_3$) δ 7.70 (ddt, *J* = 6.7, 5.0, 1.5 Hz, 4H), 7.50 – 7.36 (m, 6H), 5.19 (tq, *J* = 3.3, 1.7 Hz, 1H), 4.30–4.25 (m, 1H), 4.12 (s, 1H), 3.72 (d, *J* = 10.3 Hz, 1H), 2.33 (dd, *J* = 8.6, 7.0 Hz, 1H), 2.11 (dq, *J* = 17.5, 2.7 Hz, 1H), 2.02 (dq, *J* = 17.6, 2.5 Hz, 1H), 1.87 (dq, *J* = 7.5, 2.6 Hz, 1H), 1.80 (q, *J* = 2.1 Hz, 3H), 1.67 (d, *J* = 8.6 Hz, 1H), 1.08 (s, 9H), 1.04 (s, 3H). ^{13}C NMR (126 MHz, $CDCl_3$): δ 147.4, 136.0, 135.8, 132.9, 132.6, 130.0, 128.0, 127.9, 116.8, 78.8, 71.2, 47.0, 40.7, 31.4, 30.6, 27.0, 19.3, 17.6, 15.0; IR (thin film) 3504, 2930, 2881, 2857, 1427, 1222, 1153, 1111, 1064, 997, 882 cm^{-1}; HRMS (EI) *m/z* $[M]^{\cdot+}$ calc'd for $C_{26}H_{34}O_2Si$ 406.2323, found 406.2325.

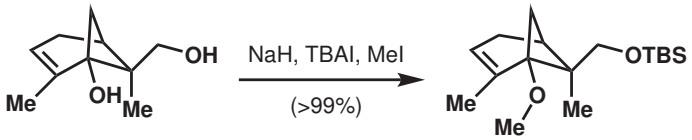

4.15 4.22

Methyl ether 4.22. To a solution of TBS ether **4.15** (31.5 mg, 0.112 mmol) in THF (0.6 mL) at room temperature was added MeI (28 µL, 0.446 mmol, 4.0 equiv) followed by NaH (60 % dispersion in mineral oil, 8.9 mg, 0.223 mmol, 2.0 equiv). After 1.5 h, more NaH (8.9 mg, 0.223 mmol, 2.0 equiv) and MeI (28 µL, 0.446 mmol, 4.0 equiv) were added and the reaction mixture

allowed to stir for an additional 3.5 h, at which point full conversion was observed by TLC. The reaction mixture was quenched by the addition of MeOH (0.5 mL), then diluted with saturated aqueous $NaHCO_3$ (2 mL) once the bubbling had stopped. The aqueous layer was washed with CH_2Cl_2 (3 x 2 mL) and the combined organic extracts dried over Na_2SO_4, filtered, and concentrated *in vacuo*. The crude material was purified by gradient flash column chromatography (6.0% EtOAc/hexanes) to afford methyl ether **4.22** (33.1 mg, >99%) as a clear oil.

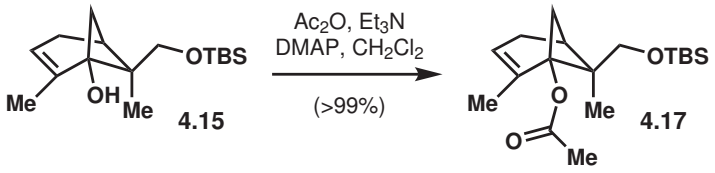

Acetate 4.17. To a solution of TBS ether **4.15** (9.8 mg, 0.0347 mmol) and DMAP (4.6 mg, 0.0347 mmol, 1.0 equiv) in CH_2Cl_2 (1.5 mL, 22 mM) was added Ac_2O (9.8 µL, 0.104 mmol, 3.0 equiv), followed by Et_3N (19 µL, 0.139 mmol, 4.0 equiv). The reaction mixture was allowed to stir at room temperature for 23 h, at which point it was quenched through the addition of saturated aqueous NH_4Cl (1 mL). The aqueous layer was extracted with CH_2Cl_2 (3 x 1 mL) and the combined organic extracts were dried over Na_2SO_4, filtered, and concentrated *in vacuo* to afford crude acetate **4.17** (11.2 mg, >99%), which was advanced as a 1.4:1 mixture of Et_3N:**4.17**. ^{1}H NMR (400 MHz, $CDCl_3$) δ 5.30 (s, 1H), 3.87 (d, *J* = 10.0 Hz, 1H), 3.63 (d, *J* = 10.0 Hz, 1H), 3.19 (s, 1H), 2.54 (dd, *J* = 9.0, 7.3 Hz, 1H), 2.40 (s, 1H), 2.18 (s, 1H), 2.08 (d, *J* = 9.6 Hz, 1H), 2.03 (s, 3H), 1.63 (s, 3H), 0.99 (s, 3H), 0.90 (s, 9H), 0.06 (s, 6H).

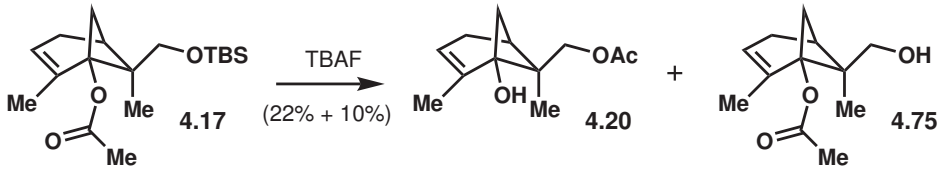

Acetates 4.20 and 4.75. TBAF (65 µL, 0.0634 mmol, 2.0 equiv) was added to a solution of acetate **4.17** (10.3 mg, 0.0317 mmol) in THF (0.3 mL, 0.1 M) under air and the resultant reaction mixture was allowed to stir at room temperature for 20 h. At this point, conversion was low based on TLC. More TBAF (130 µL, 0.127 mmol, 4.0 equiv) was added and the vial was sealed before being heated to reflux for 48 h. The reaction mixture was concentrated *in vacuo* and the crude material was purified by gradient flash column chromatography (50% EtOAc/hexanes) to afford primary acetate **4.20** (1.5 mg, 22%) as a white film and tertiary acetate **4.75** (1.0 mg, 15%) as a yellow oil.

*Primary acetate **4.20**.* ^{1}H NMR (600 MHz, $CDCl_3$) δ 5.26 (tq, *J* = 3.0, 1.7 Hz, 1H), 4.46 (d, *J* = 11.5 Hz, 1H), 4.34 (d, *J* = 11.5 Hz, 1H), 2.36 (s, 1H), 2.33 (dd, *J* = 8.8, 7.0 Hz, 1H), 2.18 (dq, *J* = 17.4, 2.6 Hz, 1H), 2.12–2.09 (m, 1H), 2.10 (s, 3H), 2.08 (dq, *J* = 17.4, 2.6 Hz, 1H), 1.76 (q, *J* = 2.0 Hz, 3H), 1.70 (d, *J* = 8.8 Hz, 1H), 0.98 (s, 3H). The spectroscopic data obtained are consistent with those previously reported in the literature.[10]

*Tertiary acetate **4.75**.* ^{1}H NMR (600 MHz, $CDCl_3$) δ 5.32 (s, 1H), 4.04 (dd, *J* = 11.4, 3.4 Hz, 1H), 3.71 (dd, *J* = 11.4, 8.7 Hz, 1H), 2.55 (dd, *J* = 9.5, 7.1 Hz, 1H), 2.29–2.18 (m, 2H), 2.13–2.08 (m, 2H), 2.07 (s, 3H), 1.70 (dd, *J* = 8.9, 3.8 Hz, 1H), 1.65 (q, *J* = 1.9 Hz, 3H), 1.10 (s, 3H).

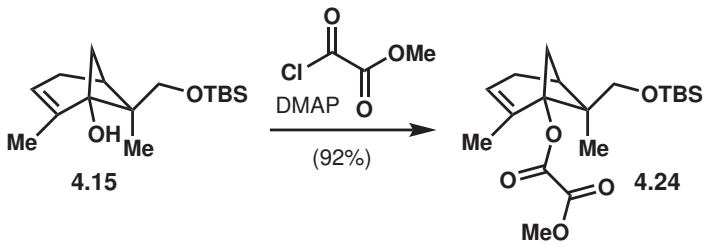

Methyl oxalate 4.24. To a solution of alcohol **4.15** (1.39 g, 4.92 mmol) in CH_2Cl_2 (50 mL, 0.1 M) was added DMAP (1.20 g, 9.84 mmol, 2.0 equiv) and methyl oxalyl chloride (0.81 mL, 8.85 mmol, 1.8 equiv) in an ice/water bath. The reaction mixture was allowed to warm to room temperature and stirred for 2 h before being quenched by the addition of water (20 mL). The aqueous layer was extracted with CH_2Cl_2 (4 x 15 mL), dried over Na_2SO_4, filtered, and concentrated *in vacuo*. The crude material was purified by flash column chromatography (10% EtOAc/hexanes) to afford methyl oxalate **4.24** (1.60 g, 92%) as a pale yellow oil. ^{1}H NMR (700 MHz, $CDCl_3$) δ 5.35 (tt, *J* = 3.1, 1.7 Hz, 1H), 3.89 (d, *J* = 1.0 Hz, 3H), 3.86 (d, *J* = 10.1 Hz, 1H), 3.70 (d, *J* = 10.1 Hz, 1H), 2.65 (dd, *J* = 9.2, 7.4 Hz, 1H), 2.43 (dq, *J* = 7.9, 2.7 Hz, 1H), 2.23 (dq, *J* = 18.0, 2.7 Hz, 1H), 2.12–2.06 (m, 2H), 1.66 (t, *J* = 2.3 Hz, 3H), 1.05 (s, 3H), 0.89 (d, *J* = 1.1 Hz, 9H), 0.05 (d, *J* = 1.3 Hz, 6H); ^{13}C NMR (156 MHz, $CDCl_3$) δ 142.5, 119.8, 87.1, 66.3, 53.5, 48.6, 38.8, 32.3, 30.8, 26.0, 25.1, 17.4, 14.9, –5.3; IR (thin film) 3501, 2955, 2930, 2886, 2856, 1767, 1741, 1450, 1320, 1205, 1163 cm^{-1}; HRMS (ESI) *m/z* [M + Na]$^+$ calc'd for $C_{19}H_{32}NaO_5Si$ 391.1911, found 391.1911.

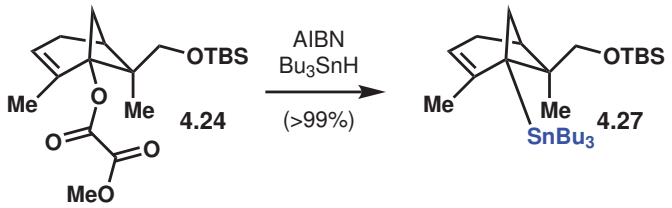

Stannane 4.27. A solution of mixed oxalate ester **4.24** (20.1 mg, 0.0545 mmol) and *n*-Bu_3SnH (73 µL, 0.273 mmol, 5.0 equiv) in degassed PhMe (3.0 mL, 18 mM) was pre-heated in an oil bath at 110 °C for 5 min. AIBN (18.0 mg, 0.109 mmol, 2.0 equiv) was then added to the solution dropwise over 1 h. The resultant reaction mixture was heated for an additional 45 min before being cooled to room temperature. The reaction mixture was concentrated *in vacuo* and loaded directly onto a SiO_2 plug. The crude material was purified by flash column chromatography (0–10–100% EtOAc/hexanes) to afford stannane **4.27** (30.5 mg, >99%) as a clear oil. ^{1}H NMR (600 MHz, $CDCl_3$) δ 5.32 (s, 1H), 3.90 (d, J = 10.2 Hz, 1H), 3.67 (d, J = 10.1 Hz, 1H), 2.64 (t, J = 8.2 Hz, 1H), 2.45 (dd, J = 7.4, 2.0 Hz, 1H), 2.22 (d, J = 18.0 Hz, 1H), 2.10–2.03 (m, 2H), 1.67 (s, 3H), 1.67–1.61 (m, 6H), 1.35 (dt, J = 21.2, 7.7 Hz, 12H), 1.04 (s, 3H), 0.91 (t, J = 7.3 Hz, 9H), 0.89 (s, 9H), 0.04 (s, 6H); ^{13}C NMR (151 MHz, $CDCl_3$) δ 142.7, 119.3, 66.1, 48.5, 38.7, 32.2, 30.8, 27.7, 27.02, 27.01, 26.0, 18.4, 17.3, 17.1, 14.8, 13.6, –5.4. HRMS was attempted, but unsuccessful.

The loss of the bridgehead oxygen atom and its replacement with a stannyl group was confirmed by 2D NMR. Assignments of ^{13}C shifts in stannane **4.27** and deoxygenated pinene **4.21** were confirmed by HSQC. HMBC correlation between H6 and C10 was used to assign the bridgehead positions of **4.21** (C4 vs C6). Comparison of ^{13}C NMR spectra of stannane **4.27** to deoxygenated product **4.21**, alcohol **4.15**, and α-pinene[33] showed that the stannyl-bearing bridge-

head carbon (C6, see Table 4.6) is unusually shielded and has a chemical shift on par with the *n*-butyl groups and with other allyl stannanes.[§]

Table 4.6: Comparison of ^{13}C NMR spectra of stannane **4.27**, deoxygenated product **4.21**, alcohol **4.15**, and α-pinene (**4.76**).

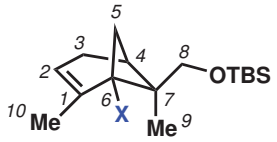

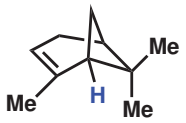

4.76
α-pinene

	4.27 (X = $SnBu_3$)	**4.21** (X = H)	**4.15** (X = OH)	α-Pinene (**4.76**)
C1	142.7	144.3	142.5	144.5
C2	119.3	116.8	119.8	116.0
C3	30.8	31.1	30.6 or 31.5	31.3
C4	32.2	36.6	30.6 or 31.5	40.7
C5	38.7	31.8	40.8	41.3
C6	**17.3**	**43.0**	**78.7**	**47.0**
C7	48.5	43.8	46.5	38.0
C8	66.1	69.3	70.9	26.4
C9	14.8	16.2	14.9	20.8
C10	17.1	23.1	17.5	23.0
TBS	–5.4	–5.2	–5.3	–
	18.4	18.6	18.3	–
	26.0	26.1	26.0	–
$SnBu_3$	13.6, 27.01, 27.02, 27.7	–	–	–

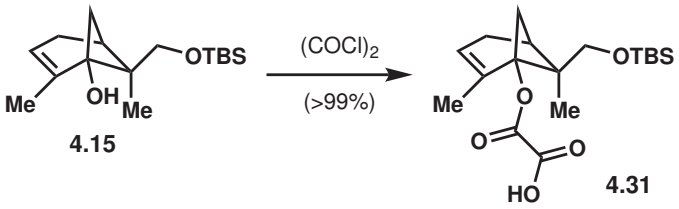

Oxalic acid 4.31. To a solution of TBS alcohol **4.15** (383 mg, 1.35 mmol) in Et_2O (10.5 mL, 0.13 M) was added oxalyl chloride (229 µL, 2.71 mmol, 2.0 equiv) dropwise at 0 °C. The reaction mixture was allowed to warm to room temperature and stirred for 3 h. The solution was cooled to 0 °C, followed by the addition of water (15 mL). The aqueous layer was extracted with Et_2O (4 x 15 mL), dried over Na_2SO_4, filtered, and concentrated *in vacuo* to afford oxalate **4.31** (480 mg, >99%) as colorless oil. The crude material was used without further purification. ^{1}H NMR (700 MHz, $CDCl_3$) δ 5.37 (tt, *J* = 3.1, 1.6 Hz, 1H), 3.83 (d, *J* = 1.3 Hz, 2H), 2.67 (dd, *J* = 9.2, 7.5 Hz, 1H), 2.37 (dq, *J* = 7.8, 2.7 Hz, 1H), 2.28–2.20 (m, 1H), 2.14–2.04 (m, 2H), 1.66 (q, *J* = 2.0 Hz, 3H), 1.07 (s, 3H), 0.89 (s, 9H), 0.06 (s, 6H). ^{13}C NMR (156 MHz, $CDCl_3$) δ 57.3, 156.7, 141.9, 119.9, 88.0, 67.0, 48.8, 38.8, 32.4, 30.7, 26.1, 18.6, 17.4, 14.8, –5.4; IR (thin film) 501, 2954, 2928, 2887, 2856, 1742, 1255, 1183, 1113, 1093, 1068, 836 cm^{-1}; HRMS (ESI) *m/z* [M + Na]$^+$ calc'd for $C_{18}H_{30}NaO_5Si$ 377.1755, found 377.1755.

[§]Representative shifts of allyl stannanes (~10–25 ppm) were obtained from the NMR website (13-C page, Stannane section) by Prof. Hans Reich (University of Wisconsin).[34]

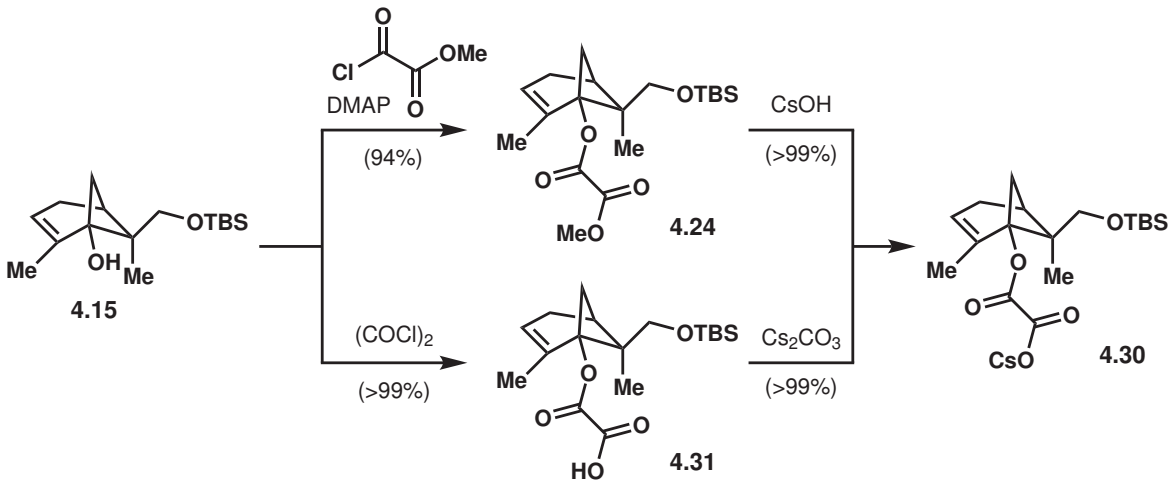

Cesium oxalate 4.30. To a solution of methyl oxalate **4.24** (85.9 mg, 0.233 mmol) in THF (1.45 mL) and H_2O (150 µL) was added a 1 M aqueous solution of CsOH (233 µL, 0.233 mmol, 1.0 equiv). The solution was stirred for 30 min at room temperature, concentrated *in vacuo* and dried with azeotropic distillation to afford cesium oxalate **4.30** (113 mg, >99%) as colorless solid.

Alternative procedure: To a solution of oxalic acid **4.31** (480 mg, 1.35 mmol) in THF (4.50 mL, 0.3 M) was added a 0.4 M aqueous solution of Cs_2CO_3 (1.69 mL, 0.677 mmol, 0.50 equiv). The solution was stirred for 30 min at room temperature, concentrated *in vacuo* and dried with azeotropic distillation to afford cesium oxalate **4.30** (657 mg, >99%) as colorless solid. ^{1}H NMR (500 MHz, $CDCl_3$) δ 5.31 (p, *J* = 2.4 Hz, 1H), 3.93 (d, *J* = 10.2 Hz, 1H), 3.64 (d, *J* = 10.1 Hz, 1H), 2.54 (dd, *J* = 9.0, 7.4 Hz, 1H), 2.46 (dq, *J* = 7.4, 2.6 Hz, 1H), 2.24 – 2.17 (m, 1H), 2.05 (dq, *J* = 17.7, 2.7 Hz, 1H), 1.98 (d, *J* = 9.1 Hz, 1H), 1.60 (q, *J* = 2.0 Hz, 3H), 1.01 (s, 3H), 0.89 (s, 9H), 0.05 (s, 6H); ^{13}C NMR (126 MHz, $CDCl_3$) δ 166.3, 163.0, 143.0, 119.5, 85.0, 66.2, 48.4, 39.0, 32.2, 31.0, 26.1, 18.5, 18.0, 15.0, –5.0; IR (neat) 3410, 2954, 2928, 2885, 2855, 1721, 1646, 1212, 1118, 1068, 836 cm^{-1}; HRMS data matched that of oxalic acid **4.31**.

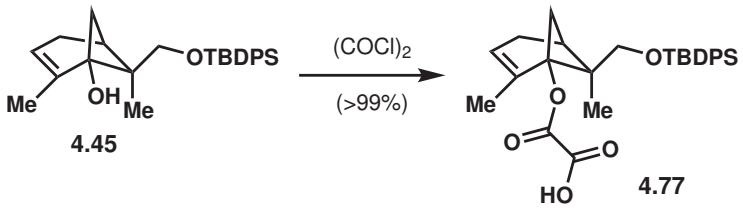

Oxalic acid 4.77. To a solution of TBDPS alcohol 115 (93.5 mg, 0.230 mmol) in Et_2O (2.30 mL, 0.1 M) was added oxalyl chloride (38.9 µL, 0.460 mmol, 2.0 equiv) dropwise at 0 °C. The reaction mixture was allowed to warm to room temperature and stirred for 5 h. The solution was cooled to 0 °C, followed by the addition of water (10 mL). The aqueous layer was extracted with Et_2O (4 x 10 mL), dried over Na_2SO_4, filtered, and concentrated *in vacuo* to afford oxalate **4.77** (103 mg, 94%) as yellow solid. The crude material was used without further purification. ^{1}H NMR (500 MHz, $CDCl_3$) δ 7.63 (m, 4H), 7.45–7.36 (m, 6H), 5.38 (tt, *J* = 3.2, 1.6 Hz, 1H), 3.90 (d, *J* = 10.4 Hz, 1H), 3.82 (d, *J* = 10.4 Hz, 1H), 2.57–2.48 (m, 2H), 2.26 (dq, *J* = 17.9, 2.6 Hz, 1H), 2.13 (dq, *J* = 17.7, 2.6 Hz, 1H), 2.04 (d, *J* = 8.1 Hz, 1H), 1.63 (q, *J* = 2.1 Hz, 3H), 1.15 (s, 3H), 1.05 (s, 9H); ^{13}C NMR (126 MHz, $CDCl_3$) δ 157.6, 156.8, 141.7, 135.8, 133.6, 129.9, 127.9, 120.2, 88.1, 67.0, 49.2,

38.7, 32.8, 32.4, 30.8, 27.0, 19.5, 17.4, 15.1; IR (neat) 2957, 2930, 2888, 2856, 1740, 1427, 1190, 1111, 1068, 822, 740, 702 cm^{-1}; HRMS (ESI) *m/z* [M - H]$^-$ calc'd for $C_{28}H_{33}O_5Si$ 477.2103, found 477.2100.

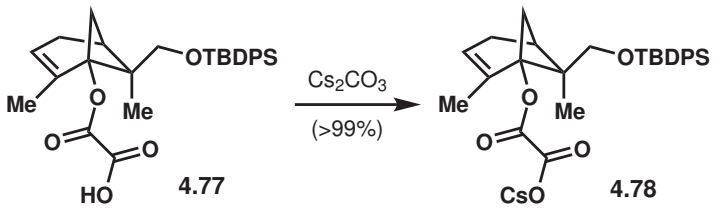

Cesium oxalate 4.78. To a solution of oxalic acid **4.77** (103 mg, 0.215 mmol) in THF (0.720 mL, 0.3 M) was added a 0.3 M aqueous solution of Cs_2CO_3 (360 µL, 0.108 mmol, 0.50 equiv). The solution was stirred for 30 min at room temperature, concentrated *in vacuo* and dried with azeotropic distillation to afford cesium oxalate **4.78** (122 mg, 93%) as colorless solid. ^{1}H NMR (500 MHz, $CDCl_3$) δ 7.65 (dt, *J* = 6.4, 1.5 Hz, 4H), 7.41–7.31 (m, 6H), 5.30–5.25 (m, 1H), 4.01 (d, *J* = 10.2 Hz, 1H), 3.70 (d, *J* = 10.2 Hz, 1H), 2.61 (dq, *J* = 7.7, 2.6 Hz, 1H), 2.42–2.35 (m, 1H), 2.23 (dq, *J* = 17.8, 2.7 Hz, 1H), 2.10 (ddt, *J* = 15.2, 6.2, 3.5 Hz, 1H), 1.95 (d, *J* = 9.2 Hz, 1H), 1.52 (d, *J* = 2.1 Hz, 3H), 1.11 (s, 3H), 1.04 (s, 9H); ^{13}C NMR (126 MHz, $CDCl_3$) δ 166.2, 162.6, 143.1, 135.7, 133.9, 129.8, 128.0, 119.3, 84.6, 67.0, 48.6, 39.0, 32.4, 31.0, 27.0, 19.6, 17.8, 15.2; IR (neat) 2957, 2929, 2887, 2856, 1724, 1427, 1281, 1171, 1112, 823, 740, 702 cm^{-1}; HRMS data matched that of oxalic acid **4.77**.

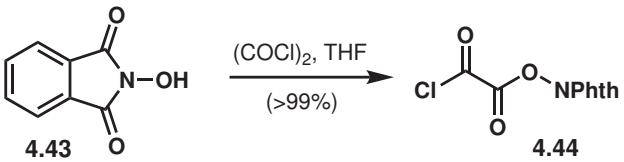

Oxalate 4.44. Oxalate **4.44** was prepared according to a procedure described by Overman and co-workers.[28] A round-bottom flask was charged with *N*-hydroxyphthalimide (196 mg, 1.20 mmol), followed by the addition of THF (20 mL, 60 mM). The resulting solution was then cooled to –78 °C and oxalyl chloride (0.508 mL, 6.00 mmol, 5.0 equiv) was added dropwise. The solution was then allowed to warm to room temperature and stirred for 18 h. The volatiles were removed under reduced pressure to yield **4.44** as a colorless solid. The crude material was dissolved in THF (20 mL) for use as a 0.06 M solution in the preparation of *t*-alkyl *N*-phthalimidoyl oxalates. ^{1}H NMR (500 MHz, $CDCl_3$) δ 7.99–7.91 (m, 2H), 7.90–7.83 (m, 2H). The spectral data were consistent with those reported in the literature.[28]

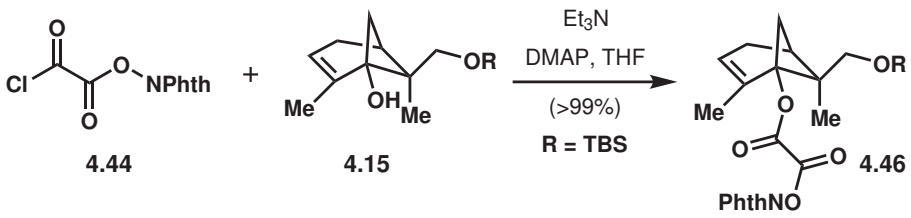

***N*-Phthalimidoyl oxalate 4.46.** A round-bottom flask was charged with alcohol **4.15** (132 mg, 0.467 mmol), and DMAP (5.70 mg, 0.0467 mmol, 0.10 equiv), followed by the addition of Et_3N

(129 µL, 0.933 mmol, 2.0 equiv). A 0.06 M solution of chloro *N*-phthalimidoyl oxalate **4.44** (15.6 mL, 0.933 mmol, 2.0 equiv) in THF was added via cannula. The resulting heterogeneous mixture was allowed to stir at room temperature for 1.5 h. The volatiles were removed under reduced pressure, and the resulting crude residue was dissolved in CH_2Cl_2 (6 mL) then poured into hexanes (200 mL). The resulting heterogeneous mixture was filtered through a cotton plug and washed with hexanes (2 x 25 mL). The filtrate was concentrated *in vacuo* to yield oxalate **4.46** as yellow oil (231 mg, 99%). ^{1}H NMR (500 MHz, $CDCl_3$) δ 7.93 (dd, *J* = 5.3, 3.1 Hz, 2H), 7.83 (dd, *J* = 5.3, 3.1 Hz, 2H), 5.39 (s, 1H), 3.92 (d, *J* = 10.1 Hz, 1H), 3.76 (d, *J* = 10.2 Hz, 1H), 2.76 (dd, *J* = 9.1, 7.5 Hz, 1H), 2.48 (dq, *J* = 8.0, 2.7 Hz, 1H), 2.30–2.21 (m, 1H), 2.16 (m, 2H), 1.73 (q, *J* = 2.1 Hz, 3H), 1.08 (s, 2H), 0.90 (s, 9H), 0.08 (s, 3H), 0.07 (s, 3H); ^{13}C NMR (126 MHz, $CDCl_3$) δ 161.0, 154.1, 153.7, 141.9, 135.2, 128.9, 124.4, 120.1, 88.8, 66.3, 49.0, 38.8, 32.3, 30.8, 26.0, 18.5, 17.5, 14.9, –5.3; IR (thin film) 2953, 2927, 2866, 2855, 1825, 1792, 1746, 1476, 1360, 1287, 1080, 835 cm^{-1}. Attempts to acquire HRMS data were unsuccessful under a variety of ionization conditions, likely due to the sensitivity of the *N*-phthalimidoyl oxalate functional group.

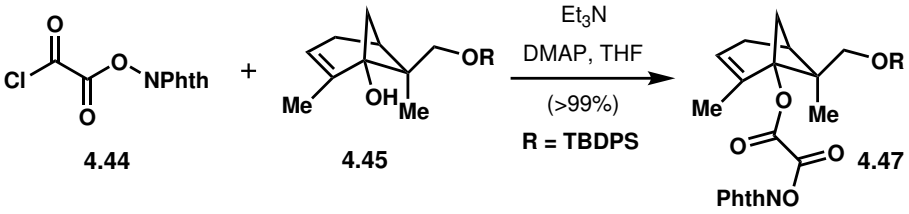

***N*-Phthalimidoyl oxalate 4.47.** A round-bottom flask was charged with alcohol **4.45** (121 mg, 0.297 mmol), and DMAP (3.63 mg, 0.0297 mmol, 0.10 equiv), followed by the addition of Et_3N (82.4 µL, 0.594 mmol, 2.0 equiv). A 0.06 M solution of chloro *N*-phthalimidoyl oxalate **4.44** (9.90 mL, 0.594 mmol, 2.0 equiv) in THF was added via cannula. The resulting heterogeneous mixture was allowed to stir at room temperature for 1.5 h. The volatiles were removed under reduced pressure, and the resulting crude residue was dissolved in CH_2Cl_2 (4 mL) then poured into hexanes (200 mL). The resulting heterogeneous mixture was filtered through a cotton plug and washed with hexanes (2 x 25 mL). The filtrate was concentrated *in vacuo* to yield oxalate **4.47** as a colorless solid (184 mg, 99%). ^{1}H NMR (500 MHz, $CDCl_3$) δ 7.91 (dd, *J* = 5.5, 3.1 Hz, 2H), 7.83 (td, *J* = 5.3, 2.1 Hz, 2H), 7.71–7.61 (m, 4H), 7.39 (m, 6H), 5.40 (dd, *J* = 3.2, 1.6 Hz, 1H), 3.98 (d, *J* = 10.4 Hz, 1H), 3.84 (d, *J* = 10.4 Hz, 1H), 2.61–2.53 (m, 2H), 2.31–2.23 (m, 1H), 2.17–2.06 (m, 2H), 1.71 (q, *J* = 2.1 Hz, 3H), 1.15 (s, 3H), 1.07 (s, 9H); ^{13}C NMR (125 MHz, $CDCl_3$) δ 160.8, 153.9, 153.7, 141.7, 135.8, 135.2, 133.7, 129.8, 129.8, 128.9, 127.9, 124.4, 120.2, 88.8, 66.9, 49.2, 38.8, 32.5, 30.8, 27.1, 19.6, 17.5, 15.0; IR (thin film) 2957, 2929, 2889, 2856, 1825, 1792, 1748, 1468, 1288, 1185, 1092, 700 cm^{-1}. Attempts to acquire HRMS data were unsuccessful under a variety of ionization conditions, likely due to the sensitivity of the *N*-phthalimidoyl oxalate functional group.

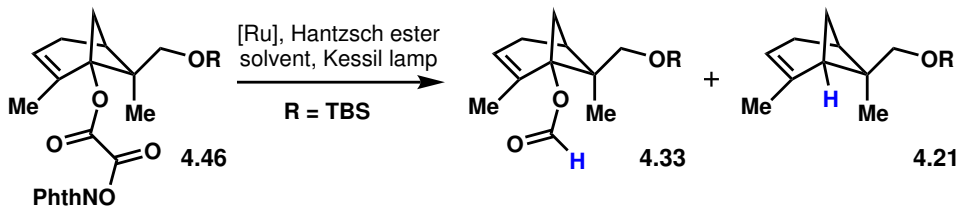

Silyl ether 4.21 and formate ester 4.33. A 20 mL vial was charged with oxalate **4.46** (230 mg, 0.461 mmol), $Ru(bpy)_3(PF_6)_2$ (5.94 mg, 0.007 mmol, 1.5 mol %), Hantzsch ester (117 mg, 0.461 mmol, 1.0 equiv), a magnetic stir bar, and nitrogen-sparged benzene (4.60 mL, 0.1 M). The heterogeneous reaction was placed into a preheated oil bath (80°C) in the center of two blue LEDs and allowed to stir at 80°C for 14 h. The reaction was filtered through a pad of silica gel, washed with CH_2Cl_2 (15 mL), and the filtrate concentrated *in vacuo*. The crude residue was purified via preparative TLC (100% hexanes) to afford **4.21** (10 mg, 8%) as colorless oil.

*Silyl ether **4.21***. ^{1}H NMR (500 MHz, $CDCl_3$) δ 5.23 (tp, *J* = 3.1, 1.6 Hz, 1H), 3.74 (d, *J* = 9.9 Hz, 1H), 3.69 (d, *J* = 9.8 Hz, 1H), 2.29–2.22 (m, 2H), 2.19 (dddt, *J* = 8.9, 5.9, 4.0, 1.9 Hz, 1H), 2.13 (dh, *J* = 16.9, 2.4 Hz, 1H), 2.03 (td, *J* = 5.6, 1.5 Hz, 1H), 1.66 (q, *J* = 2.0 Hz, 3H), 1.19 (d, *J* = 8.7 Hz, 1H), 0.90 (s, 9H), 0.87 (s, 3H), 0.06 (s, 3H), 0.06 (s, 3H); ^{13}C NMR (126 MHz, $CDCl_3$) δ 144.3, 116.8, 69.3, 43.8, 43.0, 36.6, 31.8, 31.1, 26.1, 23.1, 18.6, 16.2, –5.2; HRMS was not obtained successfully, but treatment with TASF gave cyclobutanol **4.8**.

*Formate ester **4.33***. ^{1}H NMR (500 MHz, $CDCl_3$) δ 7.98 (s, 1H), 5.30–5.26 (m, 1H), 3.81 (d, *J* = 10.1 Hz, 1H), 3.62 (d, *J* = 10.2 Hz, 1H), 2.55 (dd, *J* = 9.1, 7.4 Hz, 1H), 2.39–2.34 (m, 1H), 2.17 (dd, *J* = 17.7, 2.6 Hz, 1H), 2.06–1.99 (m, 1H), 1.96 (d, *J* = 9.1 Hz, 1H), 1.60 (q, *J* = 2.1 Hz, 3H), 0.96 (s, 3H), 0.84 (s, 9H), 0.00 (s, 6H); ^{13}C NMR (126 MHz, $CDCl_3$) δ 160.6, 142.8, 119.5, 84.8, 66.5, 48.2, 38.9, 32.4, 32.1, 26.1, 22.9, 17.9, 14.3, –5.3; IR (neat) 2955, 2924, 2853, 1729, 1461, 1255, 1170, 1115, 1090, 836 cm^{-1}; HRMS (EI) *m/z* $[M]^{\cdot-}$ calc'd for $C_{17}H_{30}O_3Si$ 309.1891, found 309.1882.

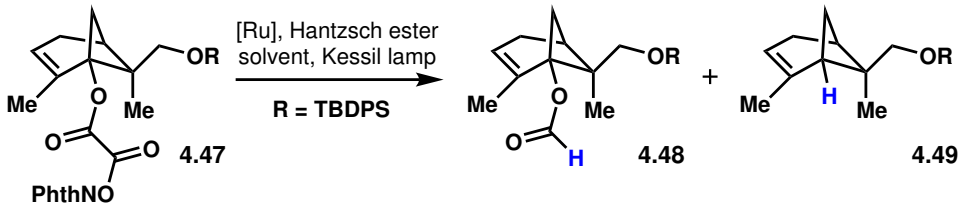

Silyl ether 4.49 and formate ester 4.48. A 20 mL vial was charged with oxalate **4.47** (184 mg, 0.295 mmol, 1.00 equiv), $Ru(bpy)_3(PF_6)_2$ (12.7 mg, 0.0150 mmol, 5 mol %), Hantzsch ester (112 mg, 0.443 mmol, 1.5 equiv), a magnetic stir bar, and nitrogen-sparged toluene (3.00 mL, 0.1 M). The heterogeneous reaction was placed into a preheated oil bath (110 °C) in the center of two blue LEDs and allowed to stir at 110 °C for 18 h. The reaction was filtered through a pad of silica gel, washed with CH_2Cl_2 (15 mL), and the filtrate concentrated *in vacuo*. The crude residue was purified via preparative TLC (100% hexanes) to afford silyl ether **4.49** as colorless oil (18 mg, 16%), along with undesired formate **4.48** (~18%).

*Silyl ether **4.49***. ^{1}H NMR (500 MHz, $CDCl_3$) δ 7.70 (dq, *J* = 6.5, 1.6 Hz, 4H), 7.45–7.37 (m, 6H), 5.24 (tq, *J* = 3.1, 1.6 Hz, 1H), 3.81 (d, *J* = 10.0 Hz, 1H), 3.76 (d, *J* = 9.9 Hz, 1H), 2.31–2.03 (m, 5H), 1.67 (q, *J* = 2.0 Hz, 3H), 1.14 (d, *J* = 8.7 Hz, 1H), 1.07 (s, 9H), 0.99 (s, 3H); ^{13}C NMR (126 MHz, $CDCl_3$) δ 144.2, 135.8, 134.3, 129.6, 127.7, 116.9, 70.1, 44.1, 43.0, 36.6, 31.7, 31.1, 27.0, 23.1, 19.6, 16.5; IR (neat) 2955, 2927, 2855, 1427, 1362, 1111, 1073, 822, 799, 701 cm^{-1}; HRMS (EI) *m/z* $[M]^{\cdot+}$ calc'd for $C_{26}H_{34}OSi$ 390.2373, found 390.2375.

*Formate ester **4.48***. ^{1}H NMR (500 MHz, $CDCl_3$) δ 7.91 (s, 1H), 7.68 (ddd, *J* = 8.1, 5.5, 1.6 Hz, 4H), 7.47–7.35 (m, 6H), 5.35 (tt, *J* = 3.1, 1.7 Hz, 1H), 3.92 (d, *J* = 10.3 Hz, 1H), 3.76 (d, *J* = 10.3 Hz, 1H), 2.52 (dt, *J* = 7.8, 2.7 Hz, 1H), 2.44 (dd, *J* = 9.1, 7.4 Hz, 1H), 2.29–2.20 (m, 1H), 2.12 (dq, *J* =

17.7, 2.7 Hz, 1H), 1.99 (d, *J* = 9.1 Hz, 1H), 1.64 (q, *J* = 2.1 Hz, 3H), 1.12 (s, 3H), 1.06 (s, 9H); ^{13}C NMR (126 MHz, $CDCl_3$) δ 160.5, 142.6, 135.8, 133.8, 129.8, 127.8, 119.4, 84.7, 67.2, 48.4, 39.0, 32.6, 31.0, 27.0, 19.6, 17.9, 15.0; IR (neat) 2957, 2929, 2887, 2856, 1724, 1427, 1281, 1171, 1112, 823, 702 cm^{-1}; HRMS (EI) *m/z* $[M]^{\cdot+}$ calc'd for $C_{27}H_{34}O_3Si$ 434.2272, found 434.2277.

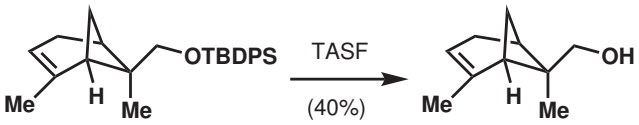

4.49 4.8

Alcohol 4.8. To a solution of silyl ether **4.49** (27.7 mg, 0.0709 mmol) in DMF (720 µL) was added TASF (78.1 mg, 0.284 mmol, 4.0 equiv) as solid in one portion. The reaction mixture was vigorously stirred for 48 h at room temperature before being quenched by the addition of brine (10 mL). The aqueous layer was extracted with EtOAc (3 x 25 mL) and the combined organic layers were washed with brine (2 mL), dried over Na_2SO_4, filtered, and concentrated *in vacuo*. The residue was purified via preparative TLC (25% EtOAc/hexanes) to afford alcohol **4.8** (4.8 mg, 44%) as colorless oil. ^{1}H NMR (500 MHz, $CDCl_3$) δ 5.25 (dq, *J* = 3.0, 1.5 Hz, 1H), 3.82 (d, *J* = 10.9 Hz, 1H), 3.77 (d, *J* = 10.9 Hz, 1H), 2.34–2.26 (m, 2H), 2.22 (ttd, *J* = 5.9, 2.7, 1.2 Hz, 1H), 2.15 (ddq, *J* = 17.3, 4.9, 2.4 Hz, 1H), 2.07 (td, *J* = 5.7, 1.5 Hz, 1H), 1.68 (q, *J* = 2.0 Hz, 3H), 1.23 (s, 1H), 0.93 (s, 3H); ^{13}C NMR (126 MHz, $CDCl_3$) δ 143.9, 117.0, 69.5, 43.6, 42.8, 36.5, 31.7, 30.9, 23.1, 15.9; IR (thin film) 3345, 2919, 2850, 1710, 1445, 1375, 1083, 1023, 788 cm^{-1}; HRMS (EI) *m/z* $[M]^{\cdot+}$ calc'd for $C_{10}H_{16}O$ 152.1196, found 152.1201.

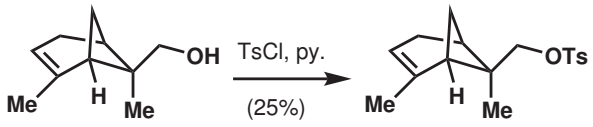

4.8 4.53

Tosylate 4.53. To a solution of alcohol **4.8** (1.9 mg, 0.0131 mmol) in pyridine (0.38 mL, 35 mM) at 0 °C was added TsCl (5.0 mg, 0.0262 mmol, 2.0 equiv). The reaction mixture was stored in a freezer at –20 °C for 11 days,* then poured into ice and extracted with Et_2O (3 x 10 mL). The combined organic extracts were washed sequentially with 1 M aqueous HCl (5 mL), $NaHCO_3$ (saturated aqueous, 10 mL) and brine (2 mL), then dried over $MgSO_4$. The mixture was then filtered and concentrated *in vacuo*. Purification by column chromatography (2.5–10% EtOAc/hexane) gave tosylate **4.53** (1.0 mg, 3.26 µmol, 25% yield) as a white film. ^{1}H NMR (600 MHz, $CDCl_3$) δ 7.82 (d, *J* = 8.0 Hz, 2H), 7.35 (d, *J* = 7.9 Hz, 2H), 5.24 (dt, *J* = 3.5, 1.7 Hz, 1H), 4.21 (d, *J* = 9.5 Hz, 1H), 4.17 (d, *J* = 9.4 Hz, 1H), 2.46 (s, 3H), 2.26 (ddd, *J* = 16.6, 4.9, 2.2 Hz, 1H), 2.23–2.17 (m, 1H), 2.15 (t, *J* = 4.6 Hz, 1H), 2.14–2.08 (m, 2H), 2.06 (t, *J* = 5.7 Hz, 1H), 1.64 (q, *J* = 1.9 Hz, 3H), 1.21 (d, *J* = 9.1 Hz, 1H), 0.86 (s, 3H); ^{13}C NMR (151 MHz, $CDCl_3$) δ 144.8, 143.1, 133.4, 130.0, 128.1, 117.2, 77.2, 42.7, 42.2, 36.6, 31.4, 30.6, 22.9, 21.8, 16.1; IR (thin film) 2594, 2924, 2854, 1733, 1710, 1598, 1447, 1358, 1175, 943, 862, 812, 789, 664, 554 cm^{-1}. *The product and starting material were not distinguishable by TLC. Reaction was likely done much sooner.

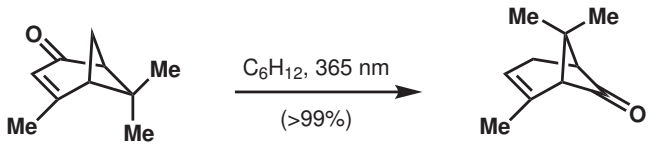

4.57
(–)-verbenone

4.60
(–)-chrysanthenone

4.5.2 Synthesis of chrysanthenol derivatives

Chrysanthenone. (–)-Verbenone (1.33 mL, 9.00 mmol) was dissolved in cyclohexane (9.0 mL, 1.0 M) under air. The stirring solution was irradiated with 365 nm light in a fan-cooled photobox for 4 h, then concentrated *in vacuo* to give a yellow oil (1.35 g, 9.00 mmol, >99% yield). This material was typically advanced without purification as significant decomposition was observed during flash column chromatography. Eluting with 0–10% EtOAc/hexanes gave chrysanthenone as a clear oil (900. mg, 5.99 mmol, 67% yield). Spectroscopic data for the purified compound matched that of the crude material. ^{1}H NMR (600 MHz, $CDCl_3$) δ 5.34 (bs, 1H), 2.66–2.62 (m, 1H), 2.62 (d, *J* = 6.6 Hz, 1H), 2.62–2.57 (m, 1H), 2.55 (dtd, *J* = 7.4, 3.2, 0.9 Hz, 1H), 1.69 (q, *J* = 2.0 Hz, 3H), 1.20 (s, 3H), 1.17 (s, 3H). ^{13}C NMR (151 MHz, $CDCl_3$) δ 206.5, 138.7, 118.6, 67.8, 62.6, 33.0, 29.9, 27.3, 23.0, 14.7. The spectroscopic data obtained and decomposition upon attempted purification are consistent with what was previously reported in the literature.[35]

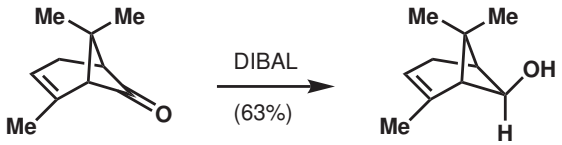

4.60 **4.56**

***cis*-Chrysanthenol.** To a stirring solution of crude chrysanthenone (225 mg, 1.50 mmol) in cyclohexane (10. mL, 0.15 M) was added a 1.0 M solution of DIBAL in hexanes (1.5 mL, 1.5 mmol, 1.0 equiv). The resultant solution was stirred at room temperature for 18 h, then quenched with a 20 wt% aqueous solution of Rochelle's salt (1 mL) and allowed to stir under air for an additional 16 h. The aqueous layer was extracted with EtOAc (3 x 0.5 mL). The combined organic extracts were dried over Na_2SO_4, filtered, and concentrated in vacuo to give 90 mg of a pale yellow oil. Purification by flash column chromatography (eluting with 0–25% EtOAc/hexane) gave *cis*-chrysanthenol **4.56** as a clear oil (151 mg, 0.992 mmol, 66% yield over 2 steps). ^{1}H NMR (600 MHz, $CDCl_3$) δ 5.20 (tq, *J* = 2.7, 1.3 Hz, 1H), 3.98 (s, 1H), 2.28 (ddd, *J* = 17.0, 4.7, 2.1 Hz, 1H), 2.23 (ddd, *J* = 17.5, 4.5, 2.6 Hz, 1H), 2.00–1.98 (m, 2H), 1.87 (bs, 1H), 1.66 (q, *J* = 2.0 Hz, 3H), 1.57 (s, 3H), 0.90 (s, 3H). The spectroscopic data obtained are consistent with those previously reported in the literature.[35]

General procedure for addition of Grignard reagents to chrysanthenone. To a solution of chrysanthenone in THF (0.2 M, including volume of Grignard solution) was added a solution of Grignard reagent in THF (2.0 or 4.0 equiv). The reaction mixture was allowed to stir at the specified temperature for 16 h, then quenched through the addition of NH_4Cl (saturated aqueous, 1 mL) and extracted with EtOAc (3 x 5 mL). The combined organic extracts were dried over Na_2SO_4, filtered, and concentrated *in vacuo* to give the crude product.

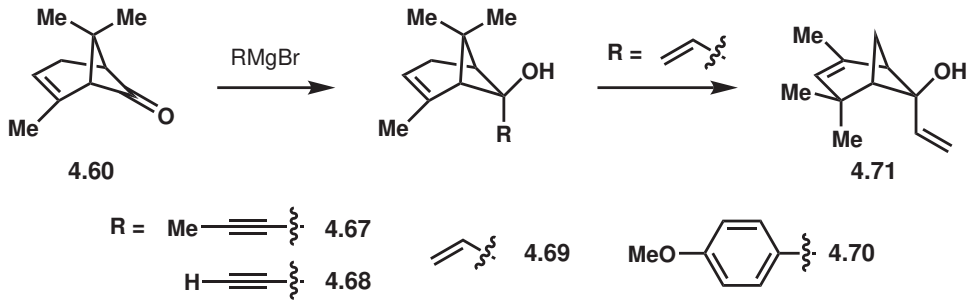

Propynyl chrysanthenol (4.67). To neat chrysanthenone (**4.60**, 30.0 mg, 0.200 mmol) was added 1-propynylmagnesium bromide (0.5 M in THF, 1.6 mL, 0.800 mmol, 4.0 equiv) at room temperature. Purification of the crude reaction mixture by flash column chromatography (eluting with 0–20% EtOAc/hexane) gave propynyl chrysanthenol (**4.67**, 36.0 mg, 95%) as a clear oil. ^{1}H NMR (600 MHz, $CDCl_3$) δ 5.28 (tt, *J* = 3.3, 1.7 Hz, 1H), 2.44 (ddd, *J* = 17.3, 5.8, 2.4 Hz, 1H), 2.23 (dtd, *J* = 16.8, 4.9, 2.4 Hz, 1H), 2.19 (dd, *J* = 6.8, 1.4 Hz, 1H), 2.16–2.08 (m, 2H), 1.80 (s, 3H), 1.66 (q, *J* = 2.0 Hz, 3H), 1.59 (s, 3H), 0.93 (s, 3H). This compound is unambiguously characterized by single crystal X-ray crystallography (see Appendix 4.B).

Ethynyl chrysanthenol (4.68). To a solution of chrysanthenone (**4.60**, 15.0 mg, 0.100 mmol) in THF (0.2 mL) was added ethynylmagnesium bromide (0.5 M in THF, 0.8 mL, 0.400 mmol, 4.0 equiv). The reaction vessel was sealed and heated in an aluminum block at 50 °C. Purification of the crude reaction mixture by flash column chromatography (eluting with 0–20% EtOAc/hexane) gave ethynyl chrysanthenol (**4.68**, 10.9 mg, 62%) ^{1}H NMR (600 MHz, $CDCl_3$) δ 5.32 (th, *J* = 3.1, 1.6 Hz, 1H), 2.49 (dq, *J* = 17.2, 2.6 Hz, 1H), 2.39 (s, 1H), 2.31–2.26 (m, 1H), 2.27 (s, 1H), 2.24 (dd, *J* = 6.8, 1.3 Hz, 1H), 2.19 (dtd, *J* = 6.9, 2.9, 1.2 Hz, 1H), 1.68 (q, *J* = 2.0 Hz, 3H), 1.61 (s, 3H), 0.94 (s, 3H).

4-Methoxy-phenyl chrysanthenol (4.70). To a solution of chrysanthenone (**4.60**, 15.0 mg, 0.100 mmol) in THF (0.6 mL) was added 4-methoxyphenylmagnesium bromide (0.5 M in THF, 0.4 mL, 0.200 mmol, 2.0 equiv). The reaction vessel was sealed and heated in an aluminum block at 50 °C. Purification of the crude reaction mixture by flash column chromatography (eluting with 0–20% EtOAc/hexane) gave aryl chrysanthenol **4.70** (24.7 mg, 96%) as a clear oil. ^{1}H NMR (600 MHz, $CDCl_3$) δ 7.06 (d, *J* = 8.6 Hz, 2H), 6.83 (d, *J* = 8.7 Hz, 2H), 4.85 (td, *J* = 3.1, 1.6 Hz, 1H), 3.79 (s, 3H), 2.51–2.42 (m, 2H), 2.23 (dq, *J* = 18.3, 2.5 Hz, 1H), 2.14 (ddd, *J* = 17.5, 4.3, 2.3 Hz, 1H), 1.74 (s, 3H), 1.70 (q, J = 2.0 Hz, 3H), 1.01 (s, 3H).

Vinyl chrysanthenol (4.69) and rearranged product 4.71. To a solution of chrysanthenone (**4.60**, 15.0 mg, 0.100 mmol) in THF (0.7 mL) was added vinylmagnesium bromide (0.7 M in THF, 0.3 mL, 0.200 mmol, 2.0 equiv) at room temperature. The reaction yielded a mixture of starting material **4.60** (18%), 1,2-addition product **4.69** (10%), and rearranged product **4.71** (45%), as determined by quantitative NMR. Full conversion to **4.71** could be obtained through either use of 4.0 equiv of vinylmagnesium bromide or heating of the reaction mixture to 50 °C.

*Vinyl chrysanthenol (**4.69**).* ^{1}H NMR (500 MHz, $CDCl_3$) δ 6.35 (dd, *J* = 17.6, 10.8 Hz, 1H), 5.24–5.22 (m, 1H), 5.20 (dd, *J* = 17.6, 1.6 Hz, 1H), 5.04 (dd, *J* = 10.9, 1.6 Hz, 1H), 2.25 (dq, *J* = 21.0, 3.3 Hz, 1H), 2.18 (dq, *J* = 21.0, 3.3 Hz, 1H), 2.11 (q, *J* = 1.1 Hz, 2H), 1.67 (s, 3H), 1.66 (d, J = 2.0 Hz, 3H), 0.95 (s, 3H). ^{13}C NMR ($CDCl_3$)* 141.4, 141.1, 119.4, 113.8, 56.8, 50.3, 35.9, 31.1, 28.0, 23.2,

22.4. *Based on correlations in HSQC and HMBC.

*Rearranged vinyl chrysanthenol (**4.71**).* ^{1}H NMR (400 MHz, $CDCl_3$) δ 6.31 (dd, *J* = 17.5, 10.9 Hz, 1H), 5.23 (dd, *J* = 17.5, 1.8 Hz, 1H), 5.07 (dd, *J* = 10.8, 1.8 Hz, 1H), 5.05 (s, 1H), 2.66 (dt, *J* = 8.3, 5.6 Hz, 1H), 2.23 (ddd, *J* = 6.5, 5.2, 1.2 Hz, 1H), 2.17 (td, *J* = 6.3, 1.9 Hz, 1H), 1.75 (bs, 1H), 1.71 (d, *J* = 1.6 Hz, 3H), 1.50 (d, *J* = 8.3 Hz, 1H), 1.04 (s, 3H), 0.97 (s, 3H); ^{13}C NMR (101 MHz, $CDCl_3$) δ 141.3, 139.9, 127.9, 113.5, 81.3, 58.2, 50.5, 39.1, 31.1, 28.9, 26.4, 22.4. This compound is unambiguously characterized by single crystal X-ray crystallography (see Appendix 4.B).

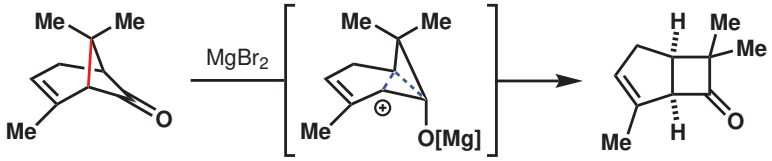

4.72 **4.73** **4.74**

Fused bicycle 4.74. To chrysanthenone (**4.60**, 34.3 mg, 0.228 mmol) was added a solution of cyclopropylmagnesium bromide (0.5 M in THF, 1.8 mL, 0.913 mmol, 4.0 equiv). The reaction vessel was sealed and heated in an oil bath at 65 °C for 24 h. The reaction mixture was quenched through the addition on NH_4Cl (saturated aqueous, 1 mL) and extracted with EtOAc (3 x 1 mL). The combined organic extracts were dried over Na_2SO_4, filtered, and concentrated *in vacuo*. Purification by flash column chromatography (eluting with 0-25% EtOAc/hexane) gave fused bicycle **4.74** (6.2 mg, 0.0413 mmol, 18% yield). ^{1}H NMR (500 MHz, $CDCl_3$) δ 5.42 (s, 1H), 4.02 (q, *J* = 3.4 Hz, 1H), 2.63 (t, *J* = 7.6 Hz, 1H), 2.57 (ddq, *J* = 15.8, 8.0, 2.4 Hz, 1H), 2.46 (d, *J* = 17.3 Hz, 1H), 1.75 (dq, *J* = 2.6, 1.4 Hz, 3H), 1.20 (s, 3H), 1.11 (s, 3H); ^{13}C NMR (126 MHz, $CDCl_3$) δ 213.9, 136.1, 127.5, 72.1, 60.8, 40.5, 33.7, 24.6, 19.3, 15.5. The spectroscopic data obtained are consistent with those previously reported in the literature.[36]

4.6 References

1. Yang, Y.; Zhang, Y.; Zhang, S.; Chen, Q.; Ma, K.; Bao, L.; Tao, Y.; Yin, W.; Wang, G.; Liu, H. *J. Nat. Prod.* **2018**, *81*, 1089–1092.
2. Wang, L.; Yang, B.; Lin, X. P.; Zhou, X. F.; Liu, Y. *Nat. Prod. Rep.* **2013**, *30*, 455–473.
3. Huang, A. C.; Kautsar, S. A.; Hong, Y. J.; Medema, M. H.; Bond, A. D.; Tantillo, D. J.; Osbourn, A. *Proc. Natl. Acad. Sci. U. S. A.* **2017**, *114*, E6005–E6014.
4. Luo, S. H.; Luo, Q.; Niu, X. M.; Xie, M. J.; Zhao, X.; Schneider, B.; Gershenzon, J.; Li, S. H. *Angew. Chem., Int. Ed.* **2010**, *49*, 4471–4475.
5. Li, C. H.; Jing, S. X.; Luo, S. H.; Shi, W.; Hua, J.; Liu, Y.; Li, X. N.; Schneider, B.; Gershenzon, J.; Li, S. H. *Org. Lett.* **2013**, *15*, 1694–1697.
6. Evidente, A.; Kornienko, A.; Lefranc, F.; Cimmino, A.; Dasari, R.; Evidente, M.; Mathieu, V.; Kiss, R. *Curr. Med. Chem.* **2015**, *22*, 3502–3522.
7. Zhang, C.; Liu, Y. *J. Nat. Med.* **2015**, *69*, 255–266.
8. Genilloud, O. *Nat. Prod. Rep.* **2017**, *34*, 1203–1232.
9. Bermejo, F. A.; Fernández Mateos, A.; Marcos Escribano, A.; Martín Lago, R.; Mateos Burón, L.; Rodríguez López, M.; Rubio González, R. *Tetrahedron* **2006**, *62*, 8933–8942.
10. Masarwa, A.; Weber, M.; Sarpong, R. *J. Am. Chem. Soc.* **2015**, *137*, 6327–6334.
11. McCombie, S. W.; Motherwell, W. B.; Tozer, M. J. *Org. React.* **2012**, *77*, 161–592.

12. Herrmann, J. M.; König, B. *Eur. J. Org. Chem.* **2013**, 7017–7027.
13. Lam, K.; Markó, I. E. *Org. Lett.* **2008**, *10*, 2773–2776.
14. Boar, R. B.; Joukhadar, L.; McGhie, J. F.; Misra, S. C.; Barrett, A. G.; Barton, D. H.; Prokopiou, P. A. *J. Chem. Soc., Chem. Commun.* **1978**, 68–69.
15. Barrett, A. G.; Godfrey, C. R.; Hollinshead, D. M.; Prokopiou, P. A.; Barton, D. H.; Boar, R. B.; Joukhadar, L.; McGhie, J. F.; Misra, S. C. *J. Chem. Soc., Perkin Trans. 1* **1981**, *0*, 1501–1509.
16. Dolan, S. C.; MacMillan, J. *J. Chem. Soc., Chem. Commun.* **1985**, 1588–1589.
17. Muehlfenzl, K. S. Toward the Total Synthesis of Somaliensene A., MA thesis, Ludwig-Maximilians Universitaet Muenchen, 2019.
18. Romero, N. A.; Nicewicz, D. A. *Chem. Rev.* **2016**, *116*, 10075–10166.
19. Zuo, Z.; Macmillan, D. W. *J. Am. Chem. Soc.* **2014**, *136*, 5257–5260.
20. Miyake, Y.; Nakajima, K.; Nishibayashi, Y. *Chem. Commun.* **2013**, *49*, 7854–7856.
21. Liu, J.; Liu, Q.; Yi, H.; Qin, C.; Bai, R.; Qi, X.; Lan, Y.; Lei, A. *Angew. Chem., Int. Ed.* **2014**, *53*, 502–506.
22. Nawrat, C. C.; Jamison, C. R.; Slutskyy, Y.; MacMillan, D. W.; Overman, L. E. *J. Am. Chem. Soc.* **2015**, *137*, 11270–11273.
23. Zhang, X.; MacMillan, D. W. *J. Am. Chem. Soc.* **2016**, *138*, 13862–13865.
24. Su, J. Y.; Grünenfelder, D. C.; Takeuchi, K.; Reisman, S. E. *Org. Lett.* **2018**, *20*, 4912–4916.
25. Okada, K.; Okamoto, K.; Morita, N.; Okubo, K.; Oda, M. *J. Am. Chem. Soc.* **1991**, *113*, 9401–9402.
26. Barton, D. H. R.; Crich, D. *Tetrahedron Lett.* **1985**, *26*, 757–760.
27. Barton, D. H. R.; Crich, D.; Kretzschmar, G. *J. Chem. Soc., Perkin Trans. 1* **1986**, 39–53.
28. Lackner, G. L.; Quasdorf, K. W.; Overman, L. E. *J. Am. Chem. Soc.* **2013**, *135*, 15342–15345.
29. Lackner, G. L.; Quasdorf, K. W.; Pratsch, G.; Overman, L. E. *J. Org. Chem.* **2015**, *80*, 6012–6024.
30. Hurst, J. J.; Whitham, G. H. *J. Chem. Soc.* **1960**, 2864–2869.
31. (a) Erman, W. F. *J. Am. Chem. Soc.* **1967**, *89*, 3828–3841; (b) Erman, W. F. *J. Am. Chem. Soc.* **1969**, *91*, 779–780; (c) Erman, W. F.; Treptow, R. S.; Bakuzis, P.; Wenkert, E. *J. Am. Chem. Soc.* **1971**, *93*, 657–665.
32. Gottlieb, H. E.; Kotlyar, V.; Nudelman, A. *J. Org. Chem.* **1997**, *62*, 7512–7515.
33. Lee, S.-G. *Magn. Reson. Chem.* **2002**, *40*, 311–312.
34. Reich, H. J. C-13 Chemical Shifts, https://www.chem.wisc.edu/areas/reich/nmr/c13-data/cdata.htm.
35. Pinhey, J. T.; Southwell, I. A. *Aust. J. Chem.* **1971**, *24*, 1311–1313.
36. Beereboom, J. J. *J. Am. Chem. Soc.* **1963**, *85*, 3525–3526.

Appendix 4.A NMR Spectral Data for Chapter 4

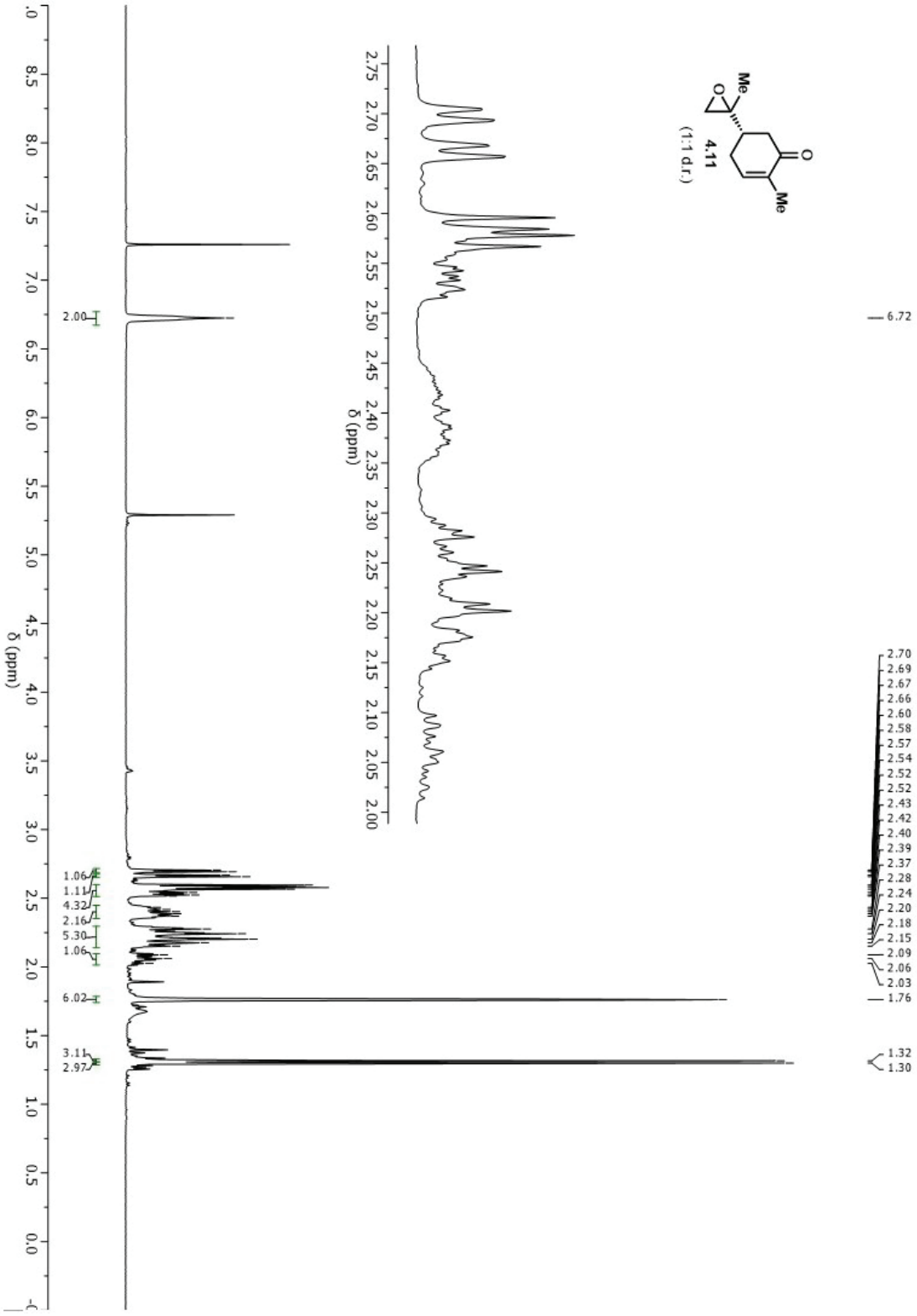

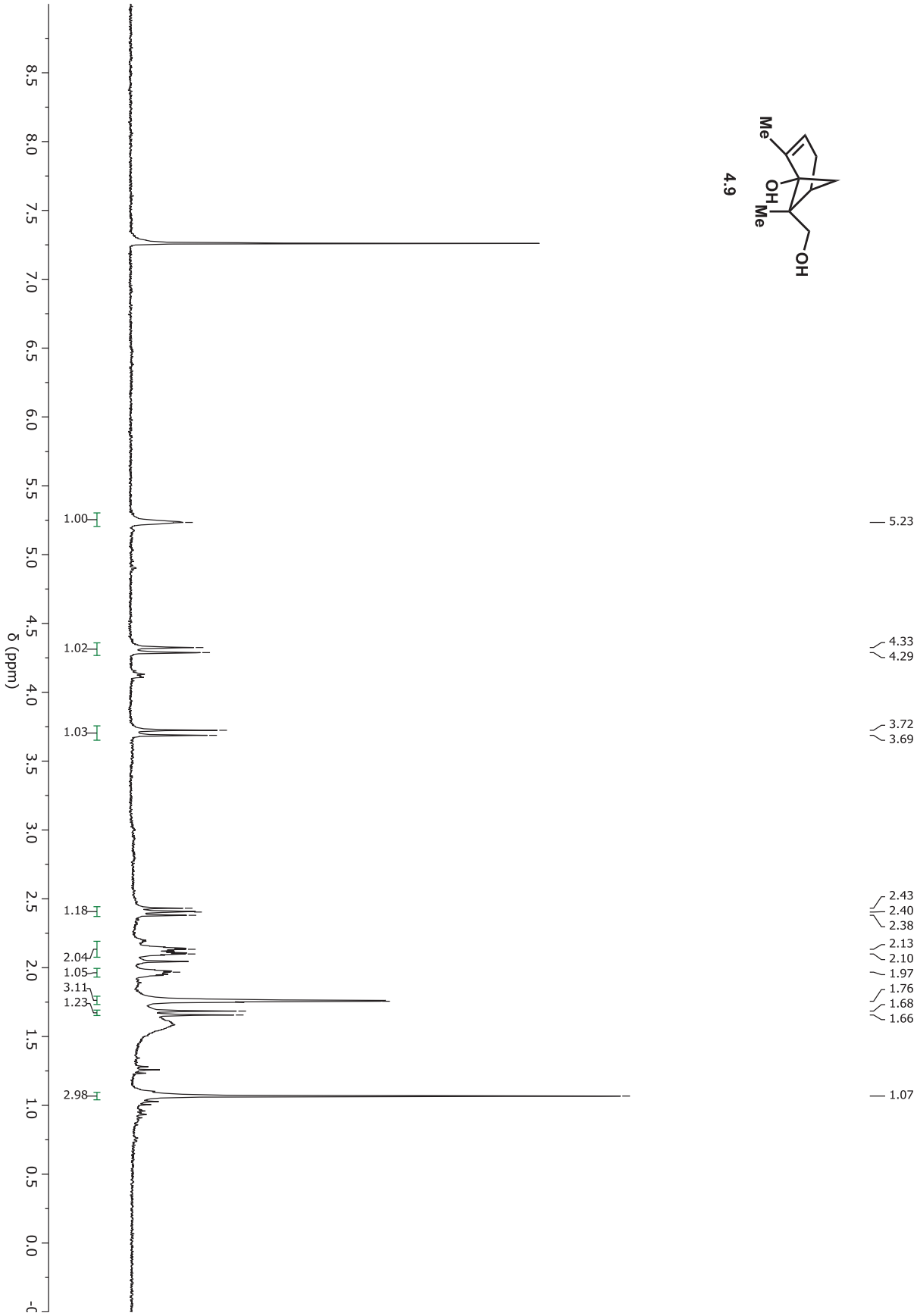
Me
OH
Me
OH
4.9
δ (ppm)
8.5
8.0
7.5
7.0
6.5
6.0
5.5
5.0
4.5
4.0
3.5
3.0
2.5
2.0
1.5
1.0
0.5
0.0
1.00
1.02
1.03
1.18
2.04
1.05
3.11
1.23
2.98
5.23
4.33
4.29
3.72
3.69
2.43
2.40
2.38
2.13
2.10
1.97
1.76
1.68
1.66
1.07

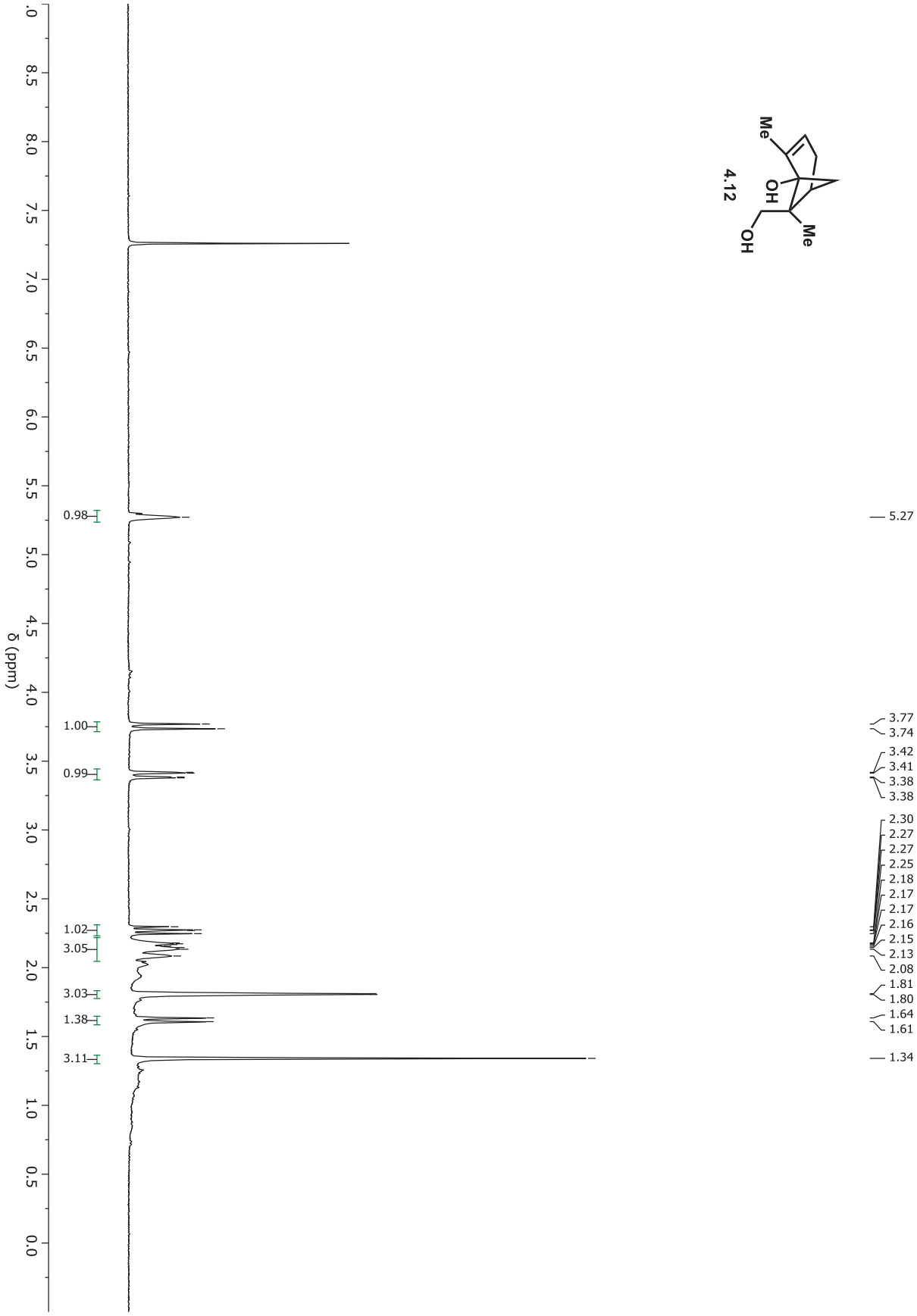
Me
OH
OH
Me
4.12
δ (ppm)
0.98
1.00
0.99
1.02
3.05
3.03
1.38
3.11
5.27
3.77
3.74
3.42
3.41
3.38
3.38
2.30
2.27
2.27
2.25
2.18
2.17
2.17
2.16
2.15
2.13
2.08
1.81
1.80
1.64
1.61
1.34

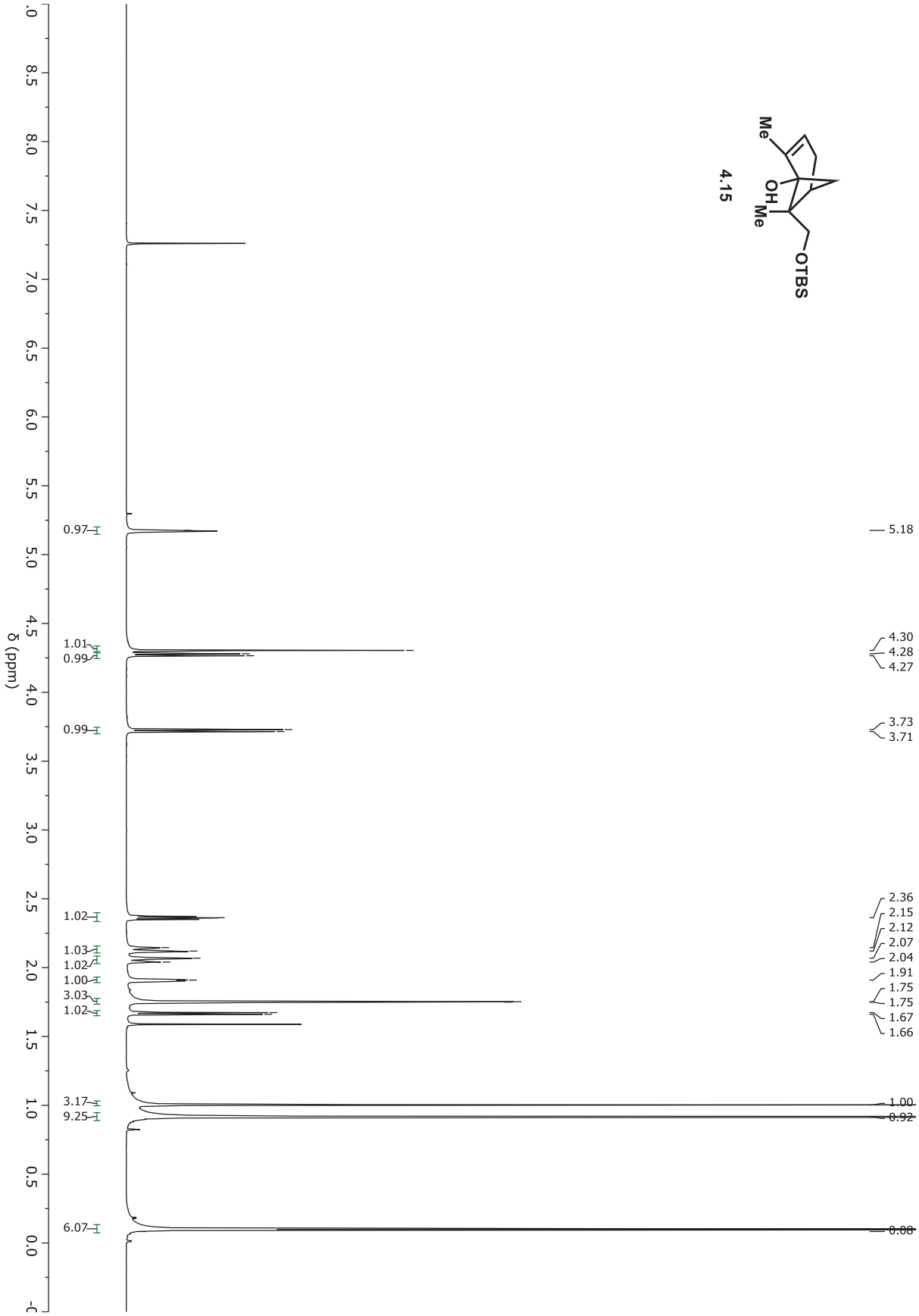
4.15
Me
OH
Me
OTBS
δ (ppm)
0.97
1.01
0.99
0.99
1.02
1.03
1.02
1.00
3.03
1.02
3.17
9.25
6.07
5.18
4.30
4.28
4.27
3.73
3.71
2.36
2.15
2.12
2.07
2.04
1.91
1.75
1.75
1.67
1.66
1.00
0.92
0.00

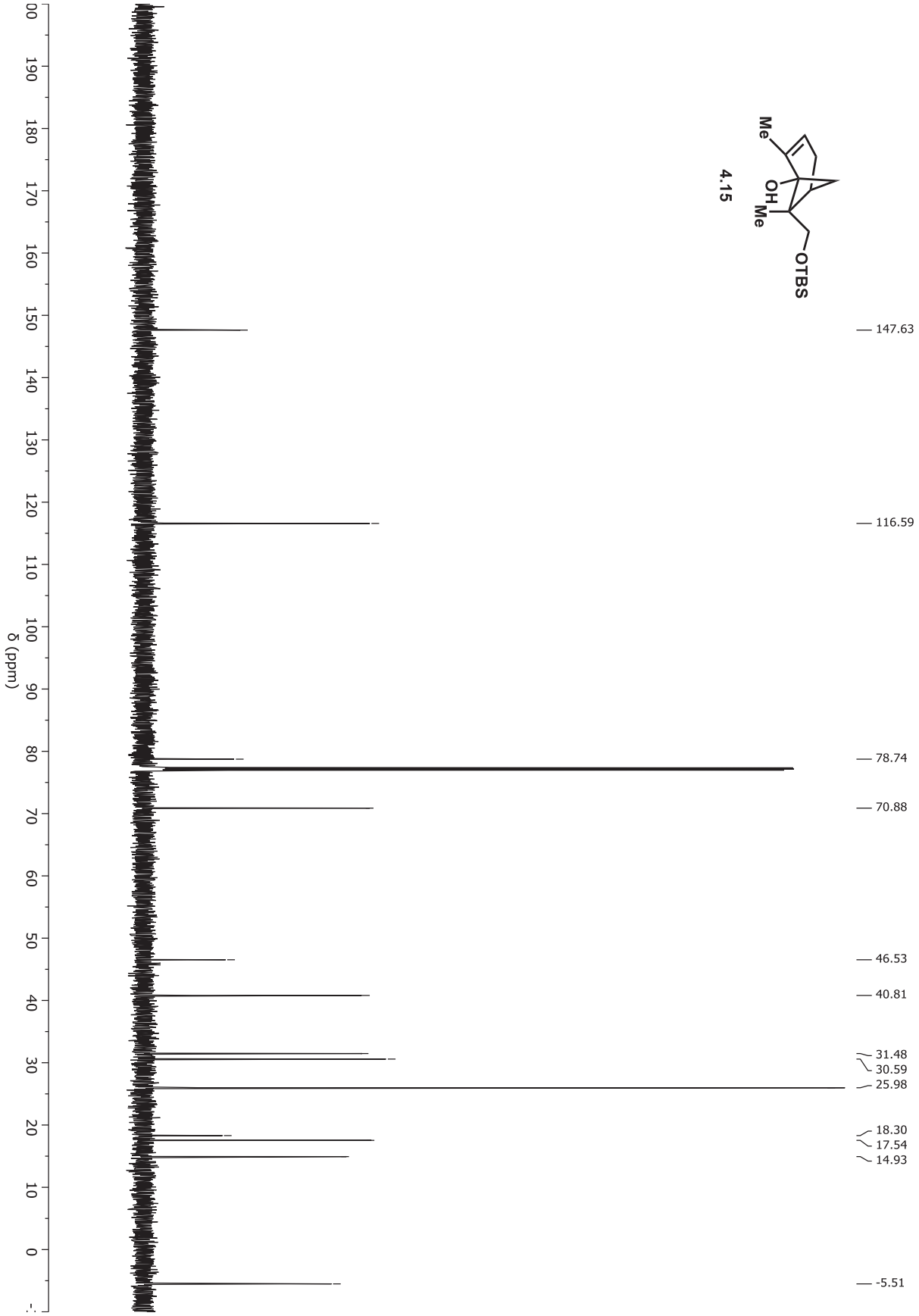
4.15
Me
OH
Me
OTBS
δ (ppm)
200
190
180
170
160
150
140
130
120
110
100
90
80
70
60
50
40
30
20
10
0
-10
147.63
116.59
78.74
70.88
46.53
40.81
31.48
30.59
25.98
18.30
17.54
14.93
-5.51

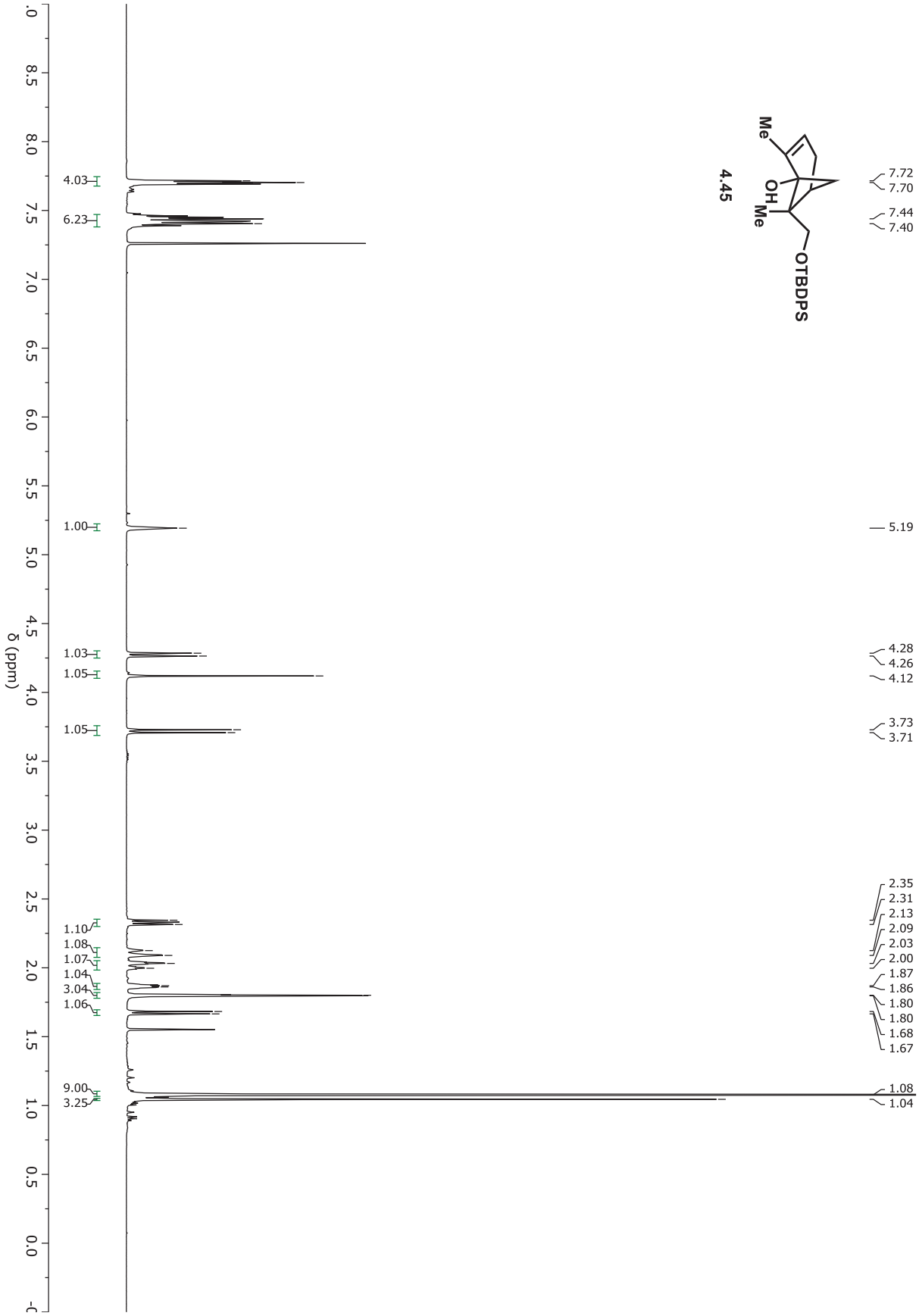
4.03
6.23
1.00
1.03
1.05
1.05
1.10
1.08
1.07
1.04
3.04
1.06
9.00
3.25
δ (ppm)
4.45
Me
OH
Me
OTBDPS
7.72
7.70
7.44
7.40
5.19
4.28
4.26
4.12
3.73
3.71
2.35
2.31
2.13
2.09
2.03
2.00
1.87
1.86
1.80
1.80
1.68
1.67
1.08
1.04

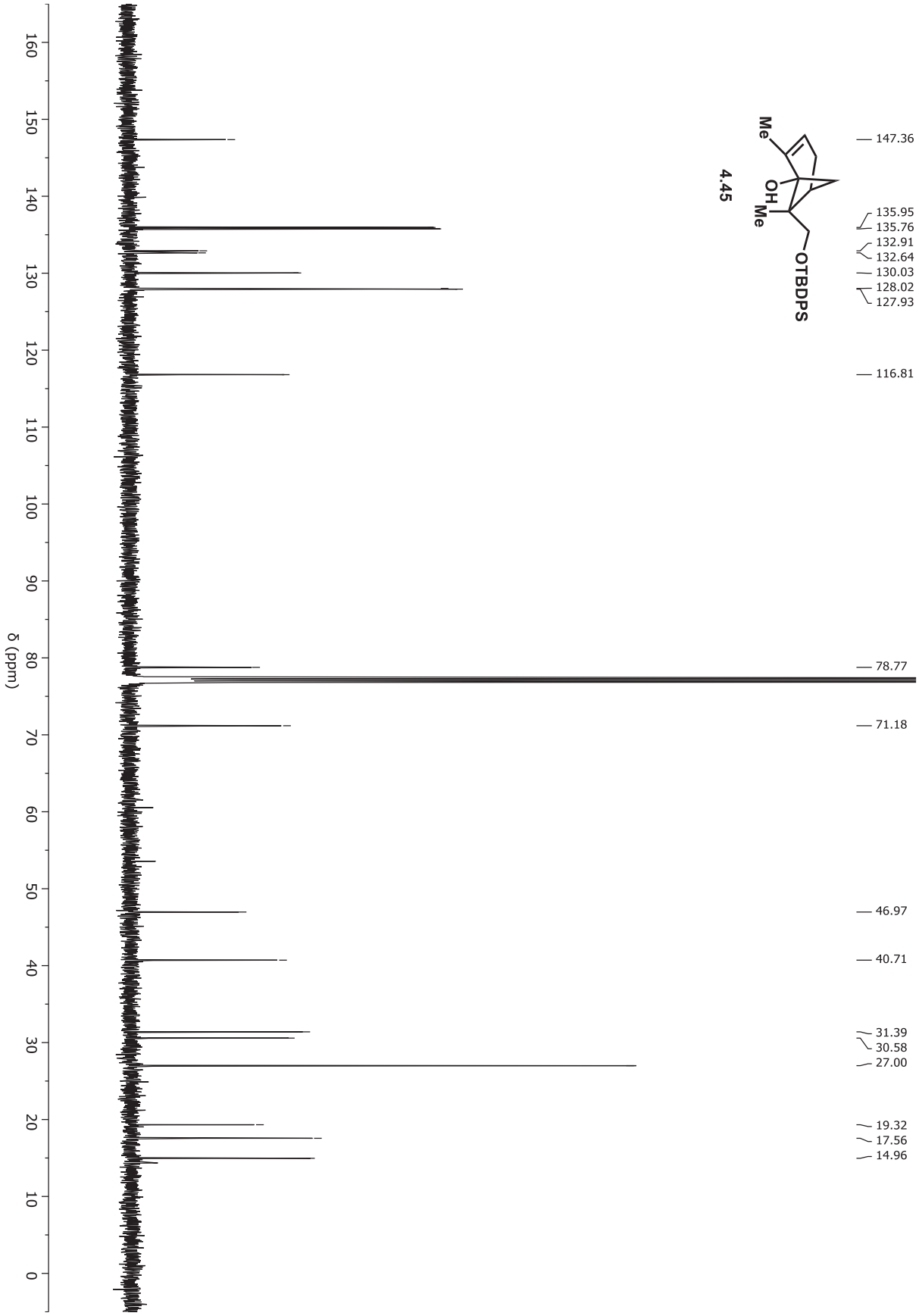
4.45
Me
OH
Me
OTBDPS
147.36
135.95
135.76
132.91
132.64
130.03
128.02
127.93
116.81
78.77
71.18
46.97
40.71
31.39
30.58
27.00
19.32
17.56
14.96
δ (ppm)
160
150
140
130
120
110
100
90
80
70
60
50
40
30
20
10
0

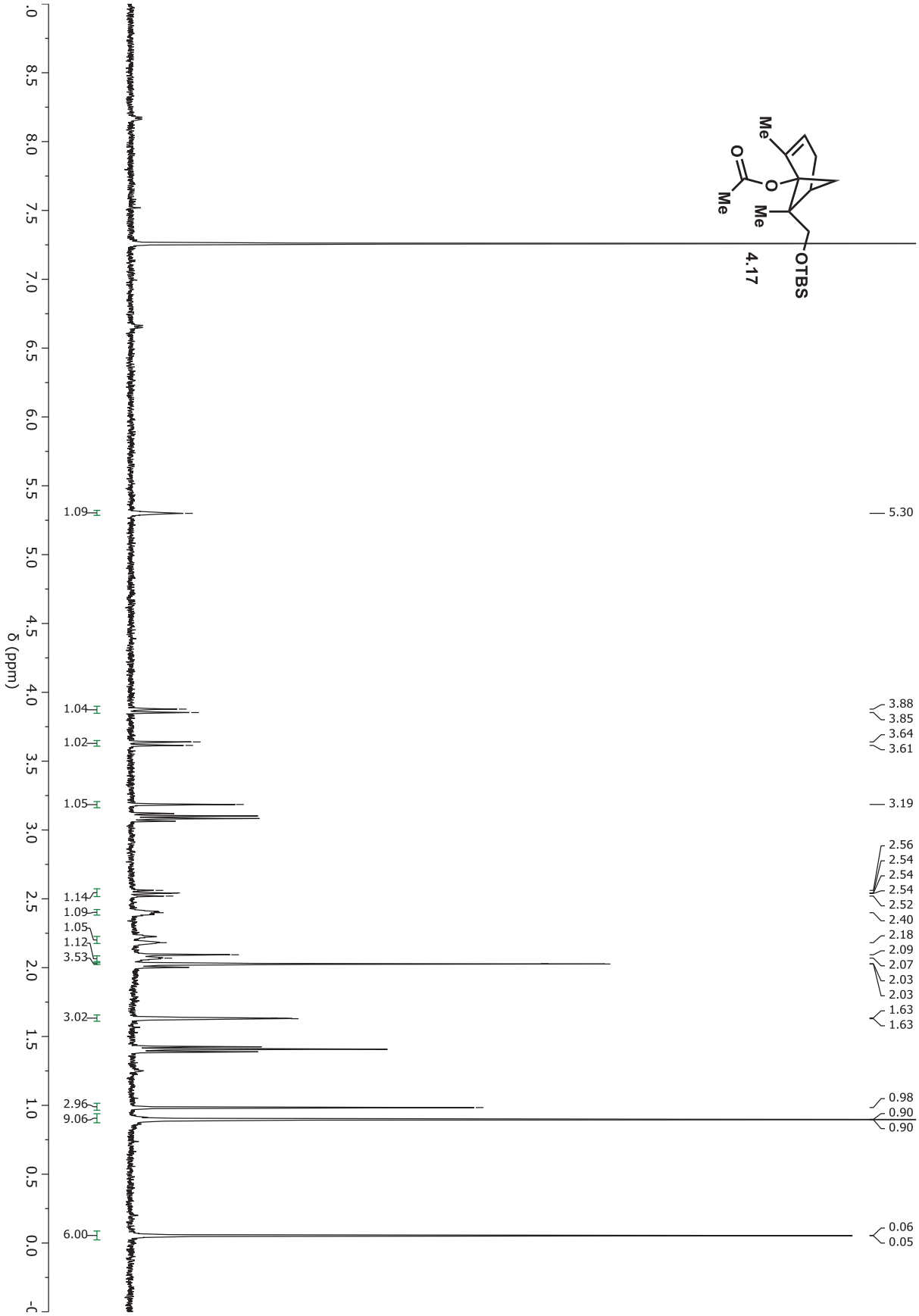
Me
O
Me
O
Me
4.17
OTBS
δ (ppm)
1.09
1.04
1.02
1.05
1.14
1.09
1.05
1.12
3.53
3.02
2.96
9.06
6.00
5.30
3.88
3.85
3.64
3.61
3.19
2.56
2.54
2.54
2.54
2.52
2.40
2.18
2.09
2.07
2.03
2.03
1.63
1.63
0.98
0.90
0.90
0.06
0.05

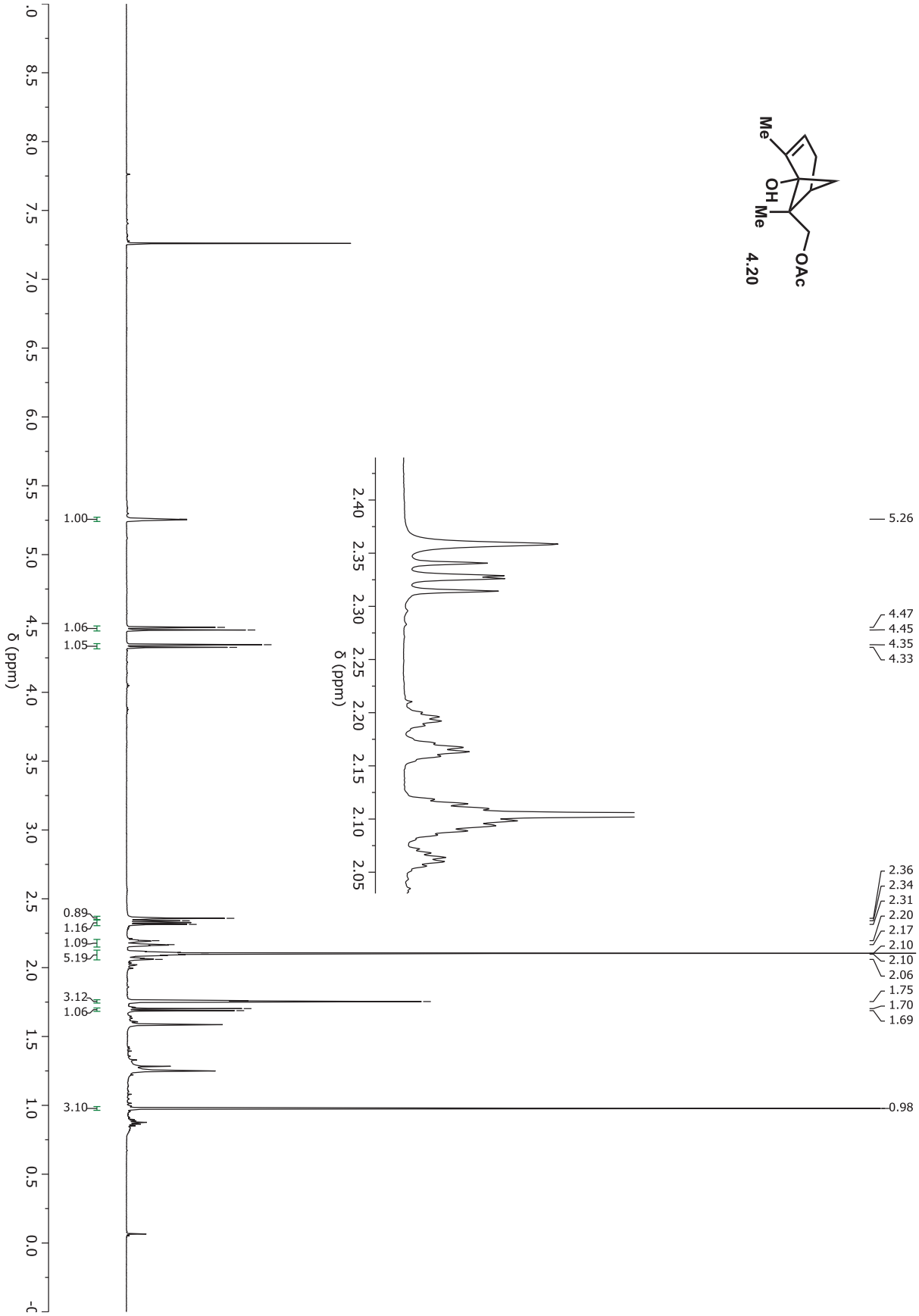
Me
OH
Me
OAc
4.20
δ (ppm)
δ (ppm)
1.00
1.06
1.05
0.89
1.16
1.09
5.19
3.12
1.06
3.10
5.26
4.47
4.45
4.35
4.33
2.36
2.34
2.31
2.20
2.17
2.10
2.10
2.06
1.75
1.70
1.69
0.98

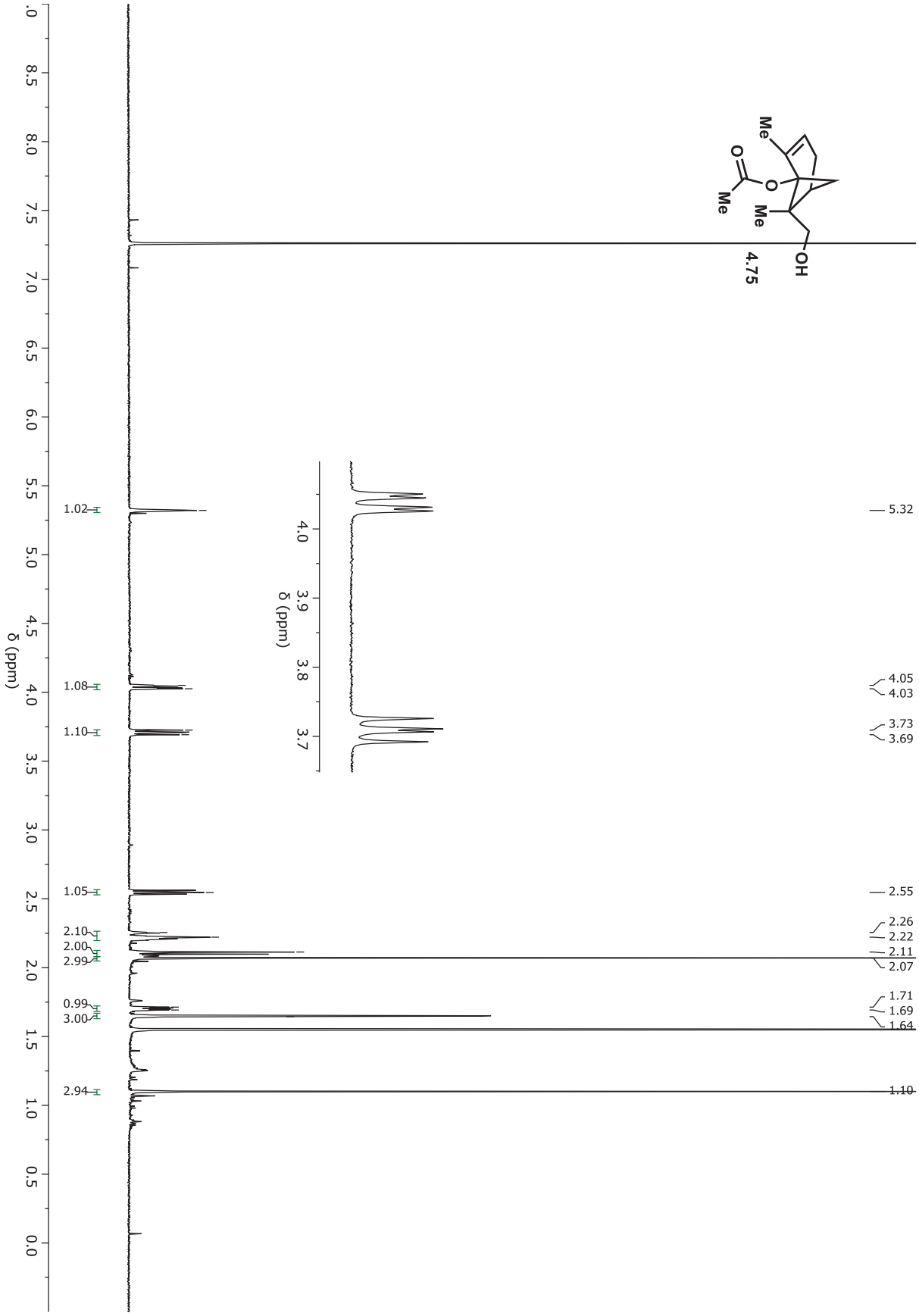
Me
O
O
Me
Me
OH
4.75
δ (ppm)
4.0
3.9
3.8
3.7
1.02
1.08
1.10
1.05
2.10
2.00
2.99
0.99
3.00
2.94
5.32
4.05
4.03
3.73
3.69
2.55
2.26
2.22
2.11
2.07
1.71
1.69
1.64
1.10

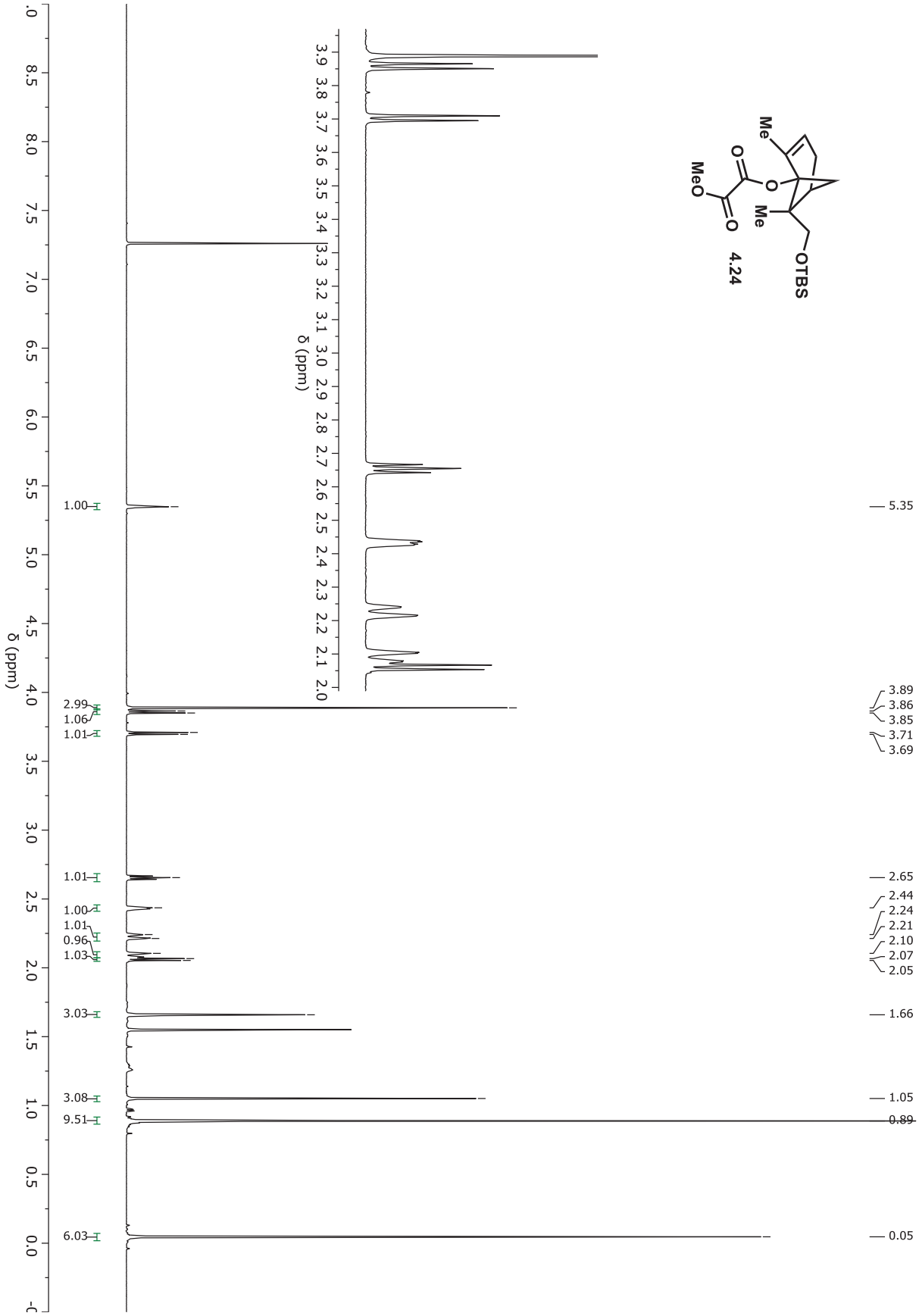
Me
O
MeO
O
O
Me
OTBS
4.24
δ (ppm)
δ (ppm)
1.00
2.99
1.06
1.01
1.01
1.00
1.01
0.96
1.03
3.03
3.08
9.51
6.03
5.35
3.89
3.86
3.85
3.71
3.69
2.65
2.44
2.24
2.21
2.10
2.07
2.05
1.66
1.05
0.89
0.05

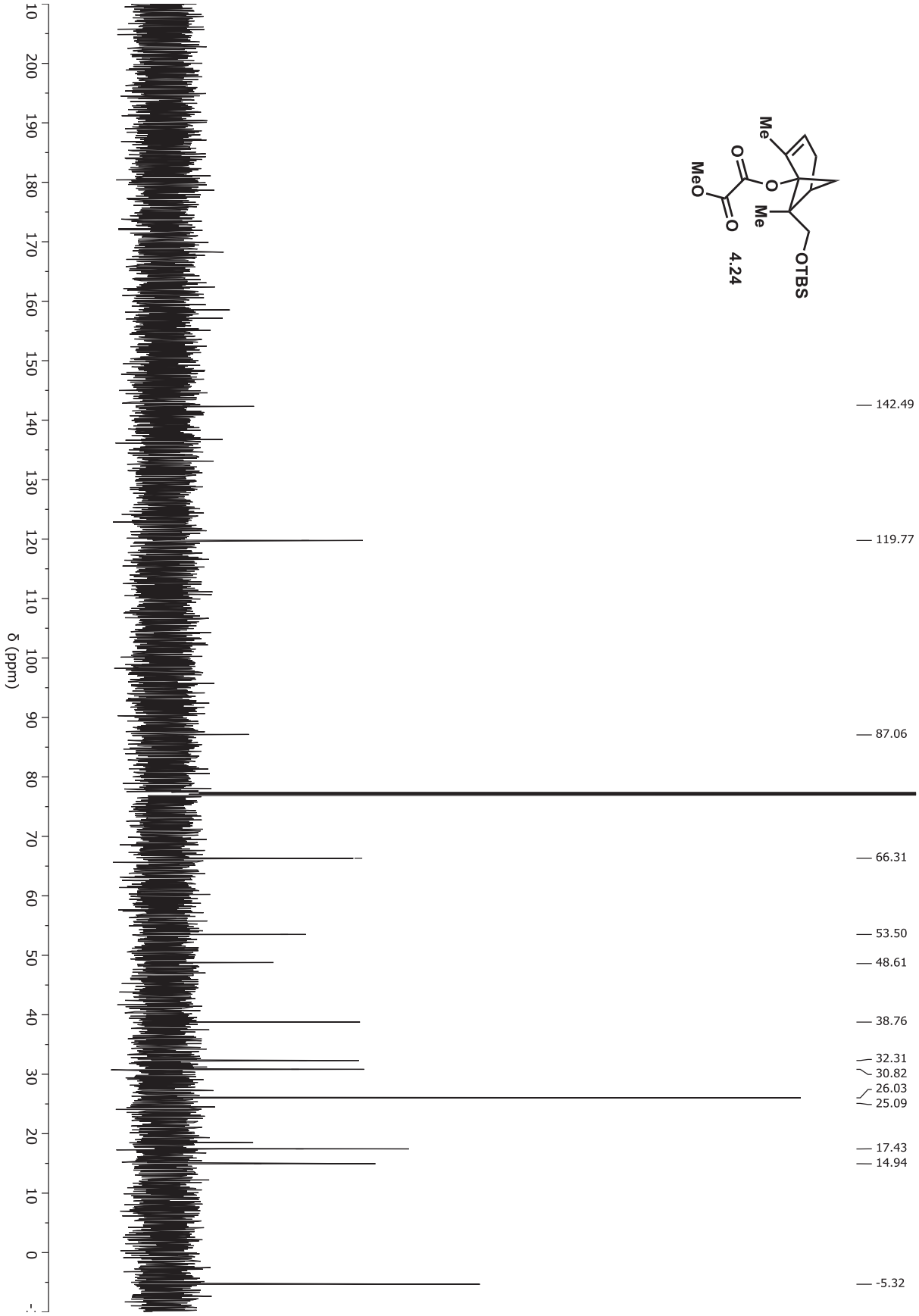
Me
O
MeO
O
O
Me
OTBS
O
4.24
δ (ppm)
142.49
119.77
87.06
66.31
53.50
48.61
38.76
32.31
30.82
26.03
25.09
17.43
14.94
-5.32

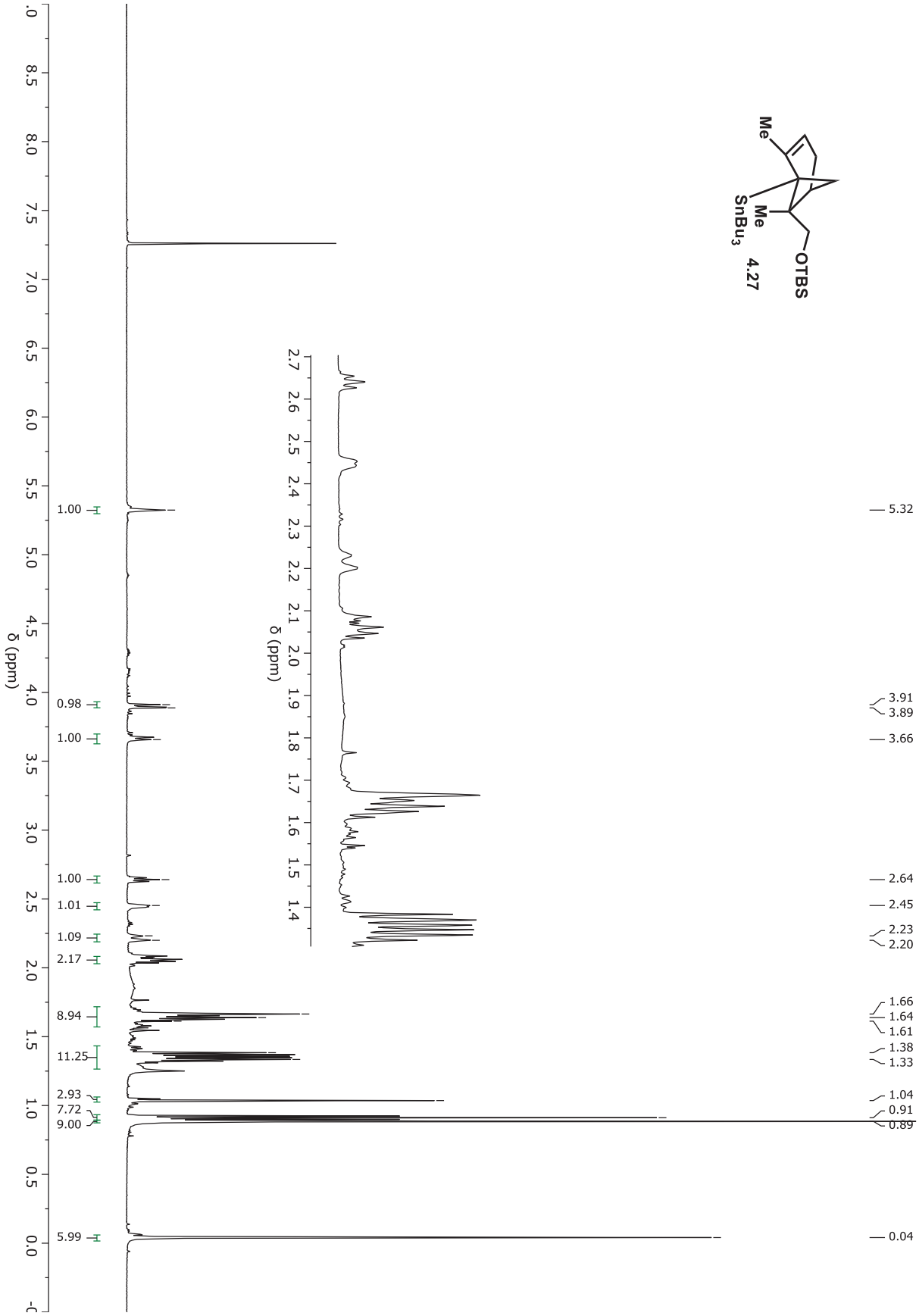
Me
Me
SnBu3
OTBS
4.27
δ (ppm)
1.00
0.98
1.00
1.00
1.01
1.09
2.17
8.94
11.25
2.93
7.72
9.00
5.99
5.32
3.91
3.89
3.66
2.64
2.45
2.23
2.20
1.66
1.64
1.61
1.38
1.33
1.04
0.91
0.89
0.04

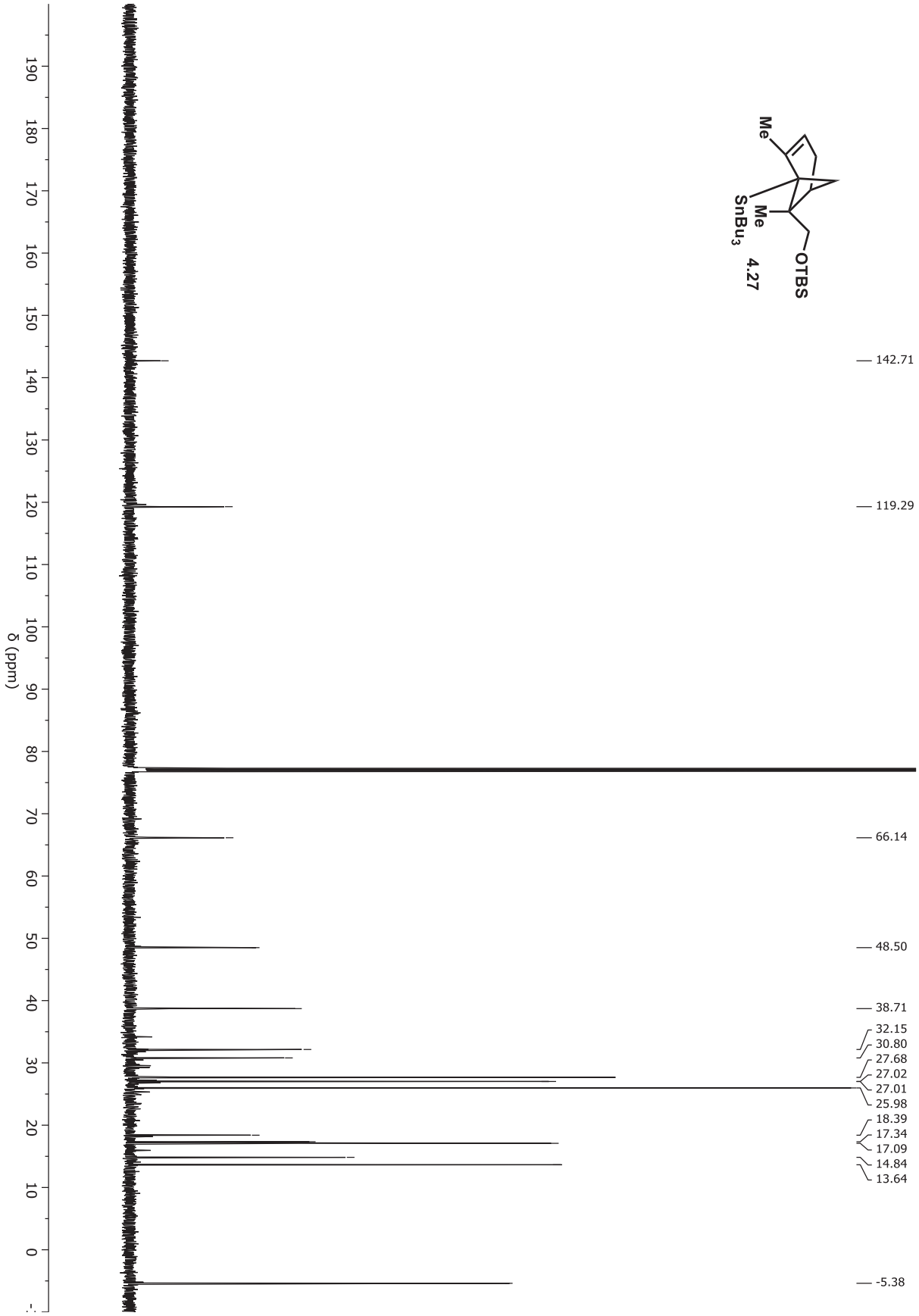
Me
Me
SnBu3
OTBS
4.27
δ (ppm)
142.71
119.29
66.14
48.50
38.71
32.15
30.80
27.68
27.02
27.01
25.98
18.39
17.34
17.09
14.84
13.64
-5.38

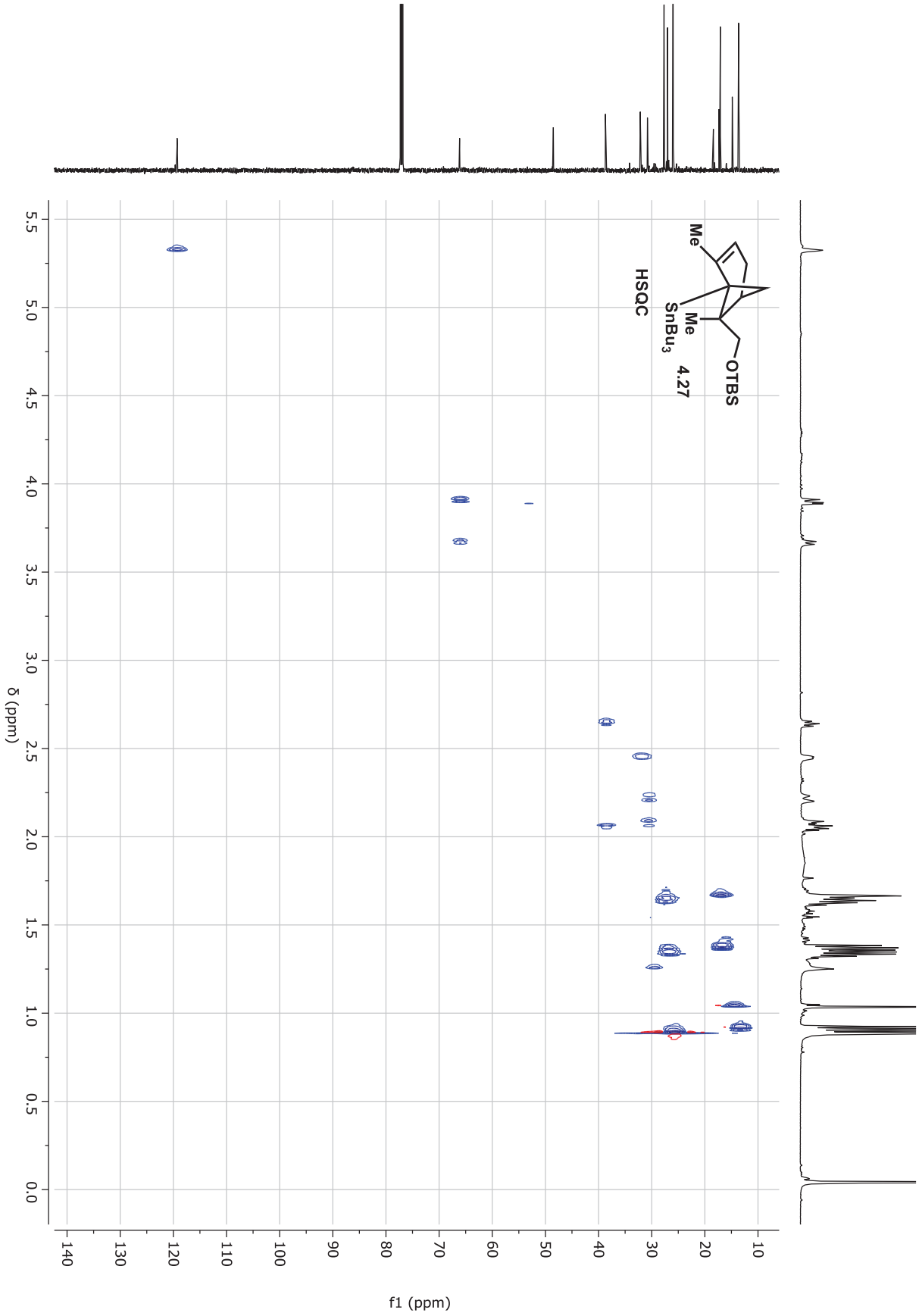
HSQC
Me
Me
SnBu3
OTBS
4.27
δ (ppm)
f1 (ppm)

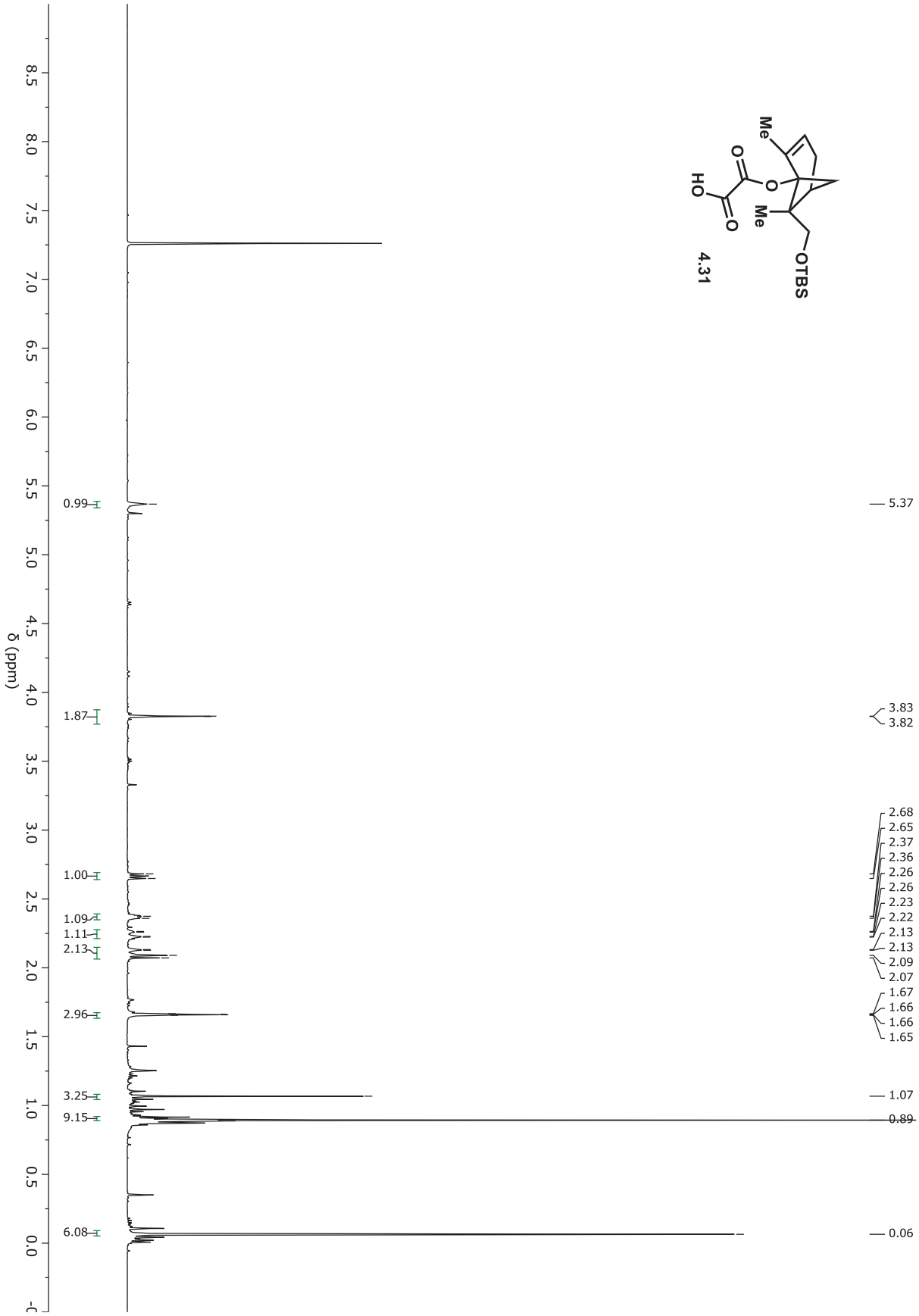
Me
O
O
HO
O
O
Me
OTBS
4.31
δ (ppm)
0.99
1.87
1.00
1.09
1.11
2.13
2.96
3.25
9.15
6.08
5.37
3.83
3.82
2.68
2.65
2.37
2.36
2.26
2.26
2.23
2.22
2.13
2.13
2.09
2.07
1.67
1.66
1.66
1.65
1.07
0.89
0.06

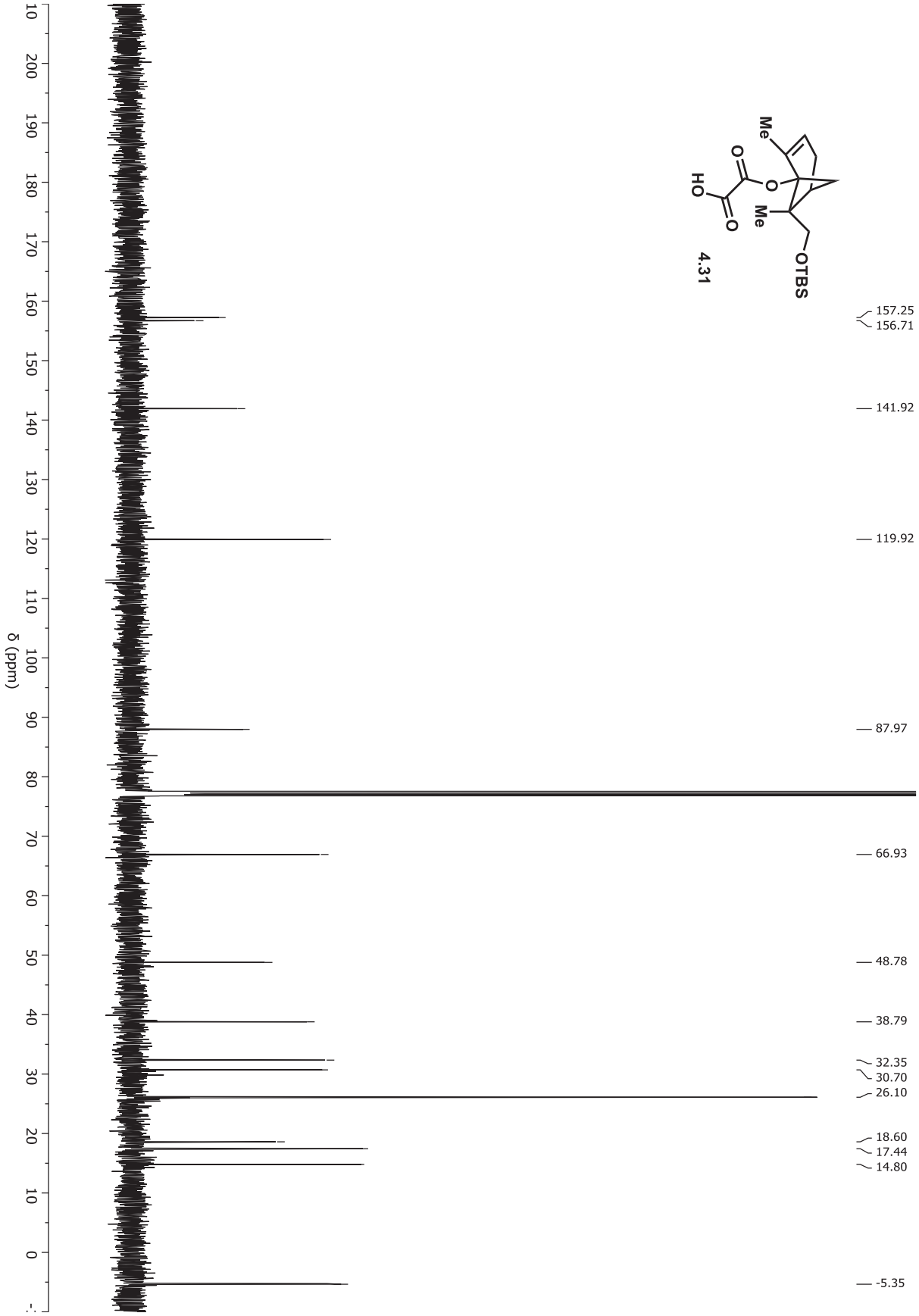
δ (ppm)
157.25
156.71
141.92
119.92
87.97
66.93
48.78
38.79
32.35
30.70
26.10
18.60
17.44
14.80
-5.35
4.31
HO
O
O
O
Me
Me
OTBS

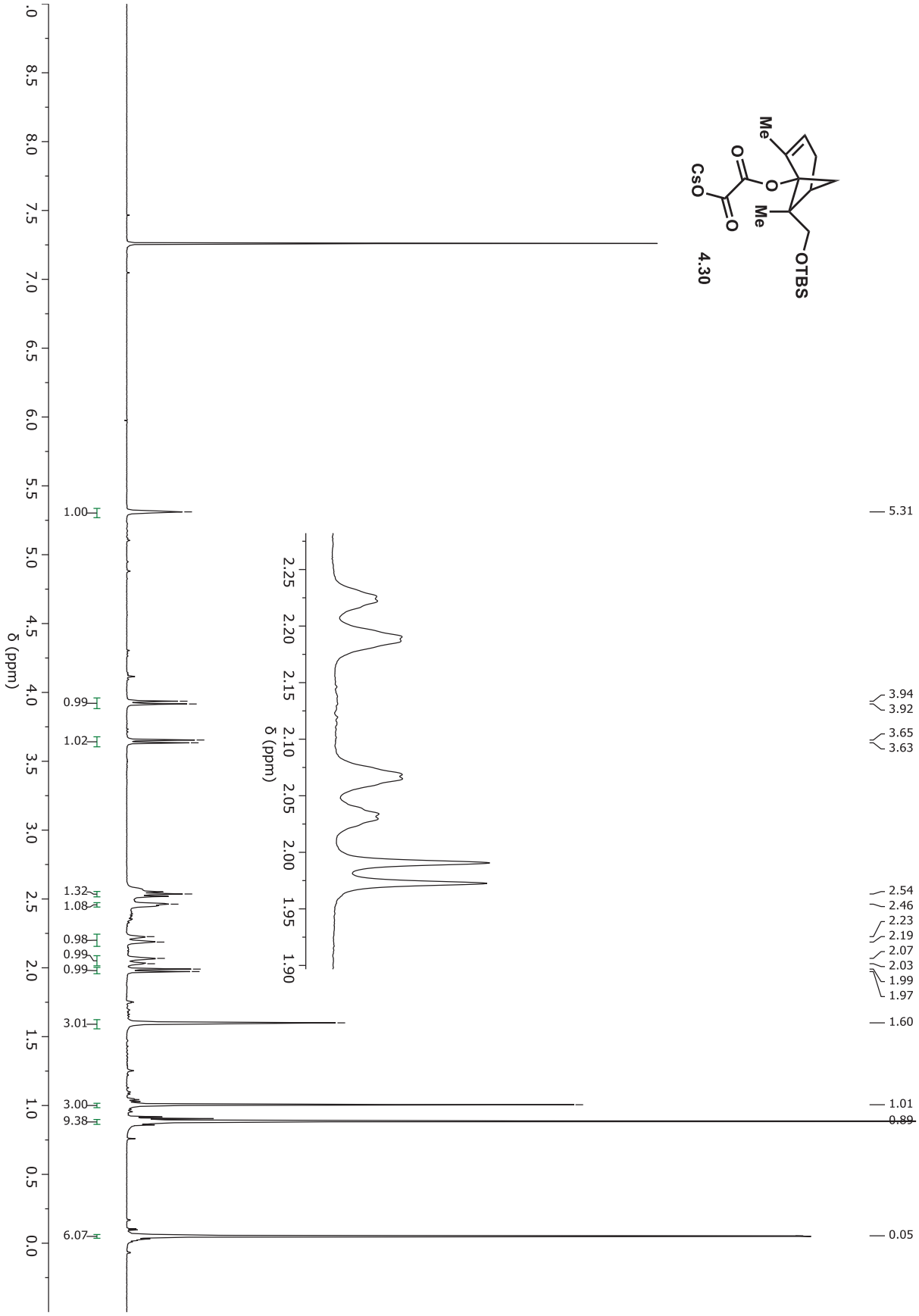
Me
O
CsO
O
O
Me
OTBS
4.30
δ (ppm)
2.25
2.20
2.15
2.10
2.05
2.00
1.95
1.90
δ (ppm)
.0
8.5
8.0
7.5
7.0
6.5
6.0
5.5
5.0
4.5
4.0
3.5
3.0
2.5
2.0
1.5
1.0
0.5
0.0
1.00
0.99
1.02
1.32
1.08
0.98
0.99
0.99
3.01
3.00
9.38
6.07
5.31
3.94
3.92
3.65
3.63
2.54
2.46
2.23
2.19
2.07
2.03
1.99
1.97
1.60
1.01
0.89
0.05

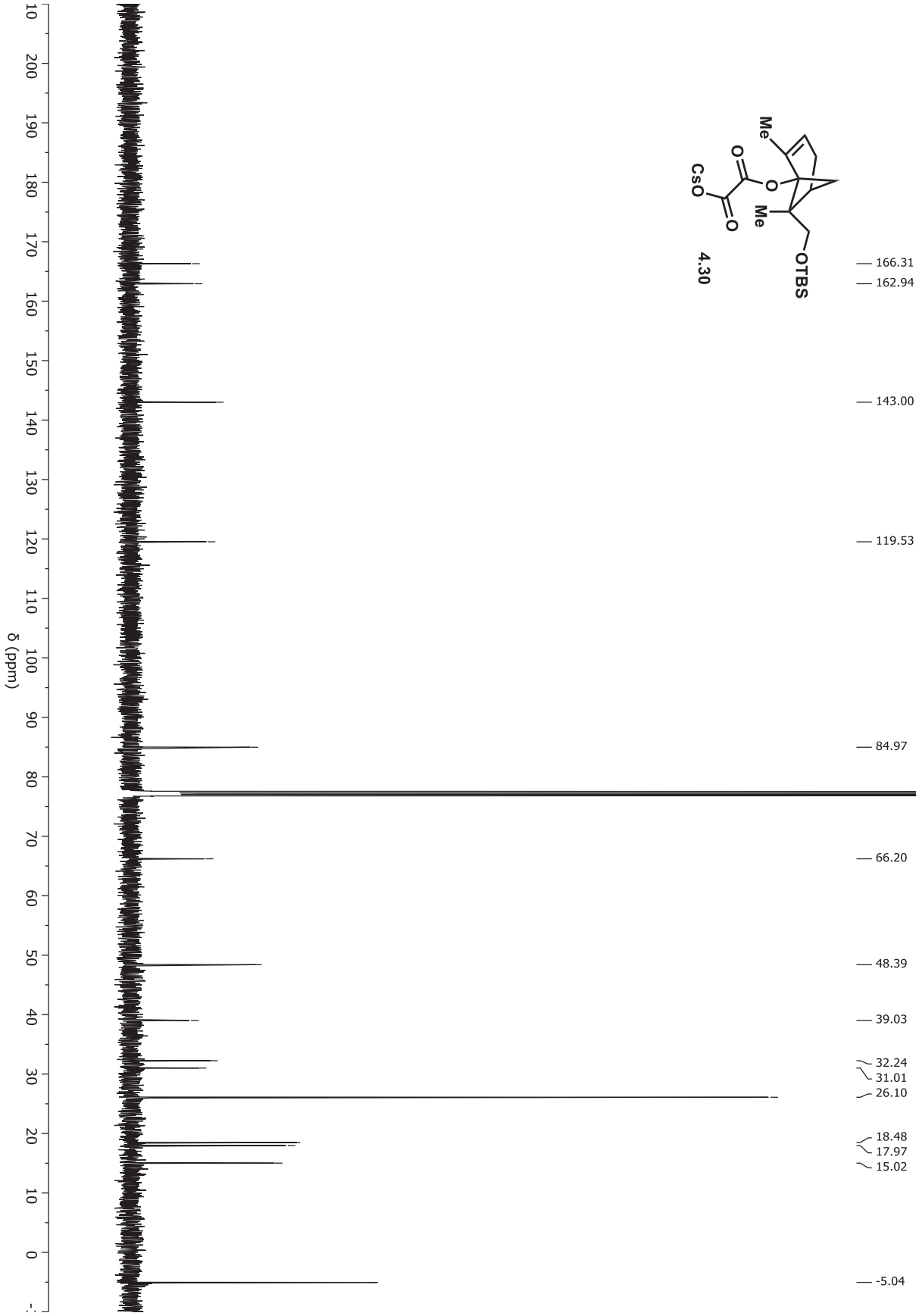
Me
O
CsO
O
O
Me
OTBS
4.30
166.31
162.94
143.00
119.53
84.97
66.20
48.39
39.03
32.24
31.01
26.10
18.48
17.97
15.02
-5.04
δ (ppm)

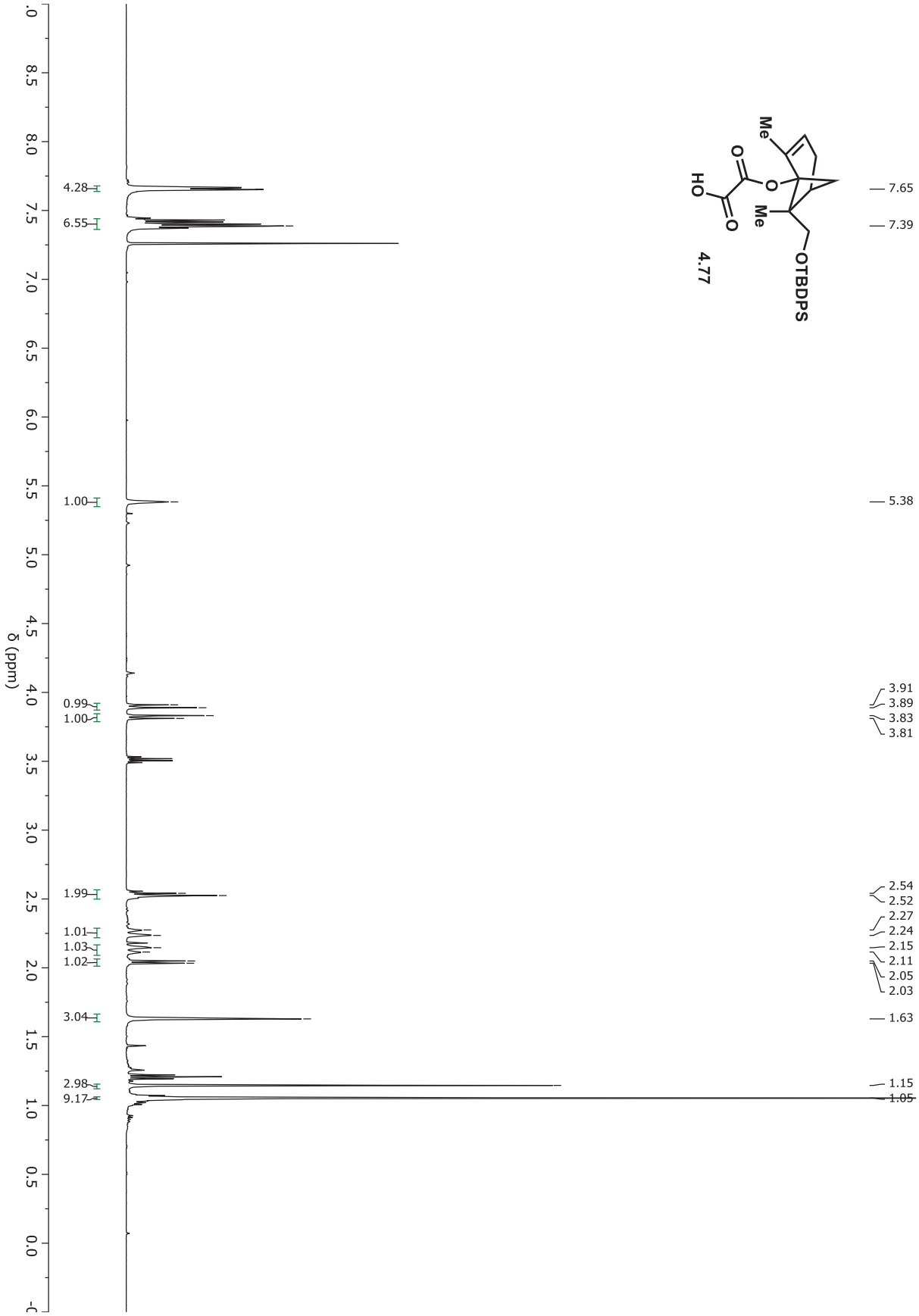
4.77
HO
O
O
O
Me
Me
OTBDPS
δ (ppm)
4.28
6.55
1.00
0.99
1.00
1.99
1.01
1.03
1.02
3.04
2.98
9.17
7.65
7.39
5.38
3.91
3.89
3.83
3.81
2.54
2.52
2.27
2.24
2.15
2.11
2.05
2.03
1.63
1.15
1.05

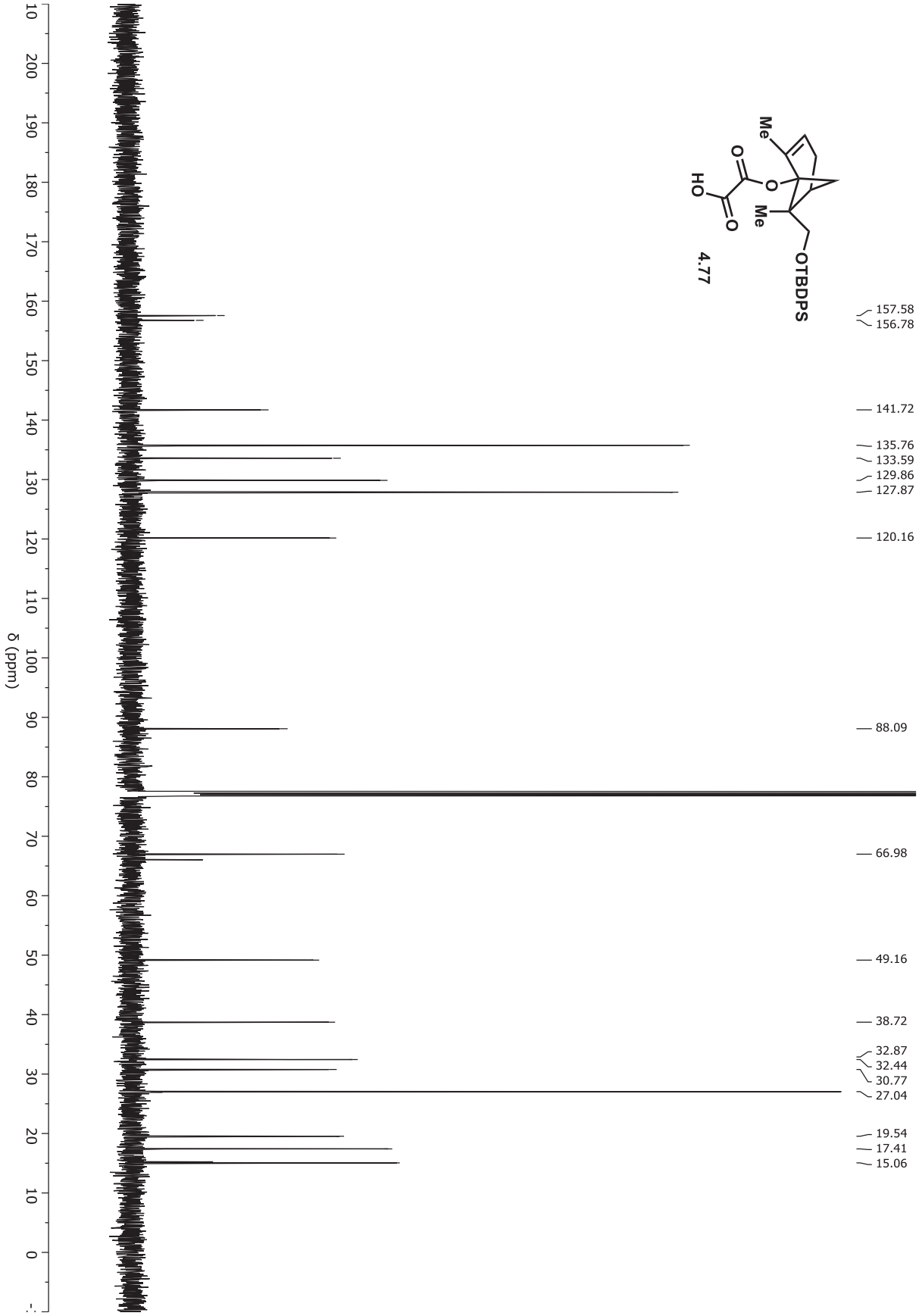
δ (ppm)
157.58
156.78
141.72
135.76
133.59
129.86
127.87
120.16
88.09
66.98
49.16
38.72
32.87
32.44
30.77
27.04
19.54
17.41
15.06
4.77
Me
O
O
HO
O
O
Me
OTBDPS

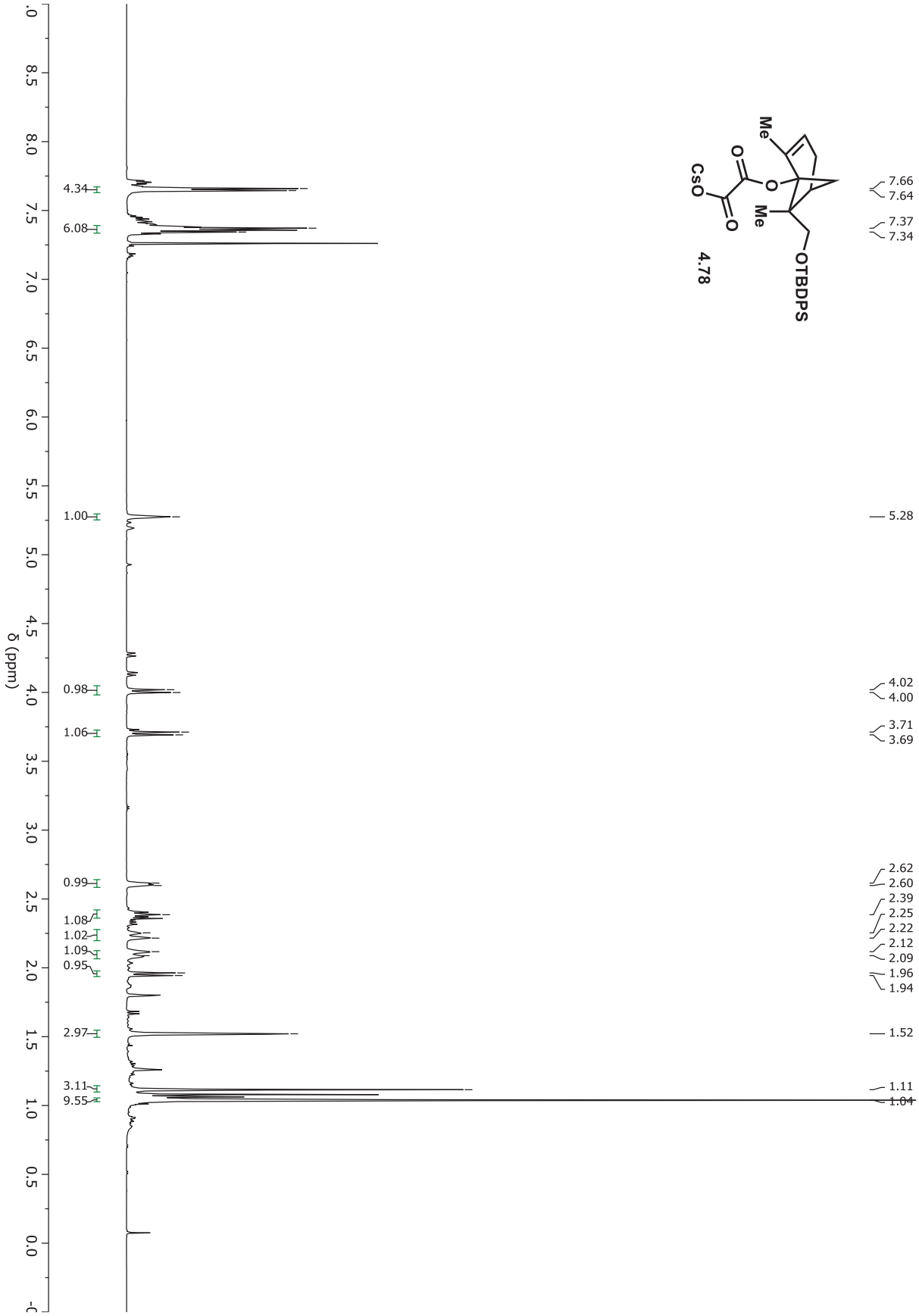
δ (ppm)
4.34
6.08
1.00
0.98
1.06
0.99
1.08
1.02
1.09
0.95
2.97
3.11
9.55
7.66
7.64
7.37
7.34
5.28
4.02
4.00
3.71
3.69
2.62
2.60
2.39
2.25
2.22
2.12
2.09
1.96
1.94
1.52
1.11
1.04
Me
O
Me
CsO
O
O
OTBDPS
4.78

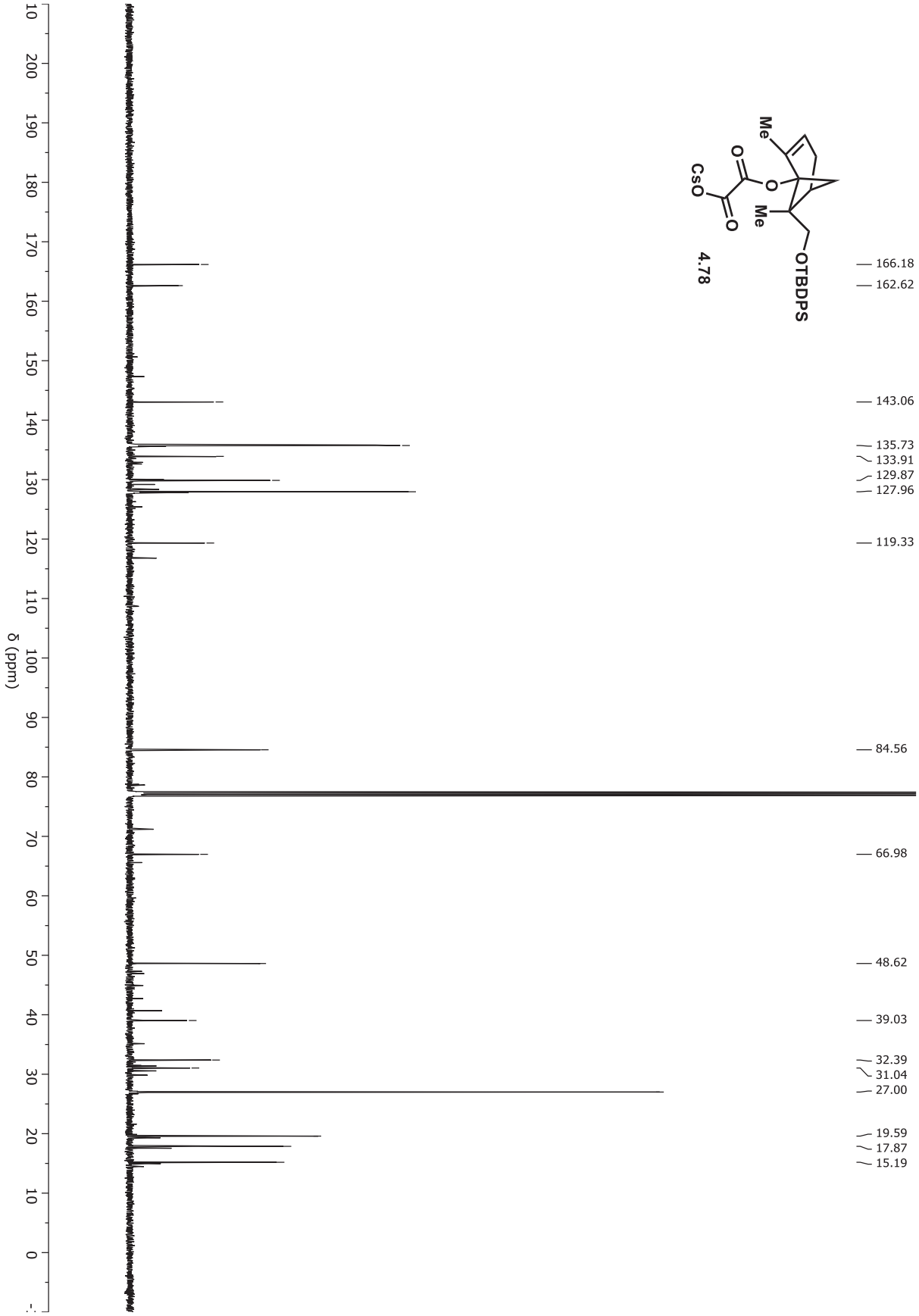
4.78
CsO
O
O
O
Me
Me
OTBDPS
166.18
162.62
143.06
135.73
133.91
129.87
127.96
119.33
84.56
66.98
48.62
39.03
32.39
31.04
27.00
19.59
17.87
15.19
δ (ppm)

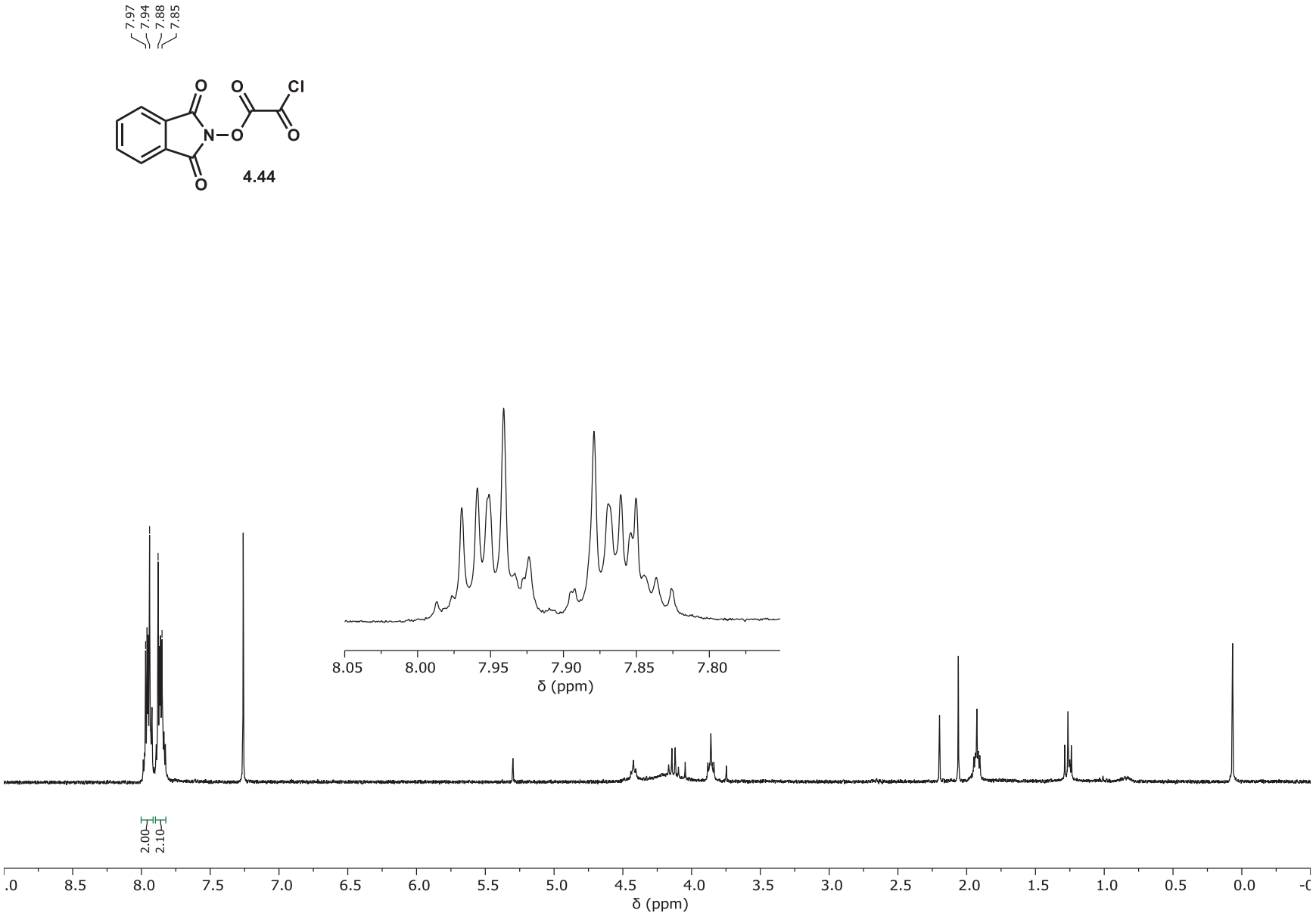
7.97
7.94
7.88
7.85
O
O
Cl
N
O
O
O
O
4.44
8.05
8.00
7.95
7.90
7.85
7.80
δ (ppm)
2.00
2.10
.0
8.5
8.0
7.5
7.0
6.5
6.0
5.5
5.0
4.5
4.0
3.5
3.0
2.5
2.0
1.5
1.0
0.5
0.0
δ (ppm)

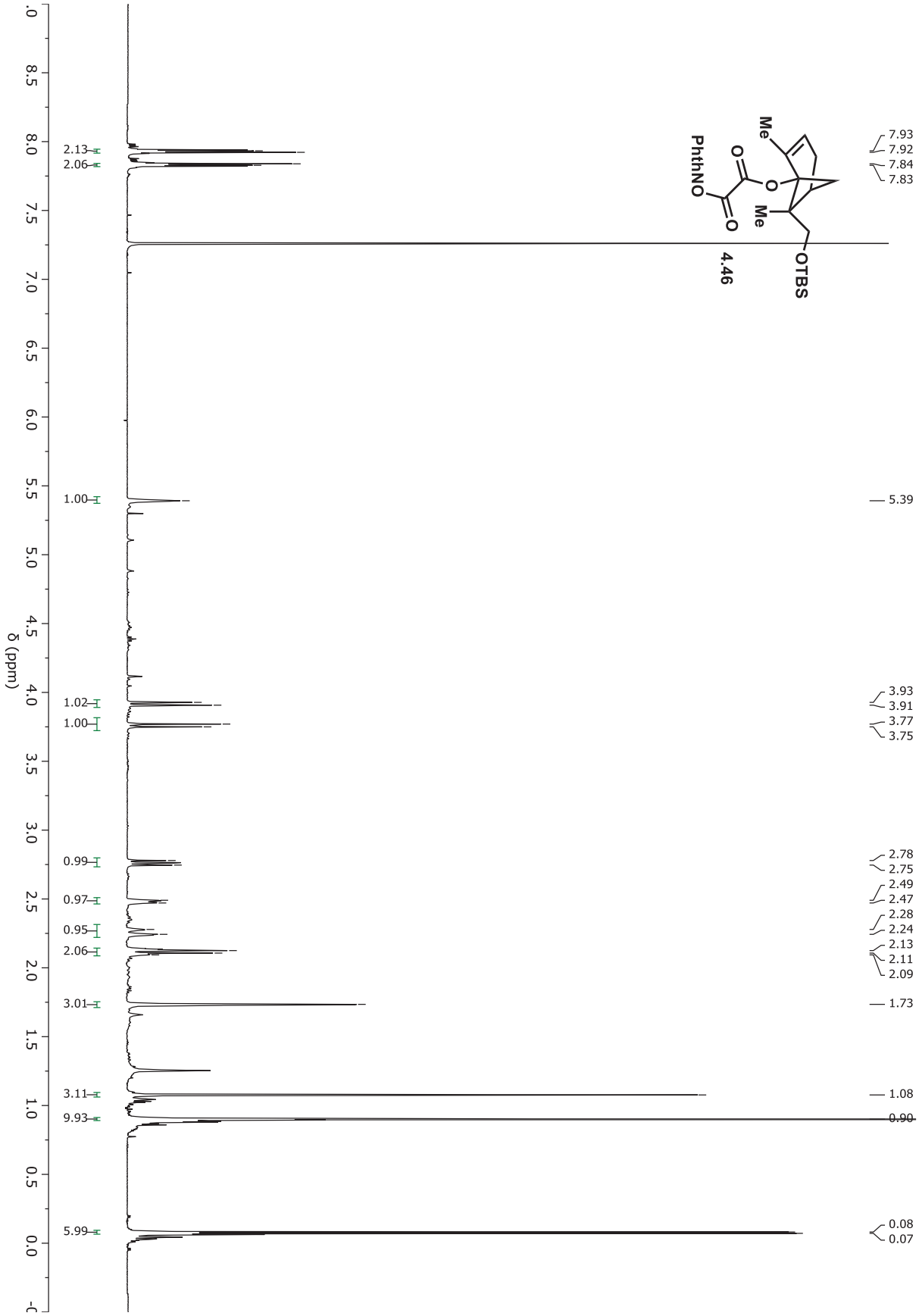
PhthNO
O
O
O
Me
Me
4.46
OTBS
δ (ppm)
2.13
2.06
1.00
1.02
1.00
0.99
0.97
0.95
2.06
3.01
3.11
9.93
5.99
7.93
7.92
7.84
7.83
5.39
3.93
3.91
3.77
3.75
2.78
2.75
2.49
2.47
2.28
2.24
2.13
2.11
2.09
1.73
1.08
0.90
0.08
0.07

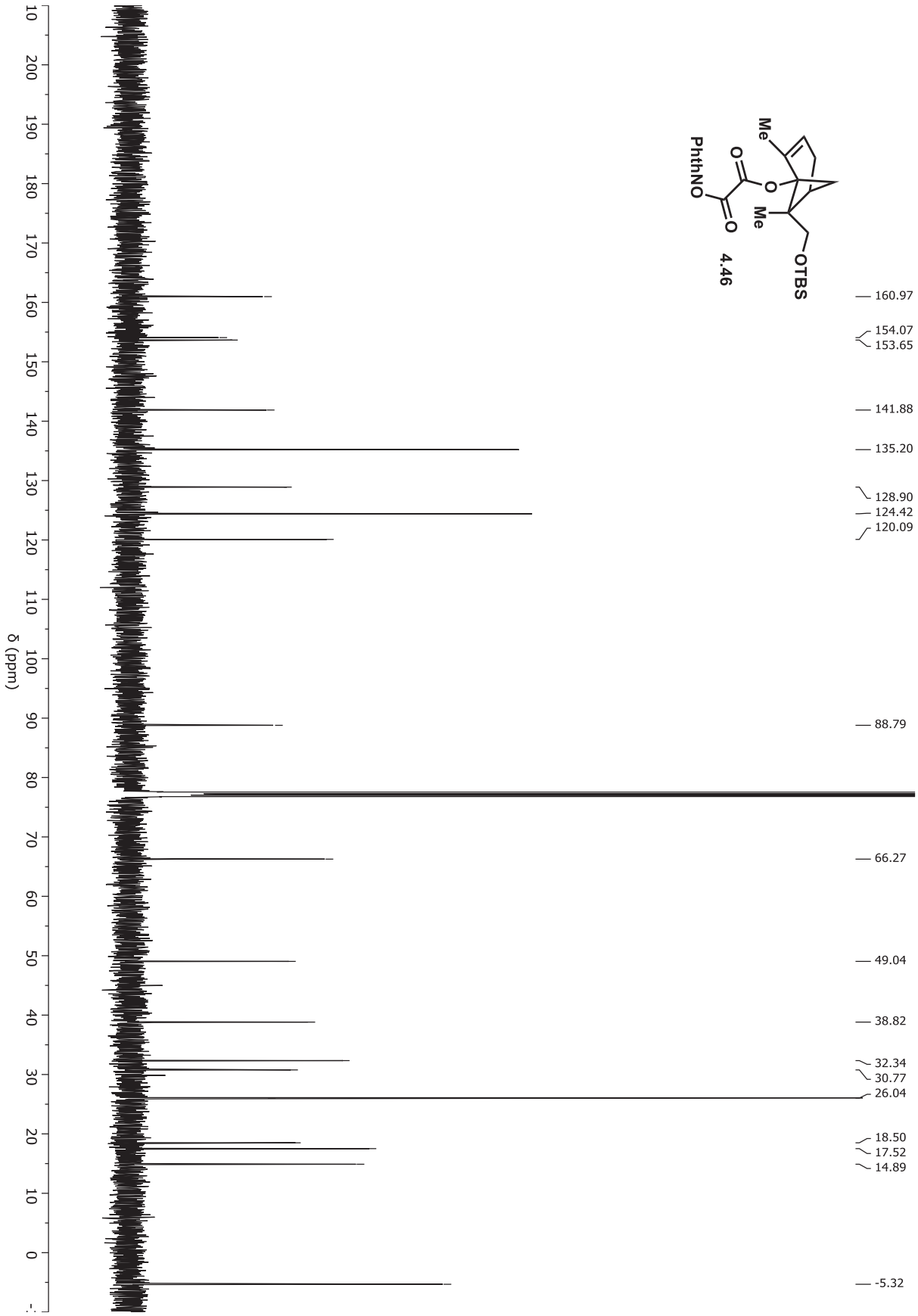
PhthNO
O
O
Me
O
Me
OTBS
4.46
160.97
154.07
153.65
141.88
135.20
128.90
124.42
120.09
88.79
66.27
49.04
38.82
32.34
30.77
26.04
18.50
17.52
14.89
-5.32
δ (ppm)

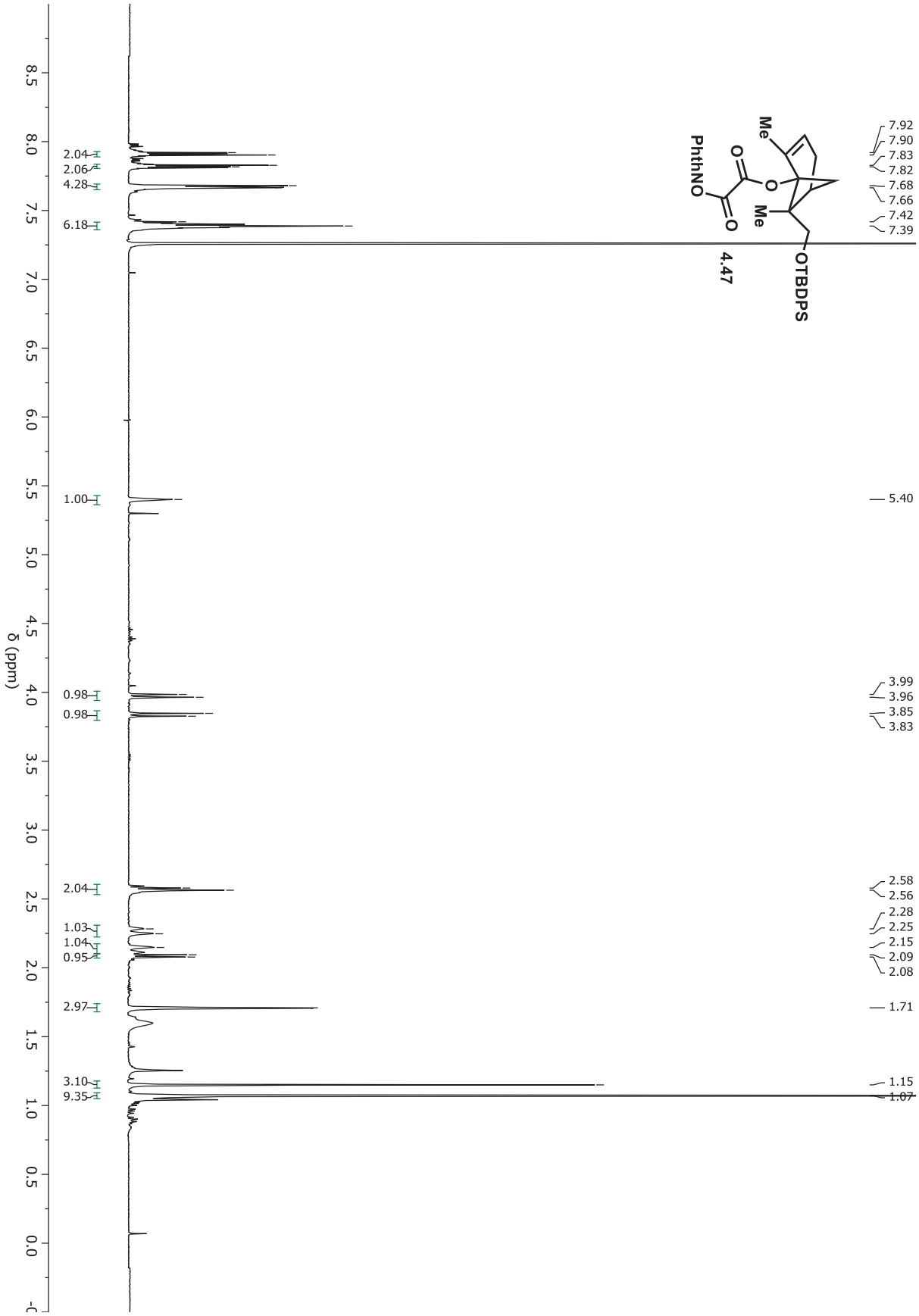
PhthNO
O
O
Me
O
Me
4.47
OTBDPS
δ (ppm)
8.5
8.0
7.5
7.0
6.5
6.0
5.5
5.0
4.5
4.0
3.5
3.0
2.5
2.0
1.5
1.0
0.5
0.0
2.04
2.06
4.28
6.18
1.00
0.98
0.98
2.04
1.03
1.04
0.95
2.97
3.10
9.35
7.92
7.90
7.83
7.82
7.68
7.66
7.42
7.39
5.40
3.99
3.96
3.85
3.83
2.58
2.56
2.28
2.25
2.15
2.09
2.08
1.71
1.15
1.07

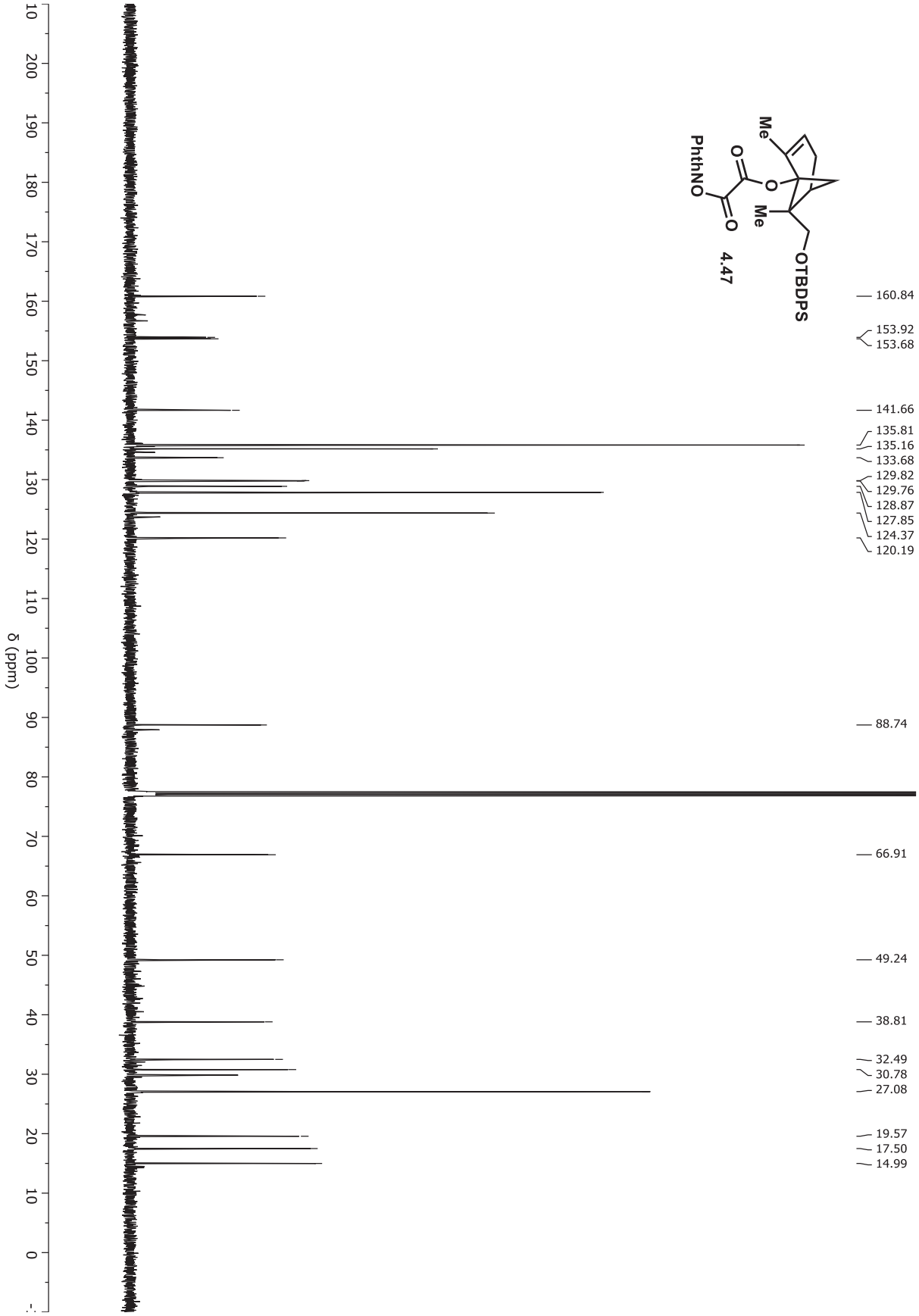
PhthNO
O
O
O
Me
Me
OTBDPS
4.47
160.84
153.92
153.68
141.66
135.81
135.16
133.68
129.82
129.76
128.87
127.85
124.37
120.19
88.74
66.91
49.24
38.81
32.49
30.78
27.08
19.57
17.50
14.99
δ (ppm)

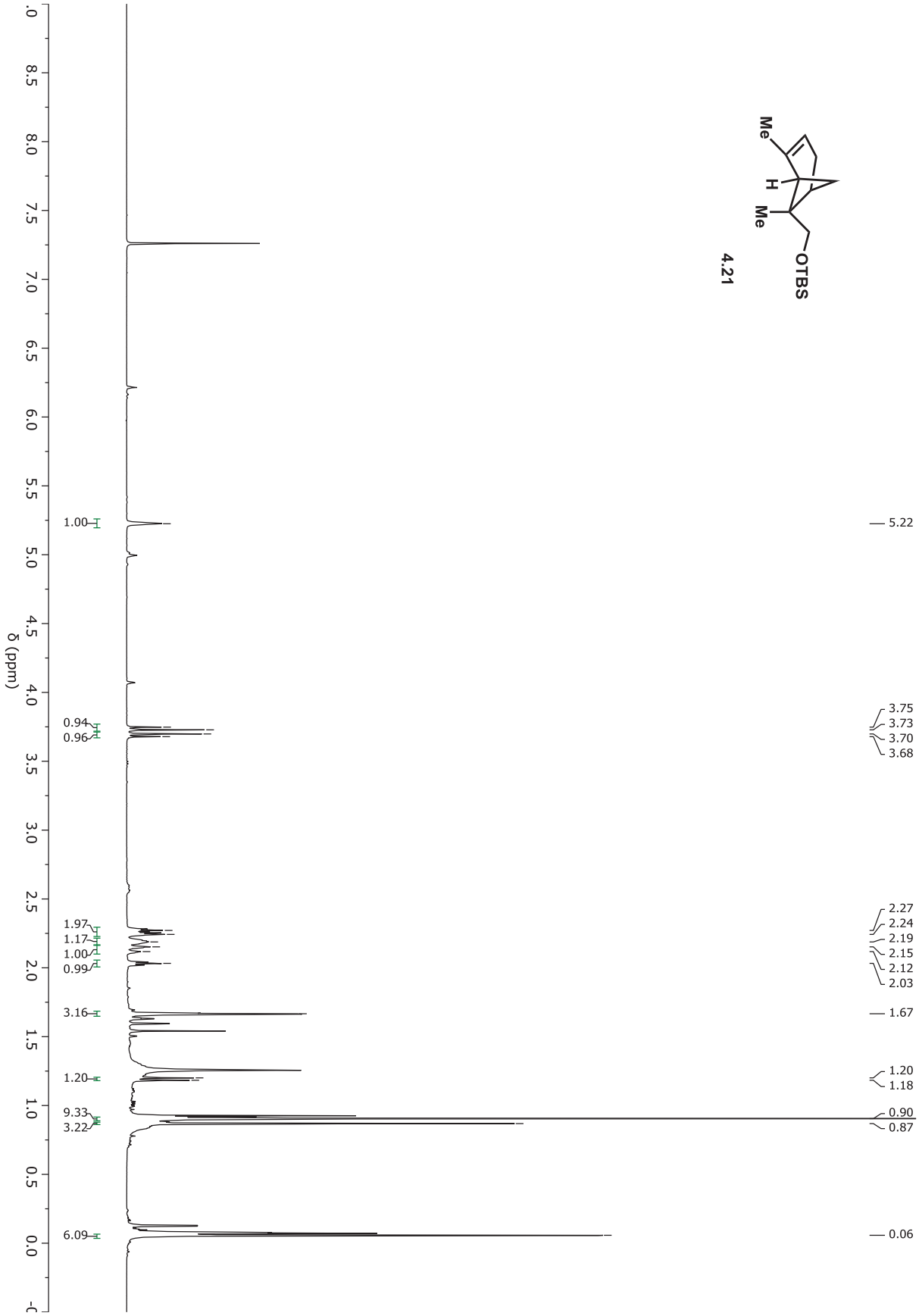
Me
H
Me
OTBS
4.21
δ (ppm)
1.00
0.94
0.96
1.97
1.17
1.00
0.99
3.16
1.20
9.33
3.22
6.09
5.22
3.75
3.73
3.70
3.68
2.27
2.24
2.19
2.15
2.12
2.03
1.67
1.20
1.18
0.90
0.87
0.06

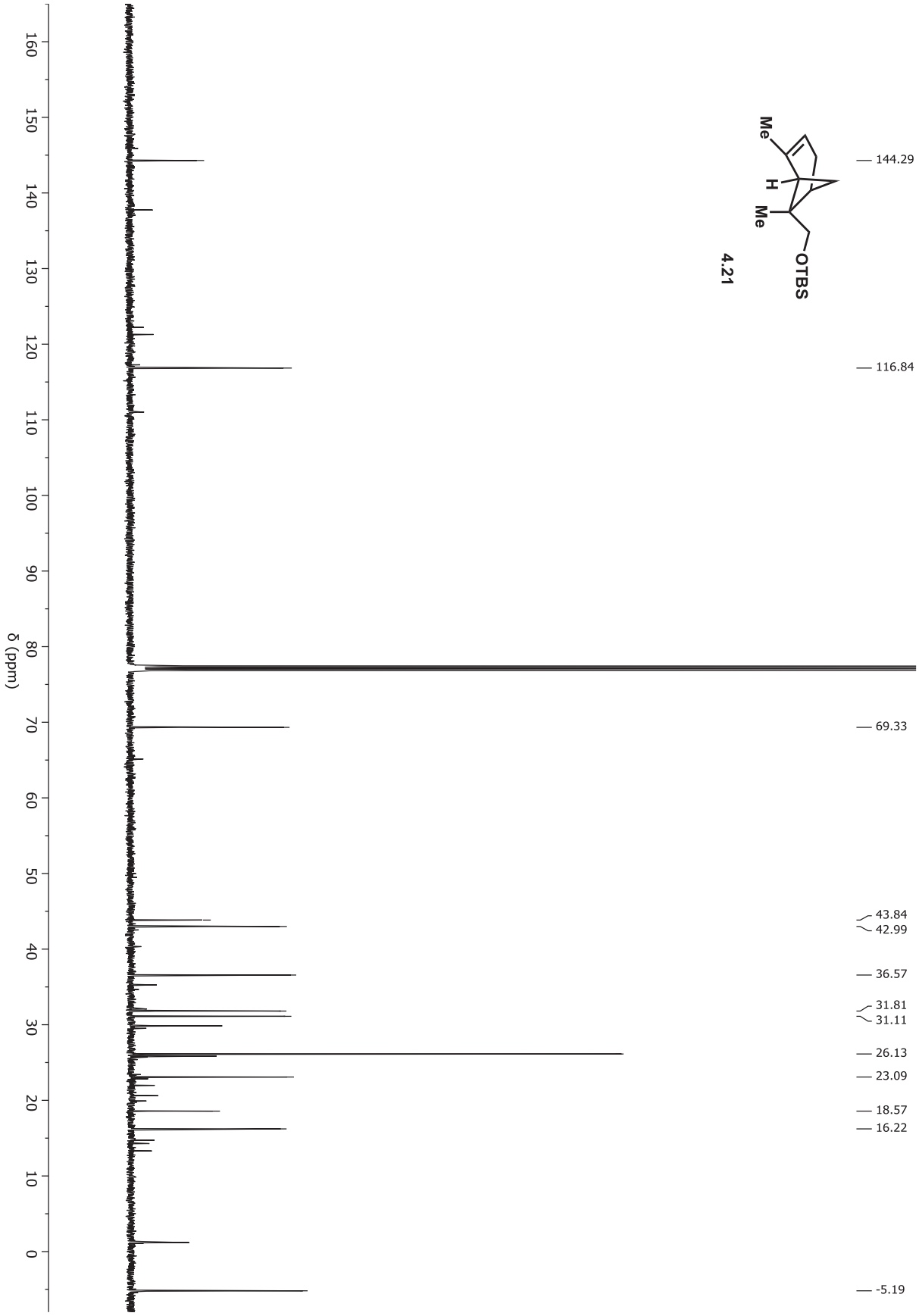
Me
H
Me
OTBS
4.21
144.29
116.84
69.33
43.84
42.99
36.57
31.81
31.11
26.13
23.09
18.57
16.22
-5.19
δ (ppm)
160
150
140
130
120
110
100
90
80
70
60
50
40
30
20
10
0

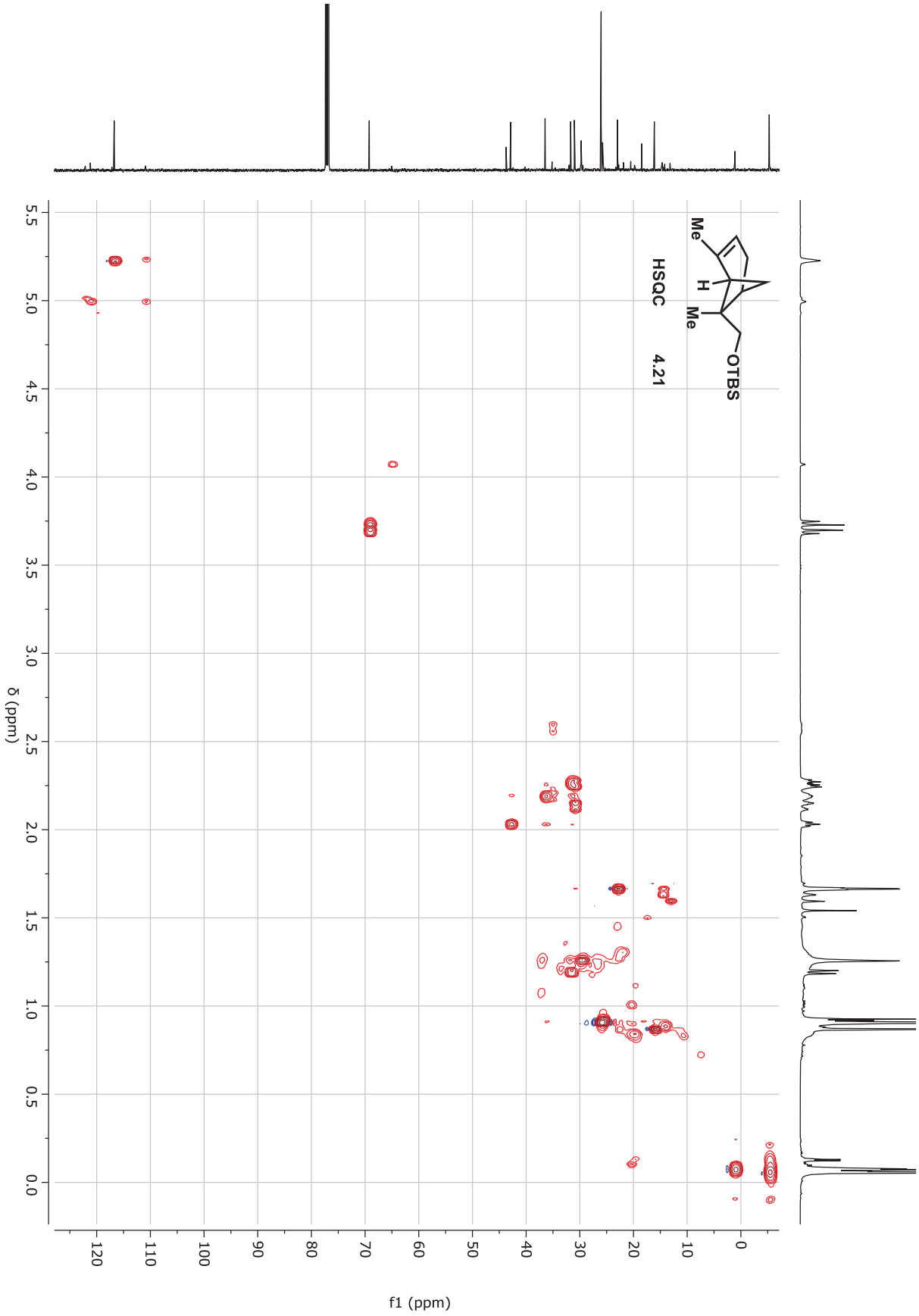
HSQC
4.21
Me
H
Me
OTBS
δ (ppm)
f1 (ppm)

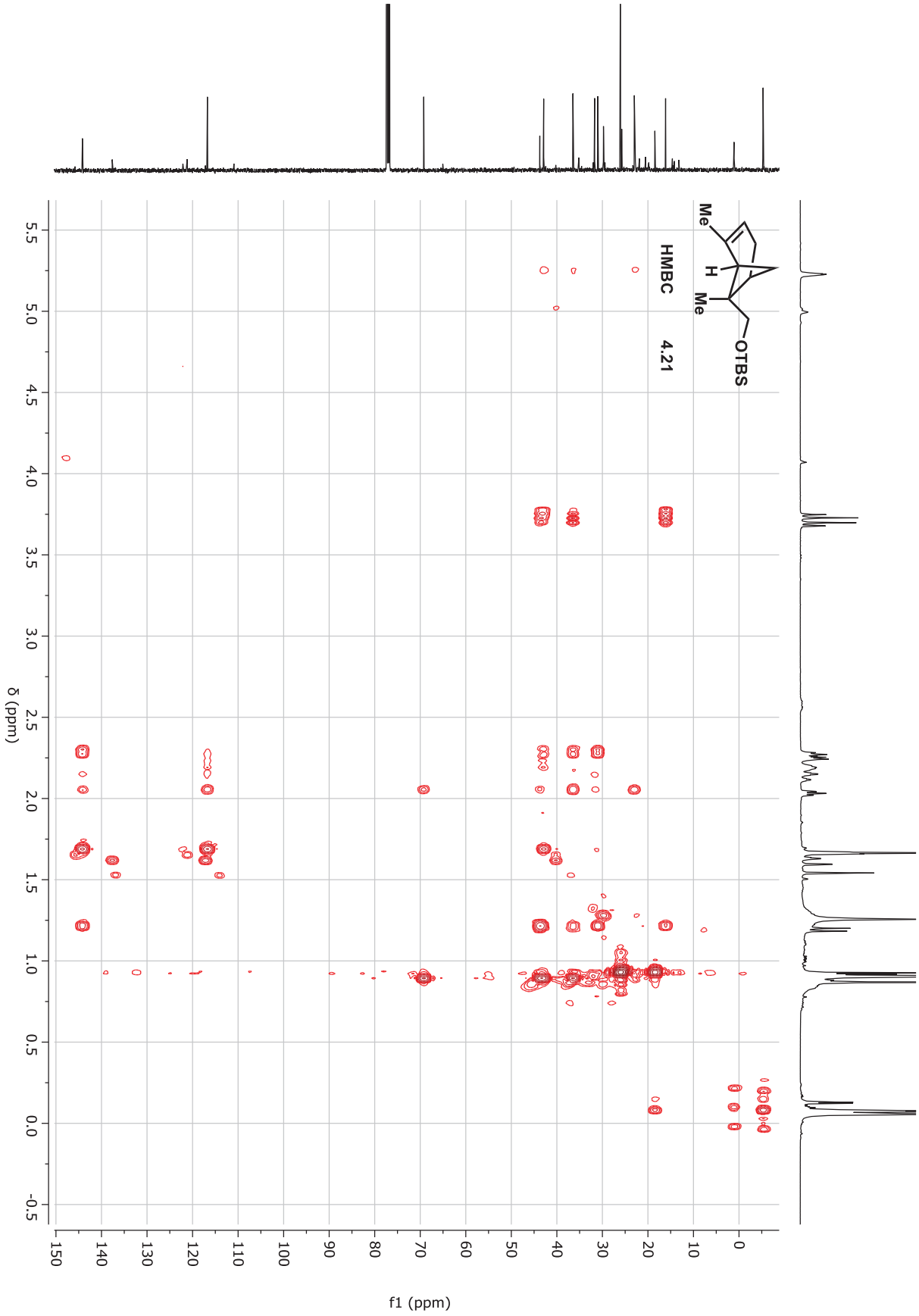
HMBC
4.21
Me
H
Me
OTBS
δ (ppm)
f1 (ppm)

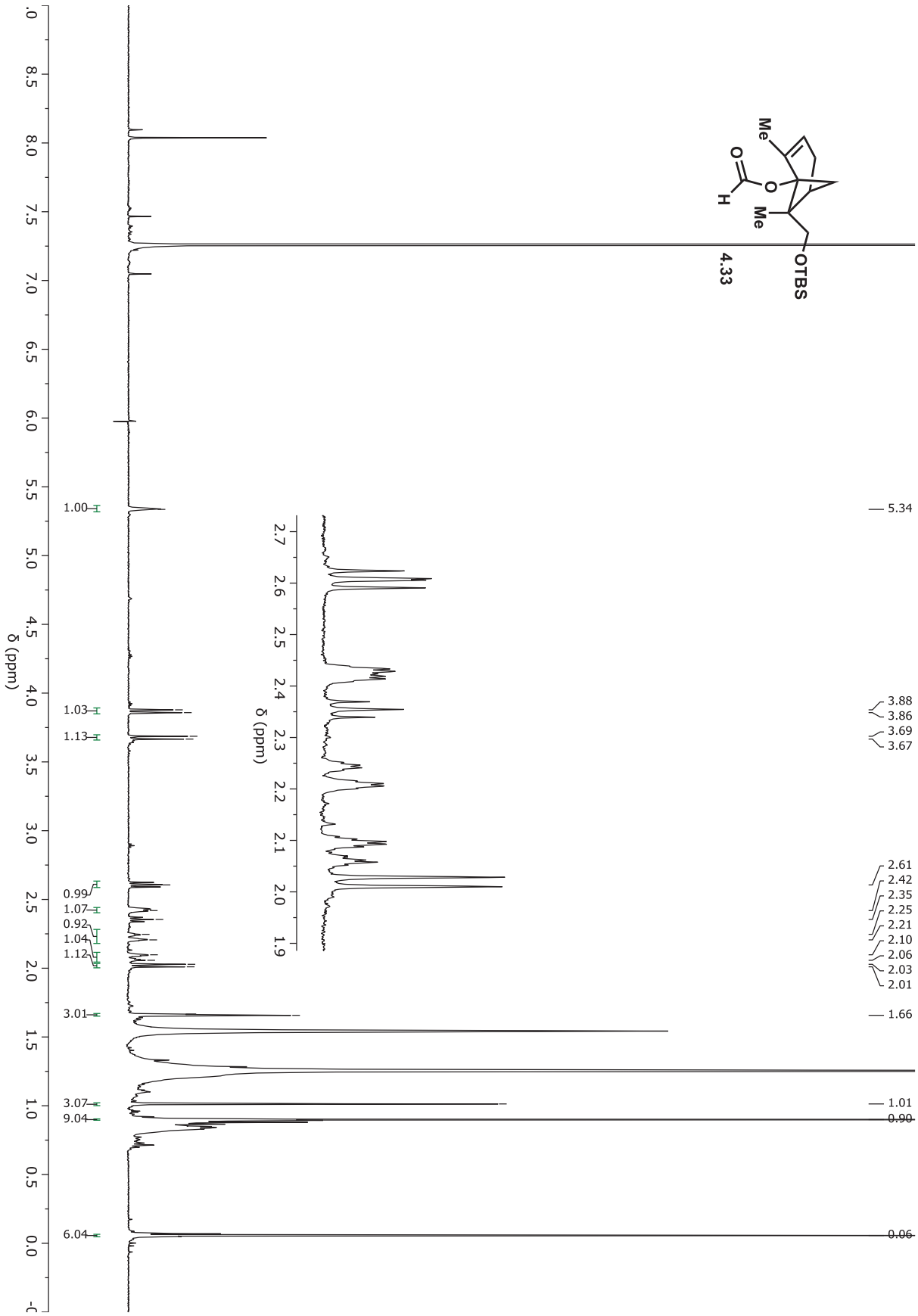
Me
O
H
O
Me
OTBS
4.33
δ (ppm)
δ (ppm)
1.00
1.03
1.13
0.99
1.07
0.92
1.04
1.12
3.01
3.07
9.04
6.04
5.34
3.88
3.86
3.69
3.67
2.61
2.42
2.35
2.25
2.21
2.10
2.06
2.03
2.01
1.66
1.01
0.90
0.06

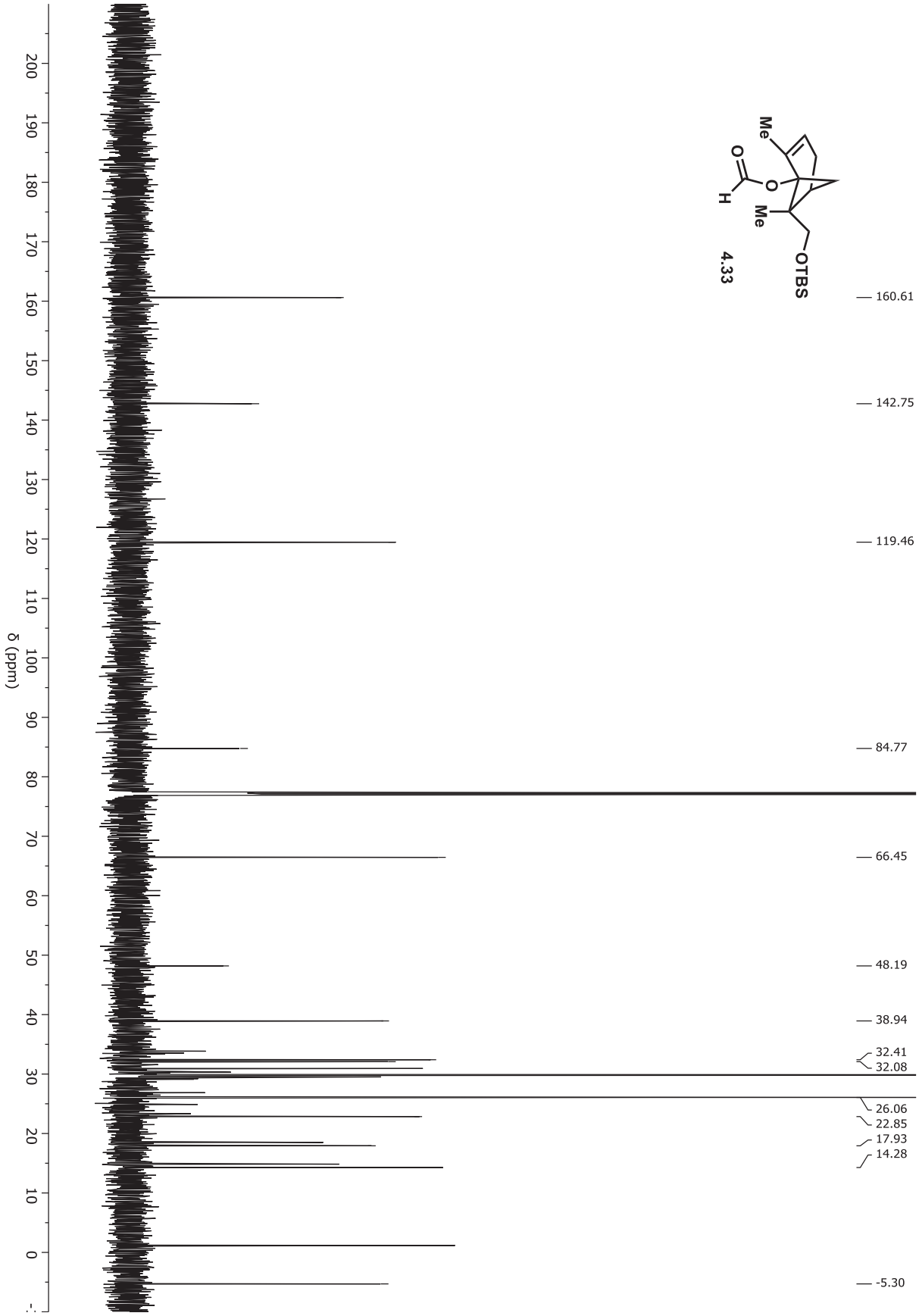
Me
O
H
O
Me
OTBS
4.33
160.61
142.75
119.46
84.77
66.45
48.19
38.94
32.41
32.08
26.06
22.85
17.93
14.28
-5.30
δ (ppm)

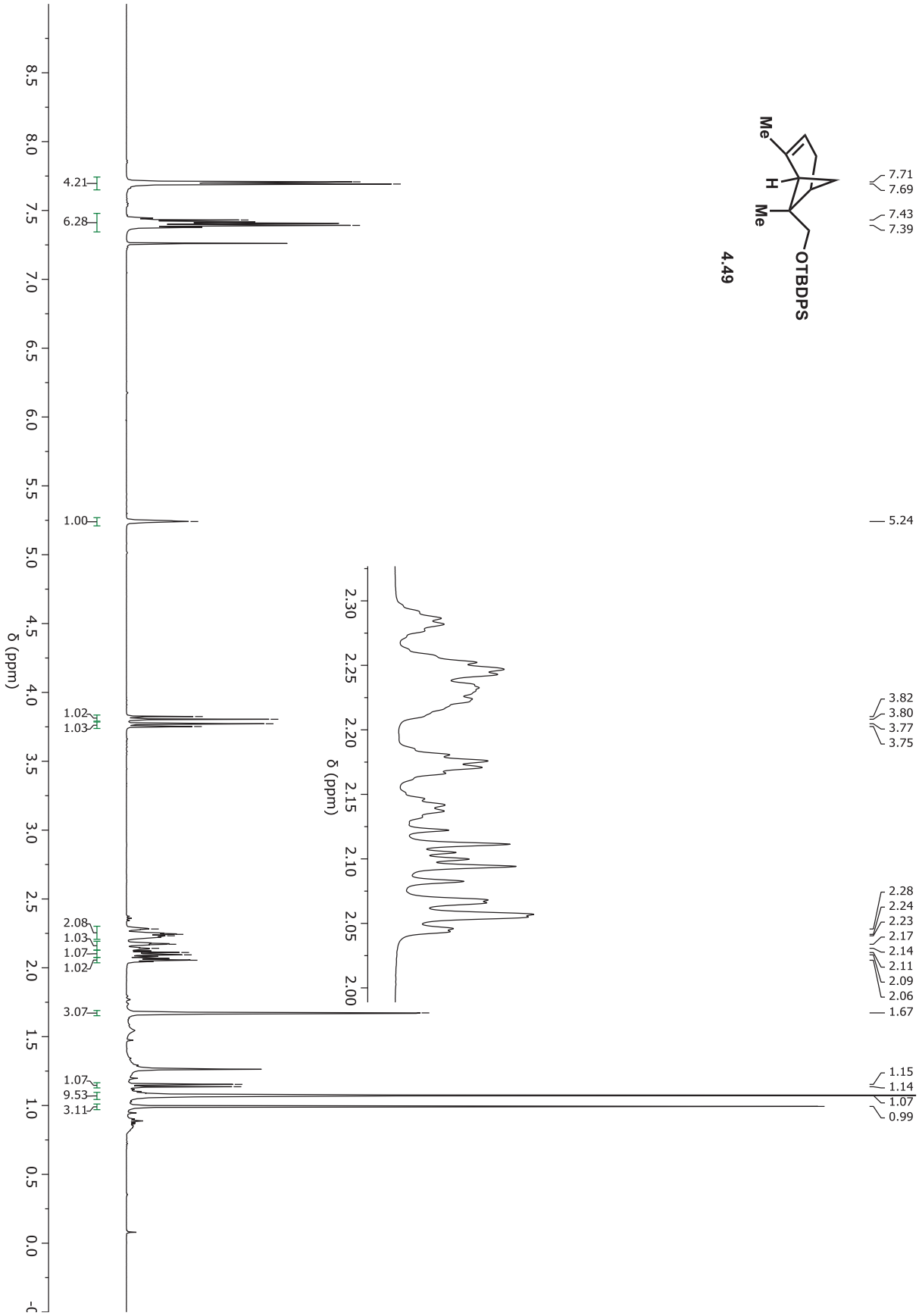
Me
H
Me
OTBDPS
4.49
7.71
7.69
7.43
7.39
5.24
3.82
3.80
3.77
3.75
2.28
2.24
2.23
2.17
2.14
2.11
2.09
2.06
1.67
1.15
1.14
1.07
0.99
4.21
6.28
1.00
1.02
1.03
2.08
1.03
1.07
1.02
3.07
1.07
9.53
3.11
δ (ppm)
δ (ppm)

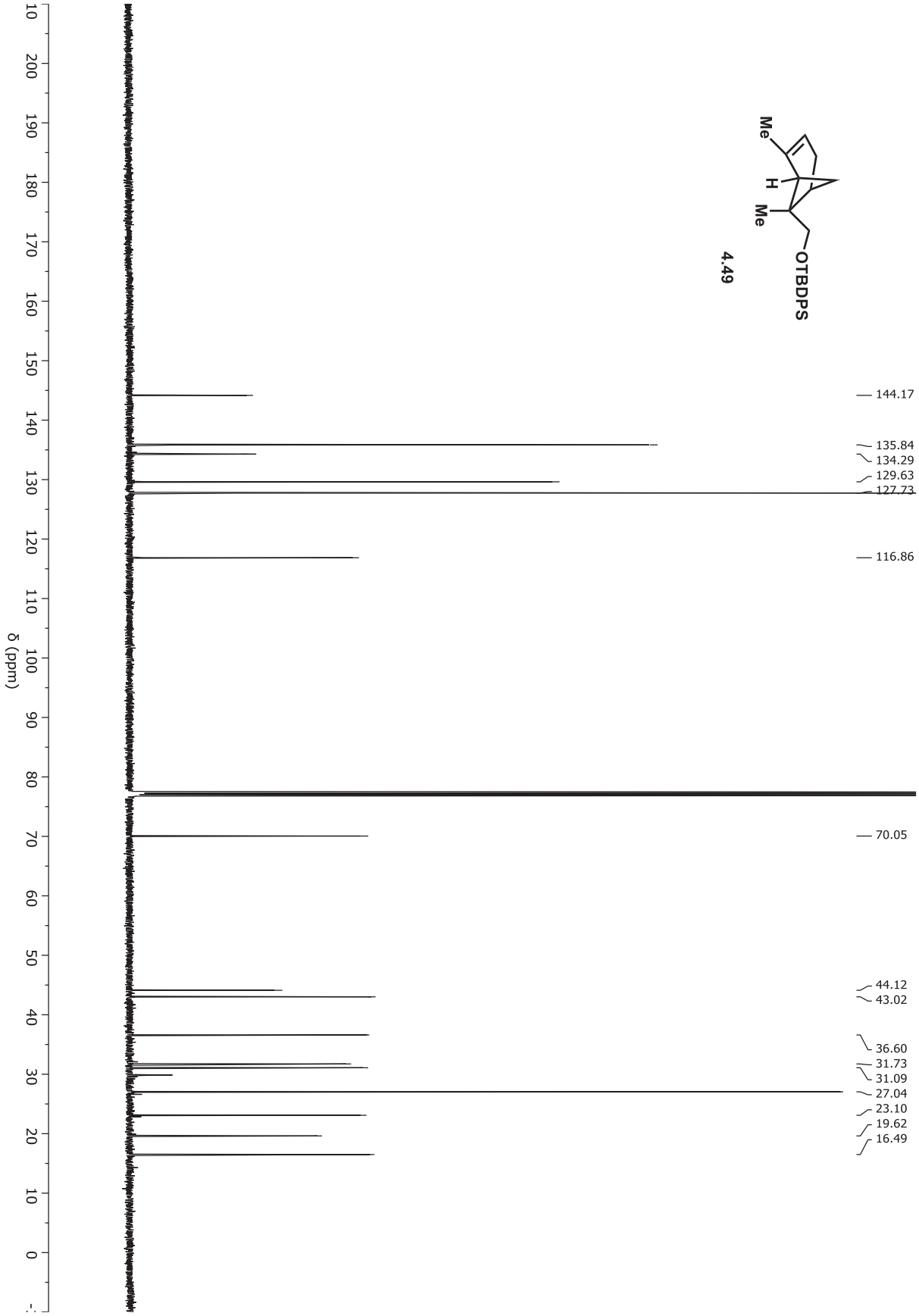
Me
H
Me
OTBDPS
4.49
144.17
135.84
134.29
129.63
127.73
116.86
70.05
44.12
43.02
36.60
31.73
31.09
27.04
23.10
19.62
16.49
δ (ppm)

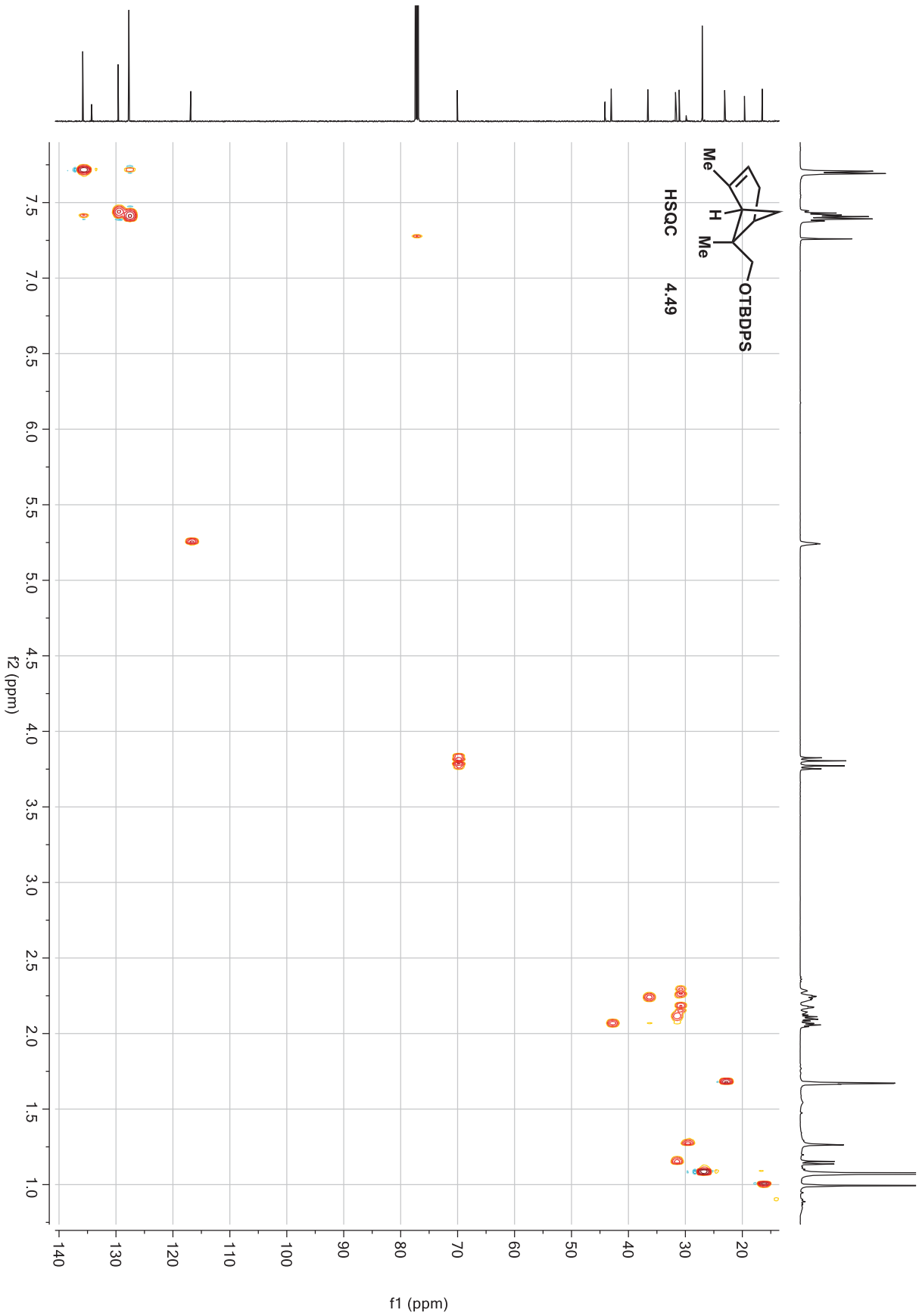
HSQC
4.49
Me
H
Me
OTBDPS
f2 (ppm)
f1 (ppm)

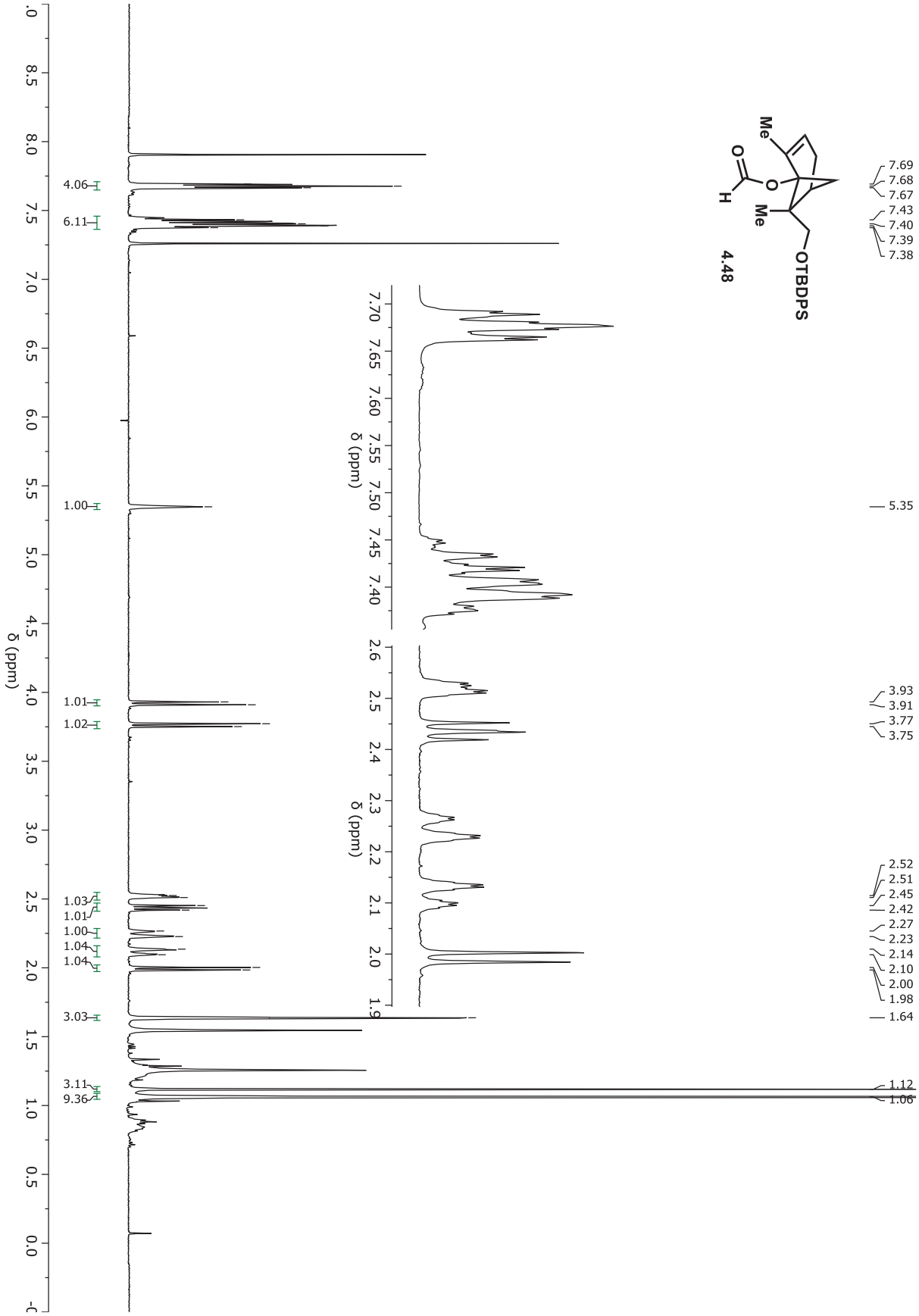
Me
O
H
O
Me
OTBDPS
4.48
δ (ppm)
4.06
6.11
1.00
1.01
1.02
1.03
1.01
1.00
1.04
1.04
3.03
3.11
9.36
7.69
7.68
7.67
7.43
7.40
7.39
7.38
5.35
3.93
3.91
3.77
3.75
2.52
2.51
2.45
2.42
2.27
2.23
2.14
2.10
2.00
1.98
1.64
1.12
1.06

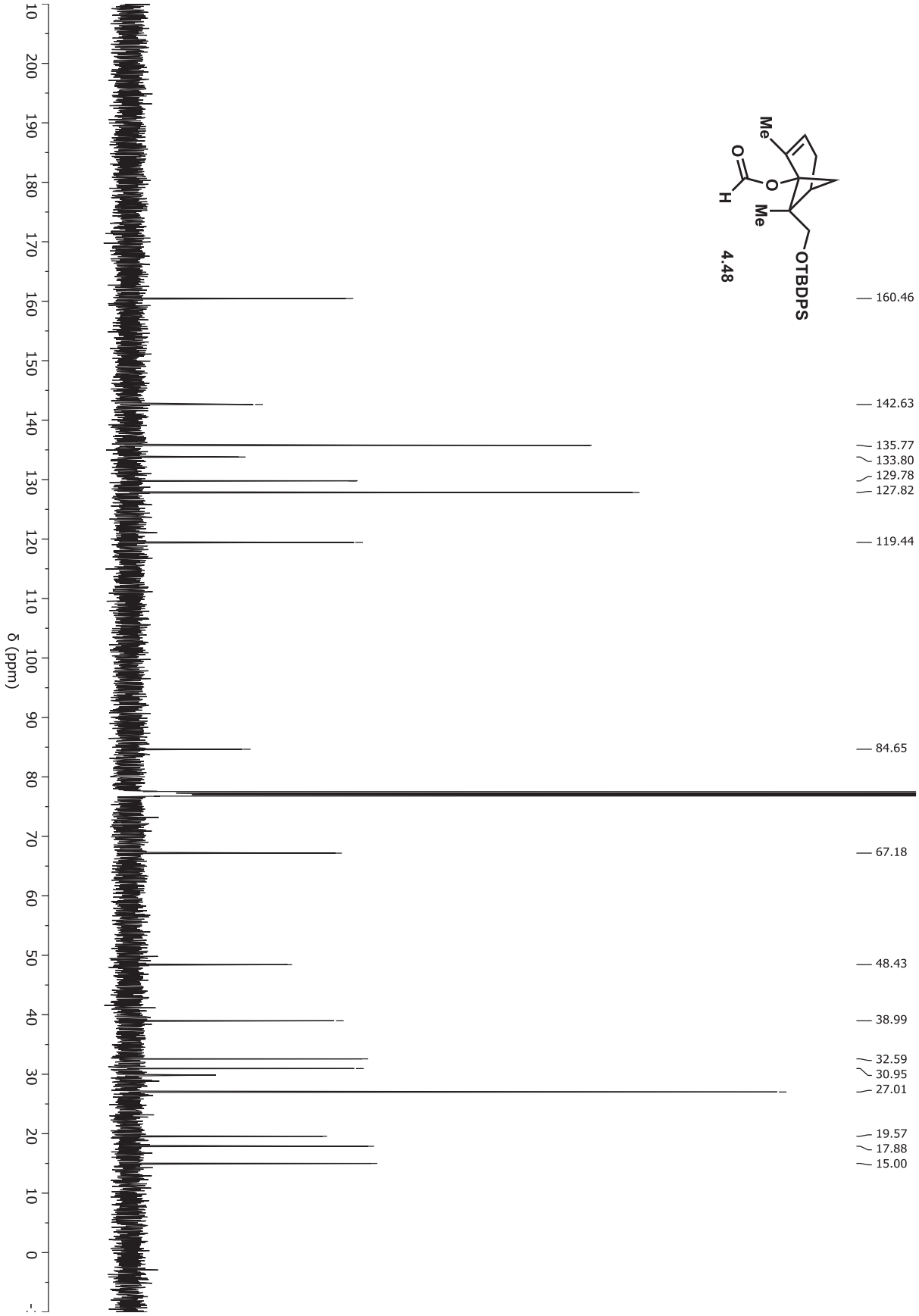
Me
O
H
O
Me
OTBDPS
4.48
160.46
142.63
135.77
133.80
129.78
127.82
119.44
84.65
67.18
48.43
38.99
32.59
30.95
27.01
19.57
17.88
15.00
δ (ppm)

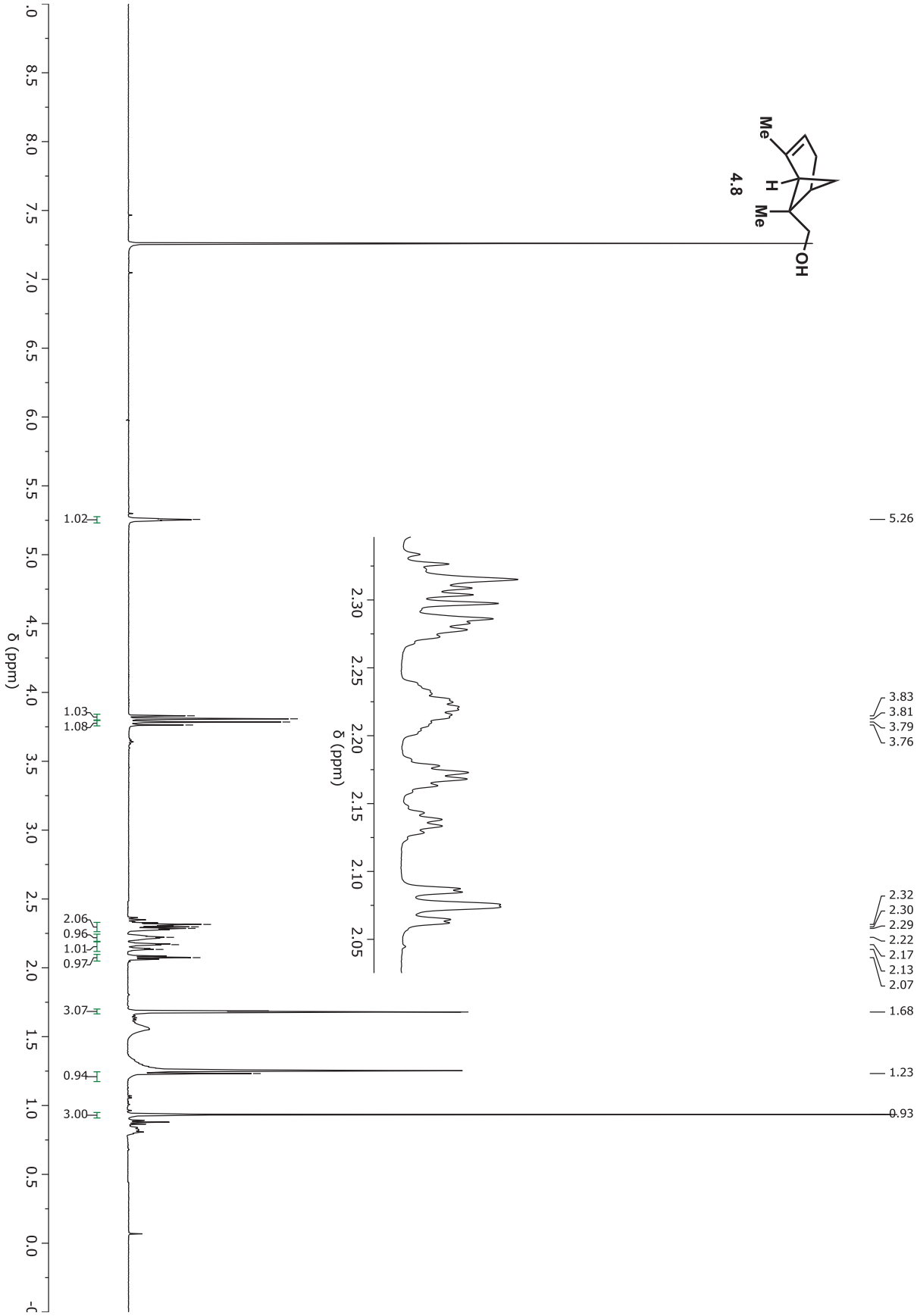
Me
H
Me
OH
4.8
δ (ppm)
1.02
1.03
1.08
2.06
0.96
1.01
0.97
3.07
0.94
3.00
5.26
3.83
3.81
3.79
3.76
2.32
2.30
2.29
2.22
2.17
2.13
2.07
1.68
1.23
0.93

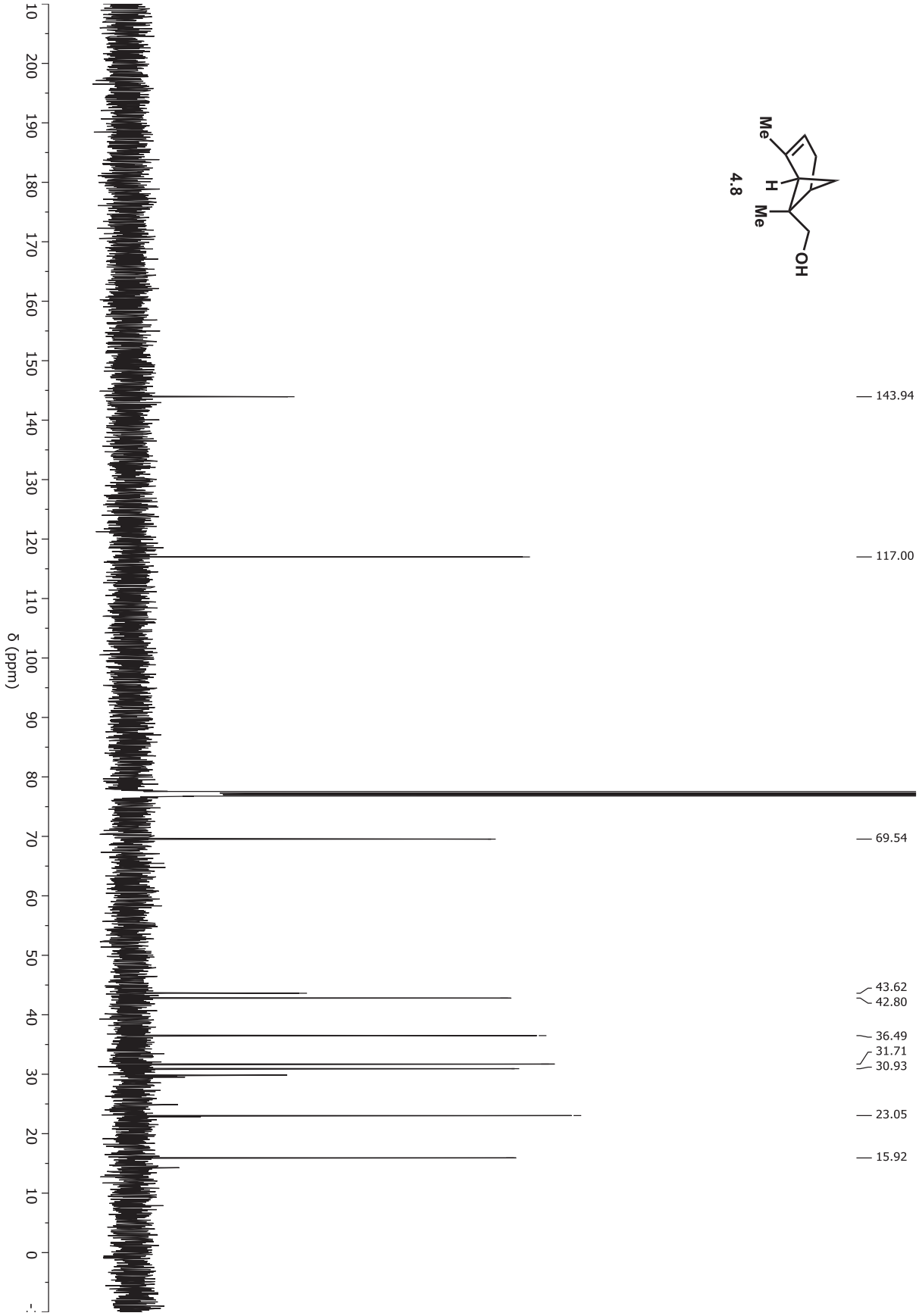
Me
H
Me
OH
4.8
δ (ppm)
143.94
117.00
69.54
43.62
42.80
36.49
31.71
30.93
23.05
15.92

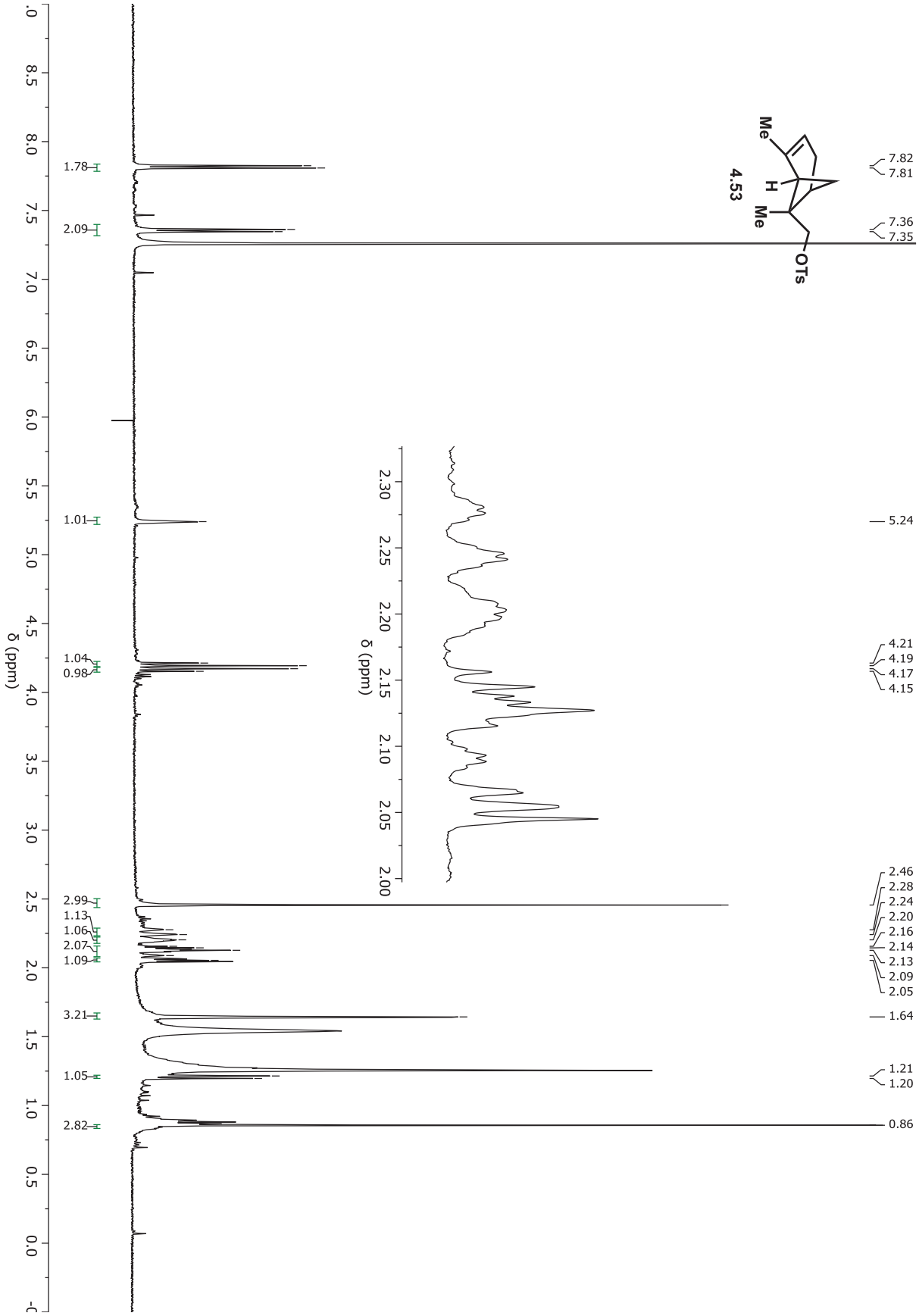
4.53
Me
H
Me
OTs
δ (ppm)
δ (ppm)
1.78
2.09
1.01
1.04
0.98
2.99
1.13
1.06
2.07
1.09
3.21
1.05
2.82
7.82
7.81
7.36
7.35
5.24
4.21
4.19
4.17
4.15
2.46
2.28
2.24
2.20
2.16
2.14
2.13
2.09
2.05
1.64
1.21
1.20
0.86

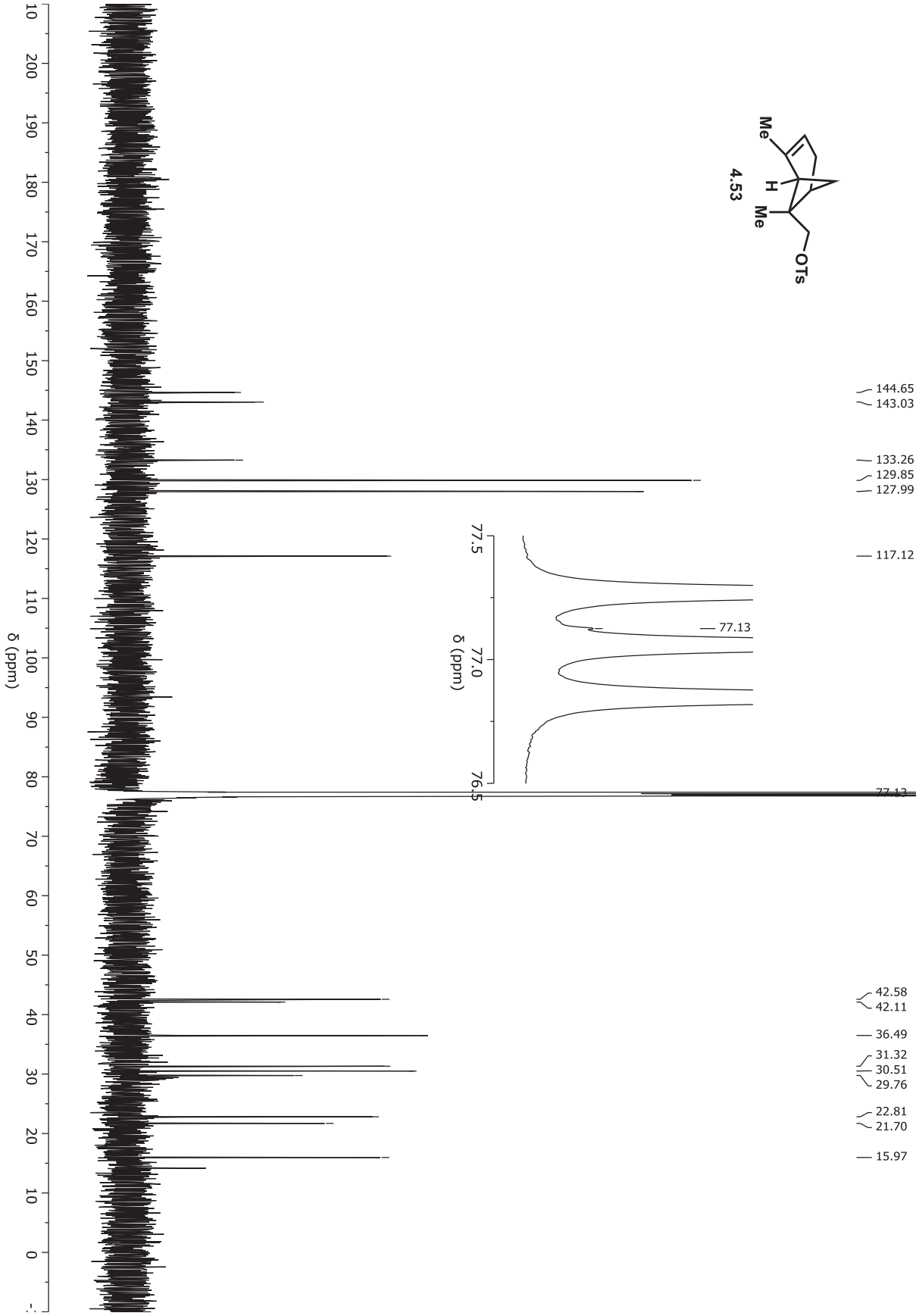
Me
H
Me
OTs
4.53
144.65
143.03
133.26
129.85
127.99
117.12
77.13
42.58
42.11
36.49
31.32
30.51
29.76
22.81
21.70
15.97
δ (ppm)

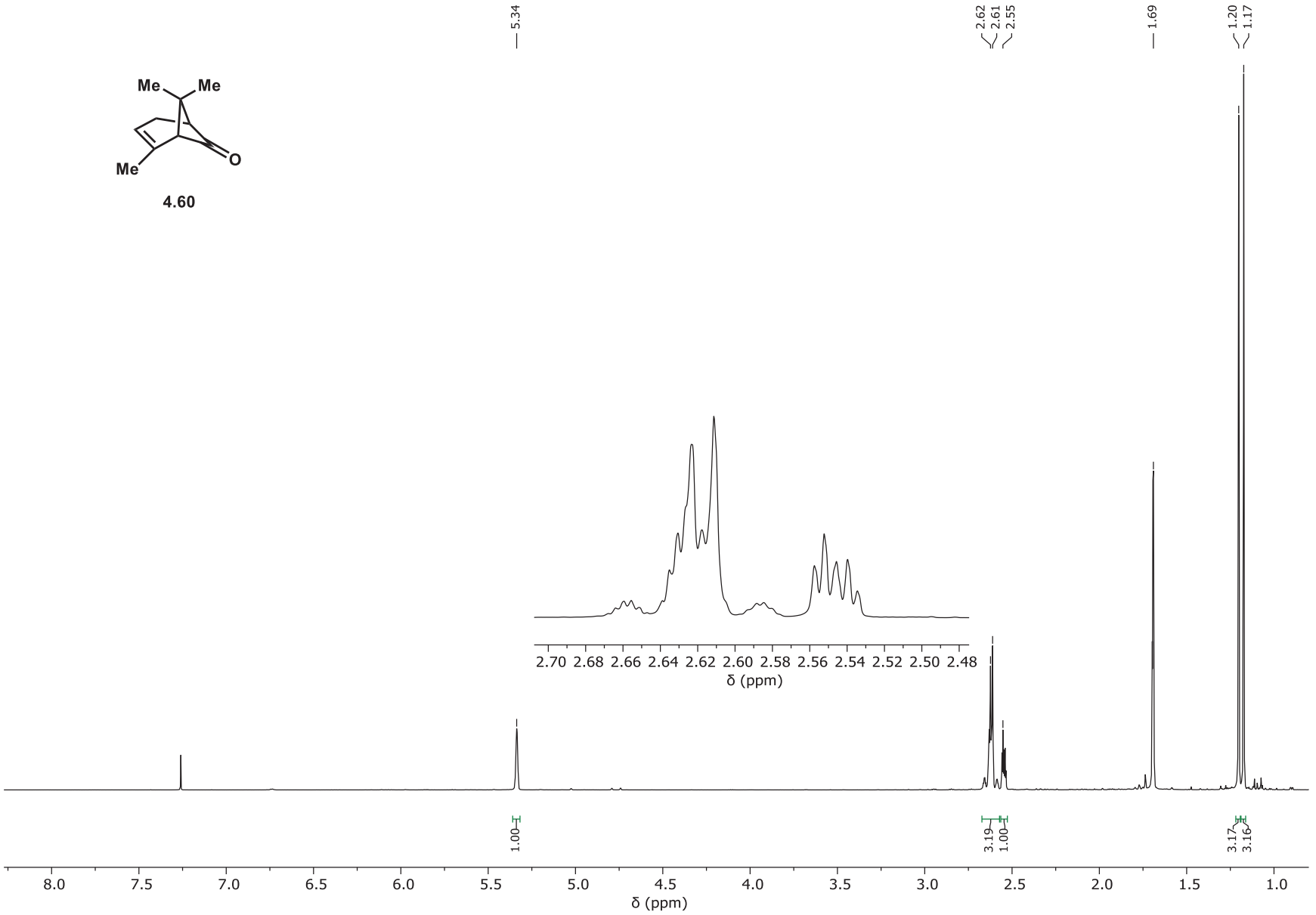
Me
Me
Me
O
4.60
5.34
2.62
2.61
2.55
1.69
1.20
1.17
2.70 2.68 2.66 2.64 2.62 2.60 2.58 2.56 2.54 2.52 2.50 2.48
δ (ppm)
1.00
3.19
1.00
3.17
3.16
8.0 7.5 7.0 6.5 6.0 5.5 5.0 4.5 4.0 3.5 3.0 2.5 2.0 1.5 1.0
δ (ppm)

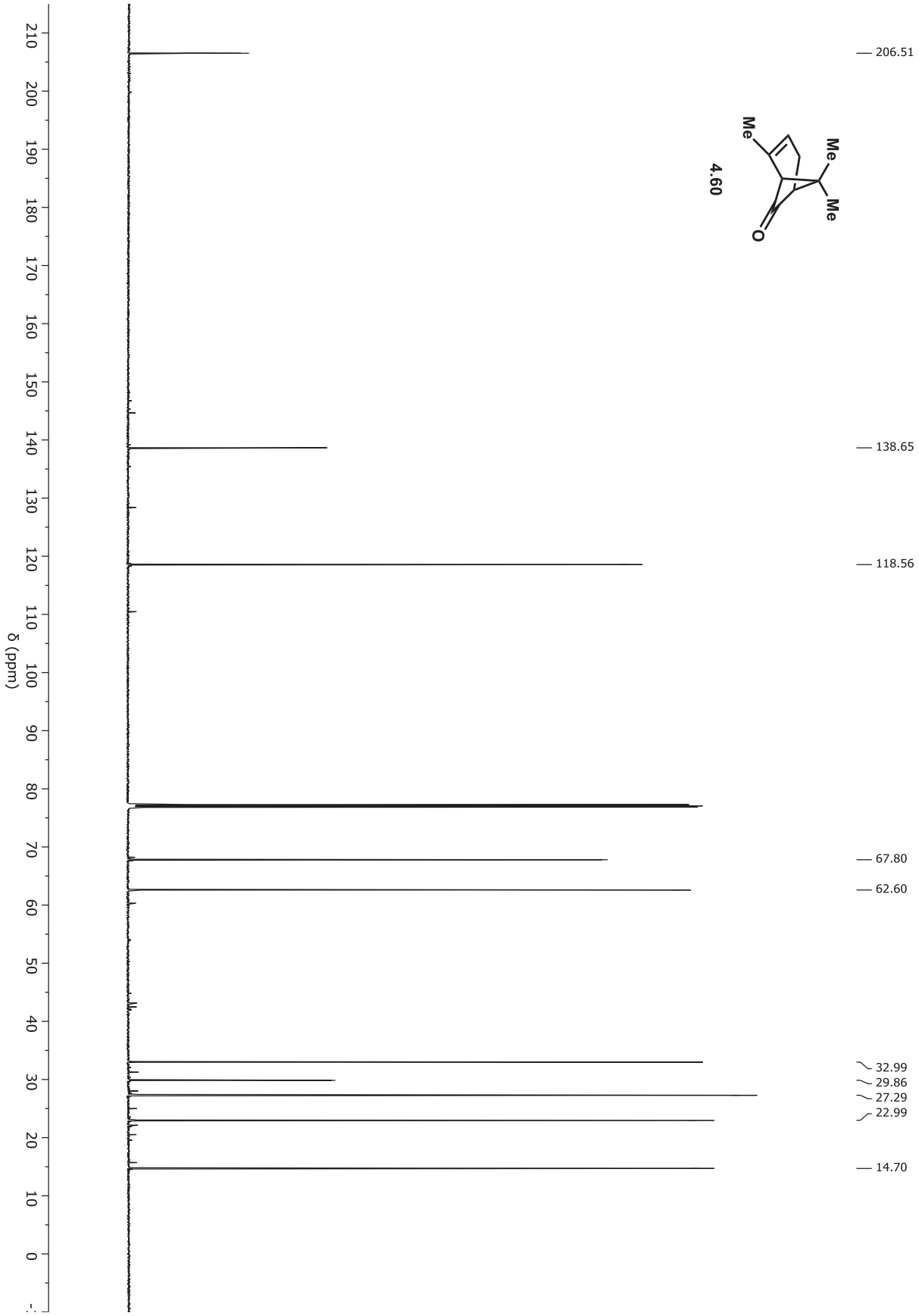
206.51
138.65
118.56
67.80
62.60
32.99
29.86
27.29
22.99
14.70
δ (ppm)
Me
Me
Me
O
4.60

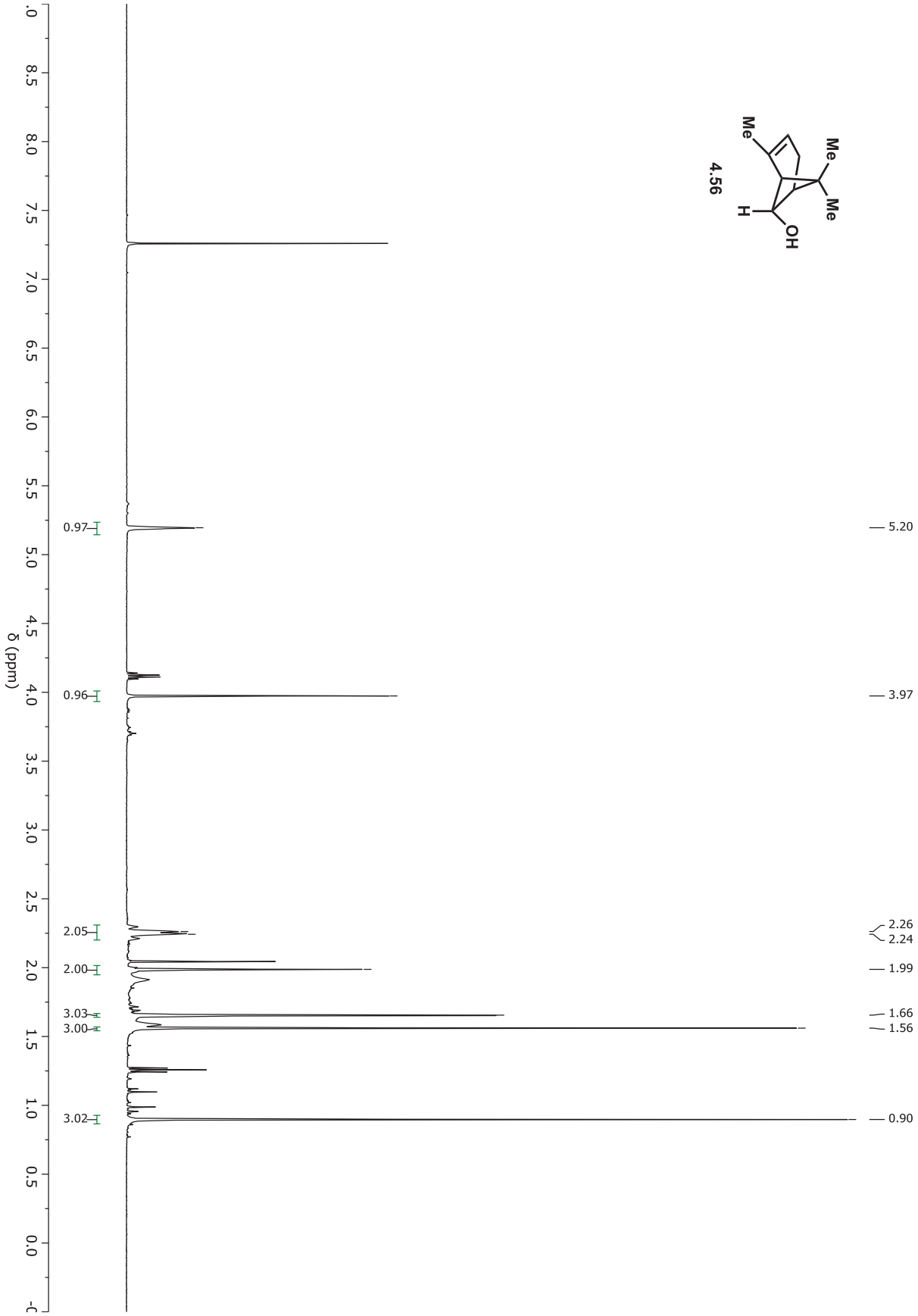
4.56
Me
Me
Me
H
OH
δ (ppm)
0.97
0.96
2.05
2.00
3.03
3.00
3.02
5.20
3.97
2.26
2.24
1.99
1.66
1.56
0.90

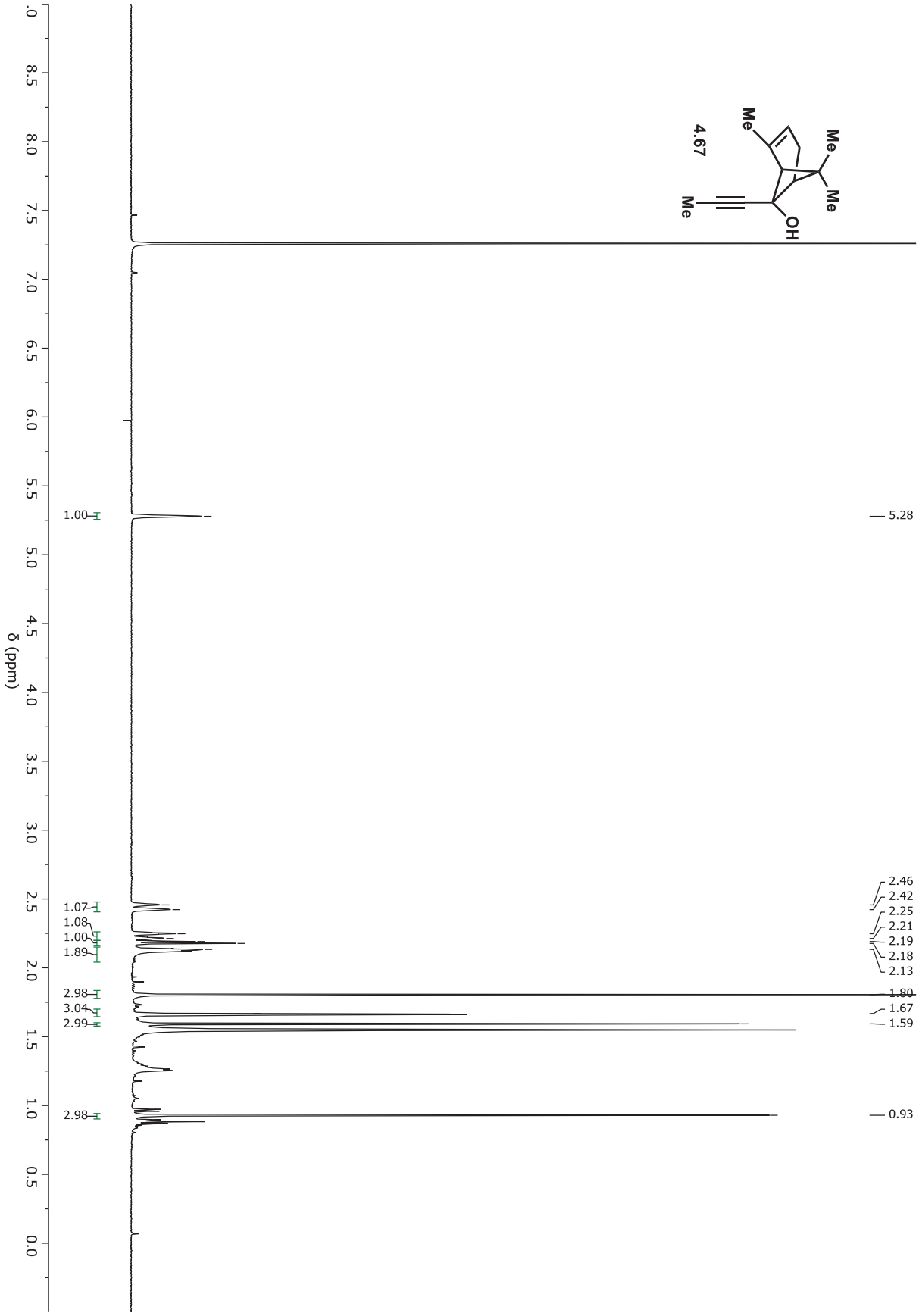
4.67
Me
Me
Me
Me
OH
δ (ppm)
1.00
1.07
1.08
1.00
1.89
2.98
3.04
2.99
2.98
5.28
2.46
2.42
2.25
2.21
2.19
2.18
2.13
1.80
1.67
1.59
0.93

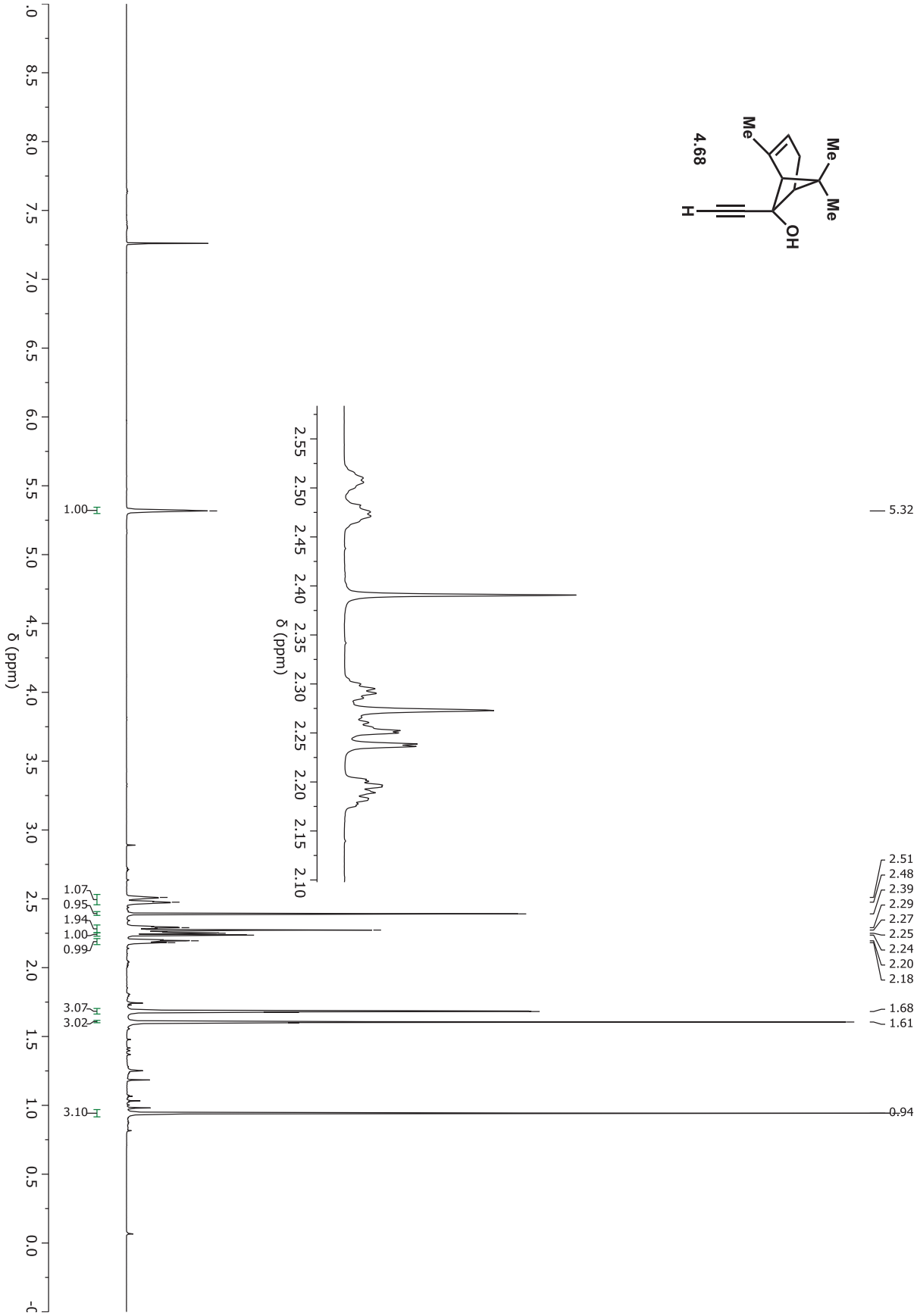
4.68
Me
Me
Me
H
OH
δ (ppm)
δ (ppm)
1.00
1.07
0.95
1.94
1.00
0.99
3.07
3.02
3.10
5.32
2.51
2.48
2.39
2.29
2.27
2.25
2.24
2.20
2.18
1.68
1.61
0.94

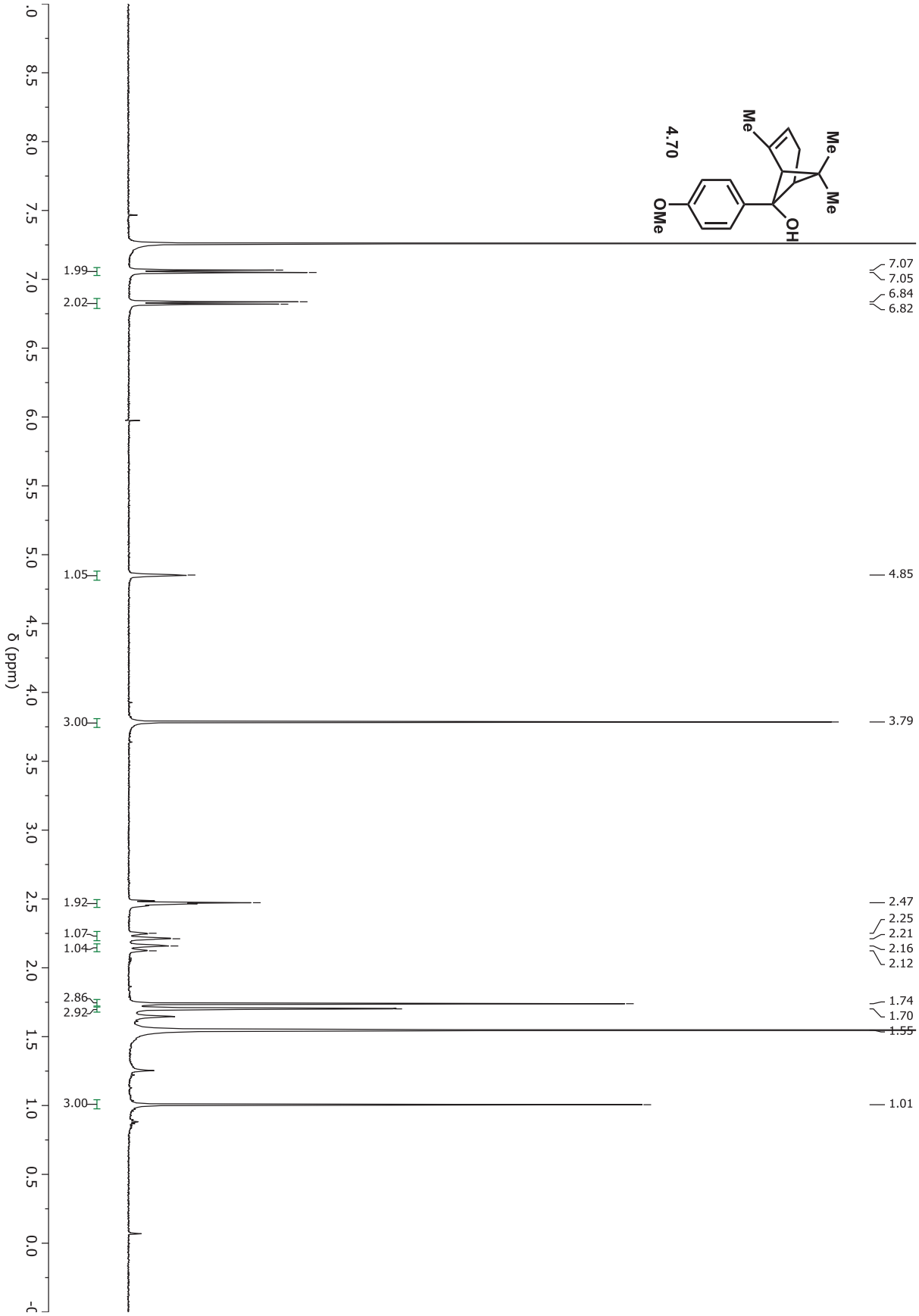
4.70
Me
Me
Me
OMe
OH
1.99
2.02
1.05
3.00
1.92
1.07
1.04
2.86
2.92
3.00
7.07
7.05
6.84
6.82
4.85
3.79
2.47
2.25
2.21
2.16
2.12
1.74
1.70
1.55
1.01
δ (ppm)

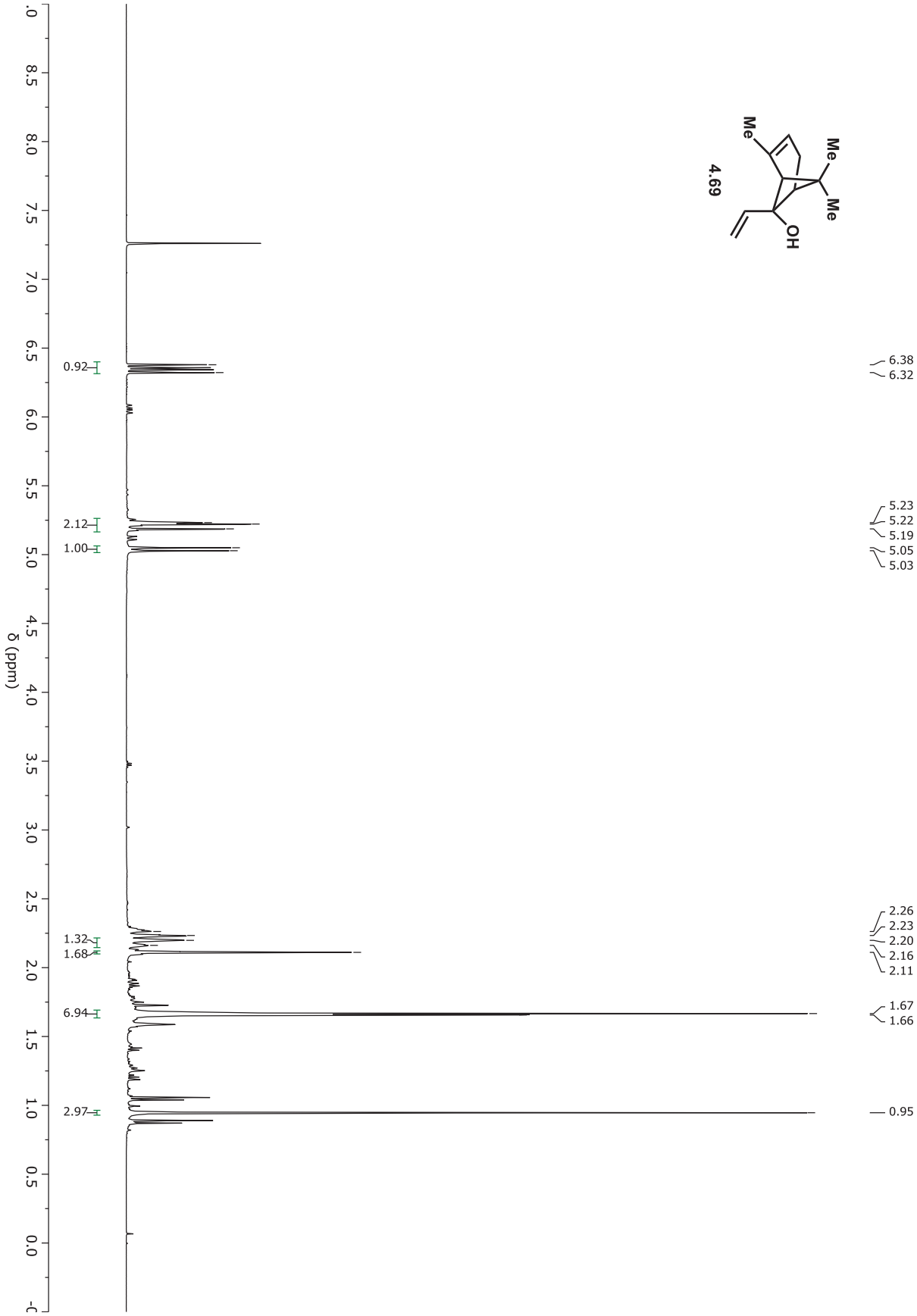
4.69
Me
Me
Me
OH
δ (ppm)
0.92
2.12
1.00
1.32
1.68
6.94
2.97
6.38
6.32
5.23
5.22
5.19
5.05
5.03
2.26
2.23
2.20
2.16
2.11
1.67
1.66
0.95

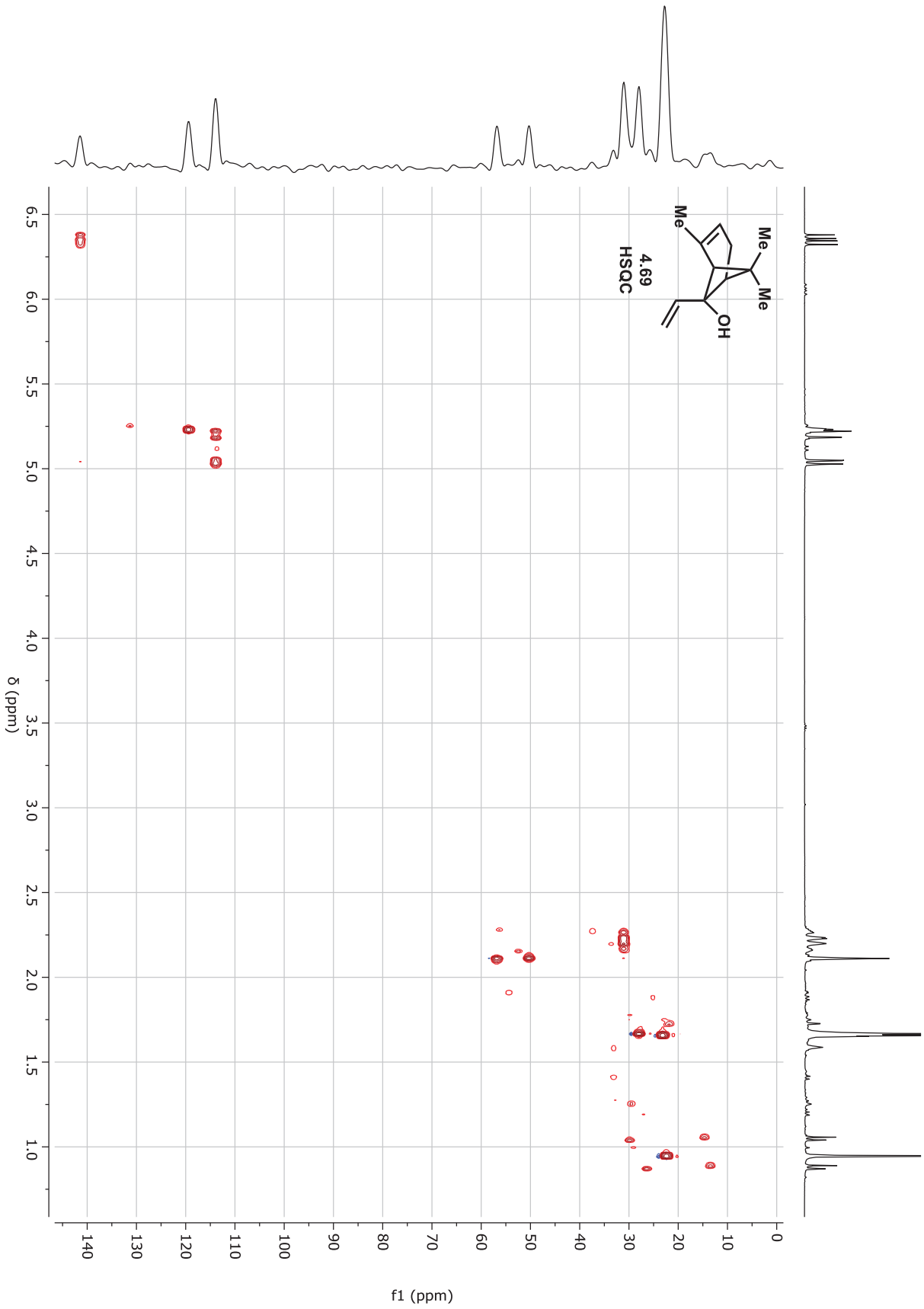
4.69
HSQC
Me
Me
Me
OH
δ (ppm)
f1 (ppm)

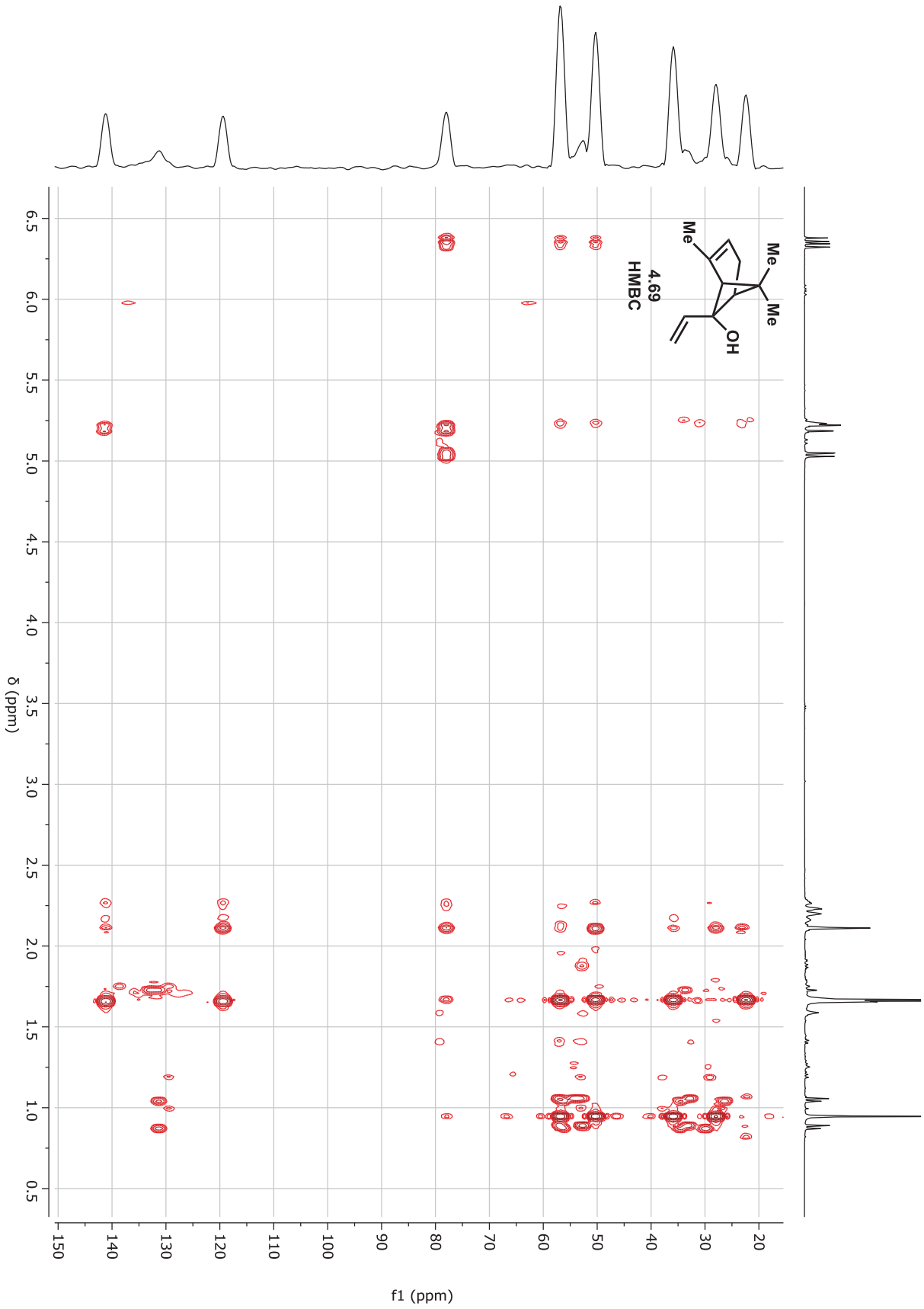
4.69
HMBC
Me
Me
Me
OH
δ (ppm)
f1 (ppm)

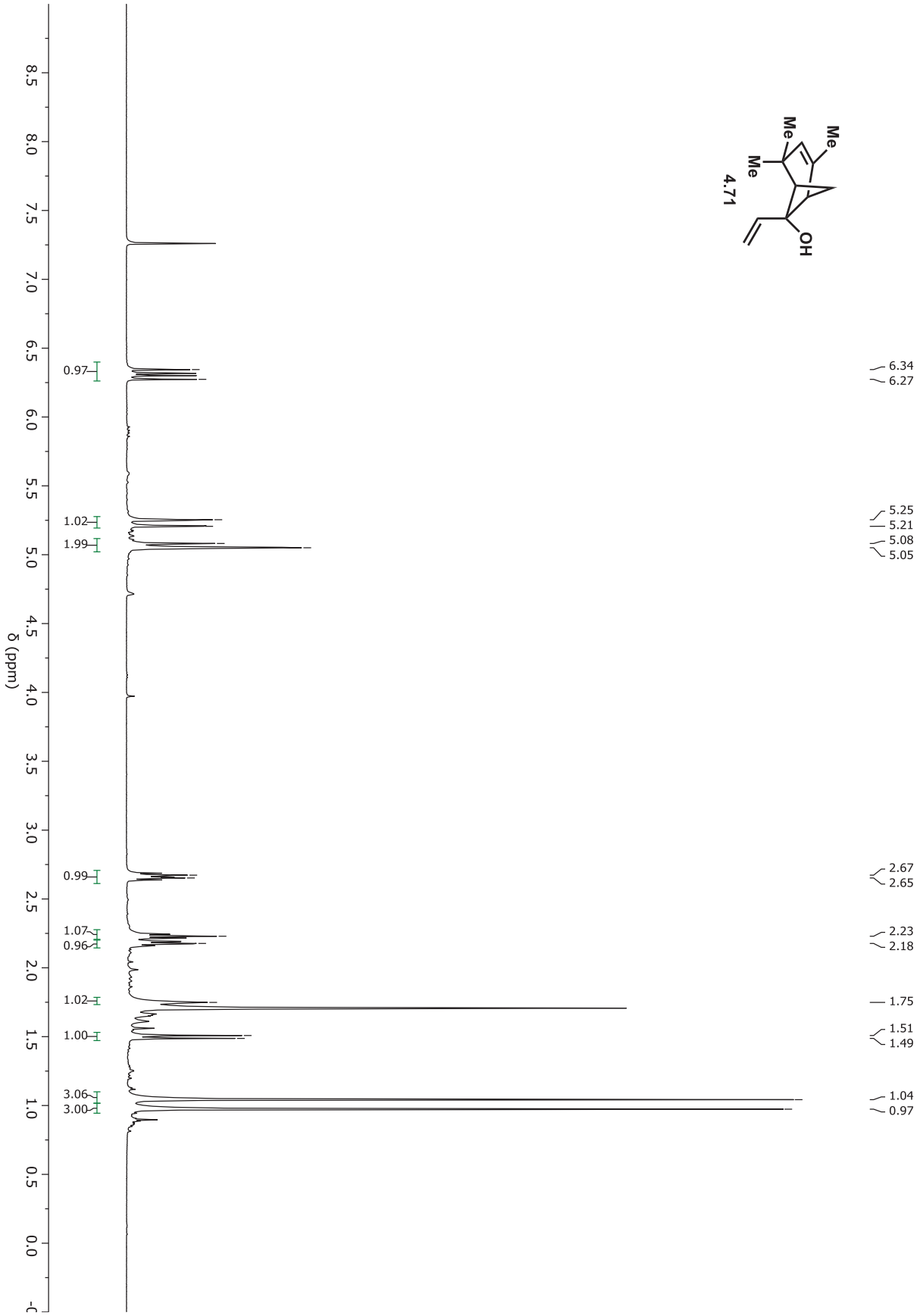
Me
Me
Me
OH
4.71
δ (ppm)
0.97
1.02
1.99
0.99
1.07
0.96
1.02
1.00
3.06
3.00
6.34
6.27
5.25
5.21
5.08
5.05
2.67
2.65
2.23
2.18
1.75
1.51
1.49
1.04
0.97

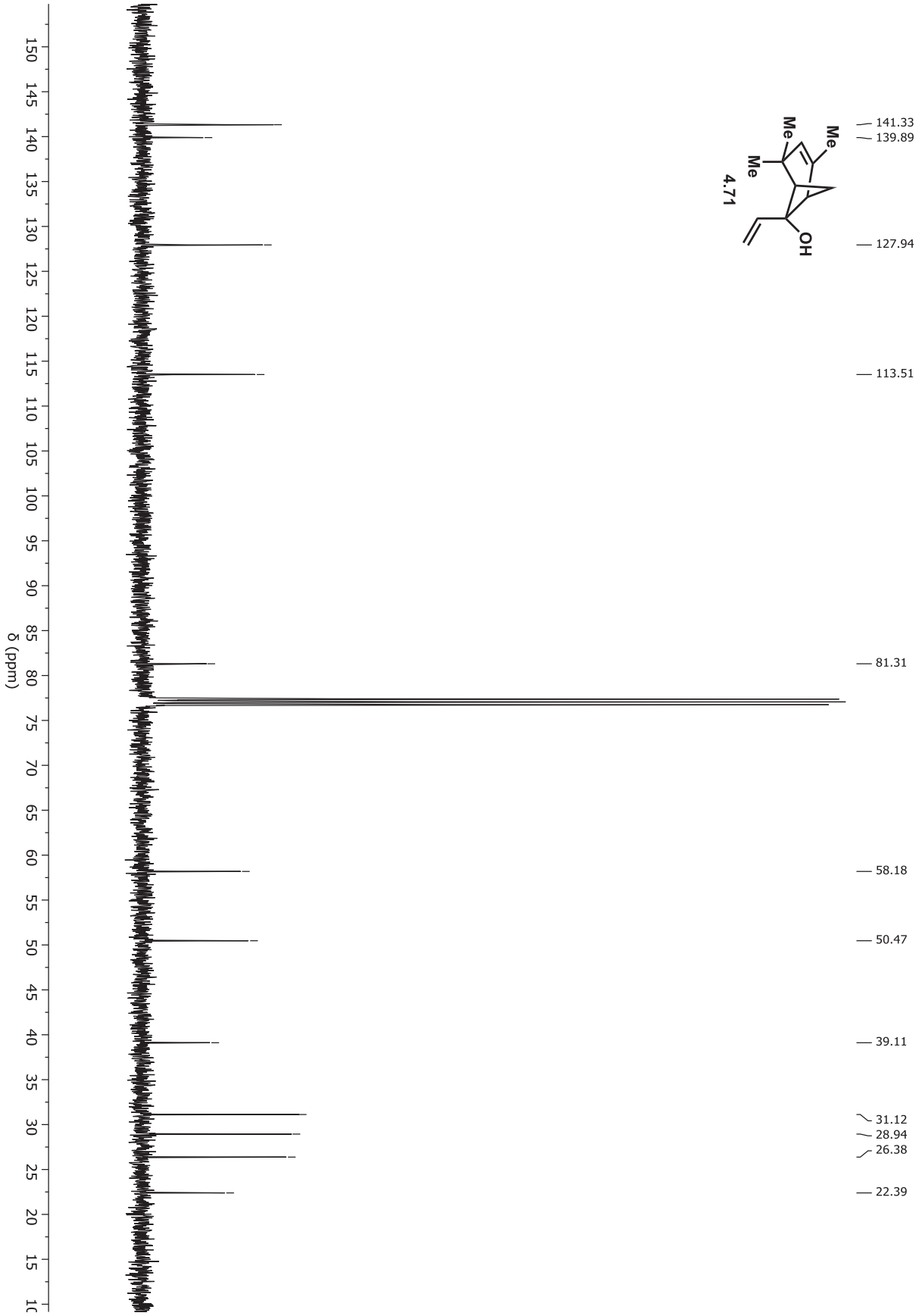
δ (ppm)
150
145
140
135
130
125
120
115
110
105
100
95
90
85
80
75
70
65
60
55
50
45
40
35
30
25
20
15
10
Me
Me
Me
OH
4.71
141.33
139.89
127.94
113.51
81.31
58.18
50.47
39.11
31.12
28.94
26.38
22.39

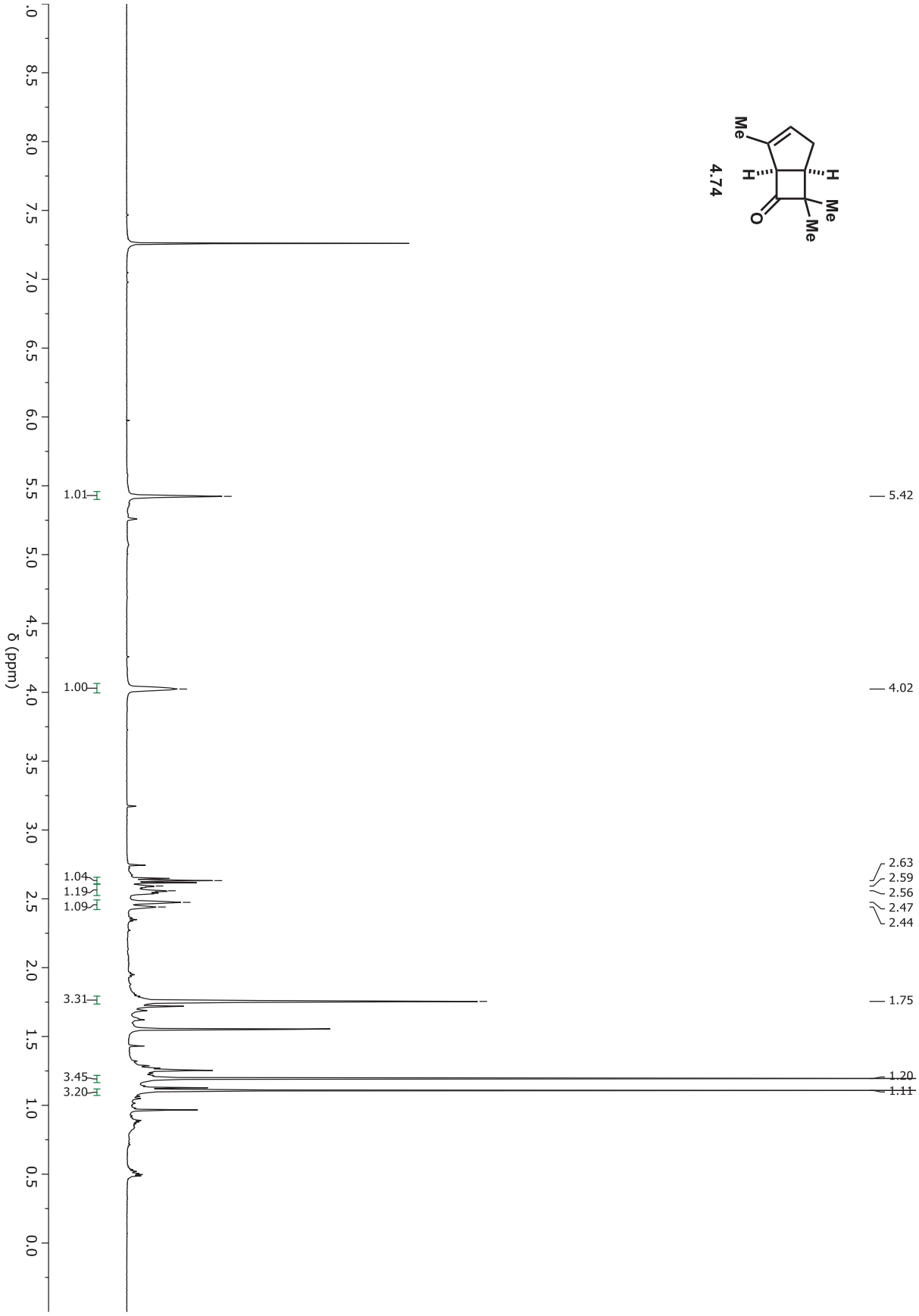
Me
H
H
Me
Me
O
4.74
δ (ppm)
1.01
1.00
1.04
1.19
1.09
3.31
3.45
3.20
5.42
4.02
2.63
2.59
2.56
2.47
2.44
1.75
1.20
1.11

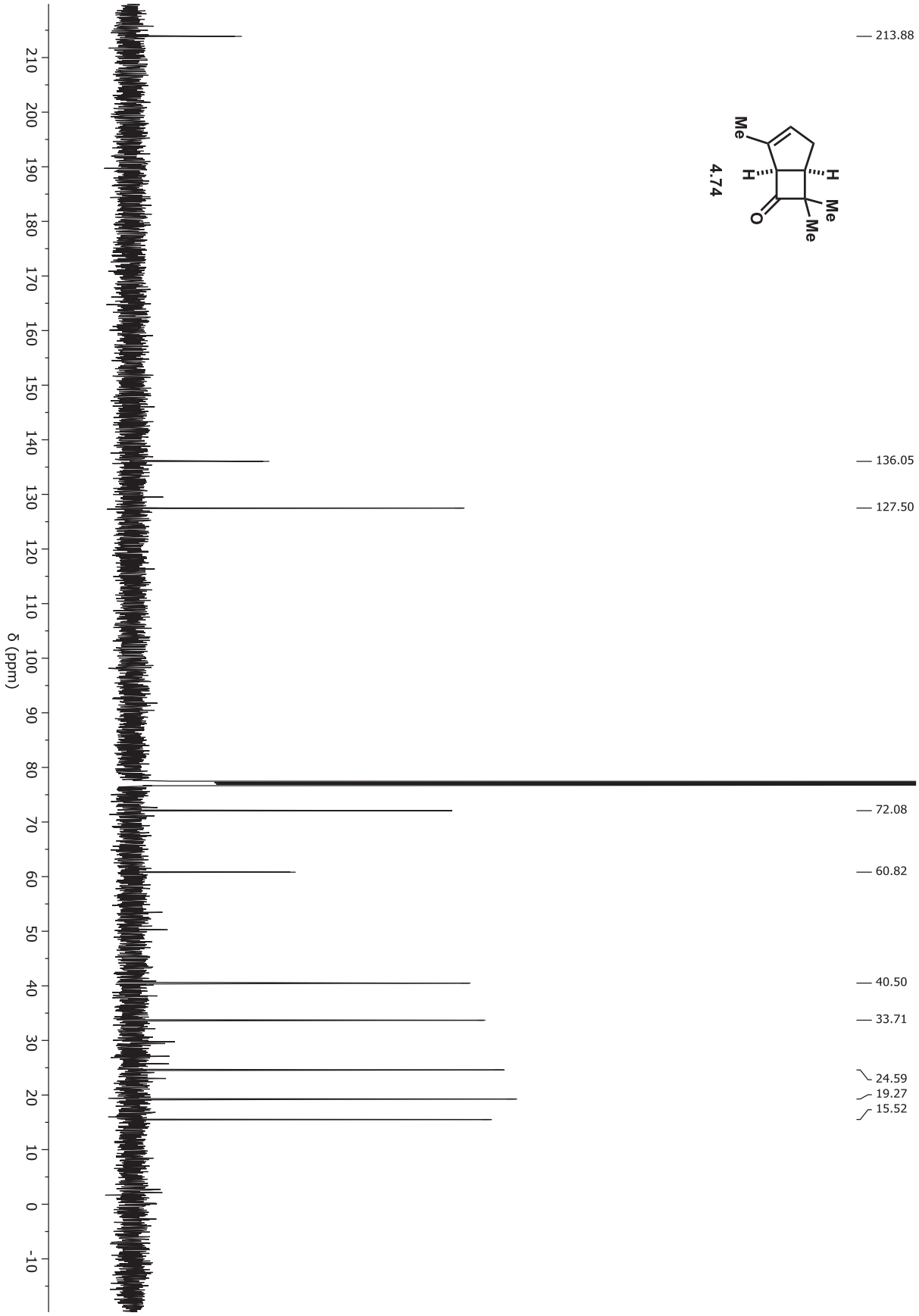
213.88
136.05
127.50
72.08
60.82
40.50
33.71
24.59
19.27
15.52
δ (ppm)
Me
H
H
Me
Me
O
4.74

Appendix 4.B X-Ray crystallography data for Chapter 4

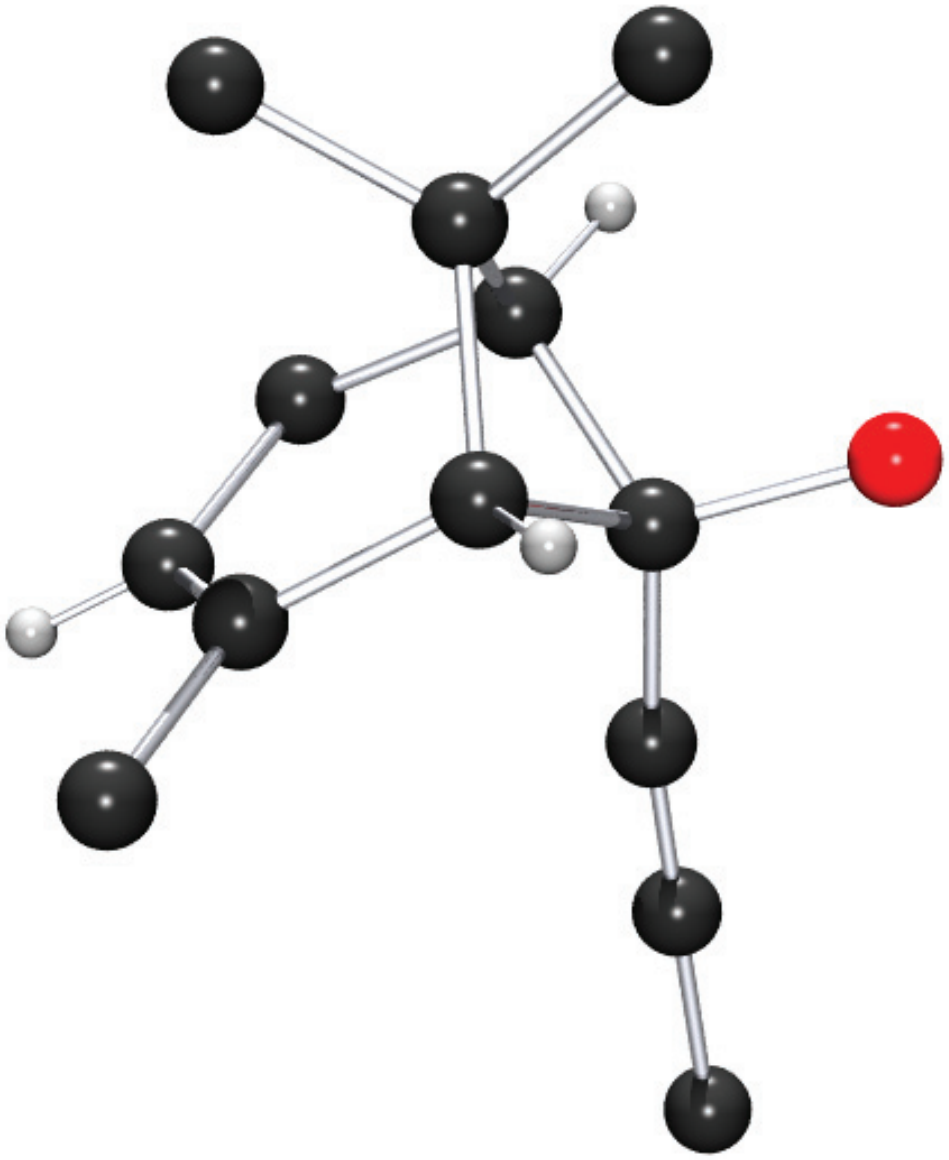

Figure 4.1: POV-Ray/ORTEP rendering of non-rearranged alkyne addition product **4.67** with ellipsoids at 50% probability. Only tertiary and vinylic hydrogens are shown for clarity.

Table 4.7: Crystal data and structure refinement for alkyne 1,2-addition product **4.67**.

Cambridge Crystallographic Data Center	Not deposited
Empirical formula	C13 H18 O
Formula weight	190.27
Temperature	100(2) K
Wavelength	1.54184 Å
Crystal system	Monoclinic
Space group	P 21/c
Unit cell dimensions	a = 10.94100(10) Å α = 90°
	b = 21.9317(2) Å β = 112.2260(10)°
	c = 10.39670(10) Å γ = 90°
Volume	2309.38(4) $Å^3$
Z	8
Density (calculated)	1.095 Mg/m^3
Absorption coefficient	0.514 mm^{-1}
F(000)	832
Crystal size	0.380 x 0.240 x 0.210 mm^3
Theta range for data collection	4.031 to 74.484°
Index ranges	-13<=h<=13, -27<=k<=26, -12<=l<=12
Reflections collected	76677
Independent reflections	4715 [R(int) = 0.0589]
Completeness to theta = 74.000°	99.8%
Absorption correction	Semi-empirical from equivalents
Max. and min. transmission	1.00000 and 0.81955
Refinement method	Full-matrix least-squares on F^2
Data / restraints / parameters	4715 / 0 / 269
Goodness-of-fit on F^2	1.051
Final R indices [I>2sigma(I)]	R1 = 0.0568, wR2 = 0.1506
R indices (all data)	R1 = 0.0573, wR2 = 0.1510
Extinction coefficient	n/a
Largest diff. peak and hole	0.816 and -0.332 $e.Å^{-3}$

Table 4.8: Atomic coordinates (x 10^4) and equivalent isotropic displacement parameters (Å^2 x 10^3) for **4.67**. U(eq) is defined as one third of the trace of the orthogonalized U^{ij} tensor.

	x	y	z	U(eq)
C(1A)	6279(2)	5767(1)	525(2)	39(1)
C(1B)	3342(2)	6007(1)	7166(2)	45(1)
C(2A)	5161(2)	5764(1)	972(2)	30(1)
C(2B)	4423(2)	6095(1)	6683(2)	32(1)
C(3A)	4249(2)	5760(1)	1339(2)	27(1)
C(3B)	5305(2)	6154(1)	6286(2)	28(1)
C(4A)	3244(2)	5714(1)	1955(2)	25(1)
C(4B)	6367(1)	6129(1)	5742(2)	25(1)
C(5A)	1841(2)	5469(1)	1074(2)	30(1)
C(5B)	7804(2)	6297(1)	6717(2)	29(1)
C(6A)	1264(2)	5903(1)	1906(2)	31(1)
C(6B)	8044(2)	6537(1)	5409(2)	30(1)
C(7A)	-122(2)	6160(1)	1124(2)	43(1)
C(7B)	8981(2)	7078(1)	5629(2)	40(1)
C(8A)	1270(2)	5647(1)	3284(2)	36(1)
C(8B)	8492(2)	6050(1)	4626(2)	36(1)
C(9A)	2498(2)	6310(1)	2080(2)	31(1)
C(9B)	6504(1)	6658(1)	4800(2)	26(1)
C(10A)	2211(2)	6670(1)	736(2)	38(1)
C(10B)	6199(2)	7241(1)	5406(2)	29(1)
C(11A)	2488(2)	7336(1)	820(2)	47(1)
C(11B)	5181(2)	7666(1)	4472(2)	33(1)
C(12A)	1716(2)	6361(1)	-434(2)	39(1)
C(12B)	6816(2)	7314(1)	6774(2)	34(1)
C(13A)	1447(2)	5688(1)	-427(2)	39(1)
C(13B)	7753(2)	6834(1)	7639(2)	36(1)
O(1A)	3794(1)	5369(1)	3203(1)	28(1)
O(1B)	6282(1)	5553(1)	5070(1)	26(1)

Table 4.9: Bond lengths [Å] for **4.67**.

C(1A)-C(2A)	1.463(2)	C(7B)-H(7BA)	0.9800
C(1A)-H(1AA)	0.9800	C(7B)-H(7BB)	0.9800
C(1A)-H(1AB)	0.9800	C(7B)-H(7BC)	0.9800
C(1A)-H(1AC)	0.9800	C(8A)-H(8AA)	0.9800
C(1B)-C(2B)	1.462(2)	C(8A)-H(8AB)	0.9800
C(1B)-H(1BA)	0.9800	C(8A)-H(8AC)	0.9800
C(1B)-H(1BB)	0.9800	C(8B)-H(8BA)	0.9800
C(1B)-H(1BC)	0.9800	C(8B)-H(8BB)	0.9800
C(2A)-C(3A)	1.196(2)	C(8B)-H(8BC)	0.9800
C(2B)-C(3B)	1.192(2)	C(9A)-C(10A)	1.531(2)
C(3A)-C(4A)	1.471(2)	C(9A)-H(9A)	1.0000
C(3B)-C(4B)	1.473(2)	C(9B)-C(10B)	1.517(2)
C(4A)-O(1A)	1.4244(17)	C(9B)-H(9B)	1.0000
C(4A)-C(5A)	1.556(2)	C(10A)-C(12A)	1.317(3)
C(4A)-C(9A)	1.573(2)	C(10A)-C(11A)	1.487(3)
C(4B)-O(1B)	1.4300(17)	C(10B)-C(12B)	1.333(2)
C(4B)-C(5B)	1.559(2)	C(10B)-C(11B)	1.496(2)
C(4B)-C(9B)	1.5622(19)	C(11A)-H(11A)	0.9800
C(5A)-C(13A)	1.531(2)	C(11A)-H(11B)	0.9800
C(5A)-C(6A)	1.571(2)	C(11A)-H(11C)	0.9800
C(5A)-H(5A)	1.0000	C(11B)-H(11D)	0.9800
C(5B)-C(13B)	1.533(2)	C(11B)-H(11E)	0.9800
C(5B)-C(6B)	1.569(2)	C(11B)-H(11F)	0.9800
C(5B)-H(5B)	1.0000	C(12A)-C(13A)	1.507(3)
C(6A)-C(7A)	1.531(2)	C(12A)-H(12A)	0.9500
C(6A)-C(8A)	1.536(2)	C(12B)-C(13B)	1.507(2)
C(6A)-C(9A)	1.571(2)	C(12B)-H(12B)	0.9500
C(6B)-C(7B)	1.528(2)	C(13A)-H(13A)	0.9900
C(6B)-C(8B)	1.531(2)	C(13A)-H(13B)	0.9900
C(6B)-C(9B)	1.581(2)	C(13B)-H(^{13}C)	0.9900
C(7A)-H(7AA)	0.9800	C(13B)-H(13D)	0.9900
C(7A)-H(7AB)	0.9800	O(1A)-H(1A)	0.85(3)
C(7A)-H(7AC)	0.9800	O(1B)-H(1B)	0.84(3)

Table 4.10: Bond angles [°] for **4.67**.

C(2A)-C(1A)-H(1AA)	109.5	H(7BB)-C(7B)-H(7BC)	109.5
C(2A)-C(1A)-H(1AB)	109.5	C(6A)-C(8A)-H(8AA)	109.5
H(1AA)-C(1A)-H(1AB)	109.5	C(6A)-C(8A)-H(8AB)	109.5
C(2A)-C(1A)-H(1AC)	109.5	H(8AA)-C(8A)-H(8AB)	109.5
H(1AA)-C(1A)-H(1AC)	109.5	C(6A)-C(8A)-H(8AC)	109.5
H(1AB)-C(1A)-H(1AC)	109.5	H(8AA)-C(8A)-H(8AC)	109.5
C(2B)-C(1B)-H(1BA)	109.5	H(8AB)-C(8A)-H(8AC)	109.5
C(2B)-C(1B)-H(1BB)	109.5	C(6B)-C(8B)-H(8BA)	109.5
H(1BA)-C(1B)-H(1BB)	109.5	C(6B)-C(8B)-H(8BB)	109.5
C(2B)-C(1B)-H(1BC)	109.5	H(8BA)-C(8B)-H(8BB)	109.5
H(1BA)-C(1B)-H(1BC)	109.5	C(6B)-C(8B)-H(8BC)	109.5
H(1BB)-C(1B)-H(1BC)	109.5	H(8BA)-C(8B)-H(8BC)	109.5
C(3A)-C(2A)-C(1A)	179.73(18)	H(8BB)-C(8B)-H(8BC)	109.5
C(3B)-C(2B)-C(1B)	178.54(18)	C(10A)-C(9A)-C(6A)	108.51(14)
C(2A)-C(3A)-C(4A)	172.51(16)	C(10A)-C(9A)-C(4A)	106.69(12)
C(2B)-C(3B)-C(4B)	171.45(16)	C(6A)-C(9A)-C(4A)	88.19(11)
O(1A)-C(4A)-C(3A)	107.80(12)	C(10A)-C(9A)-H(9A)	116.6
O(1A)-C(4A)-C(5A)	109.58(12)	C(6A)-C(9A)-H(9A)	116.6
C(3A)-C(4A)-C(5A)	120.07(13)	C(4A)-C(9A)-H(9A)	116.6
O(1A)-C(4A)-C(9A)	114.86(12)	C(10B)-C(9B)-C(4B)	106.05(11)
C(3A)-C(4A)-C(9A)	118.42(12)	C(10B)-C(9B)-C(6B)	110.05(12)
C(5A)-C(4A)-C(9A)	84.75(11)	C(4B)-C(9B)-C(6B)	87.97(11)
O(1B)-C(4B)-C(3B)	107.78(12)	C(10B)-C(9B)-H(9B)	116.4
O(1B)-C(4B)-C(5B)	112.98(12)	C(4B)-C(9B)-H(9B)	116.4
C(3B)-C(4B)-C(5B)	119.35(12)	C(6B)-C(9B)-H(9B)	116.4
O(1B)-C(4B)-C(9B)	110.70(11)	C(12A)-C(10A)-C(11A)	124.29(17)
C(3B)-C(4B)-C(9B)	119.35(12)	C(12A)-C(10A)-C(9A)	116.63(16)
C(5B)-C(4B)-C(9B)	85.36(11)	C(11A)-C(10A)-C(9A)	119.08(17)
C(13A)-C(5A)-C(4A)	109.07(13)	C(12B)-C(10B)-C(11B)	124.73(15)
C(13A)-C(5A)-C(6A)	110.76(13)	C(12B)-C(10B)-C(9B)	116.28(14)
C(4A)-C(5A)-C(6A)	88.79(11)	C(11B)-C(10B)-C(9B)	118.85(13)
C(13A)-C(5A)-H(5A)	115.1	C(10A)-C(11A)-H(11A)	109.5
C(4A)-C(5A)-H(5A)	115.1	C(10A)-C(11A)-H(11B)	109.5

C(6A)-C(5A)-H(5A)	115.1	H(11A)-C(11A)-H(11B)	109.5
C(13B)-C(5B)-C(4B)	108.75(13)	C(10A)-C(11A)-H(11C)	109.5
C(13B)-C(5B)-C(6B)	109.99(13)	H(11A)-C(11A)-H(11C)	109.5
C(4B)-C(5B)-C(6B)	88.53(11)	H(11B)-C(11A)-H(11C)	109.5
C(13B)-C(5B)-H(5B)	115.5	C(10B)-C(11B)-H(11D)	109.5
C(4B)-C(5B)-H(5B)	115.5	C(10B)-C(11B)-H(11E)	109.5
C(6B)-C(5B)-H(5B)	115.5	H(11D)-C(11B)-H(11E)	109.5
C(7A)-C(6A)-C(8A)	106.51(13)	C(10B)-C(11B)-H(11F)	109.5
C(7A)-C(6A)-C(9A)	119.21(14)	H(11D)-C(11B)-H(11F)	109.5
C(8A)-C(6A)-C(9A)	113.59(14)	H(11E)-C(11B)-H(11F)	109.5
C(7A)-C(6A)-C(5A)	116.99(14)	C(10A)-C(12A)-C(13A)	120.88(15)
C(8A)-C(6A)-C(5A)	115.46(13)	C(10A)-C(12A)-H(12A)	119.6
C(9A)-C(6A)-C(5A)	84.32(11)	C(13A)-C(12A)-H(12A)	119.6
C(7B)-C(6B)-C(8B)	106.79(13)	C(10B)-C(12B)-C(13B)	120.53(15)
C(7B)-C(6B)-C(5B)	116.98(14)	C(10B)-C(12B)-H(12B)	119.7
C(8B)-C(6B)-C(5B)	114.73(13)	C(13B)-C(12B)-H(12B)	119.7
C(7B)-C(6B)-C(9B)	118.88(13)	C(12A)-C(13A)-C(5A)	109.38(15)
C(8B)-C(6B)-C(9B)	114.22(13)	C(12A)-C(13A)-H(13A)	109.8
C(5B)-C(6B)-C(9B)	84.37(10)	C(5A)-C(13A)-H(13A)	109.8
C(6A)-C(7A)-H(7AA)	109.5	C(12A)-C(13A)-H(13B)	109.8
C(6A)-C(7A)-H(7AB)	109.5	C(5A)-C(13A)-H(13B)	109.8
H(7AA)-C(7A)-H(7AB)	109.5	H(13A)-C(13A)-H(13B)	108.2
C(6A)-C(7A)-H(7AC)	109.5	C(12B)-C(13B)-C(5B)	109.95(13)
H(7AA)-C(7A)-H(7AC)	109.5	C(12B)-C(13B)-H(^{13}C)	109.7
H(7AB)-C(7A)-H(7AC)	109.5	C(5B)-C(13B)-H(^{13}C)	109.7
C(6B)-C(7B)-H(7BA)	109.5	C(12B)-C(13B)-H(13D)	109.7
C(6B)-C(7B)-H(7BB)	109.5	C(5B)-C(13B)-H(13D)	109.7
H(7BA)-C(7B)-H(7BB)	109.5	H(^{13}C)-C(13B)-H(13D)	108.2
C(6B)-C(7B)-H(7BC)	109.5	C(4A)-O(1A)-H(1A)	111.9(16)
H(7BA)-C(7B)-H(7BC)	109.5	C(4B)-O(1B)-H(1B)	109.7(17)

Table 4.11: Anisotropic displacement parameters ($Å^2$ x 10^3) for **4.67**. The anisotropic displacement factor exponent takes the form: $-2\pi^2[h^2a^{*2}U^{11} + ... + 2\ h\ k\ a^*\ b^*\ U^{12}]$.

	U^{11}	U^{22}	U^{33}	U^{23}	U^{13}	U^{12}
C(1A)	35(1)	41(1)	52(1)	6(1)	29(1)	6(1)
C(1B)	41(1)	62(1)	43(1)	-4(1)	29(1)	-8(1)
C(2A)	30(1)	29(1)	35(1)	5(1)	18(1)	4(1)
C(2B)	35(1)	36(1)	31(1)	0(1)	18(1)	-2(1)
C(3A)	28(1)	25(1)	30(1)	4(1)	14(1)	4(1)
C(3B)	32(1)	28(1)	28(1)	3(1)	16(1)	1(1)
C(4A)	28(1)	24(1)	28(1)	5(1)	16(1)	3(1)
C(4B)	28(1)	25(1)	27(1)	2(1)	15(1)	0(1)
C(5A)	26(1)	36(1)	32(1)	2(1)	14(1)	2(1)
C(5B)	28(1)	33(1)	29(1)	4(1)	13(1)	0(1)
C(6A)	28(1)	34(1)	38(1)	5(1)	20(1)	4(1)
C(6B)	27(1)	33(1)	33(1)	5(1)	15(1)	-1(1)
C(7A)	33(1)	52(1)	52(1)	12(1)	25(1)	11(1)
C(7B)	32(1)	43(1)	46(1)	8(1)	17(1)	-7(1)
C(8A)	37(1)	41(1)	42(1)	7(1)	26(1)	4(1)
C(8B)	33(1)	42(1)	41(1)	7(1)	24(1)	5(1)
C(9A)	33(1)	28(1)	40(1)	3(1)	23(1)	3(1)
C(9B)	28(1)	25(1)	27(1)	3(1)	14(1)	-1(1)
C(10A)	33(1)	35(1)	55(1)	17(1)	27(1)	12(1)
C(10B)	32(1)	25(1)	35(1)	1(1)	19(1)	-3(1)
C(11A)	50(1)	37(1)	62(1)	11(1)	31(1)	8(1)
C(11B)	39(1)	26(1)	40(1)	2(1)	21(1)	1(1)
C(12A)	33(1)	53(1)	36(1)	15(1)	20(1)	14(1)
C(12B)	40(1)	30(1)	36(1)	-5(1)	18(1)	-5(1)
C(13A)	29(1)	59(1)	31(1)	3(1)	13(1)	6(1)
C(13B)	38(1)	40(1)	30(1)	-2(1)	13(1)	-6(1)
O(1A)	26(1)	30(1)	30(1)	8(1)	12(1)	0(1)
O(1B)	31(1)	23(1)	29(1)	4(1)	16(1)	1(1)

Table 4.12: Hydrogen coordinates (x 10^4) and isotropic displacement parameters (Å^2 x 10^3) for **4.67**.

	x	y	z	U(eq)
H(1AA)	5969	5666	-466	59
H(1AB)	6932	5464	1061	59
H(1AC)	6687	6172	680	59
H(1BA)	2577	6248	6590	67
H(1BB)	3624	6138	8136	67
H(1BC)	3100	5574	7096	67
H(5A)	1708	5024	1183	36
H(5B)	8372	5947	7213	35
H(7AA)	-175	6328	231	64
H(7AB)	-304	6482	1679	64
H(7AC)	-774	5833	961	64
H(7BA)	8996	7207	4732	60
H(7BB)	9872	6957	6249	60
H(7BC)	8677	7417	6046	60
H(8AA)	667	5298	3094	54
H(8AB)	982	5964	3771	54
H(8AC)	2166	5515	38	64 54
H(8BA)	7887	5702	4422	54
H(8BB)	9386	5915	5201	54
H(8BC)	8488	6222	3755	54
H(9A)	2890	6544	2968	37
H(9B)	6037	6601	3775	31
H(11A)	2032	7535	1355	70
H(11B)	2175	7509	-120	70
H(11C)	3441	7404	1278	70
H(11D)	5466	7815	3742	49
H(11E)	5069	8012	5014	49
H(11F)	4339	7450	4047	49
H(12A)	1526	6566	-1294	46
H(12B)	6665	7672	7206	41
H(13A)	1959	5463	-882	47
H(13B)	497	5607	-953	47
H(^{13}C)	7454	6689	8373	43
H(13D)	8646	7011	8094	43
H(1A)	4600(30)	5460(11)	3660(30)	54(7)
H(1B)	6300(20)	5270(12)	5620(30)	54(7)

Table 4.13: Torsion angles [°] for **4.67**.

O(1A)-C(4A)-C(5A)-C(13A)	-161.64(13)	O(1A)-C(4A)-C(9A)-C(6A)	-81.39(14)
C(3A)-C(4A)-C(5A)-C(13A)	-36.13(19)	C(3A)-C(4A)-C(9A)-C(6A)	149.27(14)
C(9A)-C(4A)-C(5A)-C(13A)	83.81(14)	C(5A)-C(4A)-C(9A)-C(6A)	27.77(11)
O(1A)-C(4A)-C(5A)-C(6A)	86.78(13)	O(1B)-C(4B)-C(9B)-C(10B)	164.42(12)
C(3A)-C(4A)-C(5A)-C(6A)	-147.71(13)	C(3B)-C(4B)-C(9B)-C(10B)	38.48(17)
C(9A)-C(4A)-C(5A)-C(6A)	-27.76(11)	C(5B)-C(4B)-C(9B)-C(10B)	-82.75(13)
O(1B)-C(4B)-C(5B)-C(13B)	-166.60(12)	O(1B)-C(4B)-C(9B)-C(6B)	-85.29(13)
C(3B)-C(4B)-C(5B)-C(13B)	-38.37(18)	C(3B)-C(4B)-C(9B)-C(6B)	148.77(14)
C(9B)-C(4B)-C(5B)-C(13B)	82.87(13)	C(5B)-C(4B)-C(9B)-C(6B)	27.54(11)
O(1B)-C(4B)-C(5B)-C(6B)	82.77(13)	C(7B)-C(6B)-C(9B)-C(10B)	-38.82(18)
C(3B)-C(4B)-C(5B)-C(6B)	-149.00(14)	C(8B)-C(6B)-C(9B)-C(10B)	-166.41(12)
C(9B)-C(4B)-C(5B)-C(6B)	-27.77(11)	C(5B)-C(6B)-C(9B)-C(10B)	78.97(13)
C(13A)-C(5A)-C(6A)-C(7A)	37.8(2)	C(7B)-C(6B)-C(9B)-C(4B)	-145.18(14)
C(4A)-C(5A)-C(6A)-C(7A)	147.80(14)	C(8B)-C(6B)-C(9B)-C(4B)	87.24(13)
C(13A)-C(5A)-C(6A)-C(8A)	164.40(14)	C(5B)-C(6B)-C(9B)-C(4B)	-27.39(11)
C(4A)-C(5A)-C(6A)-C(8A)	-85.64(15)	C(6A)-C(9A)-C(10A)-C(12A)	-47.15(19)
C(13A)-C(5A)-C(6A)-C(9A)	-82.14(14)	C(4A)-C(9A)-C(10A)-C(12A)	46.62(19)
C(4A)-C(5A)-C(6A)-C(9A)	27.82(11)	C(6A)-C(9A)-C(10A)-C(11A)	132.31(16)
C(13B)-C(5B)-C(6B)-C(7B)	37.64(19)	C(4A)-C(9A)-C(10A)-C(11A)	-133.93(15)
C(4B)-C(5B)-C(6B)-C(7B)	147.08(14)	C(4B)-C(9B)-C(10B)-C(12B)	48.45(17)
C(13B)-C(5B)-C(6B)-C(8B)	163.90(14)	C(6B)-C(9B)-C(10B)-C(12B)	-45.33(18)
C(4B)-C(5B)-C(6B)-C(8B)	-86.66(14)	C(4B)-C(9B)-C(10B)-C(11B)	-127.52(14)
C(13B)-C(5B)-C(6B)-C(9B)	-82.00(13)	C(6B)-C(9B)-C(10B)-C(11B)	138.70(14)
C(4B)-C(5B)-C(6B)-C(9B)	27.44(11)	C(11A)-C(10A)-C(12A)-C(13A)	-179.14(16)
C(7A)-C(6A)-C(9A)-C(10A)	-38.3(2)	C(9A)-C(10A)-C(12A)-C(13A)	0.3(2)
C(8A)-C(6A)-C(9A)-C(10A)	-165.16(13)	C(11B)-C(10B)-C(12B)-C(13B)	175.34(15)
C(5A)-C(6A)-C(9A)-C(10A)	79.50(13)	C(9B)-C(10B)-C(12B)-C(13B)	-0.4(2)
C(7A)-C(6A)-C(9A)-C(4A)	-145.34(15)	C(10A)-C(12A)-C(13A)-C(5A)	-0.3(2)
C(8A)-C(6A)-C(9A)-C(4A)	87.83(14)	C(4A)-C(5A)-C(13A)-C(12A)	-48.10(17)
C(5A)-C(6A)-C(9A)-C(4A)	-27.51(11)	C(6A)-C(5A)-C(13A)-C(12A)	48.05(17)
O(1A)-C(4A)-C(9A)-C(10A)	169.81(13)	C(10B)-C(12B)-C(13B)-C(5B)	-1.4(2)
C(3A)-C(4A)-C(9A)-C(10A)	40.47(19)	C(4B)-C(5B)-C(13B)-C(12B)	-45.59(17)
C(5A)-C(4A)-C(9A)-C(10A)	-81.02(14)	C(6B)-C(5B)-C(13B)-C(12B)	49.85(17)

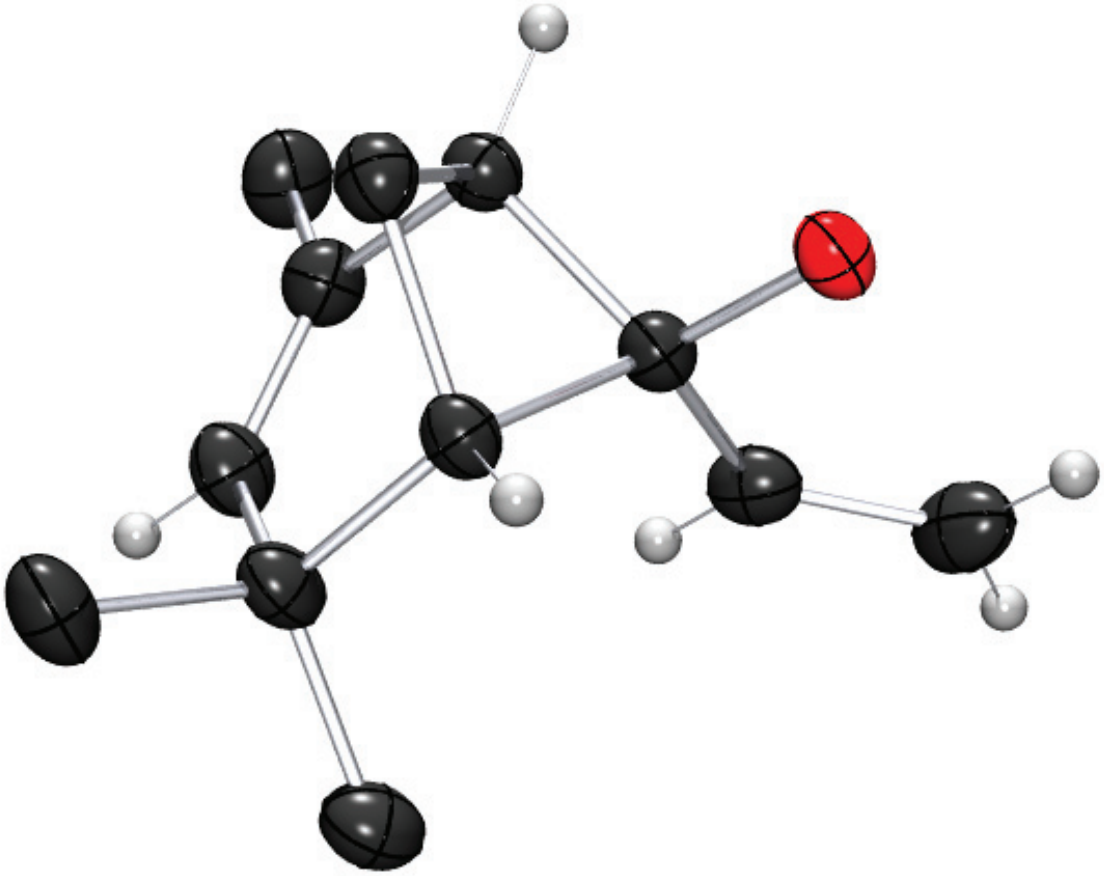

Figure 4.2: POV-Ray/ORTEP rendering of rearranged [3.1.1] bicycle **4.71** with ellipsoids at 50% probability. Only tertiary and vinylic hydrogens are shown for clarity.

Table 4.14: Crystal data and structure refinement for rearranged bicycle **4.71**.

Cambridge Crystallographic Data Center	Not deposited
Empirical formula	C12 H18 O
Formula weight	178.26
Temperature	100(2) K
Wavelength	1.54184 Å
Crystal system	Orthorhombic
Space group	P 21 21 21
Unit cell dimensions	a = 8.33890(10) Å α = 90°
	b = 11.5932(2) Å β = 90°
	c = 22.6819(3) Å γ = 90°
Volume	2192.76(5) $Å^3$
Z	8
Density (calculated)	1.080 Mg/m^3
Absorption coefficient	0.509 mm^{-1}
F(000)	784
Crystal size	0.230 x 0.100 x 0.070 mm^3
Theta range for data collection	3.898 to 74.503°
Index ranges	-6<=h<=10, -14<=k<=14, -28<=l<=22
Reflections collected	22311
Independent reflections	4430 [R(int) = 0.0605]
Completeness to theta = 74.000°	100.0%
Absorption correction	Semi-empirical from equivalents
Max. and min. transmission	1.00000 and 0.77586
Refinement method	Full-matrix least-squares on F^2
Data / restraints / parameters	4430 / 0 / 249
Goodness-of-fit on F^2	1.102
Final R indices [I>2sigma(I)]	R1 = 0.0380, wR2 = 0.1050
R indices (all data)	R1 = 0.0400, wR2 = 0.1076
Absolute structure parameter	0.07(12)
Extinction coefficient	n/a
Largest diff. peak and hole	0.182 and -0.171 $e.Å^{-3}$

Table 4.15: Atomic coordinates (x 10^4) and equivalent isotropic displacement parameters (Å^2 x 10^3) for **4.71**. U(eq) is defined as one third of the trace of the orthogonalized U^{ij} tensor.

	x	y	z	U(eq)
C(1)	7864(3)	4667(2)	4578(1)	32(1)
C(2)	7273(2)	5078(2)	5077(1)	26(1)
C(3)	6048(2)	4491(2)	5451(1)	23(1)
C(4)	6280(2)	4524(2)	6138(1)	25(1)
C(5)	4440(2)	4340(2)	6185(1)	26(1)
C(6)	4324(2)	4997(2)	5586(1)	24(1)
C(7)	4299(3)	6305(2)	5696(1)	29(1)
C(8)	4477(3)	6987(2)	5118(1)	36(1)
C(9)	2671(3)	6646(2)	5965(1)	37(1)
C(10)	5662(3)	6580(2)	6115(1)	31(1)
C(11)	6633(3)	5762(2)	6319(1)	29(1)
C(12)	8070(3)	5985(2)	6701(1)	38(1)
C(13)	10320(3)	3219(2)	6257(1)	38(1)
C(14)	9614(2)	2264(2)	6447(1)	29(1)
C(15)	8468(2)	1549(2)	6095(1)	24(1)
C(16)	8745(2)	210(2)	6102(1)	24(1)
C(17)	6946(2)	86(2)	5942(1)	26(1)
C(18)	6700(2)	1236(2)	6288(1)	24(1)
C(19)	6507(3)	977(2)	6949(1)	28(1)
C(20)	6487(3)	2099(2)	7311(1)	34(1)
C(21)	4877(3)	371(2)	7056(1)	36(1)
C(22)	7870(3)	189(2)	7129(1)	31(1)
C(23)	8948(2)	-179(2)	6738(1)	28(1)
C(24)	10345(3)	-938(2)	6882(1)	37(1)
O(1)	5774(2)	3343(1)	5248(1)	25(1)
O(2)	8314(2)	1980(1)	5510(1)	26(1)

Table 4.16: Bond lengths [Å] for **4.71**

C(1)-C(2)	1.323(3)	C(13)-H(13A)	0.9500
C(1)-H(1A)	0.9500	C(13)-H(13B)	0.9500
C(1)-H(1B)	0.9500	C(14)-C(15)	1.496(3)
C(2)-C(3)	1.492(3)	C(14)-H(14)	0.9500
C(2)-H(2)	0.9500	C(15)-O(2)	1.425(2)
C(3)-O(1)	1.427(2)	C(15)-C(16)	1.570(3)
C(3)-C(4)	1.570(3)	C(15)-C(18)	1.580(3)
C(3)-C(6)	1.582(3)	C(16)-C(23)	1.521(3)
C(4)-C(11)	1.522(3)	C(16)-C(17)	1.550(3)
C(4)-C(5)	1.553(3)	C(16)-H(16)	1.0000
C(4)-H(4)	1.0000	C(17)-C(18)	1.560(3)
C(5)-C(6)	1.560(3)	C(17)-H(17A)	0.9900
C(5)-H(5A)	0.9900	C(17)-H(17B)	0.9900
C(5)-H(5B)	0.9900	C(18)-C(19)	1.538(3)
C(6)-C(7)	1.538(3)	C(18)-H(18)	1.0000
C(6)-H(6)	1.0000	C(19)-C(22)	1.514(3)
C(7)-C(10)	1.514(3)	C(19)-C(20)	1.538(3)
C(7)-C(8)	1.538(3)	C(19)-C(21)	1.549(3)
C(7)-C(9)	1.540(3)	C(20)-H(20A)	0.9800
C(8)-H(8A)	0.9800	C(20)-H(20B)	0.9800
C(8)-H(8B)	0.9800	C(20)-H(20C)	0.9800
C(8)-H(8C)	0.9800	C(21)-H(21A)	0.9800
C(9)-H(9A)	0.9800	C(21)-H(21B)	0.9800
C(9)-H(9B)	0.9800	C(21)-H(21C)	0.9800
C(9)-H(9C)	0.9800	C(22)-C(23)	1.334(3)
C(10)-C(11)	1.330(3)	C(22)-H(22)	0.9500
C(10)-H(10)	0.9500	C(23)-C(24)	1.497(3)
C(11)-C(12)	1.502(3)	C(24)-H(24A)	0.9800
C(12)-H(12A)	0.9800	C(24)-H(24B)	0.9800
C(12)-H(12B)	0.9800	C(24)-H(24C)	0.9800
C(12)-H(12C)	0.9800	O(1)-H(1)	0.89(3)
C(13)-C(14)	1.326(3)	O(2)-H(2A)	0.93(3)

Table 4.17: Bond angles [°] for **4.71**.

C(2)-C(1)-H(1A)	120.0	C(7)-C(8)-H(8A)	109.5
C(2)-C(1)-H(1B)	120.0	C(7)-C(8)-H(8B)	109.5
H(1A)-C(1)-H(1B)	120.0	H(8A)-C(8)-H(8B)	109.5
C(1)-C(2)-C(3)	125.3(2)	C(7)-C(8)-H(8C)	109.5
C(1)-C(2)-H(2)	117.4	H(8A)-C(8)-H(8C)	109.5
C(3)-C(2)-H(2)	117.4	H(8B)-C(8)-H(8C)	109.5
O(1)-C(3)-C(2)	110.55(16)	C(7)-C(9)-H(9A)	109.5
O(1)-C(3)-C(4)	111.27(15)	C(7)-C(9)-H(9B)	109.5
C(2)-C(3)-C(4)	117.99(17)	H(9A)-C(9)-H(9B)	109.5
O(1)-C(3)-C(6)	105.18(15)	C(7)-C(9)-H(9C)	109.5
C(2)-C(3)-C(6)	124.28(17)	H(9A)-C(9)-H(9C)	109.5
C(4)-C(3)-C(6)	84.91(14)	H(9B)-C(9)-H(9C)	109.5
C(11)-C(4)-C(5)	107.57(17)	C(11)-C(10)-C(7)	121.7(2)
C(11)-C(4)-C(3)	108.32(16)	C(11)-C(10)-H(10)	119.1
C(5)-C(4)-C(3)	86.76(14)	C(7)-C(10)-H(10)	119.1
C(11)-C(4)-H(4)	116.7	C(10)-C(11)-C(12)	124.4(2)
C(5)-C(4)-H(4)	116.7	C(10)-C(11)-C(4)	117.39(19)
C(3)-C(4)-H(4)	116.7	C(12)-C(11)-C(4)	118.21(19)
C(4)-C(5)-C(6)	86.23(14)	C(11)-C(12)-H(12A)	109.5
C(4)-C(5)-H(5A)	114.3	C(11)-C(12)-H(12B)	109.5
C(6)-C(5)-H(5A)	114.3	H(12A)-C(12)-H(12B)	109.5
C(4)-C(5)-H(5B)	114.3	C(11)-C(12)-H(12C)	109.5
C(6)-C(5)-H(5B)	114.3	H(12A)-C(12)-H(12C)	109.5
H(5A)-C(5)-H(5B)	111.4	H(12B)-C(12)-H(12C)	109.5
C(7)-C(6)-C(5)	109.85(16)	C(14)-C(13)-H(13A)	120.0
C(7)-C(6)-C(3)	114.15(17)	C(14)-C(13)-H(13B)	120.0
C(5)-C(6)-C(3)	86.07(14)	H(13A)-C(13)-H(13B)	120.0
C(7)-C(6)-H(6)	114.5	C(13)-C(14)-C(15)	124.9(2)
C(5)-C(6)-H(6)	114.5	C(13)-C(14)-H(14)	117.5
C(3)-C(6)-H(6)	114.5	C(15)-C(14)-H(14)	117.5
C(10)-C(7)-C(6)	107.42(17)	O(2)-C(15)-C(14)	111.11(17)
C(10)-C(7)-C(8)	110.72(19)	O(2)-C(15)-C(16)	111.68(15)
C(6)-C(7)-C(8)	111.50(17)	C(14)-C(15)-C(16)	116.70(17)
C(10)-C(7)-C(9)	111.07(17)	O(2)-C(15)-C(18)	104.74(15)
C(6)-C(7)-C(9)	109.27(19)	C(14)-C(15)-C(18)	125.16(16)
C(8)-C(7)-C(9)	106.89(18)	C(16)-C(15)-C(18)	84.69(14)

C(23)-C(16)-C(17)	107.54(16)	C(19)-C(20)-H(20B)	109.5
C(23)-C(16)-C(15)	108.57(16)	H(20A)-C(20)-H(20B)	109.5
C(17)-C(16)-C(15)	86.98(15)	C(19)-C(20)-H(20C)	109.5
C(23)-C(16)-H(16)	116.6	H(20A)-C(20)-H(20C)	109.5
C(17)-C(16)-H(16)	116.6	H(20B)-C(20)-H(20C)	109.5
C(15)-C(16)-H(16)	116.6	C(19)-C(21)-H(21A)	109.5
C(16)-C(17)-C(18)	86.02(15)	C(19)-C(21)-H(21B)	109.5
C(16)-C(17)-H(17A)	114.3	H(21A)-C(21)-H(21B)	109.5
C(18)-C(17)-H(17A)	114.3	C(19)-C(21)-H(21C)	109.5
C(16)-C(17)-H(17B)	114.3	H(21A)-C(21)-H(21C)	109.5
C(18)-C(17)-H(17B)	114.3	H(21B)-C(21)-H(21C)	109.5
H(17A)-C(17)-H(17B)	111.5	C(23)-C(22)-C(19)	121.30(19)
C(19)-C(18)-C(17)	109.72(17)	C(23)-C(22)-H(22)	119.3
C(19)-C(18)-C(15)	114.34(16)	C(19)-C(22)-H(22)	119.3
C(17)-C(18)-C(15)	86.25(14)	C(22)-C(23)-C(24)	124.6(2)
C(19)-C(18)-H(18)	114.5	C(22)-C(23)-C(16)	117.49(19)
C(17)-C(18)-H(18)	114.5	C(24)-C(23)-C(16)	117.89(19)
C(15)-C(18)-H(18)	114.5	C(23)-C(24)-H(24A)	109.5
C(22)-C(19)-C(20)	112.00(18)	C(23)-C(24)-H(24B)	109.5
C(22)-C(19)-C(18)	107.59(17)	H(24A)-C(24)-H(24B)	109.5
C(20)-C(19)-C(18)	110.85(18)	C(23)-C(24)-H(24C)	109.5
C(22)-C(19)-C(21)	110.08(18)	H(24A)-C(24)-H(24C)	109.5
C(20)-C(19)-C(21)	106.91(19)	H(24B)-C(24)-H(24C)	109.5
C(18)-C(19)-C(21)	109.41(17)	C(3)-O(1)-H(1)	109.6(19)
C(19)-C(20)-H(20A)	109.5	C(15)-O(2)-H(2A)	109.7(18)

Table 4.18: Anisotropic displacement parameters ($Å^2$ x 10^3) for **4.71**. The anisotropic displacement factor exponent takes the form: $-2\pi^2[h^2a^{*2}U^{11} + ... + 2\ h\ k\ a^*\ b^*\ U^{12}]$.

	U^{11}	U^{22}	U^{33}	U^{23}	U^{13}	U^{12}
C(1)	28(1)	38(1)	30(1)	0(1)	6(1)	0(1)
C(2)	25(1)	26(1)	29(1)	1(1)	1(1)	-1(1)
C(3)	23(1)	22(1)	24(1)	1(1)	2(1)	0(1)
C(4)	22(1)	26(1)	25(1)	2(1)	-1(1)	0(1)
C(5)	22(1)	30(1)	24(1)	2(1)	2(1)	-1(1)
C(6)	22(1)	28(1)	23(1)	0(1)	1(1)	2(1)
C(7)	34(1)	28(1)	26(1)	0(1)	2(1)	5(1)
C(8)	47(1)	28(1)	35(1)	2(1)	2(1)	8(1)
C(9)	38(1)	41(1)	32(1)	-4(1)	1(1)	12(1)
C(10)	36(1)	27(1)	29(1)	-5(1)	6(1)	-2(1)
C(11)	28(1)	33(1)	25(1)	-2(1)	5(1)	-5(1)
C(12)	32(1)	45(1)	39(1)	-8(1)	-1(1)	-10(1)
C(13)	28(1)	35(1)	50(1)	-10(1)	3(1)	-6(1)
C(14)	22(1)	32(1)	33(1)	-6(1)	-1(1)	1(1)
C(15)	23(1)	25(1)	23(1)	1(1)	1(1)	0(1)
C(16)	22(1)	26(1)	25(1)	0(1)	1(1)	0(1)
C(17)	24(1)	28(1)	26(1)	0(1)	-1(1)	-3(1)
C(18)	20(1)	28(1)	23(1)	2(1)	0(1)	0(1)
C(19)	30(1)	33(1)	22(1)	3(1)	3(1)	3(1)
C(20)	37(1)	41(1)	25(1)	-2(1)	1(1)	5(1)
C(21)	31(1)	45(1)	32(1)	9(1)	7(1)	1(1)
C(22)	31(1)	37(1)	26(1)	6(1)	-1(1)	1(1)
C(23)	27(1)	28(1)	29(1)	2(1)	-3(1)	1(1)
C(24)	32(1)	37(1)	41(1)	7(1)	-2(1)	6(1)
O(1)	24(1)	22(1)	28(1)	-1(1)	-2(1)	1(1)
O(2)	24(1)	30(1)	24(1)	4(1)	4(1)	2(1)

Table 4.19: Hydrogen coordinates (x 10^4) and isotropic displacement parameters (Å^2 x 10^3) for **4.71**.

	x	y	z	U(eq)
H(1A)	7509	3942	4433	38
H(1B)	8644	5096	4366	38
H(2)	7660	5805	5208	32
H(4)	6976	3912	6313	29
H(5A)	3931	4746	6520	31
H(5B)	4100	3523	6166	31
H(6)	3460	4712	5317	29
H(8A)	5485	6773	4925	54
H(8B)	4483	7816	5205	54
H(8C)	3576	6808	4857	54
H(9A)	1808	6438	5692	55
H(9B)	2651	7480	6036	55
H(9C)	2519	6238	6340	55
H(10)	5827	7356	6234	37
H(12A)	8016	5495	7053	58
H(12B)	8083	6798	6820	58
H(12C)	9049	5808	6480	58
H(13A)	10111	3494	5870	45
H(13B)	11036	3627	6507	45
H(14)	9854	2016	6837	35
H(16)	9533	-102	5810	29
H(17A)	6414	-592	6122	31
H(17B)	6714	140	5515	31
H(18)	5856	1753	6120	28
H(20A)	7501	2512	7253	52
H(20B)	6353	1915	7729	52
H(20C)	5595	2586	7179	52
H(21A)	4004	879	6928	54
H(21B)	4756	201	7477	54
H(21C)	4839	-349	6830	54
H(22)	7958	-47	7529	37
H(24A)	10283	-1647	6648	55
H(24B)	10323	-1134	7303	55
H(24C)	11345	-532	6791	55
H(1)	6660(40)	2920(30)	5295(12)	43(8)
H(2A)	9270(40)	1890(30)	5310(13)	48(8)

Table 4.20: Torsion angles [°] for **4.71**.

C(1)-C(2)-C(3)-O(1)	8.9(3)	C(13)-C(14)-C(15)-O(2)	4.1(3)
C(1)-C(2)-C(3)-C(4)	138.6(2)	C(13)-C(14)-C(15)-C(16)	133.7(2)
C(1)-C(2)-C(3)-C(6)	-117.5(2)	C(13)-C(14)-C(15)-C(18)	-123.2(2)
O(1)-C(3)-C(4)-C(11)	177.73(16)	O(2)-C(15)-C(16)-C(23)	178.31(16)
C(2)-C(3)-C(4)-C(11)	48.4(2)	C(14)-C(15)-C(16)-C(23)	49.0(2)
C(6)-C(3)-C(4)-C(11)	-77.94(17)	C(18)-C(15)-C(16)-C(23)	-77.92(16)
O(1)-C(3)-C(4)-C(5)	-74.82(17)	O(2)-C(15)-C(16)-C(17)	-74.20(17)
C(2)-C(3)-C(4)-C(5)	155.88(18)	C(14)-C(15)-C(16)-C(17)	156.48(18)
C(6)-C(3)-C(4)-C(5)	29.51(14)	C(18)-C(15)-C(16)-C(17)	29.57(13)
C(11)-C(4)-C(5)-C(6)	78.30(17)	C(23)-C(16)-C(17)-C(18)	78.60(17)
C(3)-C(4)-C(5)-C(6)	-29.90(14)	C(15)-C(16)-C(17)-C(18)	-29.92(13)
C(4)-C(5)-C(6)-C(7)	-84.61(18)	C(16)-C(17)-C(18)-C(19)	-84.81(17)
C(4)-C(5)-C(6)-C(3)	29.67(14)	C(16)-C(17)-C(18)-C(15)	29.73(14)
O(1)-C(3)-C(6)-C(7)	-168.68(15)	O(2)-C(15)-C(18)-C(19)	-168.37(16)
C(2)-C(3)-C(6)-C(7)	-40.0(3)	C(14)-C(15)-C(18)-C(19)	-38.5(3)
C(4)-C(3)-C(6)-C(7)	80.64(17)	C(16)-C(15)-C(18)-C(19)	80.58(18)
O(1)-C(3)-C(6)-C(5)	81.31(16)	O(2)-C(15)-C(18)-C(17)	81.67(16)
C(2)-C(3)-C(6)-C(5)	-150.0(2)	C(14)-C(15)-C(18)-C(17)	-148.5(2)
C(4)-C(3)-C(6)-C(5)	-29.37(14)	C(16)-C(15)-C(18)-C(17)	-29.38(13)
C(5)-C(6)-C(7)-C(10)	48.8(2)	C(17)-C(18)-C(19)-C(22)	49.7(2)
C(3)-C(6)-C(7)-C(10)	-45.9(2)	C(15)-C(18)-C(19)-C(22)	-45.2(2)
C(5)-C(6)-C(7)-C(8)	170.27(17)	C(17)-C(18)-C(19)-C(20)	172.46(17)
C(3)-C(6)-C(7)-C(8)	75.6(2)	C(15)-C(18)-C(19)-C(20)	77.5(2)
C(5)-C(6)-C(7)-C(9)	-71.8(2)	C(17)-C(18)-C(19)-C(21)	-69.9(2)
C(3)-C(6)-C(7)-C(9)	-166.49(16)	C(15)-C(18)-C(19)-C(21)	-164.80(17)
C(6)-C(7)-C(10)-C(11)	0.2(3)	C(20)-C(19)-C(22)-C(23)	-123.6(2)
C(8)-C(7)-C(10)-C(11)	-121.8(2)	C(18)-C(19)-C(22)-C(23)	-1.5(3)
C(9)-C(7)-C(10)-C(11)	119.7(2)	C(21)-C(19)-C(22)-C(23)	117.6(2)
C(7)-C(10)-C(11)-C(12)	175.7(2)	C(19)-C(22)-C(23)-C(24)	178.7(2)
C(7)-C(10)-C(11)-C(4)	-2.6(3)	C(19)-C(22)-C(23)-C(16)	-0.7(3)
C(5)-C(4)-C(11)-C(10)	-43.0(2)	C(17)-C(16)-C(23)-C(22)	-44.2(3)
C(3)-C(4)-C(11)-C(10)	49.4(2)	C(15)-C(16)-C(23)-C(22)	48.5(3)
C(5)-C(4)-C(11)-C(12)	138.58(19)	C(17)-C(16)-C(23)-C(24)	136.3(2)
C(3)-C(4)-C(11)-C(12)	-128.99(19)	C(15)-C(16)-C(23)-C(24)	-131.0(2)